

# PROCEEDINGS GEOMOD 2016

26/10/2016



## Organizing Committee (France):

**S. Dominguez** (University of Montpellier, [dominguez@gm.univ-montp2.fr](mailto:dominguez@gm.univ-montp2.fr)), **B. Maillot** (University of Cergy-Pontoise), **V. Cayol** (University of Clermont-Ferrand), **D. Arcay** (University of Montpellier), **B. Guillaume** (University of Rennes), **V. Pinel** (University of Savoie Mont-Blanc), **F. Graveleau** (University of Lille). Technical Staff: **C. Romano** (University of Montpellier), **A. Delplanque** (University of Montpellier).

## Scientific Committee:

**C. Annen** (University of Bristol, U.K.), **A. Chemenda** (University of Nice-Sophia-Antipolis, France), **M. Cooke** (University of Massachusett, USA), **T. Dooley** (University of Texas at Austin, USA), **F. Funiello** (University of Roma Tre, Italy), **K. Leever** (GFZ, Potsdam, Germany), **J. Malavieille** (University of Montpellier, France), **J.-C. Ringenbach** (TOTAL, Pau, France), **S. Schmalholz** (University of Lausanne, Swiss).

## **SESSIONS :**

<b>S0 - What's up in Modelling ?</b>	p.3
<b>S1 - Geodynamics, Plate tectonics</b>	p.34
<b>S2 - Coupling Tectonic and Surface processes</b>	p.100
<b>S3 - Volcanoes: from the plumbing system to the eruptive plume</b>	p.155
<b>S4 - Seismic cycle &amp; Earthquake dynamics</b>	p.204
<b>S5 - Rheology, strain localization, folding and faulting</b>	p.242
<b>S6 - Dynamics of sedimentary Basins, Fluids &amp; Georeservoirs</b>	p.281

**GEOMOD2016 WebSite :**

<http://geomod2016.gm.univ-montp2.fr/About.html>

**GEOMOD2016 Facebook :**

<https://www.facebook.com/geomod2016/>

## **S0 - What's up in Modelling ?**

## Adequate constitutive description of geological materials is a major challenge for geomodeling: examples of deformation localization, fracturing, and faulting

Alexandre Chemenda<sup>1</sup>, Daniel Mas<sup>1</sup>, Julien Ambre<sup>1</sup>, Jinyang Fan<sup>1</sup>, J.-P. Petit<sup>2</sup>, Stephane Bouissou<sup>1</sup>

<sup>1</sup>) University of Nice-Sophia Antipolis, Observatoire de la Côte d'Azur, Geoazur, Valbonne, France

<sup>2</sup>) University of Montpellier, Géosciences Montpellier, Montpellier, France

Corresponding author: chem@geoazur.unice.fr

S0- What's up in Modelling ? (Keynote)

### Introduction:

The mechanical (constitutive) models of geomaterials become progressively more sophisticated with the progress in our understanding of rock properties, which reflects the complexity of the behavior of these materials. For example, the experimental results from the test conducted under different loading configurations corresponding to the different Lode angles  $\theta$  (axisymmetric compression, extension and true 3-D tests; Heard, 1960; Nguyen et al., 2011; Ingraham et al., 2013; Ma and Haimson, 2013) as well as a very recent theoretical analysis of these results (Chemenda and Mas, *JMPS*, 2016) show that  $\theta$  strongly affects the inelastic response and failure of geomaterials. The  $\theta$ -dependence of the rock properties as well as the evolution of the constitute parameters with inelastic deformation (damage) is typically ignored in numerical geomodeling and must be taken into account, notably when dealing with the material failure. It becomes particularly important to conduct a combined experimental and numerical (virtual) modeling complemented by the theoretical analysis and field observations to evaluate the realism of the virtual models. In this paper we present recent findings in the constitutive modeling and report the results from experimental studies and numerical modeling of faulting and fracturing resulting from a constitutive instability.

### Constitutive framework, experimental, and numerical models

A pragmatic approach consists in formulation, based on the experimental data, of the models that are as simple as possible and that capture at the same time the essential features of rock behavior. How far can we simplify? The classical Mohr-Coulomb and Drucker-Prager models with constant internal friction coefficient  $\alpha$ , cohesion, and dilatancy factor are clearly oversimplified as in reality all these parameters are not constant but evolve with both the stress state and the material damage or inelastic strain (Fig. 1).

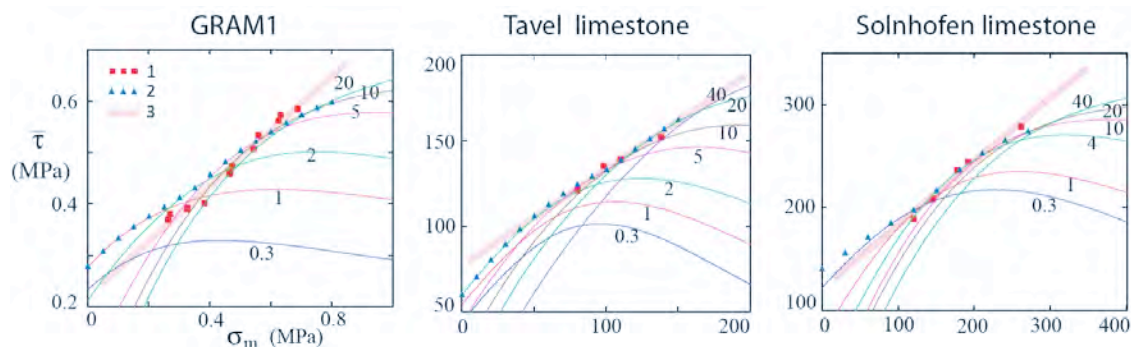


Figure 1: Iso- $\gamma$  sections of the yield surfaces with the superposed stress peak points (1) and the points corresponding to zero values of the hardening modulus (2). (3) is the linear approximation of the peak points corresponding to the failure envelopes. The slopes of these envelopes  $\alpha_{pk}$  are different from  $\alpha = \partial\bar{\tau} / \partial\sigma_m$ . The

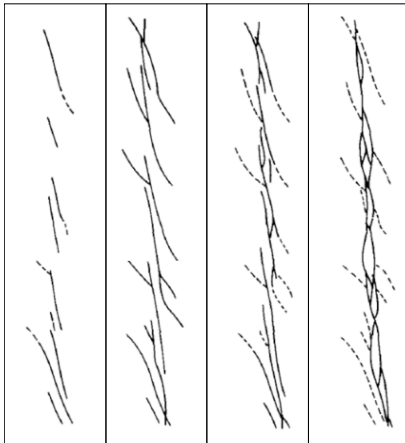
numbers on the iso- $\gamma$  sections of the yield surfaces are  $10^3 \times \gamma$ ;  $\bar{\tau}$  is the von Mises stress,  $\sigma_m$  is the mean stress, and  $\gamma$  is the accumulated inelastic strain or damage (Mas, Chemenda, *IJRMMS*, 2015).

Recent analysis of large data set for Granular Rock Analog Material GRAM1 and two limestones has revealed that not only  $\alpha$  defined from yield surfaces is not constant, but also it is not directly related to the friction coefficient  $\alpha_{pk}$  routinely defined from the failure envelopes (from the stress peaks) as is shown in Fig. 1.

The details of constitutive description strongly affect the predictions of the material failure particularly when the mean stress  $\sigma_m$  is not very small and the failure results from a material instability leading to the deformation localization. We present results from true 3-D experiments showing the formation of four types of deformation localization bands with progressively increasing  $\sigma_m$ : pure dilatant/dilatancy, shear-dilatant, pure shear, shear-compactive. These bands have different both orientation in the stress space and evolution. Only bands with dilatant component of deformation can rapidly evolve to fractures either opening or shear, whereas the bands with compactive deformation undergo a long evolution that may never result in a fracture formation.

Numerical modeling integrating evolution of the constitutive parameters with stress and strain (as shown in Fig. 1) and experimentally derived relation between the yield and plastic potential functions (Mas and Chemenda, *IJRMMS*, 2015), allows not only to reproduce all aforementioned band/fracture types, but also more complicated scenarios with evolution of band networks, differential band thickening and propagation observed in the experimental tests and in nature (e.g., Chemenda et al., *Tectophys.*, 2012). The numerical models allow also following in detail the initiation and evolution of fault systems (Fig. 2) that initiate via deformation banding of different types (Chemenda et al., 2016).

Sandbox model (Naylor et al., 1986)



Numerical model

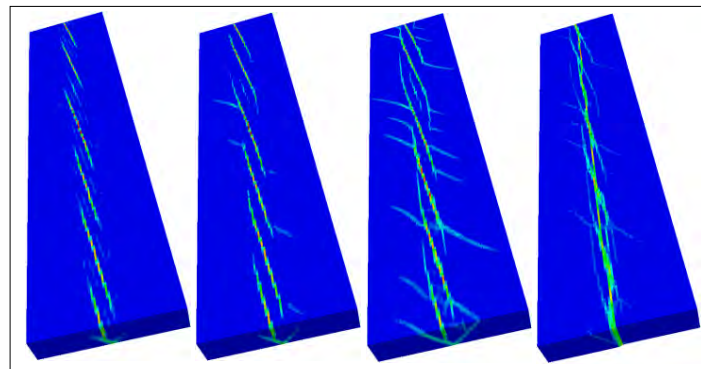


Figure 2: Comparison of the evolution of the Riedel-type faulting in analogue and numerical models

**Keywords:** Rock mechanical (constitutive) properties, rock testing, Lode angle, deformation bifurcation, strain localization, fracturing, faulting, experimental and numerical modeling, natural deformation bands.

## Laboratory characterization of thermal plumes at high Rayleigh numbers

Danielle Brand<sup>1</sup> and Anne Davaille<sup>1</sup>

<sup>1</sup>) Université Paris-Saclay, Lab. FAST, Orsay, France

Corresponding author: [Danielle.brand@u-psud.fr](mailto:Danielle.brand@u-psud.fr)

S0- What's up in Modelling ? (PS7)

### Introduction:

Thermal plumes are gravitationally buoyant instabilities which form when a layer of fluid is heated from below. Therefore, they are ubiquitous features of thermal convection and should exist in planetary mantle convection. They offer a reasonable explanation for hotspot volcanism, which could be generated by decompression melting as plumes reach the planet surface (Wilson, 1963; Morgan, 1971). Recent developments in whole-mantle seismic imaging techniques indeed show that rather broad, quasi-vertical low shear-wave velocity anomalies extending from the core-mantle boundary to the near surface exist beneath several major hotspots (French & Romanowicz, 2015). As low shear-wave velocities are usually produced by hotter material, this confirms the existence of mantle plumes. On the other hand, plume impact signatures in the lithosphere vary from triple junction and continental breakup to large oceanic plateaus to linear volcanic chains. The mechanisms leading to these different signatures are not fully understood though.

In this project, we use laboratory experiments and state of the art visualization techniques to characterize thermal plumes and their impingement under a fluid surface. The plume ascent velocity, dilation of the plume head, periodicity of plume formation, and plume morphology are systematically studied and scaling laws are derived from the experimental data. As reference cases, the fluid layer was initially homogeneous. A few additional cases were run where the plume head interacts with a thin plastic layer at the top of the experimental tank.

### Laboratory study:

Plume generation is carefully studied through fluid laboratory models in the regime of high Rayleigh numbers and intermediate viscosity ratios (applicable to Earth's mantle). We concentrate on the development of laminar, thermal plumes in temperature-dependent, viscous glucose syrups. The fluid is uniformly heated from below at a constant temperature and the studied plumes are localized on a small copper protuberance in the center of the experimental tank, 25 or 60 mm in diameter.

#### *Visualization Techniques*

In order to quantitatively characterize experimental plumes, several new techniques are employed. Temperature fields are visualized using thermo-chromatic liquid crystals (TLCs), which map five chosen isotherms and also help to define the plume shape (Figure 1). Each of the five types of TLCs reflects monochromatic light at distinct temperatures, which allows for the illumination of a cross section in any selected horizontal or vertical plane. Velocity fields are obtained using particle image velocimetry (PIV) and topographic profiles and plume ascent are imaged through time-lapse photography. Image analysis is then performed using Matlab (Figure 2).

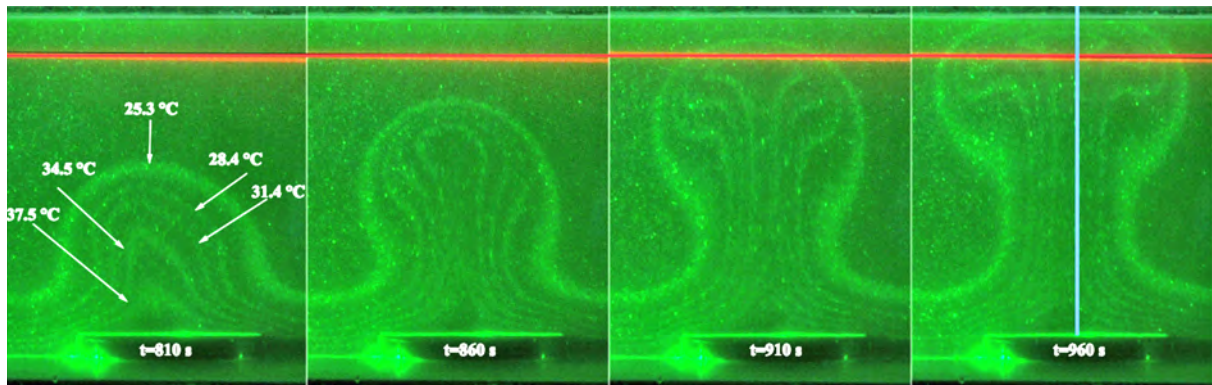


Figure 1: Development of the plume from  $t=810$  s to  $t=960$  s, visualized using TLCs. The bright lines contouring the plume are the isotherms and each isotherm consists of a different type of TLC. This depicts a cross section in the vertical plane, through the center of the plume. The red and blue lines are the horizontal and vertical axes used to construct the images presented in Figure 2. The experimental tank is heated to  $60$  °C from below.

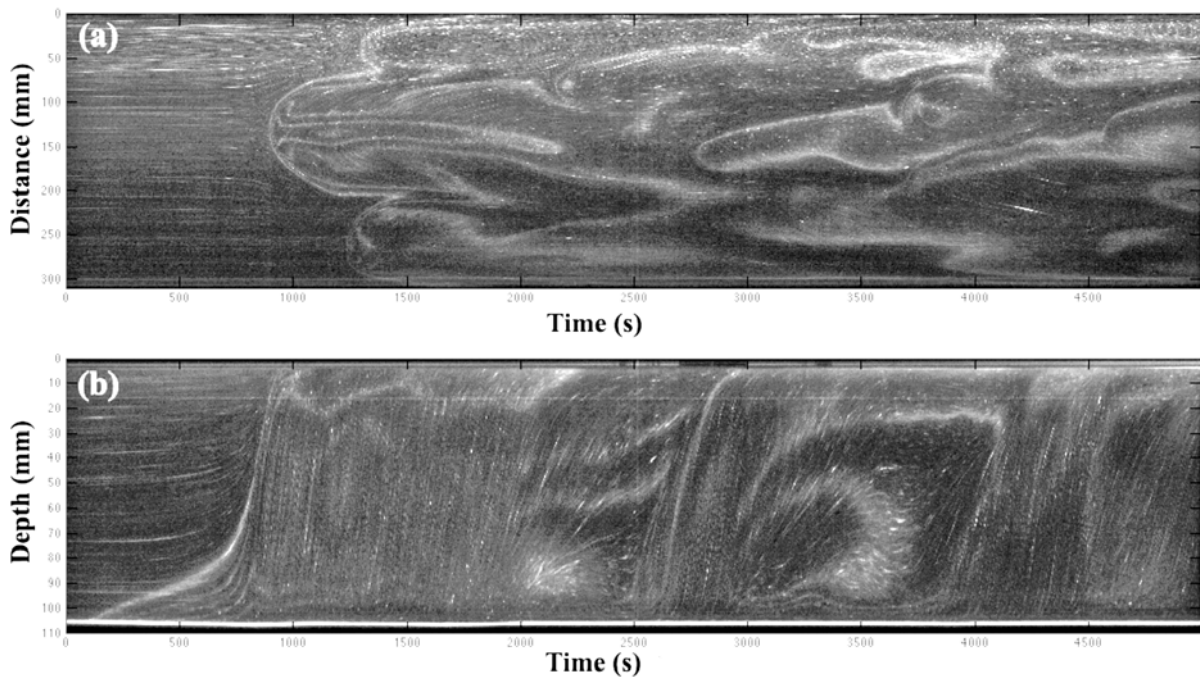


Figure 2: MatLab analysis for the experiment presented in Figure 1. **a** Development of the plume head through time along a horizontal axis (red line in Figure 1). This illustrates the construction of eight consecutive plumes over 5000 s. **b** Plume uplift through time along the vertical plume axis (blue line in Figure 1). The bright lines are the isotherms.

### References:

- French, S.W., and Romanowicz, B., 2015. Broad plumes rooted at the base of Earth's mantle beneath major hotspots, *Nature*, 525, 95-99.  
 Morgan, W.J., 1971. Convection plumes in the lower mantle, *Nature*, 230, 42-43  
 Wilson, J.T., 1963. Hypothesis of earth's behavior, *Nature*, 198, 925-929.

**Keywords:** Mantle plumes, convection, hotspots, visualization, thermo-chromic liquid crystals, laboratory experiments.

## Benchmarking numerical models of brittle thrust wedges

Susanne Buitert<sup>1</sup>, Guido Schreurs<sup>2</sup> and the GeoMod Team\*

<sup>1</sup>) Geodynamics Team, Geological Survey of Norway, 7040 Trondheim, Norway and The Centre of Earth Evolution and Dynamics, University of Oslo, 0316 Oslo, Norway.

<sup>2</sup>) Institute of Geological Sciences, University of Bern, 3012 Bern, Switzerland

Corresponding author: susanne.buitert@ngu.no

S0- What's up in Modelling ? (PS7)

Model experiments that investigate the evolution of deformation processes in the crust face specific challenges related to, among others, contrasts in material properties, the heterogeneous character of continental crust, the presence of a free surface, and large offsets on shear zones. These pose specific demands on numerical software and laboratory models. Particularly brittle deformation, with the formation and evolution of shear zones, has been challenging for especially continuum numerical techniques, resulting in different approaches to brittle material behaviour. To test the model-independence of brittle experiments and quantify the variability between their results, we performed a direct comparison of three brittle thrust wedge experiments with identical setups. We here report the results of 11 numerical experiments and compare these to the 15 analogue experiments of Schreurs et al. (2016).

Our three tests resemble setups frequently used by analogue models, which limits the amount of deformation and prescribes boundary conditions that include friction and velocity discontinuities. The first experiment tests whether codes reproduce predictions from analytical critical taper theory. Eleven codes pass the stable wedge test, showing negligible internal deformation and maintaining the initial surface slope upon horizontal translation over a frictional interface. Small deformation of the wedge toe occurs in some cases. Eight codes participated in the second experiment that examines the evolution of a wedge by thrust formation from a subcritical state to the critical taper geometry (Fig. 1). All models recover the critical taper. However, the models show two deformation modes characterised by either mainly forward dipping thrusts or a series of thrust pop-ups. We speculate that the two modes are caused by differences in effective basal boundary friction related to different algorithms for modelling boundary friction. The third experiment examines stacking of forward thrusts that are translated upward along a backward thrust. The results of the seven codes that run this experiment show variability in deformation style, number of thrusts, thrust dip angles and surface slope.

Overall, our experiments show that numerical models run with different numerical techniques can successfully simulate laboratory brittle thrust wedge models at the cm-scale. The similarity in results between the analogue and numerical models encourages using both techniques for investigating the formation and evolution of accretionary prisms and fold-and-thrust belts. In more detail, however, we find that it is challenging to reproduce sandbox-type setups numerically, because of frictional boundary conditions and velocity discontinuities. We would like to emphasize that, where shear zones are concerned, trends, rather than absolute numbers, should be used in applications of model results to natural settings. We recommend that future numerical-analogue comparisons use simple boundary conditions and that the numerical Earth Science community defines a plasticity test to resolve the variability in model shear zone spacing and dip angle.

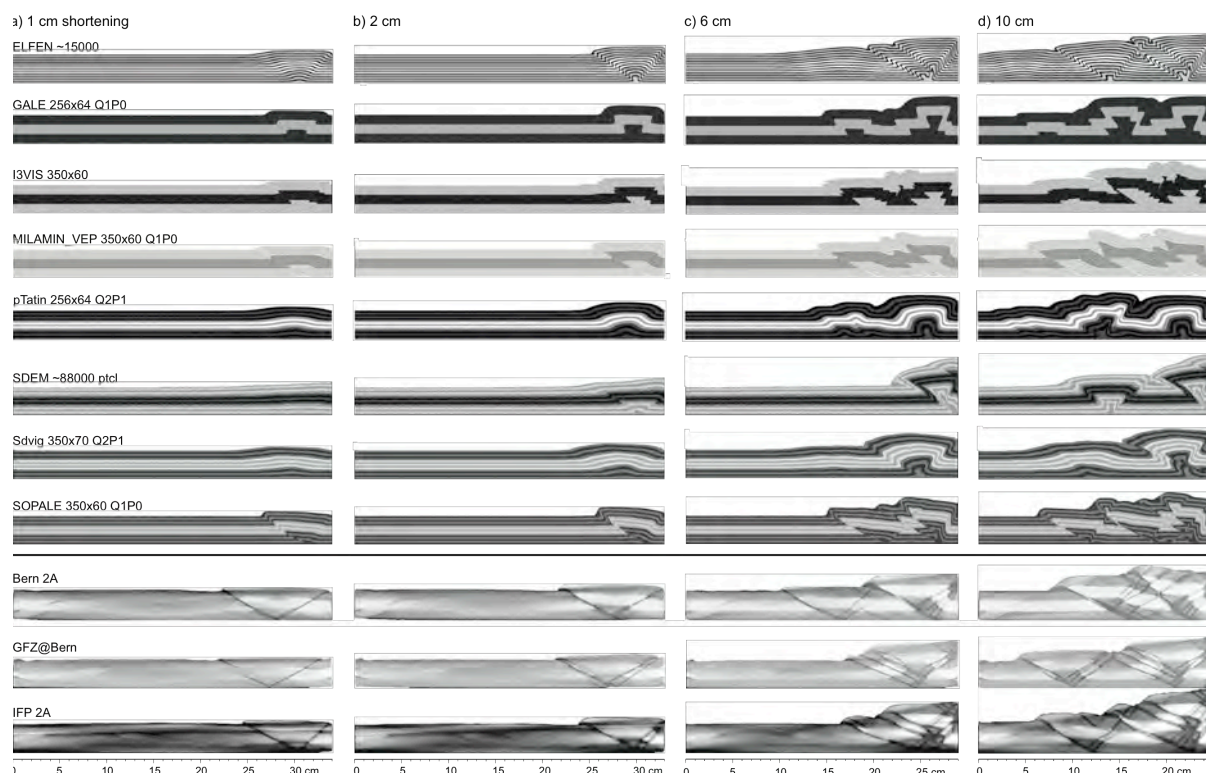


Figure 1: Results of eight numerical thrust wedge models after 1, 2, 6 and 10 cm of shortening (top). Wedge formation initiates with a pop-up structure near the mobile wall and continues with in-sequence formation of forward thrusts and backward thrusts. Analogue results of the University of Bern and IFP (as imaged in an X-ray computer tomographer) from Schreurs et al. (2016) shown below. Reprinted from *Journal of Structural Geology*, doi: 10.1016/j.jsg.2016.03.003, Buiter et al. (2016), *Benchmarking numerical models of brittle thrust wedges*, with permission from Elsevier.

## References:

- \*Buiter, S.J.H., Schreurs, G., Albertz, M., Gerya, T.V., Kaus, B., Landry, W., le Pourhiet, L., Mishin, Y., Egholm, D.L., Cooke, M., Maillot, B., Thieulot, C., Crook, T., May, D., Souloumiac, P. and Beaumont, C., 2016. Benchmarking numerical models of brittle thrust wedges, *Journal of Structural Geology*, doi: 10.1016/j.jsg.2016.03.003
- Schreurs, G., Buiter, S.J.H., Boutelier, J., Burberry, C., Callot, J.-P., Cavozi, C., Cerca, M., Chen, J.-H., Cristallini, E., Cruden, A.R., Cruz, L., Daniel, J.-M., Da Poian, G., Garcia, V.H., Gomes, V.J.S., Grall, C., Guillot, Y., Guzmán, C., Nur Hidayah, T., Hilley, G., Klinkmueller, M., Koyi, H.A., Lu, C.-Y., Maillot, B., Meriaux, C., Nilfouroushan, F., Pan, C.-C., Pillot, D., Portillo, R., Rosenau, M., Schellart, W.P., Schlische, R.W., Take, A., Vendeville, B., Vergnaud, M., Vettori, M., Wang, S.-H., Withjack, M.O., Yagupsky, D., Yamada, Y., 2016. Benchmarking analogue models of brittle thrust wedges, *Journal of Structural Geology*, doi: 10.1016/j.jsg.2016.03.005

**Keywords :** Thrust wedges, Brittle wedges, Benchmarking, Critical taper, Shear zones, Numerical modelling, Plasticity.

## Laboratory geodesy: Application of open-source photogrammetric software MicMac for monitoring surface deformation in laboratory models

Olivier Galland<sup>1</sup>, Håvard S. Bertelsen<sup>1</sup>, Frank Guldstrand<sup>1,2</sup>, Luc Girod<sup>3</sup>, Rikke F. Johannessen<sup>1</sup>, Fanny Bjugger<sup>2</sup>, Steffi Burchardt<sup>2</sup> and Karen Mair<sup>1</sup>

<sup>1</sup>) University of Oslo, Department of Geosciences, Physics of Geological Processes (PGP), Oslo, Norway.

<sup>2</sup>) Uppsala University, Department of Earth Sciences, Centre for Mineralogy, Petrology & Geochemistry, Uppsala, Sweden.

<sup>3</sup>) University of Oslo, Department of Geosciences, Oslo, Norway.

Corresponding author: olivier.galland@geo.uio.no

S0- What's up in Modelling ? (PS7)

### Abstract:

Quantifying deformation is essential in modern laboratory models of geological systems. However, high precision methods are usually costly or not straightforward to implement. This contribution presents a new laboratory monitoring method through the implementation of the open-source software MicMac, which efficiently implements photogrammetry in Structure-from-Motion (SfM) algorithms (Galland et al., 2016). Critical evaluation is provided using results from an example laboratory geodesy scenario: magma emplacement (Fig. 1). MicMac automatically processes images from synchronized cameras to compute time series of digital elevation models (DEMs) and orthorectified images of model surfaces. MicMac also implements Digital Image Correlation (DIC) to produce high-resolution displacement maps. The resolution of DEMs and displacement maps corresponds to the pixel size of the processed images. Using 24 MP cameras, the precision of DEMs and displacements is  $\sim 0.05$  mm on a  $40 \times 40$  cm surface. Processing displacement maps with Matlab<sup>®</sup> scripts allows automatic fracture mapping on the monitored surface (Fig. 2). MicMac also offers the possibility to integrate 3D models of excavated structures with the corresponding surface deformation data. The high resolution and high precision of MicMac results and the ability to generate virtual 3D models of complex structures make it a very promising tool for quantitative monitoring in laboratory models of geological systems.

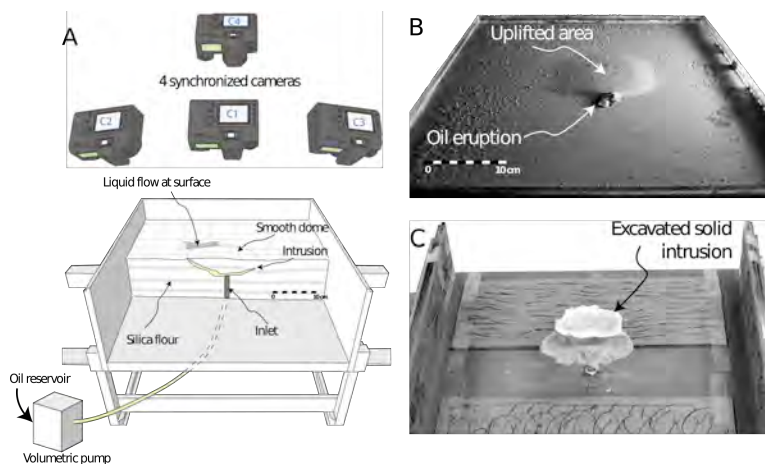


Figure 1. A. Diagram showing the experimental apparatus used for volcano geodesy (see text for explanations).

B. Representative oblique view photograph of the model surface during an experiment. The surface exhibited a smooth dome, at the rim of which the oil erupted. C. Representative oblique view photograph of an excavated solidified intrusion. As it is fully excavated, it is possible to apply photogrammetry and compute its 3D shape.

The implementation of MicMac in the laboratory is highly versatile. This laboratory geodesy platform offers great potential to study numerous geological phenomena involving surface deformation. These processes include tectonics, landslides, glacier dynamics, etc. The ultimate objective is to integrate laboratory data with real geodetic measurements to help interpreting natural data, and therefore better constrain the processes underlying surface deformation.

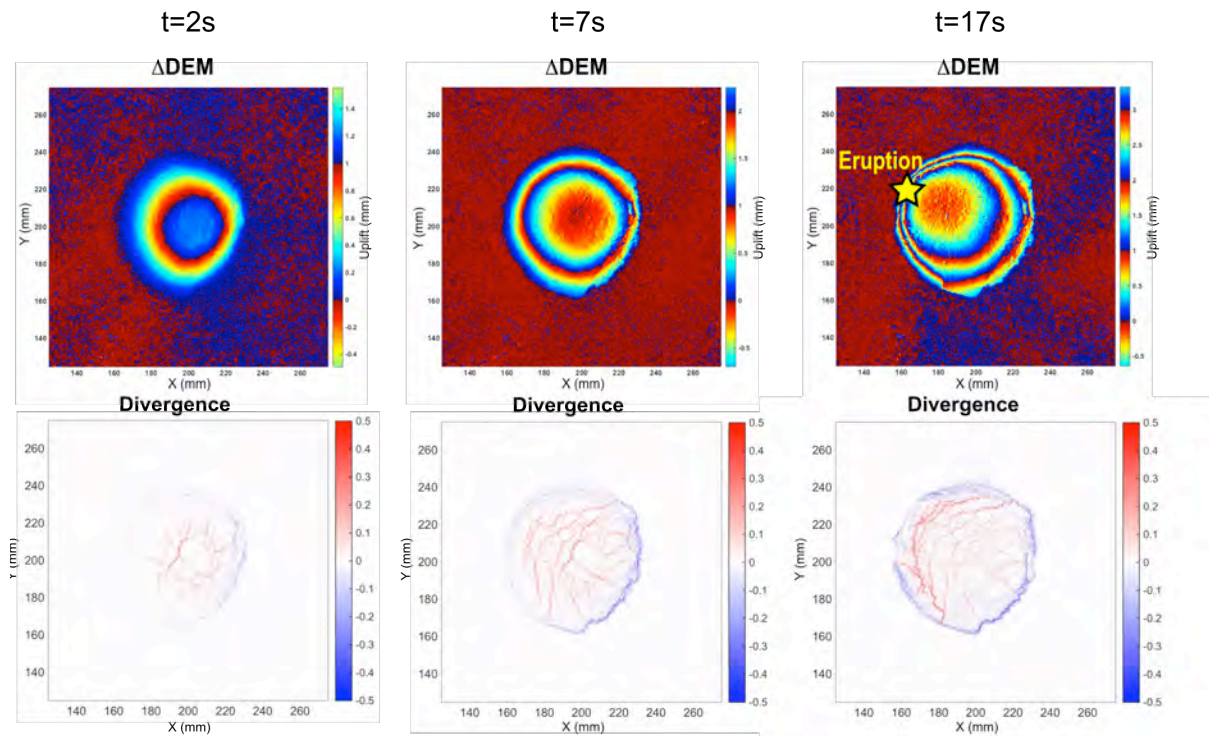


Figure 2. Plots of representative results of the surface evolution during an example magma intrusion experiment at three distinct time steps (columns). The plots display  $\Delta DEM$  (topography change with respect to initial state), and divergence field calculated from  $U_x$  and  $U_y$  field. The yellow star locates oil eruption.

**Acknowledgements:** This work was supported by a Center of Excellence grant from the Norwegian Research Council to PGP (grant no. 146031). Guldstrand's position is funded by the DIPS (Dynamics of igneous plumbing systems, grant no. 240467) project, distributed by the Norwegian Research Council. Girod was funded by the European Research Council under the European Union's Seventh Framework Programme (FP/2007–2013)/ERC grant agreement no. 320816.

### References:

Galland, O., Bertelsen, H. S., Guldstrand, F., Girod, L., Johannessen, R. F., Bjugger, F., Burchardt, S. & Mair, K. 2016. Application of open-source photogrammetric software MicMac for monitoring surface deformation in laboratory models. *Journal of Geophysical Research: Solid Earth*, 121, 2852-2872.

**Keywords:** photogrammetry, analogue models, surface deformation.

## Generating tetrahedral meshes for finite element simulations on complex geological structures

Ines Görz<sup>1</sup>, Björn Zehner<sup>2</sup>, Jana H. Börner<sup>1</sup> and Klaus Spitzer<sup>1</sup>

<sup>1</sup>) Department of Geophysics and Geoinformatics, TU Bergakademie Freiberg, Gustav-Zeuner-Straße 12, 09599 Freiberg, Germany

<sup>2</sup>) Federal Institute for Geosciences and Natural Resources (BGR), Wilhelmstraße 25-30, 13593 Berlin, Germany

Corresponding author: igo@geo.tu-freiberg.de

S0- What's up in Modelling ? (PS7)

Geological 3D models represent complex geometry and topology of geological bodies, taking into account geological concepts and data related to the subsurface. They often describe the structural model in terms of triangulated surfaces that specify the extent of objects only by their boundaries. This so-called boundary representation requires little storage and is particularly suited to the visualization of models. By contrast, a cell representation discretizes the whole volume of the modelling domain and is needed when the model is used for numerical simulations. Different types of cell representations are available. For finite element codes, unstructured tetrahedral meshes are often used that can adapt to complicated forms and be refined locally. The conversion process from the surface-based representation to the volume-based representation is complicated and still under investigation. Many methods have been developed to perform it. These methods have to fulfil requirements, such as providing a good mesh quality, allowing for local mesh adaption and the incorporation of geometry into the definition of the boundary conditions.

In our study, we tested workflows for the generation of unstructured tetrahedral meshes on a real-world geological model. The modelling area is situated in Niedersachsen (Germany) and comprises an Upper Permian salt diapir, its Mesozoic sedimentary host rock, Tertiary eroded sedimentary sequences and the Quaternary cover (NIBIS; LBEG, 2013). We use simulations of the transient electromagnetic method (TEM) to test the workflows. Each geological unit represents one homogeneous volume with constant specific electrical resistivities as input parameters for the simulation. The electric source is located at one point at the surface which represents the ground, while the receivers are placed in two virtual boreholes at points with constant distance to the source. Both source and receiver locations have to be nodes of the discretization. Since we apply a linear basis function for the TEM simulation, we have to refine the mesh around the receivers in order to avoid evaluation errors with one element.

We tested three workflows starting with the software Skua-Gocad (Paradigm, 2011) in which the structural model was created. Since the boundary surfaces are generated independently of each other in this software, the nodes of the surface's triangulation are not identical at the surface contacts, such that a conformable triangulation has to be produced prior to the volume tessellation by tetrahedrons. For the first workflow, we used the Skua Finite Element Mesh Constructor (FEMC) which automatically generated a conformable surface triangulation and a tetrahedral mesh. A local mesh refinement and the prescription of geometry for setting the boundary conditions is not possible with this workflow. The second workflow generated a conformable surface mesh by re-meshing the surfaces from a framework of surface boundaries and contact lines in the software Gmsh (Geuzane and Remacle, 2009). We refined the triangulation of the ground around the electric source and passed the conformable set of boundary surfaces to the software TetGen (Si, 2011) for tessellation. Since the mesh generated in TetGen is coincident with the surface triangulation, the resulting tetrahedral mesh is refined around the source. For the third workflow, we exported the boundary surfaces of the structural model to the computer-aided engineering software ANSYS (Ansys, 2013) where the triangulated surfaces were converted into one single NURBS. Since a NURBS is a continuous mathematical

function, the tetrahedral mesh is produced independently of the original surface triangulation and a well-controlled local adaption and refinement of the mesh around the source is possible.

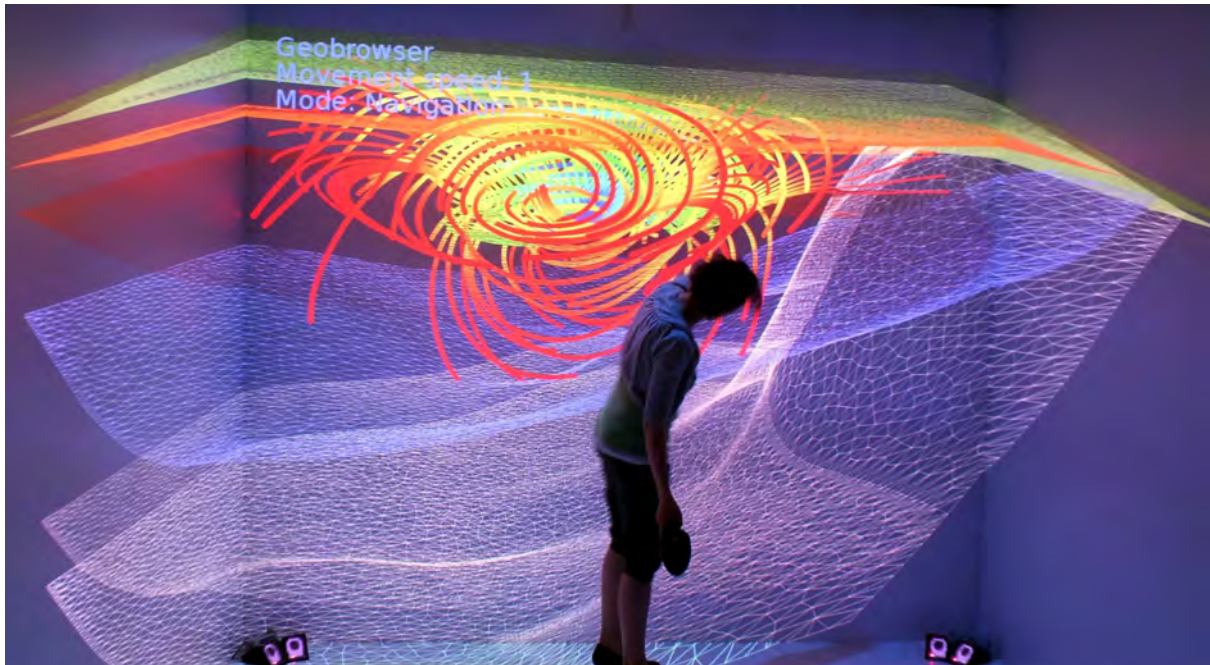


Figure 1: Visualization of the simulation results: The electrical and magnetic vector field rendered in a CAVE.

The three models we generated using the three workflows were passed to the TEM software of Afanasjew et al. (2013). The Matlab code solves the curl-curl equation for the electric field that describes the inductive response in the time domain. We ran the simulation on the three meshes produced with the three workflows and compared the simulation results. To estimate the absolute accuracy, we plotted the numerical solutions for homogeneous material parameters against the analytical solution for a homogeneous half-space (Nabighian, 1979).

The FEMC mesh is not able to image the expected circular shape of the electric field and cannot reproduce the analytical solution. The Gmsh/TetGen and Ansys meshes reproduce well the analytical solution and have the correct shape, sign and order of magnitude. Having completed this check, the geological units in the 3D model were equipped with electrical resistivities according to Schön (1996) and Archie (1942). The numerical solution for the transient electromagnetic field shows the same circular current system as in the homogeneous case, but adapted to the formation resistivities. The current system concentrates on the conductive sedimentary horizons, but does not protrude into the high-resistivity salt rocks (Figure 1). In addition, it is distorted according to the Jurassic and Cretaceous formations which were dragged upward by the rising salt. The FEMC mesh shows a different shape with a zone of high current density directly below the source. We think that the deviation of the simulation results on this mesh in comparison to the others is caused by the coarse resolution of the mesh around the electric source due to propagation errors.

We showed that all three workflows successfully yielded a discretization of the diapiric structure on which calculations robustly run. However, it could be seen that the mesh had to be adapted to the special requirements of the simulation method. In our case we needed a mesh refinement around the source, which could not be generated with the Skua FEMC. So the simulation results on this mesh were not feasible. Our example shows that each model makes special demands of the mesh and the user has to decide which workflow is best suited to the model and simulation method desired.

**References:**

- Afanasjew M., Börner R.-U., Eiermann M., Ernst O., Spitzer K. (2013): Efficient Three-Dimensional Time Domain TEM Simulation Using Finite Elements, a Nonlocal Boundary Condition, Multigrid, and Rational Krylov Subspace Methods. Expanded Abstracts, 5th International Symposium on Three-Dimensional Electromagnetics, May 7 – 9, 2013, Sapporo, Japan, 4p.
- Ansys Workbench 14.5 (2013): Ansys Inc., URL: <http://www.ansys.com>.
- Archie G.E. (1942): The electrical resistivity log as an aid in determining some reservoir characteristics. Transactions of the American Institute of Mining and Metallurgical Engineers 146, 54–62.
- Geuzaine C., Remacle J.-F. (2009): Gmsh: a Three-Dimensional Finite Element Mesh Generator with Built-in Pre- and Post-Processing Facilities. International Journal for Numerical Methods in Engineering 79, 1309 – 1331.
- PARADIGM Gocad-Skua<sup>®</sup> software (2011): URL: <http://www.pdgm.com/products/gocad.aspx>.
- Nabighian, M., 1979. Quasi-static transient response of a conducting half-space—an approximate representation. Geophysics 44(10), 1700–1705.
- NIBIS<sup>®</sup> mapserver of the LBEG Niedersachsen, Germany (2013): URL: <http://nibis.lbeg.de/cardomap3/>, data retrieved february 18th, 2013.
- Schön J. (1996): Physical properties of rocks - fundamentals and principles of petrophysics. 1 ed. Pergamon. Volume 18 of Handbook of Geophysical Exploration.
- Si H. (2011): TetGen, A Quality Tetrahedral Mesh Generator and a 3D Delaunay Triangulator. <http://tetgen.berlios.de/>, last time visited July 2011.

**Keywords:** 3D model, tetrahedral mesh, finite elements, electromagnetics, TEM.

## **Cem-GM: Cemented granular material as rock analogue to model irreversible fragmentation of rocks in landslides**

Øystein Thordén Haug<sup>1,2</sup>, Matthias Rosenau<sup>2</sup>, Karen Leever<sup>2</sup>, and Onno Oncken<sup>3</sup>

<sup>1</sup>) Physics of Geological Processes, University of Oslo, Norway

<sup>2</sup>) GFZ German Research Centre for Geoscience, Helmholtz Centre Potsdam, Germany

Corresponding author: o.t.haug@geo.uio.no

S0- What's up in Modelling ? (PS7)

### **Introduction:**

Fragmentation is the process of separating a material by fractures, and occurs in many geological systems, e.g. volcanic eruptions [e.g. Haug et al. (2013)] and landslides [e.g. Locat et al. (2006)]. Despite its common occurrence in landslides, fragmentation is rarely considered in models describing their transport. Instead, most models use granular material to study the behavior of landslides in motion [e.g. Manzella and Labiouse (2009)]. However, this means one must assume that all fragmentation occurs at the point of slope failure, and any reduction of particle size during transport is neglected. Nevertheless, models that include fragmentation [Bowman et al. (2012)] have shown that the final travel length of the front of the landslide deposit will increase with increased degree of fragmentation. This suggests that fragmentation can play an important role in the transport of landslides, and needs to be considered.

Analogue experiments are good tools to study the transport of landslides as they easily allow considering complex shapes of both the landslide body and the slope. However, existing rock analogue are either too strong (e.g. coal), so that fragmentation only occurs in an increased gravity field of a centrifuge [e.g. Bowman et al (2012)], or they allow healing (e.g. powders). Here, we present a new rock analogue that overcomes these limitations: a cemented granular material that can irreversibly fragment on a lab-scale.

### **Material properties**

The material consists of sand cemented with a weak binding material (either gypsum or potato starch). The material properties were tested using tri-axial and ring shear tests. The cohesion can be controlled from the concentration of cement, allowing us to use cohesion as a variable (Figure 1). Ring shear test showed that only the primary cohesion of the material was increased, and that the angle of friction was unchanged compared to uncemented sand.

### **Cohesion as a variable – application for fragmentation during landslides**

Since the strength of the analogue material can easily be varied, cohesion becomes an experimental variable. Experiments with varying cohesion reveal that three kinematic regimes exists (Figure 2): (1) *Immediate collapse*, The sample undergoes complete failure at the point of release, leading to a granular flow. (2) *Dynamic fragmentation*, the sample stays intact while acceleration, but fragments during an impact, leading to a transition from an elastic block to a granular flow. (3) *Elastic block*, the sample can withstand the impact, and stays largely intact during its entire travel path.

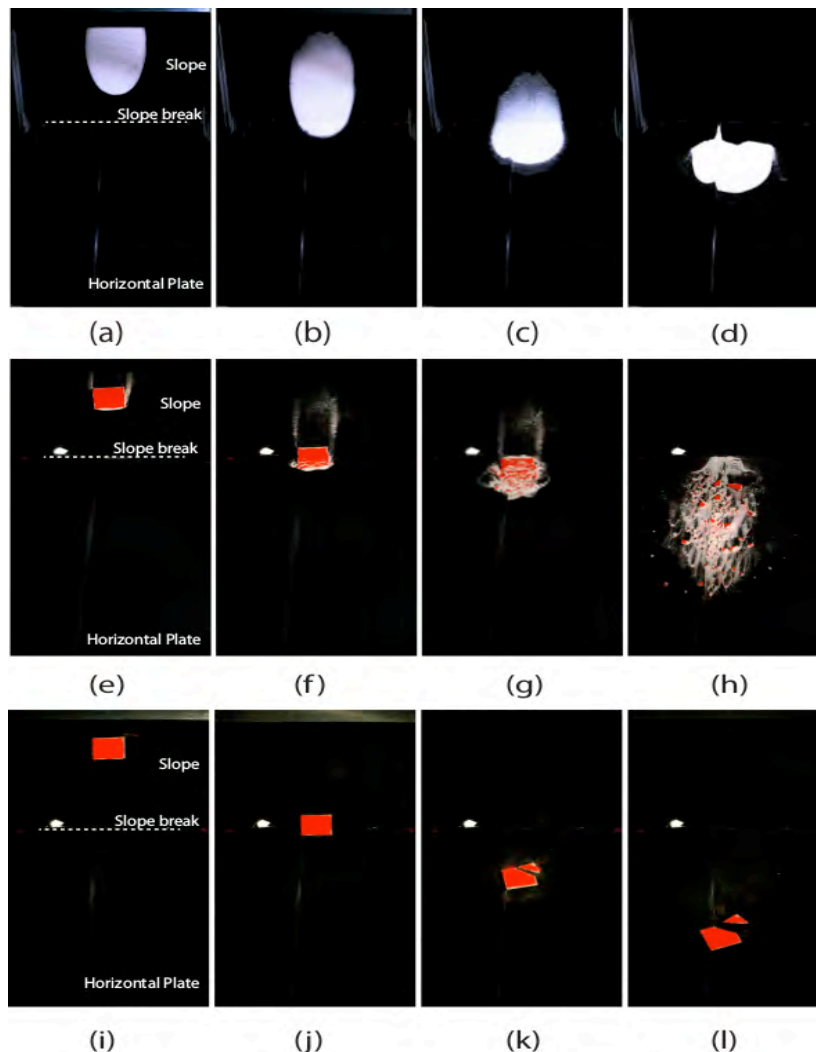


Figure 2: Cohesion as a variable reveals three kinematic regimes: (a-d) immediate collapse, (e-h) Dynamic fragmentation and (i-l) Elastic block.

### References:

- Bowman, E. T., Take, W. A., Rait, K. L., & Hann, C. (2012). Physical models of rock avalanche spreading behaviour with dynamic fragmentation. *Canadian Geotechnical Journal*, 49(4), 460–476. <http://doi.org/10.1139/t2012-007>
- Haug, Ø. T., Galland, O., & Gisler, G. R. (2013). Experimental modelling of fragmentation applied to volcanic explosions. *Earth and Planetary Science Letters*, 384, 188–197. <http://doi.org/10.1016/j.epsl.2013.10.004>
- Locat, P., Couture, R., Leroueil, S., Locat, J., & Jaboyedoff, M. (2006). Fragmentation energy in rock avalanches. *Canadian Geotechnical Journal*, 43(8), 830–851. <http://doi.org/10.1139/t06-045>
- Manzella, I., & Labiouse, V. (2009). Flow experiments with gravel and blocks at small scale to investigate parameters and mechanisms involved in rock avalanches. *Engineering Geology*, 109 (1-2), 146–158. <http://doi.org/10.1016/j.enggeo.2008.11.006>.

**Keywords:** Analogue material, fragmentation, landslides.

## **Modelling fully-coupled Thermo-Hydro-Mechanical (THM) processes in fractured geothermal reservoirs using GOLEM: a massively parallel open-source simulator.**

Antoine B. Jacquy<sup>1,2</sup> and Mauro Cacace<sup>1</sup>

<sup>1)</sup> GFZ – German Research Centre for Geosciences, Potsdam, Germany

<sup>2)</sup> RWTH Aachen University, Aachen, Germany

Corresponding author: antoine.jacquy@gfz-potsdam.de

S0- What's up in Modelling ? (PS7)

Deep geothermal resources have received increasing attention in the last decades as a source of carbon-free energy. However, extracting the heat from such low permeable reservoirs requires fluid pathways whether natural or engineered. Understanding the key processes controlling fluid and heat flow around geological discontinuities such as faults and fractures is therefore of interest in order to design safe and sustainable geothermal operations. Furthermore, numerical simulators have become indispensable in geological studies to model coupled processes and complex geological geometries. In this study, we present a new simulator GOLEM, using multiphysics coupling to characterize geological reservoirs. In particular, special attention is given to discrete geological features such as faults and fractures.

### **Multiphysics coupling:**

GOLEM is based on the Multiphysics Object-Oriented Simulation Environment (MOOSE) [Gaston et al., 2009]. The MOOSE framework provides a powerful and flexible platform to solve multiphysics problems implicitly and in a tightly coupled manner on unstructured meshes which is of interest for the considered non-linear context. Governing equations for fluid flow, heat transfer (conductive and advective), saline transport as well as deformation (elastic and plastic) have been implemented into the GOLEM application. Coupling between rock deformation and fluid and heat flow is considered using theories of poroelasticity and thermoelasticity (see Figure 1). Furthermore, considering material properties such as density and viscosity and transport properties such as porosity as dependent on the state variables (based on the International Association for the Properties of Water and Steam models) increase the coupling complexity of the problem. The GOLEM application aims therefore at integrating more physical processes observed in the field or in the laboratory to simulate more realistic scenarios.

The use of high-level nonlinear solver technology [Balay et al., 1997] allow us to tackle these complex multiphysics problems in three dimensions.

### **Discrete faults and fractures:**

To include in a three-dimensional model discrete faults and fractures, the interface elements approach is used. These geological discontinuities are considered as two-dimensional inclusions within the three-dimensional domain. By considering the aperture of such features as scaling parameter for the governing equations, one can insure that the conservations of mass and energy are respected.

This approach can be used to model fractures and faults as fluid pathways without considerable meshing efforts. Evolution of the fractures aperture is also considered based on the surrounding stress field.

Basic concepts behind the GOLEM simulator will be presented in this study as well as a few application examples to illustrate its main features.

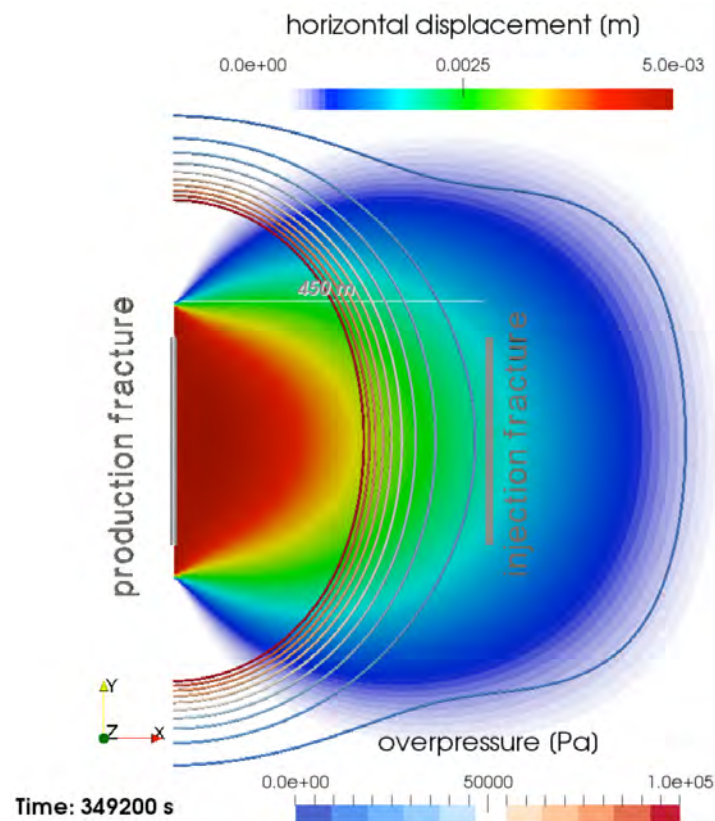


Figure 1: Example of a poroelastic response of a geothermal reservoir during hydraulic stimulation of a well.

### References:

- Gaston, D., Newman, C., Hansen, G. and Lebrun-Grandie, D.. 2009. MOOSE: A parallel computational framework for coupled systems of nonlinear equations. Nucl. Engrg. Design, 239, 1768–1778.
- Balay, S., Gropp, W. D., Curfman McInnes, L., and Smith, B. F., 1997. Efficient Management of Parallelism in Object Oriented Numerical Software Libraries. Modern Software Tools in Scientific Computing, 163-202.

**Keywords:** Coupled Thermo-Hydro-Mechanical Processes, Geothermal Reservoir, Numerical Modelling of Fractures and Faults, C++, Fully-Coupled, MOOSE.

## **The GEOMOD2008 materials benchmark 1: Properties of granular analogue model materials**

Matthias Klinkmüller<sup>1</sup>, Guido Schreurs<sup>1</sup>, Matthias Rosenau<sup>2</sup>, and Helga Kemnitz<sup>2</sup>

<sup>1</sup>) Institute of Geological Sciences, University of Bern, Switzerland

<sup>2</sup>) Helmholtz-Centre Potsdam, GFZ German Research Centre for Geosciences, Potsdam, Germany

Corresponding author: rosen@gfz-potsdam.de

S0- What's up in Modelling ? (PS7)

We report the material properties of 26 granular analogue materials used in 14 analogue modelling laboratories. We determined physical characteristics such as bulk density, grain size distribution, and grain shape, and performed ring shear tests to determine friction angles and cohesion, and uniaxial compression tests to evaluate the compaction behaviour. Mean grain size of the materials varied between (c. 100 and 400 micrometer). Analysis of grain shape factors show that the four different classes of granular materials (14 quartz sands, 5 dyed quartz sands, 4 heavy mineral sands and 3 size fractions of glass beads) can be broadly divided into two groups consisting of 12 angular and 14 rounded materials. Grain shape has an influence on friction angles, with most angular materials having higher internal friction angles (between c. 35° and 40°) than rounded materials, whereas well-rounded glass beads have the lowest internal friction angles (between c. 25° and 30°).

We interpret this as an effect of intergranular sliding versus rolling. Most angular materials have also higher basal friction angles (tested for a specific foil) than more rounded materials, suggesting that angular grains scratch and wear the foil. Most materials have a cohesion in the order of 10-100 Pa except for well-rounded glass beads, which show a trend towards a quasi-cohesionless ( $C < 10$  Pa) Coulomb-type material. The uniaxial confined compression tests reveal that rounded grains generally show less compaction than angular grains. We interpret this to be related to the initial packing density reached during sieving which is higher for rounded grains than for angular grains. Ring-shear test data show that angular grains undergo a longer strain-hardening phase than more rounded materials. This might explain why analogue models consisting of angular grains accommodate deformation in a more distributed manner prior to strain localization than models consisting of rounded grains. Also, models build with angular grains will tend to show more dilatancy during shear zone formation than models build with round grains of comparable mean grain size.

Geophysical Research Abstracts  
Vol. 18, EGU2016-3807, 2016  
EGU General Assembly 2016  
© Author(s) 2016. CC Attribution 3.0 License.



## Properties of granular analogue model materials: A community wide survey

Matthias Klinkmüller (1), Guido Schreurs (1), Matthias Rosenau (2), and Helga Kemnitz (2)  
(1) Institute of Geological Sciences, University of Bern, Switzerland, (2) Helmholtz-Centre Potsdam – GFZ Deutsches GeoForschungsZentrum, Potsdam, Germany

Geophysical Research Abstracts  
Vol. 18, EGU2016-3220, 2016  
EGU General Assembly 2016  
© Author(s) 2016. CC Attribution 3.0 License.



## Viscoelastic silicone oils in analog modeling - a rheological benchmark

Michael Rudolf (1), David Boutelier (2), Matthias Rosenau (1), Guido Schreurs (3), and Onno Oncken (1)  
(1) GFZ German Research Centre for Geosciences, Lithosphere Dynamics, Potsdam, Germany (michael.rudolf@gfz-potsdam.de), (2) School of Environmental and Life Sciences, University of Newcastle, University Drive, Callaghan, NSW2308, Australia, (3) Institute of Geological Sciences, University of Bern, Switzerland

A screenshot of a web browser window. The address bar shows the URL 'www.geodynamics.no/benchmarks/benchmark-anmaterials.html'. The browser's bookmark bar contains several items including 'SAP', 'TYPO3 GFZ', 'Articlerequest', 'Web of Science [v.5.1]', 'EndNote', 'SUBTOP', 'Epos', 'SFB', 'Google News', 'Wetter Bürgel, Thürin...', 'Wetter im Herbst / W...', and 'Weitere Lesezeichen'. The main content area of the browser has a light purple background. At the top, there is a navigation menu with links: 'Home', 'GeoMod2004 experiments', 'GeoMod2008 experiments', 'Plasticity benchmark', 'Materials benchmark', and 'Links'. Below this, the title 'Properties benchmark of granular and viscous analogue materials' is displayed in bold. The text below the title states: 'Organised by Matthias Klinkmüller (University of Bern), Matthias Rosenau (GFZ Potsdam), David Boutelier (GFZ Potsdam), Helga Kemnitz (GFZ Potsdam) and Guido Schreurs (University of Bern). The material properties are determined by Matthias Rosenau and Matthias Klinkmüller using the facilities at GFZ Potsdam. The properties of sand are determined with the Schulze Ring-Shear Tester (<http://www.dietmar-schulze.de/re.html>). The computer-controlled Ring-Shear Tester RST-01.pc serves for determining the frictional properties of granular materials including the angle of internal friction for fault initiation (first peak strength), fault reactivation (second peak strength) and fault sliding (dynamic-stable strength). The Schulze Ring-Shear Tester is certified and the apparatus and measuring procedure is described in a standard available from ASTM international (document nr. ASTM D6773-02, <http://www.astm.org>). The bulk modulus is measured with a uniaxial compression tester at GFZ Potsdam.'



Matthias Klinkmüller



Guido Schreurs



Susanne Buiter

**Analogue Laboratories (17)**

Centro de Geociencias Mexico	Mariano Cerca
Cergy-Pontoise	Bertrand Maillot
GFZ Potsdam	Matthias Rosenau
IFP	Jean-Marc Daniel
Kyoto University	Yasuhiro Yamada
Monash University	Wouter Schellart
National Taiwan University	Chia-Yu Lu
Rutgers University	Roy Schlichte, Martha Withjack
Stanford University	Leonardo Cruz
University of Bern	Guido Schreurs
University of Buenos Aires	Victor Garcia
University of Lille	Bruno Vendeville
University of Ouro Preto	Caroline J.S. Gomes
University of Parma	Cristian Cavozi
University of Salzburg	Hans Peter Steyrer
University of Toronto	Sandy Cruden
University of Uppsala	Hemin Koyi

HelTec | Helmholtz-Laboratory for Tectonic Modeling



**ARTICLE IN PRESS**  
TECTO-126911; No of Pages 16  
Tectonophysics xxx (2016) xxx–xxx  
Contents lists available at ScienceDirect  
**Tectonophysics**  
journal homepage: [www.elsevier.com/locate/tecto](http://www.elsevier.com/locate/tecto)

Properties of granular analogue model materials: A community wide survey

M. Klinkmüller<sup>a</sup>, G. Schreurs<sup>a,1</sup>, M. Rosenau<sup>b</sup>, H. Kienitz<sup>b</sup>

<sup>a</sup> Institute of Geological Sciences, University of Bern, Baltzerstrasse 1 + 3, CH-3012 Bern, Switzerland  
<sup>b</sup> Helmholtz-Zentrum Potsdam, GFZ Deutsches Geoforschungszentrum, Telegrafenberg, D-14473 Potsdam, Germany

**ARTICLE IN PRESS**  
TECTO-126862; No of Pages 11  
Tectonophysics xxx (2015) xxx–xxx  
Contents lists available at ScienceDirect  
**Tectonophysics**  
journal homepage: [www.elsevier.com/locate/tecto](http://www.elsevier.com/locate/tecto)

Rheological benchmark of silicone oils used for analog modeling of short- and long-term lithospheric deformation

Michael Rudolf<sup>a,\*,1</sup>, David Boutelier<sup>b</sup>, Matthias Rosenau<sup>a</sup>, Guido Schreurs<sup>c</sup>, Onno Oncken<sup>a</sup>

<sup>a</sup> Lithosphere Dynamics, Helmholtz Centre Potsdam, German Research Centre for Geosciences (GFZ), Telegrafenberg, D-14473 Potsdam, Germany  
<sup>b</sup> School of Environmental and Life Sciences, University of Newcastle, University Drive, Callaghan, NSW 2308, Australia  
<sup>c</sup> Institute of Geological Sciences, University of Bern, Switzerland



Open access data sets

GFZ Helmholtz-Zentrum Potsdam, Deutsches Geoforschungszentrum  
EPOS European Plate Observing System

**GeoMod2016 materials benchmark: The ring shear test dataset**  
This dataset contains the raw data from the ring shear test performed at the Helmholtz-Zentrum Potsdam, GFZ Deutsches Geoforschungszentrum. The data includes the shear stress, shear rate, and shear displacement for each sample. The data is available in the form of a CSV file and a PDF file. The data is available for research purposes only. For more information, please contact the Helmholtz-Laboratory for Tectonic Modeling.

**GeoMod2016 materials benchmark: The SEM image dataset**  
This dataset contains the SEM images of the samples used in the ring shear test. The images show the microstructure of the samples and the deformation patterns. The data is available in the form of a ZIP file. The data is available for research purposes only. For more information, please contact the Helmholtz-Laboratory for Tectonic Modeling.

**GeoMod2016 materials benchmark: The shear failure dataset**  
This dataset contains the raw data from the shear failure test performed at the Helmholtz-Zentrum Potsdam, GFZ Deutsches Geoforschungszentrum. The data includes the shear stress, shear rate, and shear displacement for each sample. The data is available in the form of a CSV file and a PDF file. The data is available for research purposes only. For more information, please contact the Helmholtz-Laboratory for Tectonic Modeling.

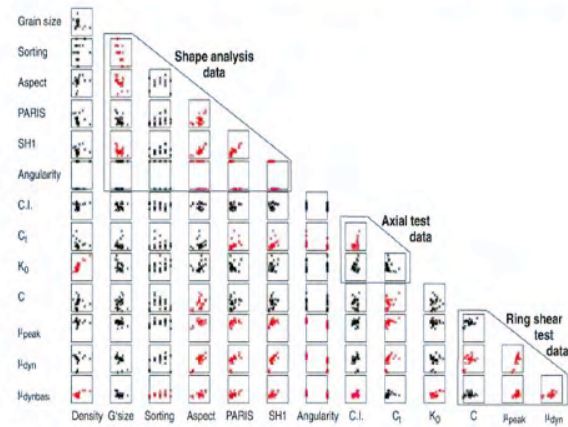
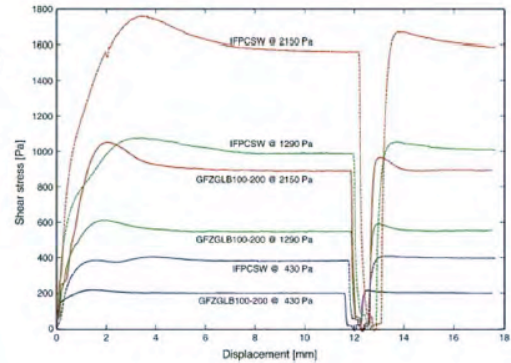
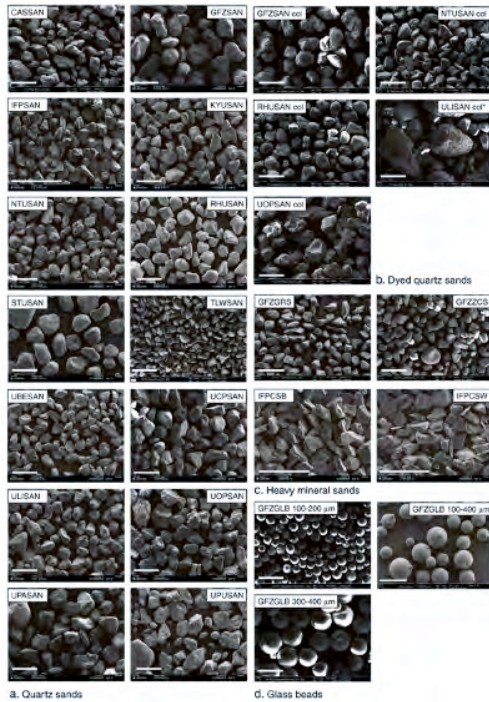
**GeoMod2016 materials benchmark: The ring shear dataset**  
This dataset contains the raw data from the ring shear test performed at the Helmholtz-Zentrum Potsdam, GFZ Deutsches Geoforschungszentrum. The data includes the shear stress, shear rate, and shear displacement for each sample. The data is available in the form of a CSV file and a PDF file. The data is available for research purposes only. For more information, please contact the Helmholtz-Laboratory for Tectonic Modeling.

**GeoMod2016 materials benchmark: The ring shear dataset**  
This dataset contains the raw data from the ring shear test performed at the Helmholtz-Zentrum Potsdam, GFZ Deutsches Geoforschungszentrum. The data includes the shear stress, shear rate, and shear displacement for each sample. The data is available in the form of a CSV file and a PDF file. The data is available for research purposes only. For more information, please contact the Helmholtz-Laboratory for Tectonic Modeling.

**Supplementary rheological benchmark of silicone oils for analog modeling of short- and long-term lithospheric deformation**  
This dataset contains the raw data from the rheological benchmark of silicone oils. The data includes the shear stress, shear rate, and shear displacement for each sample. The data is available in the form of a CSV file and a PDF file. The data is available for research purposes only. For more information, please contact the Helmholtz-Laboratory for Tectonic Modeling.

Discussion points

- Variability of material behaviors/properties
- Interdependencies of properties
- Similarity to rock & suitability for analog modelling
- ...



Time for a Remake  
of the Material Benchmark !?

## New anisotropic analogue materials for tectonics and hydraulic fracturing experiments

R. Mourgues<sup>1</sup>, A. Zanella<sup>1</sup>, P. Strzeczynski<sup>1</sup>, F. Richard<sup>1</sup>, C. Gruber<sup>1</sup>

<sup>1</sup>) Laboratoire de Planétologie et Géodynamique, LPG – UMR CNRS 6112 - Université du Maine, Le Mans, France

Corresponding author: zanella.alain@gmail.com

S0- What's up in Modelling ? (PS7)

Shales are widespread fine grained sedimentary rocks that are highly anisotropic in their mechanical behavior. This mechanical anisotropy influences faulting, hydraulic fracturing or magma emplacement in sedimentary basins and it is becoming an important issue in petroleum exploration and reservoir geophysics. However most of the time, this fundamental property remains neglected in experiments because of the lack of suitable analogue materials.

In this contribution, we describe transversely isotropic analogue materials that can be used in scaled experiments to simulate anisotropic sediments. The materials consist of mixtures of micas (muscovite), sand and gel. The sheets of muscovite give the anisotropic property, and the gel fill pores and increase cohesion. All the mixtures were prepared and all the mechanical tests were conducted under water. The materials are thus suitable for immersed experiments.

All tested materials were prepared in the same standardized way (fig.1a). We heated up water and the required quantity of gelatin powder until boiling. Then, the sand and the micas were poured into the solution and compacted by vibrating and applying a load on the surface. This vibration allowed the micas to deposit with a preferred orientation defining a plane of anisotropy. The material was then cooled down. We produced several granular cohesive materials by mixing sand and micas with different proportions and by controlling the concentration of the gel. For each material, we systematically estimated cohesion and friction at various orientations to the plane of anisotropy ( $\alpha=0^\circ$ ,  $30^\circ$ ,  $45^\circ$ ,  $60^\circ$ ,  $90^\circ$ ,  $120^\circ$ ,  $135^\circ$ ,  $150^\circ$ , fig.1).

We used a classic shear-box to determine each envelope of failure which was approximated by a linear Mohr-Coulomb law (fig.1a). For mixtures containing only micas without gel to stick the grains, we measured values of cohesion ranging between 280 Pa for  $\alpha=0^\circ$  and 580Pa for  $\alpha=90^\circ$  (fig.1b). The material was thus highly anisotropic with minimal shear strength in the bedding plane. By adding sand, the anisotropy decreased with values of C between 220 Pa for  $\alpha=0^\circ$  and 330 Pa for  $\alpha=90^\circ$  for mixture 30% micas / 70% sand. The gel within the pore increased cohesion (510Pa for  $\alpha=0^\circ$  in 100% micas mixture) but it also decreased anisotropy (fig.1b).

In order to compare the mechanical behavior of the analogue material with natural shale, we used the experimental data to compute virtual uniaxial tests and define uniaxial compressive strengths relative to the anisotropy plane (fig.1c). We calculated anisotropy ratios  $k=\sigma_{cmax}/\sigma_{cmin}$  between 0 and 3.37 for mixtures without gel and between 0 and 2.7 for mixtures with gel. These values are compatible with anisotropy degrees in shale fig.1d).

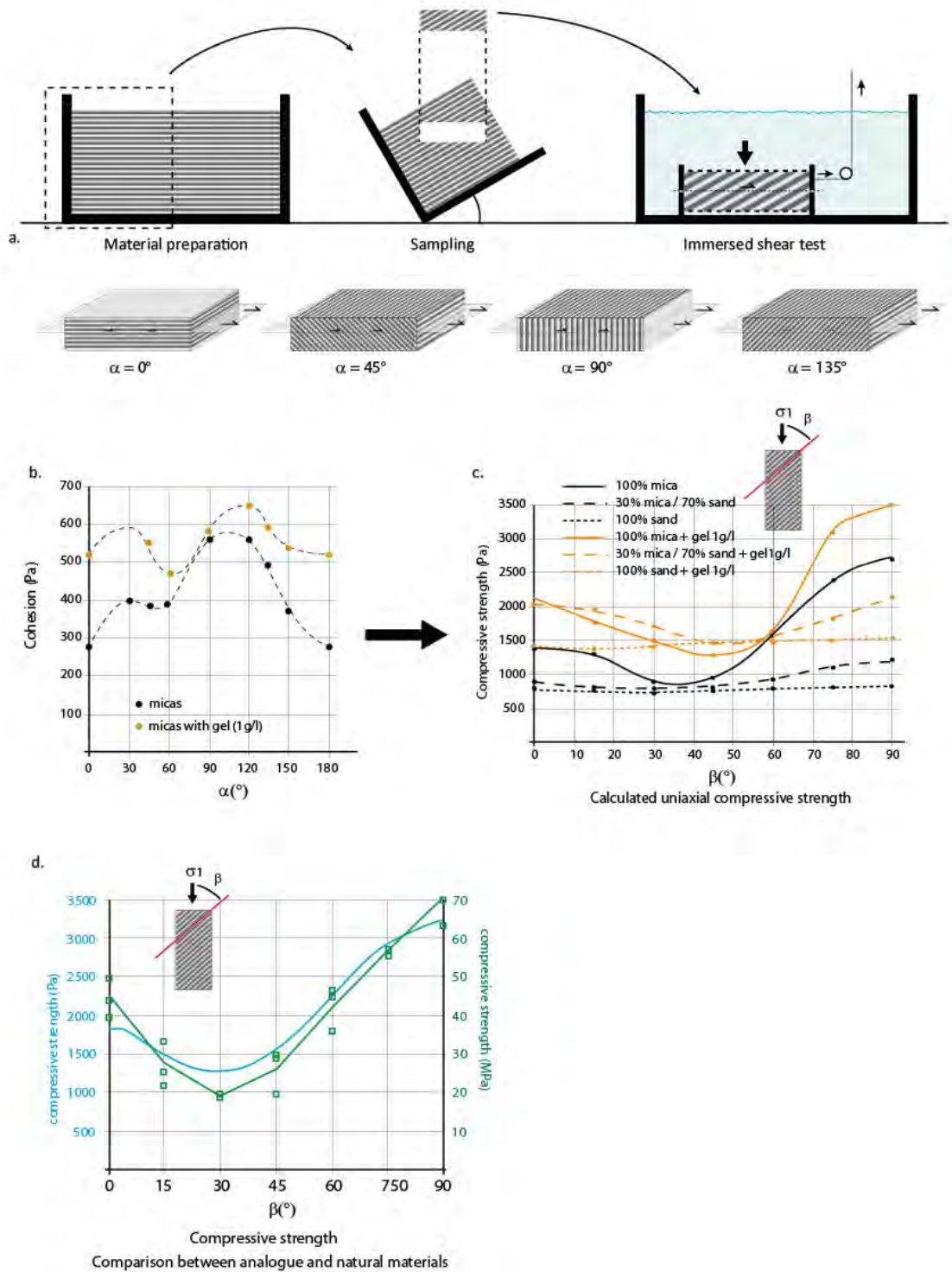


Fig1. a. Preparation of the material, sampling and shear tests. b. Cohesion measured at different orientations  $\alpha$ . c. Calculated uniaxial compressive strengths for the various mixtures. d. Comparison with a natural shale (data from Ajalloeian and Lashkaripour, 2000).

**Keywords:** Anisotropy, cohesion, friction coefficient, tensile strength, hydraulic fracturing.

## Characterising the physical properties of granular crustal analogues in laboratory experiments imaged with X-ray Computed Tomography

Sam Poppe<sup>1</sup>, Eoghan P. Holohan<sup>2</sup>, Matthias Rosenau<sup>3</sup>, Régis Mourgues<sup>4</sup>, Gert Van Gompel<sup>5</sup>, Nico Buls<sup>5</sup> and Matthieu Kervyn<sup>1</sup>

<sup>1</sup>) Vrije Universiteit Brussel, Department of Geography, Earth System Sciences, Brussels, Belgium

<sup>2</sup>) University College Dublin, UCD School of Earth Sciences, Dublin, Ireland

<sup>3</sup>) Helmholtz Center Potsdam, Helmholtz Laboratory for Tectonic Modelling, Potsdam, Germany

<sup>4</sup>) University of Main, Department of Geosciences, Le Mans, France

<sup>5</sup>) Radiology Department, Vrije Universiteit Brussel, Brussels, Belgium

Corresponding author: sam.poppe@vub.ac.be

S0- What's up in Modelling ? (PS7)

Analogue sand box models have been widely used to study geo-tectonic deformation processes. While past outcomes of analogue models have commonly comprised qualitative structural descriptions, recent work has emphasized quantifying the geometric, kinematic and dynamic parameters of the deformation. This has led to two main trends in model development over the last number of years.

Firstly, there has been an increased emphasis on 3D quantification of model deformation. While optical image analysis techniques (e.g. Structure-from-Motion (SfM) photogrammetry and Digital Image Correlation (DIC); see e.g. Galland et al. 2016) used for this purpose are limited to model surfaces, there is an emerging possibility of full 3D imaging of deformation of both the model surfaces and the model interior by X-ray Computed Tomography (XCT) (Adam et al., 2013). Complicated trade-off relations between image resolution (voxel size) and maximum object size, scanning time and high operational costs have led to very few applications of this powerful imaging technique to analogue models so far. Secondly, there has been deeper investigation of the mechanics of modeling materials, such as granular analogues for upper crustal rocks (e.g. Abdelmalak et al. 2016; Klinkmüller et al. 2016). Sand-filler mixtures used for this purpose, especially in volcano-tectonic analogue models, have not yet received detailed attention, however.

In our study, we quantified the physical and X-ray imaging properties of a range of mixtures of fine-grained fillers and silica sand. We assessed the mechanical impact of powdered gypsum (plaster) and kaolin clay as fillers, but we also tested the effect of adding more dense garnet sand into the silica sand to provide texture in XCT images. Using a Schülze Ring-Shear Tester (RST) and a Hubert-type shear box, we estimated the density, cohesion and friction coefficient of the granular materials, both as end-members and when mixed at different volumetric ratios. We tested both pouring and sieving from 20 cm height as emplacement techniques. By using medical XCT scanners, we also estimated the X-ray attenuation characteristics of the four above granular materials and three liquid or visco-elastic materials (corn oil, golden syrup, silicon putty).

We find that the handling technique (sieving vs. pouring) had a strong impact on the compositional homogeneity and mechanics of the mixed materials. In general, sieving resulted in layered (i.e. inhomogeneous) bulk materials because of the strong size and density contrast between the endmember materials (sand vs. filler). Pouring increased compositional homogeneity, but resulted in a

less dense packing of the bulk material, causing a larger amount of distributed deformation to occur before strain localisation. RST results show that the mechanical behavior of pure fillers (plaster, kaolin clay) displays complex, non-brittle components and stick-slip behavior. Adding filler to sand progressively increases the mechanical heterogeneity of the mixture. Friction coefficients increased from  $\sim 0.6$  to  $\sim 0.8$  and cohesions from few tens to few hundreds Pa. Pouring the granular materials instead of sieving resulted in a progressive deviation of the mechanics of sand-filler mixtures from the brittle Mohr-Coulomb behavior typical for granular materials (Lohrmann et al. 2003). Both the emplacement technique and the amount of filler mixed into sand hence significantly influence the mechanics of the mixture, potentially due to the contrast in their respective mean grain sizes. The approximation of sand-filler mixtures as Mohr-Coulomb-type brittle material might therefore be an oversimplification of their true rheology.

The X-ray attenuation of the tested materials varied over a range of X-ray energies and the nature of the attenuation curve differed largely between the liquids (near-linear curve) and granular materials which are of much higher density (sigmoidal curve). In this way, sand-filler mixtures provided a clear contrast with the liquid magma analogues at an X-ray energy of 100-120 KeV. These variations should be taken into account when setting up the optimal XCT scan acquisition parameters for obtaining sharp and contrast-rich XCT images of a sand box model.

Finally, we obtained a time series of XCT scans of an analogue simulation of golden syrup injection in a granular sand-plaster host, analogue to the intrusion of low-viscous magma in dense volcanic rock. We demonstrate that the constrained physical properties help to produce contrast-rich images of an analogue experiment in which the host medium, the propagating liquid body and formed structures are efficiently imaged during the ongoing injection process. The outcome of our work should serve as a useful reference for quantification of analogue model deformation in 3D by using dynamic X-ray CT.

### References:

- Abdelmalak, M. M., Bulois, C., Mourgues, R., Galland, O., Legland, J. B., Gruber, C., 2016. Description of new dry granular materials of variable cohesion and friction coefficient: Implications for laboratory modeling of the brittle crust. *Tectonophysics*, In press.
- Adam, J., Klinkmüller, M., Schreurs, G., Wieneke, B., 2013. Quantitative 3D strain analysis in analogue experiments simulating tectonic deformation: Integration of X-ray computed tomography and digital volume correlation techniques. *Journal of Structural Geology*, 55, 127–149.
- Galland, O., Bertelsen, H.S., Guldstrand, F., Girod, L., Johannessen, R., Bjugger, F., Burchardt, S., Mair, K., 2016. Application of open-source photogrammetric software MicMac for monitoring surface deformation in laboratory models. *Journal of Geophysical Research: Solid Earth*, 121:4, 2852-2872.
- Klinkmüller, M., Schreurs, G., Rosenau, M., Kemnitz, H., 2016. Properties of granular analogue materials: A community wide survey. *Tectonophysics*, 666, doi.: 10.1016/j.tecto.2016.01.017.
- Lohrmann, J., Kukowski, N., Adam, J., Oncken, O., 2003. The impact of analogue material properties on the geometry, kinematics, and dynamics of convergent sand wedges. *Journal of Structural Geology*, 25:10, 1691-1711.

**Keywords:** Analogue modeling, rheology, volcano-tectonism, X-ray Computed Tomography.

## The GEOMOD2008 materials benchmark 2: Properties of viscoelastic analogue model materials

Michael Rudolf<sup>1</sup>, David Boutelier<sup>2</sup>, Matthias Rosenau<sup>1</sup>, Guido Schreurs<sup>3</sup>, and Onno Oncken<sup>1</sup>

<sup>1</sup>) Helmholtz Centre Potsdam, GFZ German Research Centre for Geosciences, Potsdam, Germany

<sup>2</sup>) School of Environmental and Life Sciences, University of Newcastle, University Drive, Callaghan, NSW2308, Australia

<sup>3</sup>) Institute of Geological Sciences, University of Bern, Switzerland

Corresponding author: michael.rudolf@gfz-potsdam.de

S0- What's up in Modelling ? (PS7)

Tectonic analog models frequently use silicone oils to simulate viscous flow in the lower crust and mantle. Precise knowledge of the model rheology is required to ensure dynamic similarity with the prototype. We assessed the rheological properties of various silicone oils using rotational and oscillatory tests. Resulting viscosities are in the range of  $2 - 3 \times 10^4$  Pa s with a transition from Newtonian viscous to power-law, shear-thinning, around shear rates of  $10^{-2}$  to  $10^{-1}$  s<sup>-1</sup>. Maxwell relaxation times are in the range of  $10^{-1}$  s. Comparing the rheological properties of chemically similar silicone oils from different laboratories shows that they differ from laboratory to laboratory.

Furthermore, we characterized the temperature dependency of viscosity and aging effects. The samples show a reduction in zero-shear viscosity over time. This stabilizes at a certain value over several months. The dynamic moduli decrease as well, but other viscoelastic constants, such as the Maxwell relaxation time, are not affected by aging. We conclude that the aging is mainly controlled by the storage conditions and that a silicone shows no further aging when it has equilibrated with the ambient laboratory conditions. We consider all these differences as minor compared to the much larger uncertainties for estimating the lithosphere rheology.

Nevertheless, it is important that the rheological properties of the experimental materials are monitored during an experimental series that spans over several weeks to months. Additionally, the viscoelastic properties may be scaled using dimensionless parameters (Deborah number) and show a dynamically similar change from Newtonian to power-law flow, like the natural prototype. In consequence, the viscoelasticity of these silicone oils is able to mimic the change in deformation mechanism from diffusion to dislocation creep.

## Benchmarking analogue models of brittle thrust wedges

Guido Schreurs<sup>1</sup>, Susanne Buitert<sup>2</sup>, and the GeoModTeam\*

<sup>1</sup>) Institute of Geological Sciences, University of Bern, Baltzerstrasse 1 + 3, 3012 Bern, Switzerland

<sup>2</sup>) Geodynamics Team, Geological Survey of Norway, 7491 Trondheim, Norway, and The Centre for Earth Evolution and Dynamics, University of Oslo, PO Box 1048 Blindern, 0316 Oslo, Norway

Corresponding author: schreurs@geo.unibe.ch

S0- What's up in Modelling ? (PS7)

We performed a quantitative comparison of brittle thrust wedge experiments to evaluate the variability among analogue models and to appraise the reproducibility and limits of model interpretation (Schreurs et al., 2016). Fifteen analogue modeling laboratories participated in this benchmark initiative. Each laboratory received a shipment of the same type of quartz and corundum sand and all laboratories adhered to a stringent model building protocol and used the same type of foil to cover base and sidewalls of the sandbox. Sieve structure, sifting height, filling rate, and details on offscraping of excess sand followed prescribed procedures. In a companion benchmark, Buitert et al. (2016) present the results of numerical experiments reproducing the analogue model set-ups. Our analogue benchmark shows that even for simple plane-strain experiments with prescribed stringent model construction techniques, quantitative model results show variability, most notably for surface slope, thrust spacing and number of forward and backthrusts (Fig. 1 and 2). One of the sources of the variability in model results is related to slight variations in how sand is deposited in the sandbox. Small changes in sifting height, sifting rate, and scraping will result in slightly heterogeneous material bulk densities, which will affect the mechanical properties of the sand, and will result in lateral and vertical differences in peak and boundary friction angles, as well as cohesion values once the model is constructed. Initial variations in basal friction are inferred to play the most important role in causing model variability.

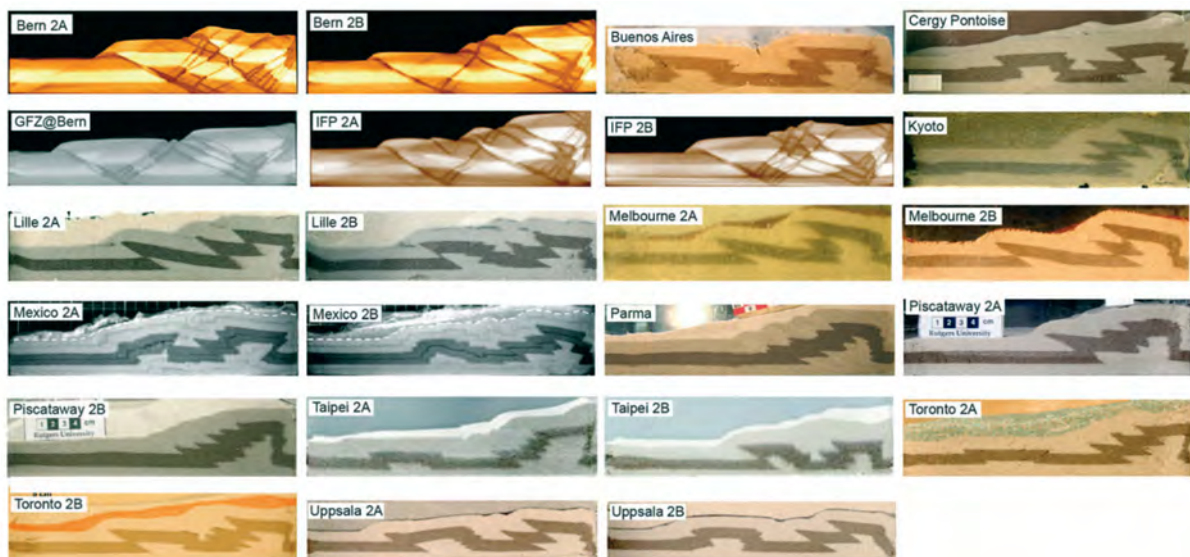


Figure 1. Cross sections through centre of thrust wedge models after 10 cm of shortening. In the experimental set-up alternating horizontal layers of quartz and corundum sand are shortened by inward movement of a mobile wall from right to left. Width of each panel shown is 25 cm. Note that some labs added a layer of sand before cutting the model. Sections of Bern, GFZ@Bern and IFP represent X-ray computed tomography slices. Figure

reprinted from *Journal of Structural Geology*, doi: 10.1016/j.jsg.2016.03.00, Schreurs et al. (2016), *Benchmarking analogue models of brittle thrust wedges*, with permission from Elsevier.

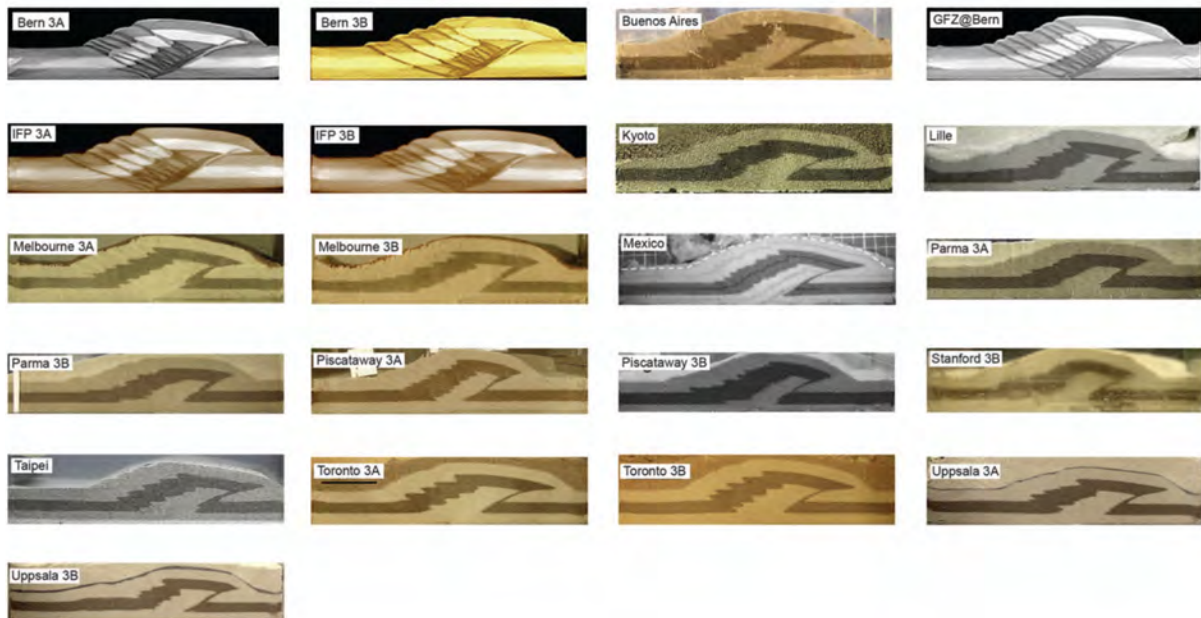


Figure 2. Cross sections through centre of thrust wedge models after 10 cm of shortening. In the experimental set-up a thin rigid sheet, 1 mm thick, and 12 cm in length is attached to the mobile wall and underlies part of the model. Movement of the mobile wall is from right to left. Width of each panel shown is 25 cm. Note that some labs added a layer of sand before cutting the model. Sections of Bern, GFZ@Bern and IFP represent X-ray computed tomography slices. Figure reprinted from *Journal of Structural Geology*, doi: 10.1016/j.jsg.2016.03.00, Schreurs et al. (2016), *Benchmarking analogue models of brittle thrust wedges*, with permission from Elsevier.

Our comparison shows that the human factor plays a decisive role, and even when one modeler repeats the same experiment, quantitative model results still show variability. Our observations highlight the limits of up-scaling quantitative analogue model results to nature or for making comparisons with numerical models. The frictional behavior of sand is highly sensitive to small variations in material state or experimental set-up, and hence, it will remain difficult to scale quantitative results such as number of thrusts, thrust spacing, and pop-up width from model to nature.

## References:

- Buiter, S.J.H., Schreurs, G., Albertz, M., Gerya, T.V., Kaus, B., Landry, W., le Pourhiet, L., Mishin, Y., Egholm, D.L., Cooke, M., Maillot, B., Thieulot, C., Crook, T., May, D., Souloumiac, P. and Beaumont, C., 2016. Benchmarking numerical models of brittle thrust wedges, *Journal of Structural Geology*, doi: 10.1016/j.jsg.2016.03.003
- \*Schreurs, G., Buiter, S.J.H., Boutelier, J., Burberry, C., Callot, J.-P., Cavoizzi, C., Cerca, M., Chen, J.-H., Cristallini, E., Cruden, A.R., Cruz, L., Daniel, J.-M., Da Poian, G., Garcia, V.H., Gomes, V.J.S., Grall, C., Guillot, Y., Guzman, C., Nur Hidayah, T., Hilley, G., Klinkmüller, M., Koyi, H.A., Lu, C.-Y., Maillot, B., Meriaux, C., Nilfouroushan, F., Pan, C.-C., Pillot, D., Portillo, R., Rosenau, M., Schellart, W.P., Schlische, R.W., Take, A., Vendeville, B., Vergnaud, M., Vettori, M., Wang, S.-H., Withjack, M.O., Yagupsky, D., Yamada, Y., 2016. Benchmarking analogue models of brittle thrust wedges, *Journal of Structural Geology*, doi: 10.1016/j.jsg.2016.03.005

**Keywords:** Thrust wedges, brittle wedges, Shear zones, Analogue models, Benchmarking, Critical taper, Sand.

## **EPOS' Multi-Scale Laboratory platform: a long-term reference tool for experimental Earth Sciences**

Daniele Trippanera<sup>1</sup>, Francesca Funiciello<sup>1</sup>, Matthias Rosenau<sup>2</sup>, Ernst Willingshofer<sup>4</sup>, Leonardo Sagnotti<sup>3</sup>, Piergiorgio Scarlato<sup>3</sup>, Telemaco Tesei<sup>3</sup>, Chris Spiers<sup>4</sup>, Martyn Drury<sup>4</sup>, Kirsten Elger<sup>2</sup>, Damian Ulbricht<sup>2</sup>, Elisa Calignano<sup>4</sup>, Mirjam Kan-Parker<sup>4</sup>, Otto Lange<sup>4</sup>, and the EPOS-IP WP16 Team.

<sup>1</sup>) Università' Rome TRE, Dipartimento di Scienze, Roma, Italy,

<sup>2</sup>) Helmholtz Centre Potsdam, GFZ – German Research Centre for Geosciences, Potsdam, Germany,

<sup>3</sup>) Istituto Nazionale di Geofisica e Vulcanologia, Roma, Italy,

<sup>4</sup>) Utrecht University, Utrecht, the Netherlands

Corresponding author: [daniele.trippanera@uniroma3.it](mailto:daniele.trippanera@uniroma3.it)

S0- What's up in Modelling ? (PS7)

The European Plate Observing System (EPOS) is a developing interdisciplinary virtual platform that aims at providing geo-scientific data and services to the worldwide community. As a part of this project, now at its implementation phase (EPOS-IP), the Work Package 16 (WP16) represents a building up community of European Geoscience “Multiscale Laboratories”. The currently participating and collaborating laboratories (Utrecht University, GFZ, Roma Tre University, INGV, NERC, CSIC-ICTJA, CNRS, LMU, UBI, ETH, CNR) embody several types of laboratory infrastructures, engaged in different fields of interest of Earth Science. They hold data covering a wide range of scales, from the continental to the molecular one. This long-view project aims at merging the top class multidisciplinary laboratories in Geoscience into a coherent and collaborative network, additionally working towards the standardization of virtual access to data, data products, and physical access to the infrastructures, i.e. laboratories. At this time, most of data produced by the different laboratories are usually available only within the related scholarly publications (often as print-version only) or they remain unpublished and inaccessible on local devices.

However, all high-quality datasets have potential value for secondary use in science, teaching and outreach. They could be of crucial importance for the exploration of geo-resources, geo-storage, geo-hazards and for the understanding of the earth system evolution in general. The EPOS multi-scale laboratory platform represents a unique opportunity to share and discover data by means of open access, DOI-referenced, online data publication including long-term storage, managing and curation services and to set up a cohesive community of laboratories.

The WP16 is starting to provide data, data services and software (DDSS) for three pilot case laboratories: (1) rock physics, (2) palaeomagnetic, and (3) analogue modelling. As a proof of concept, first analogue modelling datasets have been published via GFZ Data Services (<http://doidb.wdc-terra.org/search/public/ui?&sort=updated+desc&q=epos>). First datasets include rock analogue material properties (e.g. friction data, rheology data, SEM imagery) as well as supplementary figures, images and movies from experiments on tectonic processes. Soon, a metadata catalogue tailored to the specific communities will link the growing number of datasets to a centralized EPOS hub. Additionally, WP16 aims at creating mechanisms and procedures for trans-national access (TNA) to multi-scale laboratory facilities'. By the end of next year EPOS-IP will enter a pilot phase to test, validate, and consolidate the services and to provide a proof of concept for the operational features that will be offered beyond the completion of the EPOS IP.

Local and national repositories will be connected by means of a centralized Thematic Core Service (TCS) system associated to a metadata catalogue. The TCS communicates at higher level with the Integrated Core Service (ICS) that collects information from all the TCSs, allowing the final user to perform a complete interdisciplinary research within a web interface.

As a scenario, an experimentalist willing to decide which material is suitable for his experimental setup, can get “virtual lab access” to retrieve information about material parameters with minimum effort and then may decide to move in a specific laboratory equipped with the instruments needed. This scenario will offer the possibility to share and implement knowledge in cooperation with all the participant European laboratories.

The participation to the development of this project is open to everybody who is interested in.

## A new analogue modelling machine to study scissor tectonics

Frank Zwaan<sup>1</sup>, Guido Schreurs<sup>1</sup>, Claude Grau<sup>2</sup>, Reto Gwerder<sup>2</sup>, Rudolf Kamber<sup>2</sup>, Theodor Wüst<sup>2</sup>, Michael Ziltener<sup>2</sup>

<sup>1</sup>) Institute of Geological Sciences, University of Bern, Baltzerstrasse 1 + 3, 3012 Bern, Switzerland

<sup>2</sup>) IPEK, Hochschule für Technik Rapperswil, Oberseestrasse 10, 8640 Rapperswil, Switzerland

Corresponding author: frank.zwaan@geo.unibe.ch

S0- What's up in Modelling ? (PS7)

### Introduction:

Although tectonic modelers generally apply constant deformation velocities throughout their models, natural settings can involve along-strike velocity variations. In extensional regimes, we often observe the propagation and associated “scissor-like” opening of a rift, as older rift parts are further evolved than the rift tip (e.g. opening of the North Atlantic). In specific settings this scissor-like opening on one side of the vertical scissor axis can result in compression on the other side of the scissor axis (e.g. the Bay of Biscay-Pyrenees system).

### The two model set-ups:

To model scissor tectonics, we use an experimental machine, which allows two types of set-ups: a foam-base set-up and a rigid-base set up. The machine consists of two long sidewalls that can rotate about a vertical axis and two curved sidewalls to confine the experimental space. As the sidewalls scissor open at one side of the model (extension) they close on the other side (compression). Computer-guided motors can move the sidewalls independently from one another (velocity range: 0.1 mm/h to 8 m/h). For both types of set-ups, special components can be added to the machine. No metal parts are used to allow X-Ray CT-scanning and 3D analysis of the internal structural evolution.

When applying the foam-base set-up, the sidewalls motion deforms the foam uniformly and induces distributed deformation at the base of the overlying brittle-ductile model materials: sand and a viscous polydimethylsiloxane (PDMS)/sand mixture respectively). Lines of viscous material can be added on top of the basal model layer (seeds) to control where faulting occurs. This model set-up allows the modeling of a full scissor-tectonic system with both a compressional and extensional domain. First tests have shown that this set-up yields useful results.

The concept of the base-plate machine is more traditional, applying rigid base plates to induce deformation of the overlying model materials (brittle-ductile or brittle only) along the edges of the base plates. This is a major difference with the foam-base set-up, which allows much more freedom for the model to evolve (Zwaan et al., 2016). The shape of the standard base plate components allows some room for different base plate geometries. However, this set-up only permits extensional scissor motion. Therefore an additional internal barrier fences off one side of the experimental space.

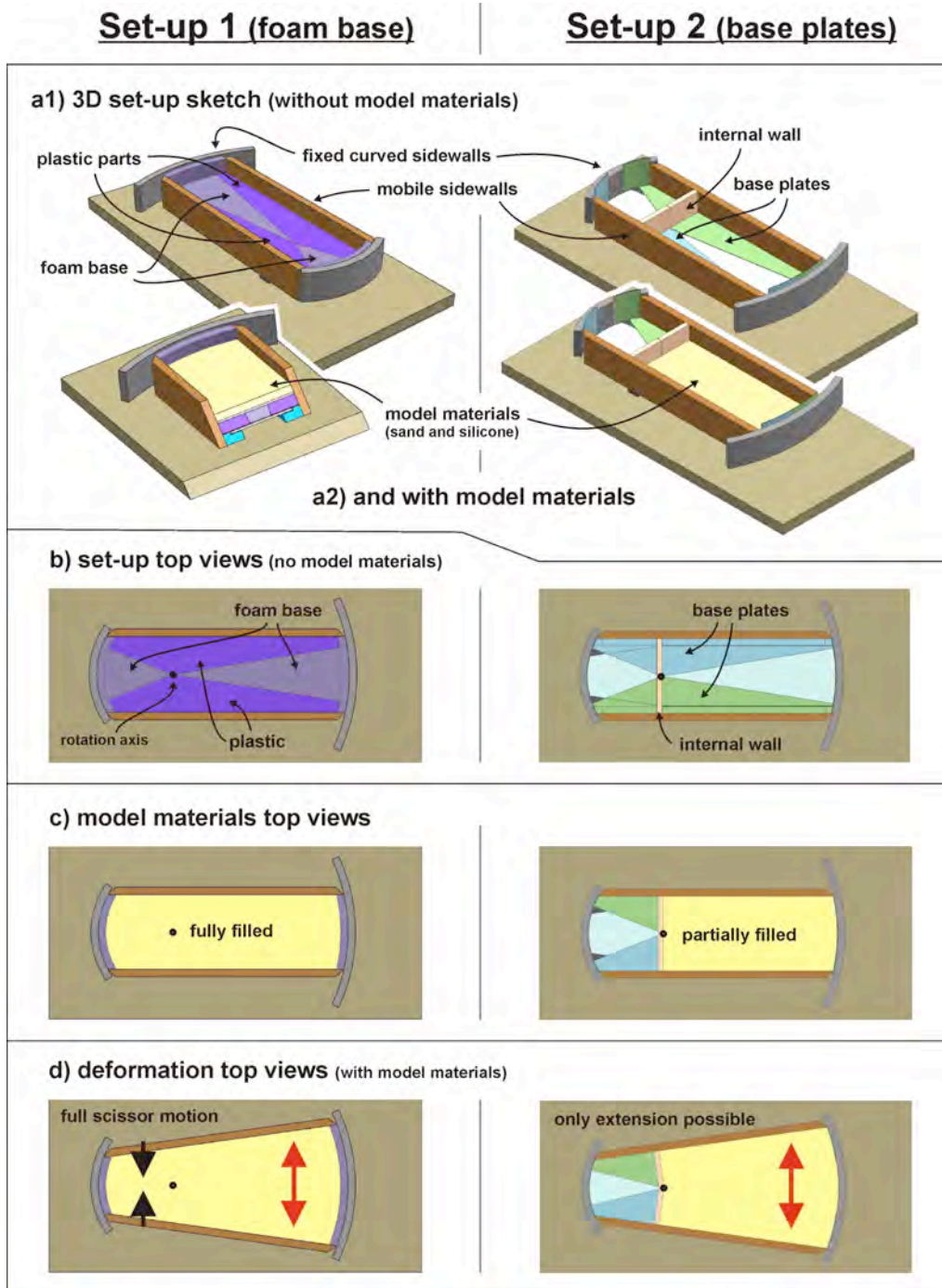


Figure 1. The two model set-ups our machine allows. Left: Foam base set-up, right: base plate set-up.

**References:**

Zwaan, F., Schreurs, G., Naliboff, J., Buitert, S.J.H., 2016. Insights in the effects of oblique extension on continental rift interaction from 3D analogue and numerical modeling, *Tectonophysics*.

**Keywords:** Oblique Extension, Transtension, Analogue Modeling, Rifting.

## **S1 – Geodynamics, Plate tectonics**

Geodynamics involves processes that may be either very fast or extremely slow (earthquakes vs. oceanic plate cooling), multi-scale and depth-dependent, which limits their study from an observational-only prospect. This is why both analogue and numerical modelings play an essential role to test hypothesis on the physics and evolution of geodynamic processes.

The ongoing development of computational and analysis capabilities in both numerical and analogue simulations allows for an improvement of the spatial and temporal resolutions and helps reducing the gap between small-scale and large-scale deformations, which results in a fast-improvement of the understanding of geodynamic problems.

In this session, we invite contributions highlighting the state-of-the-art in analogue and numerical modelings of geodynamic processes, which include, but are not limited to, deformation of the lithosphere, subduction, rifting, mantle convection, and plumes. Contributions that use the joint numerical-analogue modeling approaches are particularly welcome.

**Conveners:** Thibault Duretz (University of Lausanne, Switzerland) and Laetitia Le Pourhiet (University Pierre et Marie Curie, Paris).

**Keynote speaker:**

**"The impact of Wilson Cycle inheritance on continental rifted margins"** by Susanne Buiter (Norway Geological Survey, Norway) - [susanne.buiter@ngu.no](mailto:susanne.buiter@ngu.no)

## The impact of Wilson Cycle inheritance on continental rifted margins

Susanne Buitert<sup>1,2</sup>, Joya Tetreault<sup>3,1</sup> and Susan Ellis<sup>4</sup>

<sup>1</sup>) Geodynamics Team, Geological Survey of Norway, 7040 Trondheim (susanne.buitert@ngu.no)

<sup>2</sup>) The Centre of Earth Evolution and Dynamics, University of Oslo, Norway

<sup>3</sup>) Exploro Geoservices AS, Trondheim, Norway

<sup>4</sup>) GNS Science, Lower Hutt, New Zealand

Corresponding autor: susanne.buitert@ngu.no

S1 – Geodynamics, Plate tectonics (Keynote)

The Wilson Cycle theory describes how oceanic subduction initiates at a rifted continental margin, leading to closure of the ocean, and how future continental extension localises at the resulting continental collision zone. Each stage of the Wilson Cycle is expected to develop lithospheric heterogeneities, which can influence the next deformation phases of the cycle. We present numerical experiments that investigate the Wilson Cycle from rifting to orogenesis to rifting and use these results to discuss the effects of collisional inheritance on rifted margin architecture.

Continental rifted margins differ in margin width, onshore topography, fault patterns, and offshore sediment thickness. For example, the mid-Norwegian and Iberian margins are considered hyper-extended margins, displaying highly thinned continental crust over a wide region. Other continental margins, such as in the northern Norway and Flemish Cap regions, are much narrower. Numerical experiments of continental extension show that the width of rifted margins varies with crustal rheology and extension velocity. A strong lower crust leads to a short margin accompanied by high rift flank uplift. A weak lower crust at moderate extension rates forms a long, hyper-extended crust. However, such studies are usually aimed at systematic mapping of the sensitivities of continental rifting to parameter variations and are therefore composed of laterally homogeneous lithospheric layers. A small region of elevated temperatures and/or weak material properties ensures the initial localisation of deformation away from model boundaries, but this region does not represent collisional inheritance.

Continental collision causes structural, compositional, and thermal inheritances that can all favour localisation of rifting. Orogenic thrust faults form large-scale heterogeneities for rifts to initiate on, inherited sedimentary and magmatic sequences can act as deformation localisers, and orogens are thermally weak because of the greater amount of heat producing elements in their vertical column due to their thicker crustal root. The present-day margins of the Atlantic and Indian Oceans illustrate that continental break-up can occur on both relatively young and very old sutures, such as Morocco–Nova Scotia and East Antarctica–Australia, respectively.

Our Wilson Cycle experiments illustrate how structural and thermal inheritance impacts rifted margin architecture. A continental rift can utilize the weak former subduction interface, promoting exhumation of previously subducted oceanic crust and sediments. In tandem, elevated temperatures in the collisional orogen can weaken its crustal rheology sufficiently to localize rifting. In the latter case, the weak crust promotes the formation of a hyper-extended margin. But inheritance also lies in the sub-lithospheric mantle, where mantle flow currents produced during subduction and slab detachment influence rift development from below.

**Keywords:** Numerical modelling, Rifted margins, Continental extension, Subduction, Collision.

## Studying scissor tectonics: a 4D analog modelling approach

Frank Zwaan<sup>1</sup>, Guido Schreurs<sup>1</sup>

<sup>1</sup>Institute of Geological Sciences, University of Bern, Baltzerstrasse 1 + 3, 3012 Bern, Switzerland

Corresponding autor: frank.zwaan@geo.unibe.ch

S1 – Geodynamics, Plate tectonics (Oral)

### Introduction:

Although tectonic modelers generally apply constant deformation velocities throughout their models, natural settings can involve along-strike velocity variations. In extensional regimes (e.g. the North Atlantic), we often observe the propagation and associated “scissor-like” opening of a rift, as older rift parts are further evolved than the rift tip. In some cases, this extension can result in compression on the other side of the rotation axis to complete a full scissor tectonic system (e.g. Pyrenees).

### Methods:

To model scissor tectonics, we apply a foam base that allows distributed deformation at the base of overlying brittle-ductile model material: quartz sand sieved upon a layer of a viscous PDMS/sand mixture (Fig. 1a). Both layers are 4 cm thick (1 cm = 5 km in nature), representing upper and lower crust respectively. Rotation of the model sidewalls around a rotation point induces extension at one side of the model and compression at the other side (Fig. 1b). Seeds of ductile material (diameter ca. 1 cm) are placed on top of the basal model layer to control where faulting occurs in the overlying brittle sand (Fig. 1c). The sidewall tips are moving apart with 4 mm/h during 7.5 h for a total of 30 mm extension, which translates to 30 km of extension at a natural deformation rate. X-Ray computer tomography allows 3D analysis of the internal structural evolution (hence 4D).

### Results:

Top views show that our model produces rifting in the extensional domain, no visible deformation near the scissor axis and thrusting in the compressional domain (Fig. 1c). These structures are also well visible on a horizontal section through the brittle sand layer (Fig. 1d). It also shows the development of a second thrust as part of a pop-up structure that is evident on vertical CT-sections (Fig. 1e, panel I). The vertical CT-sections also show no deformation near the scissor axis (Fig. 1e, panel II). In the extension domain, rift structures occur (Fig. 1e, panel III). The rift becomes more developed farther away from the scissor axis, as total extension increased and rift-internal faulting occurs. Towards the model edge, we observe a 36 mm wide and 8 mm deep basin, horst structures, and a strongly deformed seed (Fig. 1e, panels IV-VI). Some boundary effects are present in the shape of extensional faulting along the sidewalls.

### Outlook

These initial model results show the functionality of our model set-up. Future modeling will involve syn-rift sedimentation, various weak zone geometries and the testing of another possible set-up with rigid base plates that our new machine allows. Both 3D surface scanning and particle-tracing analysis will be used for surface evolution mapping and to quantify surface and internal model deformation.

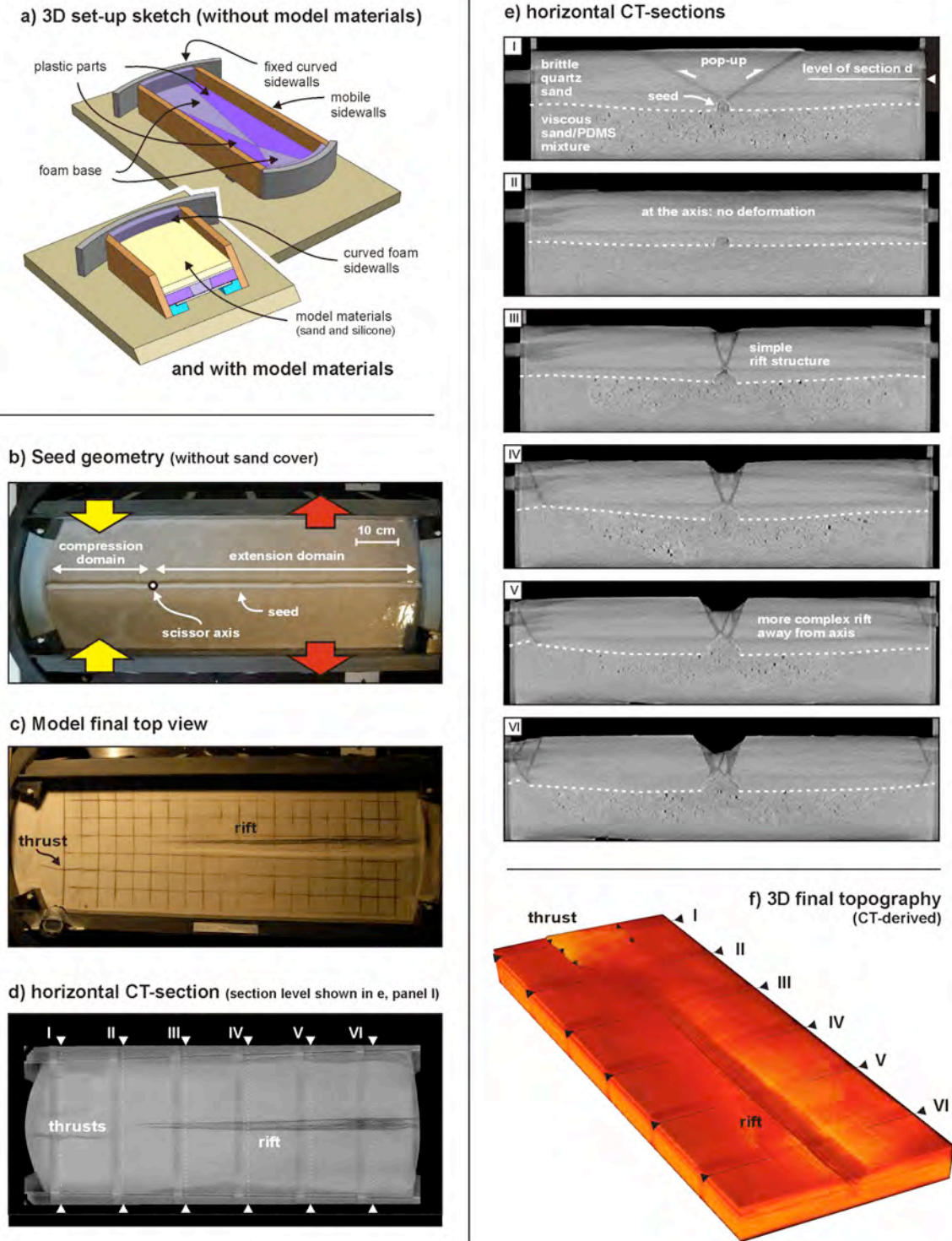


Figure 1. (a) 3D model set-up sketch. (b) Top view showing seed geometry without sand cover. (c) Final top view, showing surface structures at the end of the model run. (d) Horizontal CT-section through the sand layer, showing structures at ca. 2 cm depth (see Fig. 1e). Vertical stripes are CT-artifacts. (e) Vertical CT-sections showing internal model structures. Section locations are depicted on Figs. 1d and f. (f) CT-derived 3D topography at the end of the model run.

**Keywords:** Scissor Tectonics, Analogue Modeling, Rifting, Compression.

## Does unsteady overriding plate kinematics explain variability of slab dip and upper plate deformation ?

Solenn Hertgen <sup>1\*</sup>, Benjamin Guillaume <sup>1</sup> and Joseph Martinod <sup>2</sup>

<sup>1</sup>) Géosciences Rennes, CNRS, UMR 6118-Université de Rennes 1, Rennes Cedex 35042, France

<sup>2</sup>) ISTerre, Université de Savoie, 73376 Le Bourget du Lac cedex, France

Corresponding author: solenn.hertgen@univ-rennes1.fr

S1 – Geodynamics, Plate tectonics (Oral)

Plates reorganization associated with mantle convection leads to changes in absolute plate velocities. These changes may in turn impact the geometry of the subducting plate and the overriding plate regime of deformation, as proposed by Heuret *et al.*, (2007) on the basis of geodynamical models of subduction. These authors obtain a very good correlation between upper plate absolute motion on one hand and slab dip and upper plate deformation on the other hand. Specifically, steep slab and extension are generally associated with overriding plate moving away from the trench, while shallow slab and shortening generally occur when the upper plate goes the other way. However, these correlations are established considering models in which the motion of the overriding plate is constant and the subduction steady-state. It may not represent the general case since plate tectonic reconstructions show that in Nature plate motions change through times both at short (*i.e.*, 1-10 Ma) and long (*i.e.*, 10-100 Ma) time scales (*e.g.*, Müller *et al.*, in press). It raises some first-order questions: How does the subduction adapt to changes in the overriding plate absolute velocity? What is the impact on slab geometry and upper plate deformation? Could it explain why correlations in Nature between overriding plate absolute motion and slab dip are poorer than expected?

### Materials and methods: 3D laboratory models vs. natural subduction zones:

We conducted a series of 3D analogue models of subduction performed in the Laboratory of Experimental Tectonics of the Roma Tre University, in which we instantaneously changed the velocity of the overriding plate after a period of steady-state subduction. These variations reproduce kinematic changes that may arise from far-field changes in boundary conditions in Nature. In parallel, present-day subduction parameters (dip, velocities, slab depth) have been extracted from the global database SUBMAP (Heuret and Lallemand, 2005) for 260 transects evenly distributed all along present-day subduction zones. The evolution of overriding plate velocity for the last 5, 10 and 20 Myr have been extracted for the same transects from the tectonic reconstruction by Seton *et al.*, 2012.

### Results: comparison between analogue models and Nature:

Instantaneous changes in the overriding plate absolute velocity produce a transient stage during which both shallow and deep slab dips and upper plate deformation adjust, followed by a period of stabilization. The correlation coefficient between overriding plate velocity and upper plate deformation (including all points) is 0.88 (Fig. 1a). It only slightly increases (0.90) when discarding points corresponding to the transient stage, evidencing that deformation velocity adjusts rapidly to changes in upper plate kinematics. Correlation coefficients between overriding plate velocity and shallow and deep slab dips give values of 0.73 and 0.63, respectively (including all points; Fig.1b). The correlation largely increases when considering only the stage after slab stabilized with values of 0.85 for shallow dip and 0.93 for deep dip (Fig.1b). It shows that slab geometry requires a larger time to adjust to plate kinematic changes. For deep slab dip, our models show that this time delay is on average  $17 \pm 4$  Myr and is independent of both absolute velocity and changes in absolute velocity.

There is a systematic trend toward lower than expected slab dip when the upper plate slows down and higher than expected slab dip when the upper plate accelerates (Fig.1b). Analysis of present-day subduction zones shows the same general trends. However, in Nature, the correlations for all transects are poorer than in laboratory models ( $<0.35$ ). Correlations can be improved by discarding transects close to slab edges and for which the slab has not reached the 660 km discontinuity, similar to what found by Lallemand *et al.*, (2005). More interestingly, the distribution of slab dip as a function of overriding plate accelerations or decelerations above specific periods of time supports the idea of a global adjustment time of  $\sim 10$  Ma, close to what found in analogue models. Over this time period, deep slab dips tend to be lower than expected when the upper plate constantly decelerated, and higher than expected when it accelerated (Fig.1c). The same analysis for upper plate deformation gives a best result for an adjustment time of 5 Ma. The unsteady nature of overriding plate kinematics may explain the poor correlation in Nature between present-day subduction kinematics, slab dip and upper plate deformation, because the present-day velocities corresponds to a snapshot in the evolving history of subduction.

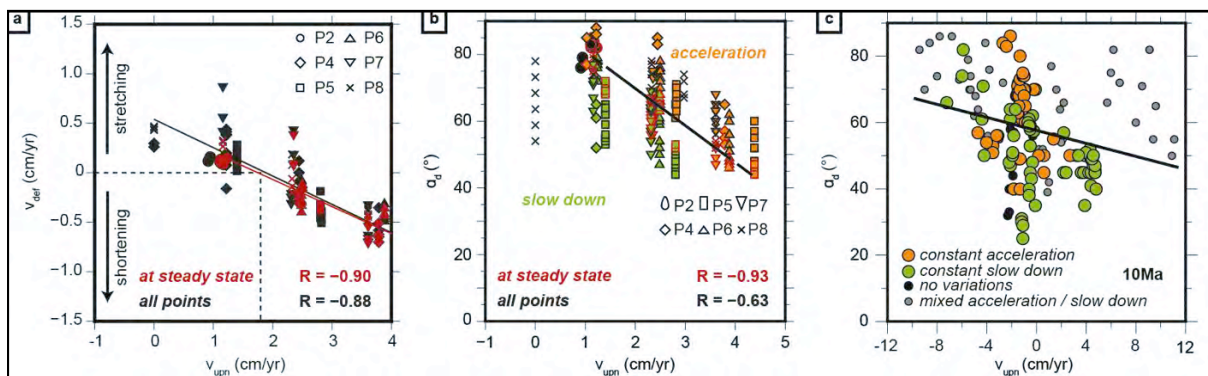


Figure 1: a) Upper plate deformation velocity vs. overriding plate absolute velocity for all models. b) Distribution of deep slab dip (330 km-depth) following overriding plate acceleration (orange) or deceleration (green) for all models. c) Distribution of deep slab dip as a function of changes in upper plate velocity over the last 10 Ma for all transects in Nature (after Heuret *et al.*, 2005 and Seton *et al.*, 2012). The black lines correspond to the linear regression line for steady-state subduction in models and for all transects in Nature.

## References:

- Heuret, A., Lallemand, S., 2005. Plate motions, slab dynamics and back-arc deformation, *Physics of the Earth and Planetary Interiors* 149, 31-51.
- Heuret, A., Funicello, F., Faccenna, C., Lallemand, S., 2007. Plate kinematics, slab shape and back-arc stress: A comparison between laboratory models and current subduction zones, *Earth and Planetary Science Letters* 256, 473-483.
- Lallemand, S., Heuret, A., Boutelier, D., 2005. On the relationships between slab dip, back-arc stress, upper plate absolute motion, and crustal nature in subduction zones, *G3* 6(9), Q09006.
- Müller, R.D., *et al.*, in press. Ocean basin evolution and global-scale plate reorganization events since Pangea breakup, *Annual Review of Earth and Planetary Sciences*.
- Seton, M., *et al.*, 2012. Global continental and ocean basin reconstructions since 200 Ma, *Earth-Science Reviews* 113, 212-270.

**Keywords:** overriding plate, plate reorganization, absolute plate velocity, slab dip, upper plate deformation, adjustment time, subduction zone.

## Finite strain sensitivity to past mantle flow

Maria Chertova<sup>1</sup> and Wim Spakman<sup>1,2</sup>

<sup>1</sup>) University Utrecht, Earth Sciences, Mantle dynamics group, Utrecht, Netherlands

<sup>2</sup>) Centre of Earth Evolution and Dynamics (CEED), University of Oslo

Corresponding author: M.V.Chertova@uu.nl

S1 – Geodynamics, Plate tectonics (Oral)

### Introduction:

Remotely forced mantle flow might significantly influence the position of the subduction zone, while keeping the slab shape relatively unaffected (Chertova et al., 2016), suggesting that the present day slab morphology may not easily reveal mantle flow that was forced elsewhere in the mantle. Here we make a first attempt to find diagnostics for the existence of past external mantle flow from the present day finite strain pattern surrounding a slab. When modeling real Earth subduction zones, these could provide a new link for understanding shear wave splitting observations, e.g. for the Gibraltar subduction region (Diaz and Gallart, 2014).

To investigate the impact of the external mantle flow on the final pattern of finite strain ellipsoid (FSE) evolution we perform numerical subduction modeling in a Cartesian domain and analyze how mantle inflow prescribed for different sides of the model affects FSE patterns. We evaluate FSE dependence on the redirection of mantle flow, which may also occur for actual subduction zones. We examine the possibility of determining of the dominant direction of past mantle flow using the present day finite strain pattern.

### Model description:

To analyze the finite strain development for the subduction zone in the presence of the external mantle flow we employ the generic model from Chertova et al. (2016) which comprises subducting and overriding plates and two side-plates at the surface of a Cartesian domain of 3000x2000 km with a depth of 1000 km. Plates are decoupled via 70 km weak zones with viscosity of  $3 \cdot 10^{20}$  Pas. The width of subducting plate varies between 600 and 1400 km. At the start of modeling the subduction angle of  $45^\circ$  and the slab reaches depth of 300 km. We use non-linear rheology, which consists of diffusion, dislocation creep, and a viscosity limiter of  $5 \cdot 10^{23}$  Pas, and include two upper mantle phase transition zones and a viscosity jump at the transition to the lower mantle. To test different mantle flow directions we prescribe a uniform in-flowing velocity of 3 cm/yr on either the western, eastern, or southern boundary of the model, while the other boundaries are open. Subduction is initially dipping east and to ensure that the slab does not get close to the side boundary due to westward rollback we prescribe a constant input velocity for the subducting plate in the range of 1.5-3 cm/yr at the western boundary.

### Dependence of the FSE pattern on the imposed mantle flow:

To evaluate the influence of the mantle flow on the final pattern of FSE, we compare models with mantle flow imposed on one particular model side with the reference model that has open boundary conditions on all sides. An example of the resulting pattern of long FSE axis is shown in figure 1. We plot two cross-sections oriented in WE direction through the center of the slab and slab edge.

In the subslab area, the model with eastern inflow is similar to the reference model showing a wide area of trench-parallel long FSE axis. We relate this effect to the same boundary conditions used for the western boundary, which is closest to the subslab region and to the “shielding” of the subslab

region by the slab. In contrast, a distinctly different pattern is observed in the mantle wedge above the slab where a wide area of trench-parallel FSE long-axis exists that is not observed in any other model. This serves as diagnostic for the existence of mantle inflow from the east. The model with western mantle inflow shows patterns of long FSE axis quite similar to the reference model. Only small differences exist in the subslab area attributable to the western inflow. The last model, with southern, or trench parallel, mantle flow demonstrates a distinctly different pattern of long FSE axis from all other models. Nowhere in the modeling domain the long axes are oriented trench parallel or lie within the symmetry plane.

Another question we address with our work is how fast the finite strain pattern responds to changes in the dominant direction of mantle flow. With our models we test changing of boundary conditions for 10 My after a strong FSE pattern is developed in the model. We show that, in the case of a well-developed finite strain pattern, we can recover the dominant direction of the past mantle flow and, to some extent, can trace the history of its variations through time. The inherited finite strain pattern is rather stable and, after changing the mantle flow direction, it will be maintained for at least 5-10 My.

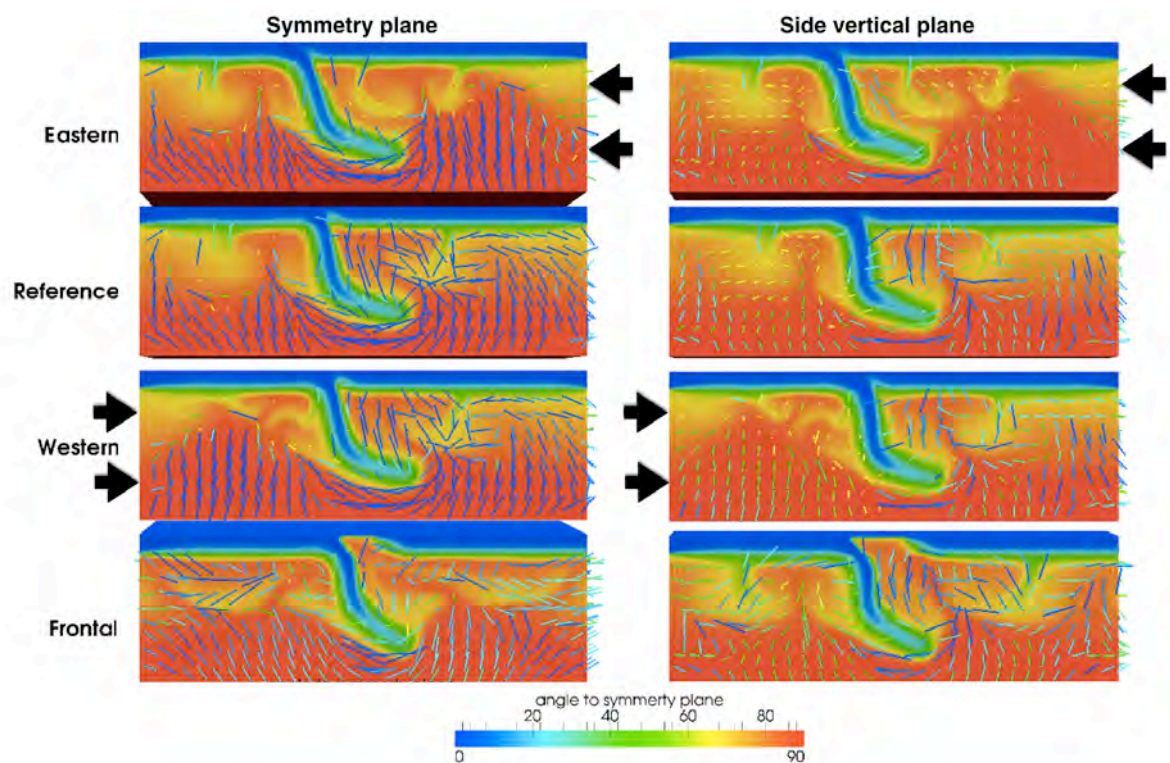


Figure 1. Long FSE axis for models with open boundaries, with western inflow, eastern inflow and frontal inflow after 25 My of the subduction evolution. Colors indicate angle between long axis and symmetry plane.

#### References:

- Diaz, J., and Gallart, J., 2014. Seismic anisotropy from the Variscan core of Iberia to the western African Craton: New constraints on upper mantle flow at regional scale. *Earth and Planetary Science Letters*, 394, 48-57.
- Chertova, M., and Spakman, W., 2016. Mantle flow influence on the evolution of subduction systems, in prep.

**Keywords:** Subduction, mantle flow, finite strain.

## Controls on continental strain partitioning above an oblique subduction zone, Northern Andes

Jorina M. Schütt<sup>1</sup> and David M. Whipp, Jr.<sup>1</sup>

<sup>1</sup> University of Helsinki, Finland

Corresponding author: jorina.schutt@helsinki.fi

S1 – Geodynamics, Plate tectonics (Oral)

### Introduction:

At obliquely convergent plate margins strain partitioning is a common tectonic process dividing oblique convergence into margin-normal slip on the plate-bounding fault and horizontal shearing on a strike-slip system parallel to the margin. In subduction zones, strain partitioning in the upper continental plate is mainly controlled by the shear forces acting on the plate interface and the strength of the continental crust (e.g., Stern, 2002). Plate interface forces are influenced by the dip angle of the subducting plate (i.e. the length of plate interface in the frictional domain) and the obliquity angle  $\gamma$  between the normal to the plate margin and the plate convergence velocity vector (Fig. 1A). The crustal strength of the continent is strongly affected by the presence or absence of a volcanic arc, with the absence of volcanic arcs being common at ‘flat slab’ subduction zones. Along the ~7000 km western margin of South America the convergence obliquity, subduction dip angles and presence of a volcanic arc all vary, and strain partitioning is only observed along parts of it. This raises the question, which are the most important subduction zone characteristics to control strain partitioning in the overriding continental plate?

In this work, we focus on the Northern Volcanic Zone (NVZ; 5°N - 2°S; Fig. 1A) of the Andes, which is characterized by a ~35° subduction dip angle with an obliquity angle of about  $\gamma = 40^\circ$ , extensive volcanism and significant strain partitioning in the continental crust.

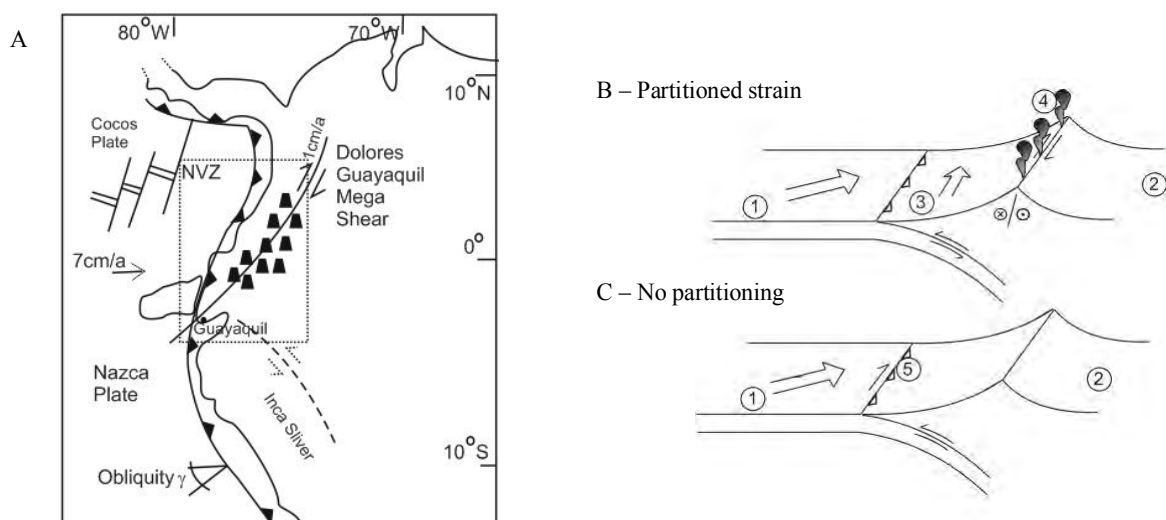


Figure 1: A: Simplified tectonic map of northern South America: Northern Volcanic Zone (NVZ) with Dolores Guayaquil Mega Shear Zone (DGM) and the southern ‘flat slab’ (south of 3°S) zone with the slowly moving Inca sliver; black polygons represent volcanoes; B: Schematic sketch of strain partitioning as in the NVZ: The oceanic Nazca Plate (1) is subducting underneath the continental South American Plate (2) with a steep and

oblique angle (3). On the continental side strain partitioning, a right lateral shear zone (DGM) and a volcanic arc (4) are observed; C: No partitioning case with oblique subduction (5).

**Model design** We use lithospheric-scale 3D numerical geodynamic experiments to investigate the influence of subduction geometry on strain partitioning above an oblique subduction zone. Herein we focus on how weaknesses in the crust change strain partitioning behavior. The numerical modelling software (DOUAR; Braun, et al., 2008) solves the Stokes flow equation for a viscous-plastic creeping flow to calculate velocity fields, rock uplift and strain rates in a 1600 km x 1600 km box with a depth of 160 km. The subduction geometry and material properties are based on a simplified, generic subduction zone similar to the northern Andes. The upper surface is initially defined to resemble Andean topography and is fixed over the entire run time (1 Ma). We consider two main model designs, one with and one without a weak zone representing the volcanic arc in the NVZ. The weakness is introduced applying a region of low friction angle in a purely mechanical frictional-viscous medium.

### Results and Conclusions:

Preliminary results shown in Figure 2A and B confirm that the weak volcanic arc is needed for significant strain partitioning to occur. We observe little strain partitioning for a uniform continental crustal strength with a friction angle of  $F = 15^\circ$  (Fig. 2B). However, strain partitioning does occur when including a weak zone in the continental crust (with  $F = 2^\circ$ ) resulting from arc volcanic activity (Fig. 2A). This results in margin-parallel northeastward translation of a continental sliver at 1.2 cm/year, which agrees well with observations of a continental sliver identified by GPS measurements in the NVZ (Veloza et al., 2012).

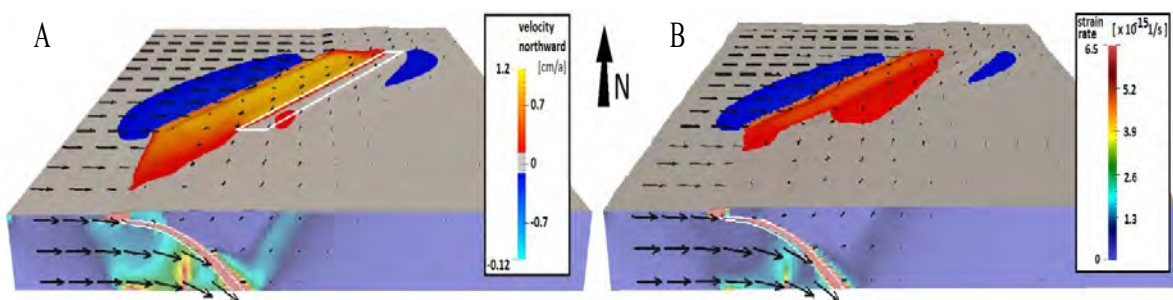


Figure 2: Oblique view of the 3D numerical experiments after 1 Ma with velocity vectors, strain rates, and the north component of surface velocities: (A) model with a volcanic arc (white outline on top surface) shows strain partitioning in the continental crust (e.g. a coherent block moving northward with about 1.2 cm/a) while (B) model without a volcanic arc does not experience clear strain partitioning. The legends are valid for both A and B: the velocity northward at the top surface and the strain at the front cross section.

### References:

- Braun, J., Thieulot, C., Fullsack, P., DeKool, M., Beaumont, C., and Huisman, R., 2008. DOUAR: A new three-dimensional creeping flow numerical model for the solution of geological problems. *Physics of the Earth and Planetary Interiors* 171, p. 76-91.
- Stern, R. J., 2002. Subduction zones. *Reviews of Geophysics*, Vol 40 No 4.
- Veloza, G., Styron, R., Taylor, M., and Mora, A., 2012. Open-source archive of active faults for northwest South America, *GSA Today*, Volume 22, Number 10.

**Keywords:** Numerical 3D modeling, Strain partitioning, Subduction, Andes.



When applied to generic-type intracontinental settings, the results from the modelling efforts are able to explain the first order characteristics of their long and, yet to be understood subsidence and reconcile all major observations common to their deformation history. Depending on the sedimentary loading history and on the level of initial thermal perturbation of the lithosphere, we demonstrate how a rheologically stratified lithosphere can subside naturally over geological time scales without the need to impose “ad hoc” geometric and/or kinematic initial conditions. 3D feedback effects of sedimentation on the thermo-mechanical structure of the plate result in a weakened lower crust, which is mechanically decoupled from the underlying upper mantle, and therefore easily reactivated even under relatively low far-field tectonic stresses (possibly enhanced by lower crustal flow) thus leading to impulse of acceleration of subsidence rates with respect to their background values (Fig. 2).

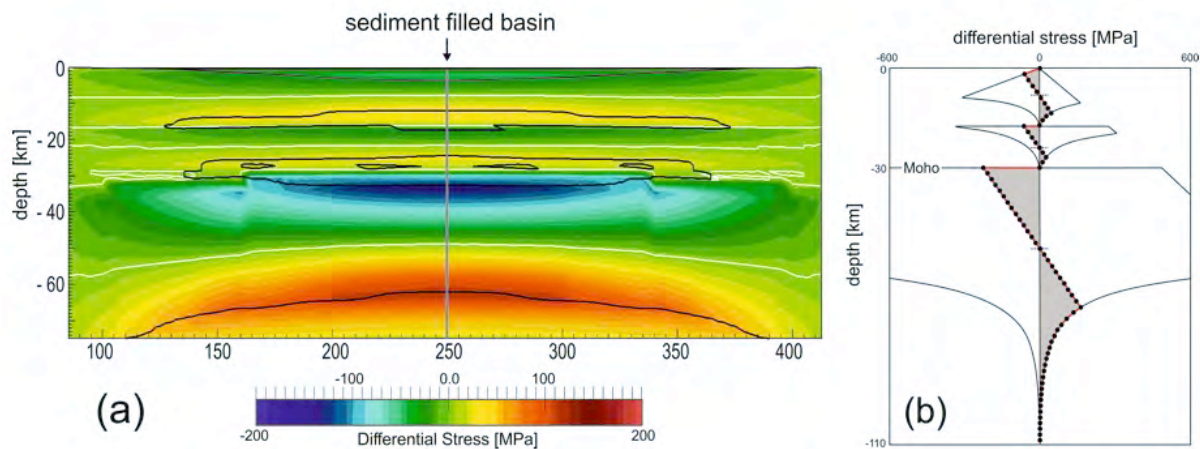


*Figure 2: Effects of loading by sediments on the mechanical configuration of the lithosphere. (a) Differential stress distribution after 150 Myr of simulation time. White curves indicate the locations of neutral flexural planes (no differential stress) at different depths. Black lines contour the extent of the domains of plastic yielding (brittle or ductile creep) due to either tensile (positive) or compressive (negative) stresses. (b) Yield strength envelope (YSE) and bending stress distribution (shaded areas) at the point of maximum bending. Thermal and mechanical effects of the sedimentary cover result in a ductile weakening of the lower crust and in a decoupling of the lithosphere across the crust-to-mantle level. This is indicated by the high values of shear stresses and by a reversal of their signs (from compression to extension) at this depth. Due to crustal-mantle decoupling, each layer behaves mechanically independently and show a separate distribution of bending stresses. Stress decay due to thermally activated olivine creep occurs at depths greater than 80 km.*

Based on the obtained results, we hypothesize that intracontinental basins should be conceived as extreme members of the rift-to-drift suite of basin, which were formed under low magnitudes extensional tectonics. Despite their longevity and long-term potential for mineral, fossil and renewable resources, intracontinental basins do represent highly dynamic systems that did not attain a state of isostatic equilibrium during any stage in their history. Therefore, their subsidence can be explained by the striving for a thermal and mechanical equilibrium that, however, is never reached.

#### References:

Cacace M, Scheck-Wenderoth M. (2016): Why intracontinental basins subside longer: 3D feedback effects of lithospheric cooling and sedimentation on the flexural strength of the lithosphere, *J. Geophys. Res. Solid Earth*, 121, 3742 – 3761, doi: 10.1002/2015JB012682.

**Keywords:** Long-term subsidence, flexural deformation, rheology, thermal cooling.

## Effects of grain size variation and mantle viscosity on fluid migration in the mantle wedge

Nestor Cerpa<sup>1</sup>, Ikuko Wada<sup>1</sup>, Cian Wilson<sup>2</sup> and Marc Spiegelman<sup>2,3</sup>

<sup>1</sup>) University of Minnesota, Department of Earth Sciences, Minneapolis, MN, USA

<sup>2</sup>) Columbia University, Lamont-Doherty Earth Observatory, Palisades, NY, USA

<sup>3</sup>) Columbia University, Department of Applied Physics and Applied Math, New York, NY, USA.

Corresponding author : ncerpagi@umn.edu

S1 – Geodynamics, Plate tectonics (Oral)

### Introduction:

Arc volcanism tends to occur in a narrow region where the vertical distance to the top of the slab is  $\sim 100 \pm 30$  km [e.g., England et al. 2004]. Slab-derived fluids are thought to trigger hydrous melting in the hot region of the mantle wedge [e.g., Grove et al. 2006]. However, numerical thermo-petrologic models for subduction zones predict fluid release from slabs over a wide depth range [Hacker et al., 2008], and the mechanism that focuses fluids and melts beneath the arcs is still highly debated [Tatsumi et al., 1986 ; Cagnioncle et al., 2007, Grove et al., 2006, Wilson et al., 2014]. Fluid migration depends on the permeability of the medium, which in turn depends on fluid fraction and mineral grain size [e.g., Wark et al., 2003]. Using a numerical fluid migration (FM) model with a uniform grain size, Cagnioncle et al. [2007] showed that finer grain size tends to drag fluids down-dip along the base of the mantle wedge due to lower permeability.

Recently, Wada and Behn [2015] adopted a grain size distribution in the mantle wedge calculated by a coupled thermal-grain size evolution (T-GSE) model in their FM model and showed that the predicted grain size distribution leads to focusing of fluids beneath the arcs. However, these models do not include the effects of matrix compaction and mantle solid rheology on fluid flow. Viscous resistance of the matrix to the volumetric strain in porous flow generates compaction pressure that partly drives fluid flow in the mantle wedge as shown by Wilson et al, [2014]. Yet the authors only considered uniform grain sizes. In the present work we aim to quantify the combined effects of grain size variation and mantle viscosity structure on FM pathways in the mantle wedge using a 2-D numerical model. We also assess the influence of slab age, slab dip, slab velocity, and fluid influx on fluid flow.

Model

We develop a 2-D mantle wedge FM model that incorporates the effects of grain size variation and mantle viscosity based on a coupled Darcy's-Stokes flow model [McKenzie, 1984]. Here, we assume uniform densities for both the fluid and solid phases and a small-porosity approximation such that the solid mantle flow is independent of the fluid flow. For the solid flow calculation, we use a kinematic-dynamic model, in which dynamic mantle flow is driven by the subduction velocity prescribed at the top of the slab. In the model, we use a composite rheology that accounts for both diffusion and dislocation creep and employ a T-GSE model to calculate the grain size distribution, following Wada and Behn [2015]. For the fluid flow calculation, we incorporate the effects of mantle compaction. We use a constant fluid viscosity based on the assumed composition of the fluids. Permeability depends on porosity and grain-size while solid matrix bulk viscosity is porosity-dependent. The fluid influx from the slab is imposed as a boundary condition at the base of the mantle wedge. We solve the governing equations of each problem with finite elements in space and finite differences in time using the software package TerraFERMA [Wilson and Spiegelman, 2015].

**Preliminary Results:**

In our preliminary work we assess the general trends of the effect of spatial variations in grain size and solid shear viscosity while keeping all other parameter values the same. Particularly, we first impose a single influx source at a prescribed depth. When influx is imposed at a relatively shallow depth (80-100 km) our models predict an initial down-dip fluid transport by the mantle velocity due to a relatively low grain size ( $\leq 1$  mm) and a relatively high matrix shear viscosity ( $>1020$  Pa.s). With increase in grain size with depth, fluids become primarily driven by buoyancy and start to migrate upwards as porosity waves. The migrating fluids tend to move towards the trench due to the mantle inflow and to pond where the solid shear viscosity becomes too high and the resulting compaction pressure gradients counterbalance buoyancy at  $\sim 50$ -60 km depth. Based on a series of model runs that we performed, these general trends are sensitive to grain size distribution, shear viscosity, and fluid flux, all of which are dependent on subduction parameters such as slab age, slab dip, and subduction rate. We thus aim to quantify the effects of subduction parameters and to provide a better understanding of fluid migration pathways beneath arcs.

**References:**

- England, P.-C., Engdahl, R., and Thatcher, W., 2004. Systematic variation in the depths of slabs beneath arc volcanoes, *Geophys. J. Int.*, 156, 377-408.
- Cagnioncle, A.-M., Parmentier, E. M., and Elkins-Tanton, L.-T., 2007. Effect of solid flow above a subducting slab on water distribution and melting at convergent plate boundaries, *J. Geophys. Res.*, 112, B09402, doi:10.1029/2007JB004934.
- Grove, T. L., Chatterjee, N., Parman, S. W., and Medard, E., 2006. The influence of H<sub>2</sub>O on mantle wedge melting, *Earth Planet. Sci. Lett.*, 249, 74-89.
- Hacker, B. R., 2008. H<sub>2</sub>O subduction beyond arcs, *Geochem. Geophys. Geosyst.*, 9(3). McKenzie, 1984. The generation and compaction of partially molten rock, *J. Petrol.*, 25, 713-765. Tatsumi, Y., 1986. Formation of the volcanic front in subduction zones, *Geophys. Res. Lett.*, 13(8), 717-720. Wada, I., and Behn, M. D., and He, J., 2011. Grain size distribution in the mantle wedge of subduction zones, *J. Geophys. Res.*, 116, doi:10.1029/2011JB008294. Wada, I., and Behn, M. D., 2015. Focusing of upward fluid migration beneath the arc: Effect of mineral grain size variation in the mantle wedge, *Geochem. Geophys. Geosyst.*, 16(11), 3905-3923.
- Wark, D. A., Williams, C. A., Watson, E. B., and Price, J. D., 2003. Reassessment of pore shapes in microstructurally equilibrated rocks, with implication for permeability of the upper mantle, *J. Geophys. Res. : Solid Earth*, 108. Wilson, C. R., Spiegelman, M., Van Keken, P. E., and Hacker, B. R., 2014. Fluid flow in subduction zone: The role of solid rheology and compaction pressure, *Earth Planet. Sci. Lett.*, 401, 261-274.
- Wilson, C. R. and Spiegelman, M., 2015. Software: TerraFERMA v1.0 – The Transparent Finite Element Rapid Model Assembler, open-source repository: [terraferma.github.io](https://github.com/terraferma)

**Keywords:** Subduction, Fluids, Porous Flow, Arcs.

## How to simulate the subduction interface in a convective and compositional model? The effects of numerical and rheological parameters

Diane Arcay<sup>1</sup>

<sup>1</sup>) Geosciences Montpellier, University of Montpellier, CNRS, Antilles University

Corresponding Author: [diane.arcay@gm.univ-montp2.fr](mailto:diane.arcay@gm.univ-montp2.fr)

S1 – Geodynamics, Plate tectonics (PS7)

### Introduction:

In a subduction zone, the properties of the interplate domain affects the seismogenic characteristics of the interplate perceivable at the time-scale of the seismic cycle. Moreover, as the interplate domain interacts with the whole subduction system, it partly controls the subduction viability. As such its structure is likely to equilibrate at the time-scale of tens of Myr. The relationships between the behaviors at these two end-member time scales are poorly known, while they may be one of the basic keys of the subduction factory. This study focuses on the processes governing the thermo-mechanical structure of the subduction interface, by performing long-term experiments (~20 Myr of convergence) in which the diving and overriding lithospheres interact with the surrounding mantle.

#### Model set-up

The 2D simulation box, 2220 km wide and 555 km deep, is made of 2 lithological layers: an 8 km thick layer covers the surface of the incoming lithosphere, while the remaining domain is made of mantle. A non-Newtonian viscous rheology and a pseudo-brittle rheology are combined. Strength depends on depth, temperature and strain rate, for both oceanic crust and mantle rocks. The crust is significantly weaker than the mantle both in the brittle and ductile realms to favor strain localization at the incoming plate surface. A constant convergence rate of 6.5 cm/yr is applied on the subducting plate far away from the subduction zone. Regarding the modelled subduction interface, a special attention is paid to the down-dip extent, labelled *zcoup*, of the domain of kinematic decoupling between the two converging plates. At depth shallower than *zcoup*, the tangential velocity is discontinuous across the subduction interface, while at deeper levels, mantle rocks are kinematically dragged down along with the subducting plate. The depth *zcoup* affects the interplate domain structure, as it is the shallowest depth reached by hot asthenosphere in the mantle wedge tip.

#### Simulated functioning of the interplate factory

Two end-member cases are considered: the subduction of an old oceanic lithosphere (~100 Myr old and ~100 km thick), on one hand, and of a young (20 Myr old) lithosphere (~ 40 km thick), on the other hand. The overriding plate is ~100 km thick in all cases. When convergence starts, the efficiency of strain localization within the weak crustal layer forming the subduction channel depends on the strength contrast between the soft crustal layer and the more or less stiff cold mantle composing the base of the fore-arc lithosphere. Simulations show that, to promote subduction, the interplate channel has to allow simultaneously for two opposite processes. At shallow depths, the subduction interface must localize deformation to sustain the kinematic discontinuity between the two converging plates.

Still, at depth close to the boundary between the upper plate and the asthenosphere, strain localization has to jump from the subduction plane to the soft asthenosphere to spatially decouple the incoming plate from the overlying lithosphere. If not, a continuous localization of deformation within the weak oceanic crust results either, for an old incoming plate, in a downward dragging of the upper plate base (“asymmetric double subduction”, Fig. 1a1), or, for a young subducting lithosphere, in an horizontal subduction since the asthenospheric “corner flow” has not been activated (Fig. 1b1).

**Case 1: Subduction of an old and cold lithosphere** This set-up is used to first highlight the influence of the numerical resolution on the modeled *zcoup* value. If the weak crustal layer is too thinned within the subduction channel, the average composition at Eulerian nodes within the crustal layer is a mix between weak crust and stiff mantle (see insert in Fig. 1a1). This numerically strengthens the interplate channel and promotes an early jump of strain into the asthenosphere. As a result, the simulated *zcoup* depth shallows because of numerical artifacts. Second, by varying the ductile strength contrast between the mantle and the weak interplate crust ( $\Delta E_a$ ), an activation energy offset between the two lithologies greater than 135 kJ/mol appears to impede the necessary strain jump into the asthenosphere, leading to subduction of the base of the arc lithosphere (Fig. 1a2). This yield an extremely cold fore-arc structure preventing mantle melting at water-saturation conditions, and thus the formation of a volcanic front.

**Case 2: Subduction of a young and warm lithosphere**

Simulating the subduction of a 20 Myr old lithosphere reveals that in this set-up, a successful initiation depends on (1) the strength difference between mantle and interplate channel ( $\Delta E_a$ ) and on (2) the density contrast between them. A too buoyant crust impedes subduction unless imposing a high to very high ductile strength contrast,  $\Delta E_a$ . However if  $\Delta E_a$  is too high, an interplate partial coupling with the upper plate base and/or and diapirism of the buoyant interplate crust (Fig. 1b2) appear.

The modeled down-dip extent of the interplate boundary, *zcoup*, is finally compared to proxies in nature: (1) slab surface depth right below the volcanic front, (2) depth of strong lateral contrast close to the slab surface in high resolution seismic tomography when available, and (3) location of the heat flow maxima observed in heat flux profiles from the trench toward the arc lithosphere.

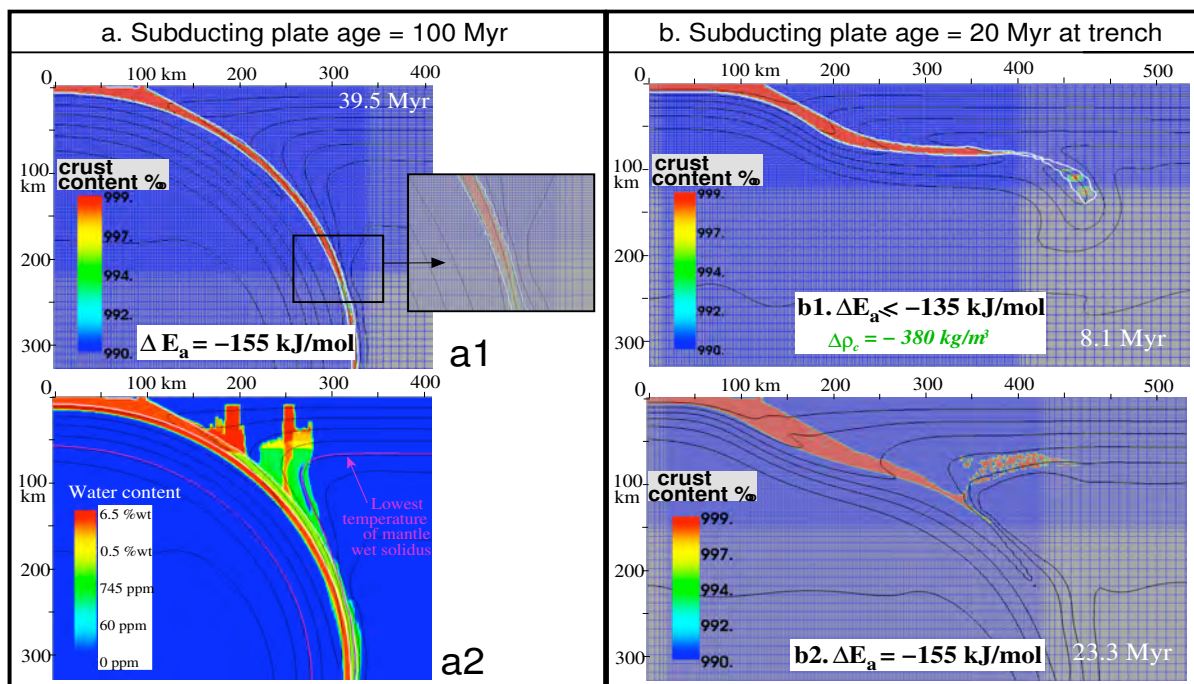


**Figure 1:** Influence of activation energy offset between crust and mantle,  $\Delta E_a$ , on the subduction mode: Zooms on the steady-state subduction. One isotherm every 200°C. The concentration in weak oceanic marker is >49% within the white line. The color scale focuses on very high content in crust marker (>990 ‰). Panel (a): Subduction of an old lithosphere for a high  $\Delta E_a$ , yielding a two-sided subduction. On the bottom row, the logarithmic water content color scale highlights very low water amounts in the asthenosphere. The pink line is the 980°C isotherm, i.e., the minimum temperature of the peridotite water-saturated solidus. Panel (b): Subduction of a 20 Myr old lithosphere as a function of  $\Delta E_a$  for a very buoyant subducting crust

**Keywords:** Subduction, interplate domain, numerical modeling.

## Hydro-thermo-mechanical numerical simulations for the control of sea floor topography on interplate strength in subduction zones

Arthur Bauville<sup>1</sup> and Mikito Furuichi<sup>1</sup>

<sup>1</sup>) Department of Mathematical Science and Advanced Technology, Japan Agency for Marine-Earth Science and Technology (JAMSTEC), 3173-25 Showa-machi, Kanazawa, Yokohama, Japan

Corresponding author: abauville@jamstec.go.jp

S1 – Geodynamics, Plate tectonics (PS7)

The subduction of rough sea floor results in lower plate coupling than the subduction of smooth sea floor (Wang and Bilek, 2011). On the other hand, rough sea floor is also associated with higher effective friction coefficient of the subduction interface than smooth sea floor (Gao and Wang 2016).

To investigate this paradoxical situation, we perform two-dimensional (2D) numerical simulation of subduction with varying rugosity of the sea floor. We focus on the shallow part of the subduction zone, in particular the subduction prism and the upper plate near the interface. We describe the variations in tectonic structures caused by sea floor rugosity and we characterize the interplate region in terms of effective strength. The effective strength of the shallow interplate region is strongly affected by the presence of water, therefore, we built a so-called hydro-thermo-mechanical numerical model (e.g. Bercovici et al., 2001; Dymkova and Gerya, 2013). The numerical scheme is based on the finite-difference staggered grid method/Marker-in-cell (e.g. Gerya and Yuen, 2003). The model describes the flow of rocks on a geological time scale, as well as the flow of water through it. The mechanical properties of the solid are described by a visco-elasto-plastic rheology, where the viscous part of the rheology is dependent on temperature. Water affects the yield criterion of the solid phase by lowering the effective pressure.

We present early results demonstrating the influence of sea floor topography on the strength and structures of the interplate region in the presence of water. We also discuss the pros and cons of parameterizing the effect of water by prescribing an effective coefficient of friction a priori rather than solving for the dynamical system.

### References:

- Bercovici, D., Ricard, Y. and Schubert, G., 2001. A two-phase model for compaction and damage: 1. General theory. *Journal of Geophysical Research: Solid Earth*, 106(B5), pp.8887-8906.
- Dymkova, D. and Gerya, T., 2013. Porous fluid flow enables oceanic subduction initiation on Earth. *Geophysical Research Letters*, 40(21), pp.5671-5676.
- Gerya, T.V. and Yuen, D.A., 2003. Characteristics-based marker-in-cell method with conservative finite-differences schemes for modeling geological flows with strongly variable transport properties. *Physics of the Earth and Planetary Interiors*, 140(4), pp.293-318.
- Gao, X. and Wang, K., 2014. Strength of stick-slip and creeping subduction megathrusts from heat flow observations, *Science*, 345(6200), pp.1038-1041.
- Wang, K. and Bilek, S.L., 2014. Invited review paper: Fault creep caused by subduction of rough seafloor relief. *Tectonophysics*, 610, 1-24.

**Keywords:** Hydro-thermo-mechanical model, seamount, subduction, lithosphere strength.

## **Plumes to initiate subduction, continental growth and plate tectonics : comparison between laboratory experiments, Venus and the Early Earth.**

Anne Davaille<sup>1</sup>

<sup>1</sup>) Laboratoire FAST (CNRS / Univ. Paris-Sud) , bat. 502, rue du Belvedere, Campus Universitaire, 91405 ORSAY, France

Corresponding author: [davaille@fast.u-psud.fr](mailto:davaille@fast.u-psud.fr).

S1 – Geodynamics, Plate tectonics (PS7)

### **Abstract:**

The necessary conditions for plate tectonics and continental growth to occur on a terrestrial planet are still debated. Both require plate failure and subduction, but understanding their onset remains a challenge due to the complexity of mantle rocks. We carried out experiments on convection in aqueous colloidal dispersions heated from below, and dried and cooled from above. The rheology of these fluids depends strongly on solid particle fraction  $\varphi_p$ , being Newtonian at low  $\varphi_p$ , and presenting memory, yield stress, elasticity, and brittle properties as  $\varphi_p$  increases (Di Giuseppe et al, 2012). Such a behaviour is analogue to the rheology of mantle rocks as temperature decreases.

When drying is sufficiently rapid in the laboratory, a visco-elasto-plastic skin ("lithosphere") forms on the fluid surface. Depending on its rheology, and on the different scales of convection existing in our laboratory mantle, we observed different modes of one-sided subduction initiation. However, not all of them lead to continuous plate tectonics. If subduction is definitely a necessary condition for plate tectonics, it is not sufficient.

Amongst the different modes of subduction initiation, we observed one of them where one-sided subduction was induced by the impingement of a hot plume under the skin, the trench being localized on the rim of the plume impingement zone under the lithosphere (fig.1). Due to the plastic/brittle character of the skin, the subduction trench will never describe a complete circle, but several tears and/or transform faults will develop as subduction and roll back proceed. Then depending on the lithospheric rheology, the nascent subduction can either stop as the result of subducted plate necking, or continue to sink smoothly.

Those experiments therefore demonstrate a strong association between plumes and subduction initiation. This could explain on Venus the association of large coronae (created by hot upwelling mantle plumes) with trenches that have topographic signatures similar to Earth's subduction trenches (Sandwell and Schubert, 1992 ; Smrekar et al, 2016). Moreover, inspection of the geological record on Earth cratons suggests that many continental growth bursts open by a plume event closely followed by generation of granitoids in a subduction environment (e.g. Arndt and Davaille, 2013 ; Condie et al, 2014). This suggests that plume-induced subduction may have been instrumental in the nucleation and growth of cratons, and in the onset of continuous plate tectonics.

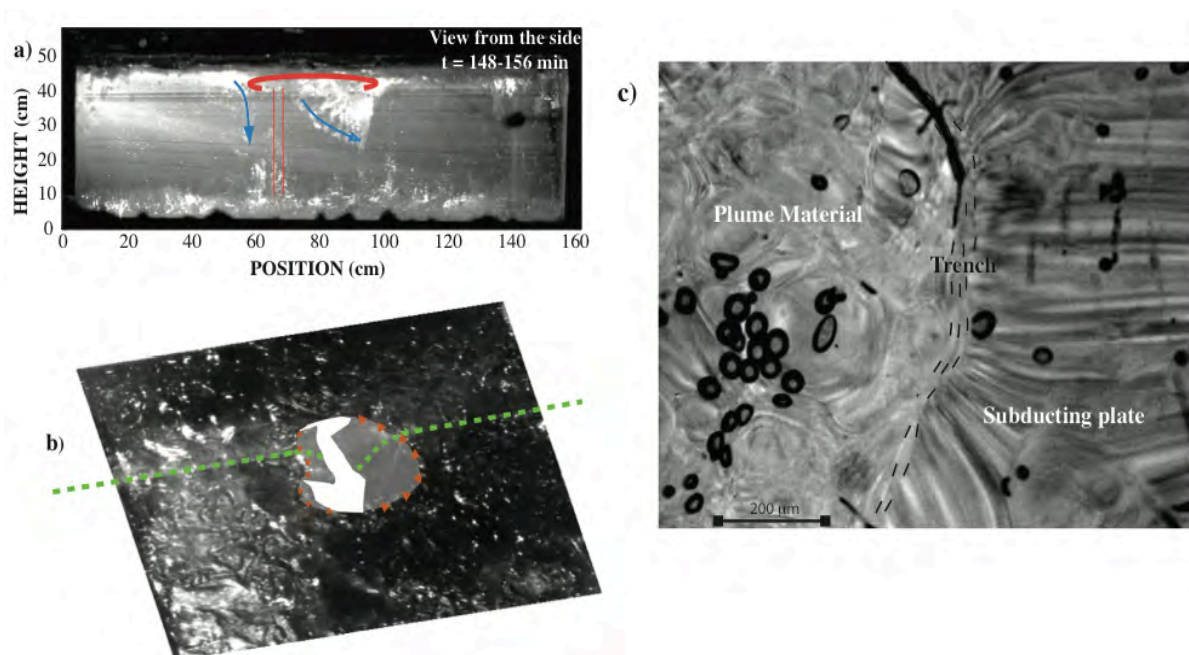


Figure 1: Plume-induced subduction in the laboratory. a) side view. 10 images have been superimposed to show the slab roll-back as the plume spreads. b) 3D view from above where the plume material has been removed. c) close up (1 cm across) on the boundary between plume material and subducting plate. Darker areas are thicker. The outer bulge close to the trench presents cracks and stripes. The trench (black dashed lines) shows faults parallel to it. The small black ovoids are spurious bubbles.

#### References:

- Arndt N, A. Davaille, 2013. Episodic Earth Evolution. *Tectonophysics*, 609,661-674.
- Condie, K.C., A. Davaille, R.C. Aster & N. Arndt (2014) Upstairs-downstairs: supercontinents and large igneous provinces, are they related?, *International Geology Review*, 57, 1341-1348.
- Di Giuseppe E. , A. Davaille, E. Mittelstaedt and M. François, 2012. Rheological and mechanical properties of silica colloids : from Newtonian liquid to brittle behaviour. *Rheol. Acta* 51(5), 451-465.
- Sandwell D.T. and G. Schubert, 1992. Evidence for retrograde lithospheric subduction on Venus, *Science*, 257, 766-770.
- Smrekar S.E., A. Davaille, S. Tomlinson, 2016. Plume-induced subduction on Venus, *Nat. Geosc.*, subm.

**Keywords:** Mantle Convection, Plume, Subduction, Plate Tectonics, Archean, Continental Growth, colloids.

## **Extension of a mechanically heterogeneous lithosphere: the role of structural softening**

Duretz Thibault<sup>1</sup>, Petri Benoit<sup>2</sup>, Mohn Geoffroy<sup>3</sup>, Schenker Filippo L.<sup>4</sup>, Schmalholz Stefan M.<sup>1</sup> and Müntener Othmar<sup>1</sup>

<sup>1</sup>) Institute of Earth Sciences, University of Lausanne, Géopolis, CH-1015 Lausanne

<sup>2</sup>) Ecole et Observatoire des Sciences de la Terre, Institut de Physique du Globe de Strasbourg – CNRS UMR7516, Université de Strasbourg, 1 rue Blessig, F–67084, Strasbourg Cedex, France

<sup>3</sup>) Département Géosciences et Environnement, Université de Cergy-Pontoise, 5, mail Gay Lussac, Neuville-sur-Oise, 95031 Cergy-Pontoise Cedex

<sup>4</sup>) SUPSI, University of Applied Sciences and Arts of Southern Switzerland, Via Trevano, CH-6952 Canobbio

Corresponding author: [thibault.duretz@unil.ch](mailto:thibault.duretz@unil.ch)

S1 – Geodynamics, Plate tectonics (PS7)

### **Introduction:**

Numerous geological and geophysical studies have drawn attention to the multi-stage and depth-dependent character of lithospheric thinning. Throughout rifting, a variety of structures are responsible for accommodating lithospheric thinning (normal faults, low angle detachments, extensional shear zones, extraction faults), resulting in the formation of complexly structured passive margins (e.g. necking zones, extremely thinned continental crust, mantle exhumation, continental allochthons). It is well documented that the lithosphere often encompasses mechanical heterogeneities inherited from previous tectonic events (e.g. orogeny). These inherited mechanical heterogeneities can cause structural softening. The impact on the dynamics of lithospheric thinning is so far incompletely understood.

### **Modelling strategy:**

We study the role of inherited mechanical heterogeneities on the development of passive margins using two-dimensional thermo-mechanical models of lithospheric thinning. The equation of energy and momentum balance for incompressible materials are solved with an implicit finite difference method. The advection is treated explicitly using the marker-and-cell method and fourth-order in space Runge-Kutta scheme. At first order, we decide to represent inherited heterogeneities by mechanical layering (km-scale). Both the crust and the upper mantle incorporate a number of mechanically strong layers. The rheologies are voluntarily kept relatively simple (temperature, stress, and strain rate-dependent visco-plastic) and do not include any material strain softening.

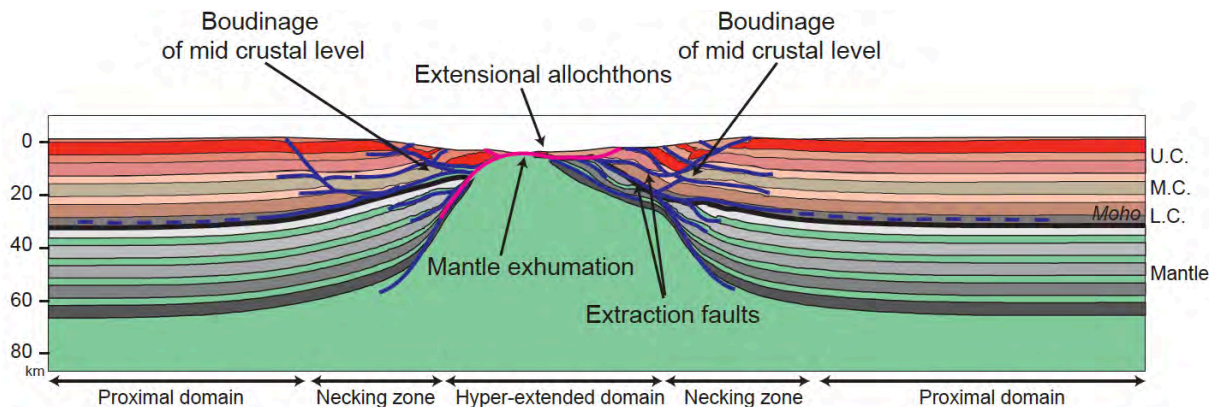


Figure 1: Geometry of the reference model after 40% extension. The different layers represent competent horizons (red to brown for crustal lithologies, white to dark grey for mantle lithologies). The black line indicates the location of the Moho and the blue and red lines symbolize the main structures that accommodate lithospheric thinning.

### Results:

The different simulations demonstrate that mechanical layering causes multi-stage and depth-dependent extension (Fig. 1). At first the deformation style is decoupled: while upper crustal and lithospheric layers undergo thinning by brittle (frictional-plastic) faults, lower crustal and lithospheric levels accommodate extension by symmetric ductile necking. In addition, competent mid-crustal levels are laterally extracted from the hyper-extended domain (Fig. 1). Secondly, as extensional structures cut across the Moho, crustal and lithospheric deformation becomes coupled leading to asymmetric extension. Subsequently, subcontinental mantle exhumation occurs along a low angle extensional shear zone that cross cuts the lithosphere. Noticeably crustal allochthons develop at the edges of the conjugate necking zone.

### Conclusions:

Our results further highlight the importance of mechanical heterogeneities and related structural softening for lithospheric thinning. Incorporating mechanical heterogeneities in lithospheric extension models allows for the formation of numerous observed geological features (necking zones, mantle exhumation, continental allochthons) despite the use of a simple rheological model. Structural softening can therefore alone explain the complex structuration of passive margins.

**Keywords:** Lithospheric extension, structural softening, mechanical heterogeneities.

## **4D analogue modeling of interaction between compressive and transcurrent structures: insights from SW Sicily and the Sicily Channel.**

Jakub Fedorik<sup>1</sup>, Frank Zwaan<sup>2</sup>, Guido Schreurs<sup>2</sup>, Giovanni Toscani<sup>1</sup>, Lorenzo Bonini<sup>3</sup>, Emanuele Lodolo<sup>4</sup>, Dario Civile<sup>4</sup>, Silvio Seno<sup>1</sup>

<sup>1</sup>) University of Pavia, Department of Earth and Environmental Sciences, Pavia, Italy

<sup>2</sup>) University of Bern, Institute of Geological Science, Bern, Switzerland

<sup>3</sup>) University of Trieste, Department of Mathematics and Geosciences, Trieste, Italy

<sup>4</sup>) National Institute of Oceanography and Experimental Geophysics, Trieste, Italy

Corresponding author: jakub.fedorik01@universitadipavia.it

S1 – Geodynamics, Plate tectonics (PS7)

Analogue models were used to investigate the 4D evolution of a transcurrent structure and its interaction with a preexisting thrust front. An analysis of 7 models applying: pure strike-slip, transtension (10/20/30 degrees) and transpression (10/20/30 degrees) kinematics, shows important structural variations in the area of transcurrent fault. The models closely resemble the geometries of natural interaction observed between the transcurrent transfer zone and the Maghrebian fold-and-thrust belt in the area of the Sicily Channel (fig. 1a).

The experimental apparatus consisted of a box with three independent rigid base plates. These plates were covered by a 4-cm-thick layer of quartz and the upper plate was sliding on the fixed plate (fig. 1b). During this first phase of deformation the thrust front was created. In the second phase the lower plate was sliding under the fixed plate. The shape of the fixed plate permitted to build a transcurrent fault and at the same time the thrust front from the first phase was reactivated and new thrust faults were formed. The analogue models were analyzed by X-Ray Computer Tomography (XRCT, fig. 1d). This technique permits visualization of the interior of a model during deformation without destroying it.

In the area of SW Sicily and northern part of the Sicily channel, two main structures, the Maghrebian fold-and-thrust belt and a transfer zone, interact. The most recent interaction was recorder during the Belice earthquake sequence in 1968 and the calculated focal mechanisms are compatible either with a pure E-W thrust plane or with a prevalently right-lateral movement on a NNW striking, WSW dipping plane. Analysis of multichannel seismic reflection profiles acquired in the northern part of the Sicily Channel were used to analyze the Sciacca fault which displays a mainly transpressional structural character. The outermost thrust sheet-Gela Nappe is interpreted by many authors as a complex, imbricate wedge, involving the sequences of a foredeep basin. The Gela Nappe is well exposed along the south coast of Sicily, where both Sciacca fault and Gela Nappe can be observed (fig. 1c).

The observations suggest that the SW of Sicily and the northern part of the Sicily channel was shaped by the occurrence of two independent tectonic processes, the Maghrebian fold-and-thrust belt and transcurrent fault which act simultaneously and overlap each other. The interpretation of seismic reflection profiles, merged in a 3-D model with the bathymetry, and its comparison with analogue models demonstrated a fair match between the model and natural case. Main equivalences are (1) the presence of well-developed flower structures along the transcurrent structure (fig. 1c-d), (2) rotation of the thrust front during deformation and (3) segmentation of transcurrent structure in the area of the thrust front.

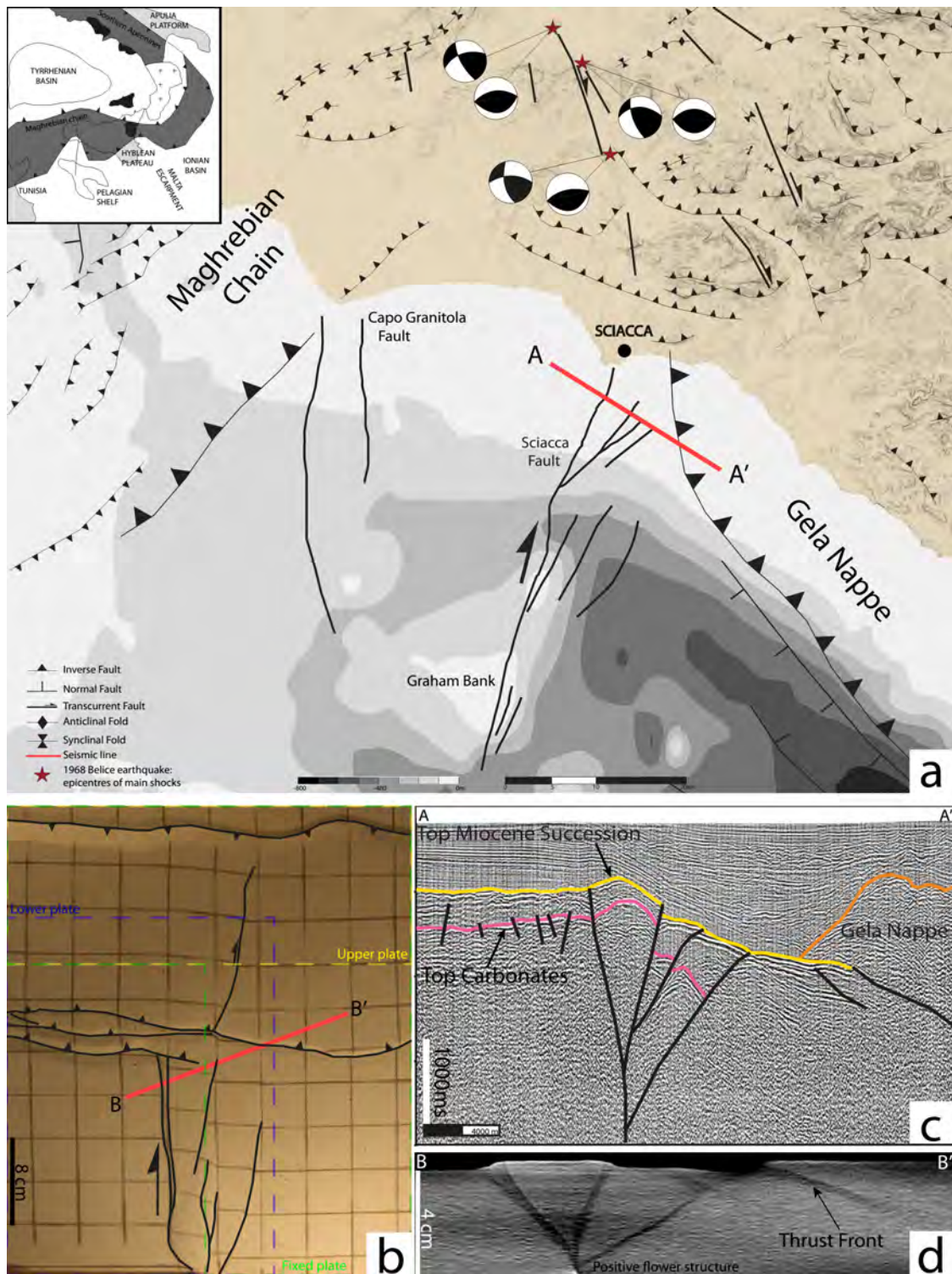


Figure 1: a) Structural map of the study area in the Sicily Channel and SW Sicily, b) top view image of analogue model. Capture shows deformation after 35mm of displacement during the 2<sup>nd</sup> phase, c) seismic line showing the complex of the transcurrent structure and the outermost thrust sheet-Gela Nappe, location red line A-A' in fig.1a, d) section view from XRCT location red line B-B' in fig.1b.

**Keywords:** Analogue modeling, transcurrent structure, thrust front, interaction, Sicily, XRCT scan.

## Three-dimensional instantaneous dynamics modeling of present-day Aegean subduction

Anne Glerum<sup>1</sup>, Wim Spakman<sup>1,2</sup>, Douwe van Hinsbergen<sup>1</sup>, Casper Pranger<sup>3</sup>, Cedric Thieulot<sup>1</sup>, Menno Fraters<sup>1</sup>

<sup>1</sup> Utrecht University, Department of Earth Sciences, Utrecht, The Netherlands

<sup>2</sup> University of Oslo, Centre of Earth Evolution and Dynamics (CEED), Oslo, Norway

<sup>3</sup> ETH Zurich, Institute of Geophysics, Zurich, Switzerland

Corresponding author: A.C.Glerum@uu.nl

S1 – Geodynamics, Plate tectonics (PS7)

### Abstract:

The Aegean region (eastern Mediterranean) has known continuous subduction for at least 100 My (van Hinsbergen et al., 2005), rendering it an ideal candidate for the study of the interaction between crustal tectonics, plate motion, subduction and mantle flow. To better understand this coupling of the tectonic evolution of the crust and the underlying mantle dynamics, we have developed 3D numerical models of the instantaneous dynamics of the present-day Aegean subduction system.

We use the finite element code ASPECT (Kronbichler et al., 2012) and have developed plugins to this code to create complex, realistic model set-ups (see figure). The initial and boundary conditions of the instantaneous models are derived from geological and geophysical data. For example, the geometry of the subducting slab is inferred from seismic tomography (Amaru, 2007) and earthquake hypocenters (NCEDC, 2014), and the plate boundary configuration is based on the tectonic map of Faccenna et al. (2014). Moreover, the models incorporate the major crustal weak zones of the overriding plate and crust and lithosphere thickness variations abstracted from Moho and LAB maps (Faccenna et al., 2014, Carafa et al., 2015).

The mantle initial temperature conditions can include variations to an adiabatic profile from conversion of seismic velocity anomalies (e.g. Steinberger and Calderwood, 2006). Mantle flow through the model boundaries is either left free through open boundary conditions (Chertova et al., 2012) or is prescribed. The bounding plate velocities are also varied based on literature propositions of relative and absolute plate motions, e.g. Le Pichon and Kreemer (2010), Doubrovine et al. (2012) and DeMets et al. (2010).

We first test the effect of different tomographic models (e.g. UU-P07 (Amaru, 2007) and TX2015 (Lu and Grand, 2016)) and methods for converting seismic velocity to temperature on model predictions of the regional flow field. Subsequent models combine representative initial conditions with constructed variations in subduction morphology, slab segmentation, fault zone geometry and boundary conditions, for which a wide range of hypotheses can be found in the literature (e.g. Biryol et al., 2011).

By comparing the resulting model predictions of velocity, stress and strain- and rotation rates to the widely available observations, such as focal mechanisms, GPS velocities and seismic anisotropy, we aim at determining the controls of mantle dynamics on present-day tectonic deformation in the Aegean region. This enables us to characterize the general sensitivity of surface observables to plate motions, mantle flow and slab dynamics and, thus, to further quantify the coupling of crust and mantle dynamics.

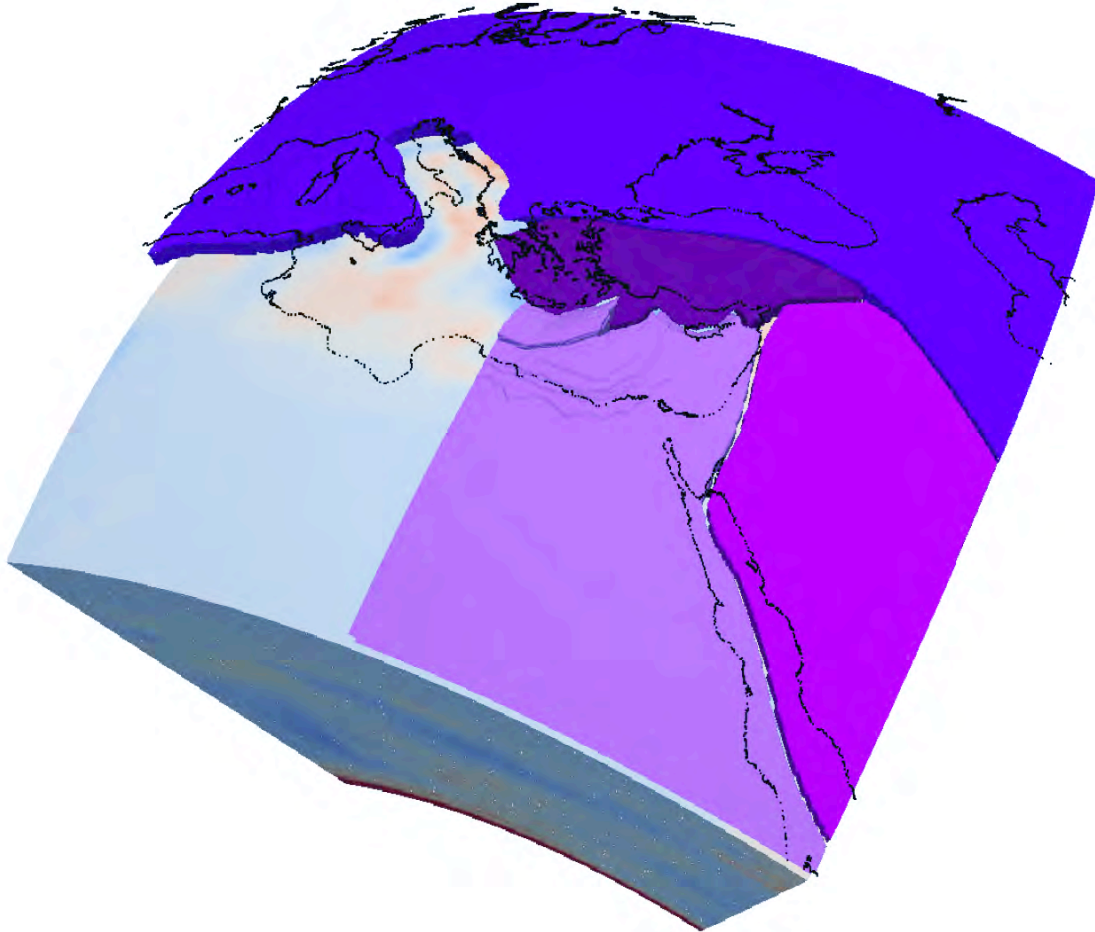


*Figure 1: Example model setup: In purple colors the four plates with variable thickness and type (oceanic versus continental). The Nubian plate is partly removed to show the initial temperature conditions from 200 km depth to the core-mantle boundary. The lateral temperature variations are based on the tomographic model UU-P07 (Amaru, 2007).*

#### **References:**

- Amaru, M. L., 2007. Global travel time tomography with 3-D reference models.
- Biryol, C. B., Beck, S. L., Zandt, G. and Özacar, A. A., 2011. Segmented African lithosphere beneath the Anatolian region inferred from teleseismic P-wave tomography, *Geophysical Journal International*, 184, 1037-1057.
- Carafa, M. M. C., Barba, S. and Bird, P., 2015. Neotectonics and long-term seismicity in Europe and the Mediterranean region, *Journal of Geophysical Research : Solid Earth*, 120.
- Chertova, M. V., Geenen, T., van den Berg, A. and Spakman, W., 2012. Using open sidewalls for modelling self-consistent lithosphere subduction dynamics, *Solid Earth*, 3, 313-326.
- DeMets, C., Gordon, R. G. and Argus, D. F., 2010. Geologically current plate motions, *Geophysical Journal International*, 181, 1-80.
- Dobrovine, P.V., Steinberger, B. and Torsvik, T. H., 2012. Absolute plate motions in a reference frame defined by moving hotspots in the Pacific, Atlantic and Indian oceans, *Journal of Geophysical Research*, 117, B09101.

- Faccenna, C., Becker, T. W., Auer, L., Billi, A., Boschi, L., Brun, J. P., Capitanio, F. A., Funiciello, F., Horvath, F., Jolivet, L., Piromallo, C., Royden, L., Rossetti, F., and Serpelloni, E., 2014. Mantle dynamics in the Mediterranean, *Reviews of Geophysics*, 52.
- Kronbichler, M., Heister, T. and Bangerth, W., 2012. High accuracy mantle convection simulation through modern numerical methods, *Geophysical Journal International*, 191, 12-29.
- Le Pichon, X. and Kreemer, C., 2010. The Miocene-to-present kinematic evolution of the Eastern Mediterranean and Middle East and its implications for dynamics, *Annual Review of Earth and Planetary Sciences*, 38, 323-351.
- Lu, C. and Grand, S. P., 2016. The effect of subducting slabs in global shear wave tomography. *Geophysical Journal International*, 205, 1074-1085.
- NCEDC, 2014. Northern California Earthquake Data Center, UC Berkeley Seismological Laboratory. Dataset.
- Steinberger, B. and Calderwood, A.R., 2006. Models of large-scale viscous flow in the Earth's mantle with constraints from mineral physics and surface observations, *Geophysical Journal International*, 167, 3, 1471-1481.
- Van Hinsbergen, D. J. J., Hafkenschied, E., Spakman, W., Meulenkamp, J. E. and Wortel, R., 2005. Nappe stacking resulting from subduction of oceanic and continental lithosphere below Greece, *Geology*, 33, 325-328.

**Keywords:** 3D, numerical modeling, subduction, instantaneous dynamics, Mediterranean, Aegean slab.

## Confronting geoid to the mantle structures in the Mediterranean.

Alexia Grabkowiak<sup>1</sup>, Olivier de Viron<sup>2</sup> and Laurent Métivier<sup>3</sup>

<sup>1</sup>) University of Paris Diderot-Paris VII, Lab. IPGP, Paris, France

<sup>2</sup>) University of La Rochelle, Lab. LIENSs, La Rochelle, France

<sup>3</sup>) IGN, LAREG, Saint-Mandé, France

Corresponding author: grabkowiak@ipgp.fr

S1 – Geodynamics, Plate tectonics (PS7)

Source separation is a key issue of gravimetric data interpretation because contributions from many sources such as crustal signal, mantle mass distribution (Richard & Hager, 1984, Hager, 1984),... are mixed together in the gravity signal. If one wants to use geoid data in order to infer information about one of the source, it requires to separate the contributions in order to isolate the relevant contribution. Ideally, this process should use as little a priori information as possible. That could be performed either by using some statistical analysis methods which separate the contributions based on a given definition of independence (Lorenz, 1956, Kutzbach, 1967), or, if some complementary dataset are available on the studied area, by using precise information about one of the contributors.

In the Mediterranean we use a tomographic model that provided an insight on how mantle structures are distributed within the 800 first kilometers of the mantle (Piromallo and Morelli, 2003). We isolate majors features of this model and confront it to the geoid's behavior in the area.

### References:

- Hager, Bradford H, 1984, Subducted slabs and the geoid - Constraints on mantle rheology and flow, *Journal of Geophysical Research*, Volume 89 - 4, Pages 6003 – 6015, doi: 10.1029/JB089iB07p06003.
- Richards, Mark A. and Hager, Bradford H., Geoid anomalies in a dynamic Earth, *Journal of Geophysical Research*, Volume 89 - 4, Pages 5987 – 6002, doi : 10.1029/JB089iB07p05987.
- Lorenz, E N, 1956, Empirical Orthogonal Functions and Statistical Weather Prediction, *Technical report Statistical Forecast Project Report 1 Department of Meteorology MIT 49*, Volume 1.
- Kutzbach, John E., 1967, Empirical Eigenvectors of Sea-Level Pressure, Surface Temperature and Precipitation Complexes over North America, *Journal of Applied Meteorology*, Volume 6 -5, Pages 791 – 802, doi: 10.1175/1520-0450(1967)006<0791:EEOSLP>2.0.CO;2.
- Piromallo, C., Morelli, A., 2003, P- wave tomography of the mantle under the Alpine-Mediterranean area, *Journal of Geophysical Research*, Volume 108, Pages 1 – 23, doi: 10.1029/2002JB001757.

**Keywords:** Gravity, mediterranean area, mantle structure, tomography.

## Impact of the overriding plate crustal rheology on convergence zones dynamics.

Solenn Hertgen<sup>1,2\*</sup>, Philippe Yamato<sup>1,2</sup> and Benjamin Guillaume<sup>1,2</sup>

<sup>1)</sup> Géosciences Rennes, Université de Rennes 1, Rennes Cedex 35042, France

<sup>2)</sup> CNRS, UMR 6118, Rennes Cedex 35042, France

Corresponding author: solenn.hertgen@univ-rennes1.fr

S1 – Geodynamics, Plate tectonics (PS7)

### Introduction:

Most of deformation at the Earth's surface is localized at plate boundaries. This deformation can be accommodated in very different ways depending on the tectonic setting.

In the case of the convergence zones, the deformation is classically classified as follows:

- i) intra-oceanic convergence (when convergence involves two oceanic lithospheres), which generally leads to the subduction/obduction initiation and to the formation of an island arc;
- ii) convergence between an oceanic and a continental lithosphere, which is generally accommodated by subduction and can also lead to the formation of a mountains range at the plate boundary and
- iii) convergence between two continental lithospheres leading to the formation of a collisional mountain range formed by the stacking of crustal slices.

Hence, different materials (*i.e.*, oceanic crust, continental crust, sediments) evolving in different contexts (*i.e.*, oceanic subduction, continental subduction, obduction) result in the formation of contrasted structures in terms of units size, morphology and metamorphism. In addition, some convergent zones from a similar tectonic context (*e.g.*, ocean/continent convergence) can produce mountains range presenting very different characteristics (*e.g.*, characterized by extension as in the Aegean or, at the opposite, by significant shortening, as in the Andes).

Although the mechanism of plate convergence appears to be the same, the structures obtained at the surface (*e.g.*, Alps, Andes, Aegean, Himalayas) seem rather unique. Rheology of both the lower subducting plate and of the plates interface is known to influence the convergence zones dynamics while very few studies have addressed the role of the overriding plate rheology in details (Heuret *et al.*, 2007; Guillaume *et al.*, 2009; Yamato *et al.*, 2009; Schellart *et al.*, 2011; Butterworth *et al.*, 2012; Iaffaldano *et al.*, 2012; Meyer and Schellart, 2013).

Nevertheless, this statement raises first order questions: What is the implication of the overriding plate rheology on the convergence zones dynamics? And more particularly, what is the influence of the crustal part on the deformation style at plate boundaries?

### Modelling approach and data constraints:

In this study, we use both numerical and analogue models. Numerical modelling is used in order to quantify the influence of vertical variations in the rheological property of the upper plate crust. Especially, the numerical tool allows to test, in 2D and at high resolution, the influence of both the initial geotherm and of non-linear rheologies. Analogue modelling are rather used to quantify the influence of lateral variations of the rheological properties and to address the problem in 3D.

These models have been constrained at best *via* a compilation of geophysical and field (*i.e.*, petrological and structural) data extracted from the literature concerning the Alps, the Andes, the Himalaya and the Aegean domain.

**References:**

- Heuret, A., Lallemand, S., 2005. Plate motions, slab dynamics and back-arc deformation, *Physics of the Earth and Planetary Interiors* 149, 31-51.
- Butterworth, N. P., Quevedo, L., Morra, G., & Müller, R. D. (2012). Influence of overriding plate geometry and rheology on subduction. *Geochemistry, Geophysics, Geosystems*, 13(6).
- Guillaume, B., Martinod, J., & Espurt, N. (2009). Variations of slab dip and overriding plate tectonics during subduction: Insights from analogue modelling. *Tectonophysics*, 463(1), 167-174.
- Heuret, A., Funiciello, F., Faccenna, C., & Lallemand, S. (2007). Plate kinematics, slab shape and back-arc stress: A comparison between laboratory models and current subduction zones. *Earth and Planetary Science Letters*, 256(3), 473-483.
- Iaffaldano, G., Di Giuseppe, E., Corbi, F., Funiciello, F., Faccenna, C., & Bunge, H. P. (2012). Varying mechanical coupling along the Andean margin: Implications for trench curvature, shortening and topography. *Tectonophysics*, 526, 16-23.
- Meyer, C., & Schellart, W. P. (2013). Three-dimensional dynamic models of subducting plate-overriding plate-upper mantle interaction. *Journal of Geophysical Research: Solid Earth*, 118(2), 775-790.
- Schellart, W. P., Stegman, D. R., Farrington, R. J., & Moresi, L. (2011). Influence of lateral slab edge distance on plate velocity, trench velocity, and subduction partitioning. *Journal of Geophysical Research: Solid Earth*, 116(B10).
- Yamato, P., Husson, L., Braun, J., Loiselet, C., & Thieulot, C. (2009). Influence of surrounding plates on 3D subduction dynamics. *Geophysical Research Letters*, 36(7).

**Keywords:** Convergence zones dynamics, overriding plate, rheology, subduction process, numerical modelling, analogue modelling.

## Role of structural inheritance in the localization of intraplate deformation: application to the Kyrgyz Tien Shan Cenozoic tectonics

Anthony Jourdon<sup>1</sup>, Laëtitia LePourhiet<sup>2</sup>, Carole Petit<sup>1</sup>, Yann Rolland<sup>1</sup>

<sup>1</sup>) University of Nice-Sophia-Antipolis, Géoazur, CNRS, Valbonne, France

<sup>2</sup>) University of Pierre et Marie Currie, IStEP, Paris, France

Corresponding author: jourdon@geoazur.unice.fr

S1 – Geodynamics, Plate tectonics (PS7)

Due to the India-Asia collision, the deformation of the Eurasian continent extends over several thousand kilometers, far away from the Himalayan belt (e.g. [Molnar and Tapponnier, 1975]). However, some areas like the Tarim craton are poorly deformed while others, as the Tien Shan belt or Tibet plateau, display large deformation rates (e.g. [Avouac et al., 1993]).

These actively deforming areas correspond to ancient plate boundaries which were previously involved in the construction of large orogenic belts. The Tien Shan is a relevant example to study the role of structural inheritance in the localization of recent deformation because of its Paleozoic tectonic history. It has been built during two consecutive orogenies (Caledonian and Variscan) which formed large scale structures (as suture zones) clearly identifiable on the field (e.g. [Hegner et al., 2010; Wang et al., 2010; Xiao et al., 2013; Loury et al., 2015]). These structures are now reworked as active deformation zones where large earthquakes can occur.

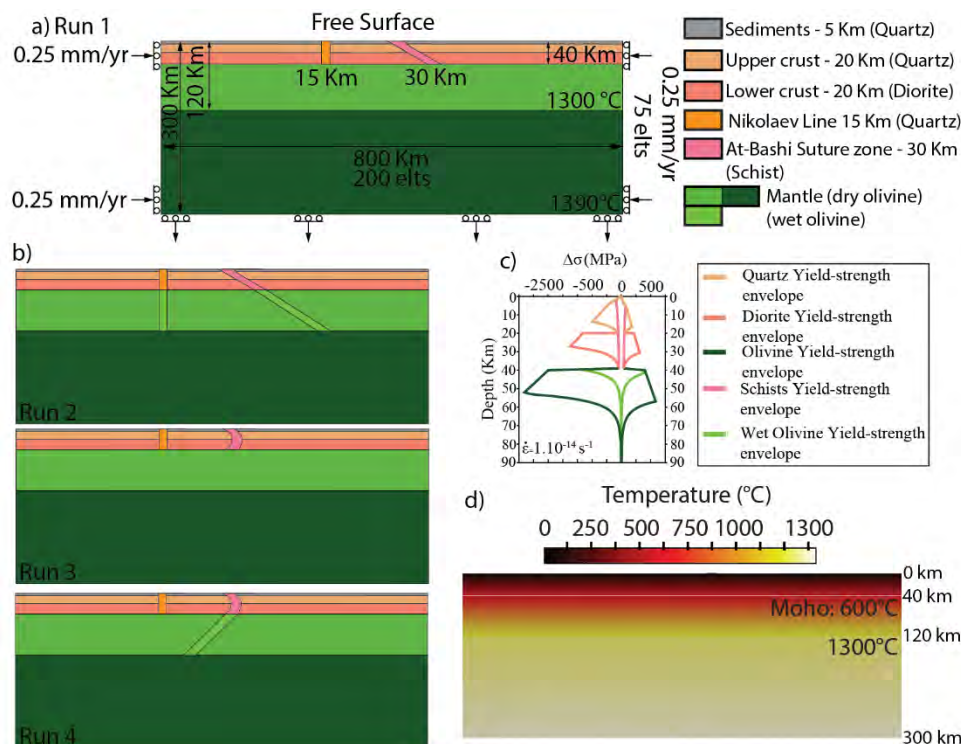


Figure 1: Initial model setup. a) Geometry of phases and boundary conditions for run1. b) Geometry of phases for runs2, 3 and 4 with same boundary conditions as for run1. c) Yield-strength envelopes. d) Initial temperature conditions.

In order to improve our understanding of the role of this structural inheritance on the Cenozoic deformation, we use the thermomechanical modeling code pTatin [May *et al.*, 2014] to simulate the lithospheric deformation of the belt depending on the geometry and rheology of inherited structures (Figure 1).

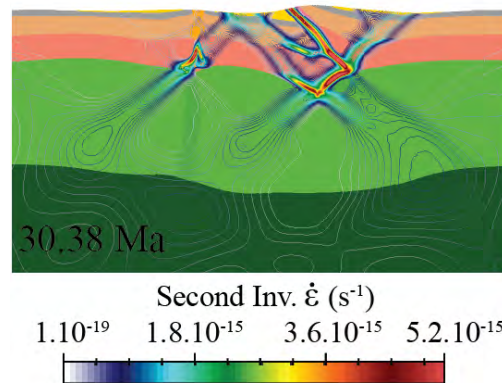


Figure 2: Final step of the run1. Colors indicate the different phases, contours represent the second invariant of the strain rate tensor.

Our results (Figure 2) show that inherited structures first localize the deformation before antithetic neofomed structures develop on the outer parts of the belt. This result is consistent with seismologic, seismic and GPS data, which show that the deformation is now localized on the borders of the belt, and especially at the South Tien Shan/ North Tarim boundary along a N-dipping top-to-the South fold and thrust belt. It suggests that all present-day structures must not be interpreted as reflecting the Paleozoic structuration of the belt.

## References:

- Avouac, J. P., P. Tapponier, M. Bai, H. You, and G. Wang (1993), Active thrusting and folding around the northern Tien Shan and late Cenozoic rotation of the Tarim relative to Dzungaria and Kazakhstan, *J. Geophys. Res.*, 98(4), 6755–6804.
- Hegner, E., R. Klemd, a. Kröner, M. Corsini, D. V. Alexeiev, L. M. Iaccheri, T. Zack, P. Dulski, X. Xia, and B. F. Windley (2010), Mineral ages and p-t conditions of late paleozoic high-pressure eclogite and provenance of mélange sediments from atbashi in the south tianshan orogen of kyrgyzstan, *Am. J. Sci.*, 310, 916–950, doi:10.2475/09.2010.07.
- Loury, C., Y. Rolland, S. Guillot, A. V Mikolaichuk, P. Lanari, O. Bruguier, and D. Bosch (2015), Crustal-scale structure of South Tien Shan : implications for subduction polarity and Cenozoic reactivation, *Geol. Soc. London, Spec. Publ.*, 427(SP427-4), doi:10.1144/SP427.4.
- May, D. A., J. Brown, and L. Le Pourhiet (2014), pTatin3D : High-Performance Methods for Long-Term Lithospheric Dynamics, in *Proceeding SC'14 Proceedings of the International Conference for High Performance Computing, Networking, Storage and Analysis*, pp. 274–284.
- Molnar, P., and P. Tapponier (1975), Cenozoic Tectonics of Asia: Effects of a Continental Collision: Features of recent continental tectonics in Asia can be interpreted as results of the India-Eurasia collision., *Science*, 189(August), 419–426, doi:10.1126/science.189.4201.419.
- Wang, B. et al. (2010), Structural and Geochronological Study of High - Pressure Metamorphic Rocks in the Kekesu Section ( Northwestern China ) : Implications for the Late Paleozoic Tectonics of the Southern Tianshan Structural and Geochronological Study of High-Pressure Metamorp, *J. Geol.*, 118(1), 59–77, doi:10.1086/648531.

Xiao, W., B. F. Windley, M. B. Allen, and C. Han (2013), Paleozoic multiple accretionary and collisional tectonics of the Chinese Tianshan orogenic collage, *Gondwana Res.*, 23(4), 1316–1341, doi:10.1016/j.gr.2012.01.012.

**Keywords:** Modeling, Structural inheritance, Tien Shan, Intraplate.

## Sea level changes in Lycia region and their effect to ancient port cities

Su Güneş Kabaklı , M. Erkan Karaman and Halil Bölük

Akdeniz University, Department of Geological Engineering, Antalya, Turkey

Corresponding author: suguneskabakli@gmail.com

S1 – Geodynamics, Plate tectonics (PS7)

Geological-tectonic- geoarchaeological researches in sea level changes on Mediterranean coasts and these changes' physical effects on coastal areas have been made from past to present. Although at the ancient age many settlements as Phaselis, Olympos, Myra, Kekova, Patara etc. and their harbour structures are established near the sea coast, today they are mostly under water (sunken city). It is obvious that the physical changes that big till ancient ages to now, were much more bigger size at expanded geological times zone. There are many parameters about the sea level changes and their physical effects on coastal areas. But their most important respond is the active tectonic movements and destroying earthquakes.

In this study, many geological-geomorphological features has been used, archaeological researches have been made in ancient harbour cities as Andriake, Patara, Phaselis, Kekova which sited in West Mediterranean Region.

In this study, the datas that achieved from the excavations before have been used. Also in this study drawn benefit from some ancient author's as Strabon's writings about region geography, the reasons and outcomes of the sea level changes on West Mediterranean Region are tried to enlightened by geological and archaeometric datas obtained today.

On the other hand, present and ancient ages' sea levels are compared to each other, in the light of the foregoing determined that the sea level changes made important destruction on the ancient cities. Ancient ports' geomorphological structure and coastal formation during the ancient process are tried to enlightened on the account of earthquakes, volcanic activities on the near islands, plate movements and climate events.

With this report, in light of geology-archaeology-geoarchaeology datas, sea level changes have been occur of tectonic reasons and results are mentioned in West Mediterranean ancient ports. Natural disasters, plate movements and river flows' effects on ancient cities are analyzed. Datas from ancient cities are compared. For example as in present some parts of Kekova are under water Patara Harbour is filled with alluvium. With this report West Mediterranean shorelines preassessments will be made by benefiting from the geological and archaeological datas of the site.

### References:

Duggan, T.M.P. 2004. A Short Account of Recorded Calamities ( earthquakes and plaques) in Antalya province and Adjacent and Related Areas Over The Past 2300 Years an Incomplete List Comments and Observations, ADALYA VII, 123-170.

### 3-D Computational Modelling of Oblique Continental Collision near South Island, New Zealand

Lev Karatun<sup>1</sup>, Russell Pysklywec<sup>1</sup>

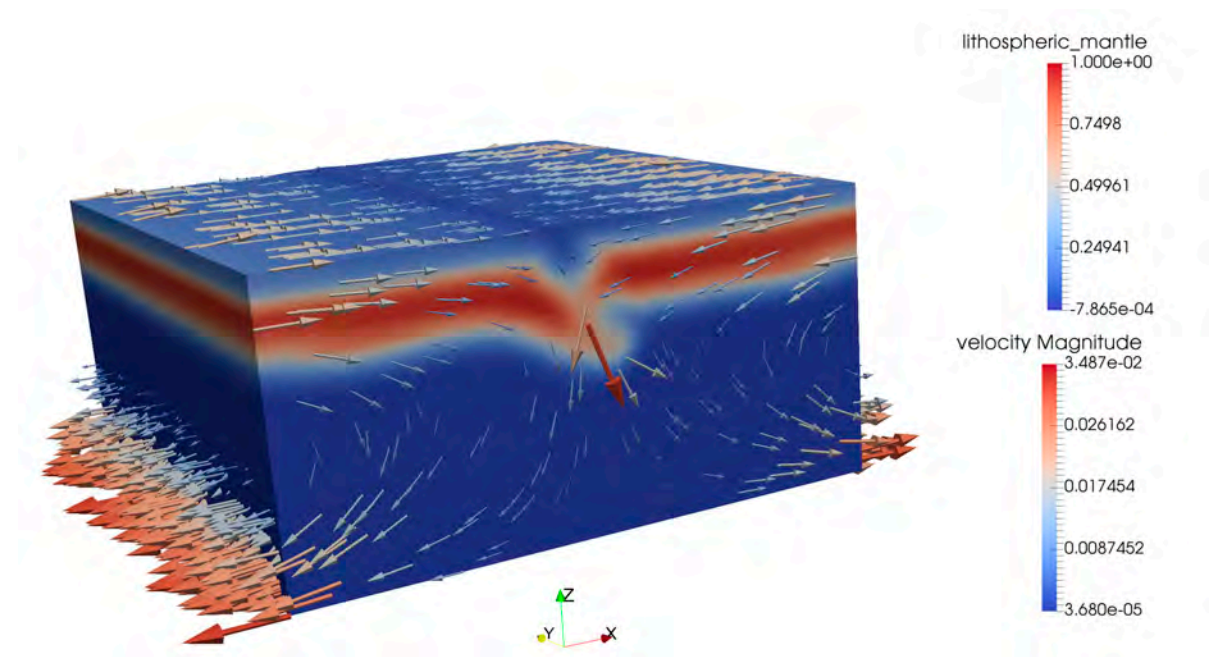
<sup>1</sup>) University of Toronto, Department of Earth Sciences, Toronto, Canada

Corresponding author: lev.karatun@gmail.com

S1 – Geodynamics, Plate tectonics (PS7)

The research explores the highly oblique continental convergence at the South Island of New Zealand, considering the fundamental geodynamic mechanisms of sub-crustal lithospheric deformation during the orogenesis. In addition to the high velocity of along-strike plate motion, the oppositely verging subduction zones bounding the collision make the problem inherently three-dimensional. To study such factors during orogenesis, we conduct 3D computational modelling and present the results of a series of new experiments configured for the oblique South Island collision.

The geodynamic modelling uses ASPECT – a robust highly-scalable and extendable geodynamic code featuring adaptive mesh refinement and complex rheologies. The model domain is defined by a box with prescribed velocities on the left and right faces with varied ratio of convergent versus strike-slip components, periodic boundary conditions for the front and back faces, free surface on top, and free slip at the bottom. Visco-plastic rheology (P-, T- and strain rate-dependent) is being used for the entire domain, with varied material parameters determining the prevailing behaviour of crustal, lithospheric and sublithospheric rocks. The obtained results provide insight into the behaviour of the lithosphere under the situation of young oblique convergence.



*Collision model at 5 Myr. Colour field shows the lithospheric mantle material plot (dimensionless), vectors show the velocity field (in m/year)*

We focus on the development of the mantle lithosphere, considering how the morphology of the sub-crustal orogenic root evolves during the convergent/strike-slip plate motions. The numerical experiments explore the dependence of this process on rheological parameters of crust and mantle and ratio of convergent versus strike-slip motion at the plate boundary. The resulting topography is also tracked to determine how the deep 3D tectonics may manifest at the surface.

**Keywords:** continental collision, lithosphere, plate tectonics, oblique convergence, ASPECT.

## **Tectonic scenarios of the Halls Creek Orogen, Western Australia – insight from geodynamic numerical modeling**

Fariba Kohanpour<sup>1</sup>, Weronika Gorczyk<sup>1</sup>, Mark Lindsay<sup>1</sup>, Sandra Occhipinti<sup>1</sup>

<sup>1</sup>) Center for Exploration Targeting, School of Earth and Environment, the University of Western Australia.

Corresponding author: Fariba.kohanpour@research.uwa.edu.au

S1 – Geodynamics, Plate tectonics (PS7)

### **Introduction:**

Deciphering the development of ancient geologic terranes is difficult and multiple scenarios are often proposed to explain their formation through time. Numerical modelling can play an important role in developing and testing geodynamic hypotheses and help us explain the evolution of terranes. The Halls Creek Orogen (HCO) is a well-preserved and well-exposed Paleoproterozoic orogenic belts which can provide insight into the assembly of the Kimberley Craton to the edge Diamantina Craton during the Nuna amalgamation. Therefore, here Hall Creek Orogen is used as a case study to reveal the tectonic evolution of a Precambrian orogeny using numerical modelling.

### **Geology and tectonic evolution of the study area:**

The Halls Creek Orogen (HCO) forms part of the 1910-1805 Ma Lamboo province and is developed between Kimberley and North Australian cratons in the north of Australia. It consists of three parallel, north-northeast trending zones (western, central and eastern) that are each interpreted as distinct tectonostratigraphic terranes. These zones contain geological units formed during the early Paleoproterozoic that may have originated in different settings and times, and were likely juxtaposed during the 1870-1850 Ma Hooper and 1835-1805 Ma Halls Creek orogenies.

There is some controversy as to how the Halls Creek Orogen developed. The 1865 Ma Tickalara Metamorphics seem to be a key unit within the Halls Creek Orogen for solving this. The formation of the protolith sedimentary and igneous rocks of central zone have been described as either forming in (1) an oceanic island arc setting above an easterly dipping subduction zone outboard of Kimberley Craton, or in (2) an ensialic marginal basin located closer to the margin of Kimberley Craton (Sheppard et al., 1999).

If the Tickalara Metamorphics represent an oceanic island arc, an east dipping subduction may have formed towards an over-riding North Australian Craton. Retreat of the subduction zone and then reversal of subduction polarity may have followed until the 1835-1805 Ma Halls Creek Orogeny, which resulted in the collision of the eastern and central zones. In contrast, the ensialic marginal basin may have been initiated due to the westward subduction zone stepping back following collision of a continent fragment sometimes before 1900 Ma.

### **Results of Numerical Experiments:**

The two plausible tectonic scenarios of the Halls Creek Orogen are examined through 33 2D thermo-mechanical-petrological numerical experiments based on I2VIS code (Gerya and Yuen, 2003). The initial constraints for model setup are appropriate to the inferred tectonic environment for the protoliths to the Tickalara Metaomorphics in an intra-ocean subduction or ocean-continent subduction/collision.

These numerical models allowed us to examine the conceptual models of geodynamic setting scenarios of the Halls Creek Orogen through time. With this approach we were able to determine experiments with specific physical parameters that are compatible with the geology observed in the Halls Creek Orogen. Finding the model most compatible with the geology can reveal processes which led to the generation of key lithological units and major structures during the tectonic evolution of the Halls Creek Orogen (Fig. 1).

The results indicate that the most plausible processes that represents the inferred tectonic evolution of the Halls Creek Orogen and geology is represented by the ensialic marginal basin scenario (ocean-continent subduction/collision setting). Finally, the results presented here have implications for assembly of the Australian continent and the early formation of the Nuna supercontinent.

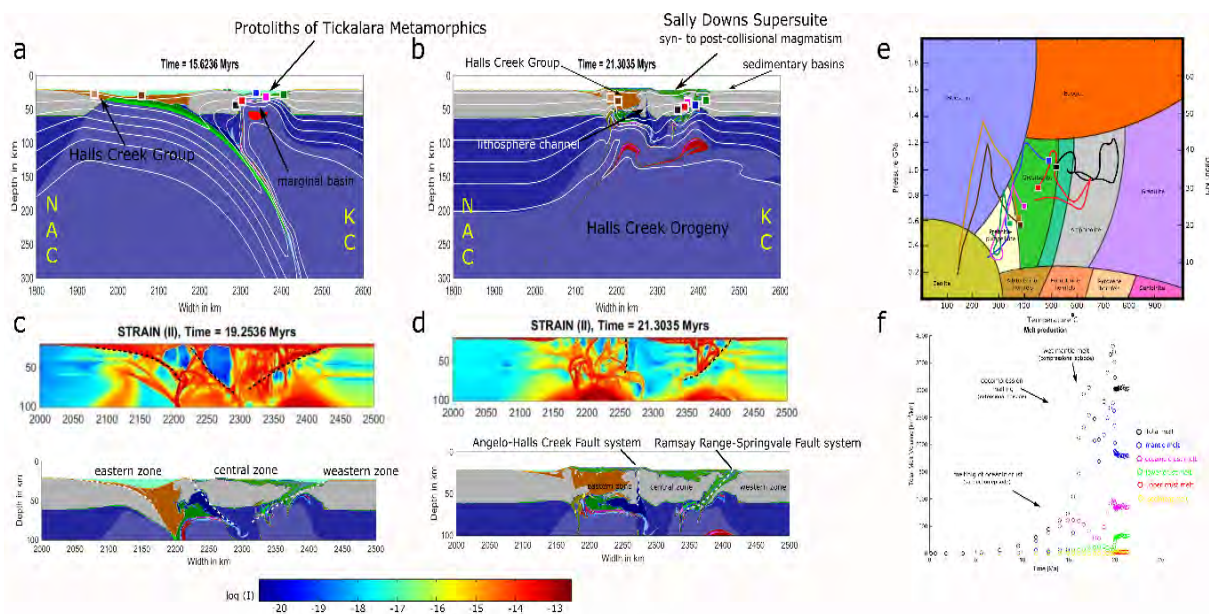


Figure 1. (a-b) Major lithological units during the evolution of numerical experiments (colored squares represent rock markers with propagation of P-T paths traced in window e; (c-d) second invariant strain models represent major structures; (e) P-T evolution from numerical model at several locations using markers; (f) Magmatic evolution of the numerical model.

## References:

- Gerya, T. V., Yuen, D.A. 2003. Characteristic-based marker-in-cell method with conservative finite-difference schemes for modelling geological flows with strongly variable transport properties. *Physics of the Earth and Planetary Interiors*, v.140, p.293-318.
- Sheppard, S., Tyler, I.M., Griffin, T.J. and Taylor, W.R. 1999. Palaeoproterozoic subduction-related and passive margin basalts in the Halls Creek Orogen, northwest Australia. *Australian Journal of Earth Sciences*, v. 46, p. 679-690.

**Keywords:** Halls Creek Orogen, Geodynamic numerical modelling, Paleoproterozoic orogeny, Nuna, Kimberley.

## Dynamics of lithospheric scale accommodation zones in oblique rift system

Laetitia Le Pourhiet<sup>1</sup>, Lucas Huiles<sup>1</sup>, Dave May<sup>2</sup>, Sylvie Leroy<sup>1</sup>

<sup>1</sup>) Sorbonne Universités, UPMC Univ Paris 06, CNRS, Institut des Sciences de la Terre de Paris (iSTeP), 4 place Jussieu 75005 Paris, France

<sup>2</sup>) Department of Earth Sciences, ETH Zürich, Zürich, Switzerland.

Corresponding author: laetitia.le\_pourhiet@upmc.fr

S1 – Geodynamics, Plate tectonics (PS7)

### Introduction:

The conceptual model of transform margin is an adaptation of the model of transform plate boundary and was first proposed by Francheteau and Le Pichon (1972) based on plate kinematic reconstruction. It was then adopted by marine geologists to conceptualize the dynamic of extremely oblique passive margins (e.g. Basile et al., 1993). In this "kinematic model", the direction of transport is everywhere parallel to the relative plate motion with a sharp change of sign at the divergent boundary and across the transform boundary. With this velocity field there is no internal deformation except thinning at divergent margin and no oblique structures are expected. Using this simple model to reconstruct plates is known to fail along large off-set oblique margins where attempts to match conjugate margins typically lead to isolated pockets of oceanic crust along rifted segments (e.g., Unternehr et al. 1988) or overlapping (Moulin et al., 2010). This lack of match is typically explained by pre-break up deformation or a delayed break-up along oblique segment. In both case, it is clear that the deviation from rigid kinematic block model should find an explanation in the dynamic of break up in oblique rifting context. Here, we revisit the classical kinematic model of the formation of transform margins using both new concepts in tectonic inheritance and newly available massively parallel computational techniques (May et al., 2015).

### Model Set up:

The set-up of the models is the classic off-set weak notch, but we can now run the models with 4km cube resolution at sufficient scale (600 km by 1200 km by 200 km) to avoid border effects and for sufficient time (30 Myr) to simulate all the tectonic phase from rifting to break-up. In order to study the impact of tectonic inheritance on the dynamic of the oblique margins, two different type of crust have been tested. One regular crust which is homogeneous in composition and one post-orogenic crust, in which the lower crust is made of less mafic material, in order to simulate the presence of upper crustal material underplated during a previous orogenic event. This post orogenic crust was previously showed to amplified strain localization on strike slip segment in 3D and to favor the occurrence of asymmetric detachment structure in extension. *Figure 1: Modeling set up*

### Results:

In 3D, the decoupling between the upper crust and the upper mantle leads to an obliquity between the different level of necking and results without any change in the other all kinematics in the boundary in three main faulting direction with time which reflects jumps of the strength of the lithosphere from one necking level to the other. The time scale and the apparition of different orientation of faults are controlled mainly by the stratification of the lithosphere. The models display a systematic asymmetry of spreading at the onset of the oblique margin that impacts the heat flow.

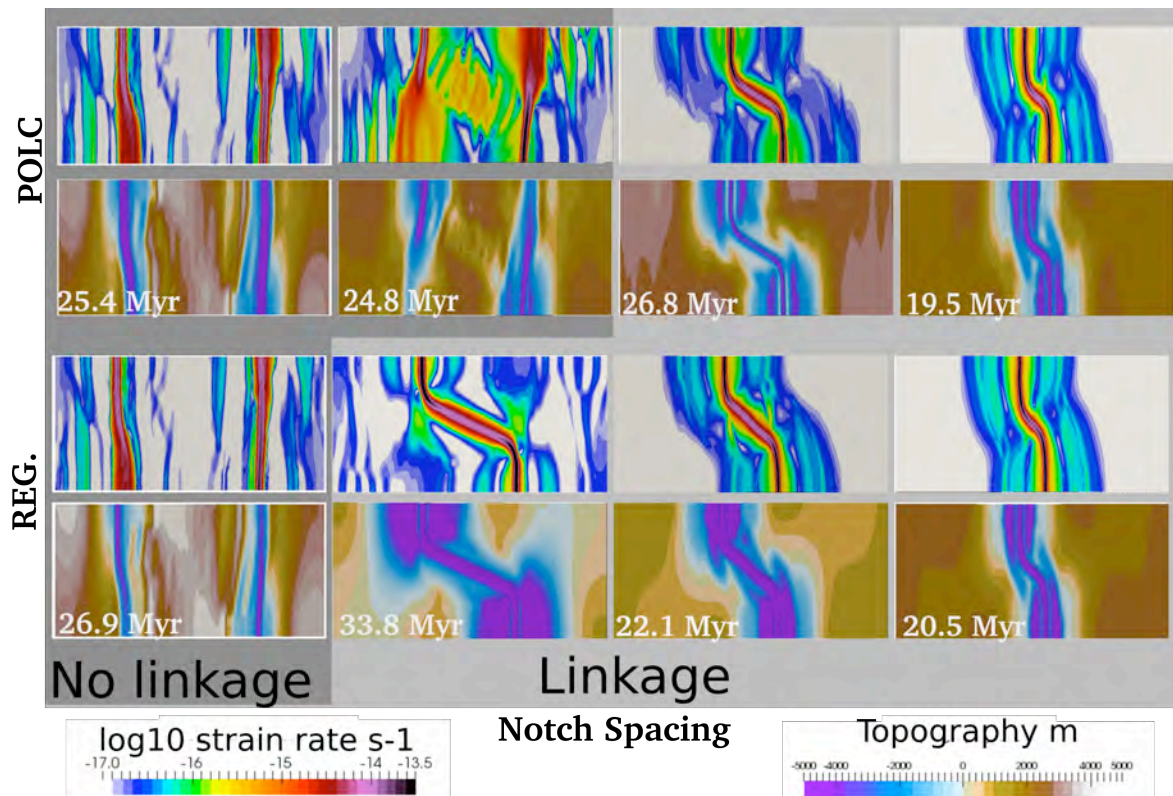


Figure 2: Results of the parametric study showing the strain rate and the topography of the models according to the nature of the lower crust and the spacing between the weak zones. The larger strength of the lithosphere favours linkage.

We detail our finding with interpretative cross-sections of models which are compared to natural dataset from the Gulf of Aden and other published section from the Central Atlantic. We discuss in detail the relationship between fault orientation and length of the margin as well as the timing, location and intensity of heat pulse affecting the margin just after the continental break-up.

#### References:

- Basile, C., Mascle, J., Popoff, M., Bouillin, J.P. and Mascle, G., 1993. The Ivory Coast-Ghana transform margin: a marginal ridge structure deduced from seismic data. *Tectonophysics*, 222(1), pp.1-19.
- Francheteau, J. and Le Pichon, X., 1972. Marginal fracture zones as structural framework of continental margins in South Atlantic Ocean. *AAPG Bulletin*, 56(6), pp.991-1007.
- May, D.A., Brown, J. and Le Pourhiet, L., 2015. A scalable, matrix-free multigrid preconditioner for finite element discretizations of heterogeneous Stokes flow. *Computer Methods in Applied Mechanics and Engineering*, 290, pp.496-523.
- Moulin, M., Aslanian, D. and Unternehr, P., 2010. A new starting point for the South and Equatorial Atlantic Ocean. *Earth-Science Reviews*, 98(1), pp.1-37.
- Unternehr, P., Curie, D., Olivet, J.L., Goslin, J. and Beuzart, P., 1988. South Atlantic fits and intraplate boundaries in Africa and South America. *Tectonophysics*, 155(1-4), pp.169-179.

**Keywords:** 3D numerical models, oblique passive margins, massively parallel simulation.

## Extrusion tectonics at plate corner in northern Taiwan: an example from field observations and sandbox models

Chia-Yu Lu <sup>1</sup>, Jian-Cheng Lee <sup>2</sup>, Zhi-nuo Li <sup>1</sup>, Chia-Hung Yeh <sup>1</sup> and Ching-An Lee <sup>1</sup>

<sup>1</sup>Geosciences Department, National Taiwan University, <sup>2</sup>Institute of Earth Sciences, Academia Sinica

Corresponding author:

S1 – Geodynamics, Plate tectonics (PS7)

In northern Taiwan, contraction, extension, transcurrent shearing, and block rotation are four major tectonic deformation mechanisms involved in the progressive deformation of this arcuate collision mountain belt. The neotectonic evolution of the Taiwan mountain belt is controlled not only by the oblique convergence between the Eurasian plate and the Philippine Sea plate but also the corner shape of the plate boundary.

Based on field observations and analyses, and taking geophysical data (mostly GPS) and results of experimental modelling into account, we interpret the curved belt of northern Taiwan as a result of contractional deformation (with compression, thrust sheet stacking & folding, back thrust duplex & back folding) that induced horizontal and vertical extrusion, combined with increasing transcurrent & rotational deformation (with transcurrent faulting, bookshelf-type strike-slip faulting and block rotation) that induced transcurrent/ rotational extrusion and extension deformation which in turn induced extensional extrusion.

As a consequence, a special type of extrusional folds was formed in association with contractional, transcurrent & rotational and extensional extrusions subsequently. The extrusion tectonics in northern Taiwan reflects a single, albeit complicated, regional pattern of deformation. The crescent-shaped mountain belt of Northeastern Taiwan develops in response to oblique indentation by an asymmetric wedge indenter, retreat of Ryukyu trench and opening of the Okinawa trough. We performed three types of analog sandbox modeling to analyze the kinematics of these structures (e.g. Fig below).



*Fig.: Sandbox model designed to simulate deformation induced by a double detachment. Silicone layers simulate weak and strong detachment such as overpressured shales and evaporites. Compression rate 1cm / hr; natural scale ratio 1cm = 1km, total advance 47.1cm, 2mm initial layers of silicone in the bottom and middle (viscosity,  $1 \times 10^4$  and  $2 \times 10^4$  Pa s respectively), sandwich among the middle and top 1cm each with colored dry quartz sand.*

## Mountain building in Taiwan, insights from analog models

Jacques Malavieille<sup>1,2</sup>, Stéphane Dominguez<sup>1,2</sup>, Serge Lallemand<sup>1,2</sup>, Chia-Yu Lu<sup>2,3</sup>, Kuo-Jen Chang<sup>2,4</sup> and Chih-Tung Chen<sup>2,3</sup>

<sup>1</sup> Géosciences Montpellier, CNRS, UMR 5243 Université Montpellier, 34095 Montpellier, France

<sup>2</sup> LIA D3E, C.N.R.S.-M.O.S.T. France-Taiwan International Laboratory

<sup>3</sup> Dept. of Geology, National Taiwan University, Taipei, Taiwan

<sup>4</sup> Dept. Civil Engineering, National Taipei University of Technology, Taipei, Taiwan.

Corresponding author: malavieille@gm.univ-montp2.fr

S1 – Geodynamics, Plate tectonics (PS7)

In Taiwan, obliquity of plate convergence involves the progressive subduction of the thinned continental margin of China under the Philippine Sea Plate (PSP). Geological observations and insights from analog models allow us to propose a tectonic evolutionary model for this typical accretionary orogen. From south to north, transition from oceanic to continental subduction induces the growth of the Taiwan belt. (1) To the South, where the Ocean Continent Transition (OCT) domain is involved in the subduction, basal accretion of basement slices (from oceanic and continental origin) induces wedge thickening and subsequent eastward backthrusting and shortening of the forearc domain against the Luzon arc. (2) In central Taiwan, where subduction of the extended Chinese continental lithosphere is mature, the continental orogenic wedge grows whereas accretion of deformed parts of the volcanic arc edifice occurs along the retro-wedge.

During more than 20 years, analog models have been realized in Géosciences Montpellier in collaboration with the department of Earth Sciences of the National Taiwan University in Taipei, to better understand the dynamics of the Taiwan orogenic wedge. Numerous advances have been achieved thanks to combined geological studies - analog modeling approaches. They help us to propose general models which outline the impact of first order processes such as continental subduction, arc accretion, mélanges formation, coupling between tectonics and surface processes.

A new scenario is proposed for mountain building in Taiwan.

Geological observations show that the forearc domain is very narrow along eastern Taiwan and that the arc is probably absent to the north of 24°N, suggesting that the frontal part of the arc lithosphere has been subducted. In the core of the growing wedge, metamorphic rocks of the Central Range were progressively exhumed in a few My rising through the overlying rocks of the former oceanic wedge. Strain partitioning caused by the combined effects of basal accretion at depth and surface erosion favored exhumation in the hinterland. During uplift, eroding rocks of the oceanic wedge (including ophiolite blocks of former mélanges) are removed and became the source for the olistostromal blocks included in the Lichi mélange which outline now the place of forearc subduction. Simultaneously, sediments are deposited in collisional basins and continuously deformed during shortening of the forearc domain. Then subduction controlled asymmetrical mechanisms of wedge growth by forward thrusting that had been operating in the Taiwan region up to this time is replaced by a more symmetrical evolution with significant backthrusting and backfolding in the retro-wedge.

At this stage, the tip of the PSP arc basement enters in the collision process, deeply indenting the Central Range, which is cut by an east-dipping, out-of-sequence crustal fault. Today, a major west-dipping shear zone develops in response to indentation by the arc lithosphere cutting through the continental lithosphere of the China margin and resulting in a subduction reversal.

## Strength and Deformation Rate of Plate Boundaries

Laurent G. J. Montési<sup>1</sup> and Frédéric Gueydan<sup>2</sup>

<sup>1</sup>) University of Maryland, Department of Geology, College Park, Maryland, USA

<sup>2</sup>) Géosciences Montpellier, UMR 5243, University of Montpellier, France

Corresponding author: montesi@umd.edu

S1 – Geodynamics, Plate tectonics (PS7)

### Introduction:

Geodetic and moment release data have been used to compile global maps of lithospheric strain rate (Kreemer et al., 2014). Plate tectonics is clearly evident on these maps, which highlight the contrast between plate boundaries and plate interiors. While plate interior display strain rates less than  $10^{-18} \text{ s}^{-1}$ , diffuse plate boundaries deform at rates up to almost  $10^{-15} \text{ s}^{-1}$ , continental deformation zones somewhat faster, and narrow plate boundaries at  $10^{-12} \text{ s}^{-1}$  or faster (e.g. Gordon, 2000). We develop rheological models that can explain the strain rate contrasts of a factor of 1000 between stable plate interiors, diffuse plate boundaries, and narrow plate boundaries based on the concepts of shear zone localization and the evolution of rock structure upon strain. We find that grain size evolution alone can explain the deformation rate of oceanic diffuse plate boundaries and, combined with layer development, the rate of continental deformation zones. However, an additional localization process, possibly serpentinization or stress enhancement due to variations in lithospheric thickness, is needed to explain narrow plate boundaries.

### Mechanical analysis of localization in ductile shear zones:

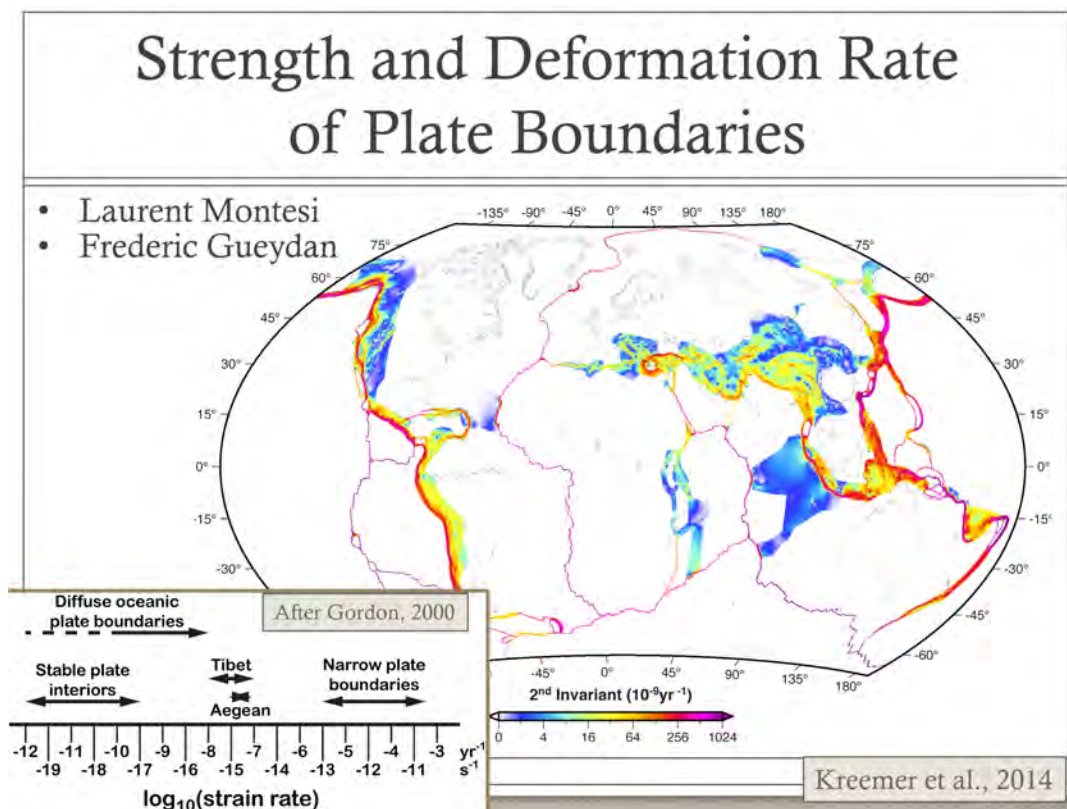
Ductile shear zones constitute a mechanical paradox in the lithosphere. The very definition of a ductile rock implies that deformation remains distributed. As the plastic deformation mechanism active in ductile shear zones are all characterized by strain rate hardening, it is energetically favorable for the rock to deform at low strain rate and low stress, which, for a given velocity, implies a broad zone of deformation. Localized ductile shear zones requires either a localized forcing (locally high stress) or a temperature or structural anomaly in the shear zone (Montési and Zuber, 2002). Either origin of localization can be inherited or develop progressively, as rock structure and temperature can change as deformation proceeds, and a shear zone nucleus can produce a stress, helping it propagate in a manner akin to a crack.

To quantify the efficiency of various localization processes, Montési (2013) proposed the definition of a localization criterion. Starting from a reference condition, where a thickness  $H$  of material in a reference state is shearing at a velocity  $V$  and stress  $\sigma$ , we determine the thickness  $h$  of a perturbed material that would also shear at velocity  $V$  and stress  $\sigma$ , therefore dissipating the same energy as the reference material. The nature of the perturbation is extremely flexible and can include a grain size change, a temperature increase, the development of layers, or metamorphism. The localization potential  $L=H/h$  indicates how narrow a shear zone might become if the prescribed change were to take place. Although the full localization potential is unlikely to be realized, it is possible to identify the most efficient localization process at each level of the continental lithosphere. (Gueydan et al., 2014). In the upper crust and middle crust, rocks fabric, including damage and alignment of phyllosilicates controls localization. Grain size reduction is the most efficient mechanism in the uppermost mantle, while the lower crust features no significant localization process, absent melting.

### Localization at the scale of the lithosphere:

In the analysis of Montési (2013) and Gueydan et al. (2014), the shear zone develops under specific pressure, temperature and stress conditions, isolated from the rest of the lithosphere. However, the analysis can be generalized to consider a complete lithospheric section. We assume that the lithospheric deformation zone is characterized by a strain rate that is invariant with depth. The strength of the lithosphere is represented by the vertically integrated stress, where the integration is conducted to a depth sufficient for the lower viscosity to be considered “asthenospheric”. We generate curves of integrated stress vs. strain rate for both reference and modified conditions and calculate the increase in strain rate associated with the perturbation at a given constant integrated strength. This assumption is motivated by the understanding that the stress level is controlled by the global convective system and plate driving forces, and they does not change upon localization.

We may start with a model of the oceanic lithosphere with a grain size coarse enough for the lithosphere to deform in grain-size insensitive dislocation creep. We then let the grain size decrease to a value in agreement with the stress level (piezometer) while letting that stress vary from depth to depth all the while subjected to the constraints that the strain rate is constant with depth and the integrated stress remains the same. The resulting structure lets lithosphere deforms at a rate about a thousand times faster than originally. This difference can explain the speed of diffuse plate boundaries. If a continental crust is added to the model, grain size reduction is slightly less effective. However, the possibility of fabric development in the mid-crust compensate for that loss, explaining the development of continental plate boundaries.



Narrow plate boundaries deform faster than can be explained by fabric and grain size reduction alone. An additional weakening process must be identified. For example, the high heat flux near mid-ocean ridge implies a thin lithosphere, which enhances stress. Stress focusing related to plate thickness variations can increase strain rate by another three orders of magnitude, explaining the stability of narrow plate boundaries. However, another process must generate the lithospheric thickness variation

in the first place. One possibility is serpentinization, which reduces the strength of the brittle crust, especially when coupled with the development of a fabric in brittle faults.

## References:

- Gordon, R., 2000. Diffuse oceanic plate boundaries: strain rates, vertically averaged rheology, and comparisons with narrow plate boundaries and stable interiors, in M. Richards, R. Gordon, R. van der Hilst (Eds.), *The History and Dynamics of Global Plate Motions*, Geophysical Monograph 121, American Geophysical Union, Washington, D.C., pp. 143-159.
- Gueydan, F., Précigout, J., and Montési, L.G.J., 2014. Strain weakening enables continental plate tectonics, *Tectonophysics*, 631, 189-196, doi: 10.1016/j.tecto.2014.02.005
- Kreemer, C., Blewitt, C.D., and Klein E.C., 2014. A geodetic plate motion and global strain rate model, *Geochemistry, Geophysics, Geosystems*, 15, 3849-3889, doi:10.1002/2014GC005407.
- Montési, L.G.J., 2013. Fabric development as the key for forming ductile shear zones and enabling plate tectonics, *Journal of Structural Geology* 50, 254-266, doi:10.1016/j.jsg.2012.12.011.
- Montési, L.G.J. and Zuber, M.T., 2002. A unified description of localization for application to large-scale tectonics, *Journal of Geophysical Research*, 107, 2045, doi:10.1029/2001JB000465.

**Keywords:** Localization, Plate boundaries, Plate-driving forces, Rheology.

## Analogue modelling of double polarity subduction

Mireia Peral<sup>1</sup>, Ágnes Király<sup>2</sup>, Sergio Zlotnik<sup>3,4</sup>, Francesca Funiciello<sup>2</sup>, Manel Fernandez<sup>1</sup>, Claudio Faccenna<sup>2</sup>

<sup>1</sup>) Group of Dynamics of the Lithosphere, Institut de Ciències de la Terra Jaume Almera (ICTJA-CSIC), Barcelona, Spain.

<sup>2</sup>) Laboratory of Experimental Tectonics, Department of Sciences, Università degli Studi Roma Tre, Rome, Italy.

<sup>3</sup>) Department of Civil and Environmental Engineering, Universitat Politècnica de Catalunya, Barcelona, Spain.

<sup>4</sup>) School of Ocean and Earth Sciences, Tongji University, China.

Corresponding author: mperal@ictja.csic.es

S1 – Geodynamics, Plate tectonics (PS7)

### Introduction and objectives:

The interaction of two subducting plates having opposite vergence has been proposed in the literature in several regions of the Earth (e.g., Lallemand et al., 2001; Lamb, 2011; Vignaroli et al., 2008). Recently, Vergés and Fernández (2012) proposed a new interpretation of the tectonic history of the Western Mediterranean that involves two subducting plates with opposite polarity. The goal of this work is to understand the dynamics of such a subduction system and its observable geotectonic consequences, with the aim of estimating its feasibility in the context of the Western Mediterranean.

### Laboratory model setup:

A series of analogue models based on viscous syrup (representing the mantle) and silicone putty (representing the subducting plate) have been designed to simulate the evolution of a double subduction system. The models were recorded and post-processed to obtain subduction velocities, retreat rates, trench curvatures and plate separation, all being functions of experimental time. Moreover, single subduction systems with similar properties were preliminarily developed as reference models, such that we can identify those behaviors that are produced as a consequence of the interaction between plates.

The basic setup contains a pair of plates subducting in opposite directions (Figure 1). The plates are fixed at their back edge to enforce a slab rollback behavior. Subduction is started by deflecting manually the leading edge of the plate (i.e., initial slab pull). Different setups were designed to test the influence of two variables on the system: i) the width of the plates and ii) the lateral distance between the two subducting plates. These parameters were chosen in order to compare our results with the numerical experiments of Kiraly et al., (2016).

The width of the plates varies from 10 cm (i.e., 600 km in nature) to 30 cm (i.e., 1800 km in nature). The lateral distance, on the other hand, varies from 10 to 0.5 cm (i.e., 30 km in nature).

### Results:

The evolution of the models is characterized, according to Kiraly et al. (2016), by three different phases: (1) initial stage of subduction, corresponding to the evolution of the system until the plates reach the base of the model box; (2) approaching trenches until they pass each other; (3) diverging trenches, until the retreating of plates is over. The duration of the phases is tuned by the relative distance between the subducting plates.

Preliminary results show that trench velocities increase during phase 2 and then decrease during phase 3, indicating a constructing interaction of the mantle flows produced by the two retreating slabs. Moreover, the lateral distance between plates remains constant along time, indicating that no effective lateral stress is produced when the opposing plates have similar dimensions.



Figure 1: Top view of a double-polarity subduction experiment. The image corresponds to the transition stage between phase 2 and phase 3 of the evolution. The plates are initially spaced 0,5 cm and both are 10 cm width.

#### References:

- Kiraly A., Capitanio F.A., Funicello F., Faccenna C.,: (doi:10.1130/G37912.1).
- Lallemand, S., Font, Y., Bijwaard, H., and Kao, H.: New insights on 3-D plates interaction near Taiwan from tomography and tectonic implications, *Tectonophysics*, 335, 229-253, 2001.
- Lamb, S.: Cenozoic tectonic evolution of the New Zealand plate-boundary zone: A paleomagnetic perspective, *Tectonophysics*, 509, 135-164, 2011.
- Vergés, J. and Fernández, M.: Tethys-Atlantic interaction along the Iberia-Africa plate boundary: The Betic-Rif orogenic system, *Tectonophysics*, 579, 144-172, 2012.
- Vignaroli, G., Faccenna, C., Jolivet, L., Piromallo, C., and Rossetti, F.: Subduction polarity reversal at the junction between the Western Alps and the Northern Apennines, Italy, *Tectonophysics*, 450, 34-50, 2008.

**Keywords:** Double-polarity subduction, Western Mediterranean, analogue modelling, laboratory experiments.

## **Tectonic inversion of the North African margin (Algeria) and possible subduction inception: insights from numerical thermo-mechanical models**

Carole Petit<sup>1</sup>, Lamine Hamai<sup>1,2</sup>, Laetitia Le Pourhiet<sup>3</sup>, Abdelkamim Yelles-Chaouche<sup>2</sup> and Abdeslam About<sup>2</sup>

<sup>1</sup>) Université Côte d'Azur, CNRS, OCA, IRD, Géoazur, France

<sup>2</sup>) Centre de Recherches en Astronomie, Astrophysique et Géophysique, Alger, Algérie

<sup>3</sup>) Université Pierre et Marie Curie, CNRS, UPMC, IStEP, France

Corresponding author: petit@geoazur.unice.fr

S1 – Geodynamics, Plate tectonics (PS7)

Whereas oceanic subduction is one of the most important processes of plate tectonics, understanding how and where it begins is still a matter of debate, mostly because examples of incipient oceanic subduction worldwide are scarce (e.g., Gerya, 2011, and references therein). Northern Algeria currently undergoes a slow compressional deformation due to the on-going Africa-Eurasia convergence. Deformation occurs on its continental margin (Frizon de Lamotte *et al.*, 2011), as evidenced by active seismicity recorded both on land and at sea (Yelles *et al.*, 2006; Domzig, 2006). The North African margin in Algeria may therefore represent a transitional stage between active and passive margin settings (e.g., Jolivet *et al.*, 2006). Published data from four wide-angle seismic profiles showed evidence of active or recent compressive deformation along the margin. Models of isostatic anomalies showed that the North Algerian margin displays isostatic anomalies close to that of an active margin (Hamai *et al.*, 2015). From these observations, two questions arise: i) what rheological and thermal parameters control compressional strain localization at the foot of the former passive margin? ii) are those parameters suitable for a long-term evolution of the North Algerian margin towards a mature subduction zone ?

In this study, we use the thermo-mechanical code pTatin (May *et al.*, 2014) to test the effect of thermal and rheological parameters on the tectonic inversion of a passive margin characterized by a young, hot oceanic domain adjacent to a cooler continental plate, following a setting similar to the North Algerian margin. As there is no evidence for a typical ocean-continent transition made of exhumed mantle, we simply consider a ~20 km wide transition zone between the oceanic and continental lithosphere, that can be either of oceanic affinity (implying a sharp transition between the oceanic and the continental domain) or of continental affinity (implying the presence of extended continental crust). This transition zone may be either vertical or dipping toward the continent. Finally, we test the effect of a smooth thermal gradient between the ocean and the continent as well as a sharp vertical boundary between the oceanic and continental geotherms.

Our results indicate that tectonic inversion may evolve towards subduction, when the transition zone is dipping towards the continent (Figure 1), or towards an indentation of the continental lower crust by the oceanic lithosphere, when the transition zone is vertical. In both cases, strain localization at the foot of the margin occurs only when it is sufficiently heated by the adjacent oceanic domain.

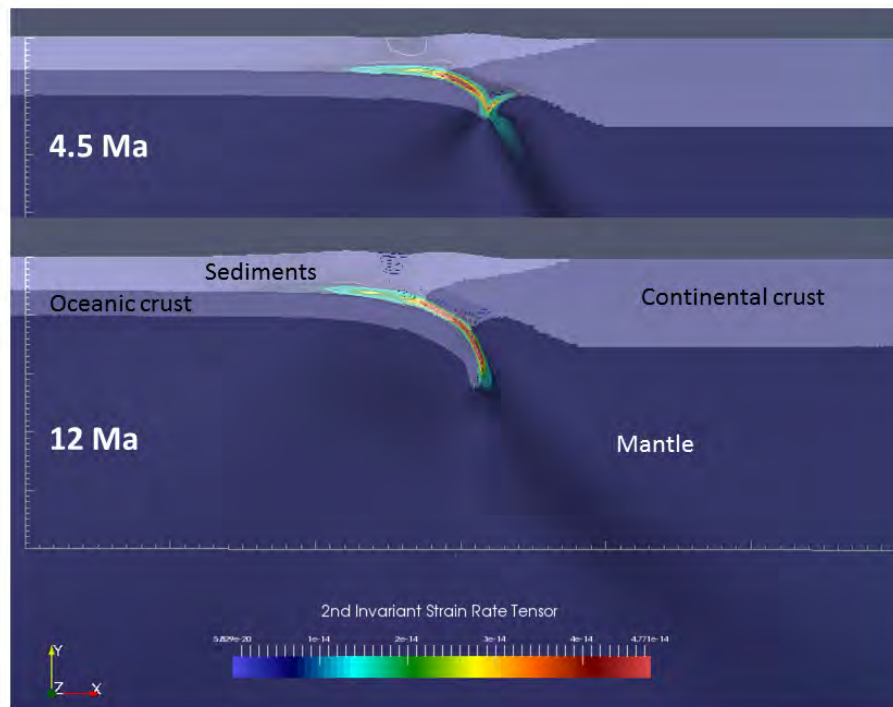


Figure 1: Results of the reference model with a transition zone dipping towards the continent and a hot geotherm; blue color scale corresponds to the different model phases; rainbow color scale is the second invariant of the 2D strain rate tensor.

#### References:

- Domzig A., K. Yelles, C. Le Roy, J. Déverchère, J.-P. Bouillin, R. Bracene, B. Mercier de Lepinay, P. Le Roy, E. Calais, K. Kherroubi, V. Gaullier, B. Savoye, H. Pauc, 2006. Searching for the Africa-Eurasia Miocene boundary onshore Western Algeria (Maradja'03 cruise), *C. R. Geosci.*, **338**, 80–91.
- Frizon de Lamotte, D., Raulin, C., Mouchot, N., Wrobel-Daveau, J.C., Blanpied, C., Ringenbach, J.C., 2011. The southernmost margin of the Tethys realm during the Mesozoic and Cenozoic: initial geometry and timing of the inversion processes. *Tectonics*, **30**, TC3002, doi: 10.1029/2010TC002691.
- Gerya, T., 2011. Future directions in subduction modeling. *J. Geodyn.*, **52**, 344–378.
- Hamai, L., Petit, C., Abtout, A., Yelles-Chaouche, A., and Déverchère, J., 2015. Flexural behaviour of the north Algerian margin and tectonic implications, *Geophys. J. Int.*, 201, 1426-1436, doi:10.1093/gji/ggv098.
- Jolivet, L., R. Augier, C. Robin, J. P. Suc, and J. M. Rouchy, 2006. Lithospheric-scale geodynamic context of the Messinian salinity crisis, *Sediment. Geol.*, 188-189, 9–33.
- May, D., Brown, J. and Le Pourhiet, L., 2014. pTatin3D: high performance methods for long-term lithospheric dynamics, SC14: International Conference for High Performance Computing, Networking, Storage and Analysis, New Orleans.
- Yelles-Chaouche A.K., A. Boudiaf, H. Djellit, R. Bracène, 2006. La tectonique active de la région nord-algérienne, *C.R. Geoscience*, 338, pp. 126–139.

**Keywords:** North Algerian margin inversion; incipient subduction; thermo-mechanical models.

## The effect of oblique trenches on temperature in subduction zones

Alexis Plunder<sup>1</sup>, Cédric Thieulot<sup>1</sup>, Wim Spakman<sup>1</sup> and Douwe van Hinsbergen<sup>1</sup>

<sup>1</sup> Utrecht University, Dept. of Earth sciences, Utrecht, The Netherlands

Corresponding author: a.v.plunder@uu.nl

S1 – Geodynamics, Plate tectonics (PS7)

### Introduction:

The geotherm of a subduction zone is thought to vary as a function of subduction rate and the age of the subducting lithosphere (Kirby et al., 1991; Peacock and Wang, 1999). Along a single subduction zone the rate of subduction can strongly vary due to changes in the angle between the trench and the plate convergence vector, namely the subduction obliquity. This phenomenon is observed all around the Pacific (*i.e.*, Marianna, Sunda-Sumatra, Aleutian...) and is supposed in the geological record of Turkey (van Hinsbergen et al., 2016). However due to observed differences in subducting lithosphere age or lateral convergence rate in nature, the quantification of temperature variation due to obliquity is not obvious and need to be better constrained (Bengtson and Van Keken, 2012; Morishige and van Keken, 2014).

### Modelling approach:

In order to investigate this effect, 3D generic numerical models were carried out using the finite element code ELEFANT (Thieulot, 2014). We designed a simplified setup to avoid interaction with other parameters. An ocean/ocean subduction setting was chosen and the domain is represented by a  $400 \times 500 \times 200$  km Cartesian box. The trench geometry is prescribed by means of a simple arc-tangent function. The mantle flow is computed in the mantle wedge by solving the equation of mass conservation. The energy conservation equation is solved in the entire domain and the results are analysed after steady state is reached. Depths-temperature trajectories along are computed in order to quantify the influence of obliquity on the temperature of the subduction interface.

### Results:

First results show that the effect of the trench curvature on the geotherm with respect to the convergence direction is not negligible (Figure 1). A small obliquity yields isotherms that are slightly deflected upwards where the obliquity is maximum. With an angle of  $\sim 30^\circ$ , the isotherms are deflected upwards of about 10 kilometres. Strong obliquity (*i.e.*, angles from  $60^\circ$  to almost  $90^\circ$ ) reveals extreme effects of the position of the isotherms. Further model will include other parameter as the dip of the slab and convergence rate to highlight their relative influence on the geotherm of subduction zone.

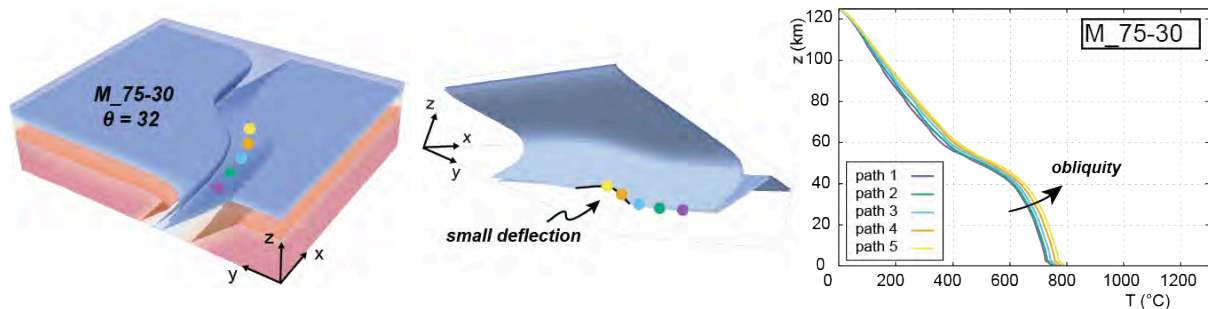


Figure 1: Left panel: top view of temperature in the model and location of depth-temperature paths. Middle panel: bottom view of the 450°C isotherm; note the deflection in link with the geometry. Right panel: Depths-temperature path along the interface showing a ca. 100°C difference as function of obliquity.

## References:

- Bengtson, A.K., Van Keken, P.E., 2012. Three-dimensional thermal structure of subduction zones: Effects of obliquity and curvature. *Solid Earth*, 3, 365–373. doi:10.5194/se-3-365-2012
- Kirby, S.H., Durham, W.B., Stern, L.A., 1991. Mantle Phase Changes and Deep-Earthquake faulting in subducting lithosphere. *Science*, 252, 216–225.
- Morishige, M., van Keken, P., 2014. Along-arc variation in the 3-D thermal structure around the junction between the Japan and Kurile arcs. *Geochemistry Geophys. Geosystems* 18, 1–16. doi: 10.1002/2014GC005356.Received
- Peacock, S.M., Wang, K., 1999. Seismic Consequences of Warm Versus Cool Subduction Metamorphism: Examples from Southwest and Northeast Japan. *Science*, 286, 937–939. doi: 10.1126/science.286.5441.937
- Thieulot, C., 2014. ELEFANT: a user-friendly multipurpose geodynamics code. *Solid Earth*, 6, 1949–2096.
- van Hinsbergen, D.J.J., Maffione, M., Plunder, A., Kaymakçı, N., Ganerød, M., Hendriks, B.W.H., Corfu, F., Gürer, D., de Gelder, G.I.N.O., Peters, K., McPhee, P.J., Brouwer, F.M., Advokaat, E.L., Vissers, R.L.M., 2016. Tectonic evolution and paleogeography of the Kırşehir Block and the Central Anatolian Ophiolites, Turkey. *Tectonics*, 35, 1–32. doi:10.1002/2015TC004018.Received

**Keywords:** Numerical modelling, obliquity in subduction zones, temperature.

## Testing the thermal state of Biella pluton country rocks via numerical model of magma cooling

Manuel Roda<sup>1</sup> and Davide Zanoni<sup>1</sup>

<sup>1</sup>) Università degli Studi di Milano, Dep. of Earth Sciences, Via Mangiagalli, 34 - 20133 Milano, Italy

Corresponding author: manuel.roda@unimi.it

S1 – Geodynamics, Plate tectonics (PS7)

### Abstract:

The Biella pluton (30-31 Ma) is a Periadriatic intrusive of the Alps, emplaced in the internal part of the HP continental Sesia Lanzo Zone (Berger et al., 2012). Pluton cooling involved contact metamorphism overprinting eclogitic to greenschist facies assemblages in country rocks. Multiscale structural analysis combined with thermos-barometric estimates suggest that magma intrusion took place at shallow crustal levels (Zanoni et al., 2008; Zanoni et al., 2010; Zanoni, 2015).

The emplacement history indicates that the intrusion of Biella body occurred when the Sesia Lanzo Zone had almost completed its exhumation under low thermal state consistent with an ongoing subduction (e.g. Roda et al., 2012 and refs therein). The mechanism proposed for triggering the Periadriatic magmatism are either subduction (Tiepolo et al., 2014) or slab break-off (e.g. Von Blanckenburg & Davies, 1995). However recent numerical modeling (Freeburn et al., 2015) suggests that a slab break-off related melting does not result in the widespread magmatism characterizing many collisional belts.

In order to unravel the thermal state of the Biella stock country rocks at the intrusion time we develop a preliminary 2D thermal model of pluton cooling testing four different thermal gradients of the host rocks. We compare the extent and the variation in the thermal peak of the contact aureole recorded in the country rock (Fig. 1) with the results of the numerical simulations.

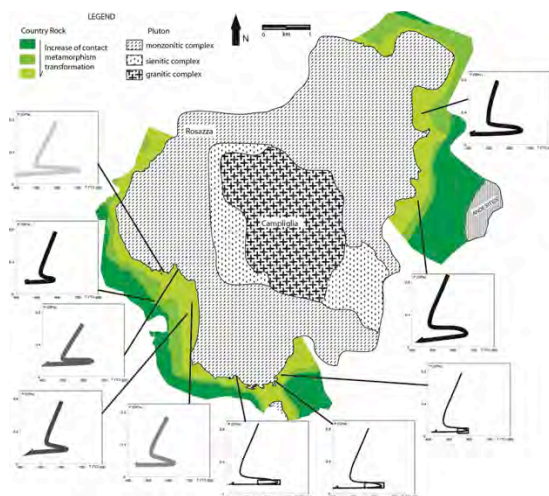


Figure 1: Summary of P-T evolution in Biella aureole at different distances from the pluton margin. Thick line: P-T from calculated petrogenetic grids; thin line: P-T from independent thermobarometry only.

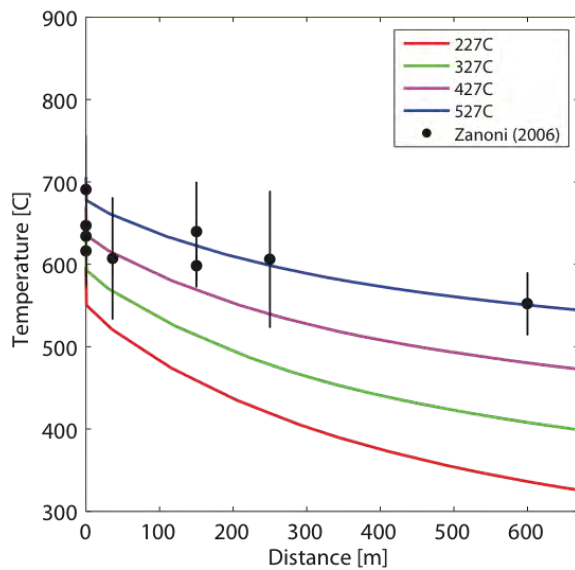


Figure 2: Spatial distribution of  $T_{max}$  due to heat conduction from the pluton to host rock for different base temperatures (lines) and comparison with natural data (dots).

The computed thermal boundary of the aureole is between 300 and 400°C and is wider than the mapped one due to the difficulty to distinguish between contact and greenschists regional metamorphism at such low temperatures. The best fit occurs for the simulation accounting for temperatures between 427 and 527°C (700 and 800 K) at 8 km depth (Fig. 2), assuming conduction as the only effective heat transfer mechanism. This indicates that the emplacement occurred under thermal gradients between 55 and 65°C/km that would exclude a syn-subductive magmatism. The suggested thermal gradient for the country rock of the Biella pluton would represent the constraint for testing different scenarios responsible for the generation of Periadriatic magmatism.

### References:

- Berger A., Mercolli I., Kapferer N., and Fugenschuh B., 2012. Single and double exhumation of fault blocks in the internal Sesia-Lanzo zone and the Ivrea-Verbano zone (Biella, Italy), *International Journal of Earth Sciences*, 101(7):1877–1894, 2012.
- Freeburn R., Van Hunen J., Maunder B.L., Magni V., and Bouilhol P., 2015. Constraining Slab Breakoff Induced Magmatism through Numerical Modelling, AGU Fall meeting, DI22A-04.
- Roda M., Spalla M.I., and Marotta A.M., 2012. Integration of natural data within a numerical model of ablative subduction: a possible interpretation for the Alpine dynamics of the Austroalpine crust, *J. metamorphic Geol.*, 30, 973–996.
- Tiepolo M., Tribuzio R., Ji W.-Q., Wu F.-Y. & Lustrino M., 2014. Alpine Tethys closure as revealed by amphibole-rich mafic and ultramafic rocks from the Adamello and the Bergell intrusions (central Alps), *Rend. Online Soc. Geol. It.*, 31, 450.
- Von Blanckenburg F. & Davies J.H., 1995. Slab breakoff. A model for syncollisional magmatism and tectonics in the Alps, *Tectonics*, 14, 120-131.
- Zanoni D., Bado L., Spalla M.I., Zucali M. & Gosso G., 2008. Structural analysis of the Northeastern margin of the Tertiary intrusive stock of Biella (Western Alps, Italy), *Ital. J. Geosci.*, 127, 125-140.
- Zanoni D., Spalla M.I. and Gosso G., 2010. Structure and PT estimates across late-collisional plutons: constraints on the exhumation of western Alpine continental HP units, *Inter. Geol. Rev.* 52, 1244-1267.
- Zanoni D., 2015. Structure and petrography of the southwestern margin of the Biella pluton, Western Alps, *Journal of Maps*, DOI: 10.1080/17445647.2015.1056259.

**Keywords:** Austroalpine, Contact aureole temperature, Periadriatic intrusives, Slab break-off, Western Alps.

## **Tectonic inversion of a basement-involved fold-and-thrust belt: Numerical modelling applied to the Kopet Dagh Mountains**

Jonas B. Ruh<sup>1</sup>, Jaume Vergés<sup>1</sup>

<sup>1</sup>) Institut de Ciències de la Terra Jaume Almera, Consejo Superior de Investigaciones Científicas, Barcelona, Spain

Corresponding author: jruh@ictja.csic.es

S1 – Geodynamics, Plate tectonics (PS7)

### **Introduction:**

In the last decades, much effort has been made towards understanding thin-skinned evolution of mountain belts, i.e. without taking into account any involvement of basement deformation, applying analogue, numerical, and analytical solutions (Davis et al., 1983; Gwinn, 1964; Hsu, 1979). Recent studies have shown that basement-involvement during orogenic growth can strongly influence the structural and mechanical evolution of mountain belts (e.g., Bauville and Schmalholz, 2015). Furthermore, focus is often limited on purely compressive systems, although new studies emphasize the importance of inversion of pre-orogenic extensional basins and inheritance of basement normal faults for the dynamics of evolving mountain belts (e.g., Boutoux et al., 2014). Numerical studies show proposed that even old and thermally strong basins can potentially be inverted if they are associated to weak shear zones (Buiter et al., 2009).

### **Natural example: Kopet Dagh Mountains, NE Iran**

The Kopet Dagh mountain belt in NE Iran is an excellent example of an inverted fold-and-thrust belt and suits perfect to investigate and understand long-term processes and evolution of a basement-involvement and tectonic inversion (Figure 1; Robert et al., 2014, and references therein). The Kopet Dagh underwent a short period of extension in the Middle Jurassic, when the northern branch of the Tethys (Paleotethys) closed. Subduction of the southern branch of the Tethys (Neotethys) initiated and the Kopet Dagh Mountains developed although their timing is not clear yet: late Eocene-Oligocene or Miocene during continental collision. Therefore, the temporal and structural evolution of the Kopet Dagh is an important key towards understanding the large-scale tectonic history of the Arabia-Eurasia continental collision.

### **Applied numerical model**

We apply a fully-staggered, marker-in-cell, finite difference numerical code with a framework written after a text book for numerical geodynamic modelling (Gerya, 2010) that was further developed. The presented model exhibits a visco-elasto-plastic rheology and simplified strain-dependent plastic softening. Initial extension and subsequent tectonic inversion towards convergence is applied to a 30 km thick crustal sequence (Figure 2). Syn-tectonic sedimentation during extension as well as filling-up of the basin during the tectonically quiet phase is applied to investigate the effect of deep-rooted inherited basement faults on the structural evolution of the overlying sedimentary sequence (Figure 1). We test the effects of varying thermal gradients, crustal rheology, and amount of (non-physical) rock softening.

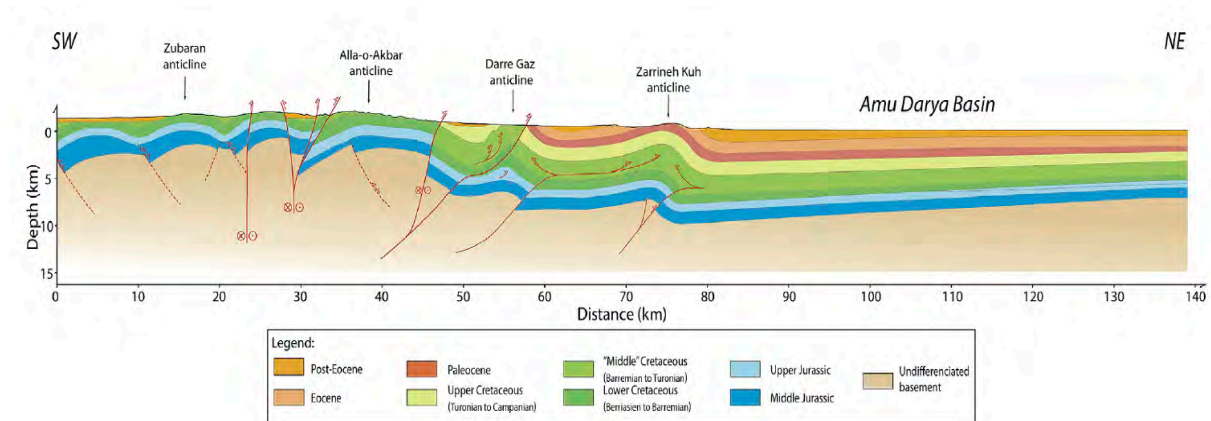


Figure 1: Regional cross-section showing inversion of inherited basement structures in the Kopet Dagh. Structural framework of Mesozoic and Cenozoic stratigraphy is strongly dependent on basement deformation. Adapted from Robert et al. (2014).

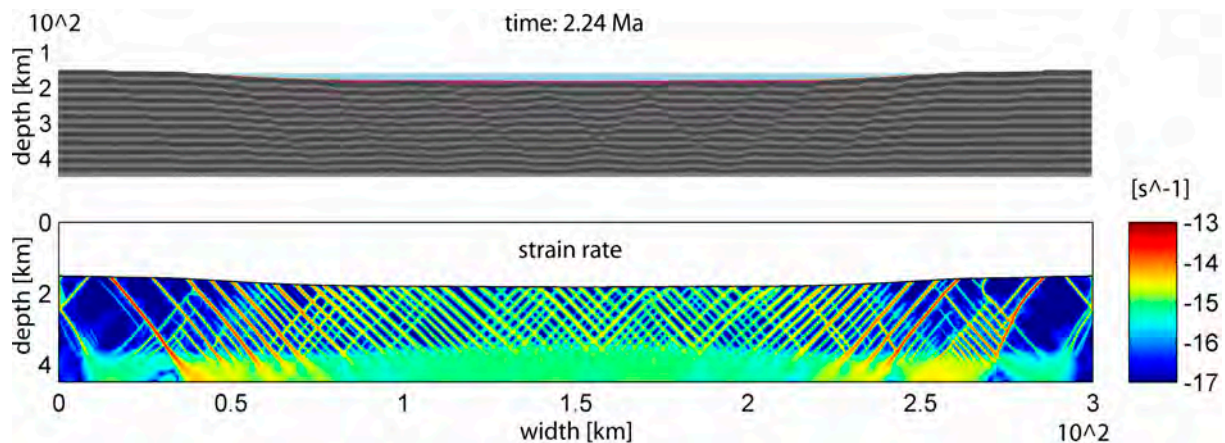


Figure 2: Preliminary numerical result after extensional phase. Top: Composition shows 500 m to 1 km normal fault offset. Reddish color indicate syn-tectonic sedimentation. Bottom: Second invariant of the strain-rate tensor.

## References:

- Bauville, A., and S. M. Schmalholz (2015), Transition from thin- to thick-skinned tectonics and consequences for nappe formation: Numerical simulations and applications to the Helvetic nappe system, Switzerland, *Tectonophysics*, 665, 101-117.
- Boutoux, A., N. Bellahsen, O. Lacombe, A. Verlaquet, and F. Mouthereau (2014), Inversion of pre-orogenic extensional basins in the external Western Alps: Structure, microstructures and restoration, *J Struct Geol*, 60, 13-29.
- Buiter, S. J. H., O. A. Pfiffner, and C. Beaumont (2009), Inversion of extensional sedimentary basins: A numerical evaluation of the localisation of shortening, *Earth Planet Sc Lett*, 288(3-4), 492-504.
- Davis, D., J. Suppe, and F. A. Dahlen (1983), Mechanics of Fold-and-Thrust Belts and Accretionary Wedges, *J Geophys Res*, 88(Nb2), 1153-1172.
- Gerya, T. (2010), *Introduction to Numerical Geodynamic Modelling*, 345 pp., Cambridge University Press.
- Gwinn, V. E. (1964), Thin-Skinned Tectonics in the Plateau and Northwestern Valley and Ridge Provinces of the Central Appalachians, *Geol Soc Am Bull*, 75(9), U863-&.

- Hsu, K. J. (1979), Thin-Skinned Plate Tectonics during Neo-Alpine Orogenesis, *Am J Sci*, 279(4), 353-366.
- Robert, A. M. M., J. Letouzey, M. A. Kavooosi, S. Sherkati, C. Muller, J. Vergés, and A. Aghababaei (2014), Structural evolution of the Kopeh Dagh fold-and-thrust belt (NE Iran) and interactions with the South Caspian Sea Basin and Amu Darya Basin, *Mar Petrol Geol*, 57, 68-87.

## Influence of spreading ridge's subduction on plate dynamics: insights from laboratory models

Méline Salze<sup>1</sup>, Benjamin Guillaume<sup>2</sup>, Joseph Martinod<sup>3</sup>, Jean-Jacques Kermarrec<sup>2</sup>, Christian Sue<sup>1</sup>

<sup>1</sup> Chrono-environnement, CNRS-UMR6249, Université de Franche-Comté, 16 route de Gray, 25030 Besançon cedex, France

<sup>2</sup> Géosciences Rennes, CNRS-UMR6118, Université de Rennes 1, 263 avenue du Général Leclerc, Campus de Beaulieu, Bâtiment 15, 35042 Rennes cedex, France

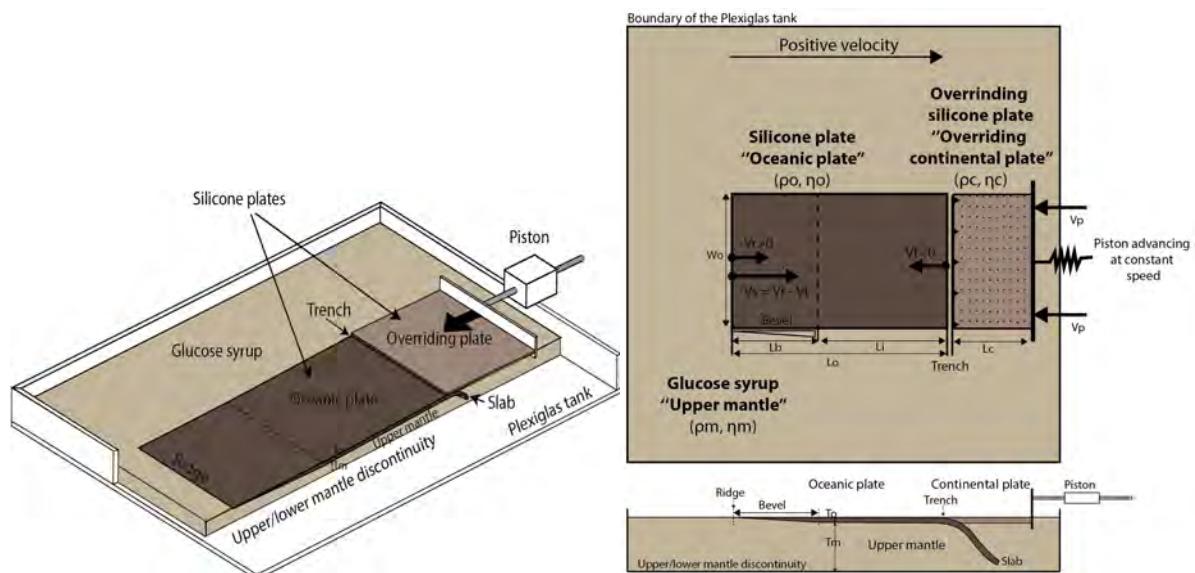
<sup>3</sup> ISTerre, Université de Savoie Mont-Blanc, 73376 Le Bourget du Lac cedex, France

Corresponding author: meline.salze@univ-fcomte.fr

S1 – Geodynamics, Plate tectonics (PS7)

### Abstract:

A series of 3-D analogue models have been conducted in the laboratory in order to simulate the arrival at trench of a spreading ridge and understand its effect on plate kinematics, slab geometry and overriding plate deformation. These models are made of a two-layered linearly viscous system including a lithosphere (PDMS silicone) and an asthenosphere (glucose syrup). To reproduce a progressive decrease of the oceanic lithosphere age approaching the trench and the associated lithosphere thickness decrease, the thickness of the oceanic plate in the model is gradually reduced from the equivalent of ~80 km to 0, eventually completing the ridge subduction. We measure i) trench, subduction and plates velocities, ii) slab dip at different depths, and iii) deformation of the overriding plate. We specifically study the effect of the overriding plate by both including it or not in the system and by changing its absolute motion. We also test the effect of a variable plate width. These models are finally confronted to natural subduction zones where an interaction with an active spreading ridge has been documented (e.g., Chile Ridge subduction beneath Patagonia since the Miocene).



**Keywords:** Analogue modeling, subduction, ridge, lithosphere, Patagonia.

## Control of Hikurangi plateau-Chatham rise and free northern slab edge on evolution of the Tonga-Kermadec-Hikurangi subduction zone

Vincent Strak<sup>1,2</sup>, Wouter P. Schellart<sup>1,3</sup>

<sup>1</sup>) School of Earth, Atmosphere and Environment, Monash University, Melbourne, Australia

<sup>2</sup>) Earthquake Research Institute, University of Tokyo, Tokyo, Japan

<sup>3</sup>) Faculty of Earth and Life Sciences, Vrije Universiteit Amsterdam, Amsterdam, Netherlands

Corresponding author: [vincent.strak@monash.edu](mailto:vincent.strak@monash.edu)

S1 – Geodynamics, Plate tectonics (PS7)

### Introduction:

We present results of analogue subduction models in which we investigate the effect of the Hikurangi plateau-Chatham rise and free northern slab edge on evolution of the Tonga-Kermadec-Hikurangi subduction zone. The Tonga-Kermadec-Hikurangi subduction zone presents a marked along-trench variation in trench retreat and subduction velocities, which increase gradually from south to north to reach very fast velocity close to the northern slab edge. The origin of this kinematic asymmetry is intriguing. However, when placed in a geodynamic framework, the kinematic asymmetry can be thought as produced by lateral variation in subducting plate density, and by different boundary conditions between the southern and the northern lateral slab edges. Presence of the Chatham rise and the Hikurangi plateau born by the subducting plate to the south of the subduction zone are in particular expected to induce a strong positive density anomaly locally, whereas there is a free lateral slab edge to the north.

### Method:

Using three-dimensional fully dynamic subduction models, we study how the presence of the Hikurangi plateau and Chatham rise affects the dynamics of the Tonga-Kermadec-Hikurangi subduction zone. We vary systematically the thickness of both the Hikurangi plateau and Chatham rise as their thickness is not perfectly constrained from geophysical observation. We measure subducting plate kinematics such as trench retreat and subduction velocities. We also use a stereoscopic Particle Image Velocimetry (sPIV) technique to map the 3 components of the subduction-induced mantle flow velocity field in the middle of the upper mantle, focusing on the associated production of upwellings around the free northern slab edge. We then study how the presence or absence of the Hikurangi plateau and Chatham rise and their different possible thicknesses affect the geometry and kinematics of the subducting plate, and the resulting subduction-induced mantle flow around the northern free slab edge.

### Results:

Our model results show that presence of the Hikurangi plateau and Chatham rise strongly affect the evolution of the subduction models. Without these geological features subduction occurs symmetrically with a trench curvature evolving from quasi-linear to slightly convex towards the overriding plate in the centre of the subduction zone. This geometry is characteristic of subduction zones with intermediate trench-parallel slab extent (Schellart et al., 2007; Strak and Schellart, 2016). When including the Hikurangi plateau and Chatham rise subduction slows down and/or ceases in the south but continues in the north (Figure 1), resulting in a trench-parallel increase in trench retreat and subduction velocity from south to north. When increasing the thickness of the Hikurangi plateau and Chatham rise, we observe a stronger velocity gradient in trench retreat and subduction velocity along

the trench. Furthermore, maps of the subduction-induced mantle flow show that an upwelling is produced around the northern free slab edge (Figure 1). This upwelling always stays focused close to the northern slab edge during progressive slab rollback and follows an easterly path. It can in part explain volcanism observed at the northern termination of the Tonga-Kermadec-Hikurangi subduction zone, where mantle decompression melting and interaction between the melt and slab produce an adakite signature.

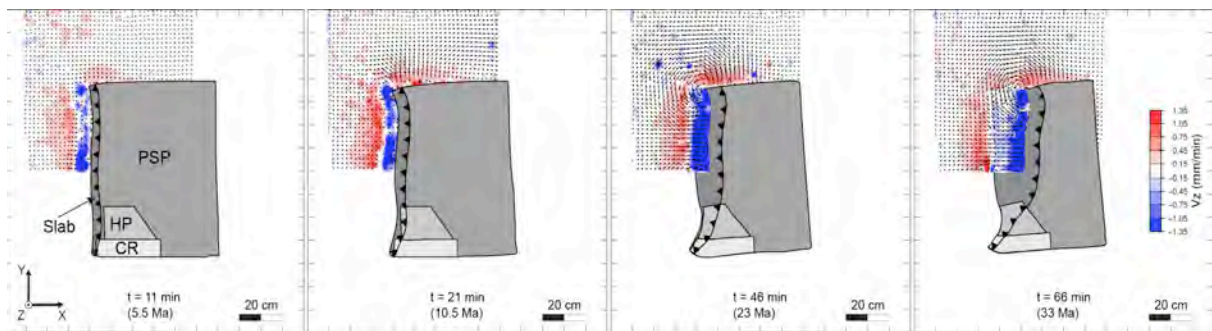


Figure 1: Line drawing and mantle flow velocity field from top views of analogue model to study subduction of the Pacific Subducting Plate (PSP) at the Tonga-Kermadec-Hikurangi subduction zone, with inclusion of the Hikurangi Plateau (HP) and Chatham rise (CR) born by the subducting plate. The 3 components of the mantle flow velocity field have been measured at a depth of 5.5 cm (scaling to 275 km) using a stereoscopic particle image velocimetry technique. The black vectors indicate the in-plane components ( $x$  and  $y$ ) and the colour map shows upwellings in red and downwellings in blue ( $z$ ). Note that 1 mm/min in the model scales to 1 cm/yr in nature. A black dashed line indicates the contour of the slab below the colour map.

## References:

- Schellart, W.P., Freeman, J., Stegman, D., Moresi, L., May, D., 2007. Evolution and diversity of subduction zones controlled by slab width, *Nature*, 446 (7133), 308–311.
- Strak, V., Schellart, W.P., 2016. Control of Slab Width on Subduction-Induced Upper Mantle Flow and Associated Upwellings: Insights from Analog Models, *Journal of Geophysical Research: Solid Earth*, 121, doi:10.1002/2015JB012545.

**Keywords:** Tonga-Kermadec-Hikurangi subduction zone, Hikurangi plateau-Chatham rise, Free northern slab edge, Along-trench velocity variation, Subduction-induced mantle flow, Mantle upwellings, Analogue modelling, Stereoscopic Particle Image Velocimetry technique.

## **Lithospheric-scale shear zone development in convergent setting: time-evolution and switches in dominant rheological behaviour**

Yamato Philippe<sup>1</sup> and Duretz Thibault<sup>1,2</sup>

<sup>1</sup>) Geosciences Rennes, UMR CNRS 6118, Université de Rennes 1, 35042 Rennes Cedex, France.

<sup>2</sup>) Institute of Earth Sciences, University of Lausanne.

Corresponding author: philippe.yamato@univ-rennes1.fr

S1 – Geodynamics, Plate tectonics (PS7)

### **Introduction:**

Lithospheric-scale shear zones are responsible for mechanical decoupling of tectonic plates and therefore represent prominent tectonic features. Paradoxically, the way they develop both in space and time remains poorly constrained and constitutes a challenging issue in tectonics. Here, we focus on lithospheric shear zones developing in a convergent setting. The aim of our study is to follow the complete evolution of a lithospheric shear zone from its genesis. A special attention is paid on identifying the dominant rheological behaviours (brittle vs. ductile) active during the evolution of the shear zone and how they alternate both in space and time.

### **Modelling strategy:**

We performed numerical simulations by using a thermo-mechanical code that solves for 2D incompressible Stokes flow and the energy conservation equation. These equations are discretized on a Eulerian-staggered grid encompassing a free surface. Advection is treated explicitly using a set of Lagrangian markers, which are used for (i) tracking material properties over time and (ii) recording stress and temperature sustained by the rocks throughout the simulations. All lithologies are characterized by a visco-elasto-plastic rheology and combine different flow laws (i.e., diffusion, dislocation, and exponential creep). We do not impose any parameterised material strain softening. We include thermal softening, which arises from the principle of energy conservation (i.e. shear heating).

Throughout the simulation we identify the dominant rheological behaviour, which is responsible for accommodating the deformation at any given location in the model (see Figure 1). The stress state is also recorded in order to quantify the strength (differential stress) evolution within the modelled lithospheric shear zones.

### **Results:**

Our results show that deformation within lithospheric shear zones is not necessarily ductile, even in (U)HP-LT conditions, as commonly believed. If ductile behaviour generally occurs after a first stage of brittle deformation this transition is strongly dependent on the amount of shear heating. As a consequence, the dominant deformation behaviour at a given location is transient. During convergence the state of stress in the shear zone depends on the far field forces applied on the lithosphere but also on the local temperature conditions. As these parameters vary in space and time, the strength within shear zones is highly variable.

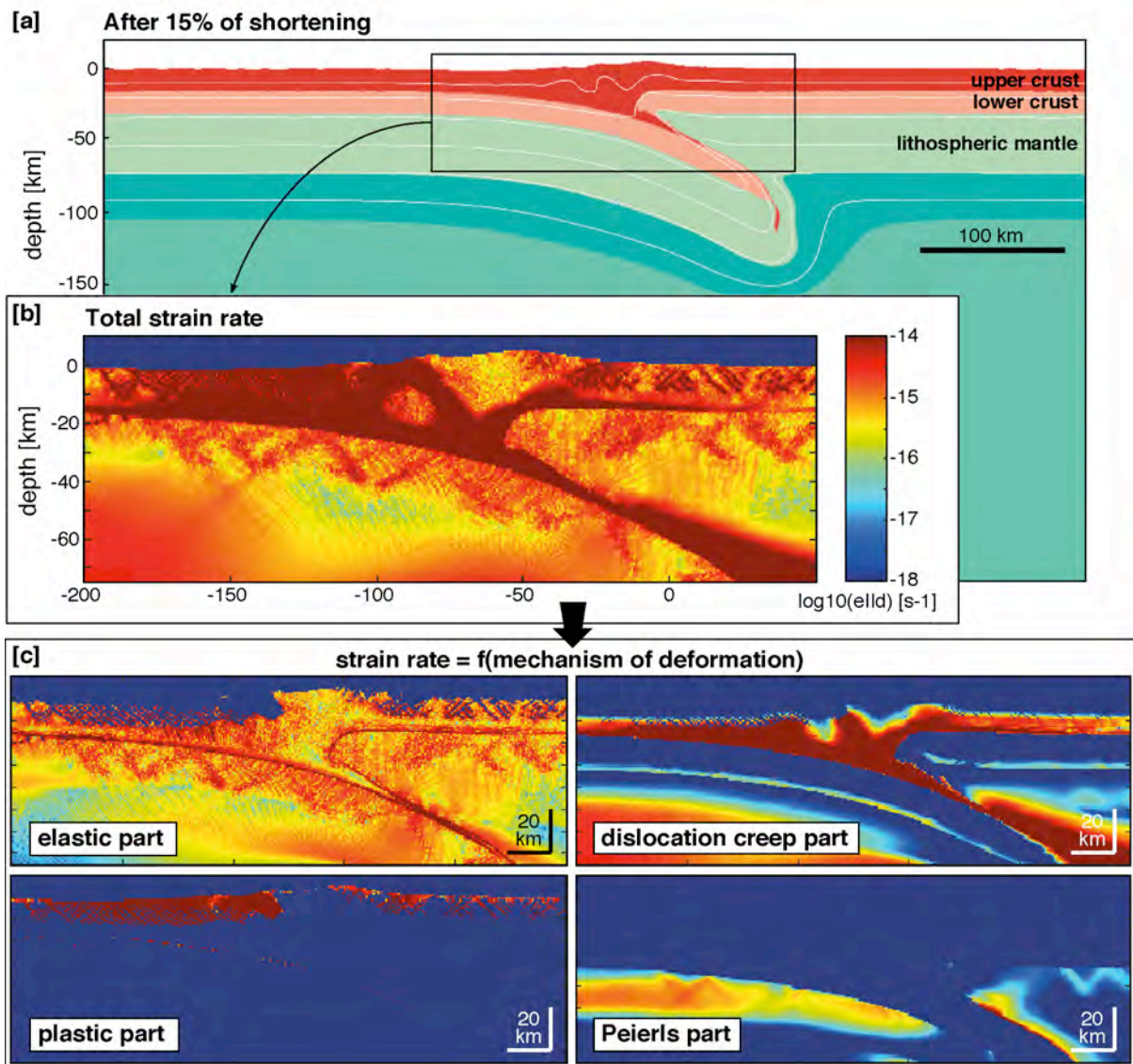


Figure 1: Example of deformation maps extracted from a continental collision model. [a] Material configuration after 15% of shortening. [b] Effective strain rate (second invariant) in the collision zone. [c] Strain rate partitioning between the various rheological behaviours (colour scale is the same as for b).

#### Implications for convergence zones:

Our models present how dominant rheological behaviours are distributed during continental collision and how the stress state evolves within (and close to) a lithospheric-scale shear zone. They particularly highlight the spatial and temporal variations of the location of brittle-ductile transitions. The implications of our study for (U)HP-LT metamorphism and deep seismicity will be discussed.

**Keywords:** Lithospheric shear zones, Rheology, Convergence zones dynamics.

## **Influences of oblique extension and structural inheritance on rift interaction: a 4D analog modeling study**

Frank Zwaan<sup>1</sup>, Guido Schreurs<sup>1</sup>

<sup>1</sup> Institute of Geological Sciences, University of Bern, Baltzerstrasse 1 + 3, 3012 Bern, Switzerland

Corresponding author: frank.zwaan@geo.unibe.ch

S1 – Geodynamics, Plate tectonics (PS7)

### **Introduction:**

During the early stages of rifting, rift segments may form along non-continuous and/or offset pre-existing structures. They can link in various ways to form a continuous rift system. Here we test the effects of 1) dextral and sinistral oblique extension as e.g. observed in the East African Rift System and 2) various geometries of structural inheritance on rift segment linkage. We use a similar method as Zwaan et al. (2016) that allows distributed deformation in the overlying model materials: sand layers for the brittle upper crust and a viscous sand/silicone mixture for the lower crust. Above the basal viscous layer we apply right stepping offset lines (seeds) of the same viscous mixture, representing inherited weaknesses in the sand, along which deformation focuses. Selected models are run in a CT-scanner to reveal their 3D internal evolution (hence 4D).

### **Results:**

Our models show that rift segments initially form along the main seeds and subsequently propagate ca. parallel to the extension direction (Fig. 1a). With sinistral transtension they grow apart, orthogonal extension has them propagating in a parallel fashion and with dextral transtension rift segments grow together. When we apply a secondary seed that connects the main seeds, the former seed seldom activates. This is in contrast with previous studies (e.g. Acocella et al., 1999), but in line with the notion that inherited structures do not always reactivate during a next tectonic phase (e.g. Nalpas & Brun, 1995). Furthermore, in our sinistral transtension models without rift-connecting seeds and with the initial seeds laterally far apart, a surprising phenomenon occurs: instead of rifts that grow apart, a strike-slip transfer zone develops, connecting both rift segments (Fig. 1a<sub>x1-4</sub> and 1b). In some models, a hybrid system develops, with both a strike-slip transfer zone and a rift arm propagating away. This might indicate that these models are close to a transition between two modes: propagating apart or strike-slip transfer zone mode. The latter bears resemblance to the Tanganyika-Malawi fault zone in East Africa (Fig. 1c): we observe 1) a similar extension direction, 2) a strike-slip transfer zone with the same motion with 3) a similar orientation to the main rifts and 4) rift segments that grow apart.

### **References:**

- Acocella, V., Facenna, C., Funicello, R., Rosetti, F., 1999. Sand-box modelling of basement-controlled extensional domains. *Terra Nova*, 11, 149-156.
- Nalpas, T., Le Douaran, S., Brun, J.-P., Unternehr, P., Richter, J.-P., 1995. Inversion of the Broad Fourteens Basin (offshore Netherlands), a small-scale model investigation. *Sedimentary Geology*, 95, 237-250.
- Zwaan, F., Schreurs, G., Naliboff, J., Buiters, S.J.H., 2016. Insights in the effects of oblique extension on continental rift interaction from 3D analogue and numerical modeling, *Tectonophysics*.

**Keywords:** Oblique Extension, Transtension, Analog Modeling, Rifting.

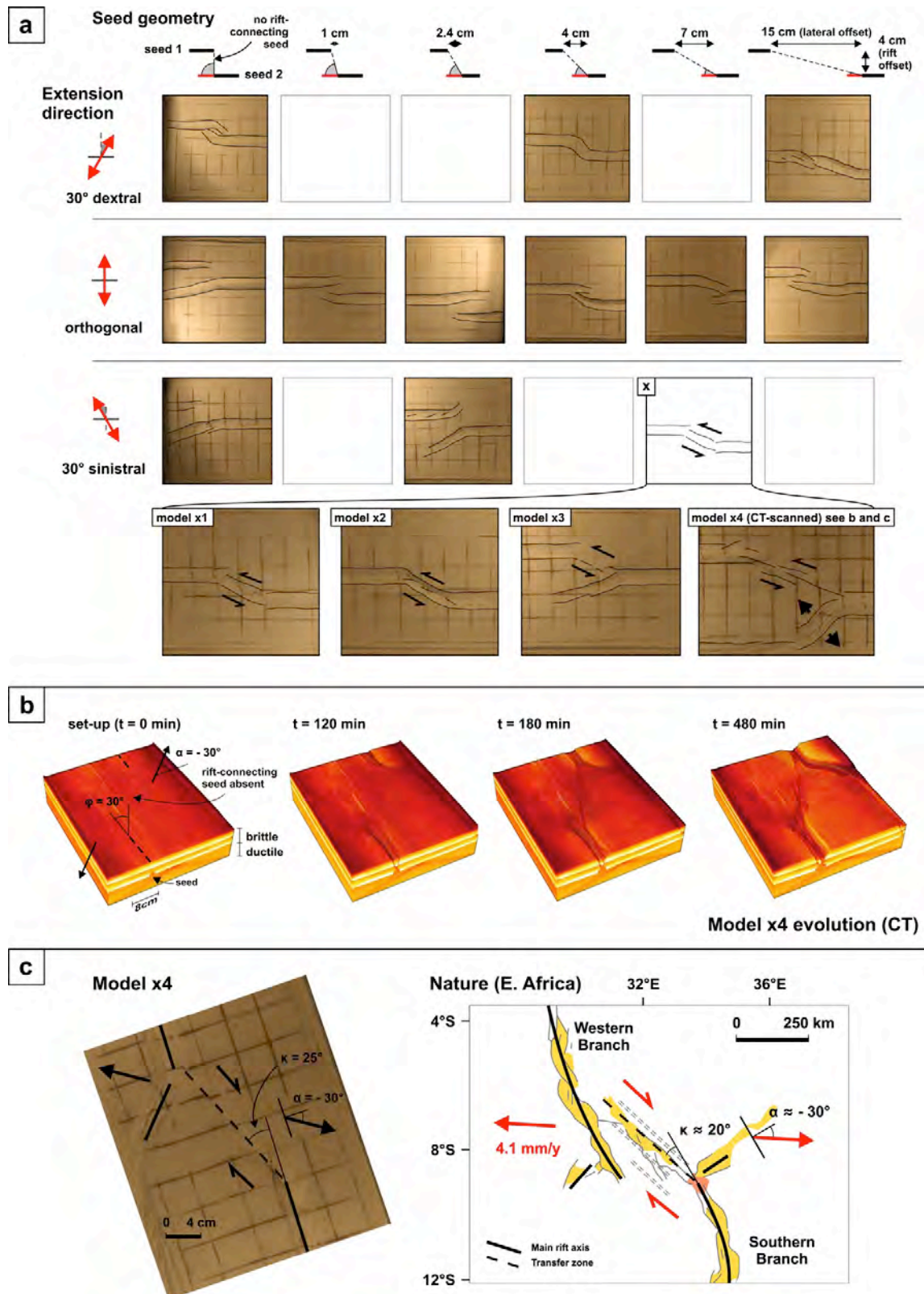


Figure 1. a) Final top view structures as a function of seed geometry and extension direction; b) CT-derived 3D evolution of model x4 (NB: mirrored with respect to Fig. 1a-b); c) Model-nature comparison, image modified after Acocella et al., 1999.

## **Neotectonics characterization of the South Kabylia fault zone Mila- region (Eastern Algeria)**

Sahra Aourari

Algerian Centre of Research Applied for Earthquake Engineering (CGS) - Algeria

Corresponding author: sahourari@hotmail.com

S1 – Geodynamics, Plate tectonics (PS7)

### **Abstract:**

The aim of the work is to describe the neotectonics indications observed near the thrust fault nominated Chevauchement Sud Kabyle (SKF). The fault is a segment of a regional Miocene front thrusting which separates the internal zones from external zones of Maghrebides in Eastern Algeria. The fault is E-W direction and north dipping, has been identified by Bouillin. It is visible between Beni Haroun and Kantour in Mila- Skikda areas. The fault reveals direct and indirect plausible indications of its activity during the Pliocene and Quaternary. A number of small earthquakes with Magnitudes  $M_s$  less than 4 which have occurred during the last century in the vicinity of the fault can argue in favour of its activity.

### **Introduction:**

The Maghrebides chain is extending from North Africa to the Far East regrouping the perimediterranean orogens. It is derived from opening then closure of the Tethys ocean [Mc Kenzi, 1972, De Mets, 1990, Stampfl and al., 2002]. It is related to the convergence of African, European plates and interposition of blocks or microplates Alkapeca [Durand Delga, 1974, 1980; Raoult, 1979; Vila, 1980; Bouillin, 1983; Wildi, 1984].

The Miocene paroxysmal phase produced significant folds distinguished in two principal directions NE- SW and E-W. According to Vila [1980], in the Eastern Algerian Maghrebides, the alpine tectonics took place in several phases: Priabonian phase generated the «front thrust» accident in which is expressed epizonal metamorphism, the flysch overthrust nappe, Tellian nappes and the folding of parautochthon domain. The Burdigalian phase generated olistostromes, Numidian flysch and plicative structures in internal zone. The Tortonian phase is expressed by decametric thrusting. The neotectonic phase has been initialized from the middle Miocene by distension creating major post nappes basins and marked by calc-alkaline magmatism. The Pliocene is particularly distinguished by a continental sedimentation.

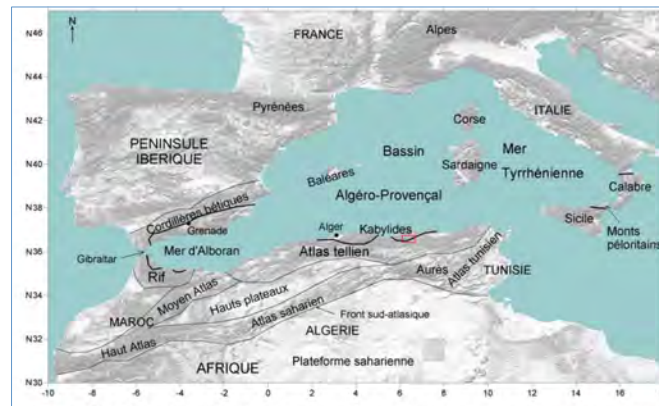


Figure 1: Map of the geomorphological domains of North Algeria: Maghrébides [(Alpine chain regroups Tell Atlas and High Plateaus) and Saharan Atlas (Hercynian, Meso-Cenozoic chain)] [Domzig, 2006]. Study area [36.80° - 36.25° N], [5.50° - 7.00° E] located inside the red square.

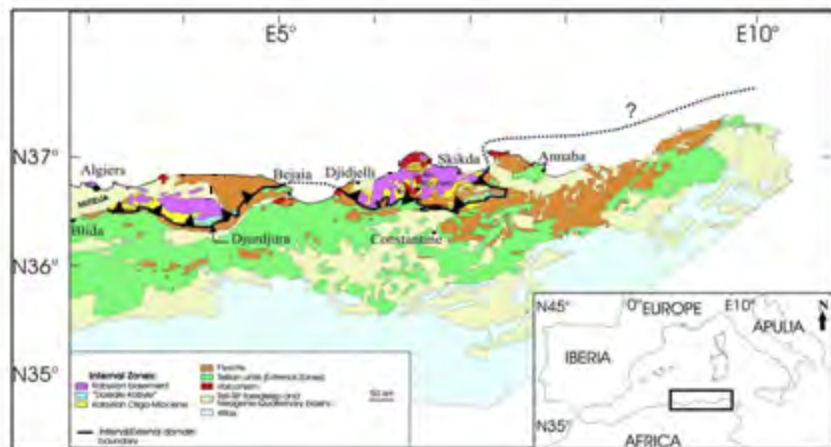


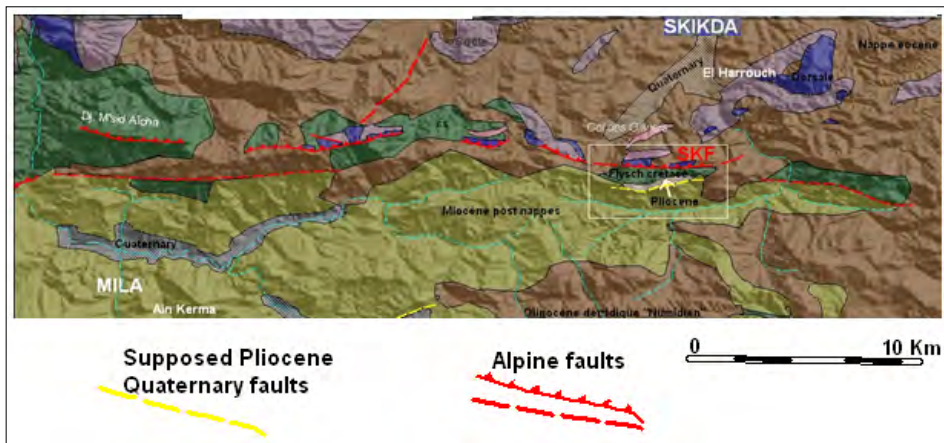
Figure 2: The main geological units of the Maghrébides chain 1 - internal zones (Paleozoic basement, Mesozoic Dorsale + Oligo-Miocène), 2 - Flyshs Southern (Meso-Cenozoic), 3 - external zones (Tellian massifs + the High Plateaux Meso-Cenozoic) (in Kharoubi, 2006)

**Tectonic setting:**

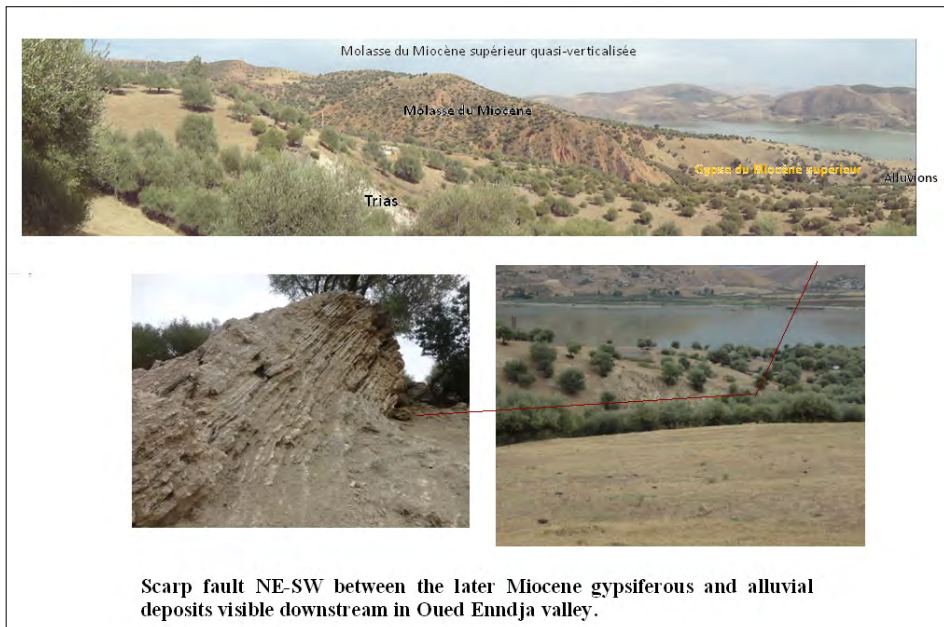
The Alpine tectonic structures correspond mainly to NE-SW, NW- SE system faults, E–W Thrust faults and NE-SW folds. The recent tectonics can be highlighted by reactivation of certain NE-SW reverse faults and E-W strike-slip faults.

**Neotectonic indications**

The obviousness related to the Pliocene and Quaternary activities of the South kabylian fault (SKF), It is marked by deformation of Pliocene; in southern Skikda and Mila areas.

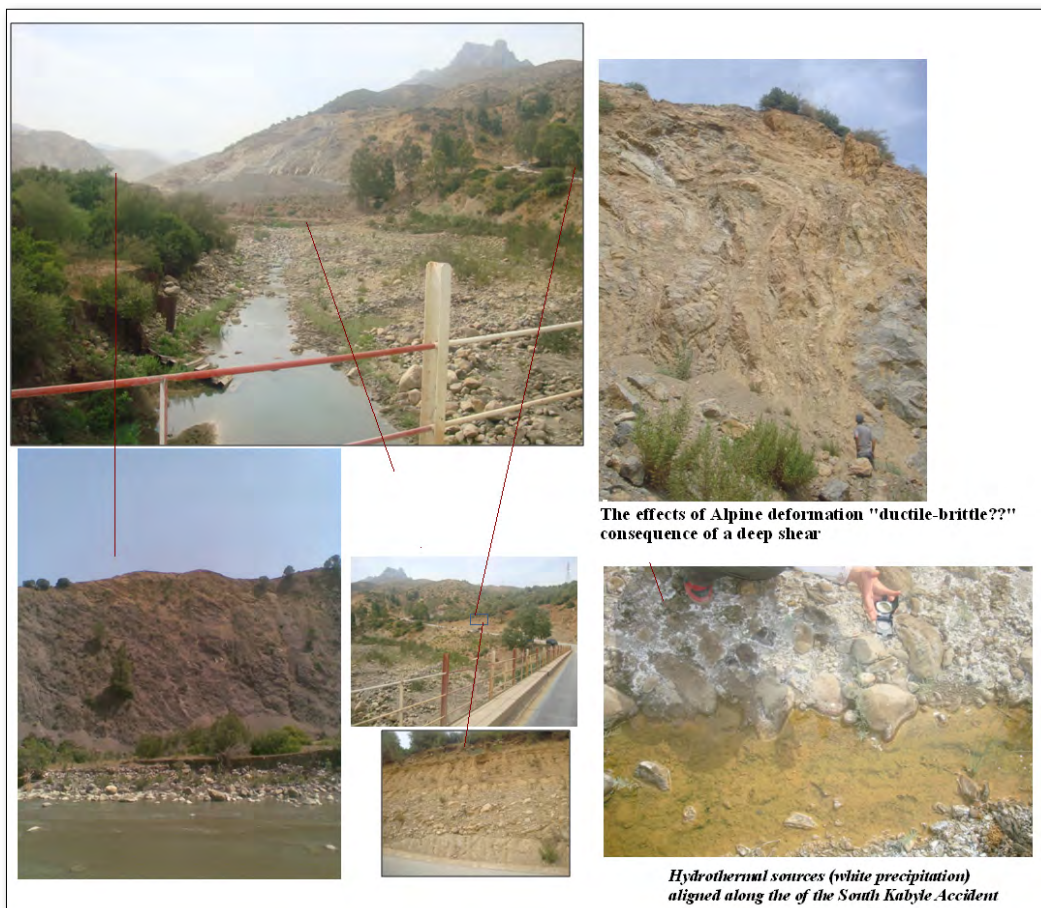


Deformation lamella marking the Pliocene suggesting the proximity of a fault which has functioned during the Pliocene-Quaternary period.





Pliocene of Mila: Monoclinical structure



**Keywords:** alpine tectonic, neotectonic indications, geomorphological indication, historical seismicity.

## **S2 - Coupling Tectonic and Surface processes**

Tectonic deformation and climate-driven erosion control the shape and evolution of continental topography. In turn, landscapes and sedimentary records offer valuable archives of the dynamics of these processes and of their potential couplings. However, unravelling the respective influence of mantle or lithosphere dynamics, erosion, sedimentation, climatic changes and structural inheritance remains a major challenge in the Geosciences.

This partly results from a lack of understanding of how integrating short- and fine-scale processes into the big picture of topography building, basin development and structural evolution. To address this issue, numerical and experimental modelling is required both to refine our understanding of the dynamics of the Earth's surface and sub-surface and to guide future geophysical, geochemical and field-based observations. To this session, we welcome studies that develop one or both approaches, as well as innovative contributions addressing technical and theoretical challenges.

We particular warmly welcome studies 1) that model processes occurring on short time scales (earthquakes, typhoons or floods) or on fine spatial scales (fracturing, landsliding or river avulsion) or 2) that integrate these short- or fine-scale processes into longer- or larger-scale models to investigate how the wide spectrum of couplings between deformation, climate and surface processes shape the Earth's topography.

**Conveners:** Philippe Steer (University of Rennes, France) and Oriol Ferrer (University of Barcelona, Spain).

### **Keynote speaker:**

**"Scale-independent self-organization in channelized transport systems"** by Chris Paola (University of Minnesota, USA) - [cpaola@umn.edu](mailto:cpaola@umn.edu)

## Scale-independent self-organization in channelized transport systems

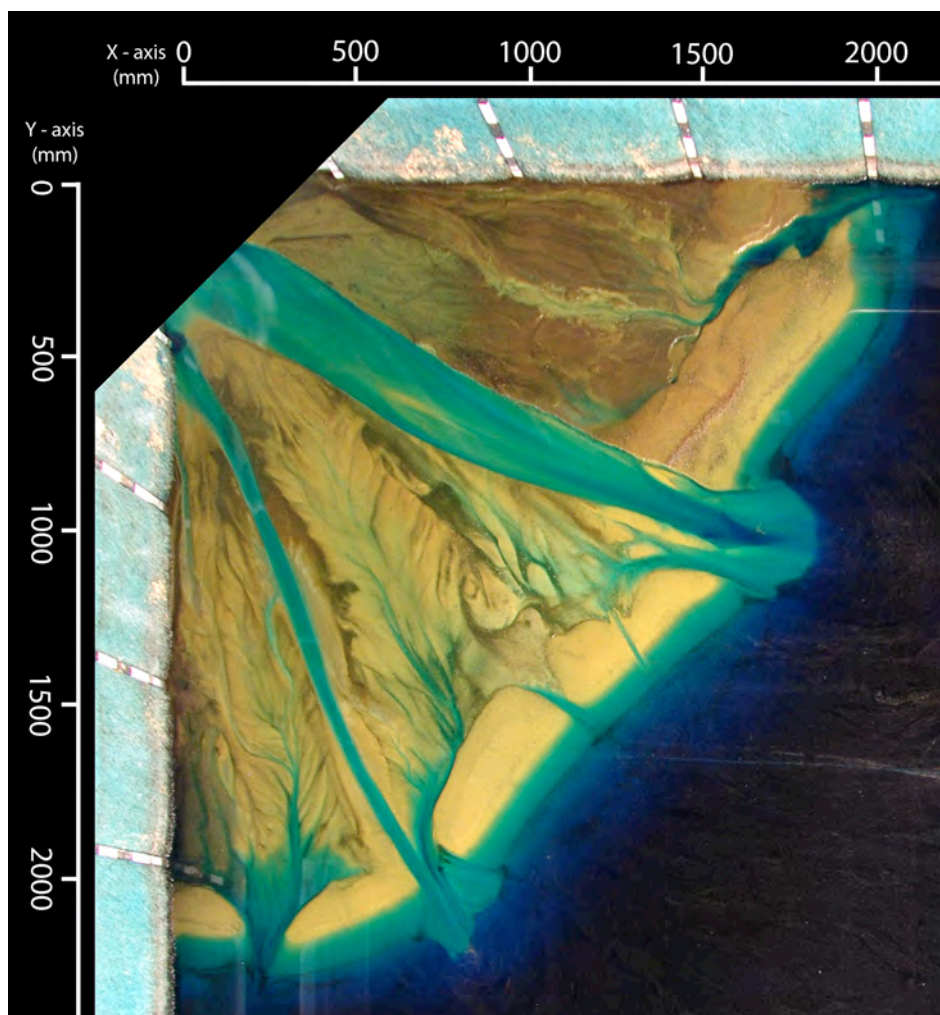
Chris Paola

University of Minnesota, Department of Earth Sciences, Newton Horace Winchell School of Earth Sciences, Minneapolis MN 55455, USA.

Corresponding author: cpaola@umn.edu

S2 - Coupling Tectonic and Surface processes (Keynote)

Major elements of the dynamics of channelized systems, from erosional landscapes to the deep ocean, appear to replicate themselves in more or less similar form across scales and environments. Among other things this allows simplified experiments and simplified dynamical models to contribute a surprising amount of useful insight. We will review examples from experiments on wave and tide influence on deltas, and on the interplay of tectonics and rivers. We will consider parallels between experiments and simplified models, as well as what these examples of "unreasonable effectiveness" can tell us about scale-independence or, perhaps, detail-independence in channelized systems.



*Overhead image of a delta produced under the combined influence of rivers, waves and tides. Can you guess the relative proportions? (Image credit: Sarah Baumgardner)\**

## Stratigraphic Signatures of Forearc Basin Formation Mechanisms

Utsav Mannu<sup>1</sup>, Kosuke Ueda<sup>2</sup>, Sean Willett<sup>1</sup>, Taras Gerya<sup>2</sup> and Michael Strasser<sup>3,1</sup>

<sup>1</sup>Geological Institute, ETH Zürich, 8092 Zürich, Switzerland

<sup>2</sup>Institute of Geophysics, ETH Zürich, 8092 Zürich, Switzerland

<sup>3</sup>Institute of Geology, University of Innsbruck, A-6020 Innsbruck, Austria

Corresponding author: utsav.mannu@erdw.ethz.ch

S2 - Coupling Tectonic and Surface processes (Oral)

### 1. Introduction:

State-of-the-art reflection seismics and borehole data give us an exceedingly detailed picture of the stratigraphic development within forearc and wedge-top basins and the underlying accretionary wedges [Strasser et al., 2009; Gulick et al., 2010; Moore et al., 2015]. Stratigraphic patterns within these basins reveal that instead of being passive, undeformed basins, basins are being constantly shaped by varying influences ranging between wedge tectonics and hinterland sediment flux. As the forearc and wedge-top basins are formed on top of the accretionary wedge, their basins stratigraphy proves to be an invaluable repository of past tectonic movements of the underlying accretionary prism [Beaudry and Moore, 1985]. However, a comprehensive interpretation on the evolution of accretionary wedges predicated upon basin stratigraphy can be contentious, because reconstructed tectonic movements could be dynamically inconsistent with wedge mechanics. Here, we present a methodology to generate synthetic stratigraphy consistent with dynamics of the accretionary wedge using the assumption that stratal surfaces and unconformities identified in reflection seismics are generated by vertical aggradation of sediments and can be approximated by isochronal surfaces [Vail, Todd & Sangree, 1977]. This synthetic stratigraphy is then compared to reflection seismics and borehole data obtained within the IODP (Integrated Ocean Drilling Program) Nankai Trough Seismogenic Zone Experiment (NanTroSEIZE) offshore SW Japan, to ascertain the self-consistency of some of the interpretation for the Nankai accretionary prism underlying the Kumano Forearc basin [Strasser et al., 2009; Gulick et al., 2010; Moore et al., 2015].

### 2. Method:

In this study, we use a dynamic 2D, high-resolution, thermo-mechanical, subduction model (I2VIS [Gerya and Yuen, 2003]) coupled to an adaptive irregular surface grid to model the free surface. The numerical method is similar to the approach used in Mannu et al. (submitted). In addition, we track basin stratigraphy developing in the wedge top basins atop the accretionary prism by emplacing lines of Lagrangian markers at discrete times along the upper surface of the model, which subsequently are buried, transported, and deformed according to the velocity field generated in the model.

### 3. Results:

We observe that the development of forearc basins in wedges with low and high taper angle follow different mechanisms. We find that, in models with low décollement strength ( $\mu_D \leq 0.05$ ) and thus low taper angle, the predominant mechanism of forearc basin formation is due to the formation of negative alpha basin (Figure 1a;d;f). These basins exhibit a landward basin uplift due to landward wedge thickening with time, resulting in seaward tilt of the basin strata (Figure 1d). On the contrary, in models with high décollement strength ( $\mu_D \geq 0.15$ ) and high taper angle, forearc basins form due to creation of accommodation space landward to an active OOST (Out-of-sequence Thrust) (Figure 1 b;e;g). OOST formation is triggered by high trench sedimentation in initial phases of hinterland sedimentation. Basin uplift due to OOST activity produces a landward basin tilting (Figure 1e)

accompanied by a seaward slope basin. Hypothetical boreholes in forearc basin and slope basin exhibit multiple unconformities which indicate an interplay between hinterland sediment flux and accommodation space.

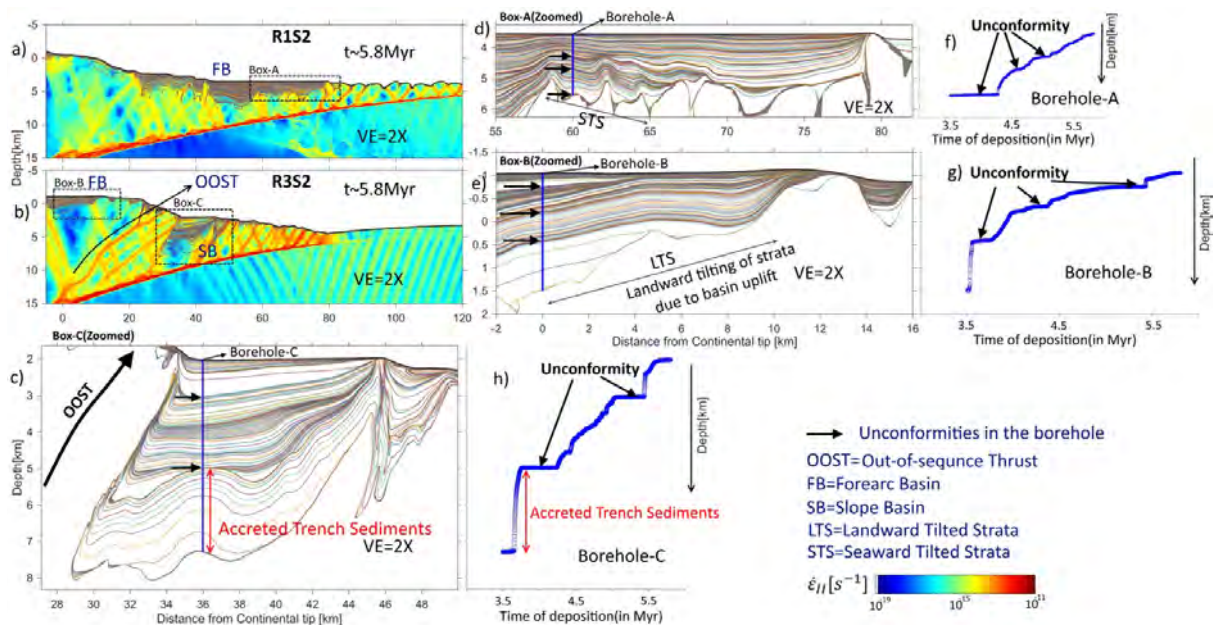


Figure 1: Forearc and slope basins with their stratigraphy. a) Strain-rate invariant plot for model R1S2 ( $\mu_D=0$ ). b) Strain-rate invariant plot for model R3S2 ( $\mu_D=0.2$ ). c) Stratigraphy of slope basin in model R3S2. d) Stratigraphy of forearc basin in model R1S2. e) Stratigraphy of forearc basin in model R3S2. f) Borehole-A time log. g) Borehole-B time log. h) Borehole-C time log.

## References:

- Beaudry, D., and G.F. Moore, 1985, Seismic stratigraphy and Cenozoic evolution of West Sumatra fore-arc basin: AAPG Bulletin, v. 69, p. 742-759.
- Gerya, T. V., & Yuen, D. A. (2003). Characteristics-based marker-in-cell method with conservative finite-differences schemes for modeling geological flows with strongly variable transport properties. *Physics of the Earth and Planetary Interiors*, 140(4), 293-318.
- Gulick, S. P. S., N. L. B. Bangs, G. F. Moore, J. Ashi, K. M. Martin, D. S. Sawyer, H. J. Tobin, S. Kuramoto, and A. Taira (2010), Rapid forearc basin uplift and megasplay fault development from 3D seismic images of Nankai Margin off Kii Peninsula, Japan, *Earth Planet. Sci. Lett.*, 300(1-2), 55–62.
- Moore, G. F., Boston, B. B., Strasser, M., Underwood, M. B., & Ratliff, R. A. (2015). Evolution of tectono-sedimentary systems in the Kumano Basin, Nankai Trough forearc. *Marine and Petroleum Geology*, 67, 604-616.
- Mannu, Utsav, et al. "Impact of sedimentation on evolution of accretionary wedges: insights from high-resolution thermo-mechanical modeling." (submitted).
- Strasser, M. et al. (2009), Origin and evolution of a splay fault in the Nankai accretionary wedge, *Nat. Geosci.*, 2(9), 648–652.
- Vail, P. R., R. G. Todd, and J. B. Sangree. "Seismic stratigraphy and global changes of sea level: Part 5. Chronostratigraphic significance of seismic reflections: Section 2. Application of seismic reflection configuration to stratigraphic interpretation." (1977): 99-116.

**Keywords:** Sedimentation in accretionary wedges, Stratigraphy.

## **Erosion changes throughout glacial cycles contribute to the magma production by continental unloading and associated volcanic activity**

Pietro Sternai<sup>1,2</sup>, Luca Caricchi<sup>3</sup> and Sébastien Castelltort<sup>3</sup>

<sup>1</sup>) University of Cambridge, United Kingdom

<sup>2</sup>) California Institute of Technology, USA

<sup>3</sup>) University of Geneva, Switzerland

Corresponding author: [psternai@caltech.edu](mailto:psternai@caltech.edu)

S2 - Coupling Tectonic and Surface processes (Oral)

### **Introduction:**

Observed peaks of igneous activity worldwide during the current interglacial (e.g., Huybers and Langmuir, 2009) suggest that climate oscillations affect the melting of the Earth's interior. A deglacial-triggering hypothesis (Hardarson and Fitton, 1991), according to which continental unloading owing to the melting of ice-caps during the transition to interglacials leads to enhanced magma production, is currently the most accredited explanation for this correspondence. The impact of climate oscillations on magma production, however, has been evaluated regardless of surface erosion although the density of upper crustal rocks and sediments exceeds that of ice by approximately three times. Such a density difference implies that the melting of 1 km of ice leads to the same increase of basalt production as the removal ~0.3 km of upper crustal rocks by erosion, provided that such unloading occurs during similar time intervals.

### **Methodology:**

We use datasets relating to the evolution of erosion rates (e.g., Hallet et al., 1996; Herman et al., 2013) to calibrate numerical models of surface erosion processes and evaluate the relative dynamic contributions of erosion and ice building/melting to continental loading/unloading during a 100 ka glacial-interglacial climate oscillation. Assuming that the Earth possess a linear rheology, a time invariant geothermal gradient and negligible deviatoric stresses at depth, variations of the melt production at any given depth due to surface ice building/melting and erosion can be inferred from modelled loading/unloading histories beneath an eroding ice sheet responding to such a climate signal.

### **Results:**

Our numerical experiments are capable of linking self-consistently short- and long-term observational constraints and suggest that the observed rates of glacial erosion imply comparable contributions to the magma production by continental unloading from ice melting during the deglaciation and surface erosion.

### **Implications:**

Degassing associated with mantle melting injects chemically and physically active gases and aerosol particles into the atmosphere, which affect climate and weather changes (Cole-Dai, 2010). The decompression of volatile saturated magmas also drives gas exsolution, which increases the probability of eruption and degassing events to occur as well as the amount of volatiles potentially released in the atmosphere (Jellinek and De Paolo, 2003). While many other physical and biological feedbacks in the ocean are certainly involved, our results suggest that erosion may play a role as important as that of ice building/melting in controlling the emissions of greenhouse gases from the solid Earth across continental domains. Although the forcing of climate oscillations on submarine

volcanisms is debated (Olive et al., 2015), sea-level rise following continental ice melting seems able to reduce the magma production of mid oceanic ridges (Crowley et al., 2015), in turn buffering the increased subaerial volcanic and degassing activity owing to continental unloading by the deglaciation (e.g., Huybers and Langmuir, 2009). Such a buffering mechanism, however, does not apply to continental unloading by erosion because loading by sediment deposition in the ocean is unlikely to occur atop of oceanic ridge. Therefore continental erosion may have greater net effects than ice building/melting on the CO<sub>2</sub> outflux and magma production from the solid Earth.

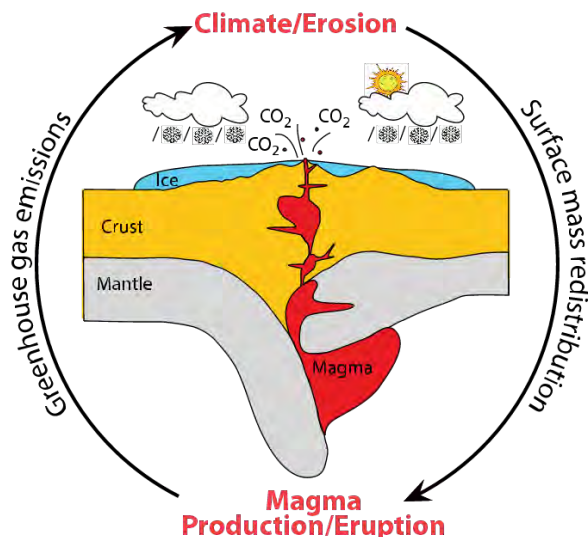


Figure 2: Schematic representation of the proposed feedback between surface and deep processes. Building and melting of erosive continental glaciers and ice-sheets throughout climate cycles control the redistribution of ice, water and rock masses across the Earth's surface and affect the magma production by mantle decompression melting. In turn, the eruption of magma at the Earth's surface affects the atmospheric greenhouse gas budget and feedbacks on climate and weather.

## References:

- Cole-Dai, J. 2010. "Volcanoes and Climate." Wiley Interdisciplinary Reviews: Climate Change 1(6): 824-839.
- Crowley, J. W., R. F. Katz, P. Huybers, C. Langmuir, and S-H Park. 2015. "Glacial cycles drive variations in the production of oceanic crust." *Science* 347(6227):1237-1240.
- Hallet, B., L. Hunter, and J. Bogen. 1996. "Rates of erosion and sediment evacuation by glaciers: A review of field data and their implications." *Global and Planetary Change* 12:213-235.
- Hardarson, B. and G. Fitton. 1991. "Increased mantle melting beneath Snaefellsjökull volcano during Late Pleistocene deglaciation." *Nature* 353:62-64.
- Herman, F., D. Seward, P. G. Valla, A. Carter, B. Kohn, S. D. Willett, and T. A. Ehlers. 2013. "Worldwide acceleration of mountain erosion under a cooling climate." *Nature* 504.
- Huybers, P. and C. Langmuir. 2009. "Feedback between deglaciation, volcanism, and atmospheric CO<sub>2</sub>." *Earth and Planetary Science Letters* 286:479-491.
- Jellinek, A. M. and D. J. De Paolo. 2003. "A model for the origin of large silicic magma chambers: precursors of caldera-forming eruptions." *Bulletin of Volcanology* 65(5):pp.363–381.
- Lisiecki, L. E. and M. E. Raymo. 2007. "Plio–Pleistocene climate evolution: trends and transitions in glacial cycle dynamics." *Quaternary Science Reviews* 26:56-69.
- Olive, J-A., M. D., Behn, G., Ito, W. R., Buck, J., Escartín, & S., Howell. 2015. "Sensitivity of seafloor bathymetry to climate-driven fluctuations in mid-ocean ridge magma supply." *Science* 350.6258: 310-313.

**Keywords:** Glacial cycles, erosion, magma production, volcanic activity, solid Earth-atmosphere geochemical exchange.

## Evolution of drainage and patterns of sedimentation in an experimental wedge

Marc Viaplana-Muzas<sup>1,2</sup>, Julien Babault<sup>2</sup>, Stephane Dominguez<sup>3</sup>, Jean Van Den Driessche<sup>4</sup> and Xavier Legrand<sup>5</sup>

<sup>1</sup>) Universitat de Barcelona. Facultat de Geologia, 08028, Barcelona, Spain.

<sup>2</sup>) Universitat Autònoma de Barcelona. Departament de Geologia, 08193 Bellaterra, Spain.

<sup>3</sup>) Université Montpellier. Géosciences Montpellier, II, F-34095, Montpellier, France.

<sup>4</sup>) Université de Rennes 1. Géosciences Rennes, Campus de Beaulieu, Rennes, France.

<sup>5</sup>) Petronas CariGali, Twin Tower KLCC, 50088, Kuala Lumpur, Malaysia.

Corresponding author: marc.via.mu@gmail.com

S2 - Coupling Tectonic and Surface processes (Oral)

### Introduction:

We used a deformation and erosion device that allows reproducing and monitoring the interactions between tectonics, erosion and sedimentation during the development of successive thrust sheets at different convergence and rainfall rates. We generated a synthetic mountain front that evolves with time and gives us the chance to study the evolution of the fluvial network and the landscape evolution associated with active tectonics. Our experiments adapt the experimental set-up proposed by Graveleau and Dominguez (2008). The deformation device is constituted by a basal film pulled beneath a static buttress. The film is overlaid by synthetic material made of glass microbeads, silica powder and plastic powder (PVC), which models the upper crust. The shortening induces deformation in the synthetic material and generates an accretionary wedge composed of imbricated thrusts. The rainfall system consists of sprinklers that produce water micro-droplets over the model. We monitored deformation during the experiments with an optical measurement bench composed by photograph cameras coupled to a laser interferometer that allows generating a Digital Elevation Model (DEM) and quantifying surface deformation.

### Drainage network evolution and implications on the patterns of sedimentation:

Drainage network exerts a first order control on erosion in mountain ranges. In a source-to-sink system, rivers erode source areas and transport the sediments to the adjacent basin (sink). The pathway of the drainage network within a mountain range defines the sediment pathway. During mountain building, the interactions between deformation and natural drainage-network evolution can result in river diversions, thus controlling the spacing between outlets and alter the patterns of sedimentation in basins. By varying the ratio of rainfall rate over shortening rate we can observe substantial differences in both; the drainage organization and along-strike variations in sedimentation patterns. With higher ratios between rainfall and shortening transverse channels are not diverted and they produce a line-source dispersal system developed in front of the active structure. At lower ratios channels merge in the backlimb of frontal structures, producing gridiron drainage patterns and in point-sourced depositional systems (Fig.1) separated by areas fed only by small channels developed in the external limbs (Viaplana-Muzas et al., 2015). The adjustment of the rivers to uplift rate and/or climate can reorganize the drainage network by divide migration and capture processes, as interpreted in some active mountains (Babault et al., 2012, Struth et al., 2015) where an early longitudinal drainage network is substituted by a new transverse drainage network. A river capture modifies the size of the catchments, resulting in rapid change in the sediment routing system and spatial distribution of erosion which potentially modify the sedimentation rates in the outlets and the composition of the sediments that infill the basins.

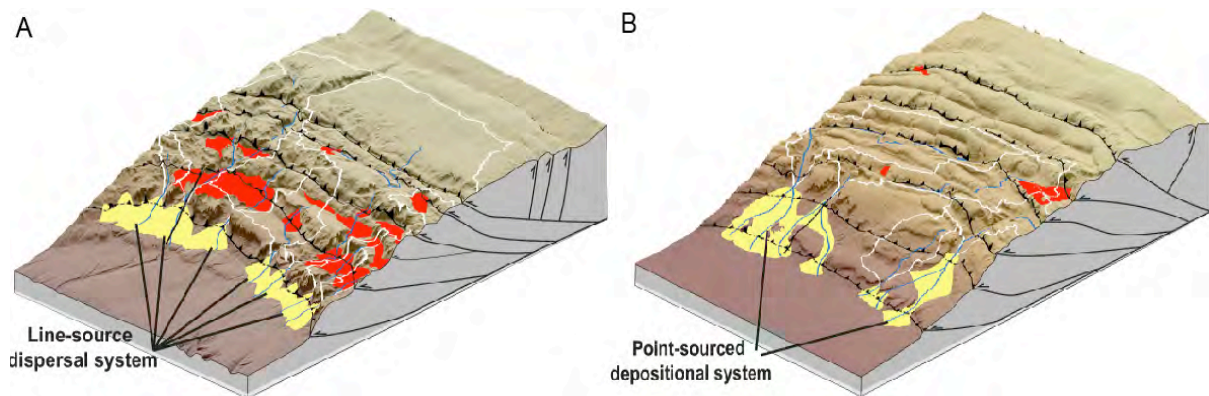


Figure 1. Patterns of sedimentation in two experiments run under low shortening rate (A) and high shortening rate (B). Rainfall rate is 9 mm/h in all experiments.

### References:

- Babault, J., Van Den Driessche, J., and Teixell, A., 2012, Longitudinal to transverse drainage network evolution in the High Atlas (Morocco): The role of tectonics: *Tectonics*, v. 31, no. 4, p. TC4020.
- Graveleau, F., and Dominguez, S., 2008. Analogue modelling of the interaction between tectonics, erosion and sedimentation in foreland thrust belts: *Comptes Rendus. Geoscience*, v. 340, no. 5, p. 324-333.
- Struth, L., Babault, J., and Teixell, A., 2015. Drainage reorganization during mountain building in the river system of the Eastern Cordillera of the Colombian Andes. *Geomorphology*, 250, 370-383.
- Viaplana-Muzas, M., Babault, J., Dominguez, S., Van Den Driessche, J., and Legrand, X., 2015. Drainage network evolution and patterns of sedimentation in an experimental wedge. *Tectonophysics*, 664, 109-124.

**Keywords:** Drainage network reorganization, source-to-sink system, sediment routing system, captures.

## Impact of pre-salt seamounts on supra-salt deformation of a salt-bearing passive margin: modelling the Western Mediterranean

Oriol Ferrer<sup>1</sup>, Oscar Gratacós<sup>1</sup>, Eduard Roca<sup>1</sup> and Josep Anton Muñoz<sup>1</sup>

<sup>1</sup>) Geomodels Research Institute. Grup de Geodinàmica i Anàlisi de Conques. Departament de Dinàmica de la Terra i l'Oceà. Universitat de Barcelona, Barcelona, Catalogne, Spain.

Corresponding author: joferrer@ub.edu

S2 - Coupling Tectonic and Surface processes (Oral)

### Introduction:

The Northwest Mediterranean Basin includes a thick Messinian salt sequence formed by three evaporitic units: 1) Lower Units (LU) including clastic turbidites with resedimented gypsum; 2) Mobile Unit (MU) composed by halite; and 3) Upper Unit (UU) containing dolomitic marls, marls and anhydrites (Lofi et al., 2011). The MU acts as a gravitational detachment favoring the downdip failure of the overlying sediments. As a result the structure of this margin is characterized by an upper extensional domain with basinward-dipping listric normal faults and a lower contractional domain that accommodates up-dip extension by folding, salt inflation or diapir squeezing. Nevertheless, this classic structural zonation can be locally disrupted by Lower to middle Miocene calc-alkaline volcanic edifices (Martí et al., 1992) that acting as a “barriers” awkward early gravitational gliding and hinder downslope salt drainage. These pre-salt reliefs modify the downslope salt flow and constraint the subsequent deformation of supra-salt cover during gravitational failure.

Using an experimental approach (sand-box models) this study aims to analyze the role played by these seamounts during the kinematic evolution of passive margins and how they alters salt flow and supra-salt deformation during gravitational gliding.

#### Experimental procedure

The experimental program consisted on seven analogue models including seamounts with different heights. Models were carried out in a glass-sided deformation rig that was 110 cm-long, 50 cm-wide and up to 15 cm-deep. The seamounts were built with plasticine and were attached to a basal plastic sheet remaining fixed throughout the experiment. The geometry of the analog salt basin consisted in an upslope panel dipping 30° and a vertical downslope edge built above four layers of 2.5 mm-thick. The LU was modeled using a 5 mm-thick layer of a volumetric mixture of sand and a silicone polymer giving a higher effective viscosity than pure polymer. Different colored polymer plugs located around the seamount were used as passive markers to trace the flow of the pure polymer during gravitational gliding (Dooley et al., 2009). The MU, was simulated using a 10mm-thick layer of pure polymer. Finally two layers of 2.5 mm-thick of green and white silica sand were used as analog of the UU. Gravitational gliding started after to tilt the baseboard of the rig 4.5°. Different syn-kinematic layers of white and red silica sand were added at intervals of two hours.

### Results and conclusions:

The presence of a seamount favors the early development of two gravitational sub-systems up- and downslope with their corresponding extensional and contractional pairs. Whereas upslope the contraction is characterized by polymer inflation and thrusting, a listric normal growth fault dipping basinwards developed in the downdip flank. This listric fault constraints the development of a basin on its hangingwall. As the margin failure continue the cover overthrusts the seamount and is passively transported downdip by gliding using the pure polymer as a detachment. When this occurs, the

previous sub-systems are reconnected as a unique system. The structural style of the experiments dramatically changes when salt depletion took place below the basin. Overthrusting and welding force the development of a second contractional zone downdip of the seamount (Fig. 1). A local unconformity developed above this contractional zone formed by a break-back thrust system (Fig. 1).

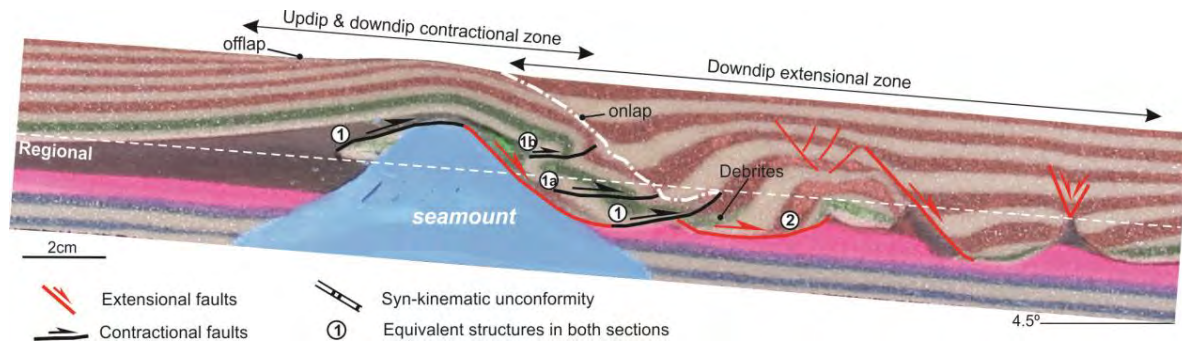


Figure 1: Detailed cross-sections of experiment 5 after 18 hours showing the main structures produced by the seamount during gravitational gliding. Whereas the pure polymer (blackish color) acts as a detachment, the pink layer (mixture of sand and pure polymer) was deformed after the depletion of pure polymer.

The kinematic evolution is clearly controlled by polymer flow velocity during gravitational gliding and by the dip differences between the flanks and the edge of the seamount. According to the evolution pattern we have defined a new deformation mechanism we called “roller coaster” by the similarity between both. During early gravity gliding, flow velocity upslope the seamount is basically reduced by buttressing. This is clearly dependent on the seamount shape. When the polymer reaches the apex of the seamount, the flow accelerates and descends rapidly throughout the downdip flank. On the seamount edge the flow velocity decrease again especially if the thickness of the source layer is progressively reduced by welding.

## References:

- Dooley, T.P., Jackson, M.P.A., Hudec, M.R., 2009. Inflation and deflation of deeply buried salt stocks during lateral shortening, *Journal of Structural Geology*, 31, 582-600.
- Lofi, J., Déverchère, J., Gaulier, V., Gillet, H., Gorini, C., Guennoc, P., Loncke, L., Maillard, A., Sage, F., Thinon, I., 2011. Seismic atlas of the “Messinian Salinity Crisis” markers in the Mediterranean and Black Seas. Commission for the Geological Map of the World (CGMW). Mémoires de la Société Géologique de France, 179, 72pp. 1CD.
- Martí, J., Mitjavila, J., Roca, E., Aparicio, A., 1992. Cenozoic magmatism of the Valencia Through (Western Mediterranean): relationship between structural evolution and volcanism, *Tectonophysics*, 203, 145-165.

## **Landsliding of rock columns by thermo-mechanical wedging-ratcheting: Study cases from the ‘Grands Causses’ gorges (Southern France)**

Alfredo Taboada<sup>1</sup>, Hadrien Ginouvez<sup>1</sup>, Mathieu Renouf<sup>2</sup>, Pierre Azemard<sup>3</sup>

<sup>1</sup> Laboratoire Géosciences Montpellier, UMR 5243, Université de Montpellier, France

<sup>2</sup> Laboratoire de Mécanique et Génie Civil, UMR5508, Université de Montpellier, France

<sup>3</sup> CEREMA, Direction Territoriale Méditerranée, Laboratoire d'AIX en Provence, France

Corresponding author: taboada@gm.univ-montp2.fr

S2 - Coupling Tectonic and Surface processes (Oral)

### **Abstract:**

The ‘Grands Causses’ is located in the southern part of the Massif Central (France) and it comprises several plateaux that are extensively incised by gorges showing vertical cliffs of decametric scale (10 – 100 m). Cliff geometry is mostly controlled by preexisting discontinuities (fractures and joint sets) that cut across massive limestone and dolomitic layers.

The observed erosion mechanisms in the bounding cliffs involve landslide processes such as rock falls, rock topples and slides. Field observations suggest that landslides are initiated by the incremental enlargement of steeply dipping discontinuities that progressively detach and separate rock columns or larger cliff portions in the direction of the free boundary. Discontinuities (e.g., fractures) have varying scales, and may cut across the entire cliff, and may be enlarged up to metric distances.

The incremental enlargement of fractures is linked with seasonal temperature oscillations in relation with movement of rock blocks that are blocked inside the fractures. The mechanism involves two successive stages in which rock blocks create a wedging and a ratcheting effect on the rock column.

Wedging is associated with compressional forces acting on the rock column, resulting from temperature increase and dilation of shallow rock material in the uphill main cliff, the blocks and the emerged part of the rock column. On the contrary, the base of the rock column, which is often buried beneath a thick layer of talus deposits, remains at relatively constant temperature and exhibits negligible volume changes. Thermal dilation tends to close the fracture inducing compressional forces in the blocks and an active lateral pressure on the rock column; if compressional forces are large enough the rock column moves outward an incremental (submillimetric) distance along a basal shear surface (e.g. a landslide) while the fracture is enlarged.

Ratcheting is associated with the downward displacement of blocks by gravity to a new equilibrium position, resulting from temperature decrease and contraction of the cliff – blocks – rock column system. Downward block movement sets the initial condition for the next wedging cycle as the temperature rises.

The model involving thermo-mechanical wedging-ratcheting is based on many field observations and it has been constrained with data from an instrumented rock column 50 m high for which displacement and temperature measurements are available over 3 years. The annual displacement shows an overall concave geometry, and the net displacement is roughly 1.6 mm/yr dipping downward 30° toward the free boundary. Temperature cycles composed of cooling and heating phases have periods between 3-15 days. The amplitudes of cooling and heating phases vary over the seasons, and control the enlargement of the fracture and plastic deformation along the shear plane beneath the rock column. Different behaviors are observed during three distinctive periods (winter, spring to summer and summer to autumn).

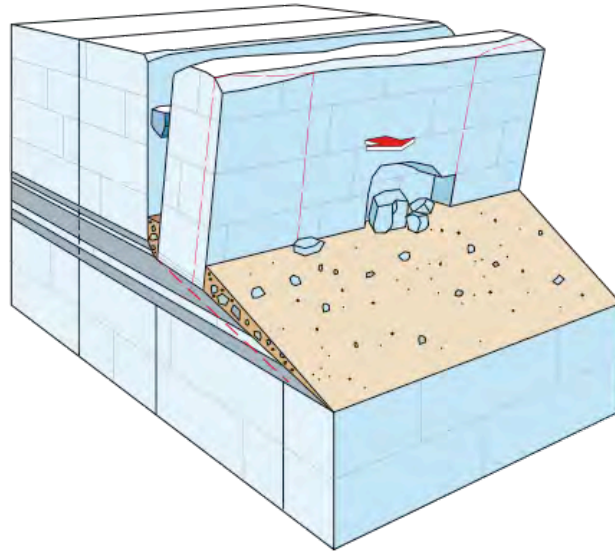


*Figure 1: Block-diagram illustrating the wedging effect of blocks located inside a vertical fracture; the external portion of the cliff moves outward as temperature rises and external rock material dilates.*

## Long-term crustal relaxation of large meteorite impact structures: influence of rheological layering of target rock on crater floor fracture patterns

Stephanie Teuber<sup>1</sup>, Matthias Rosenau<sup>2</sup>, Sascha Brune<sup>2</sup> and Ulrich Riller<sup>1</sup>

<sup>1</sup>) University of Hamburg, Hamburg, Germany

<sup>2</sup>) Helmholtz Centre Potsdam, GFZ – German Research Centre for Geosciences, Potsdam, Germany

Corresponding author: rosen@gfz-potsdam.de

S2 - Coupling Tectonic and Surface processes (Oral)

### Introduction:

Hypervelocity meteorite impact is now recognized as a fundamental geological process of the solar system. In particular, large meteorite impact is paramount for understanding (1) the evolution of the early Earth, (2) the geological modification of Earth's crust and surface, (3) the evolution of life and (4) the formation of giant natural resource deposits. The largest known terrestrial impact structures, Chicxulub (Mexico), Sudbury (Canada) and Vredefort (South Africa), are on the order of 200 km in diameter and formed within less than 10 minutes. Hypervelocity impact processes of this caliber require a transient loss in target rock cohesion, which is typically modelled using hydro codes.

The presence of fractures in crater floors of the Moon and Mercury (Fig. 1d - f) and dikes in target rock of the Vredefort and Sudbury impact structures consisting of largely differentiated impact melt indicates that impact structures, notably large ones, undergo long-term crustal relaxation associated with discontinuous deformation. The duration of this process, which entails post-impact cooling and isostatic re-equilibration of crust, as well as the cause for the variable geometry of crater floor fractures showing radial, concentric and polygonal patterns are not well known. We focus on the isostatic component of crustal re-equilibration on floor fracture patterns by means of analogue modeling using viscous and granular materials scaled respectively to a terrestrial lower and upper crust. Analogue modelling is complemented by numerical modelling in order to constrain the influence of cooling and strain rates on the crustal strength profile. The study highlights the significance of rheological layering on the formation of distinct crater floor fracture patterns. Our results may help to constrain pre-impact target rock configurations on other planets.

### Method:

The starting conditions driving isostatic relaxation of model crust are flat topographic depressions (Fig. 1a-c) resembling crudely the morphology of large craters imparted in brittle layers. In nature, viscous flow in the lower crust and the yield strength of brittle crust resist isostatic re-equilibration on crustal scale. We set up experiments in which we varied the thicknesses of brittle layers, composed of a sand-flour mixture, and the viscous layers, modelled by silicon oil. The density difference  $\Delta\rho$  of these layers is approximately 2-3 %. Except for the area occupied by the model crater, the initial total layer thickness is 10 cm, corresponding to 35 km in nature, in all experiments. To explore the geometric variation of floor fractures with crater diameter and crater depth, both were varied respectively from 80 to 120 mm and from 5 to 10 mm. Surface deformation was monitored by Particle Image Velocimetry at micrometer resolution.

### Results:

The numerical models indicate that thermal relaxation of the impact lasts on the order of 10 Myr. However, because of the high initial strain rates and rapid surficial cooling, a thin (<5 km thick) brittle crust is attained within less than 10 kyr. The decrease in strain rate and simultaneous cooling of the

deeper crust causes the crustal strength profile to be rather stable during the first 1 Myr (e.g. a strain rate decrease by one order of magnitude counterbalances cooling by 50°C). This result justifies our starting condition of a brittle layer with uniform thickness to model the geometric evolution of crater floor fractures caused by long-term crustal relaxation.

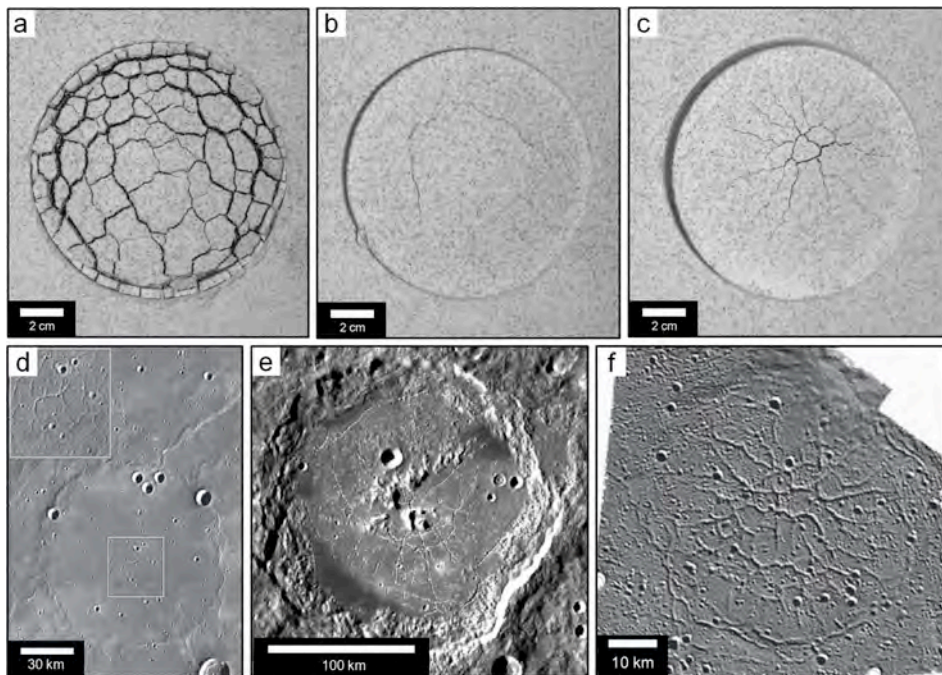


Fig. 1: Experimental (a - c) and equivalent natural (d - f) crater floor fracture patterns, which are polygonal (a, d), concentric (b, e) and radial (c, f). (d) and (e) are from Watters et al. (2012). (d) is from Jozwiak et al. (2012).

The analogue experiments show three distinct crater floor fracture patterns, which can be attributed to combinations of a specific rheological layering and crater depth. Pattern 1 is characterized by polygonal fractures (Fig. 1a) and occurs in deep craters hosted in thin brittle layers. Pattern 2 is made up of concentric fractures (Fig. 1b) and is more prominent in shallow craters imparted in thin brittle layers. Pattern 3 is displayed by radial fractures (Fig. 1c) and is observed in deep craters hosted in thick brittle layers. Shallow craters embedded in thick crust did not result in any measurable surface deformation, let alone visible fractures in model craters. Our analogue modelling results indicate that isostatic equilibration of material underlying the model crater and fracture-induced dilation are non-linear. This deformation is characterized by a uniform deceleration in strain rate until approximately 15 minutes, corresponding to ca. 10 kyr in nature, after onset of relaxation. Uplift of the crater floor is consistent with Airy isostasy modified by a yield criterion corresponding to the integrated strength of the brittle upper crust below the crater floor.

#### References:

- Jozwiak, L.M., Head, J.W., Zuber, M.T., Smith, D.E., Neumann, G.A., 2012. Lunar floor -fractured craters: Classification, distribution, origin and implications for magmatism and shallow crustal structure. *Journal of Geophysical Research* 117, E11005.
- Watters, T.R., Solomon, S.C., Klimczak, C., Freed, A.M., Head, J.W. Ernst, C.M., Blair, D.L., Goudge, T.A., Byrne, P.K., 2012. Extension and contraction within volcanically buried impact craters and basins on Mercury. *Geology* 40, 1123-1126.

**Keywords:** Meteorite impact, crustal relaxation, isostasy, fracturing, numerical, analogue, modelling.

## **Transverse- to longitudinal-dominated drainage network reorganization process: from nature to experimental modelling**

Julien Babault<sup>1</sup>, Marc Viaplana-Muzas<sup>2</sup>, Stéphane Dominguez<sup>1</sup>, Jean Van Den Driessche<sup>3</sup> and Xavier Legrand<sup>4</sup>

<sup>1</sup>) Université Montpellier. Géosciences Montpellier,II, F-34095, Montpellier, France

<sup>2</sup>) Universitat de Barcelona. Facultat de Geologia, 08028, Barcelona, Spain

<sup>3</sup>) Université de Rennes 1. Géosciences Rennes, Campus de Beaulieu, Rennes, France

<sup>4</sup>) Petronas CariGali, Twin Tower KLCC, 50088, Kuala Lumpur, Malaysia

Corresponding author: Julien.Babault@gmail.com

S2 - Coupling Tectonic and Surface processes (PS7)

### **Introduction:**

Accretionary orogens are generally considered as Coulomb wedges that display a taper geometry with a general slope from the backstop to the front of deformation. The mechanical properties of the material accreted in a wedge are known to control the magnitude of the taper angle. Surface processes have been shown in numerical and experimental models to be capable of controlling the patterns of fault propagation and exhumation style.

But it is generally accepted that in accretionary orogens rivers follow the regional slope (taper angle). This view has been supported by a compilation of drainage network organization that shows most of rivers in orogens to be transverse, i.e., perpendicular to tectonic trend. However, thrusts emerge at the front of accretionary wedges and preexisting transverse rivers may be diverted where they can't incise uplifting folds and thrusts resulting in longitudinal reaches in backlimbs. Natural examples and models of accretionary wedges that combine surface processes and mechanical processes show that the ability to incise or not uplifting thrust sheets controls the number of diversions, and by extension drainage organization.

Studies of drainage dynamics during mountain building based on natural examples in the western High Atlas (Babault et al., 2012), the Colombian Andes and in the Central Range of Papua New Guinea (Figure 1) show that longitudinal drainage, inherited from early stages of fluvial organization, is replaced by transverse-dominated one. It has been proposed that regional slope amplification enhances the potential energy for erosion in transverse rivers by increasing their local slopes leading to captures of longitudinal reaches.

Such evolution from a longitudinal to a transverse-dominated drainage may represent a common mechanism of fluvial network development during mountain building. Here we validate these interpretations using an experimental approach.

The experimental set-up is described in Viaplana-Muzas et al (2015). The analogue material is composed of three different materials: glass microbeads, silica powder and plastic powder (PVC). It is submitted to shortening and erosion. Shortening induces material deformation and generates an accretionary wedge composed of imbricated thrusts. Rainfall in the experiment allows water runoff to generate both diffusive erosion processes on hillslopes and incision/lateral erosion in channels. The models described in this study are a selection of the experiments analyzed in Viaplana-Muzas et al (2015) where all the models evolved under constant shortening rate and constant rainfall rate.

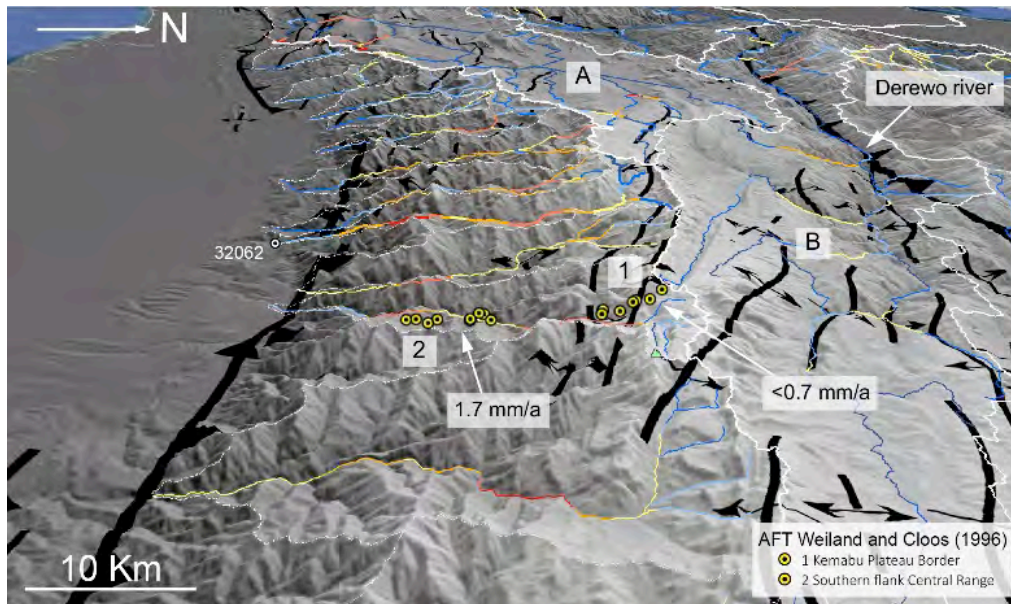


Figure 1: 3D view to the West of the upper Derewo river (catchment B) in the Central Range of Papua New Guinea. Colors indicate the steepness index values. The transverse rivers in the southern flank where erosion rate is 1.7 mm/a threaten to capture longitudinal reaches in the smooth and slowly eroding Kemabu plateau.

**Experimental set-up:**

**Drainage reorganization during accretionary wedge building:**

When a new thrust sheet emerges the topographic surface is folded. The external limb is incised by transverse channels. These transverse channels are the downstream part of preexisting transverse channels diverted by the emerging thrust sheet. The headwaters of these transverse channels propagate in the uplifting thrust by headward erosion toward the internal part of the wedges (ch2 in Figure 2). Headward erosion induces the migration of the water divide shared by longitudinal reaches in the backlimbs and transverse reaches in the forelimbs. A capture occurs when the headwater of a transverse channel reaches a longitudinal reach of another channel whose basin is located at a higher elevation. A capture creates an elbow of capture above the thrust sheet and the captured longitudinal reach suddenly starts to flow toward the captor's drainage basin.

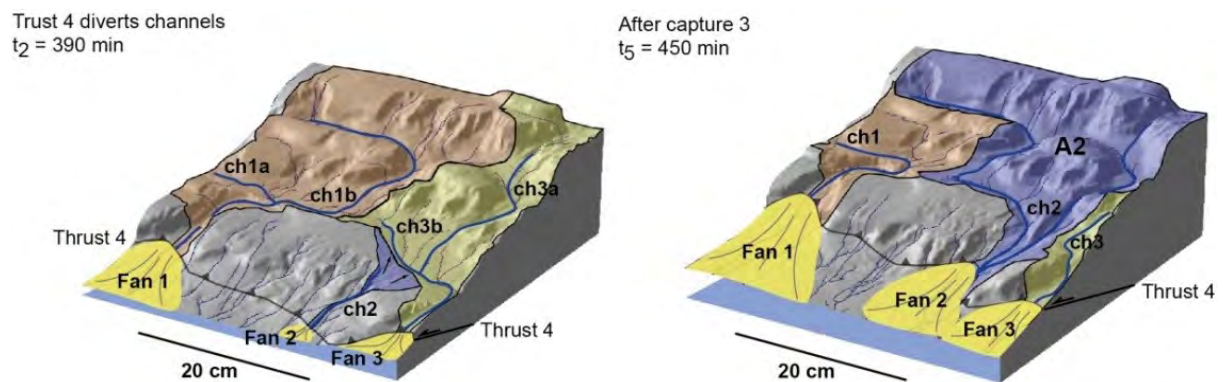


Figure 2: 3D view of an experiment showing drainage network reorganization during accretionary prism building under steady external forcing. Transverse channel ch2 captures the longitudinal reaches of channels

*ch3b and ch1b by headward erosion and three successive captures. This process is triggered by the surface uplift above thrust 4.*

Experiments show that reorganization from longitudinal to transverse drainage networks occurs under steady rainfall and shortening conditions. This behavior is controlled by the relation between mean headward erosion velocity and uplift rate. These results confirm the view that the evolution from a longitudinal to a transverse-dominated drainage is a transient stage of drainage evolution during mountain building.

## **References:**

- Babault, J., Van Den Driessche, J., and Teixell, A., 2012, Longitudinal to transverse drainage network evolution in the High Atlas (Morocco): The role of tectonics: *Tectonics*, v. 31, no. 4, p. TC4020.
- Viaplana-Muzas, M., Babault, J., Dominguez, S., Van Den Driessche, J., and Legrand, X., 2015, Drainage network evolution and patterns of sedimentation in an experimental wedge: *Tectonophysics*, v. 664, p. 109-124.

**Keywords:** Drainage network, rivers, analogue modelling, capture, mountain building, surface uplift, erosion.

**How to localize deformation in a salt detached foreland basin: results from analogue models and study of the Chazuta Thrust in the Huallaga Basin (Peru)**

Sandra Borderie<sup>1</sup>, Bruno C. Vendeville<sup>1</sup>, Fabien Graveleau<sup>1</sup>, César Witt<sup>1</sup>, and Pierre Dubois<sup>1</sup>

<sup>1</sup> Univ. Lille, CNRS, Univ. Littoral Cote d'Opale, UMR 8187, LOG, Laboratoire d'Océanologie et de Géosciences, F 59000, France

Corresponding author: [sandra.borderie@gmail.com](mailto:sandra.borderie@gmail.com)

S2 - Coupling Tectonic and Surface processes (PS7)

During mountain growth, fold-and-thrust belt widening generally occurs through a propagation of deformation toward the foreland basin. The accommodation of shortening is mainly localized and partitioned along faults and folds that detach on one or several décollements. This dynamics of deformation propagation depends on several parameters, such as the décollement's strength, the bulk rheology of the sedimentary pile, the intensity of surface processes (erosion, sedimentation), among others (Graveleau et al., 2012). In some rare cases, deformation can be very poorly partitioned but instead focuses on a very few structures. This is notably the case in the Huallaga Basin in the Sub-Andean zone of north Peru, where the major Chazuta Thrust accommodates more than 40 km of horizontal displacement, which represents more than 50% of the total shortening imposed to the foreland (Calderon et al., submitted). The Chazuta Thrust involves a salt-related detachment and is associated to a major syntectonic depocenter, the Biabo syncline. Interestingly, the allochthonous Chazuta thrust sheet has remained remarkably intact with little or no internal deformation (faults or folds) despite having been translated tens of km (Fig. 1.A).

In order to unravel the complex kinematic relationships between the Biabo syncline and the Chazuta Thrust, and with it the dynamics of highly localized deformation in a foreland basin, we have undertaken an analogue modeling study deforming a brittle sedimentary cover (made of dry sand) above a viscous décollement (made of silicone polymer). The experimental box was 85 cm long and 60 cm wide. The deformation rate was 5 mm/h. The 1.5 cm high basal silicone layer pinched out at 60 cm from the movable backstop, and was covered by either a constant thickness of brittle cover or a forward tapering brittle cover. We also tested lubrication along glass sidewalls, erosion, and sedimentation in some models. Our goal was to investigate the influence of these different parameters on the mechanisms of strain localization.

Model results confirm that the number of structures decreases (hence deformation is more localized) when the thickness of the brittle sedimentary cover increases (Liu et al., 1992). Additionally, a tapered brittle sequence above the viscous detachment (forming a brittle sedimentary wedge) favors the localization of deformation at the distal silicone pinchout. Finally, high syncontraction sedimentation, combined with local erosion of the deformation front contributes also to increase the amount of slip along the frontal thrust. We also tested the potential influence of the early subsidence of a synform located at the rear of the foreland domain. Interestingly, once the syncline had subsided into the viscous layer and touched the viscous layer's base, it acted as a bulldozer, causing silicone to thicken and flow toward the frontal thrust. It allows for alimenting continuously the frontal thrust in silicone and favors an unusually large horizontal slip, and the emplacement of a thick silicone layer in an allochthonous position. Finally, combining syncontractual erosion and sedimentation, and early backward subsidence led to the formation of a wedge where only one major thrust accommodates all the shortening (30% of the initial length) (Fig. 1.B).

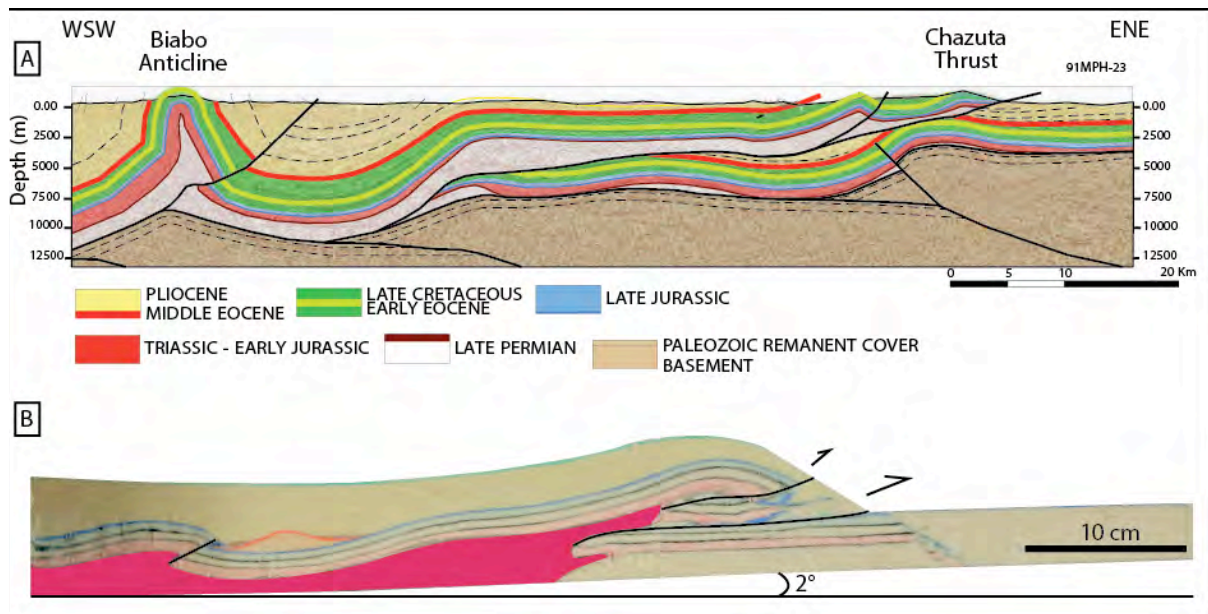


Figure 1: A: Cross-section of the Chazuta Thrust in the Huallaga Basin (Peru). The Chazuta Thrust involves a salt-related detachment (in white on the cross-section). B: Cross-section in a model which combined syncontractional erosion and sedimentation, and early backward subsidence. The viscous décollement is in pink.

This investigation helps to understand which mechanisms have likely controlled the formation of the Chazuta Thrust in the Huallaga basin. Our results suggest that an early high sedimentation rate at the rear of the Huallaga basin and a subsequent continuous sedimentation and erosion of the progressing Chazuta thrust sheet can explain the structural geometry and kinematics of the central part of the basin. The preservation of a thick syntectonic sedimentary series in the Biabo syncline seems to have played a crucial role in controlling the evolution of the Chazuta Thrust. Indeed, it contributed to thickening the evaporites under the Chazuta Thrust, helping him to accommodate more displacement.

## References:

- Calderon, Y., Baby, P., Vela, Y., Hurtado, C., Eude, A., Roddaz, M., Brusset, S., Calvès, G., Bolanos, R., Soumis, Petroleum systems restoration of the Huallaga-Maranon Andean retroforeland basin, Peru : p.1-38
- Graveleau, F., Malavieille, J., Dominguez, S., 2012. Experimental modelling of orogenic wedges: A review. *Tectonophysics* 538-540, 1–66. doi:10.1016/j.tecto.2012.01.027
- Liu, H., McClay, K., Powell, D., 1992. Physical models of thrust wedges, in: *Thrust Tectonics*. Springer, pp. 71–81.

**Keywords:** Huallaga Basin, Chazuta Thrust, analogue modeling, strain localization, surface processes.

## The Effect of syntectonic sedimentation on fold geometry: Insights from numerical modelling

Ana Carmona<sup>1</sup>, Oscar Gratacós<sup>1,3</sup>, Miguel López-Blanco<sup>1</sup>, Josep Anton Muñoz<sup>1</sup>, Roger Clavera-Gispert<sup>1</sup>, Pau Arbues<sup>1</sup>, Stuart Hardy<sup>1,2</sup>

<sup>1</sup>) GEOMODELS Research Institute, Universitat de Barcelona, Departament de Dinàmica de la Terra i de l'Oceà, Facultat de Ciències de la Terra

<sup>2</sup>) ICREA, Institució Catalana de Recerca i Estudis Avançats, Catalonia, Spain

Corresponding author: ogratacos@ub.edu

S2 - Coupling Tectonic and Surface processes (PS7)

### Introduction:

Syntectonic sediments have been widely studied to decipher the kinematic evolution of different geological systems and structures. Nonetheless, the control of sediment on the structural style or on fold geometry is more difficult to determine, since it is complicated to derive conclusions directly from the geological record, as only the final stage can be observed. Considering this, a numerical model is used to study the effect of syntectonic sedimentation on fold geometry specifically related to a delta progradation surrounded by two growing anticlines. The study is performed using a numerical model (Carmona et al. 2010) that merges deformation (DE code, Hardy et al. 2005) and sedimentation (SFM code, Gratacós et al., 2009).

Initial set-up and boundary conditions

The initial DE model (figure 1A) is defined with initial cohesion and a detachment level at the base of the model (with low cohesion). The model is tilted 1.6 degrees with an increasing bathymetry in y direction ranging from 51 to 861 m. Different shortening rates are defined perpendicular to y-axis from right to left, corresponding to fold growth rates of 0.1, 0.5, 1 and 2 mm/y. At the base, two velocity discontinuities (figure 1B) perpendicular to the shortening direction are defined acting as breaking points, which unleash in the formation of two folds. Total simulation time is 800ky. To this initial configuration, three different cases are considered, one without sediments, and two with the addition of syntectonic sediments and considering two different rates of sea-level rise (0.25mm/y and 0.5mm/y). The incoming water and sediment points are located in the boundary with the lowest bathymetry (figure 1A).

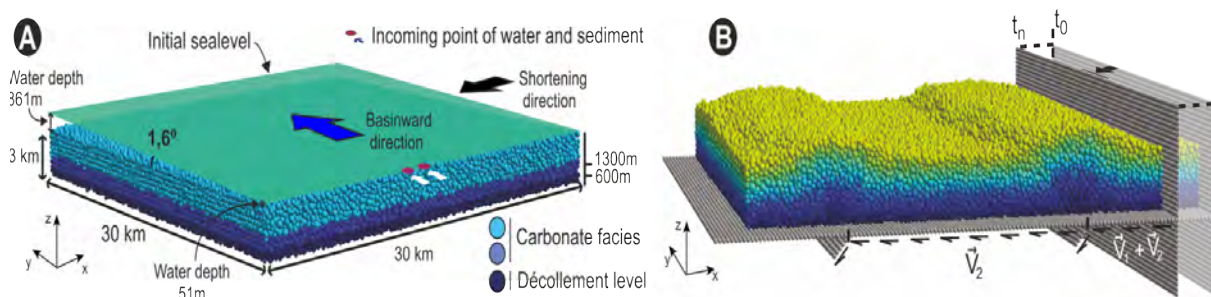


Figure 1: A - Initial set-up: the 3D DEM model colored by facies, tilted 1,6°. The reddish dots indicate the incoming point for water and sediment. B - DEM after 800ky illustrating the shortening direction and the discontinuities at the base. DEM is colored by layers, which are just for a visualization purpose, and they does not attend to any mechanical property.

**Results and conclusions:**

Example without sedimentation: two detachment anticlines with box-fold geometry are obtained over the discontinuities defined at the base of the model (figure 2A).

Example with sedimentation and a sea-level rise of 0.25m/y (figure 2B): the deposition of the new materials clearly controls the geometry of the left-side fold, showing a left-vergent asymmetric wide anticline. Moreover, the strain suggests that this anticline is passing from a detachment fold to a fault propagation fold basinwards. Structural changes are more noticeable where sediment settling is higher.

Example with sedimentation and a sea-level rise of 0,5 mm/y (figure 2C): the control of the syntectonic unit over the left-side anticline is more evident as a consequence of the increase in the accommodation space, e.g. the more proximal cross-section a-a' now is showing a fold-propagation fold instead of a detachment fold. Furthermore, the right-side anticline now is showing a right-vergent asymmetric geometry (cross-section b-b' figure 2C).

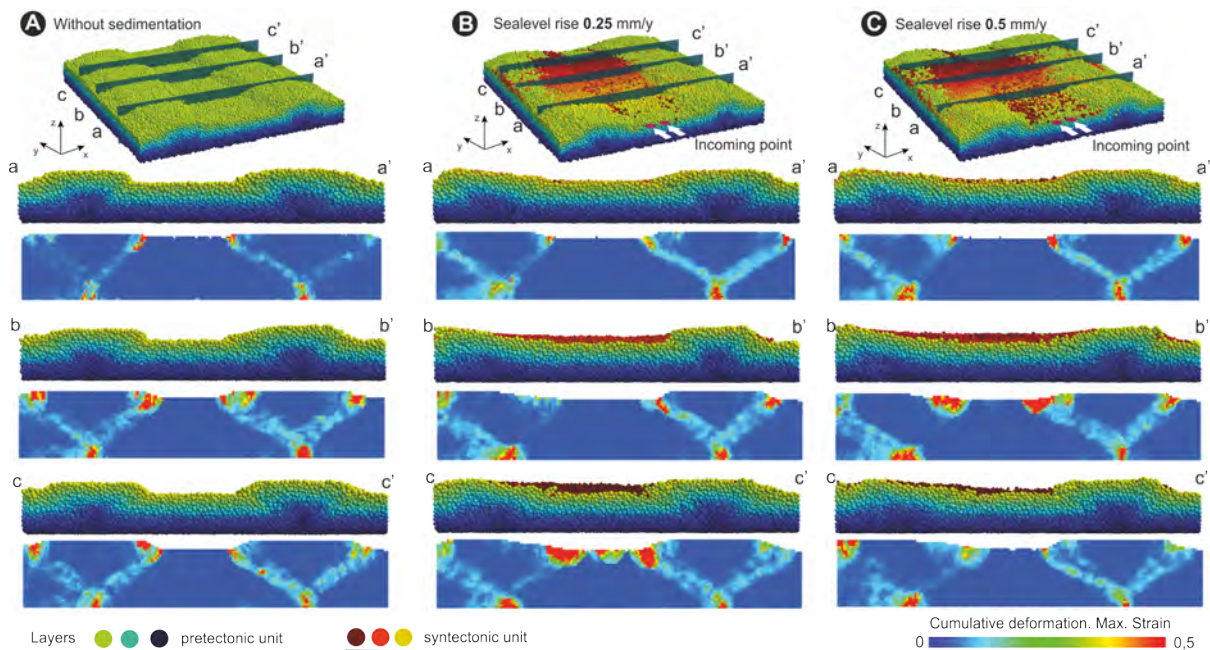


Figure 2- Cross-sections from the DE model for each sample experiment considering a fold growth rate of 1mm/y: without sediments (A) and two with syntectonic sedimentation considering two different sea-level rise, 0,25mm/y (B) and 0,5mm/y (C). Pre-tectonic unit is colored by layers, Yellow and reddish layers represent the syntectonic sediments added by SFM. The maximum strain for the pre-tectonic unit is also computed using the SSPX program.

**References:**

Carmona A., Clavera-Gispert R., Gratacós O., Hardy S., 2010. Modelling syntectonic sedimentation: combining a discrete element model of tectonic deformation and a process-based sedimentary model in 3D. *Mathematical Geoscience*, 42, 519-534

Gratacós O., Bitzer K., Cabrera L., Roca E., 2009. SIMSAFADIM-CLASTIC: a new approach to mathematical 3D forward simulation modelling for clastic and carbonate sedimentation. *Geologica Acta*, 7, 311-322

Hardy S., Finch E., 2005. Discrete-element modelling of detachment folding. *Basin Research*, 17, 507-520

**Keywords:** Syntectonic sedimentation, kinematic mechanics, fold geometry.

## Influence of ice shelf collapse on the flow of ice sheets grounded below sea-level: insights from analogue modelling

Giacomo Corti<sup>1</sup>, Antonio Zeoli<sup>2</sup>

<sup>1</sup>) Institute of Geosciences and Earth Resources, National Research Council of Italy (CNR), Florence Italy

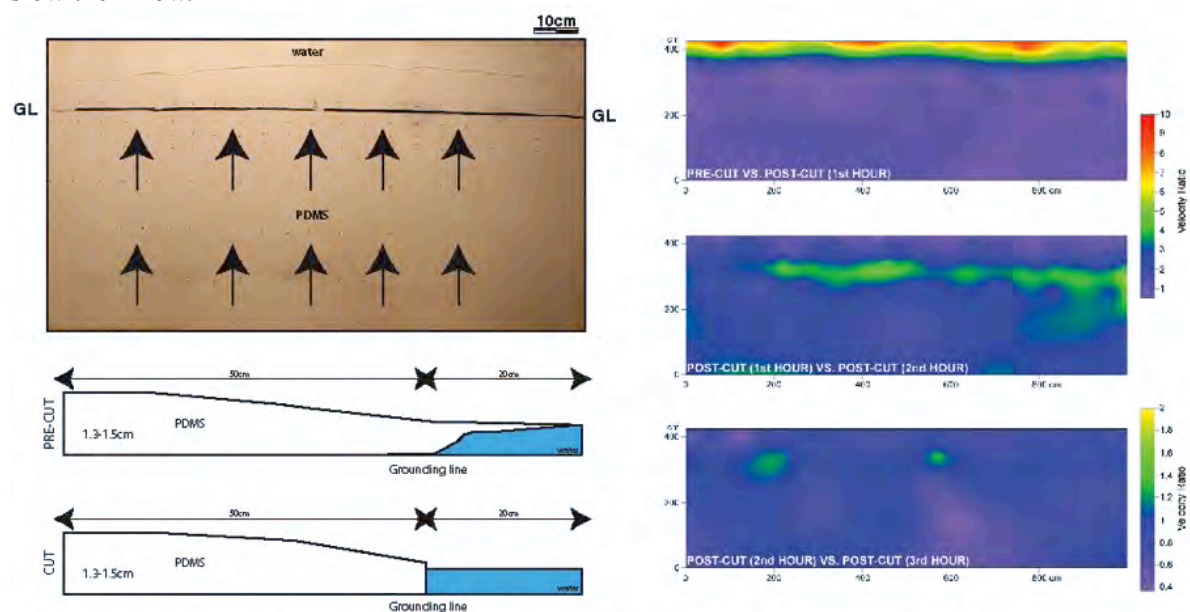
<sup>2</sup>) Museo Nazionale Antartide, Università degli Studi di Siena, via del Laterino, 8, 53100 Siena, Italy

Corresponding author: giacomo.corti@unifi.it

S2 - Coupling Tectonic and Surface processes (PS7)

The sudden breakup of ice shelves is expected to result in significant acceleration of inland glaciers, a process related to the removal of the buttressing effect exerted by the ice shelf on the tributary glaciers. This effect has been tested in previous analogue models, which however applied to ice sheets grounded above sea level (e.g., East Antarctic Ice Sheet; Antarctic Peninsula and the Larsen Ice Shelf).

In this work we expand these previous results by performing small-scale laboratory models that analyse the influence of ice shelf collapse on the flow of ice streams draining an ice sheet grounded below sea level (e.g., the West Antarctic Ice Sheet). The analogue models, with dimensions (width, length, thickness) of 120x70x1.5cm were performed at the Tectonic Modelling Laboratory of CNR-IGG of Florence, Italy, by using Polydimethylsiloxane (PDMS) as analogue for the flowing ice. This transparent, Newtonian silicone has been shown to well approximate the rheology of natural ice. The silicone was allowed to flow into a water reservoir simulating natural conditions in which ice streams flow into the sea, terminating in extensive ice shelves which act as a buttress for their glaciers and slow their flow.



**Left:** Top-view photo (upper panel) and schematic cross-sections (bottom panel) of the experiments. GL: grounding line; PDMS: Polydimethylsiloxane. **Right:** Velocity ratio among different stages of model evolution. Note the tenfold increase in velocity in the first hour after the floating platform has been removed

The geometric scaling ratio was  $10^{-5}$ , such that 1cm in the models simulated 1km in nature; a velocity of PDMS of 1 mm/hr simulated natural velocities of 100 m/year. Instability of glacier flow was induced by manually removing a basal silicone platform (floating on water) exerting backstresses to

the flowing analogue glacier: the simple set-up adopted in the experiments isolates the effect of the removal of the buttressing effect that the floating platform exerts on the flowing glaciers, thus offering insights into the influence of this parameter on the flow perturbations resulting from a collapse event.

The experimental results showed a significant increase in glacier velocity close to its outlet following ice shelf breakup, a process similar to what observed in previous models. However, this transient effect did not significantly propagate upstream towards the inner parts of ice sheet, and rapidly decayed with time. The process was also accompanied by significant ice thinning close to the grounding line. Models results suggest that the ice sheet is almost unaffected by flow perturbations induced by ice shelf collapse, unless other processes (e.g., grounding line instability induced by warm water penetration) are involved.

## Experimental drainage basins as markers of large-scale horizontal deformation

Laure Guerit<sup>1,\*</sup>, Stéphane Dominguez<sup>2</sup>, Jacques Malavieille<sup>2</sup>, Sébastien Castellort<sup>1</sup>

<sup>1</sup>) Département des Sciences de la Terre, Université de Genève, Rue des Maraîchers 13, 1205 Geneva, Switzerland.

<sup>2</sup>) Université de Montpellier, Géosciences Montpellier UMR5243, F-34095 Montpellier, France.

\*) current address: Géosciences Environnement Toulouse, 14 avenue Edouard Belin, 31000 Toulouse, France.

Corresponding author: laure.guerit@get.omp.eu

S2 - Coupling Tectonic and Surface processes (PS7)

The morphology of a fluvial landscape is a balance between its own dynamics and external forcings, and it can be used to reveal tectonic pattern or climate evolution. In particular, rivers have long been recognized as markers of localized horizontal deformation in strike-slip context and used to estimate fault slip velocity. However, deformation is not always partitioned on major faults only and in oblique context, it can be distributed over larger areas, as it is the case in the Southern Alps of New Zealand (Castellort et al, 2012). To better document and understand the regional dynamics of such systems, reliable markers of the horizontal tectonic motion over geological time scales are needed. River networks are able to record a large amount of distributed strain and they can thus be used to reconstruct the mode and rate of distribution away from major active structures.

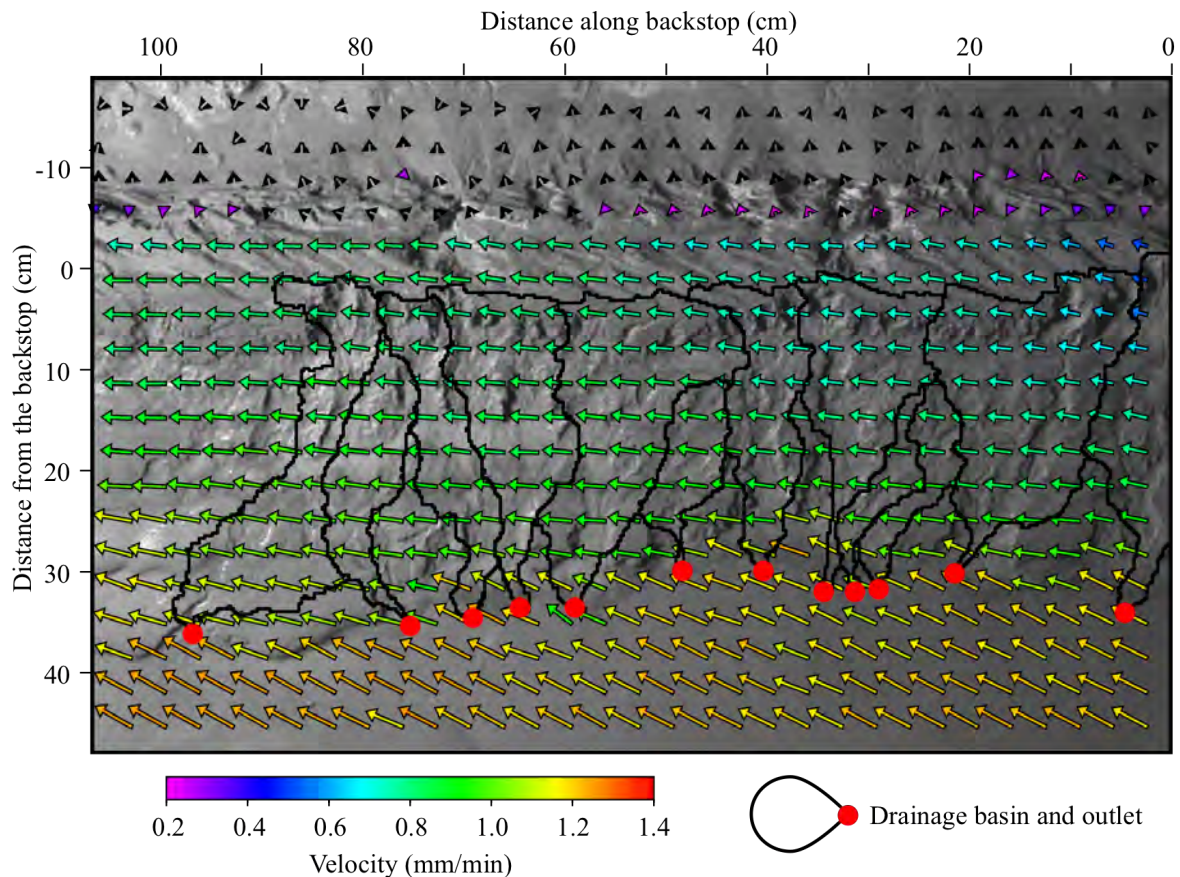


Figure 1: Main drainage basins developed on the surface of the experimental wedge and typical velocity field map from image correlation between two pictures. In response to the deformation field, the basins are rotated clockwise.

To explore the controls on river resilience to deformation, we used a sand-box experiment equipped with a rainfall system to model the evolution of a drainage network over a doubly-vergent orogenic wedge growing in a context of oblique convergence. Inspired by the geological and geodynamical context of the Southern Alps of New Zealand, we developed a new experimental material. This new granular mixture has a ductile behavior and allows the propagation of the deformation insuring a continuous growth of the wedge. However, when it reaches the surface, erosion takes place and drainage pattern can develop on its surface.

During the experiment, drainage basins are clearly rotated clockwise (Figure 1, Guerit et al, 2016). Image analysis of the time-space evolution of the landscape shows how the velocity field decreases toward the fault both in amplitude and in obliquity (Figure 1), and we show that this pattern is responsible for the rotation of the main trunk valleys. However, the rivers do not record the whole imposed rotation rate, suggesting that the channel dynamics competes with the passive deformation.

## References:

- Castelltort, S., Goren, L., Willett, S., Champagnac, J-D., Herman, F. and Braun, J., 2012. River drainage patterns in the New Zealand Alps primarily controlled by plate tectonic strain, *Nature Geoscience*, 5(10), 744-748.
- Guerit, L. and Dominguez, S. and Malavieille, J. and Castelltort, S., 2016. Deformation of an experimental drainage network in oblique collision, *Tectonophysics*, doi:10.1016/j.tecto.2016.04.016.

**Keywords:** Analogue experiment, Oblique collision, Drainage network, Deformation, New Zealand.

## **Active deformation and kinematics of the Calabria accretionary wedge (Ionian Sea): Constraints from high-resolution bathymetry and analog modeling**

Marc-Andre Gutscher<sup>1</sup>, David Dellong<sup>1,2</sup>, Heidrun Kopp<sup>3</sup>, Stephane Dominguez<sup>4</sup>, and Jacques Malavieille<sup>4</sup>

<sup>1</sup>) IUEM, Univ. Brest, CNRS, Laboratoire Domaines Oceaniques, Plouzane, France,

<sup>2</sup>) Géosciences Marines, Ifremer, Centre de Brest, Plouzané, France,

<sup>3</sup>) Helmholtz Center for Marine Research, Geomar, Kiel, Germany,

<sup>4</sup>) Geosciences Montpellier, Univ. Montpellier, Montpellier, France

Corresponding author: gutscher@univ-brest.fr

S2 - Coupling Tectonic and Surface processes (PS7)

### **Abstract:**

The Calabrian subduction in the central Mediterranean is a type example of a highly arcuate roll-back subduction. There is ongoing debate as to the geometry and activity of the associated lateral slab tear faults (Fig. 1). Two recent studies propose major dextral strike-slip displacement along two different NW-SE oriented structures; the North and South Alfeo faults (Gutscher et al., 2016) (Fig. 1B) or the Ionian Fault which forms the limit between the E and SW lobes of the accretionary wedge (Polonia et al., 2016) (Fig. 1C).

In the first model the entire accretionary wedge would be active, with deformation and thrusting throughout the external wedge caused by the SE-ward advance of both the Calabrian and the Peloritan blocks, serving as active backstops (Fig. 1B).

In the second hypothesis, the Peloritan backstop has become fixed and only the Calabrian backstop advances, thus driving compression in the E-lobe and large-scale dextral shear along the Ionian Fault (Fig. 1C). Results from several recent geophysical surveys provide complete coverage of the seafloor bathymetry at a resolution of 60m and reveal morpho-sedimentary and tectonic structures in unprecedented detail (Fig. 1A).

Analog modeling using granular materials was applied to answer specific questions as to the kinematics of candidate faults. In one experiment silicone was used as well to represent the rheological behavior of the external Calabrian wedge formed over a detachment at the base of the Messinian evaporites. One experiment indicates that clockwise rotation predicted by large-scale dextral shear along the proposed Ionian Fault cannot produce the counterclockwise vortex-like morphology observed at the boundary between the two lobes of the accretionary wedge. A pair of experiments applied to the intersection of the W Mediterranean Ridge and Calabrian wedge suggests ongoing activity of both systems and thus favors continued shortening in the SW lobe of the accretionary wedge.

Finally, an experiment examined the origin of radial slip-lines observed to emanate from the sharp corner-shaped indenter formed by the internal clastic wedge and propagating 60-80 km into the external evaporitic wedge (Fig. 2). The experiment suggests this pattern can be caused by dextral shear along the South Alfeo Fault (Fig. 1B).

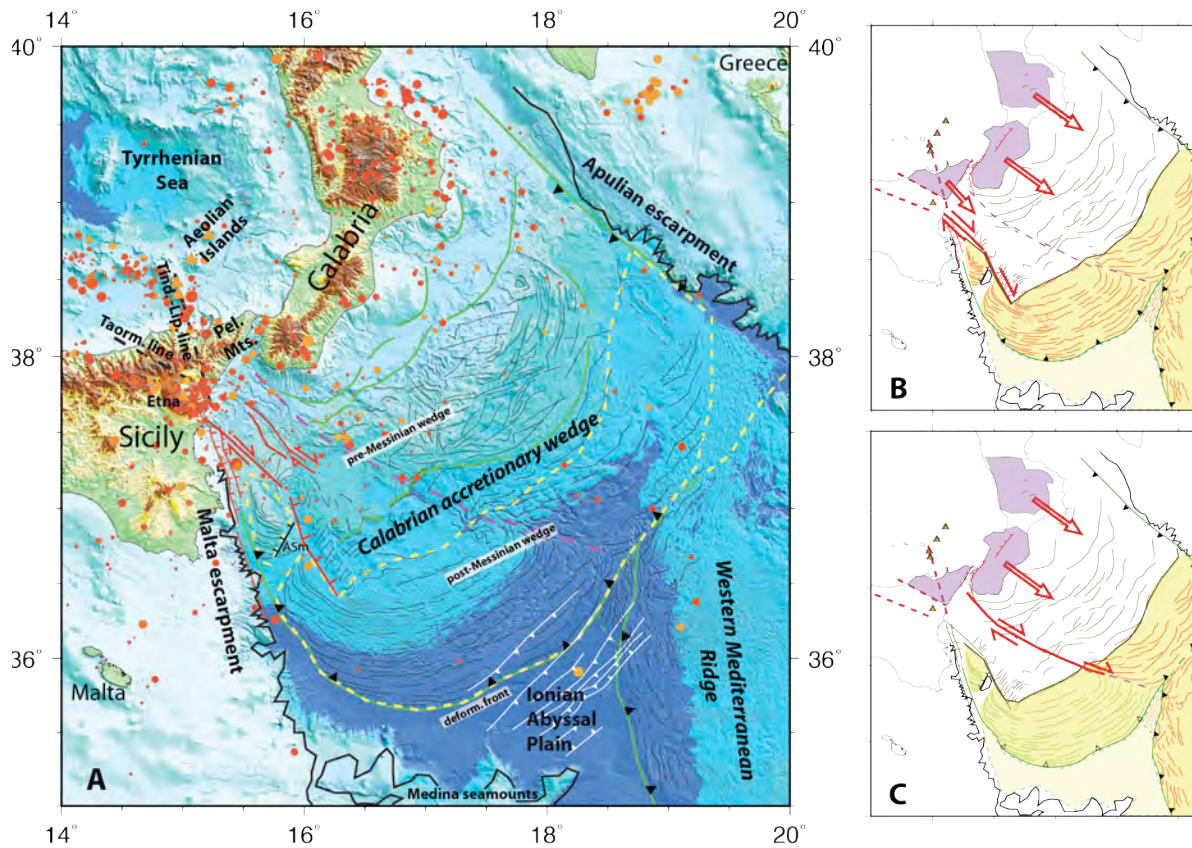


Figure 1: A: Tectonic map of the Calabrian arc/ Ionian Sea region with seismicity (NEIC Catalog 1973-2016) and relief (SRTM topography and a new bathymetric compilation at a 60m grid spacing). B: Kinematic model where the lateral slab tear fault is expressed by large-scale dextral strike slip motion along the North and South Alfeo faults (Gutscher et al., 2016). Compression occurs throughout the external wedge (thin red lines). C: Kinematic model where the major slab tear fault causes dextral strike slip motion along the Ionian Fault (dashed purple line) forming the limit between the E and SW lobes of the accretionary wedge (Polonia et al., 2016). Compression occurs only in the Eastern Lobe (thin red lines).



Figure 2: Analog modeling experiment with dextral strike slip along the lateral ramp of a modeled thrust wedge. (At left) The boundary between the backstop (pink) and the clastic (sand) wedge (green). Shortening causes thrusting in both the internal (clastic) wedge and an external viscous wedge (sand overlying a silicon layer). (At right) Slip-lines (transensional linear faults with minor displacement) propagate through the thrust wedge and towards the deformation front. These radiate from the rheologically stronger corner of the clastic wedge similar to the radial slip lines observed in the bathymetry (Fig. 1).

References:

Gutscher, M.-A., Dominguez, S., Mercier de Lepinay, B., Pinheiro, L., Gallais, F., Babonneau, N., Cattaneo, A., LeFaou, Y., Barreca, G., Micallef, A., and Rovere, M., 2016. Tectonic expression of an active slab tear from high-resolution seismic and bathymetric data offshore Sicily (Ionian Sea). *Tectonics*, v. 35, n.1, doi:10.1002/2015TC003898.

Polonia, A., Torelli, L., Artoni, A., Carlini, M., Faccenna, C., Ferranti, L., Gasperini, L., Klaeschen, D., Monaco, C., Neri, G., Nijholt, N., Orecchio, B., Wortel, R., Govers, R., 2016, The Ionian and Alfeo–Etna fault zones: New segments of an evolving plate boundary in the central Mediterranean Sea? *Tectonophysics*, v. 675, 69-90, doi:10.1016/j.tecto.2016.03.016.

**Keywords:** Subduction, accretionary wedge, Calabrian arc, Ionian Sea, Mediterranean, analog modeling, high-resolution bathymetry, lateral slab tear, strike-slip faults, indenter, slip-lines.

## The effect of fragmentation on rock avalanches: travel and deposit length

Øystein Thordén Haug<sup>1,2</sup>, Matthias Rosenau<sup>2</sup>, Karen Leever<sup>2</sup>, and Onno Oncken<sup>3</sup>

<sup>1</sup>) Physics of Geological Processes, University of Oslo, Norway

<sup>2</sup>) GFZ German Research Centre for Geoscience, Helmholtz Centre Potsdam, Germany

Corresponding author: o.t.haug@geo.uio.no

S2 - Coupling Tectonic and Surface processes (PS7)

### Introduction :

Rock avalanches are very large volume landslides (larger than  $10^6$  m<sup>3</sup>) with long travel lengths [Hsü, (1975)], which can cause dramatic changes to a landscape. The triggering of rock avalanches is often related to tectonic processes: they often fail along planes of weakness such as faults, and can be triggered by earthquakes. For an accurate description of their contribution to a landscape, one needs to understand the processes that control primary parameters, such as their travel length and the length of their deposits. The exceptional long travel lengths suggest that a weakening mechanism is at work during emplacement, which reduces the effective basal friction. Several mechanisms have been suggested in the literature, ranging from air cushioning to acoustic fluidization [see e.g. Legros (2002) and references therein]. A well-established observation is that travel length depends on the volume of the rock avalanche. However, large scatter in the data is observed: even for similar volume, the travel lengths are seen to span several orders of magnitude.

The deposits of rock avalanches are found to consist of highly fragmented material. Fragmentation has been suggested to increase their travel lengths, either by reducing basal friction by exploding fragments [Davies and McSavaney (2009)], reducing frictional interactions by fluidization of fine material, or simply by becoming more flow-like the smaller the particles become [Locat et al. (2006)]. However, no correlation has been found between the degree of fragmentation and the travel lengths [Locat et al. (2006)], and the effect of fragmentation on rock avalanches remains enigmatic. So how does the fragmentation affect the transport of rock avalanches? Here, we present simple analogue experiments of fragmenting analogue rock slabs that aim to answer this question.

### Experiments:

Taking advantage of a newly developed rock analogue material, we perform a series of experiments in a chute (see Figure 1). We vary the cohesion and geometry of the experimental samples, and measure the travel length of their front and deposit length and compare these to the degree of fragmentation.

To study the effect of fragmentation on similar conditions as a natural rock avalanche, we hypothesize a mechanism exists that lowers the basal friction, and use a basal coefficient of friction of 0.15. To quantify the degree of fragmentation we use the parameter ( $m_c$ ), which is the ratio between the sample's mass before an experiment and the mass of the largest fragment. Though very simple, it is a convenient measure, where  $m_c=1$  represent an intact sample and an increasing value represent an increasing degree of fragmentation.

### Competition between spreading and internal friction:

We present the travel length and deposit length of our experimental samples normalized by their fall height (Figure 2). The results show that between  $m_c=1$  and  $m_c=5$ , both the travel and deposit length increase, however, for higher values of  $m_c$  they decrease again. Careful visual inspection of the experiments suggests that these trends may result from a competition between spreading induced by

the fragmentation while at the same time the internal interaction between particles increase the more the material fragments. We compare our result to a set of natural data set from the literature [Locat et al. (2006)]. From this set of 9 rock avalanches, only 6 have comparable slope geometry as our setup. These 6 selected natural cases are seen to follow the same trend as our experiments, which provide confidence in our experimental results. The volumes of the 6 selected natural cases range over 2 orders of magnitude. That they are seen to follow the same trend as the experimental data, which we know have a constant basal friction, suggest that the variation of runout length may not depend on variations of basal friction, but rather on the degree of fragmentation.

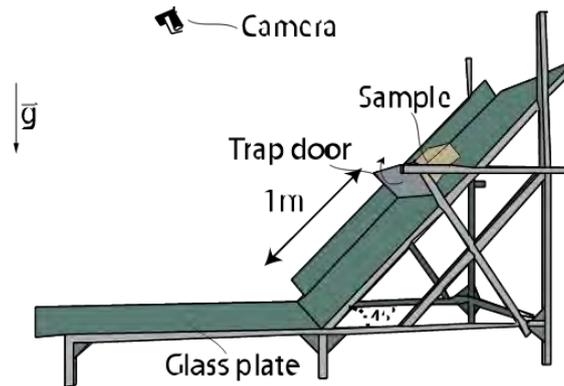


Figure 1: Experimental setup. A rectangular sample is released by opening the trap door, and it accelerates down the slope. When impacting on the horizontal plate, fragmentation may occur. After the impact, the sample slides on the horizontal plate before coming to rest. A camera captures the travel of the sample, and image analysis is used to quantify the travel length of the front and center of mass, and deposit length.

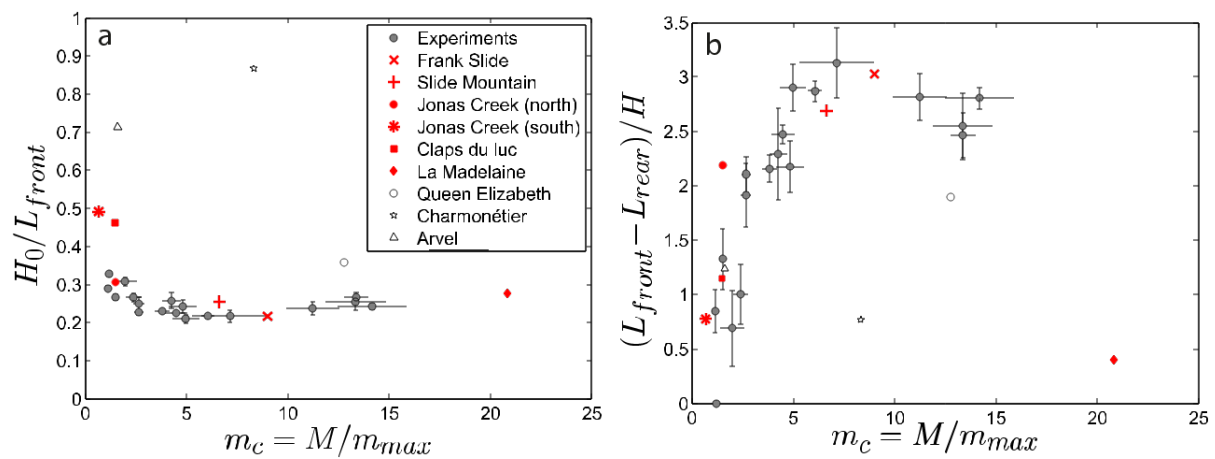


Figure 2: The relative travel length (a) and deposit length (b) of experimental (gray circles) and natural (red and open symbols) rock avalanches versus the degree of fragmentation. The experiments are observed to follow the same trend as the rock avalanches of comparable slope geometry (red symbols).

### References:

Davies, T. R., & McSaveney, M. J. (2009). The role of rock fragmentation in the motion of large landslides. *Engineering Geology*, 109(1-2), 67–79.

- Hsü, K. J. (1975). Catastrophic debris streams (sturzstroms) generated by rockfalls. *Geological Society of America Bulletin*, 86(50117), 129–140. Retrieved from <http://bulletin.geoscienceworld.org/content/86/1/129.short>
- Legros, F. (2002). The mobility of long-runout landslides. *Engineering Geology*, 63(3), 301–331. Retrieved from <http://www.sciencedirect.com/science/article/pii/S0013795201000904>
- Locat, P., Couture, R., Leroueil, S., Locat, J., & Jaboyedoff, M. (2006). Fragmentation energy in rock avalanches. *Canadian Geotechnical Journal*, 43(8), 830–851. <http://doi.org/10.1139/t06-045>

## Calibration of the landsliding numerical model SLIPOS and prediction of the seismically induced erosion for several large earthquakes scenarios

Louise Jeandet<sup>1</sup>, Dimitri Lague<sup>1</sup>, Philippe Steer<sup>1</sup>, Philippe Davy<sup>1</sup> and Mark Quigley<sup>2</sup>

<sup>1</sup>) University of Rennes 1, Geosciences Rennes, Rennes, France

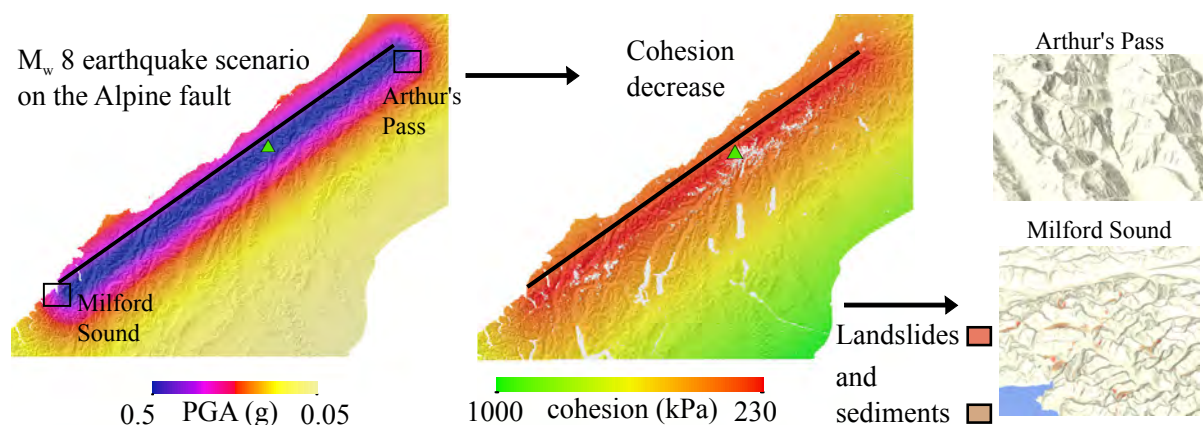
<sup>2</sup>) University of Melbourne, School of Earth Science, Melbourne, Australia

Corresponding author: philippe.steer@univ-rennes1.fr

S2 - Coupling Tectonic and Surface processes (PS7)

Coseismic landsliding is an important contributor to the long-term erosion of mountain belts. If the scaling between earthquake magnitude and the volume of eroded material is well known, the resulting geomorphic consequences, such as divide migration or valley infilling, are still poorly understood. Indeed, the prediction of the location of co-seismic landslides sources and deposits is a challenging issue and algorithms accounting for triggering of landslides by ground shaking are needed. Peak Ground Acceleration (PGA) has been shown to control at first order the spatial density of landslides. PGA can trigger landslides by two mechanisms: the direct effect of seismic acceleration on forces balance, and a transient decrease in hillslope strength parameters.

To test the accuracy of modelling seismic waves effect by a cohesion drop, we use SLIPOS, an algorithm of bedrock landsliding based on a simple stability analysis (Culmann criteria) applied at local scale, to model the spatial distribution of co-seismic landslides. The model is able to reproduce the landslide area-volume scaling relationship and the area-frequency distribution of natural landslides. Co-seismic landslide triggering is accounted for in SLIPOS by imposing a cohesion drop that is defined as a function of PGA. The spatial distribution of PGA is modeled using empirical relationships between earthquake source and PGA.



*Numerical modeling of earthquake-triggered landslide in the case of a magnitude 8 scenario for the Alpine fault in New-Zealand. Mechanical triggering of co-seismic landsliding is here modeled by a cohesion drop that we empirically express as a function of the seismic peak-ground acceleration.*

We run the model (i) on the Mw 7.6 Chi-Chi earthquake (1999) to quantitatively test the accuracy of the predictions and (ii) on earthquake scenarios (Mw 6.5 to 8) applied to the Alpine fault of New-Zealand to predict the volume of landslides associated with large magnitude earthquakes.

We demonstrate for the Alpine fault scenarios that simulating the effect of ground acceleration on landsliding using a cohesion drop leads to a realistic scaling between the volume of sediments and the earthquake magnitude.

**Keywords:** Landslides, earthquakes, numerical modeling, New-Zealand.

## What controls deformation in a bent three-dimensional orogen? An example from the Bolivian Andes

Lars Kaislaniemi<sup>1</sup>, David Whipp<sup>1</sup>

<sup>1</sup>) University of Helsinki, Department of Geosciences and Geography, Helsinki, Finland

Corresponding author: lars.kaislaniemi@helsinki.fi

S2 - Coupling Tectonic and Surface processes (PS7)

### Bolivian Andes:

The “Bolivian orocline” is a change in the orientation of the central Andes from N-S south of ~18°S in central Bolivia to roughly NW-SE to the north (Figure 1A). This bend coincides with ~50 % reduction in the width of the orogen east of the Altiplano, a significant increase in the yearly precipitation (Figure 1B), and the presence of a basement arch that reduces the thickness of relatively weak Paleozoic sediments upon which the orogen detaches. This has led to uncertainty about whether the growth of the orogen is controlled primarily by climate (erosion) or tectonics (e.g. Whipple and Gasparini 2014).

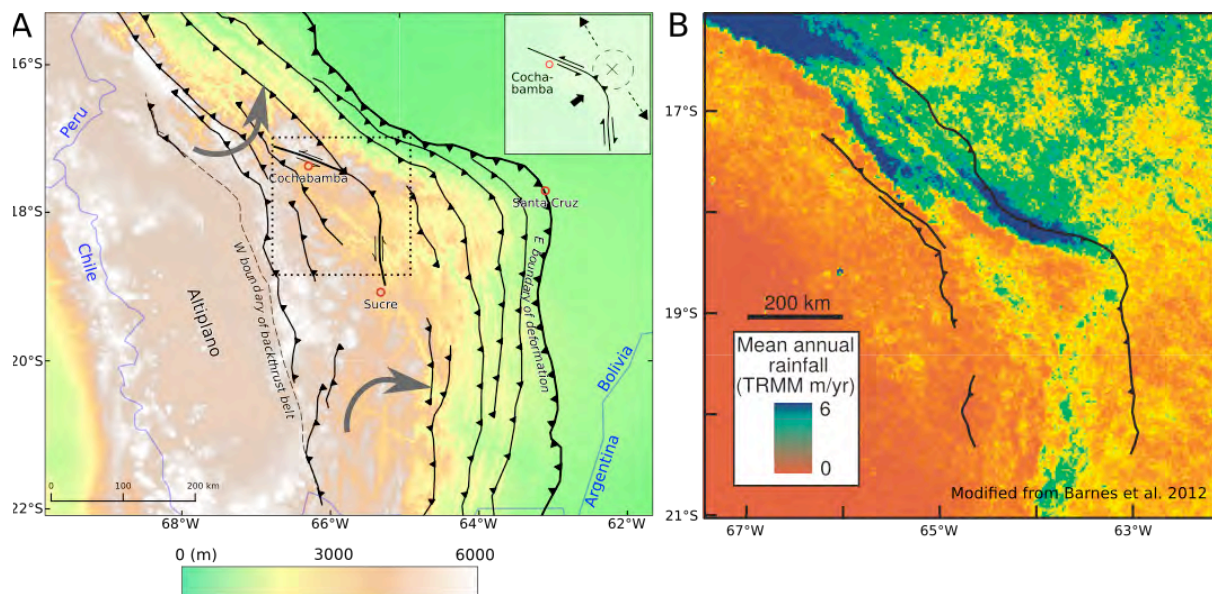


Figure 1: A) Topography of the Bolivian Andes with major structural features (from McQuarrie, 2002). Inset: Strike-slip faults near cities of Cochabamba and Sucre possibly accommodate shortening (after Dewey and Lamb, 1992). Gray arrows show direction of the rotational field deduced from paleomagnetic studies. B) Rainfall pattern in the Bolivian Andes region. Note the correlation between rainfall and width of the backthrust region. (Modified from Barnes et al. 2012).

The study of the kinematics in such three-dimensional oroclines is complicated by the fact that they are inherently three-dimensional and cannot be reduced to 2-D vertical cross-sections to reconstruct deformation. We aim to study deformation in a curved orogen to better understand how along-strike variations in rainfall and basal detachment strength affect orogen deformation. The presence of a rotational velocity/strain field near the orocline core is one of the manifestations of the orogen's 3D structure that complicate the experiments in the study area. Possibly caused by gradients in the amount

of shortening, radial material displacement, and local strain partitioning, these rotational fields south (clockwise) and north (counter-clockwise) of the orocline core (Figure 1A), deduced from paleomagnetic data, are still present and observable in GPS measurements.

### Methods and preliminary results

We use finite element code DOUAR (Braun et al. 2008) to solve the visco-plastic deformation in the retro-wedge of a curved Andean-style orogen, integrated with the surface process model FastScape (Braun and Willett 2013). Model setup comprises the crust in a 1000x1000x50 km box, including the fold-and-thrust belt east of the Altiplano and the basement of the western edge of the South American plate. A basal detachment zone with a change in its orientation is prescribed as an initially strain-softened (weak) region. Strain softening also allows development of new faults elsewhere and evolution of the geometry of the detachment zone. The effects of varying rock strength in the detachment zone and in the overlying rocks, orocline angle, and varying erosion rates (precipitation) along the orogen are considered to determine the primary control(s) on the geometry and evolution of curved orogens.

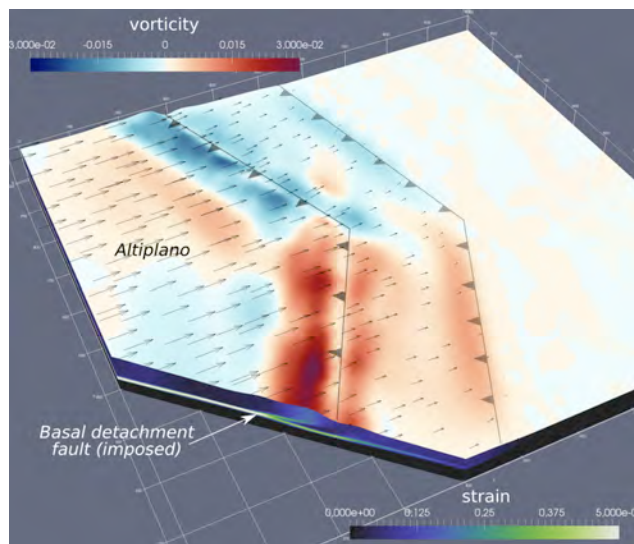


Figure 2: Preliminary results from a model where along-strike material properties are kept constant show a rotational velocity field (vorticity, in cyan-red, negative values counter-clockwise; black arrows: surface velocity) in the Andean orogenic wedge east of the Altiplano plateau, compatible with observations from the Bolivian Andes.

Preliminary results (Figure 2) with rotational fields of opposite directions south and north of the orocline bend show first-order similarity with the observed velocity/strain field. Minor along-strike mass transfer takes place along the length of the orogen, feeding material into the apex of the orocline.

### References:

- Braun, J., Thieulot, C., Fullsack, P., DeKool, M., Beaumont, C., Huismans, R., 2008. DOUAR: A new three-dimensional creeping flow numerical model for the solution of geological problems. *Physics of the Earth and Planetary Interiors*, 171, 76-91.
- Braun, J., Willett, S. D., 2013.. A very efficient  $O(n)$ , implicit and parallel method to solve the stream power equation governing fluvial incision and landscape evolution. *Geomorphology*, 180-181, 170–179.
- Dewey, J. F., Lamb, S. H., 1992. Active tectonics of the Andes. *Tectonophysics*, 205, 79-95.
- McQuarrie, N., 2002. The kinematic history of the central Andean fold-thrust belt, Bolivia: Implications for building a high plateau. *Bulletin of the Geological Society of America*, 114(8), 950–963.
- Whipple, K. X., Gasparini, N. M., 2014. Tectonic control of topography, rainfall patterns, and erosion during rapid post-12 Ma uplift of the Bolivian Andes. *Lithosphere*, 6(4), 251–268.

## Deep-seated Gravitational Slope Deformations in Pienza (Tuscany, Italy): Insights from 3D Modeling and Physical Analogue Experiments

A. Lazzarotto<sup>1</sup>, S. Izzo<sup>1</sup>, R. Aquè<sup>1</sup>, E. Tavarnelli<sup>1</sup> & G. Calabresi<sup>2</sup>

<sup>1</sup>) Dipartimento di Scienze Fisiche, della Terra e dell’Ambiente (DSFTA), Università degli Studi di Siena, Via Laterina 8, I-53100, Siena, Italy

<sup>2</sup>) ISSMGE Technical Committee 301 core member

Corresponding author: [senatro.izzo@unisi.it](mailto:senatro.izzo@unisi.it)

S2 - Coupling Tectonic and Surface processes (PS7)

### Introduction:

We attempt at modeling the effects of recent and active, deep-seated landslide movements that affect a historic-artistic Renaissance site, namely the city centre of Pienza (southern Tuscany, Italy), UNESCO heritage site. The site is located on the western edge of a relief of regional importance, the Chianti-Rapolano-Mt.Cetona Ridge, that corresponds to a positive structural high consisting of a mesozoic substratum. The city itself is built on a calcareous-arenaceous plateau some tens m thick, that overlies a pelitic unit of Lower Pliocene age. The city of Pienza owes its name to, and was committed by Pope Pius II, Enea Silvio Piccolomini (1405-1464) to the florentine architect Bernardo di Matteo Gambarelli, known as “il Rossellino” (1409-1464), who worked at the project between 1459 and 1462. Of particular artistic relevance is the Cathedral (Duomo) complex, flanked by the Bishop Palace and the Piccolomini Palace, that bound a trapezoid-shaped square; the peculiar shape of the square was designed to achieve a prospective convergence of its lines towards the horizon. The Cathedral (Duomo) complex is built on the south-western edge of the calcareous-arenaceous plateau, that laterally terminates in a sub-vertical cliff. The middle and absidal parts of the Cathedral (Duomo) are affected by a set of sub-vertical, sub-parallel fractures developed above the trace of a WNW-ESE trending normal fault belonging to a regionally important extensional fault system whose lateral continuity is interrupted and segmented by a ca. NE-SW trending transfer fault set. Creep along the abovementioned normal fault, already documented during the construction of the city, determined a slow downthrow and tilt of the absidal part of the Duomo, associated to development of several fractures in its walls. Initially “il Rossellino” thought that these fractures were due to hardening and dissection of the cement that covered the wall of the Duomo; however, Pius II rejected this explanation, correctly thinking that the cause for the development of fractures, instead, was due to instability of the calcareous-arenaceous plateau on which the Duomo was built. Soon the architect tried to remedy to the problem, in order to limit its effects, already visible on the structure of the Cathedral, especially on its internal and external walls. During the last five centuries many important restorations, based on geological, hydrogeological, geomorphological and geotechnical investigations (Spighi, 1910; Barbacci, 1956; Brandi, 1980), and supported by drainage and consolidations of the foundations of the Duomo have been subsequently performed; however, slow and steady-state movements keep affecting the absidal part of the Cathedral, as indicated by high-resolution geometric and geodetic surveys (Calabresi et al., 1988; Guidi, 1992; Izzo et al., 1992; Calabresi et al., 1995).

### Experimental models:

Using the methods described by several Authors during the last decades (e.g. Hubbert, 1937; Ramberg, 1981; Schellart, 2000; Buitter & Schreuers 2006), modified to take local complexities into due account, we present the results of mass- and time-scaled physical analogue experiments performed in the Laboratory of Modeling at the University of Siena, aimed at reproducing the effects of gravitational movements experienced by the absidal part of the Pienza Cathedral and by neighbouring historical palaces. Our approach is based on compilation of an original, detailed, 1:10.000 scale geological map

of the city of Pienza and vicinities, coupled to cross-sections whose deep structure is constrained by seismic profiles acquired for petroleum exploration.

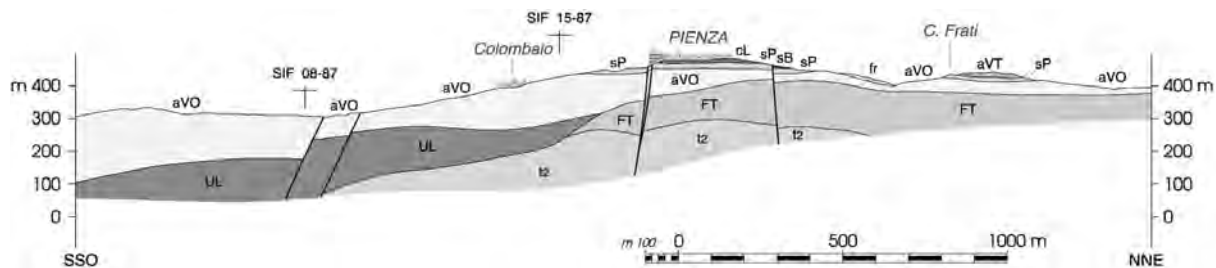


Figure 1. Across the Pienza fault system : *t2*-Anidriti di Burano (Tias sup.); *FT*-Falda Toscana (Mesozoico-Terziario); *UL*-Unità Luguri (Cretaceo-Eocene); *aVO*-Argille della Val d'Orcia (Pliocene); *sP*-Sabbie gialle e arenarie di Pienza e S. Quirico (Pliocene); *cL*-Calcare organogeno (Pliocene); *sP*-Sabbie a brachiopodi (Pliocene); *aVT*-Argille della Val di Tuoma (Pliocene); *fr*-Frana superficiale (Quaternario).

The geological map, the cross-sections and the seismic profiles provided the main source of information to build a computer-generated 3D model using the Move-TM Structural Modeling & Analysis Software (courtesy of Midland Valley Inc.). The 3D visualisation of the main geological structures provided the basis for construction of a mass- and time-scaled sandbox analogue physical model acquired under conditions of stable static equilibrium. Several evolutionary steps during the analogue physical modeling experiment were image-monitored thanks to the use of the Velocimetry Particle Imaging (PIV) high-resolution technique (Adam et al., 2005), whose results made it possible to reconstruct and constrain the kinematic evolution of phenomena reconstructed in the model.

Our findings suggest that the movements experienced by the absidal part of the Duomo and flanking historical buildings in Pienza are the direct manifestation of a Deep Seated Gravitational Slope Deformation (DSGSD), a phenomenon that has been widely recognised and reported in the geological literature. Such movements are likely to be triggered by slip along a slow-moving, actively creeping normal fault.

## References:

- Adam J. & Urai J.L. (2005) – Shear localization and strain distribution during tectonic faulting - new insight from granular-flow experiments and high-resolution optical image correlation technique. *Journal of Structural Geology*, 27, 283-301.
- Buiter S.J.H. & Schreurs G. (2006)- Analogue and numerical modelling of crustal- scale processes. *Spec. Publ. 253 Geological Society London*.
- Calabresi G. (2013) – The role of Geotechnical Engineers in saving monument and historic sites. *Proceedings of the 18<sup>th</sup> International Conference on Soil Mechanics and Geotechnical Engineering, Paris 2013*.
- Calabresi G., Lazzarotto A. & Micheluccini M. (1988) – The Cathedral of Pienza, Italy, and its foundation soils. In: *Proceedings of an international Symposium Organized by the Greek National Group of IAEG-Engineering Geology of Ancient Works, Monuments and Historical Sites*. Marinos & Koukis eds.; Balkema, Rotterdam: 459-468.
- Calabresi G., Izzo S., Lazzarotto A., Menicori P. & Pieruccini U. (1995) – Movimenti gravitativi nell'area di Pienza. *Boll. Soc. Geol. It.*:50, 67-82.
- Guidi F. (1992) – Studi topografici con livellazione geometrica di alta precisione. In: *Il Duomo di Pienza, 1459-1984, Studi e Restauri*. Cantini Ed.- Firenze: 106-109.
- Hubbert, M.K. (1937) -Theory of scale models as applied to the study of geological structures. *Geological Society of America Bull.*, 48, 1459-1520.

- Izzo S., Lazzarotto A. & Menicori P. (1992) – Elementi geologici dell'area di Pienza. In: Il Duomo di Pienza, Cinque Secoli di Restauri. Atti Conv. Pontignano – 6 giugno 1992 – Centrooffset Siena: 21-35.
- Ramberg H. (1981) – Gravity deformation and the Earth's crust. Academic Press, London.
- Schellart W.P. (2000) – Shear test results for cohesion and friction coefficients for different granular materials: scaling implications for their usage in analogue modelling. *Tectonophysics*, 324, 1-16.

## Analog modelling of pressurized subglacial water flow: Implications for tunnel valley formation and ice dynamics

Thomas Lelandais<sup>1</sup>, Régis Mourgues<sup>1</sup>, Edouard Ravier<sup>1</sup>, Stéphane Pochat<sup>2</sup>, Pierre Strzeczynski<sup>1</sup> and Olivier Bourgeois<sup>2</sup>

<sup>1</sup> Université of Maine, L.P.G. Le Mans, 72085 Le Mans, France

<sup>2</sup> Université of Nantes, L.P.G.N, 44322 Nantes, France

Corresponding author: thomas.lelandais@univ-lemans.fr

S2 - Coupling Tectonic and Surface processes (PS7)

Subglacial meltwater flow, occurring at the ice-bed interface or as groundwater flow, exerts a major control on basal erosion and ice dynamics. The understanding of the subglacial meltwater drainage system is therefore a major issue to reconstruct the dynamics of glacial paleo-environment and to predict the evolution of modern glacial systems. Tunnel valleys are an important component of this subglacial drainage system and exhibit specific characteristics including for examples: U-shaped cross-sectional profile with flat bottom, abrupt flank slopes, constant width, longitudinal profile with local adverse slopes. So far, most of tunnel valley studies were based on field and subsurface data analysis or numerical simulation and contributed to the establishment of three main models of formation. All these models underline the necessity of an over pressurized water flow at the base of the ice although the mechanisms of formation differ between these three models.

This contribution is based on analog modelling and presents an innovative approach in the study of subglacial water circulation. This experimental approach allows the formation of tunnel valleys and their morphologic evolution to be monitored.

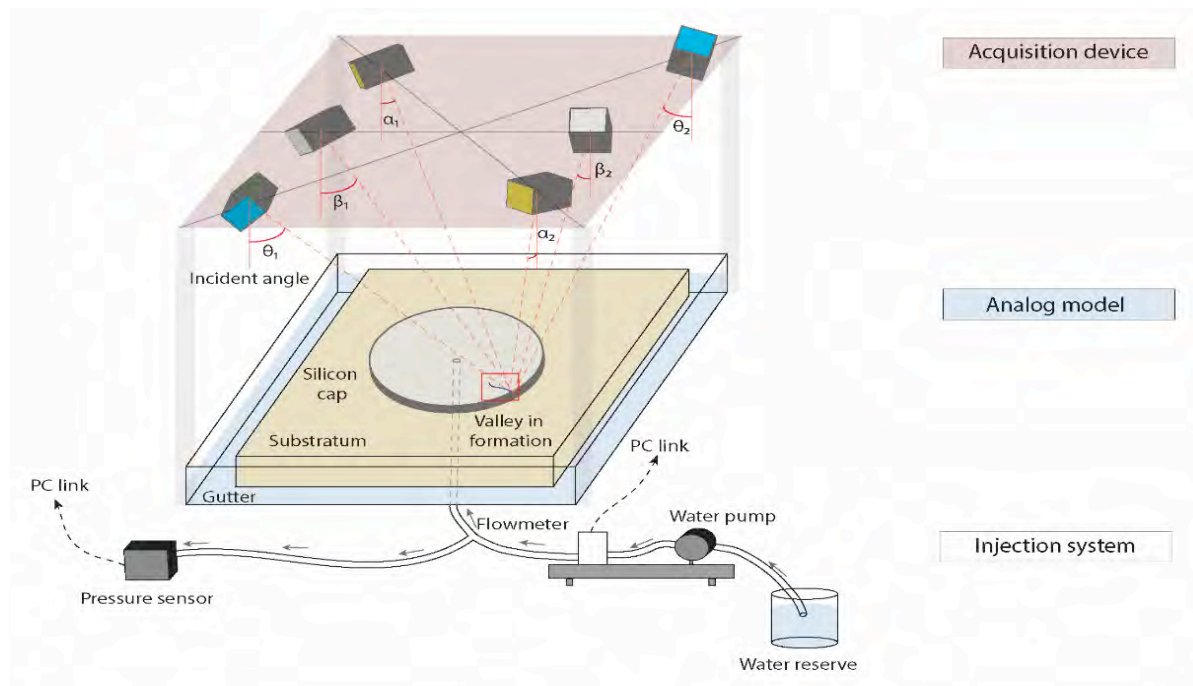


Figure 1: Acquisition device, analog model and water injection system used in this study.

In our experiments the ice is simulated by a circular and transparent lid of silicon, an impermeable material whose viscosity simulates the glacial dynamic on a reasonable timescale. Substratum is simulated with a porous sand of fine grain size (110  $\mu\text{m}$ ). Meltwater production is modeled by a punctual injection of water in the substratum at the center of the model (Figure 1).

For reduced injection discharge, low water pressure is recorded and water is evacuated as groundwater without any associated drainage features at the silicon-sand interface. For increasing injection discharge, water pressure exceeds the lithostatic stress, leading to the decoupling of the sand/silicon interface. This decoupling episode is associated with a relatively large zone where meltwater can be evacuated at the interface.

This rapid episode is followed by silicon-sand recoupling and establishment of a channelized drainage system morphologically resembling to tunnel valleys. Morphological analysis of these tunnel valley analogs are based on DEM generation (stereophotogrammetry methods) of the valley geometries using six cameras device taking simultaneous high resolution photographs of the experiments (Figure 2). The influence of various parameters such as lid thickness, water discharge and water discharge variations on valley dimensions were tested experimentally to analyse the impact of ice thickness variations or meltwater production rate changes on tunnel valley morphologies. In parallel, we also examined the impact of subglacial meltwater drainage evolution on ice dynamics by realizing silicon flow velocity maps during injection of water below the silicon lid. These maps were achieved using ultraviolet markers positioned at the base, within and at the surface of the lid. Ultraviolet markers were preferred in order to follow simultaneously the drainage features characteristics evolution by transparency (in “white light”) and the silicon flow evolution by evaluating the displacement of ultraviolet markers between different photographs (in “black light”). This method gives the opportunity to associate the 3D reconstruction of drainage features including tunnel valleys and the evolution of ice flow velocities through time.

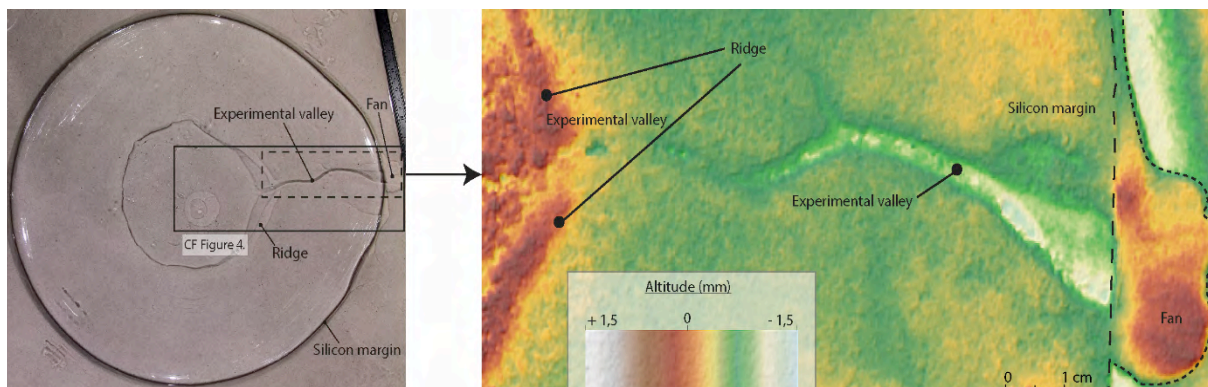


Figure 2: Example of a digital elevation model for an experimental valley

## Impact of surface processes on large scale faulting and folding in fold and thrust belts: analogue models and case studies

<sup>1,2</sup>Jacques Malavieille, <sup>1,7</sup>Clément Perrin, <sup>4</sup>Luca Clemenzi, <sup>1</sup>Audrey Taillefer, <sup>1,5</sup>Méline Salze, <sup>1</sup>Corentin Noël, <sup>1</sup>Xavier Tohane, <sup>3</sup>Giancarlo Molli, <sup>1,2</sup>Stéphane Dominguez, <sup>1,2</sup>Alfredo Taboada and <sup>6,2</sup>Chiayu Lu.

<sup>1</sup>) Géosciences Montpellier, Université Montpellier 2, Place E. Bataillon, 34095 Montpellier, France

<sup>2</sup>) LIA D3E, C.N.R.S.-M.O.S.T. France-Taiwan International Laboratory

<sup>3</sup>) Dipartimento di Scienze della Terra, Università di Pisa, 56126 Pisa, Italy

<sup>4</sup>) Dipartimento di Fisica e Scienze della Terra, Università degli Studi di Parma, 43100 Parma, Italy

<sup>5</sup>) Chrono-environnement, Université de Franche-Comté, Besançon, France.

<sup>6</sup>) Dept. of Geology, National Taiwan University, Taipei, Taiwan.

<sup>7</sup>) Columbia University, New York City, NY, United States

Corresponding author: jacques.malavieille@gm.univ-montp2.fr

### S2 - Coupling Tectonic and Surface processes (PS7)

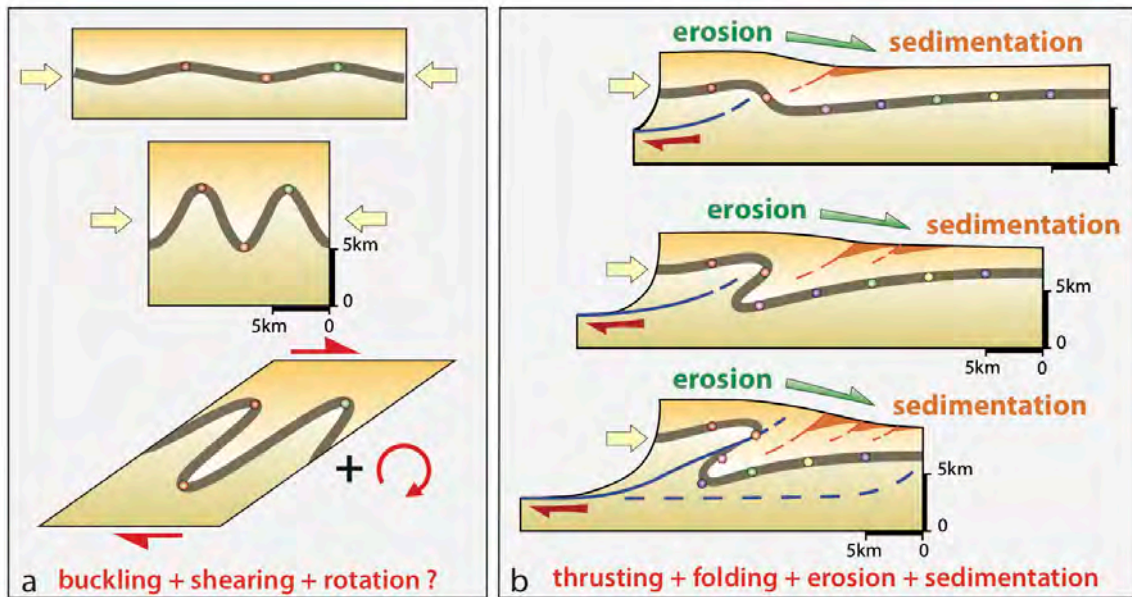
The building of fold and thrust belts (FTB) is mainly controlled by the general mechanics of continental subduction and by the interactions between tectonics and surface processes that modify wedge dynamics through material transfer. Because subduction orogens suffer large convergence, the long-term deformation is intense and generates specific structures. Among them, the way large-scale recumbent fold-nappes observed in FTB grow and evolve remains enigmatic as much as antiformal stacks of thrust units and subsequent frontal klippen. What mechanisms control large scale folding, basal accretion and its cyclicity remain an open question. Basal accretion activity is generally not constant during the long-term convergent history of orogenic wedges, alternating underthrusting of new tectonic slices with the internal deformation of the already accreted ones, or even with the migration of the underplating locus to a new place. Such a cyclical underplating behavior could promote, at a whole wedge scale, an alternate change from supercritical to subcritical taper condition.

Deformation mechanisms, long-term kinematics and evolution of FTB submitted to erosion and/or sedimentation are studied through 2D analog experiments (figure) involving large convergence. First order parameters tested include: i) décollements and/or plastic layers interbedded at different location within analog materials; ii) synconvergence surface erosion and sedimentation.

In the experiments, weak layers, favor deformation partitioning characterized by the simultaneous development of: i) underplating domains in the inner part of the wedge (basal accretion); ii) frontal accretion where the wedge grows forward. Development of antiformal thrust stacks is controlled by underplating. Thin plastic layers induce folding processes.

Recumbent and overturned folds, with large inverted limbs, develop in shear induced asymmetric deformation regime via progressive unrolling of synclinal hinges. Surface erosion and underplating at depth induce further rotation (passive tilting) and horizontalization of fold limbs.

Models give insights to discuss the mechanisms responsible for the large-scale structures (i.e., antiformal nappe stacks, klippen and kilometer scale recumbent fold-nappes) encountered in several mountain belts such as the Montagne Noire (French Massif Central), the Hercynian Pyrénées and Galicia belt (Spain), the Western Alps or the Northern Apennines (Italy).



*What deformation processes in Fold and Thrust Belts ?*

## Modeling the interaction between slip events, erosion and sedimentation along an active strike-slip fault in New Zealand: insights from morphotectonic experiments

<sup>1</sup>Malavieille, J., <sup>1</sup>Dominguez, S., <sup>2</sup>Graveleau, F., <sup>3</sup>Manighetti, I., <sup>1</sup>Ferdinand, A., <sup>1</sup>Romano, C.

<sup>1</sup>Université Montpellier 2, CNRS UMR 5243, Lab. Géosciences Montpellier, 34095 Montpellier cedex 5, France and LIA D3E, C.N.R.S.-M.O.S.T. France-Taiwan International Laboratory

<sup>2</sup>Université Lille 1, CNRS UMR 8187, LOG, F59655 Villeneuve d'Ascq, France

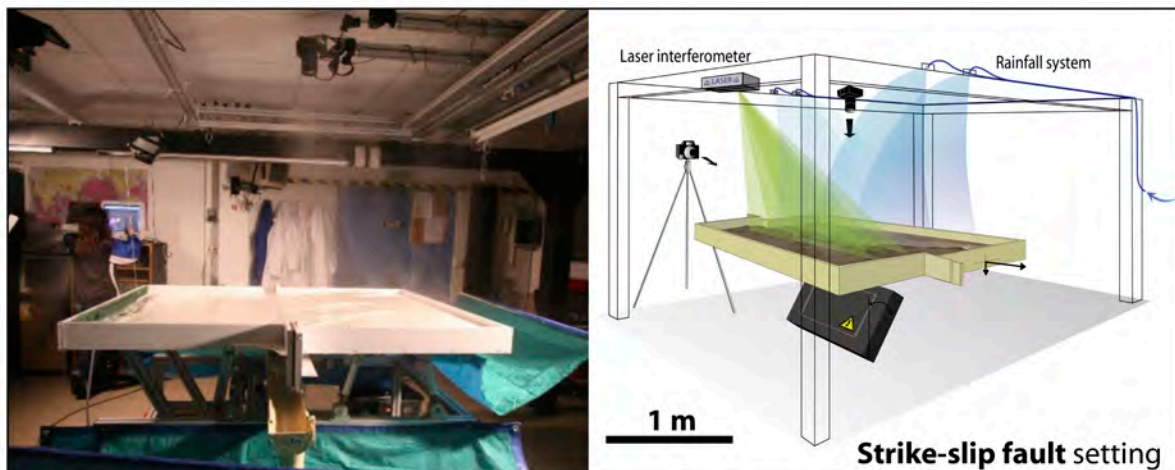
<sup>3</sup>GEOAZUR-OCA-CNRS, Nice, France

Corresponding author: jacques.malavieille@gm.univ-montp2.fr

S2 - Coupling Tectonic and Surface processes (PS7)

Tectonically controlled landforms develop morphologic features that provide useful markers to investigate rates of tectonic deformation and mechanisms of relief growth. Most of the morphological, structural and sedimentary markers observed along major seismogenic faults, result from the impact of repeated large earthquakes. Recovering information on past (i.e., last  $10^2$ - $10^4$  yrs) large earthquakes on faults is a challenge and our capability to recognize similar markers on either side of a fault in turn greatly depends on the 'evolution' that these markers may have sustained subsequently to their very first slip disruption.

To better understand and document the nature and 'evolution' of the morphological markers that are commonly used in morphotectonic and paleoseismological analyses, we have developed an original experimental set-up made to simulate repeated slip events on a strike-slip fault placed in a wet environment (rainfall system) sustaining sedimentation and erosion. The analog material is a mix of granular materials, whose mechanical properties lead to a geometric scaling of about 1:10 000 and to a temporal scaling on the order of one second equivalent to a few dozens of years. We survey the formation and evolution of a strike-slip fault from its immature stages up to one hundred repeated slip events.

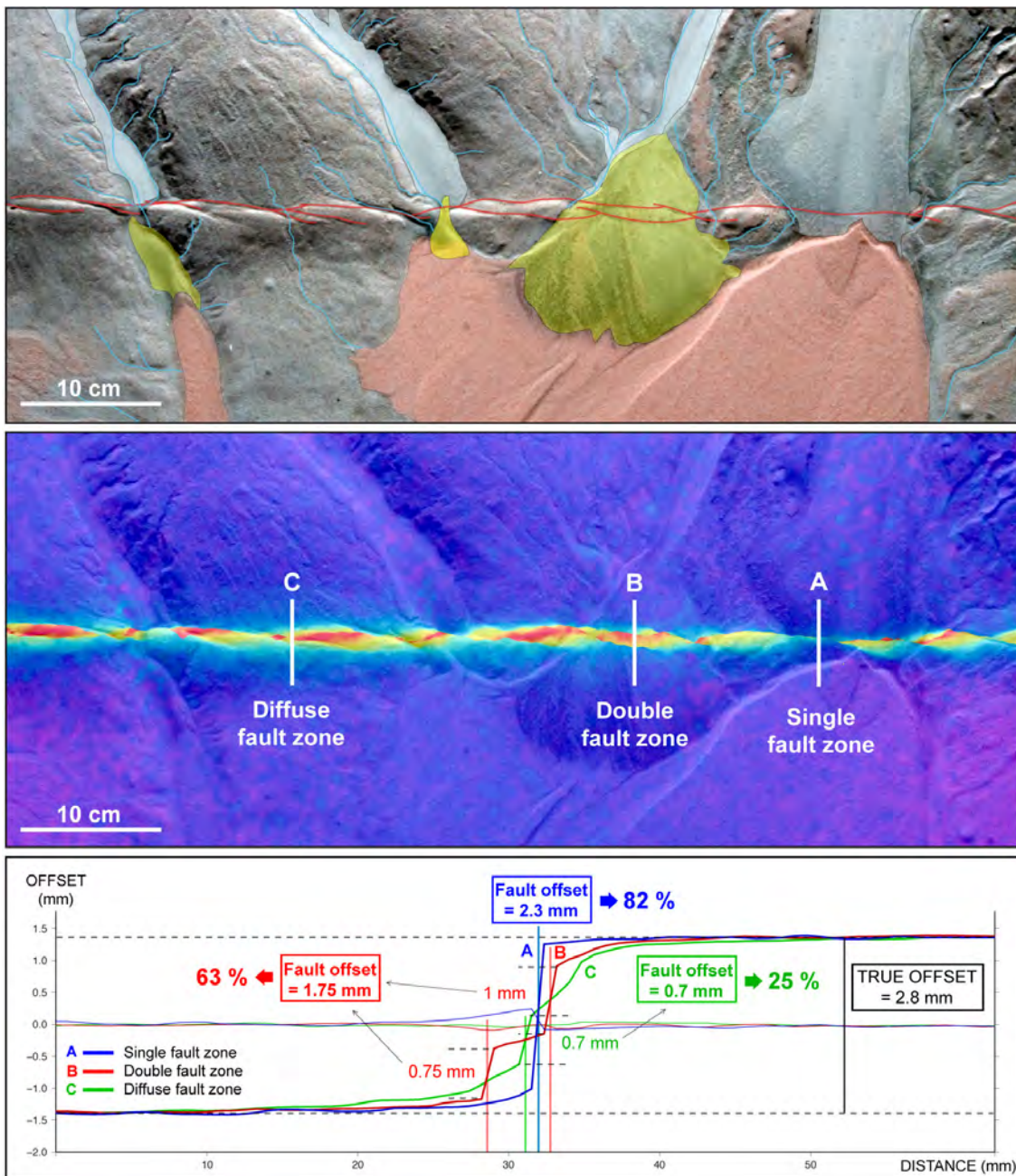


*Experimental set up*

Under the combined effects of accumulating slip, erosion and sedimentation, the model surface exhibits tectonic and morphological structures similar to natural features (Riedel's shears, pressure and shutter ridges, pull-apart basins, alluvial fans, terrace risers, braided rivers, etc), whose space and time evolution can be precisely analyzed. Deformation partitioning, sequential formation of alluvial

terraces, stream captures, development of ‘traps’ filling with sediments, etc, are observed. The control on the imposed amplitude and frequency of the rainfall cycles allows us to examine the impact of these rainfalls on the fault morphology and the evolution of the associated morphological markers.

Finally, we can compare the imposed slip events (number, amplitudes, repeat times) with the cumulative offsets eventually visible and measurable at the model surface. Marked discrepancies are found between imposed and final apparent offsets that shed light on the uncertainties that may affect the morphological and paleoseismological analyses performed on natural cases. We apply our results to further analyze several natural fault sites in New Zealand.



Quantifying fault offset for instance at a trench site faces several limitations related to the local complexity of the fault trace and the amount of diffuse deformation accommodated off the main fault.

## Diapiric architecture controlled by syn- and post-extension prograding sedimentary wedges

Mar Moragas<sup>1</sup>, Jaume Vergés<sup>1</sup>, Thierry Nalpas<sup>2</sup>, Eduard Saura<sup>1</sup>, Juan-Diego Martín-Martín<sup>3</sup>, Grégoire Messenger<sup>4</sup>, David William Hunt<sup>4</sup>

<sup>1</sup>) Group of Dynamic of the Lithosphere (GDL), Institute of Earth Sciences Jaume Almera, ICTJA-CSIC, Lluís Solé i Sabarís s/n, 08028 Barcelona, Spain

<sup>2</sup>) Géosciences Rennes, Université de Rennes 1, UMR 6118 CNRS, Campus de Beaulieu, 35042 Rennes cedex, France

<sup>3</sup>) Grup de Geologia Sedimentària, Departament de Geoquímica, Petrologia i Prospecció Geològica. Universitat de Barcelona (UB), Martí i Franquès s/n, 08028 Barcelona, Spain

<sup>4</sup>) Statoil, TDP RDI CPR CP, Sandsliveiein 90, 5020, Bergen, Norway

Corresponding author: mmoragas@ictja.csic.es

S2 - Coupling Tectonic and Surface processes (PS7)

### Introduction:

Analogue modelling has been previously applied to the analysis of the impact of the progradation of a sedimentary system above a ductile layer (McClay et al., 1998). Commonly, diapiric architecture increases in complexity with: (i) lobe progradation, where the radial shape of the prograding system causes a complex network of polygonal or circular depocenters separated by salt ridges (Gauillier and Vendeville, 2005); (ii) basement topography beneath the ductile layer (Ge et al., 1997); and (iii) the confluence of two sedimentary wedges (Guerra and Underhill, 2012). The outstanding results obtained in all these models, however, did not consider ongoing tectonic processes during diapirism.

We present 2 models with two phases (extension and post-extension phases) with different timing of progradation of sedimentary wedge in order to analyse how the time relationship between extension and sedimentary progradation control the formation of diapiric structures and their geometries.

### Results:

The Model 1 (Fig 1) illustrates the evolution of a basin with homogeneous sedimentation in the central graben during the extension phase and axial progradation of a sedimentary wedge during the post-extension stage. This configuration implies that the progradation occurs on top of a thick sand layer. In this model, the diapirs developed along the borders of the central graben as continuous diapiric ridges during the extension stage. However, the geometry of these diapirs (salt walls) varies along the strike of the central graben. In the proximal domain, where sedimentation rate is equal to the diapir growth rate, the diapirs are inward leaning, with very steep walls. Contrarily, the resulting diapirs in the distal domains, where sedimentation rate is lower than the diapir growth rate, are inward leaning, with very steep walls but with well-developed extrusions.

The Model 2 (Fig. 1) illustrates the evolution of a basin with progradation of a sedimentary wedge from the onset of the extension up to the end of the post-extension stage, and consequently on top of a ductile layer covered by a thin sand layer. This model shows well-developed diapiric structures in the proximal part of the model. Contrarily, diapirs are stagnated in the reactive phase formed during the extension and do not evolve to more mature diapiric phases in the distal domain. Additionally, the loading of the progradation wedge causes the collapse of the sedimentary pile in the proximal domain and the growth of a transversal silicone dome in the central part of the system.

### Concluding remarks:

The ratio between diapir growth and sedimentation rates, as well as the amount of sedimentary loading on top of a ductile layer influence the shape of the diapirs, enhance or hamper the formation of diapiric extrusions, and have a clear impact on the evolution of incipient diapiric structures to more evolved phases. Additionally, our results also highlight that the time of the onset of the progradation of the sedimentary wedge and the relative thickness of the sedimentary cover beneath the prograding system have a major impact on the final distribution of diapirs in a basin.

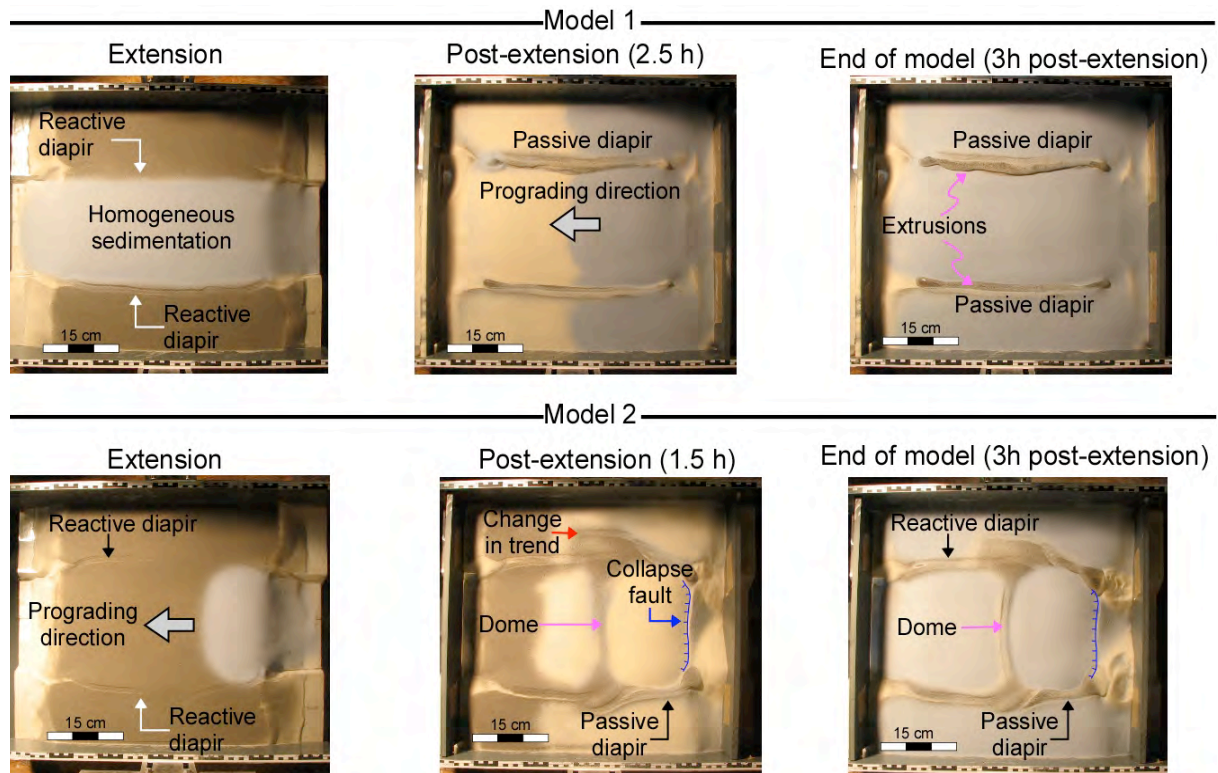


Figure 1: Top view of 3 steps of model 1 and 2. In model 1 the progradation started during the post-extension phase. In model 2, the inception of the sedimentary wedge progradation is coetaneous to the onset of the extension phase.

#### References:

- Gaullier, V., and Vendeville, B. C., 2005, Salt tectonics driven by sediment progradation: Part II - Radial spreading of sedimentary lobes prograding above salt: AAPG Bulletin, v. 89, no. 8, p. 1081-1089.
- Ge, H., Jackson, M. P. A., and Vendeville, B. C., 1997, Kinematics and dynamics of salt tectonics driven by progradation: AAPG Bulletin, v. 81, no. 3, p. 398-423.
- Guerra, M. C. M., and Underhill, J. R., 2012, Role of halokinesis in controlling structural styles and sediment dispersal in the Santos Basin, offshore Brazil: Geological Society, London, Special Publications, v. 363, no. 1, p. 175-206.
- McClay, K., Dooley, T., and Lewis, G., 1998, Analog modeling of progradational delta systems: Geology, v. 26, no. 9, p. 771-774.

**Keywords:** Analogue modelling, extension, prograding sedimentary wedge, diapir geometry.

## Export of earthquake-triggered landslides in active mountain ranges: insights from 2D morphodynamic modelling.

Thomas Croissant<sup>1</sup>, Dimitri Lague<sup>1</sup>, Philippe Davy<sup>1</sup> and Philippe Steer<sup>1</sup>

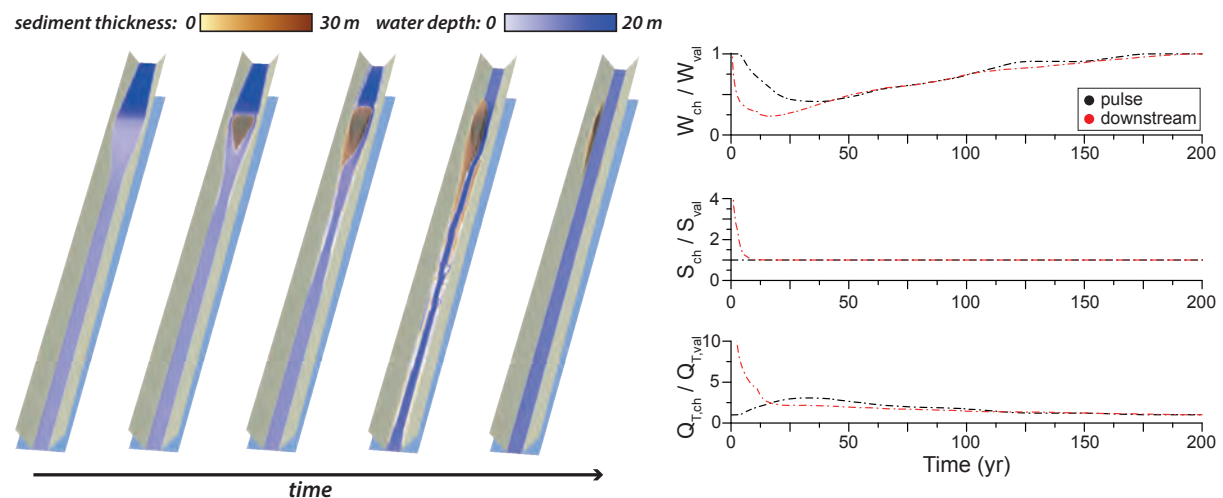
<sup>1</sup>) University of Rennes 1, Geosciences Rennes, Rennes, France

Corresponding author: philippe.steer@univ-rennes1.fr

S2 - Coupling Tectonic and Surface processes (PS7)

In active mountain ranges, large earthquakes ( $M_w > 5-6$ ) trigger numerous landslides that impact river dynamics. These landslides bring local and sudden sediment piles that will be eroded and transported along the river network causing downstream changes in river geometry, transport capacity and erosion efficiency. The progressive removal of landslide materials has implications for downstream hazards management and also for understanding landscape dynamics at the timescale of the seismic cycle. The export time of landslide-derived sediments after large-magnitude earthquakes has been studied from suspended load measurements but a full understanding of the total process, including the coupling between sediment transfer and channel geometry change, still remains an issue. Note that the transport of small sediment pulses has been studied in the context of river restoration, but the magnitude of sediment pulses generated by landslides may make the problem different.

Here, we study the export of large volumes ( $>10^6$  m<sup>3</sup>) of sediments with the 2D hydro-morphodynamic model, Eros. This model uses a new hydrodynamic module that resolves a reduced form of the Saint-Venant equations with a particle method. It is coupled with a sediment transport and lateral and vertical erosion model. Eros accounts for the complex retroactions between sediment transport and fluvial geometry, with a stochastic description of the floods experienced by the river.



*Numerical modeling of landslide export by river transport using the hydro-morphodynamic model Eros.*

Moreover, it is able to reproduce several features deemed necessary to study the evacuation of large sediment pulses, such as river regime modification (single-thread to multi-thread), river avulsion and aggradation, floods and bank erosion. Using a synthetic and simple topography we first present how granulometry, landslide volume and geometry, channel slope and flood frequency influence 1) the dominance of pulse advection vs. diffusion during its evacuation, 2) the pulse export time and 3) the

remaining volume of sediment in the catchment. The model is then applied to a high resolution (5-10 m) digital elevation model of the Poerua catchment in New Zealand which has been impacted by the effect of a large landslide during the last 15 years.

We investigate several plausible Alpine Faults earthquake scenarios to study the propagation of the sediment along a complex river network. We characterize and quantify the sediment pulse export time and mechanism for this river configuration and show its impact on the alluvial plain evolution. Our findings have strong implications for the understanding of aggradation rates and the temporal persistence of induced hazards in the alluvial plain as well as of sediment transfers in active mountain belts.

**Keywords:** River dynamics, landslides, sediment export times, earthquakes, numerical modeling, New-Zealand, hazards.

## Co-evolving complexity in coupled geomorphological-thermomechanical models

Kosuke Ueda<sup>1</sup>, Taras Gerya<sup>1</sup>, Sean Willett<sup>1</sup> and Dave May<sup>1</sup>

<sup>1</sup>) ETH Zurich, Department of Earth Sciences, Zurich, Switzerland

Corresponding author: kosuke.ueda@erdw.ethz.ch

S2 - Coupling Tectonic and Surface processes (PS7)

In tectonically active regions, topography, and stresses, are altered by tectonics and surface processes redistributing mass. Their interaction can be explored numerically by integrating (thermo-)mechanical with landscape evolution models (LEM) into a fully coupled geomorphological-thermomechanical (GmTM) approach (Ueda et al., 2015). A substantial open question is whether and how complexities and asymmetries, structural or geomorphic, can be related to system coupling including with feedback. High-resolution (thermo-)mechanical models are coupled both with a new regular, continuous-grid diffusion LEM, and an irregular, non-continuous fluvial LEM with topologic relationships between fluvial channels and hillslopes (Fig. 1). In both extensional and convergent settings, geometric complexity (structure, topography) is accentuated with the fluvial approach (Fig. 1a,e,f), e.g. by localizing thrusts at incising rivers. Efficient large-scale use of the regular LEM characterizes geodynamic surface expressions, and shows surface-process influence on deep subduction (Fig. 1e). Potential is also shown to trace characteristic basin evolution during complex rifting (Fig. 1b), where continental break-up may take place under a range of different far-field and active mantle contributions.

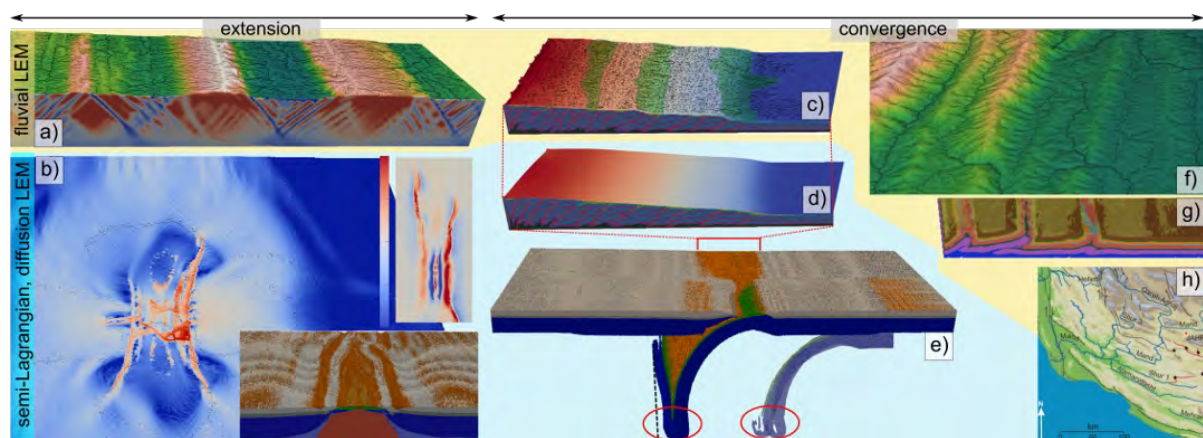


Figure 1: Representative model results. a) regional extension, 80x34 km wide block. b) break-up, 1000x1000 km continent (second strain rate invariant). Lower inset composition cut (plume red, sediment brown, ocean formation green), right inset erosion/deposition rate +/- 5 cm/a. Convergent settings: e) subduction zone, two domains of different LEM efficiency, varying slab angle (inset: front/back). c,d) LEM comparison, same wedge; note more complex (back-)thrust pattern for fluvial LEM (c). f,g) Surface, composition of model comparable to Zagros simply folded zone depicted in h) (from Walker et al., 2011).

### References:

- Ueda, K., Willett, S., Gerya, T., Ruh, J., 2015. Geomorphological–thermo-mechanical modeling: Application to orogenic wedge dynamics, *Tectonophysics* 659, 12-30.  
 Walker, R.T., Ramsay L.A., Jackson, J., 2011. Geomorphic evidence for ancestral drainage patterns in the Zagros Simple Folded Zone and growth of the Iranian plateau, *Geol. Mag.* 148, 901-910.

**Keywords:** Numerical modeling, coupling tectonics and surface processes, subduction, accretion, rifting, basins

## Evolution of morphotectonic parameters in an experimental wedge

Marc Viaplana-Muzas<sup>1,2</sup>, María Ortuño<sup>1</sup>, Vicente Perez-Peña<sup>3</sup>, José Pedro Galve<sup>3</sup>, Julien Babault<sup>2</sup>, Jean Van Den Driessche<sup>4</sup> and Stephane Dominguez<sup>5</sup>

<sup>1</sup>) RiskNat and Geomodels groups. Universitat de Barcelona. Facultat de Geologia, 08028, Barcelona, Spain.

<sup>2</sup>) Universitat Autònoma de Barcelona. Departament de Geologia, 08193 Bellaterra, Spain

<sup>3</sup>) Universidad de Granada. Campus de Fuentenueva, 18071 Granada, Spain.

<sup>4</sup>) Université de Rennes 1. Géosciences Rennes, Campus de Beaulieu, Rennes, France.

<sup>5</sup>) Université Montpellier. Géosciences Montpellier, I I, F-34095, Montpellier, France.

Corresponding author: marc.via.mu@gmail.com

S2 - Coupling Tectonic and Surface processes (PS7)

### Introduction:

The morphometry of geomorphological features along mountains front has been classically applied to characterize the regional degree of tectonic activity. The analysis of the shape and slope of alluvial fans as well as the geometry and distribution of the rivers and drainage basins is useful to detect enhanced/decreased uplift and ongoing tectonic deformation on mountain areas worldwide. The most common calculated parameters refer to the sinuosity of mountains front (Smf), the valley floor to width ratio (Vf), the stream-length gradient index (SL) or the percentage of dissection (Fd). Recently, new morphotectonic parameters, such as the Chi have permitted to better localize interest areas of tectonic activity.

All the previous studies, however, have analyzed the morphometry of the present-day landscape, this is, a snapshot of the whole history of changes experienced in active areas. Thus, the spatial comparison between areas undergoing different tectonic activity has been the only way to infer the expected changes in morphometry in the landscape. This “static” approach has to face the limitations related to controlling factors that vary in space such as lithology, structure and climate.

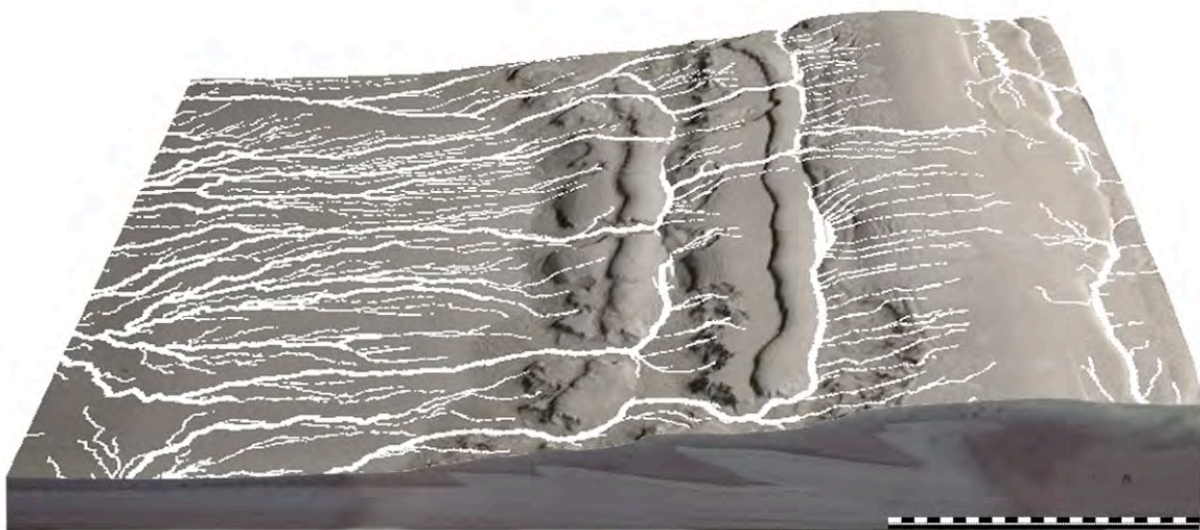


Figure 1. 3D view of a model run under 8 cm/h of shortening rate and 9 mm/h of rainfall rate, after the third thrust activity. The photographs are overlapped on the DEM. Drainage network is superimposed in white.

**Variation in time of morphometric parameters:**

We propose to use the Digital Elevation Models (DEMs) obtained for a set of experiments generating an artificial synthetic mountain front evolving with time. The system experienced orogenic growth at different rates and under different rainfall conditions, allowing us to reproduce and to monitor the interactions between tectonics, erosion and sedimentation. During the experiments, wedges were monitored by an optical measurement bench composed of photograph cameras coupled to a laser interferometer that allows quantifying surface deformations and generating DEMs. The experimental set-up used is adapted from the setup used by Graveleau and Dominguez, (2008). The deformation device is constituted by a basal film pulled beneath a static buttress. The film is overlaid by the analogue material, composed of glass microbeads, silica powder and plastic powder (PVC), which models the upper part of the crust. Shortening induces material deformation and generates an accretionary wedge composed of imbricated thrusts (Fig.1). The rainfall system is composed of sprinklers that deliver water micro-droplets over the model.

The experimental channels adjust to uplift rate by both increasing their slope and narrowing their channels as it is observed in nature above active faults. This analogy is evidenced by the values, in the erosion law, of exponents on the slope “ $n$ ”, that is  $1.5 \pm 0.2$ , and on the drainage area “ $m$ ”, that is  $0.8 \pm 0.2$  (Viaplana-Muzas et al., 2015). A set of 8 different analogue models coupling deformation and erosion were analyzed and changes in morphotectonic parameters were studied following, among others, the approach proposed by Pérez-Peña et al. (2009) for natural systems inspected using GIS tools. Results confirm that this type of modeling reproduces accurately the erosion dynamics of an active natural setting. Thus, morphotectonics of mountain fronts are analyzed for the first time in an experimental approach. This methodology emerges as a powerful way to study quantitatively the evolution of the landscape and permits to get some insights in the changes of active tectonics through the analysis of the different DEMs obtained synthetically.

**References:**

- Graveleau, F., and Dominguez, S., 2008. Analogue modelling of the interaction between tectonics, erosion and sedimentation in foreland thrust belts: *Comptes Rendus. Geoscience*, v. 340, no. 5, p. 324-333.
- Pérez-Peña, J.V., Azañón, J.M., Azor, A., Delgado, J., González-Lodeiro, F., 2009. Spatial analysis of stream power using GIS: SLk anomaly maps. *Earth Surface Processes and Landforms*, vol. 34, issue 1, pp. 16-25
- Viaplana-Muzas, M., Babault, J., Dominguez, S., Van Den Driessche, J., and Legrand, X., 2015. Drainage network evolution and patterns of sedimentation in an experimental wedge. *Tectonophysics*, 664, 109-124.

**Keywords:** Analogue modeling, Morphometric parameters, Active tectonics, Active mountain fronts.

## **Forearc deformation induced by aseismic ridge subduction and impact on river networks at continental margins using 3D finite-element models**

Stefanie Zeumann<sup>1</sup> and Andrea Hampel<sup>1</sup>

<sup>1</sup>) Leibniz Universität Hannover, Institut für Geologie, Hannover.

Corresponding author: zeumann@geowi.uni-hannover.de

S2 - Coupling Tectonic and Surface processes (PS7)

### **Introduction:**

Subduction of aseismic oceanic ridges causes considerable deformation of the forearc (e.g. Spikings and Simpson 2014; references therein). Using three-dimensional finite-element models solved with the commercial software ABAQUS we investigate the forearc deformation and impact on the river network caused by ridge subduction. Following the approach of Cailleau and Oncken (2008) we use a cylindrical shape for the subducting plate which carries the oceanic ridge and subducts beneath a wedge-shaped forearc (Figure 1a, Zeumann and Hampel, 2015, 2016). Since the focus is on the deformation of the forearc we consider the oceanic plate as rigid. The ridge is arc-shaped with its maximum height at the ridge crest. To investigate the impact on the river networks in continental forearcs we implement landscape evolution (erosion/sedimentation) using the CASQUS tool (Kurfesß and Heidbach, 2009) which links the landscape evolution model CASCADE (Braun and Sambridge, 1997) with three-dimensional models of ABAQUS.

### **General results:**

Generally, ridge subduction induces vertical and horizontal displacement, forearc indentation, and both contractional and extensional strain. The distribution of displacement and strain depends on ridge orientation related to convergence direction and margin (Zeumann and Hampel, 2015). The amount of deformation depends on ridge geometry (height/width), the frictional coupling along the plate interface, and rheological parameters of the forearc (Zeumann and Hampel, 2016).

### **Impact on river networks:**

The landscape evolution model includes diffusive hillslope processes and fluvial erosion and deposition. It calculates the amount of erosion and sedimentation for each time step at each node based on given parameters as e.g. diffusion constant or constant of stream erosion times net precipitation rate. Using the adaptive meshing technique the elevation of each node is changed due to the surface processes and a river network develops at the forearc surface after some time.

Figure 1b clearly shows the influence of ridge subduction at the river system. In regions without ridge influence the rivers run more or less straight downward the forearc wedge, which has a slope of 2°. Preliminary results show, that the ridge uplifts the forearc and redirects the rivers toward the ridge flanks. The rivers near the ridge crest show the strongest deflection whereas the rivers near the ridge toe seem nearly unaffected in their flow direction.

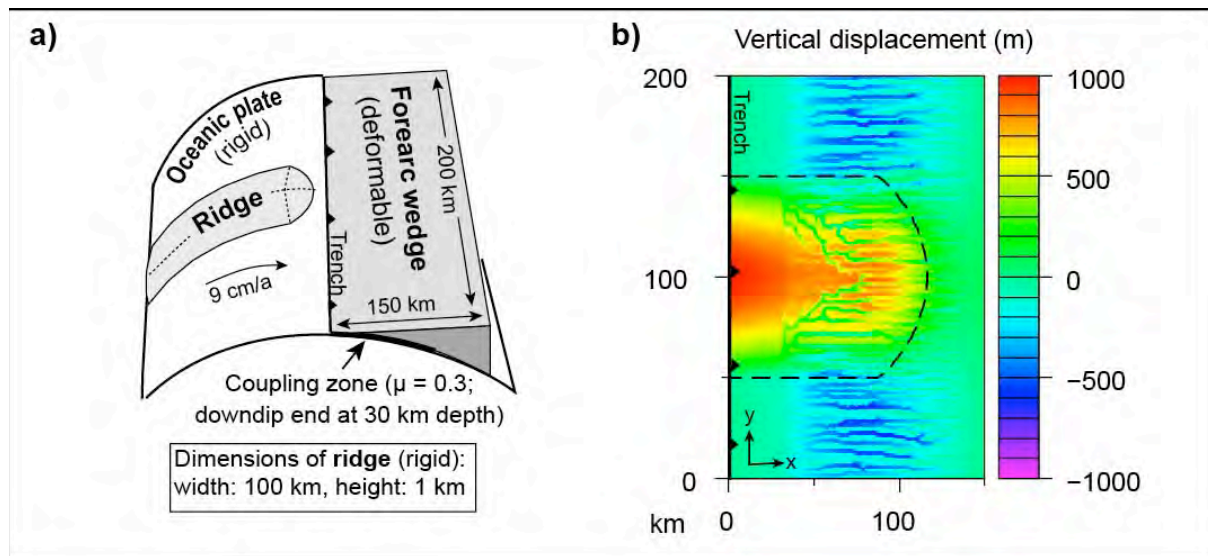


Figure 1: a) Model setup. Density  $2700 \text{ kg/m}^3$ , Young's modulus  $10 \text{ GPa}$  for the 1-km-thick upper sediment layer and  $60 \text{ GPa}$  for the lower part of the wedge. The slope of the forearc wedge is  $2^\circ$  and the friction coefficient along the plate interface is  $\mu=0.3$ . b) Top view of the vertical displacement after 1.5 Ma of ridge subduction with a convergence velocity of  $9 \text{ cm/a}$ . Surface processes start after 400 ka of subduction with time steps of 10 ka. Parameters for surface processes are diffusion constant of  $0.3 \text{ m}^2/\text{a}$  and stream erosion times net precipitation rate of  $0.01 \text{ m/a}$ . Dashed black line indicates the ridge position beneath the forearc wedge.

## References:

- Braun, J., Sambridge, M., 1997. Modelling landscape evolution on geological time scales: a new method based on irregular spatial discretization, *Basin Res.*, 9, 27-52.
- Cailleau, B., Oncken, O., 2008. Past forearc deformation in Nicaragua and coupling at the megathrust interface: Evidence for subduction retreat?, *Geochem. Geophys. Geosys.*, Q03016, doi: 10.1029/2007GC001754.
- Kurfeß, D., Heidbach, O., 2009. CASQUS: A new simulation tool for coupled 3D finite element modeling of tectonic and surface processes based on ABAQUS™ and CASCADE, *Computers and Geosciences*, 1959-1967.
- Spikings, R., Simpson, G., 2004. Rock uplift and exhumation of continental margins by the collision, accretion, and subduction of buoyant and topographically prominent oceanic crust, *Tectonics*, 33, 635-655, doi:10.1002/2013TC003425.
- Zeumann, S., Hampel, A., 2015. Deformation of erosive and accretive forearcs during subduction of migrating and non-migrating aseismic ridges: Results from 3-D finite element models and application to the Central American, Peruvian, and Ryukyu margins, *Tectonics*, 34, 1769-1791, doi: 10.1002/2015TC003867.
- Zeumann, S., Hampel, A., 2016. Three-dimensional finite-element models on the deformation of forearcs caused by aseismic ridge subduction: The role of ridge shape, friction coefficient of the plate interface and mechanical properties of the forearc, *Tectonophysics*, doi:10.1016/j.tecto.2015.12.022.

**Keywords:** Forearc deformation, oceanic ridge subduction, river networks, finite-element models.

## **S3 – Volcanoes: from the plumbing system to the eruptive plume**

Eruptions dynamics is controlled by magma discharge rates and by magma physical properties when reaching the Earth's surface. Magmas are complex 3 phases mixtures of liquid, gas and crystals. Their physical properties and their ability to reach the surface depend not only on their composition but also on how they interact with the crust during their journey from depth.

Experimental, analytical and numerical approaches are required to capture the physics of magma transfer and stalling in the crust, the building and destruction of volcanic edifices, and the transport of the erupted products at the Earth's surface or in the atmosphere. Models should aim to explain and reconcile a diversity of geological, geophysical and geochemical observations characterized by various uncertainties.

This session welcomes contributions describing progresses in volcano and volcanic hazard modeling, and that relies on improved model complexities, on the integration of physical observations, or on the characterization of uncertainties.

**Conveners:** Francesco Maccaferri (GFZ, Potsdam, Germany) and Catherine Annen (University of Bristol, U.K.).

**Keynote speaker:**

"**Shallow magmatic intrusions in planetary crusts**" by Chloe Michaut (IPGP, Paris, France) - michaut@ipgp.fr

## Shallow magmatic intrusions in planetary crusts

Chloé Michaut<sup>1</sup> and Clément Thorey<sup>1</sup>

<sup>1</sup>Institut de Physique du Globe de Paris, Université Paris Diderot, Sorbonne Paris Cité, Paris, France.

Corresponding author: michaut@ipgp.fr

S3 – Volcanoes: from the plumbing system to the eruptive plume (Keynote)

Shallow magmatic intrusions make room for themselves by lifting up their overlying roof, creating characteristic surface deformations that can be observed at the surface of planets.

We develop a model for magma flow below an overlying elastic layer characterized by a flexural wavelength  $\Lambda$  and study the dynamics and morphology of such a magmatic intrusion. We demonstrate that, depending on its size, the intrusion can show two different shapes and thickness-to-radius relationships (Michaut, 2011). In a first regime, the elasticity of the overlying layer is the main source of driving pressure in the flow; the intrusion is bell-shaped and its thickness is close to being proportional to its radius (Figure 1). When the intrusion radius becomes larger than 4 times  $\Lambda$  the flow enters a gravity current regime and progressively develops a pancake shape with a flat top (Figure 1).

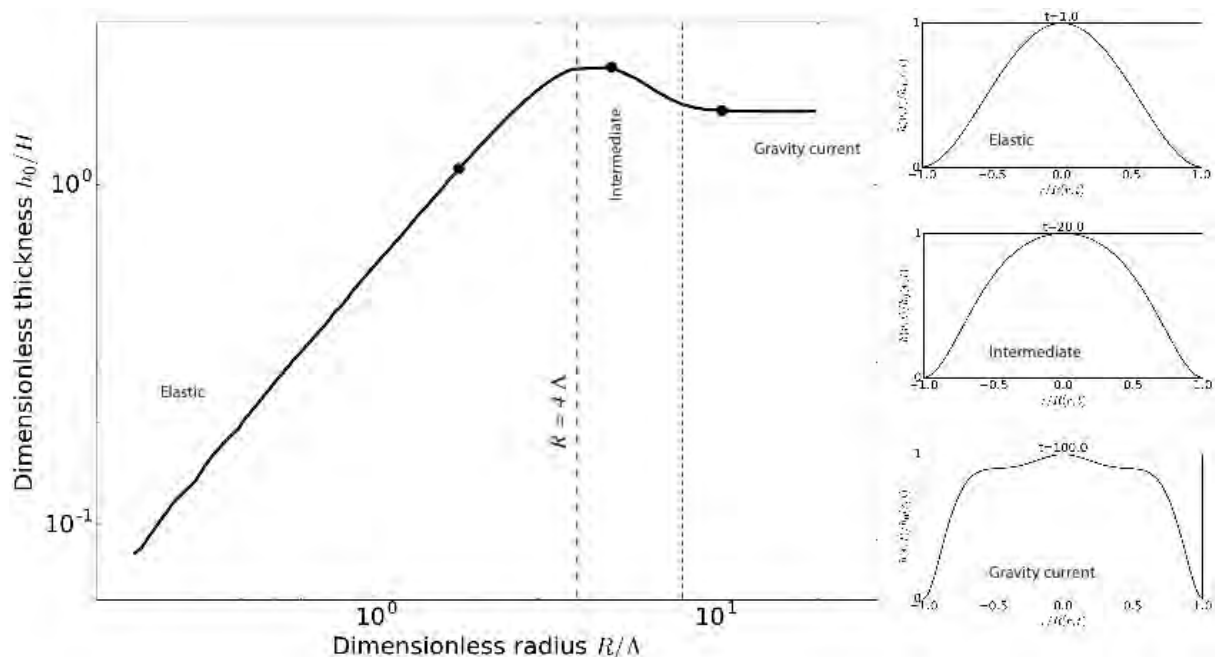


Figure 1: Maximum thickness of an intrusion normalized by the characteristic thickness of a gravity current as a function of the intrusion radius normalized by the flexural wavelength (Left); three regimes of propagation are identified, characterized by specific thickness to radius power-law relationships and specific shapes (Right).

We then account for the cooling of the intrusion and temperature-dependence of the magma viscosity and show that this does not modify the successive shapes of the intrusion. Our simulations show that, during the elastic-dominated regime, the flow effective viscosity is the average viscosity of a thin

peeling region at the tip of the flow. The effective flow viscosity thus rapidly increases as the flow cools, which could rapidly stop its spreading in this regime. We also show that spreading is influenced by the presence of a positive topography on the overlying elastic layer (Thorey and Michaut, 2014).

The model is applied to understand and characterize the dynamics of emplacement of laccoliths and saucer-shaped sills in the upper crust on Earth. We further use our results to detect and characterize shallow magmatic intrusions in the crust of planets.

## References:

- Michaut, C. 2011, Dynamics of magmatic intrusions in the upper crust: Theory and applications to laccoliths on Earth and the Moon, *J. Geophys. Res. (Solid Earth)* 116, B05205, doi:10.1029/2010JB008108.
- Thorey, C. and C. Michaut, 2014, A model for the dynamics of crater-centered intrusions: application to lunar floor-fractured craters, *J. Geophys. Res. (Planets)* 119(1), doi:10.1002/2013JE004467, p. 286-312.

## **Measuring host-rock deformation and fluid flow in an evolving model volcanic plumbing system: Insights from PIV, DIC and high-resolution laser scanning**

Janine L. Kavanagh<sup>1</sup>, David J.C. Dennis<sup>2</sup>, Alec Burns<sup>2</sup> and Sam Hignett<sup>1</sup>

<sup>1</sup>University of Liverpool, School of Environmental Sciences, Liverpool, UK

<sup>2</sup>University of Liverpool, School of Engineering, Liverpool, UK

Corresponding author: Janine.kavanagh@liverpool.ac.uk

S3 – Volcanoes: from the plumbing system to the eruptive plume (Oral)

The mechanics of magma transport are important for understanding magma distribution within the shallow crust and the tendency for intrusion or eruption. We will present the results from a series of layered gelatine analogue experiments analysed by Particle Image Velocimetry (PIV) and Digital Image Correlation (DIC) to document the fluid flow and small-scale surface and sub-surface deformation processes that occur during dyke and sill emplacement.

Gelatine is a viscoelastic material that displays predominantly elastic deformation when used at low temperatures (5-10 °C) and mid-to-low concentrations (2-5 wt%) (Kavanagh et al., 2013). To study dyke propagation and sill formation we have used a combination of Particle Image Velocimetry (PIV) and Digital Image Correlation (DIC) to characterise the dynamics of fluid flow within the intrusion and contemporaneous subsurface deformation of the host gelatine (e.g. Figure 1). Experiments are prepared by filling a 40x40x30 cm<sup>3</sup> clear-Perspex tank with a gelatine mixture that has been seeded with neutrally buoyant fluorescent particles. Water, also seeded with tracer particles, is then injected into the solid gelatine from below under a constant flux or constant head pressure. This causes a vertical penny-shaped crack (dyke) to propagate through the gelatine and erupt at the surface.

During the experiment, a vertical high-power laser sheet positioned along the centre of the tank is triggered to illuminate the seeding particles with short intense pulses, and two Dantec CCD cameras record successive images. Surface deformation profiles of the gelatine are also obtained during injection by a Micro-Epsilon laser scanner positioned above the experiment tank. Using PIV and DIC, vector fields of fluid flow within the intrusion and strain within the gelatine host is calculated by cross-correlation between successive images at a defined time interval. The experiments indicate that, prior to eruption, dyke propagation is characterised by rapid centralised and upwards fluid flow with accompanying downwards motion at the intrusion margin. The viscosity and rheology of the intruding fluid is also significant. Deformation of the gelatine solid is focused at a small head region, with the tail remaining relatively static as the dyke grows. Upon eruption, rapid centralised fluid evacuation occurs with contemporaneous contraction of the dyke and relaxation of the host gelatine.

Models that simultaneously monitor fluid dynamics and host deformation during magma ascent and eruption make an important step towards improving our understanding of the dynamics of magma transport through the crust, and may help to constrain the tendency for eruption. This work has important implications for interpreting field observations of volcanic plumbing systems, and for understanding the surface and sub-surface deformation associated with magma flow.

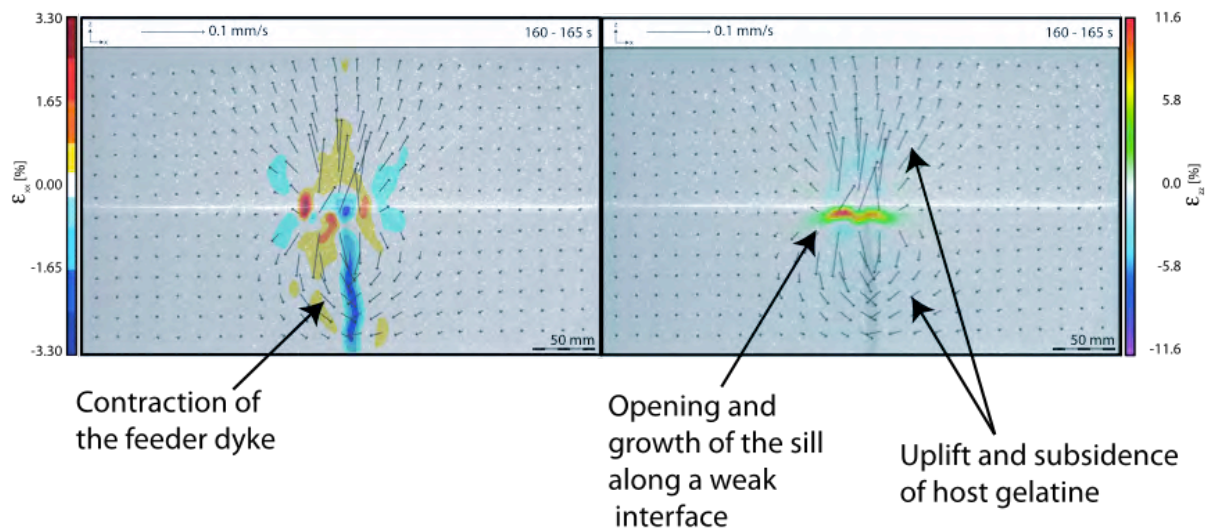


Figure 1: Colour-map of incremental strain and vector field of displacement of a two-layered elastic gelatine intruded by water (Kavanagh et al., 2015). Digital image correlation is used to capture the characteristics of host-deformation when a vertically propagating dyke turns to intrude as a sill along a weak interface between layers. The gelatine layers have equal Young's modulus.

#### References:

- Kavanagh, J., Menand, T. & Daniels, K.A., 2013. Gelatine as a crustal analogue: Determining elastic properties for modelling magmatic intrusions. *Tectonophysics*, 582, pp.101–111.
- Kavanagh, J.L., Boutelier, D. & Cruden, A.R., 2015. The mechanics of sill inception, propagation and growth: Experimental evidence for rapid reduction in magmatic overpressure. *Earth and Planetary Science Letters*, 421, pp.117–128.

**Keywords:** dyke, sill, analogue experiment, gelatine, digital image correlation, particle image velocimetry.

## The control of host rock strength on sill and laccolith emplacement

T. Schmiedel<sup>1</sup>, O. Galland<sup>1</sup>, and C. Breitzkreuz<sup>2</sup>

<sup>1</sup>) Physics of Geological Processes, Department of Geosciences, University of Oslo, Oslo, Norway

<sup>2</sup>) Geological Institute, Technical University Bergakademie Freiberg, 09599 Freiberg, Germany

Corresponding author: tobias.schmiedel@geo.uio.no

S3 – Volcanoes: from the plumbing system to the eruptive plume (Oral)

Igneous intrusions in sedimentary basins exhibit a great diversity of shapes from thin sheets (e.g. sills, cone sheets), to massive intrusions (e.g. laccoliths, plugs). Presently, none of the established models of magma emplacement has the capability to simulate this diversity (Galland et al., 2015), showing that our understanding of the general mechanisms of magma emplacement in the brittle crust is limited.

In the literature, two types of mechanical models of magma emplacement exist. On one hand, models for sheet intrusions consider “relatively low” (often neglected) viscosity magma into elastic rock (e.g. Pollard and Johnson, 1973). On the other hand, models for massive intrusions consider very viscous magma intruding into a weak plastic host rock (e.g. Roman-Berdiel et al., 1995). However, natural rocks are complex elasto-plastic materials, and field observations and seismic data evidence that both elastic and plastic deformation commonly accommodate the emplacement of magma. Therefore, the “elastic” and “plastic” end member models are not sufficient to simulate the complex host rock behaviour during the emplacement of igneous intrusions, explaining why they fail to reproducing the natural diversity of intrusion shapes.

In this study, we present new results of quantitative laboratory models of magma emplacement in the brittle crust. In this experimental series, we use Coulomb dry granular materials of variable cohesion as model host rock; we use molten vegetable oil, which solidifies after the end of the experiments, as model magma. In the models, a horizontal flexible net positioned at the injection inlet represents a weak strata, along which the oil initially intrudes. We investigate the effects of the host cohesion on magma emplacement through a series of experiments, in which the cohesion of the host is varied systematically and the injection depth and flow rate are kept constant. We show that when the host rock is strong (high cohesion), the resulting intrusions are thin, flat-lying saucer-shaped sills, and their emplacement is dominantly accommodated by elastic bending of the host. Conversely, when the host rock is weak (low cohesion), the resulting intrusions are massive laccolithic plugs and their emplacement is dominantly accommodated by shear failure of the host.

Our experiments also suggest that combined elastic/shear failure deformation modes control the emplacement of cone sheets. To our knowledge, our models are the first that spontaneously simulate both sheet intrusions and massive intrusions, therefore they fill a long-lasting gap between the established “elastic” and “plastic” end member models of magma emplacement. Our models highlight that accounting for the complex elasto-plastic behavior of the host rock is essential for unraveling the complex dynamics of magma emplacement in the Earth’s brittle crust.

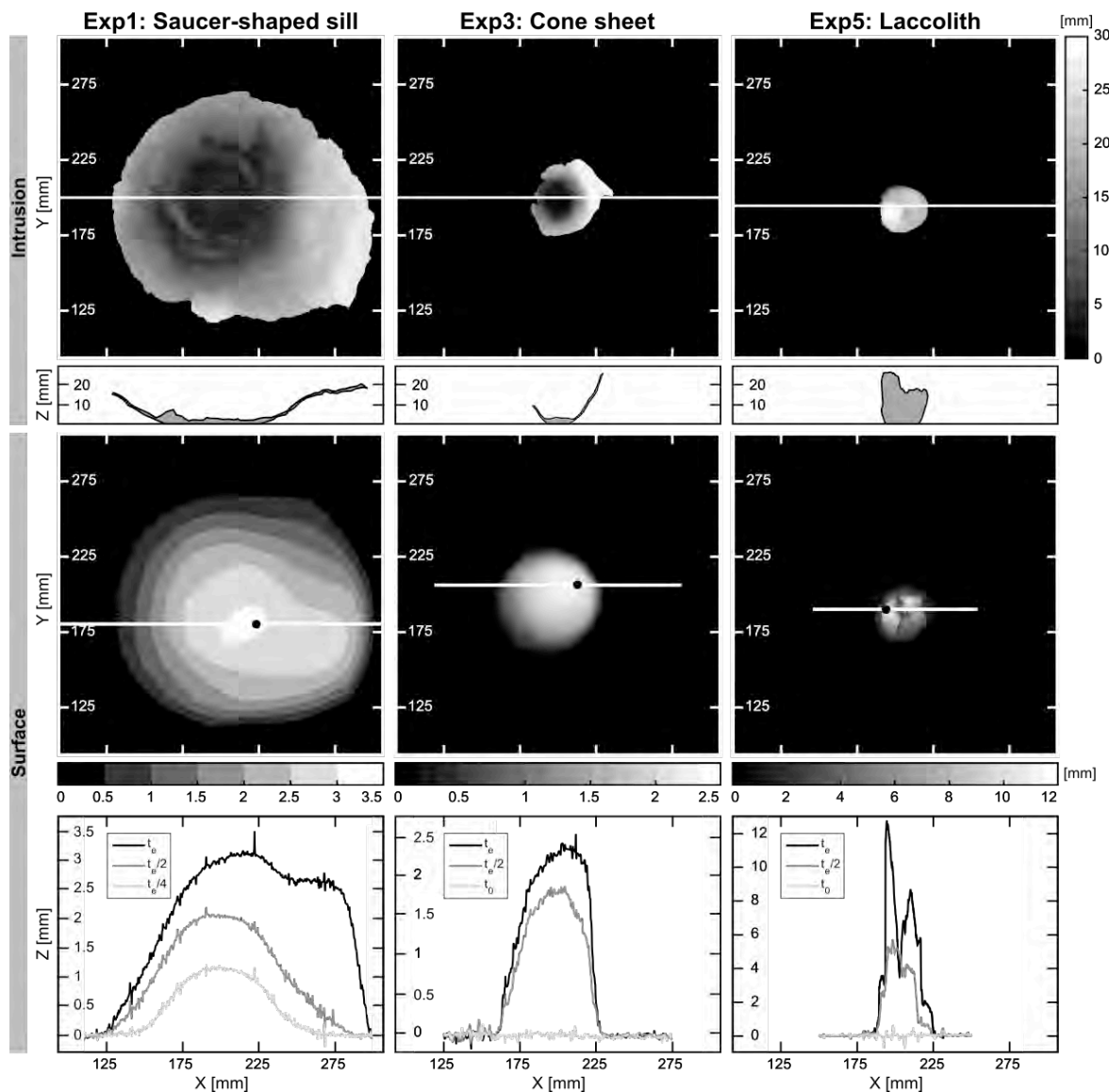


Figure 1: Topographic maps of excavated intrusions (top row), profiles of excavated intrusions (second row), topographic map of the model surface (third row), and plots of the surface uplift in over time (fourth row) for three characteristic experiments (columns). White lines in topographic maps locate the cross sections of the profiles and plots. Black dots locate the point of maximum uplift. Experiment duration  $t_e$ .

## References:

- Galland, O., Holohan, E., van Wyk de Vries, B., and Burchardt, S., 2015, Laboratory Modelling of Volcano Plumbing Systems: A Review, Springer Berlin Heidelberg, p. 1-68, doi: 10.1007/11157\_2015\_9.
- Pollard, D. D., and Johnson, A. M., 1973, Mechanics of growth of some laccolithic intrusions in the Henry mountains, Utah, II: Bending and failure of overburden layers and sill formation: Tectonophysics, v. 18, no. 3–4, p. 311-354, doi: 10.1016/0040-1951(73)90051-6.
- Roman-Berdiel, T., Gapais, D., and Brun, J. P., 1995, Analogue models of laccolith formation: Journal of Structural Geology, v. 17, no. 9, p. 1337-1346, doi: 10.1016/0191-8141(95)00012-3.

**Keywords:** Laboratory models, magma intrusions, cohesive granular materials, sill, laccolith.

## Dynamics of dikes versus cone sheets in volcanic systems

O. Galland<sup>1</sup>, S. Burchardt<sup>2</sup>, E. Hallot<sup>3</sup>, R. Mourgues<sup>4</sup>, C. Bulois<sup>5</sup>

<sup>1</sup>) Physics of Geological Processes, Department of Geosciences, University of Oslo, Oslo, Norway

<sup>2</sup>) Mineralogy, Petrology and Tectonics, Department of Earth Sciences, University of Uppsala, Uppsala, Sweden

<sup>3</sup>) Géosciences Rennes, Université de Rennes1, Rennes, France

<sup>4</sup>) L.P.G.N., Université du Maine, Le Mans, France

<sup>5</sup>) Ecole Normale Supérieure de Paris, Paris, France

Corresponding author: olivier.galland@geo.uio.no

S3 – Volcanoes: from the plumbing system to the eruptive plume (Oral)

Swarms of hundreds to thousands of igneous sheet intrusions represent the main magma pathways through the Earth's brittle crust. Igneous sheet intrusions of various shapes, such as dikes and cone sheets, coexist as parts of complex volcanic plumbing systems likely fed by common sources. How they form is fundamental regarding volcanic hazards, but yet no dynamic model simulates and predicts satisfactorily their diversity. Here we present scaled laboratory experiments that reproduced dike and cone sheet intrusion geometries under controlled conditions (Galland et al., 2014). The model rock is fine-grained, cohesive Coulomb crystalline silica flour. The model magma is a molten vegetable oil injected at constant flow rate. After the experiments, the oil solidifies and the intrusion is excavated to observe its shape.

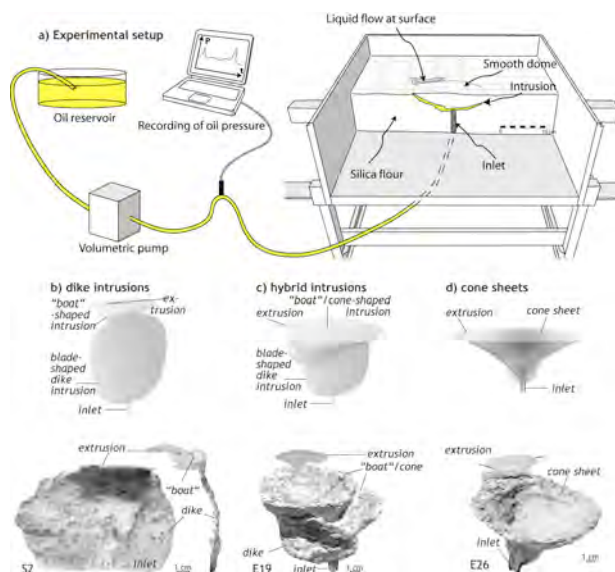


Figure 1. a) Drawing of the experimental apparatus used in this study. b) Schematic drawing (top) and photograph (bottom) of a typical dike produced during the experiments and excavated from the host-powder after solidification of the oil. The dike initiated from the inlet at the bottom and fed an elongated v-shaped, or “boat”-shaped, sheet intrusion to the very top. c) and d) Schematic drawings (top) and photographs (bottom) of typical excavated hybrid and cone sheet intrusions, respectively.

We present the results of 52 experiments, in which we varied independently three controlled parameters: the depth of the injection inlet ( $h$ ) below the free surface, the diameter of the injection inlet ( $d$ ), and the oil injection velocity ( $v$ ). The experiments produced two basic sheet intrusion morphologies that compare to natural dikes and cone sheets, as well as a transitional type of intrusion referred to as hybrid intrusions (Figure 1). We performed a dimensional analysis of the studied system and identified two dimensionless parameters that account for the coupling between the host rock and the magma source: a geometric dimensionless ratios ( $\Pi_1=h/d$ ), which describes the geometry of the magma source, and a dynamics dimensionless ratio ( $\Pi_2=v\eta/Cd$ ), which compares the local viscous stresses in the flowing magma to the host-rock strength. Here  $\eta$  is the magma viscosity and  $C$  the host

cohesion. Plotting our experiments against these two numbers results in a phase diagram evidencing a dike and a cone-sheet field, separated by a sharp transition that fits a power law (Figure 2).

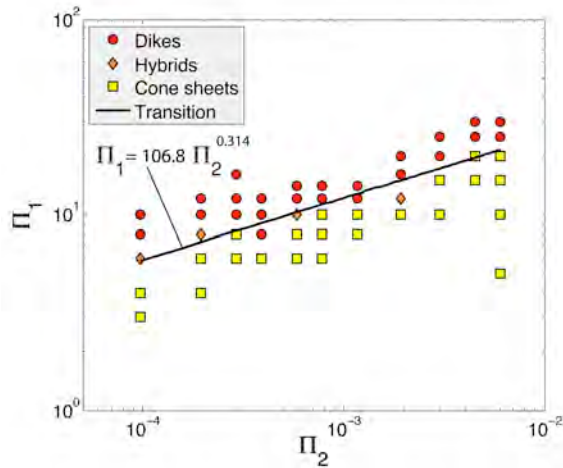


Figure 2. Log-log dimensionless phase diagram distinguishing the intrusion shapes obtained in the 52 experiments of this study: dikes (red circles), hybrid intrusions (orange lozenges), and cone sheets (yellow squares).  $\Pi_1=h/d$  and  $\Pi_2=v\eta/Cd$ . The dikes and cone sheet experiments plot in two distinct fields, separated by a line, expressed by the power law  $\Pi_1=106.8\times\Pi_2^{0.314}$ .

In order to test the relevance of our empirical law highlighted in Figure 2, we extrapolate it over the geological ranges of  $\Pi_1$  and  $\Pi_2$ , and compare it with magmatic feeders of dikes and cone sheets of different scales and shapes in nature (Figure 3). Our experimental results match very well with geological data, which indicates that our experimental models capture general magma emplacement mechanisms, reconciling existing specific models of distinct magmatic feeding systems.

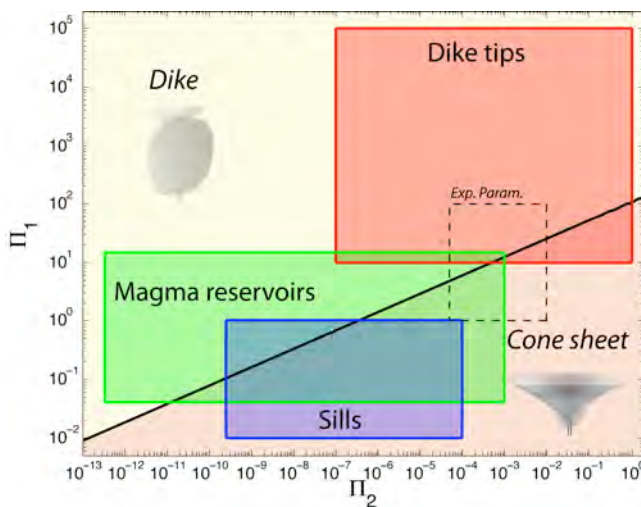


Figure 3. Graph comparing the experimental results of this study (dashed line box) to characteristic geological values of  $\Pi_1$  and  $\Pi_2$ . The dike-to-cone sheet transition is extrapolated from experimental phase diagram of 2. Geological boxes correspond to dike tips (red), magma reservoirs in volcanoes (green) and shallow sills in sedimentary basins (blue).

**References:**

Galland, O., Burchardt, S., Hallot, E., Mourgues, R., Bulois, C., 2014. Dynamics of dikes versus cone sheets in volcanic systems. *Journal of Geophysical Research: Solid Earth*, 2014JB011059.

**Keywords:** Laboratory models, magma intrusions, dikes, cone sheets, dimensional analysis.

## 4D imaging of volcano deformation during viscous magma intrusion using X-ray computed tomography.

Marta Rincón<sup>1</sup>, Álvaro Márquez<sup>1</sup>, Raquel Herrera<sup>1</sup>, Ana Alonso-Torres<sup>2</sup>, Jose Luis Granja-Bruña<sup>3</sup>, Benjamin van Wyk de Vries<sup>4</sup>

<sup>1</sup>) Universidad Rey Juan Carlos, Laboratorio de Modelización Análoga, Madrid, España.

<sup>2</sup>) Hospital Rey Juan Carlos, Radiodiagnóstico, Madrid, España.

<sup>3</sup>) Universidad Complutense de Madrid, Dpto. Geodinámica, Madrid, España.

<sup>4</sup>) University of Clermont-Ferrand, Lab. Magmas et Volcans, Clermont-Ferrand, France

Corresponding author: marta.rincon@urjc.es

S3 – Volcanoes: from the plumbing system to the eruptive plume (Oral)

Analogue models have been used since the 19th century to investigate geological processes, and where first models focused on the qualitative understanding of the process. Since then a more quantitative approach with description of the experiment results has been developed. So several techniques have been developed for monitoring of the spatio-temporal evolution of scaled analogue volcanic models. A geological process where analogue models play a fundamental role in research is the deformation of volcanic edifices during viscous magma intrusion. Quantitative monitoring of these experiments is a current challenge with the opportunity to integrate such models with geodetic volcano monitoring. Such *analogue monitoring* must include time evolution of 3D surface displacements and internal structure of the model. We show here our approach for such a complete 4D monitoring.

Previous experiments of volcano deformation during viscous magma intrusions (e.g. Donnadieu & Merle 1998; Kervyn et al. 2009) have intruded silicone or Golden Syrup in a volcanic cone of granular material. To study the internal structure of such experiments, researchers have cut cross sections. However, the obtained vision is strongly determined by the direction and timing of the section. In other volcanic models, Kervyn et al. (2010) introduced the use of computed X-ray microtomography ( $\mu$ CT) to observe the models internal structure. On one hand, only 3D data of the final result of the model can be obtained due to long time required for the scanning. On the other hand, X-Ray Computerized Axial Tomography (XRCT) using medical scanners has been successfully applied for years in tectonic models to visualize the internal structure and temporal evolution of analogue models involving granular material (e.g. Adam et al., 2013). We have explored the feasibility of XRCT, which has not been yet applied to the study of volcano models, for the monitoring of our experiments.

Our experimental device consists in the intrusion of magma at the base of a volcanic cone (Figure 1A). We used a sand-plaster mixture for the volcano and Golden Syrup for the magma analogue. We have scaled our models so experiments simulated intrusion in a 1100 m high volcano with natural magmas viscosity of  $1 \times 10^8$ – $1 \times 10^{10}$  Pa s. Flow rates were scale to 1-100 m<sup>3</sup>/s (e.g. the dacitic cryptodome at St Helens in 1980). We have used a medical Spiral CT Scanner Siemens Definition AS at the Hospital Rey Juan Carlos (Móstoles, Spain; Figure 1A). During each scan sequential slices were obtained perpendicular to the mobile table. Each slice produces a 512x512 pixel image giving quantitative information on density distribution of the scanned volume. Each slice is 1 mm thick, so our final volume is formed by around 300 slices. Images are produced in DICOM format and processed using Oxiris free software. We tested the feasibility of scanning experiments with continuous Syrup flow, and checked if scanner table movement introduced any undesirable influence. We obtained a scanning time of 26 seconds long, and scanned the device each 2 or 5 minutes during experiments between 12 to 50 minutes long.

We have obtained XRCT data from 14 intrusion experiments and laboratory data of 25 similar experiments. We have only modified the flow rate, repeating each experiment several times to

compare monitoring results from the hospital and the laboratory. From those comparisons we can confirm that our XRCT scanning monitoring procedure does not disturb the experiments. Due to the 3D nature of the XRCT data, we can analyze the coeval model interior and (Figure 1B). We can identify the intrusion-induced faulting of the edifice as faults are lower density zones, darker in the images, analyzing their 3D spatial pattern and temporal evolution by comparing successive volumes. We can also observe the intrusion and a zone around with very high pixel values (Figure 1B). Our XRCT data show that this technique allows the 4D reconstruction of the experiment, obtaining internal structural information, the evolving morphology of the intrusion and the connection of internal deformation with surface features of the model.

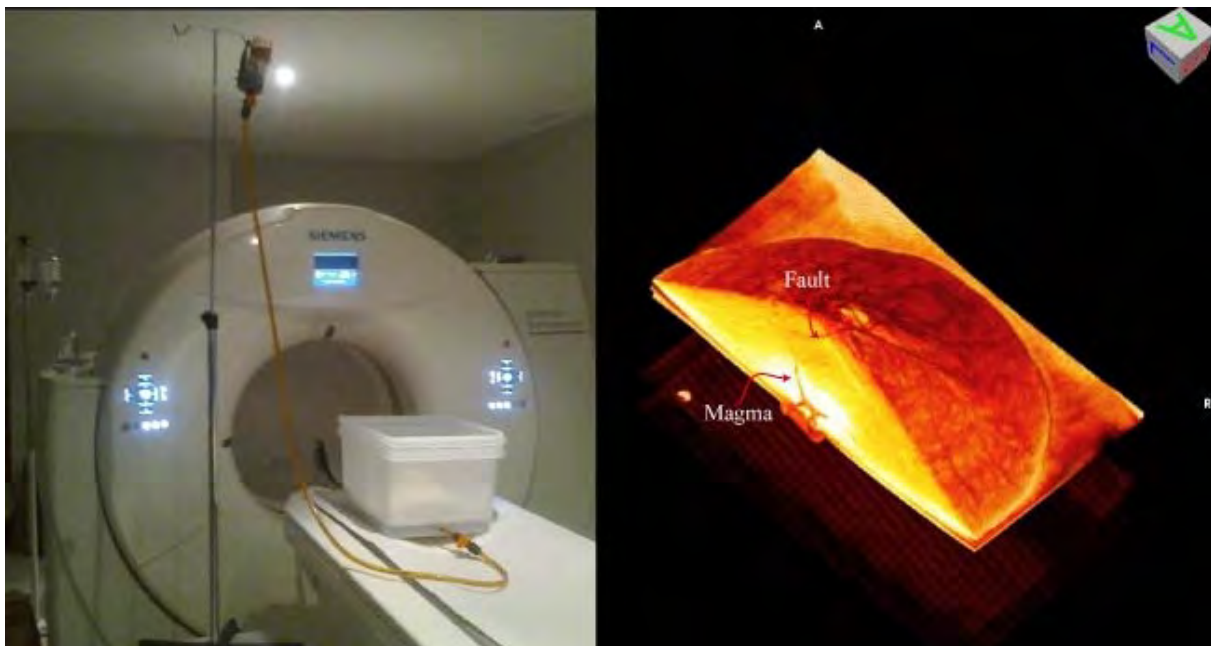


Figure 1: A: Experimental device at the XRCT. B: 3D reconstruction of an experiment.

#### References:

- Adam, J., Klinkmüller, M., Schreurs, G., & Wieneke, B. (2013). Quantitative 3D strain analysis in analogue experiments simulating tectonic deformation: Integration of X-ray computed tomography and digital volume correlation techniques. *Journal of Structural Geology*, 55, 127-149.
- Donnadieu, F., & Merle, O., 1998. Experiments on the indentation process during cryptodome intrusions: new insights into Mount St. Helens deformation. *Geology*, 26, 79-82.
- Kervyn, M., Ernst, G. G. J., van Wyk de Vries, B., Mathieu, L., & Jacobs, P., 2009. Volcano load control on dyke propagation and vent distribution: Insights from analogue modeling. *Journal of Geophysical Research: Solid Earth*, 114(B3).
- Kervyn, M., Boone, M. N., de Vries, B. V. W., Lebas, E., Cnudde, V., Fontijn, K., & Jacobs, P., 2010. 3D imaging of volcano gravitational deformation by computerized X-ray micro-tomography. *Geosphere*, 6, 482-498.

**Keywords:** Volcano analogue model, XRCT.

## Temporal evolution of magma flow and degassing conditions during dome growth, insights from 2D numerical modeling.

Laure Chevalier<sup>1</sup>, Marielle Collombet<sup>1</sup>, Virginie Pinel<sup>1</sup>, Alain Burgisser<sup>1</sup>

<sup>1</sup>) University of Savoie Mont-Blanc, IRD, CNRS, ISTerre, Le Bourget du Lac, France

Corresponding author: laure.chevalier@univ-smb.fr

S3 – Volcanoes: from the plumbing system to the eruptive plume (Oral)

### Background:

At andesitic volcanoes (e.g. Soufrière Hills Volcano, Merapi), quiescence periods with effusive lava flows and dome emplacement alternate with explosive, sometimes very violent events. Magma gas content is a controlling parameter for eruption style, that mainly depends on the ability for magma to loose gas while rising toward the surface. Understanding magma degassing evolution during an eruption is then essential to improve forecasting of effusive/explosive regime transitions.

Lava domes frequently form during effusive phases, inducing a pressure increase both within the conduit and in the surrounding rock, causing magma flow and degassing conditions to evolve (fig. 1a). To quantify dome influence on magma flow and degassing, we couple magma and gas flow in a 2D (axisymmetry) numerical model, using Comsol multiphysics software.

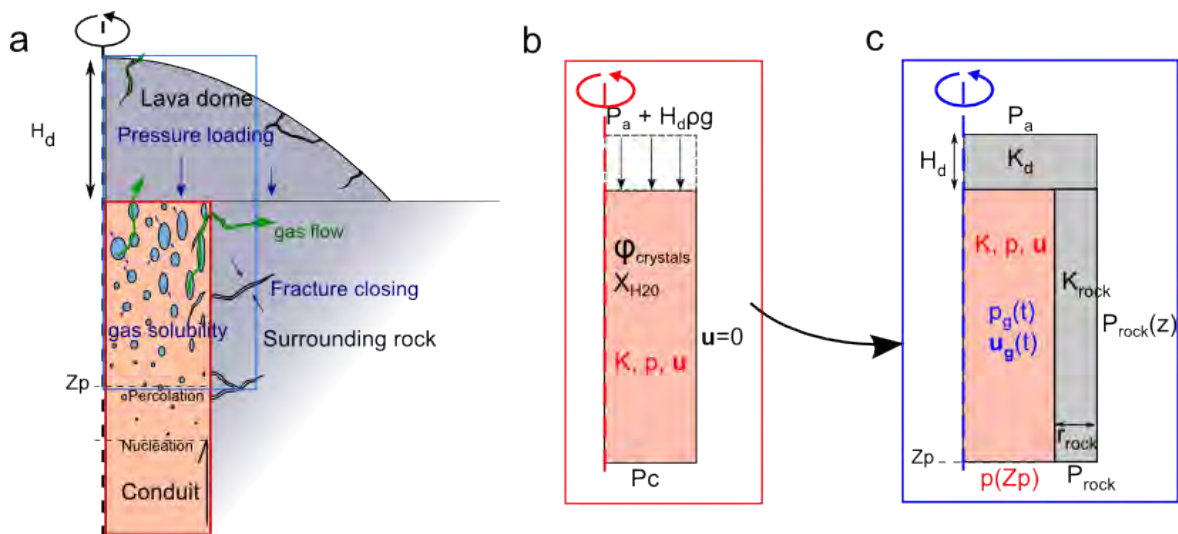


Figure 1: (a) is a global sketch of magma and gas flow inside the volcano and dome possible effects on conduit and surrounding rock conditions. Numerical models for magma and gas flow are respectively presented in (b) and (c). Boundary conditions, as well as fixed parameters are specified (black font). Parameters in red come from magma flow conditions solution, blue parameters come from gas flow solution. (modified from Chevalier et al., 2016).

### Numerical modeling:

#### Magma flow conditions

Mass and momentum conservation equations (Navier-Stokes) for magma flow are first solved in 2D axisymmetry (fig. 1b). Magma is represented as a single compressible phase, the bulk properties of which (density, viscosity) depend on the properties and interaction of the gas, melt and crystal phases.

### Gas flow conditions

Resulting magma flow conditions (magma permeability  $K$ , velocity  $u$  and pressure  $p$ ) are used as initial conditions to calculate time-dependent gas flow conditions (fig. 1) in 2D. Magma gas content evolves due to (i) water exchanges between the melt and gas phases, (ii) magma flow that advects bubbles, and (iii) Darcian gas flow through the permeable magma and surrounding rock. Gas flow conditions are solved for the top part of the conduit, where gas flow through the permeable magma, the rock surrounding the conduit and the dome (fig. 1c).

### Dome emplacement effects

From realistic initial magma flow conditions in effusive regime (Collombet, 2009), we apply increasing pressure at the conduit top. Since volatile solubility increases with pressure, dome growth is associated with an increase of magma dissolved water content at a given depth, which corresponds with a decrease of magma porosity and permeability. Although dome permeability has almost no influence on magma degassing, pressure increase in the surrounding rock as well as magma permeability decrease in the conduit limit gas leak at the conduit walls, thus causing gas pressurization in the upper conduit by a few tens of MPa (fig. 2). Magma permeability decrease and gas pressurization rise magma explosivity and hazard in case of a rapid decompression due to dome collapse.

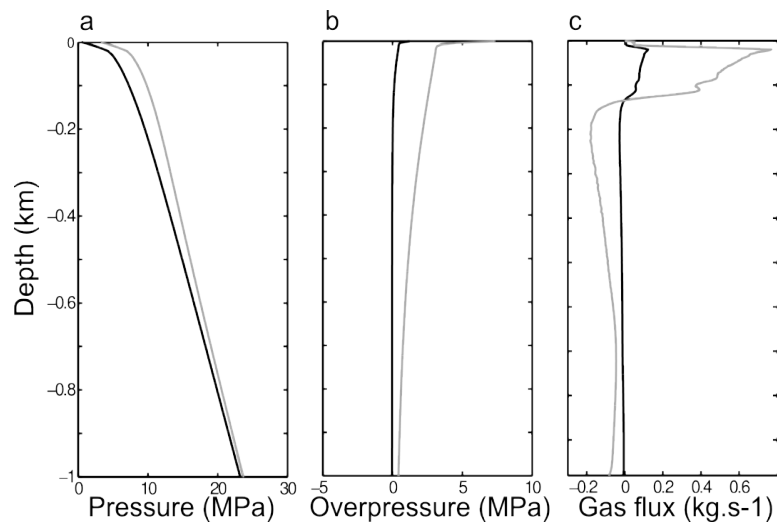


Figure 2 : Effects of pressure increase in the surrounding rock on gas flow. (a) Pressure boundary condition imposed to the surrounding rock (see fig. 1c), corresponding with dome heights of 50m (gray curve) and 300m (black curve). (b) Overpressure in the conduit (compared with effusive conditions) at gas flow equilibrium. (c) Gas flux evolution (difference with effusive conditions) at the conduit boundary, at equilibrium. Gas loss is limited at depth due to increased pressure in the surrounding rock. Gas pressure then increases in the conduit. At the conduit top, gas pressurization in the conduit is maximal, and is associated with an increased gas flux toward the surrounding rock.

### Perspectives:

Domes mostly affect magma flow and degassing by limiting gas exchange with the surrounding rock. Magma permeability has a great influence on the ability of the gas to flow and escape. Recent work

(Burgisser et al., 2016) that led to a better understanding of magma permeability development could be integrated to the model. We will discuss the implications of such changes in permeability laws. Magma permeability is extremely dependent on flow conditions and on volatile content. Coupling magma and gas flow in a full way is thus primordial, and is one of our major current task.

## References:

- Burgisser, A., Chevalier, L., Gardner, J. E., Castro, J. M., 2016 (in prep.). The percolation threshold and permeability evolution of ascending magmas.
- Chevalier, L., Collombet, M., Pinel, V., 2016 (submitted). Temporal evolution of magma flow and degassing conditions during dome growth, insights from 2D numerical modeling. *Journal of Volcanology and Geothermal Research*.
- Collombet, M., 2009. Two-dimensional gas loss for silicic magma flows: toward more realistic numerical models, *Geophysical Journal International*, 177, 309–318.

## Damage and strain localization in modelling pre-eruptive deformation

Jean-Luc Got<sup>1</sup>, Aurore Carrier<sup>1</sup>, David Marsan<sup>1</sup>, David Amitrano<sup>2</sup>, François Jouanne<sup>1</sup>, Sigrun Hreinsdottir<sup>3</sup>, Kristin Vogfjörd<sup>4</sup>

<sup>1</sup>) Université Savoie Mont-Blanc, ISTerre, Le Bourget du Lac, France

<sup>2</sup>) Université Grenoble Alpes, ISTerre, Grenoble, France

<sup>3</sup>) University of Iceland, Institute of Earth Sciences, Reykjavik, Iceland

<sup>4</sup>) Icelandic Meteorological Office, Reykjavik, Iceland

Corresponding author: jlgot@univ-smb.fr

S3 – Volcanoes: from the plumbing system to the eruptive plume (Oral)

### A time analysis of the non-linear magma-edifice coupling at Grimsvötn volcano:

Continuous monitoring of seismicity and surface displacement on active basaltic volcanoes reveals important features of the eruptive cycle. At Piton de la Fournaise volcano, based on averages performed over 22 eruptions, Schmid et al. (2012) showed that seismicity rate and displacement rate were increasing in the days and weeks preceding the eruption.

At Grimsvötn volcano, high-quality earthquake and continuous GPS data were recorded and exhibit remarkable patterns : acceleration of the cumulated earthquake number, and a 2-year exponential decrease in displacement rate followed by a 3-year constant inflation rate (Figure 1). The 2-year exponential decrease in displacement rate may be explained by the pressurization of a superficial reservoir fed by magma through a cylindrical vertical conduit and may be modelled using a linear elastic model. In that case, reservoir overpressure and surface displacement reach a limited value for large times.

This model however can not explain the constant inflation rate that follows. A constant inflation rate corresponds to a constant volume increase rate, that is, a constant input magma flow. Imposing a constant magma flow condition in the reservoir in a linear elastic medium leads to the magma pressure linearly – and infinitely – increasing with time. However real rock strength is limited and rupture occurs. Rock mechanics experiments show that rupture is preceded by a damage phase, during which anelastic deformation increases and micro-rupture number accelerates. During this phase, rock behaves partly elastically, but Young's modulus is no more constant and has to be replaced by an effective modulus, decreasing with strain. Therefore understanding the pre-eruptive process needs to understand the rupture process and the non-linear magma-edifice coupling, by taking account for damage and introducing an effective modulus.

Damage laws express the decrease of the effective modulus with strain. We show that Kachanov's damage law may be used, in the pre-eruptive case, to express the decrease of the effective shear modulus with time. Using this law and the pressurization model (spherical reservoir pressurized through a magma conduit), we found simple analytical solutions for magma reservoir overpressure, surface displacement and magma flow in the case where magma is incompressible (Figure 1). Critical time  $t_c$  may be estimated from the fit of the seismicity model to the data, and parameters  $a$ ,  $\tau_0$  and  $u_{el}$  are estimated from the fit of the displacement model to the data. Results (Figure 1) show how the shear modulus decreases with time; they also show that overpressure and magma flow remain constant for  $\sim 1000$  days, and respectively decreases and increases before the rupture and eruption. Overpressure decrease is controlled by damage and shear modulus decrease. Displacement increases, although overpressure is decreasing, because shear modulus decreases more than overpressure. Characteristic time  $t(t)$  shows a maximum ; before this maximum the order of magnitude of  $\tau$  is controlled by magma transfer, and after it is controlled by damage – this is true for overpressure,

magma flow and displacement. When magma is incompressible and  $\tau_0$  sufficiently large, the final stage of the pre-eruptive process is controlled by damage.

**Damage and strain localization around a pressurized magma reservoir:**

When a rock sample is submitted to increasing compression, shear or tension, damage appears and strain progressively localizes. We used finite element modelling of an initially elastic volcanic edifice pressurized by a spherical magma reservoir, and Kachanov’s damage law to decrease the effective modulus of each element with strain. A complex strain localization pattern appears (Figure 2).

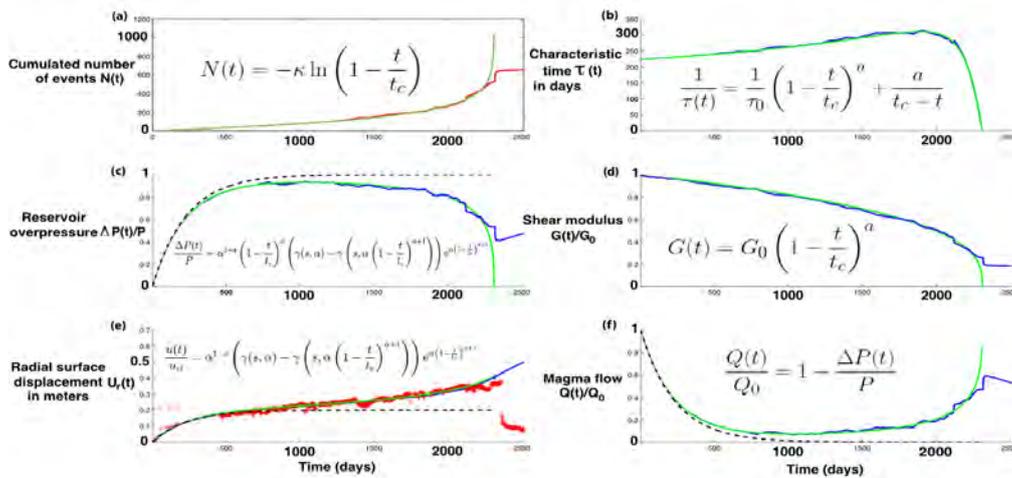


Figure 1 : Model variables as a function of time from 01/12/2004 to 31/12/2011. Data are represented in red, Runge-Kutta (RK) numerical solution in blue, analytical solution in green, linear elastic solution in dashed black.  $t_c$  is estimated from  $N(t)$ ,  $\tau_0$ ,  $u_{el}$  and  $a$  from  $u(t)$ .  $\gamma$  : incomplete  $\gamma$  function.

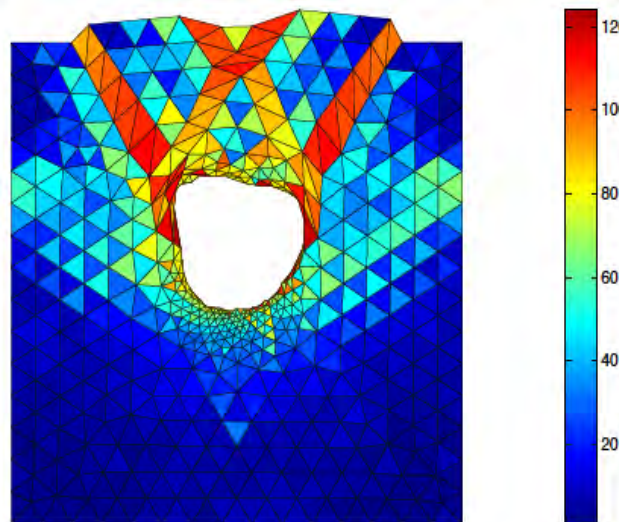


Figure 2: Number of ruptures per cell, in a 2D finite element model showing the deformation of a volcanic edifice pressurized (constant pressure) by an initially circular magma reservoir (no horizontal displacement of the model vertical boundaries). Modeling follows Amitrano et al. (1999)’s algorithm: rupture in a cell occurs when the Mohr-Coulomb criterion is fulfilled; the corresponding effective modulus is decreased. Damage and strain localization occur progressively. Inverse and normal faults appear, as well as an undeformed wedge just above the pressurized reservoir. This pattern is observed in analog experiments and on the field.

## References:

- Amitrano, D., Grasso, J.-R., Hantz, D., 1999. From diffuse to localised damage through elastic interaction, *Geophys. Res. Lett.*, 26, 14, 2109-2112.
- Schmid, A., Grasso, J.-R., Clarke, D., Ferrazzini, V., Bachèlery, P., and Staudacher, T., 2012. Eruption forerunners from multiparameter monitoring and application for eruption time predictability, *J. Geophys. Res.*, 117, B11, 203, doi:10.1029/2012JB009167.

**Keywords:** Eruption, damage, deformation, rupture, magma-edifice coupling, earthquake, volcano, Grimsvötn.

## Stress-strain relationships in intruded viscoelastic media: insights from analogue modeling

Håvard S. Bertelsen<sup>1</sup>, Benjamin Roger<sup>1</sup>, Olivier Galland<sup>1</sup>, Fanny Bjugger<sup>1</sup> and Karen Mair<sup>1</sup>

<sup>1</sup>) University of Oslo, Physics of Geological Processes, Oslo, Norway

Corresponding author: haavasb@mail.uio.no

S3 – Volcanoes: from the plumbing system to the eruptive plume (PS7)

Contrasting magma intrusion morphologies are evident in field exposures, ranging from mushroom-shaped diapirs to blade-like dykes. Currently, no common theory is able to account for such morphological diversity: only end-member models exist. On the one hand, diapiric rise is often simplified as creeping, viscous flow of the intruded host rock around a magma body. On the other hand, dykes are assumed to propagate as fractures in an elastic host rock. However, natural rocks are complex visco-elasto-plastic materials. The current theories of magma emplacement are therefore crude simplifications of reality, explaining why they do not account for the natural diversity of igneous intrusion shapes. In an attempt to fill the gap between the end-member theories, we use laboratory models of magma emplacement in visco-elasto-plastic media. Particularly, we will pay attention to constraining the visco-elasto-plastic deformation field accommodating magma emplacement. This is achieved using combined polarimetry and digital image correlation to quantify the stress-strain relationships in the host matrix and map the distribution of the visco-elasto-plastic deformation accommodating magma emplacement (Bertelsen 2014).

In our analogue model the host rock is represented by laponite, a synthetic smectite clay, which in aqueous suspension can display a wide range of rheological properties through varying concentration, ionic content, pH, and curing time. Olive oil or water was used as magma analogues. A linear Hele-Shaw cell is filled with a laponite matrix and left to cure to a viscoelastic gel form (Figure 1). After an appropriate curing period the matrix is intruded by the viscous magma analogue. The intrusion is driven by a syringe pump and maintained at a constant flow rate. When strained, the particles forming the elastic phase of the laponite matrix realigns causing birefringence. During experiments, birefringence maps are periodically captured with a polariscope composed of a camera and crossed polarizers, backlit with a uniform diffused white light source. In addition, the laponite matrix contains markers, the displacements of which can be calculated by digital image correlation.

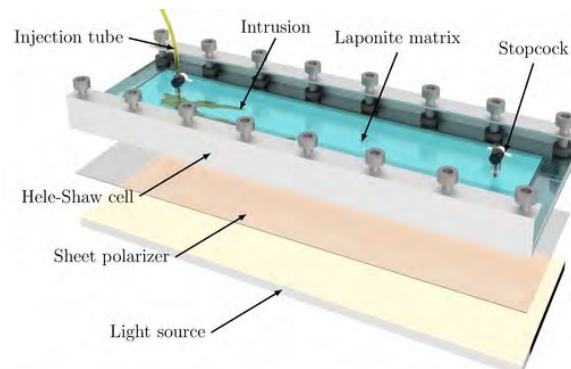


*Figure 1: Experimental setup. A linear Hele-Shaw cell filled with a viscoelastic laponite matrix is intruded by a viscous medium: oil or water. The cell is backlit using a uniform diffused white light source. Strain-induced birefringence in the otherwise transparent matrix, as well as particle and interfacial movement is captured using a camera and crossed polarizers. Intrusion flow rate is controlled with a syringe pump. Stopcocks at the inlet and outlet isolate the laponite sample during gel curing to avoid interaction with air.*

Characteristic results from the experiments are shown in Figure 2. The intrusions formed broad, lobe-like Rayleigh-Taylor fingers and narrow, magma-filled fractures in viscous and elastic host materials respectively, and more complex intrusion geometries in intermediate visco-elasto-plastic host media. The birefringence patterns are indicative of the strain taken up in the elastic network of the gel, while tracer particle movement shows the bulk flow in the continuous water phase of the gel. Importantly, optical refraction allows us to observe hairline fracture features that are invisible to the human eye.

Therefore, our experiments evidence the coeval occurrence of brittle features and elastic when observed through a polariscope. Altogether, these experiments are very promising to unravel the complex visco-elasto-plastic response of natural rocks to magma intrusions. The experiments presented here also show that the rheological response in a gel matrix subjected to fluid injection is indeed dependent on viscosity ratio. Moreover, laponite has proven to be a viable material for studying intrusive processes in the visco-elasto-plastic regime, as well as other geological processes taking place in complex rheological regimes.

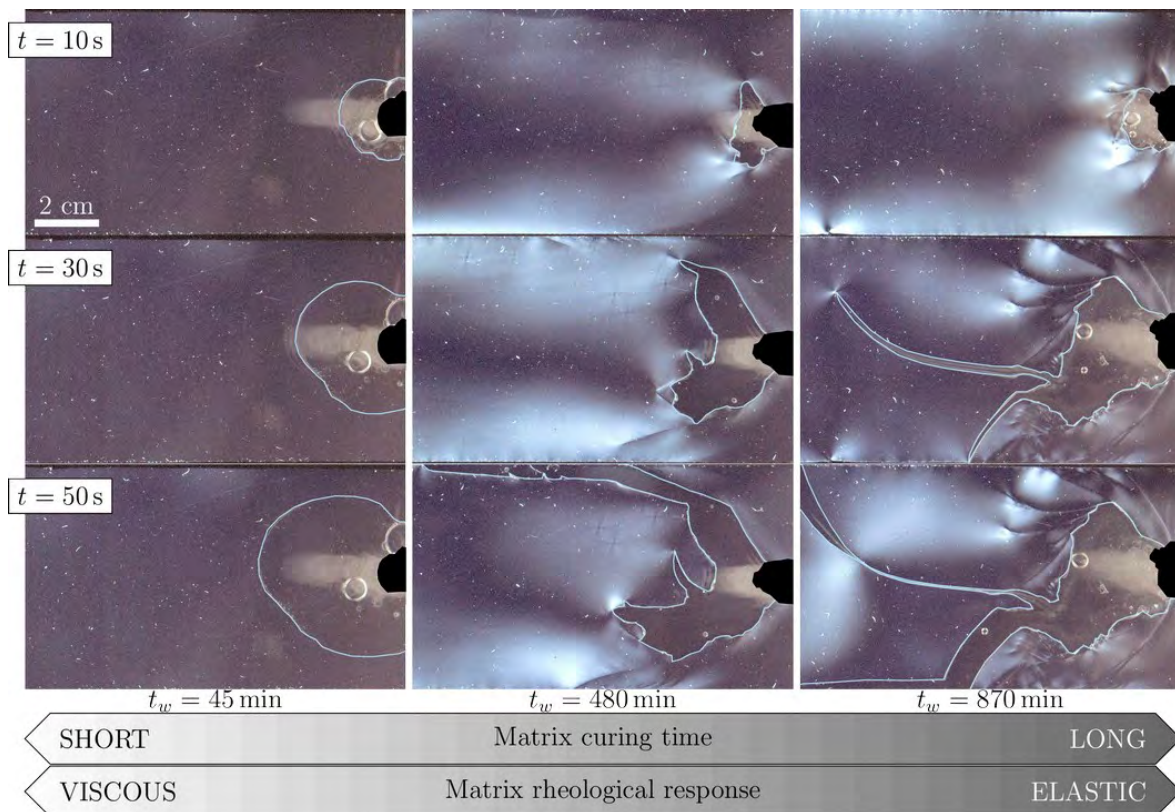


Figure 2: Top three rows: representative images showing the intrusion evolution and matrix response for three different matrix curing times at different time steps. Intrusion contours are outlined in light blue. The birefringence (white) highlight domains of distributed deformation separated by hair-thin cracks, invisible to human eyes.

## References:

Bertelsen, H. S., 2014. Blowing the Viscoelastic Trumpet: Experiment Design for Mapping Stress-Strain Patterns in Viscoelastic Hydrofracture, master thesis, permanent link: <http://urn.nb.no/-45994>

**Keywords:** Magma plumbing systems, magma intrusion, hybrid fracturing, hybrid intrusion, laponite, host rheology, photoelasticity.

## The link between circumferential dikes and eruptive fissures around calderas: insights from analog and numerical models

Fabio Corbi<sup>1\*</sup>, Eleonora Rivalta<sup>1</sup>, Virginie Pinel<sup>2</sup>, Francesco Maccaferri<sup>1</sup> and Valerio Acocella<sup>3</sup>

<sup>1)</sup> GFZ German Centre for Geosciences, Section 2.1, Telegrafenberg, 14473 Potsdam, Germany.

<sup>2)</sup> ISTerre, Université Savoie Mont-Blanc, IRD, CNRS, Campus Scientifique, Le Bourget du Lac F73376, France.

<sup>3)</sup> Roma Tre University, Laboratory of Experimental Tectonics, Dip. Scienze, Rome, Italy.

<sup>\*</sup>) now at University of Montpellier, Géosciences Montpellier Laboratory, Montpellier, France.

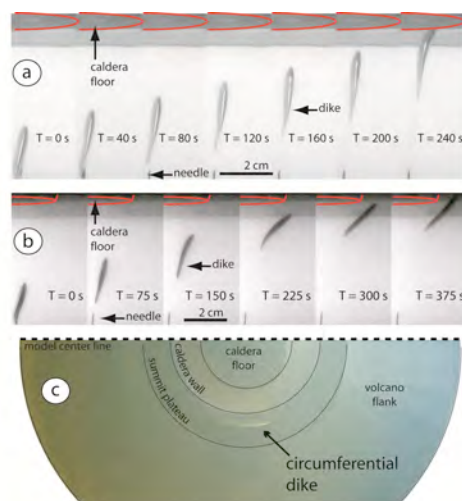
Corresponding author: fabio.corbi3@gmail.com

S3 – Volcanoes: from the plumbing system to the eruptive plume (PS7)

### Abstract:

Active calderas are seldom associated with circumferential eruptive fissures along their rim, but eroded portions of extinct magmatic complexes reveal widespread evidence of circumferential dikes. This discrepancy suggests that, while the conditions to emplace circumferential dikes below volcanoes are easily met, mechanisms must exist to arrest the dikes before they reach the surface.

Here we explain this discrepancy with laboratory experiments of air injection into a gelatin medium shaped to mimic a volcanic edifice with caldera. Our models show that the ascending dikes experience a variable degree of deflection, depending on the competition between dike overpressure,  $P_e$ , and the forcing induced by the topographic load,  $P_l$ . When  $P_l/P_e = 4.3 - 4.5$  the analog dikes proceed almost insensitive to the stress rotation and erupt within the caldera. When  $P_l/P_e = 4.8 - 5.3$  the analog dikes closely propagate orthogonal to the least compressive stress  $\sigma_3$  and stall below the caldera rim in a circumferential arrangement.



Progressive buoyancy increase through repeated supply of fluid is fundamental for the occurrence of circumferential fissures. Complementary numerical models explain the observed circumferential arrangement and validate the experiments. These results contribute defining the shallow magma transfer and related hazard assessment within calderas.

**Keywords:** Circumferential dikes, Eruptive fissures, Caldera, Unloading, Dike trajectory.

## Are igneous sheet intrusions really mode I elastic fractures?

O. Galland<sup>1</sup>, M.M. Abdelmalak<sup>2</sup>, J. Spacapan<sup>3</sup>, R. Mourgues<sup>4</sup>, H.A., Leanza<sup>5</sup>, S. Planke<sup>2,6</sup>

<sup>1</sup>) Physics of Geological Processes, Department of Geosciences, University of Oslo, Oslo, Norway

<sup>2</sup>) Centre for Earth Evolution and Dynamics, University of Oslo, Oslo, Norway

<sup>3</sup>) Universidad Nacional de La Plata-CONICET-Fundación YPF, La Plata, Argentina

<sup>4</sup>) Museo Argentino de Ciencias Naturales - CONICET, Buenos Aires, Argentina

<sup>5</sup>) L.P.G.N., Université du Maine, Le Mans, France

<sup>6</sup>) Volcanic Basin Petroleum Research, Oslo, Norway

Corresponding author: olivier.galland@geo.uio.no

S3 – Volcanoes: from the plumbing system to the eruptive plume (PS7)

### Introduction:

Igneous sheet intrusions, such as dykes and sills, represent dominant magma transport and emplacement channels through the Earth's crust. Because of their low thickness-to-length aspect ratios, sheet intrusions are commonly assumed to be hydraulic fractures. Consequently, most models of dyke and sill emplacement only account for elastic deformation of the host rock, and their propagation is considered to occur by tensile opening (Rivalta et al., 2015). In this contribution, we integrate detailed field observations and quantitative laboratory models to suggest instead that sheet intrusions might propagate as a viscous indenter by shear failure (mode II) of the host rock.

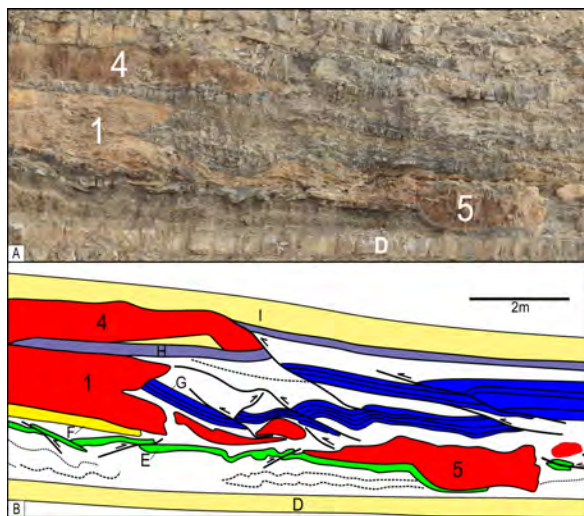


Figure 1. A. Detailed ortho-rectified photograph of the Chihuido outcrop, Neuquén Basin, Argentina, displaying two Fingers (4 and 5) and the tip of a Sill, and the surrounding structures in the host rock (Spacapan et al., submitted). B. Detailed map of A, displaying parts of layers D (bottom pale yellow), E (green) and F (yellow), G (deep blue), H (purple) and I (top pale yellow) and their associated structures. The most noticeable feature is the duplications of layer G. This is a small part of a ~50 m long outcrop, along which many intrusions and each layer of the host rock have been mapped in detail (Spacapan et al., submitted). The structures show that the host rock accommodated the emplacement of the sill by shortening, not by opening.

### Field observations:

First, we report on detailed field observations of spectacularly exposed intrusions emplaced in shale at Cuesta del Chihuido, in the Neuquén Basin, Argentina. Exceptional outcropping conditions allow detailed descriptions of both (1) intrusions sections from tip to tip, and (2) deformation structures accommodating intrusion propagation in the host rock (Spacapan et al., submitted). All intrusions exhibit irregular, blunt or rectangular tips (Figure 1). In addition, the structures in the host rock show clear evidence of both brittle and ductile deformation accommodating the propagation of the intrusions, and this deformation systematically relates to shortening and even rock wedging. Our observations suggest that the studied intrusions have propagated by pushing the host rock ahead, as a

viscous indenter. None of our observations are in agreement with the established tensile elastic fracture model.

### Laboratory modelling:

In addition to field observations, we performed dynamic two-dimensional laboratory experiments of sheet intrusion emplacement (here dykes). Our experimental setup consists of a Hele-Shaw cell, in which a model magma is injected into a cohesive model crust. Using an optical image correlation technique (PIV), we measured the displacements and the strain field induced by magma emplacement within the host rock. Dyke emplacement exhibits two stages. During the first stage corresponds to the emplacement of in a vertical dyke at depth; its propagation was controlled by both shear deformation and tensile opening. During the second stage, the intrusion gradually rotates, forming an inclined sheet dipping between 45 to 65°. This rotation results in asymmetrical surface uplift and shear failure upon the tip of the dyke. The intrusion of magma results in surface uplift, which can be accommodated by reverse faults. Our study suggests that dykes propagate as viscous indenters, rather than linear elastic fracturing.

Both field observations and modelling results contradict the established tensile elastic models. Our results therefore suggest that elastic models lack some fundamental aspects of the complex dynamics of the emplacement of sheet intrusions.

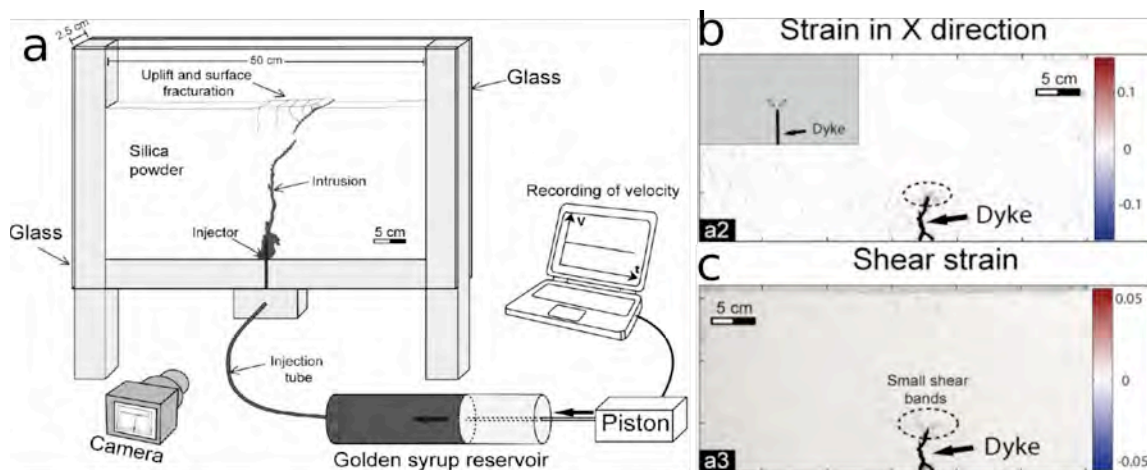


Figure 2. a. Drawing of the laboratory setup, after Abdelmalak et al. (2012). b and c. Characteristic maps of strain in X direction and shear strain associated with the propagation of a dyke. The show small-scale reverse shear bands at the dyke tip, showing that the dyke indents its overburden instead of opening it in a tensile manner.

### References:

- Abdelmalak, M.M., Mourgues, R., Galland, O., Bureau, D., 2012. Fracture mode analysis and related surface deformation during dyke intrusion: Results from 2D experimental modelling. *Earth Planet. Sci. Lett.* 359-360, 93-105.
- Rivalta, E., Taisne, B., Bungler, A.P., Katz, R.F., 2015. A review of mechanical models of dike propagation: Schools of thought, results and future directions. *Tectonophysics* 638, 1-42.
- Spacapan, J.B., Galland, O., Leanza, H.A., Planke, S., submitted. Igneous sill emplacement mechanism in shale-dominated formations: a field study at Cuesta del Chihuido, Neuquén Basin, Argentina. *Journal of the Geological Society of London*.

**Keywords:** Igneous sheet intrusions, field mapping, laboratory modeling, viscous indenter.

## Laboratory modeling of volcano plumbing systems: A review

O. Galland<sup>1</sup>, E. Holohan<sup>2</sup>, B. van Wyk de Vries<sup>3</sup>, S. Burchardt<sup>4</sup>

<sup>1</sup>) Physics of Geological Processes, Department of Geosciences, University of Oslo, Oslo, Norway

<sup>2</sup>) Géosciences Rennes, Université de Rennes1, Rennes, France

<sup>3</sup>) Observatoire de Physique du Globe de Clermont-Ferrand, Blaise Pascal University, Clermont-Ferrand, France

<sup>4</sup>) Solid Earth Geology, Department of Earth Sciences, University of Uppsala, Uppsala, Sweden

Corresponding author: olivier.galland@geo.uio.no

S3 – Volcanoes: from the plumbing system to the eruptive plume (PS7)

Since the XIX century, Earth scientists have tried to replicate geological processes in controlled laboratory experiments. This contribution (Galland et al., 2015) reviews such laboratory models of the complex development and dynamics of volcano plumbing systems (Figure 1).

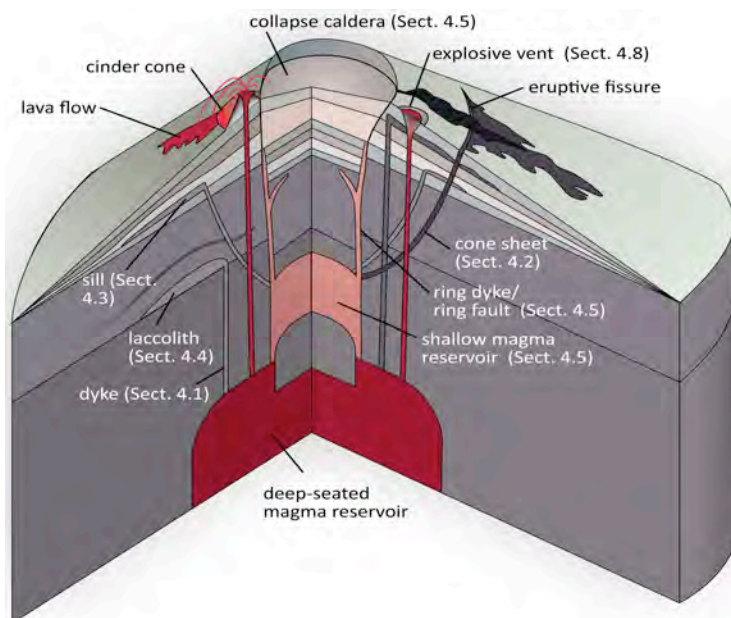


Figure 1. Schematic drawing illustrating the main characteristics of volcano plumbing systems. These include dykes, cone sheets, sills, laccoliths, caldera-related structures and intrusions, magma-fault interactions, and explosive volcanic vents. The numbering correspond to the sections developed in the review by Galland et al. (2015).

The first step of laboratory modelling is the choice of relevant model materials for rock and magma. We outline a broad range of suitable model materials used in the literature, and list their mechanical properties. These materials exhibit very diverse rheological behaviours, so their careful choice is crucial for proper experiment design.

The second step is model scaling, which successively calls upon: (1) the principle of dimensional analysis, and (2) the principle of similarity. The dimensional analysis aims to identify the dimensionless physical parameters that govern the underlying processes. The principle of similarity quantifies the extent to which the models are representative of the geological systems they intend to simulate. The application of these two steps ensures a solid understanding and geological relevance of the laboratory models. In addition, this procedure shows that laboratory models are not designed to exactly mimic a given geological system, but to understand underlying generic processes, either individually or in combination, and to identify or demonstrate physical laws that govern these processes.

From this perspective, we discuss past applications of laboratory models that aimed to understand the development of key features of volcanic plumbing systems, such as dykes, cone sheets, sills, laccoliths, caldera-related structures, ground deformation, magma/fault interactions, and explosive vents (Figure 2).

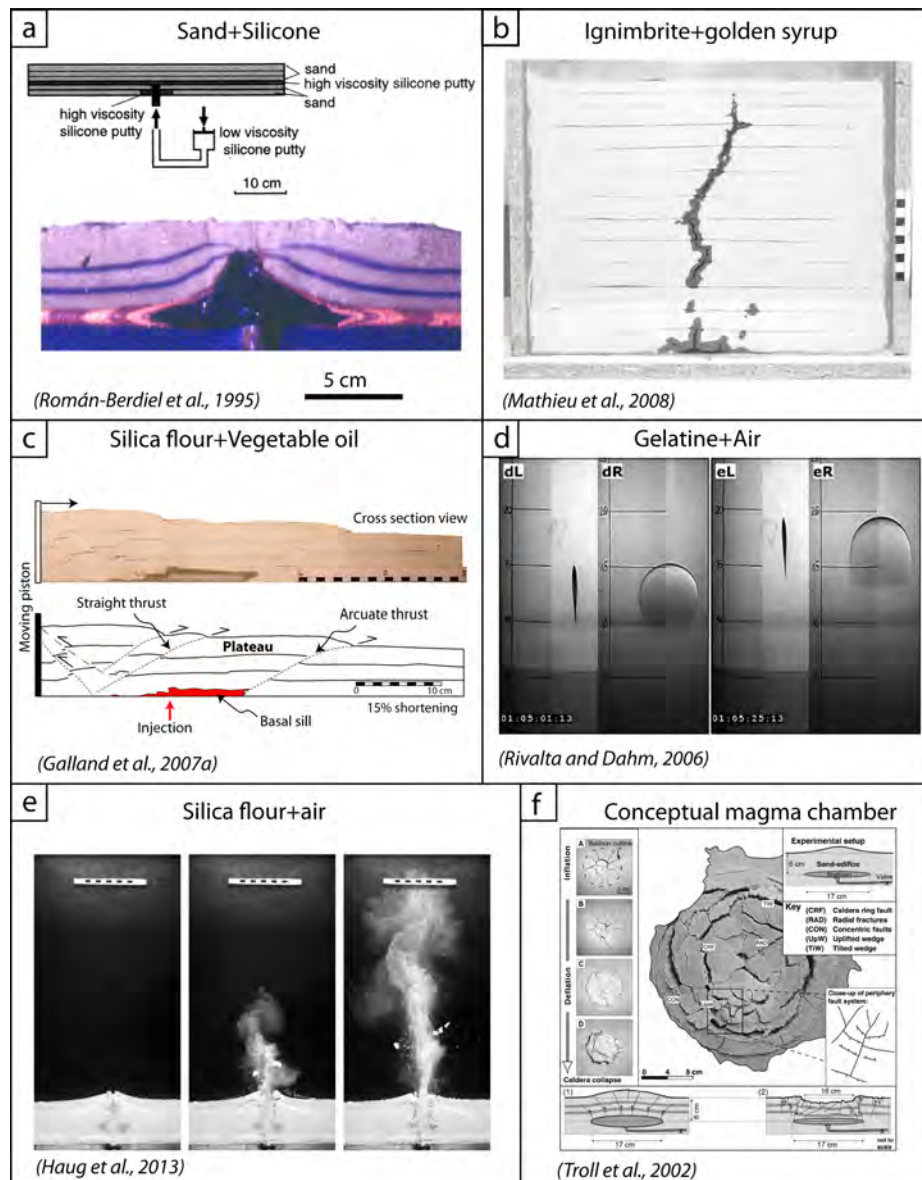


Figure 2: Characteristic examples of laboratory models of volcano plumbing systems using various model materials. a. Sand+silicone experiments for models of laccoliths. b. Ignimbrite+Golden Syrup experiment for dykes. c. Silica-flour+vegetable oil model for magma emplacement in a deforming brittle crust. d. Gelatine+air experiments for dykes in elastic host rock. e. Silica flour+air 2D experiments for explosive volcanism. f. Conceptual magma chamber using a balloon for the replenishment and draining of a magma chamber.

References:

Galland, O., Holohan, E.P., van Wyk de Vries, B., Burchardt, S., 2015. Laboratory Modelling of Volcano Plumbing Systems: A Review, in: Breikreuz, C., Rocchi, S. (Eds.), *Physical Geology of Shallow Magmatic Systems - Dykes, Sills and Laccoliths*. Springer Berlin Heidelberg, pp. 1-68.

**Keywords:** Laboratory models, volcano plumbing systems, review.

## Predicting Volcanic Eruption Locations Based on Surface Deformation Precursors

Frank Guldstrand<sup>1</sup>, Olivier Galland<sup>1</sup>, Erwan Hallot<sup>2</sup> and Steffi Burchardt<sup>3</sup>

<sup>1</sup>) University of Oslo, Department of Geosciences, Physics of Geological Processes, Oslo,

<sup>2</sup>) Université de Rennes 1, Geosciences Rennes, UMR 6118, CNRS, Rennes, France

<sup>3</sup>) Uppsala University, Department of Earth Sciences, Centre for Mineralogy, Petrology and Geochemistry, Uppsala, Sweden

Corresponding author: f.b.b.guldstrand@geo.uio.no

S3 – Volcanoes: from the plumbing system to the eruptive plume (PS7)

Prior to an eruption, the ground of active volcanic zones deforms as a result of the intrusion of magma from below. Appropriate terrestrial or space-based geodetic monitoring used to detect and survey ongoing surface deformations while magma is displacing at depth and approaching the surface, is thus of primary interest to predict where, *in fine*, the magma should breach the Earth's surface. Assessing and mitigating the hazards of an eruption can be greatly improved if an estimated eruption location can be determined as it poses a great threat to human lives and property if it occurs in the vicinity of populated areas. However, the conventional methods used to analyze surface deformation do not allow for forecasting eruption location in real time or verifiably constraining the geometry of the magma feeder prior to an eruption (Wright et al., 2006, Amelung et al., 2000).

The approach suffers from crucial limitations in the aspect of eruption location and hazard assessment: (1) modeling is mostly performed a significant time after data acquisition, such that real-time analysis is out of reach. Consequently, it has poor potential for forecasting the eruption location. (2) The current practice within geodetic monitoring does not have the combined high spatial and temporal resolution required to perform the analysis we suggest. (3) Does not provide a verified pre-eruption estimate of magma feeder geometry from measured surface, which would allow for a first order estimate of the style of eruption.

We show, using surface deformation from 43 scaled laboratory models, how the simple geometric aspects of center of uplifted area (C) and maximum uplift (M), acquired at high spatial and temporal resolutions, can be used to follow magma pathways at shallow depth and predict eruption locations in real time (Fig 1 A, B). From (C) and (M) we define a vector  $\vec{V}_{MC}$  that, along with the norm  $|\vec{V}_{MC}|$  allows us to predict the eruption location before the eruption and a verified intrusion geometry (here dykes or cone sheets).

Our modeling approach and results highlight the dynamic nature of the surface deformation associated with shallow magma emplacement processes. Resolving surface deformation both at high spatial and temporal resolutions has the potential to identify simple geometric features, such as points of maximum uplift, which constitute proxies for magma ascent locations. As long as such geometrical features develop in a significant time prior to eruption they have the potential to be used as precursors, indicative for the potential location of a forthcoming volcanic eruption. Extracted only from surface data, these precursors are purely geometrical and relevant for various magma feeder geometries. This implies that costly computational surface data modeling, which is based on a, *a priori*, defined magmatic source geometry, is not necessary for eruption location forecasting purposes.

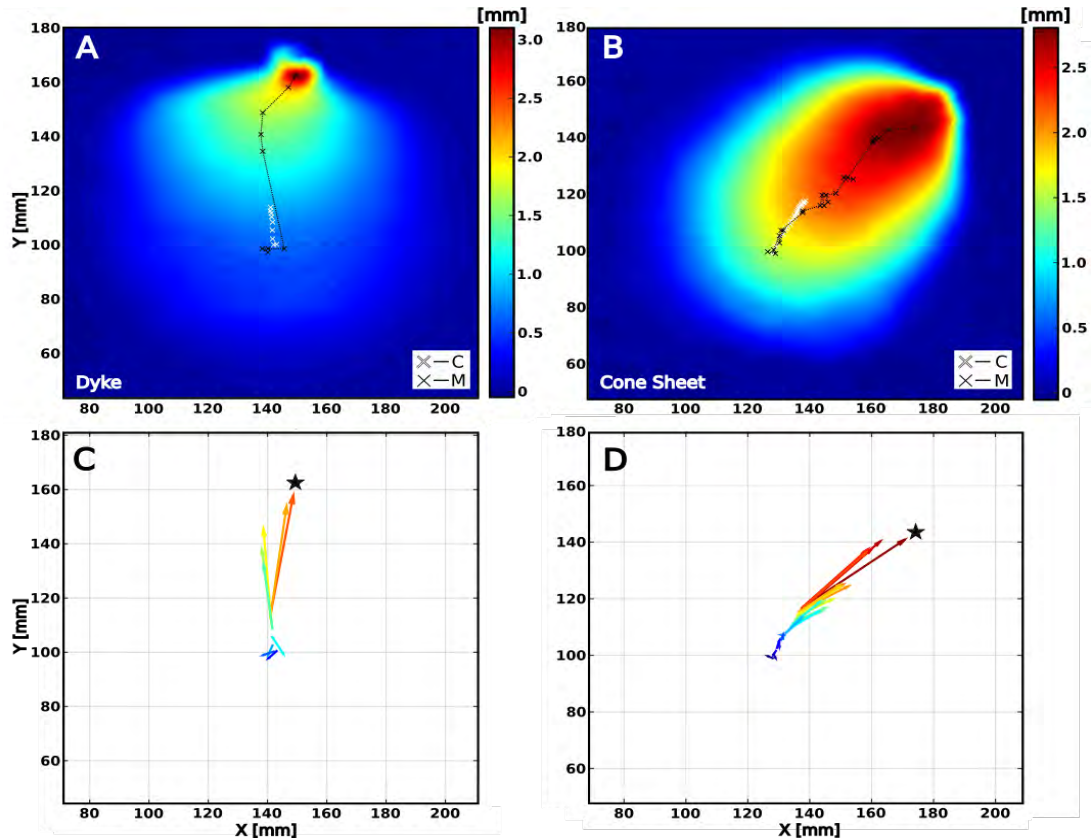


Figure 1. (A,B)  $\Delta$ DEM at the final timestep for 2 representative experiments, corresponding to a Dyke and a Cone Sheet, (uplift in mm) and corresponding vectors VMC at each timestep (C, D). (A, B) White crosses locate the center of the uplifted area at each timestep. Connected Black crosses (and lines) show the successive locations (and trajectory) of the maximum during the experiments. The final point of maximum uplift marks the point of eruption. (C, D) The color-code for VMC follows the timesteps from dark blue to dark red as time proceeds. The random orientation of the short vectors in the initial timesteps evolves, prior to the eruption, into a trends pointing towards the points of eruption (shown by a black star).

#### Acknowledgements:

Guldstrand's position is funded by the DIPS (Dynamics of Igneous Plumbing Systems, grant no. 240467) project from the Norwegian Research Council. This work was supported by a MeMoVoc exchange visit grant from the European Science Foundation (grant no. 4251).

#### References:

- Amelung, F., Jónsson, S., Zebker, H. & Segall, P. 2000. Widespread uplift and 'trapdoor' faulting on Galapagos volcanoes observed with radar interferometry. *Nature*, 407, 993-996.
- Wright, T. J., Ebinger, C., Biggs, J., Ayele, A., Yirgu, G., Keir, D. & Stork, A. 2006. Magma-maintained rift segmentation at continental rupture in the 2005 Afar dyking episode. *Nature*, 442, 291-294.

**Keywords:** Surface Deformation, Analogue Modeling, Eruption Location Forecasting.

## **Dynamics of Surface Deformation Induced by Dyke and Cone Sheet Emplacement in Laboratory Models**

Frank Guldstrand<sup>1</sup>, Olivier Galland<sup>1</sup>, Erwan Hallot<sup>2</sup> and Steffi Burchardt<sup>3</sup>

<sup>1</sup>) University of Oslo, Department of Geosciences, Physics of Geological Processes, Oslo, Norway

<sup>2</sup>) Université de Rennes 1, Geosciences Rennes, UMR 6118, CNRS, Rennes, France

<sup>3</sup>) Uppsala University, Department of Earth Sciences, Centre for Mineralogy, Petrology and Geochemistry, Uppsala, Sweden

Corresponding author: f.b.guldstrand@geo.uio.no

S3 – Volcanoes: from the plumbing system to the eruptive plume (PS7)

### **Introduction:**

The hazardous nature of volcanoes promotes the development and implementation of various monitoring techniques. In particular, geodetic methods such as GNSS and InSAR consist of monitoring surface deformation as a response to the dynamics of volcanic plumbing systems at depth. However, none of these methods offer both high spatial and temporal resolution of the surface deformation data. The consequence of these limitations is that the complex dynamics of surface deformation due to, for example, the emplacement of a magma intrusion is poorly understood. In this contribution, we present quantitative laboratory modeling results of surface deformation induced by the emplacement of shallow magma intrusions, here dykes and cone sheets. We show that surface deformation exhibits a complex dynamics that reflects the complex evolution of magma path at depth. Our results also demonstrate that surface deformation data at both high spatial and temporal resolutions are necessary to capture the dynamics of surface deformation associated with magma emplacement.

### **Method:**

Our laboratory setup uses fine-grained silica flour and a vegetable oil to simulate host rock and magma, respectively (Fig. 1). The surface uplift due to intrusion is monitored using a moiré projection apparatus (Bréque et al., 2004). This setup allows us to simulate the emplacement of various intrusion geometries in the shallow elasto-plastic crust and to quantitatively measure: (1) the pressure of the magma analogue through time; (2) the high-resolution and high-precision surface deformation induced by the emplacement of magma through time (Galland, 2012); (3) the 3D shape of the intrusion, as the magma analogue solidifies after the end of the experiment and the intrusion can be excavated. In addition, our models are able to simulate spontaneously various intrusion shapes, including dykes and cone sheets (Galland et al., 2014) in a controlled systematic manner.

### **Results and Conclusion:**

We produced 43 experiments, among which 22 produced cone sheets, 19 produced dykes and two classified as hybrids (Galland et al., 2014). During each experiment, a topographic map of the model surface is computed every 1.5 s. We performed a quantitative analysis of this substantial surface deformation data set, and reveal the dynamic evolution of surface uplift associated with dykes and cone sheets. We analyzed the dynamics of the maximum uplift (Fig. 2), the uplifted area, and uplifted volume, and quantified the asymmetry of the uplift pattern, and show that the surface deformation associated with dykes and cone sheets exhibit clearly distinctive, systematic signatures.

The results are highly relevant in the context of volcano geodesy for comparison, evaluation and development of current geodetic models. We are convinced that our quantitative laboratory data will become very valuable for helping interpreting geodetic data monitored at active volcanoes.

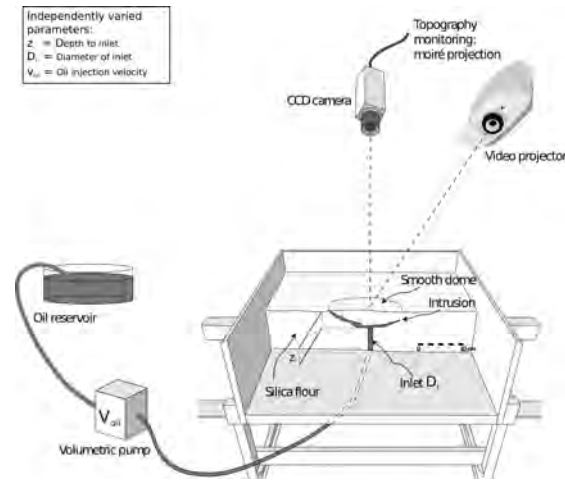


Figure 1. Diagram showing the experimental apparatus consisting of a 40 cm wide experimental box into which silica flour is poured and compacted. Vegetable Oil (Végétaline) is intruded using a constant flow rate driven by a volumetric pump. Each experiment lasts for about ~1 min or less ending with oil erupting at the surface. Topography monitoring is done through projecting a set of moving fringes recorded by the capture camera enabling a monitoring ever 1.5 s. The model is left to cool for ~45 min after which it is excavated to verify intrusion geometry. In this case, either sub-vertical planar dykes, of which some exhibit a hull shape, or inverted cone sheets.

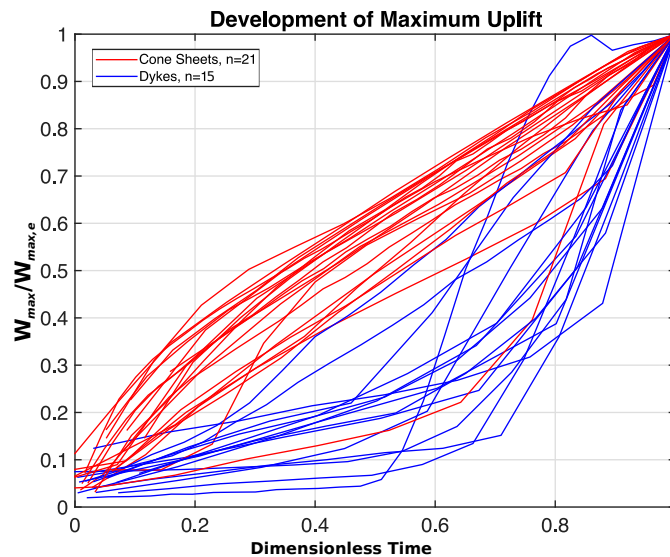


Figure 2. Scaled maximum uplift over dimensionless time for dykes (blue) and cone sheets (red). An intrusion that has been classified as a cone sheet appears in the lower dyke regime. This due to it having developed a late stage hull-shaped feature on top of the sub-vertical planar dyke. A more robust definition is thus based on using the dynamic evolution surface deformation as a definition for the two end-member regimes and the overlapping hybrids. Experiments with more than five timesteps have been plotted.

**Acknowledgements:**

Guldstrand's position is funded by the DIPS (Dynamics of Igneous Plumbing Systems, grant no. 240467) project from the Norwegian Research Council. This work was supported by a MeMoVolc exchange visit grant from the European Science Foundation (grant no. 4251).

## References:

- Bréque, C., Dupe, J.-C. & Bremond, F. 2004. Calibration of a system of projection moiré for relief measuring: biomechanical applications. *Optics and Lasers in Engineering*, 41, 241-260.
- Galland, O. 2012. Experimental modelling of ground deformation associated with shallow magma intrusions. *Earth and Planetary Science Letters*, 317, 145-156.
- Galland, O., Burchardt, S., Hallot, E., Mourgues, R. & Bulois, C. 2014. Dynamics of dikes versus cone sheets in volcanic systems. *Journal of Geophysical Research: Solid Earth*, 119, 6178-6192.
- Galland, O., Cobbold, P. R., Hallot, E., De Bremond D'Ars, J. & Delavaud, G. 2006. Use of vegetable oil and silica powder for scale modelling of magmatic intrusion in a deforming brittle crust. *Earth and Planetary Science Letters*, 243, 786-804.

**Keywords:** Surface Deformation, Analogue Modeling, Dykes, Cone Sheets.

## Modeling viscous flow using discrete particles: limits and applications to magma intrusions

Øystein Thordén Haug<sup>1</sup>, Alban Souche<sup>1</sup>, Olivier Galland<sup>1</sup>, Karen Mair<sup>1</sup>, and Steffen Abe<sup>2</sup>

<sup>1</sup>) Physics of Geological Processes, Department of Geosciences, University of Oslo, Norway

<sup>2</sup>) Institute for Geothermal Resources Management, Mainz, Germany

Corresponding author: o.t.haug@geo.uio.no

S3 – Volcanoes: from the plumbing system to the eruptive plume (PS7)

### Introduction:

Magmatic intrusions involve magma flowing through a host rock by the opening and propagation of fractures. Numerical modeling of such fluid-driven fracturing processes poses challenges: one has to account for the fracturing and opening of the host, the viscous flow of magma, as well as the coupling between them. The fracturing process may involve both localized damage such as opening of a fracture, and distributed damage such as compaction and zones of micro-fractures. In addition, the magma viscosity may significantly influence the specific fracturing process operating in the host rock, e.g. low viscosities can lead to hydro-fracturing, whereas higher viscosities can lead to non-negligible shear stresses at the fluid-host interface and cause the magma to act as viscous indenters.

The Discrete Element Method (DEM) is a widely used numerical technique for the study of fracturing of geomaterials. However, the implementation of viscous fluid flow in discrete element models is not trivial. In this study, we attempt to model quasi-viscous fluid flow behavior using Esys-Particle software (Abe et al., 2004). We build on the methodology presented by Abe and Urai (2012) where a combination of elastic repulsion and dashpot interactions between the discrete particles is used. Several benchmarks will be presented to illustrate the validity of the approach. We present two such tests: the pure shear test (figure 1) and the Poiseuille flow test (figure 2). These results show promise for the use of discrete elements to model viscous flow.

Further testing regarding the breakdown of the methodology for a relative length scale (ratio between particle size and fracture aperture) will be presented. The results will also highlight the benefits of using DEM for the application of magmatic intrusions as well as the inherent pitfalls of methodology encountered during benchmarking.

### Material testing:

#### *Pure shear tests*

We run two-dimensional pure shear tests by confining an assemblage of particles in an initially square box. The upper and lower walls are moved towards each other until a desired stress is achieved, which is then kept constant for the rest of the test. After reaching the desired stress, the left and right walls start moving away from each other with a constant velocity. By measuring the wall positions and forces acting on them, we calculate the strain rate and the differential stress. Figure 1 displays the measured differential stresses versus the corresponding strain rate for five such assemblages. A linear correlation is observed, the slope of which represents the bulk viscosity for the particle assemblage.

#### *Poiseuille flow tests*

While the pure shear tests allow us to calibrate the models, i.e. measure a bulk viscosity, the Poiseuille flow test compares the flow of the quasi-viscous particle to the analytical expression of an incompressible flow. This therefore serves as a test to assess how well the DEM particles can be used to model the type of fluid flow that may be expected for magma during intrusion. Figure 2 shows a snapshot of the displacement of quasi-viscous particles pushed by a piston through a channel. The displacement field is seen to be qualitatively comparative to the analytical parabolic displacement profile.

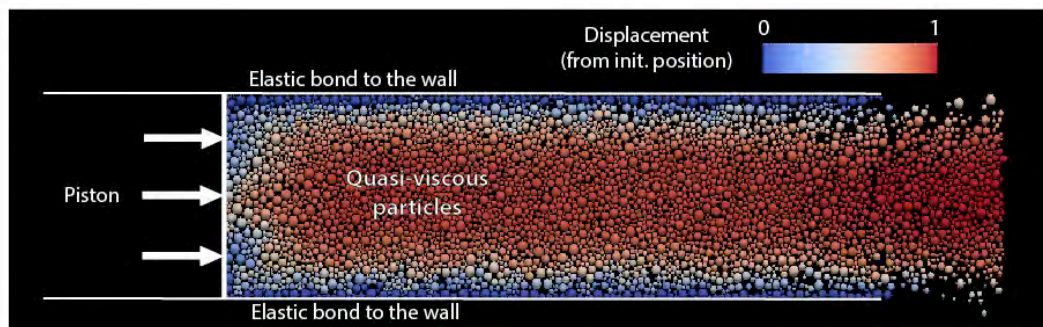


Figure 2: Poiseuille flow tests: A piston pushes the particle assemblage with a constant velocity producing a parabolic displacement profile along cross sections of the pipe.

#### References:

- Abe, S., Place, D., & Mora, P. (2004). A parallel implementation of the lattice solid model for the simulation of rock mechanics and earthquake dynamics. *Pure and Applied Geophysics*, 161(11-12), 2265–2277. <http://doi.org/10.1007/s00024-004-2562-x>
- Abe, S., & Urai, J. L. (2012). Discrete element modeling of boudinage: Insights on rock rheology, matrix flow, and evolution of geometry. *Journal of Geophysical Research: Solid Earth*, 117(1), 1–13. <http://doi.org/10.1029/2011JB008555>

**Keywords:** Magmatic intrusions, DEM, quasi-viscous particles, calibration.

## Quantitative experimental modeling of fragmentation during phreatic and phreatomagmatic eruptions

Øystein Thordén Haug<sup>1</sup>, Olivier Galland<sup>1</sup>, and Galen Gisler<sup>1</sup>

<sup>1</sup>) Physics of Geological Processes, University of Oslo, Norway

Corresponding author: o.t.haug@geo.uio.no

S3 – Volcanoes: from the plumbing system to the eruptive plume (PS7)

### Introduction:

During phreatic and phreatomagmatic, the sudden evaporation of water leads to a rapid volume increase, which may lead to explosive eruptions. These explosions cause fragmentation of the magma and/or the host rock, resulting in coarse-grained (lapilli) to very fine-grained (ash) material.

The products of the explosions, i.e. the fragments, are classically described by their fragment size distribution, which commonly follows power laws of exponent  $D$  (Kaminski and Jaupart, 1998). Such descriptive approach, however, considers the final products only and do not provide information on the dynamics of fragmentation. The aim of this contribution is thus to address the following fundamental questions. What are the physics that govern fragmentation processes? How fragmentation occurs through time? What are the mechanisms that produce power law fragment size distributions? And what are the scaling laws that control the exponent  $D$ ?

### Experimental setup and observations:

To address these questions, we performed a quantitative experimental study. The setup consists of a Hele-Shaw cell filled with a layer of cohesive silica flour, at the base of which a pulse of pressurized air is injected, leading to fragmentation of the layer of flour. The fragmentation process is sequentially monitored through time using a high-speed camera ( $f = 4$  kHz).

To study the dynamics of the fragmentation process, we developed a Matlab-based image analysis tool, which automatically retrieves the number and sizes of the fragments at each time step of the image sequence (Figure 1). This therefore allows monitoring the evolution of the fragment size distribution over time in the experiments providing quantitative insights into the fragmentation process.

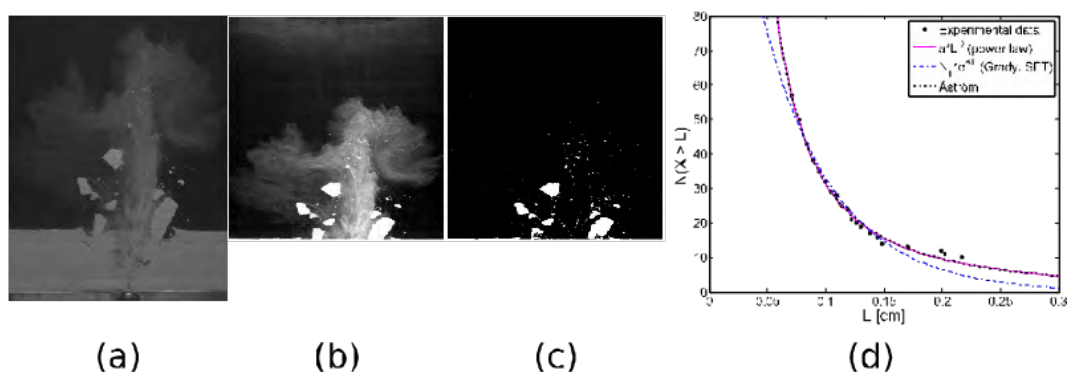


Figure 1: Image analysis: (a) Image taken during an experiment showing the production of fragments and dusty plume. (b) The image is cropped and its contrast increased. (c) Binary image, giving fragments a value of 1 while the background is set to 0. (d) From the binary image, the size of the fragments are determined, the distribution of which closely resembles a power law with an exponent  $D$ .

The image analysis tool allows us to capture the exponent  $D$  of the fragment size distribution, the average size of fragments ( $A$ ) and the number of fragments ( $N$ ), all through time (Figure 2). Based on these observations, we are able to propose scaling laws for these parameters as function of time and pressure in the air tank (Haug et al., 2013).

### Conclusions:

The fragment size distributions in our experiments as in nature are described by power law distributions of exponents  $D$  (Figure 1). For the first time, we here determined the scaling laws that govern the number of fragments ( $N$ ), the average size of the fragments ( $A$ ) and  $D$ . We show that (1)  $N$  scales with  $P^{1/2}$ , (2)  $A$  scales with  $P^{-2/3}$ , (3)  $D$  scales with  $P^{1/5}$ . Our experimental procedure thus appears as a unique tool to unravel the complex physics of fragmentation during phreatic and phreatomagmatic explosions.

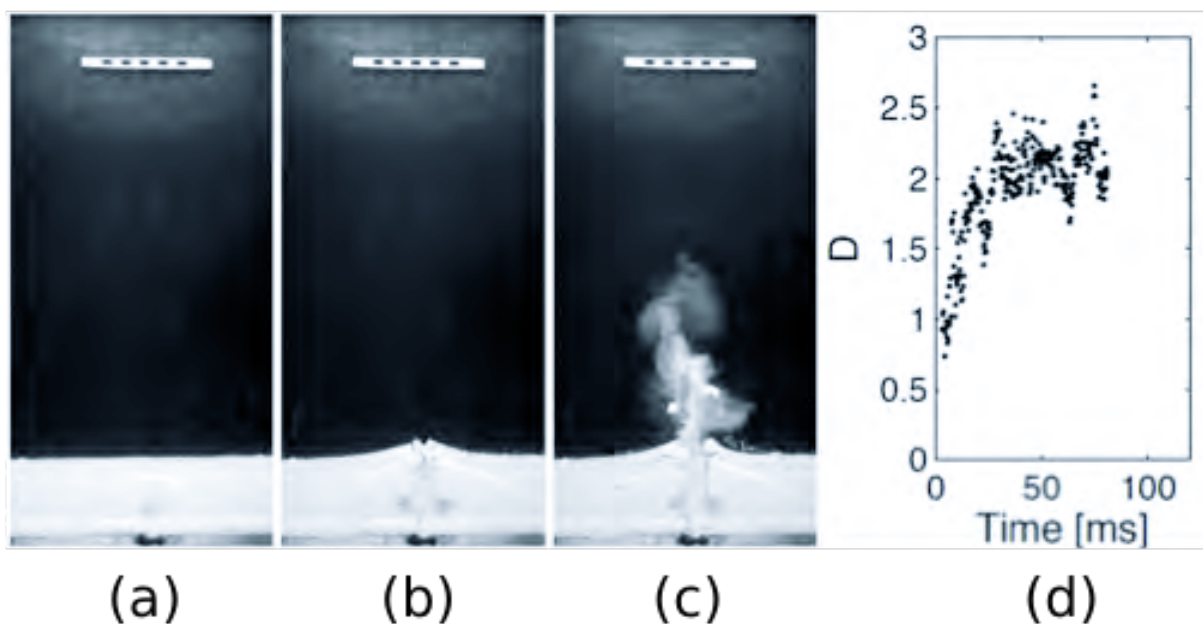


Figure 2: Results: (a-c) Three snapshots of an experiment showing the air carving through the layer of silica flour and ejecting fragments into the air. (d) The exponent of the power law fragment size distributions ( $D$ ) is plotted through time. It is first observed to increase until it reaches a steady state.

### References:

- Haug, Ø. T., Galland, O., & Gisler, G. R. (2013). Experimental modelling of fragmentation applied to volcanic explosions. *Earth and Planetary Science Letters*, 384, 188–197. <http://doi.org/10.1016/j.epsl.2013.10.004>
- Kaminski, E., & Jaupart, C. (1998). The size distribution of pyroclasts and the fragmentation sequence in explosive volcanic eruptions. *Journal of Geophysical Research*, 103(B12), 29759. <http://doi.org/10.1029/98JB02795>

## From sill to radial dike systems on Venus: the role of upward flexure environments and elliptical magma reservoirs

Nicolas Le Corvec<sup>1</sup>, Patrick J. McGovern<sup>2</sup> and Eric B. Grosfils<sup>3</sup>

<sup>1</sup>) University of Clermont-Ferrand, Lab. Magmas et Volcans, Clermont-Ferrand, France; <sup>2</sup>) Lunar and Planetary Institute, Houston, TX, USA; <sup>3</sup>) Geology Department, Pomona College, Claremont, CA, USA

Corresponding author: lecorvec@opgc.fr

S3 – Volcanoes: from the plumbing system to the eruptive plume (PS7)

### Introduction:

Magma accumulation in the lithosphere leads to the formation of magmatic reservoirs. The shape of these reservoirs is complex and evolves with their growth and failure, which is controlled by the depth of the reservoir within the lithosphere [Grosfils, 2007], the tectonic environment [Galgana *et al.*, 2013], and the mechanical properties of the lithosphere [Le Corvec *et al.*, 2015]. These studies principally consider the reservoirs to be spherical, however calderas on Venus demonstrate that the underlying reservoir shapes tend to be elliptical (e.g., Sacajawea Patera, Ishtar Terra). The caldera diameters range commonly between 40 and 80 km in diameter [Head *et al.*, 1992]. In addition to the formation of calderas, Venusian volcano-tectonic complexes possess intriguing giant radiating dike systems [Grosfils and Head, 1994], which have been recently constrained by new studies showing that tectonic environments affected by upward flexure tend to promote the formation of radial dikes for shallow magma chambers [Galgana *et al.*, 2013; Le Corvec *et al.*, 2015].

### Methodology:

Following previous methodology [Galgana *et al.*, 2013; Grosfils, 2007], axisymmetric finite element models (FEMs) using COMSOL Multiphysics [COMSOL] were used to study the stability of elliptical reservoirs (Fig. 1). The models are gravitationally loaded with lithostatic pre-stress, constrained horizontally with rollers at the outer edge of the model. The lithosphere is initially lying in equilibrium on top of the asthenosphere (modeled as a boundary condition) [Galgana *et al.*, 2013].

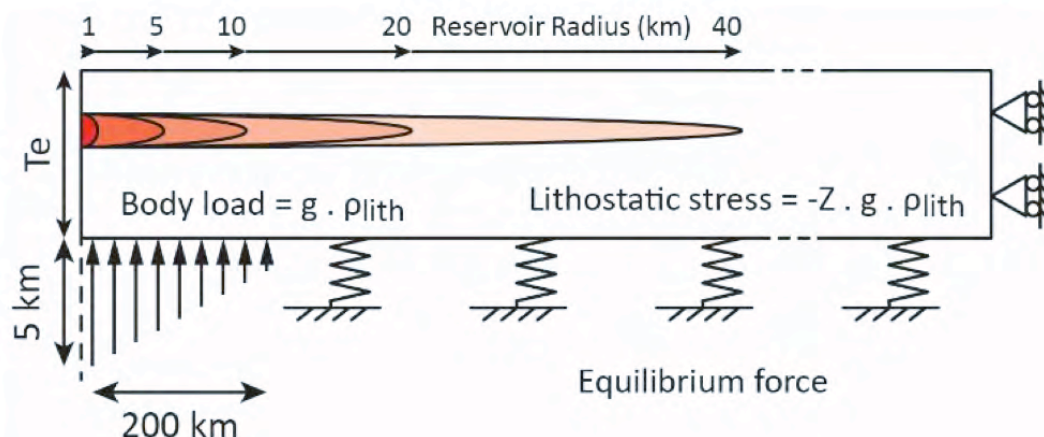


Figure 1: FEM boundary condition for an upward flexure environment. The magma reservoir has a vertical axis ( $R_a$ ) of 1 km, and a horizontal axis ( $R_b$ ) of 1, 5, 10, 20 and 40 km. The reservoir is pressurized until it reaches tensile failure. The depth of the reservoir varies from 3 to 9 km, and 6 to 18 km for a 20 km and 40 km thick lithosphere, respectively.  $\rho_{lith} = 2800 \text{ kg/m}^3$  and  $g = -8.87 \text{ m/s}^2$ . Not to scale.

The uplift deformation is created with a conical load applied at the base of the lithosphere (height 5 km, radius 250 km) (Fig. 1). Embedded within the lithosphere, magma reservoirs are pressurized to reach failure of its surrounding material. We tested the influence of ellipticity on the amount of overpressure needed to reach failure through different axis ratios ( $R_a/R_b = 1:1, 1:5, 1:10, 1:20$  and  $1:40$ ). The elastic properties were defined with their Young's Modulus ( $E = 1e11$  Pa), Poisson's ratio ( $\nu = 0.25$ ) and density ( $\rho_{\text{lith}} = 2800$  kg/m<sup>3</sup> equivalent to a basaltic composition).

### Results:

We observed that spherical magma reservoirs, when stable (i.e., overpressure  $> 0$  MPa), fail at their summit. Tensile failure is controlled by the hoop stress, and will promote the formation of vertical dikes. These results are in accordance with previous work [Galgana *et al.*, 2013]. Increasing the elliptical shape of the reservoirs moves the location of failure from their summit to their midsection and decrease the amount of overpressure required to reach tensile failure. Tensile failure is in these cases controlled by the tangential stress, which will promote the formation of sills.

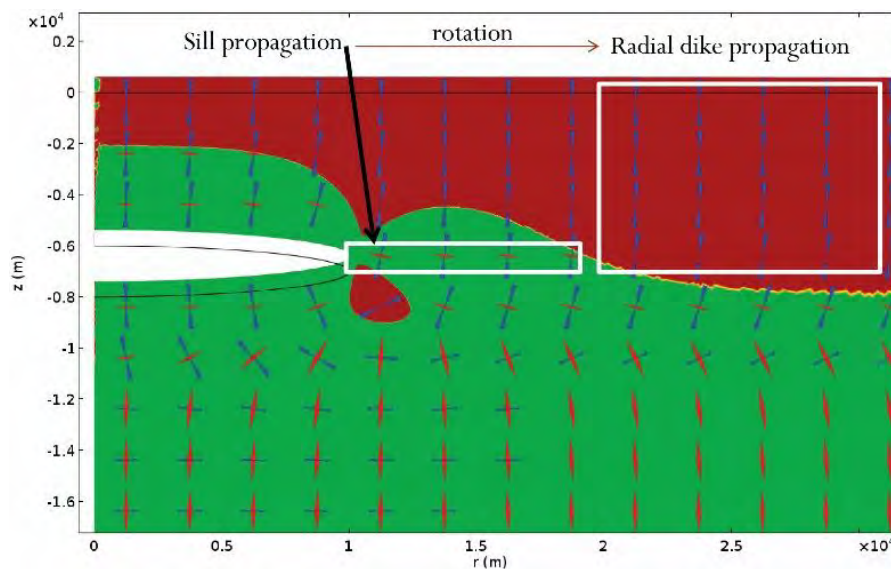


Figure 2: State of stress within a model subjected to upward flexure. The reservoir has a  $R_a/R_b$  ratio of 1:10. Red and blue cones represent the orientation of the minimum and maximum compressional stress, respectively. The background dark red and green colors represent the orientation of the minimum compressional stress in the  $\phi$ -direction, dark red: out of plane and green: in plane.

We observe that the state of stress within models having an elliptical reservoirs and subjected to upward flexure allow the propagation to sills for a short distance (Fig. 2, green background color). The magma will further away encounter a state of stress favoring the formation of radial dikes (Fig. 2, dark red back ground color). We observe that the amount of overpressure relative to the tectonic stresses allows the intrusion to rotate from sill to dike and that the distances between the tip of elliptical reservoir and the radial dike zone are similar to natural examples on Venus (e.g., Tumas Corona).

### References:

COMSOL Multiphysics Modeling and Simulation Software, *Version 4.3b*, 2013, doi:Export Date 28 May 2013.

- Galgana, G. A., E. B. Grosfils, and P. J. McGovern (2013), Radial dike formation on Venus: Insights from models of uplift, flexure and magmatism, *Icarus*, 225(1), 538-547, doi:<http://dx.doi.org/10.1016/j.icarus.2013.04.020>.
- Grosfils, E. B. (2007), Magma reservoir failure on the terrestrial planets: Assessing the importance of gravitational loading in simple elastic models, *Journal of Volcanology and Geothermal Research*, 166(2), 47-75, doi:10.1016/j.jvolgeores.2007.06.007.
- Grosfils, E. B., and J. W. Head (1994), The global distribution of giant radiating dike swarms on Venus: Implications for the global stress state, *Geophysical Research Letters*, 21(8), 701-704, doi:10.1029/94gl00592.
- Head, J. W., L. S. Crumpler, J. C. Aubele, J. E. Guest, and R. S. Saunders (1992), Venus volcanism: Classification of volcanic features and structures, associations, and global distribution from Magellan data, *Journal of Geophysical Research: Planets*, 97(E8), 13153-13197, doi:10.1029/92je01273.
- Le Corvec, N., P. J. McGovern, E. B. Grosfils, and G. Galgana (2015), Effects of crustal-scale mechanical layering on magma chamber failure and magma propagation within the Venusian lithosphere, *Journal of Geophysical Research: Planets*, 120(7), 2015JE004814, doi:10.1002/2015je004814.

**Keywords:** Venus, Volcanism, Tectonics, Numerical Modeling.

## Structural control on fluid pathways close to shallow magma intrusions: clues from analogue models

Domenico Montanari<sup>1</sup>, Andrea Agostini<sup>1\*</sup>, Marco Bonini<sup>1</sup> and Giacomo Corti<sup>1</sup>

<sup>1</sup>) Institute of Geosciences and Earth Resources, National Research Council of Italy (CNR), Florence Italy

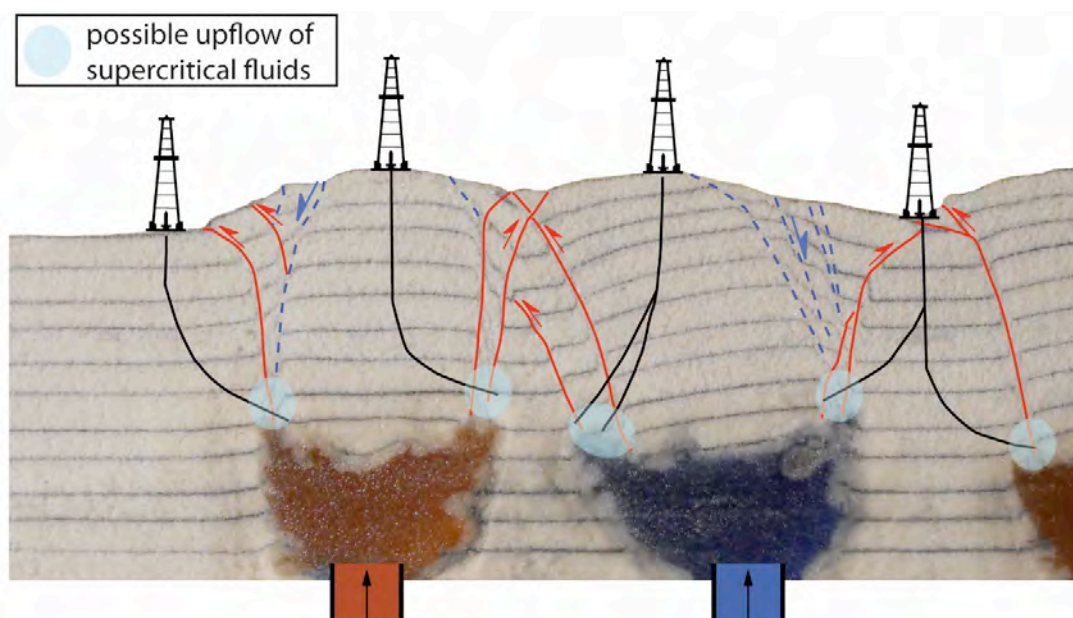
\* now at: Istituto Nazionale di Geofisica e Vulcanologia (INGV), Pisa, Italy

Corresponding author: domenico.montanari@gmail.com

Session S3 - Volcanoes: from the plumbing system to the eruptive plume (PS7)

The simple concept at the base of our research is that superhot geothermal fluids circulate very close to magma intrusions and, possibly, within the fractures associated with the magma migration and emplacement. Magma overpressure at the time of the emplacement at shallow crustal levels may lead to deformation (i.e. forced folding, fracturing and faulting) in the country rock both at local and regional scale (e.g. Senger et al., 2015).

Previous studies on magma emplacement and the evolution of caldera/resurgent domes in different tectonic contexts were mainly addressed to the analysis of the system evolution, magma depth, intrusion shape, etc., and rarely on the analysis of the brittle deformation of the overburden (e.g. Galland 2012). To get insights into these processes, we explored in the laboratory the development of fracture/fault networks associated with the emplacement of magma at shallow crustal levels. We used a mixture of quartz sand and K-feldspar fine sand as an analogue for the brittle crust, and polyglycerols for the magma. Polyglycerols are interesting new analogue ductile materials, in that they allow the reproduction of a wide range of viscosities. The modeling apparatus is a modified version of that developed by Montanari et al. (2010), to which the reader is referred for the scaling approach.



*Analogue models suggest that possible supercritical fluid pathways, apart from the fluids circulating within the metamorphic aureole, could be found within the structures related to magma emplacement, and consequently coeval and geometrically associated to emplacing magma. Inward dipping annular reverse faults are expected to significantly influence the distribution and migration of supercritical geothermal fluids near the edge of the magma intrusions.*

The presented modeling approach produced interesting results, providing useful hints for geothermal researches. In particular, sets of anular faults and fractures developed in close connection with the emplacement of the analogue magma, and are expected to significantly influence the distribution and migration of superhot geothermal fluids near the edge of the magma intrusion. These structures can therefore be considered as possible targets for geothermal and/or mineral deposits exploration, with evidence by analogue models providing geometric and conceptual constraints useful also for the 3D seismic interpretation.

The research leading to these results has received funding from the European Community's Seventh Framework Programme under grant agreement No. 608553 (Project IMAGE).

## References:

- Galland, O., 2012. Experimental modelling of ground deformation associated with shallow magma intrusions, *Earth Planet. Sci. Lett.* 317–318, 145–156.
- Senger, K., Buckley, S.J., Chevallier, L., Fagereng, Å., Galland, O., Kurz, T.H., Ogata, K., Planke, S., Tveranger, J., 2015. Fracturing of doleritic intrusions and associated contact zones: Implications for fluid flow in volcanic basins, *J. of African Earth Sciences*, 102, 70-85.
- Montanari, D., Corti, G., Sani, F., Del Ventisette, C., Bonini, M., Moratti, G., 2010. Experimental investigation on granite emplacement during shortening, *Tectonophysics* 484, 147–155

**Keywords:** Analogue modeling, magma emplacement in the shallow crust, geothermal exploration.

## Lithospheric flexure and gravity spreading of Olympus Mons volcano, Mars

S. Musiol<sup>1</sup>, E. P. Holohan<sup>2,\*</sup>, B. Cailleau<sup>3</sup>, T. Platz<sup>1,4,+</sup>, A. Dumke<sup>1</sup>, T. R. Walter<sup>2</sup>, D. A. Williams<sup>5</sup>, and S. van Gasselt<sup>1</sup>

<sup>1</sup>) Planetary Sciences and Remote Sensing, Institute of Geological Sciences, Freie Universität Berlin, Berlin, Germany

<sup>2</sup>) Physics of Earthquakes and Volcanoes, GFZ German Research Centre for Geosciences, Potsdam, Germany

<sup>3</sup>) Geophysics, Institute of Geological Sciences, Freie Universität Berlin, Berlin, Germany

<sup>4</sup>) Planetary Science Institute, Tucson, Arizona, USA

<sup>5</sup>) Ronald Greeley Center for Planetary Studies, School of Earth and Space Exploration, Arizona State University, Tempe, Arizona, USA

<sup>\*</sup>) now at University College Dublin, Dublin, Ireland

<sup>+</sup>) now at Max Planck Institute for Solar System Research, Göttingen, Germany

Corresponding author: stefanie.musiol@fu-berlin.de

Session S3 - Volcanoes: from the plumbing system to the eruptive plume (PS7)

### Abstract:

The structural architecture of large volcanoes is governed substantially by gravity-driven deformation that is manifest as distinct processes such as basement flexure or volcanic spreading. Temporal effects and the mutual interplay of these processes have been investigated only to a limited extent, and so we present novel numerical models of the time-dependent deformation associated with them. The models simulate the combined effects of lithospheric flexure and volcanic spreading during growth increments of an elastoplastic volcanic cone. Different spreading scenarios are considered by a variable coupling decoupling behavior at the interface between volcano and basement. We apply our models to Olympus Mons on Mars, which is characterized by upper to middle flank terraces on the shield, is encircled by a basal scarp that has an average slope of 30° and is surrounded by distant deposits that resemble large-scale slumping features on Earth.

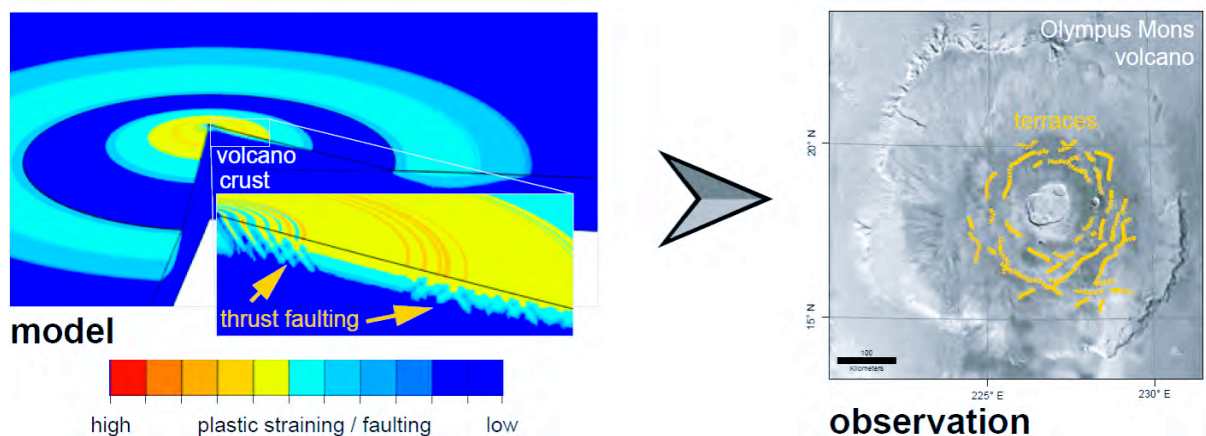


Figure 1: Concentric inward- and outward-dipping thrust faults on the model volcano surface, caused by edifice-induced lithospheric flexure, resemble observations of terraces on the shield of Olympus Mons volcano, Mars.

Our results are consistent with the interpretation that terraces on Olympus Mons' flanks form by thrust faulting that results from lithospheric flexure (Figure 1). The presence and expression of terraces

depend on the coupling of volcano and basement, on the time of volcano growth relative to mantle relaxation, and on the cohesion of the edifice. The encircling scarp may be related to a very low friction detachment at the edifice base, which leads to a normal fault regime on the lowermost flanks. With time and volcano growth, predicted stress and faulting regimes migrate only slightly, indicating that the structural architecture of volcanoes is largely set in the very early stages of formation.

## **Reference:**

Musiol, S., E. P. Holohan, B. Cailleau, T. Platz, A. Dumke, T. R. Walter, D. A. Williams, and S. van Gasselt (2016), Lithospheric flexure and gravity spreading of Olympus Mons volcano, Mars, *J. Geophys. Res. Planets*, 121, 255–272, doi:10.1002/2015JE004896.

## **Acknowledgements:**

The work was supported by the DLR Space Administration on behalf of the Federal Ministry for Economic Affairs and Energy, grants 50QM1001 and 50QM1301 (HRSC on Mars Express). S.M. acknowledges additional support by the German Academic Exchange Service DAAD for an international collaboration with Arizona State University. B.C. was supported by the German Science Foundation DFG (CA459/2-1). T.P. was partially supported by the Helmholtz Association through the research alliance 'Planetary Evolution and Life' (grant HA-203). This project was motivated in part by NASA MDAP grant NNX09AM94G to D.A.W. to produce a 1:1M-scale geologic map of Olympus Mons.

## **Magma propagation modeling: towards the coupling of rock fracturing and fluid dynamics.**

Virginie Pinel<sup>1</sup>, Francesco Maccaferri<sup>2</sup>, Eleonora Rivalta<sup>2</sup>, Alexandre Carrara<sup>1</sup>, Fabio Corbi<sup>3</sup>

<sup>1</sup>) ISTerre, Université Savoie Mont-Blanc, IRD, CNRS, Campus Scientifique, Le Bourget du Lac F73376, France

<sup>2</sup>) GFZ German Centre for Geosciences, Section 2.1, Telegrafenberg, 14473 Potsdam, Germany

<sup>3</sup>) University of Montpellier, Géosciences Montpellier Laboratory, Montpellier, France.

Corresponding author: virginie.pinel@univ-smb.fr

S3 – Volcanoes: from the plumbing system to the eruptive plume (PS7)

### **Introduction:**

Analog experiments show that both dyke trajectories and dyke propagation velocities are influenced by the magma driving pressure and by the external stress field (Watanabe et al., 2002). It follows that the temporal evolution of magma propagation inferred from seismic and geodetic data can be used to constrain the magma overpressure and the local stress field. Numerical models for dyke propagation can be divided in two general categories based on different approaches, one in which the behavior is controlled by fluid dynamics and the other which focuses on rock fracturing.

The first set of models, based on fluid dynamics, are 1D and provide an information about the propagation velocity, whereas the second set, based on rock fracturing, are 2 D and estimate the magma path depending on the crustal properties, stress field and buoyancy forces. Here we couple a static numerical model solving for magma pathway (Maccaferri et al., 2011) with a dynamical model of dyke propagation (Pinel & Jaupart, 2000) providing velocities in order to study the effect of a surface load on magma transport.

This model is compared to analogue experiments and applied to the dyke responsible for the Etna's 2001 eruption.

### **Model description:**

This is a two-step model where the magma trajectory is first estimated for a given stress field and density contrast between the magma and the surrounding crust. The amplitude of the normal stress component applied on a surface parallel to this trajectory, which correspond to the stress the magma have to counterbalance for the dyke to open is also estimated. In a second step, we model the fluid dynamic propagation along the trajectory considering a Newtonian, incompressible viscous magma in a laminar regime.

### **Results:**

Our model is applied to the surface loading case, similarly to previous analog models (Watanabe et al., 2002). We confirm that surface loading tends to attract the magma. The rising dyke is all the more deflected as the ratio between the applied load and the magma driving pressure is large (Figure 1). Besides the dynamical calculation clearly shows that when the dyke enters the compressive stress field induced by the load it velocity decreases (Figure 2).

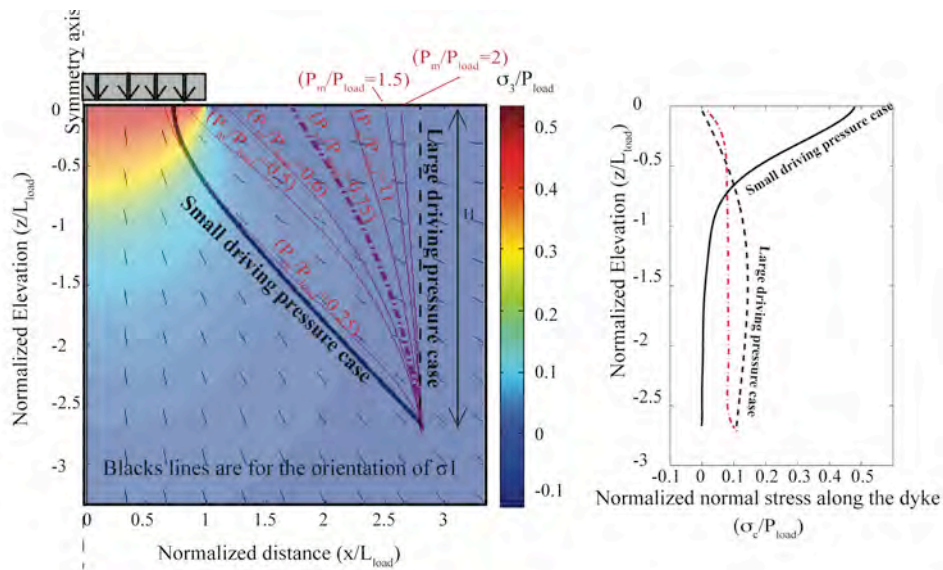


Figure 1: Dyke trajectories in a crust loaded at the surface for a dyke starting at a normalized depth of 2.7 and a normalized radial distance of 2.8 from the axis of the load. The magma path depends on the ratio between the magma driving pressure and the load applied ( $P_m/P_{load}$ ) (from Pinel et al, in prep.).

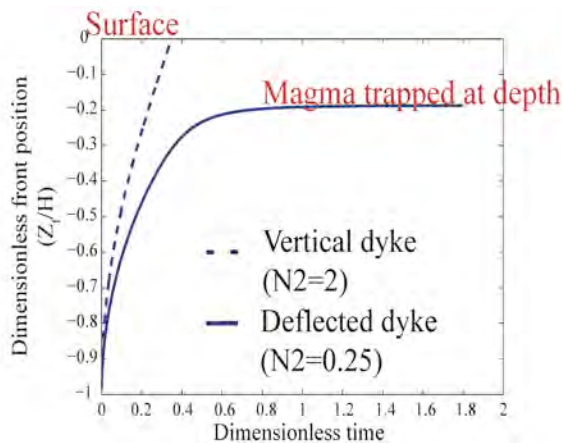


Figure 2: Front position as a function of time for two end-member trajectories.  $N_2$  is the ratio between the magma driving pressure and the load applied ( $P_m/P_{load}$ ).

The model is then applied to the July 2001 eruption of Etna, for which the final dyke deflection had been previously interpreted as due to the topographic load by Bonaccorso et al. (2010). We show that the velocity decrease observed during the last stage of the propagation can also be attributed to the local stress field. We use the dyke propagation duration to estimate the magma overpressure at the dyke bottom to be less than 4 MPa

**References:**

Bonaccorso, A., G. Currenti, C. Del Negro, and E. Boschi, 2010, Dike deflection modelling for inferring magma pressure and withdrawal, with application to Etna 2001 case, Earth Planet. Sci. Lett., 109, 121-129, doi.org/10.1016/j.epsl.2010.02.030.  
 Maccaferri, F., M. Bonafede, and E. Rivalta, 2011, A quantitative study of the mechanisms governing dike propagation, dyke arrest and sill formation, J. Volcanol. Geotherm. Res., 208, 39-50, doi: 10.1016/j.jvolgeores.2011.09.001.  
 Pinel, V., and C. Jaupart, 2000, The effect of edifice load on magma ascent beneath a volcano, Phil.

Trans. R. Soc. Lond. A, 358, 1,515-1,532.

Pinel, V., Carrara A., Maccaferri F., Rivalta, E., Corbi, F., A two-step model for dynamical dyke propagation in two-dimensions: Application to the July 2001 Etna eruption.

Watanabe, T., T. Masuyama, K. Nagaoka, and T. Tahara, 2002, Analog experiments on magma-filled cracks: Competition between external stresses and internal pressure, Earth Planet. Sci. Lett., 54, 1,247-1,261

**Keywords:** Magma path, propagation velocity, numerical modeling.

## Volcanology of Phlegrean Fields: a Continuous and Fractional Wavelet Approach

G. Pucciarelli<sup>1</sup>, E. Guariglia<sup>2</sup>

<sup>1,2</sup> *Dept. of Physics “E. R. Caianiello” – University of Salerno*

Corresponding author: [gpucciarelli@unisa.it](mailto:gpucciarelli@unisa.it)  
email: [eguariglia@unisa.it](mailto:eguariglia@unisa.it)

S3 – Volcanoes: from the plumbing system to the eruptive plume (PS7)

The Phlegrean Fields are an area in the west of Naples (Italy), with a huge interest in Geophysical community being a volcanic caldera among the most dangerous in the world. Reason of this is high exposure of people who live in that area (550,000 inhabitants ca.). Various techniques of monitoring exist. Among all, the control of ground deformations and variations in sea level have a considerable importance. The first one are used to verify the presence of possible traces related to a magma resurgence which could precede an eventual eruption, while the second one comes in handy to check the phenomenon of the bradyseism, which afflicts in a particular way this volcanic area.

We have analysed time series of ground deformation and tidal data in this area to highlight this important geophysical features and comparing these results with those obtained from similar data in other time periods. With regard to first mentioned, we have analyzed tiltmetric data. These one come from the tiltmeter network sited in Pozzuoli (that is, Pozzuoli North Tunnel and Pozzuoli South Tunnel). The second typology of data, namely tidal data, come from the tide gauge in Pozzuoli. Both time series have been analysed by means of a conventional Fourier Transform and we have obtained a Power Spectral Density (PSD) for each specific period in which we have subdivided data. But, given that data at our disposal are not stationary, it is clear that a conventional Fourier Analysis is not adequate for having a complete picture of frequencies which are present in our signals. Then, another goal we want to reach is maintenance of time information, goal which is impossible to obtain with Fourier Analysis.

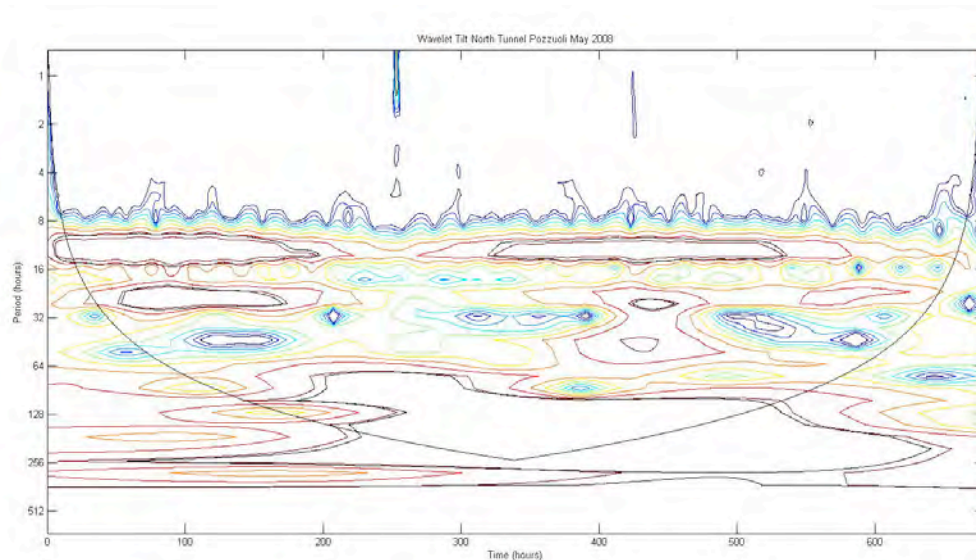
Therefore, in order to realize an advance analysis of these experimental data, we have used a wavelet approach. We have preferred choice of this kind of analysis because it allows to have information not only on frequencies but even on time. Then, it is an efficient method to obtain all the frequencies which have present in signal with a good resolution. This factor is relevant in choice of a wavelet approach. For example, the Short Time Fourier Transform is time-frequency localized, but the introduction of the window function to cover signals brings with it resolution problems. So, spectral analysis has been obtained by a wavelet approach: results are a local spectrum, for each scale in which signal has been decomposed, and a global one achieved by average on each period of local spectrum.

At this proposal, we have used the Continuous Wavelet Transform and, as so-called “Wavelet Mother”, we have opted for Gabor-Morlet wavelet. We have made this choice because Gabor-Morlet wavelet is a complex function modulated by a Gaussian window: this characteristic makes it extremely suitable for the Geophysical applications.

But, the only use of CWT could be not sufficient to obtain a complete picture of all frequencies which are in signals.

So, we have made use of Fractional Wavelet Transform, too. This for a particular reason. Continuous Wavelet Transform, which we have used, has made of components that are a sort of scaled bandpass filter in frequency domain. So, CWT results to be limited in the time-frequency plane. Then, we have analysed time series by means of Fractional Wavelet Transform proposed by Shi J. et al (2012). Through this FWT, we could obtain a more complete picture of all frequencies which are in signals.

For each time series, we have the principal harmonic constituents: lunar semidiurnal (M2), solar semidiurnal (S2) and lunar diurnal (K1). Besides, time series show peaks for some frequencies higher than 1/hour. These peaks highlight the presence of seiches, which are standing waves occurring in total or partial enclosed body water, as Gulf of Naples is. Studies about occurrence of these seiches are very important in volcanic areas, because these oscillations could be link up with generation of discrete plumes of rising magma.



*Wavelet spectrogram of tiltmeter data registered in May 2008 by North Tunnel Pozzuoli Tiltmeter*

Frequencies at which we notice these seiches are in agreement with previous studies. In this case, spectra obtained by means of FWT individuate variations in variance which are similar to which obtained by means CWT. These two kinds of variation underline the presence of principal harmonic constituents and of seiches, respectively. Since Wavelet analysis preserve time information about happening of these frequencies, we can obtain time periods where seiches recur in an evident way. So, we perform another kind of wavelet analysis and particularly we perform fractional derivative of CWT according to Caputo's approach. We notice that spectra obtained from this kind of analysis underline presence of seiches which we are not present in “traditional” CWT and FWT analysis. For the future, we would perform this kind of analysis for other time series (not necessarily Phlegrean Fields time series) to verify if results of it have a physical meaning or are only a mathematical effect.

**Keywords:** Phlegrean Fields, tiltmeters, tides, Fourier Analysis, Power Spectral Density, Gabor-Morlet wavelet, Fractional wavelet transform.

## The role of magma viscosity on the faulting mechanism around magma intrusions: a 2D FEM study

Alban Souche<sup>1</sup>, Øystein Thordén Haug<sup>1</sup>, Olivier Galland<sup>1</sup>, Marcin Dabrowski<sup>1,2</sup>

<sup>1</sup>) Physics of Geological Processes, University of Oslo, Norway

<sup>2</sup>) Computational Geology Laboratory, Polish Geological Institute, Poland

Corresponding author: [alban.souche@geo.uio.no](mailto:alban.souche@geo.uio.no)

S3 – Volcanoes: from the plumbing system to the eruptive plume (PS7)

### Introduction:

Host-rock failure during magma intrusion is commonly assumed to occur by tensile fractures. However, in some cases, complex structures such as shear bands, rock wedging, or imbricated thrusts can form in sedimentary rocks around sills and dikes (i.e., Galland et al. (in this session); Pollard, 1973). These structures, which developed during the intrusion event, suggest that the faulting mechanism of the host-rock can be dominated by shear stresses near the intrusion interface and highlight the impact of the magma viscosity on the host-rock deformation. A number of studies have investigated the fracturing pattern of host-rocks around magmatic intrusions within the framework of elasto-plasticity or rigid-plasticity theory (i.e., Gerbault et al., 1998, 2012; Pollard, 1973). However, the coupling of the intrusive magma dynamic on the system is often simplified and implemented as hydrostatic pressure acting normally on the host-rock interface.

In this study, we numerically solve the viscous fluid flow of the magma with the deformation of the host-rock and quantify the effect of the shear stresses along the intrusion interface on the failure mechanism of the host-rock. Thus, we aim to investigate under which condition failure may shift from different propagation modes (mode I versus mode II) during the growth of the intrusion. Special consideration will be given to the viscosity of the magma, the crack-tip geometry, and the rheological heterogeneities of the host-rock.

### Numerical approaches:

We numerically explore the onset of a fluid-driven fracturing process where a viscous fluid (the magma) intrudes an elasto-plastic medium (the host-rock). The traction imposed by the fluid at the interface is fully resolved by solving for Stokes flow within the intrusion. Two numerical finite element approaches are tested to approximate the plastic deformation:

1) using an effective viscosity approach (e.g., Kaus, 2010), where the entire domain is discretized with a visco-elasto-plastic formulation with dominant viscous and elasto-plastic behavior for the magma and host-rock respectively. 2) using an incremental procedure based on a Newton-Raphson algorithm with a consistent tangent operator (Yarushina et al., 2009). In this approach, the viscous fluid flow of the magma is coupled to the mechanical deformation of the host-rock by imposing a traction boundary condition along the intrusion interface.

### Results:

We present preliminary results obtained from the numerical code using an effective viscosity approach to the plastic deformation (first approach described above). Figure 1 shows the results of two simulations where only the viscosity of the intruding magma is changed, and where the rheological parameters of the host-rock and the injection rate are kept the same. While the pattern of the developing shear bands may be influenced by the prescribe boundary conditions at the limit of the domain, we observe an interesting result regarding the positions of the developing shear bands along

the interface. For relatively low viscosity ( $\mu = 1e5$  Pa.s, panel A) the shear bands develop from the intrusion tip, while for larger viscosity ( $\mu = 1e8$  Pa.s, panel B) the shear bands initiate away from the intrusion tip due to the shear stresses acting along the interface. This illustrates the importance of the shear stresses induced by the viscous magma flow during the emplacement mechanism.

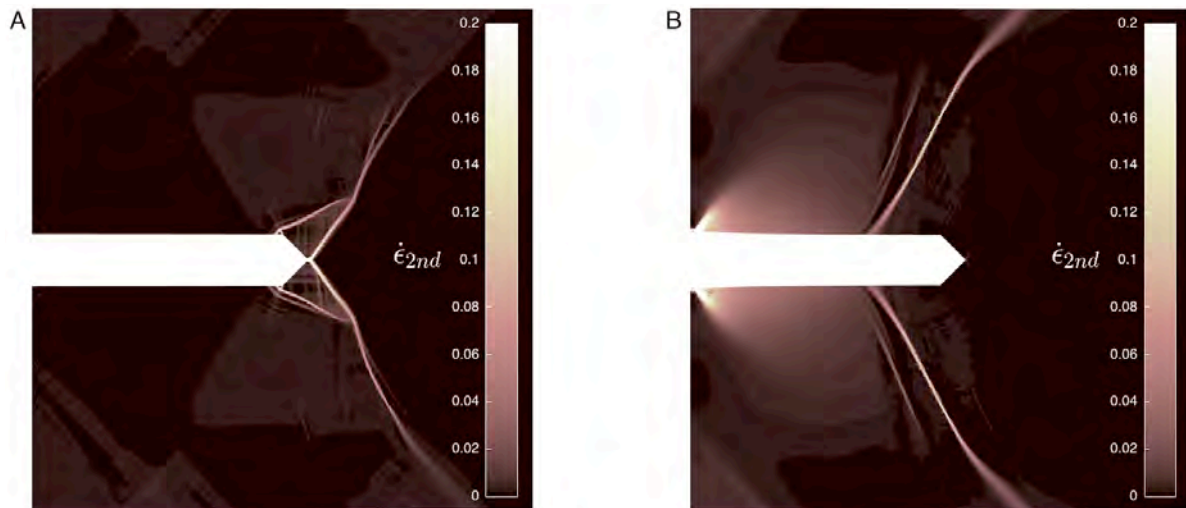


Figure 1: Second invariant of the deviatoric strain rate [s<sup>-1</sup>] obtained for two simulations with different magma viscosity ( $\mu = 1e5$  Pa.s, panel A, and  $\mu = 1e8$  Pa.s, panel B). A Poiseuille flow profile is imposed at the left side of the intrusion with maximum x-velocity of 10 cm/s. The results are obtained after 0.6 s of injection. The domain size is 2x2 m and the thickness of the intrusion is 20 cm. Left boundary condition with free slip along the y-direction, right boundary condition with no slip, and free surface on the top and bottom.

### References:

- Galland, O., Adbelmalak, M. M., Spacapan, J., Mourgues, R., Leanza, H. A., Planke, S., 2016, Are igneous sheet intrusions really mode I elastic fractures?, GeoMod 2016 conference, session 3.
- Gerbault M., Poliakov, A. N. B., Daignieres, M., 1998, Prediction of faulting from the theories of elasticity and plasticity: what are the limits?, *Journal of Structure Geology*, 20, 301-320.
- Gerbault M., Cappa, F., Hassani, R., 2012, Elasto-plastic and hydromechanical models of failure around an infinitely long magma chamber, *Geochemistry, Geophysics, Geosystems*, 13(3).
- Kaus, B. J., 2010, Factors that control the angle of shear bands in geodynamics numerical models of brittle deformation, *Tectonophysics*, 484(1), 36-47.
- Pollard, D. D., 1973, Derivation and evolution of a mechanical model for sheet intrusions, *Tectonophysics*, 19, 233-269.
- Yarushina, V. M., Dabrowski, M., Podladchikov, Y. Y., 2010, An analytical benchmark with combined pressure and shear loading for elastoplastic numerical models, *Geochemistry, Geophysics, Geosystems*, 11(8).

**Keywords:** Sill intrusion, crack tip deformation, mixed mode fracturing, elasto-plastic finite element modeling.

## **S4- Seismic cycle & Earthquake dynamics**

Destructive earthquakes, like the Haiti earthquake (2010, Mw=7, >230000 deaths), Tohoku earthquake (2011, Mw=9.1, >15000 deaths) or the recent Nepal earthquake (2015, Mw7.8, > 9000 deaths), generate heavy human, economic and environmental losses. A better understanding of these natural disasters represents, then, a major societal and scientific challenge.

Nowadays, new technological advances in satellite imagery measurements as well as the development of dense geodetic and seismologic networks allow now for detailed analyses of surface kinematics associated with these deformation phases. Earthquake study faces, however, major limiting factors related to the difficulty to access the deep source of earthquake and to integrate the characteristic time scales of deformation processes that extend from seconds to thousands of years.

Numerical and analog modeling are often the only and best approaches to interpret the observations and improve our understanding of such geological processes. All contributions dealing with the seismic cycle, earthquake dynamics, seismic source processes, active fault kinematics, co-seismic surface deformations, ... are more than welcome.

**Conveners:** Rodolphe Cattin (University of Montpellier, France) and Matthias Rosenau (GFZ German Research Centre for Geosciences, Potsdam, Germany).

Keynote speaker:

**"Dynamics of crustal deformation and seismicity, a Himalayan perspective"** by Jean-Philippe Avouac (Caltech, USA) - avouac@gps.caltech.edu

## Dynamics of crustal deformation and seismicity, a Himalayan perspective

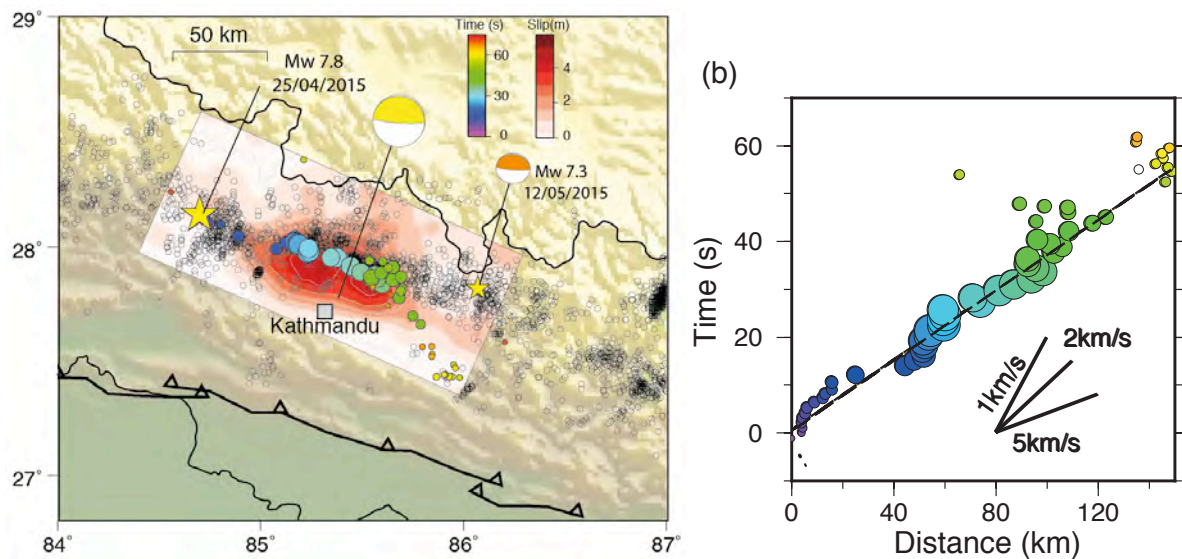
Jean-philippe Avouac

Seismological Laboratory, California Institute of Technology, Pasadena, CA 91125, USA

Corresponding author: avouac@gps.caltech.edu

### S4- Seismic cycle & Earthquake dynamics (Keynote)

Thanks to advances in numerical methods and improved computational resources, major progress have been made over the last few decades with regard to dynamic modelling of crustal deformation and the seismic cycle. We also now have access to various techniques from seismology, GPS geodesy, radar and optical remote sensing to measure seismic and aseismic deformation. Validating and calibrating dynamic models of crustal deformation and the seismic cycle from observations remains a major challenge yet. This is due in particular to the difficulty of isolating the contribution to the measured deformation of elastic and anelastic processes and to tell apart different anelastic deformation processes (frictional sliding vs viscous deformation for example). I will review these difficulties and avenues to solve these difficulties based on the Himalayan example. I'll focus in particular on interseismic, co-seismic and postseismic deformation related to the Mw7.8 Gorkha earthquake of 2015. We will discuss what constraints on the frictional properties of crustal faults and bulk rheology of the crust and upper mantle can be derived from the observations at hands and what observations would be needed to better constrain these properties.



*Slip rate on the Main Himalayan Thrust during the Mw7.8 Gorkha earthquake rupture, Nepal. The dots show the sources of high frequency (~1Hz) seismic waves. It is based on Avouac et al (NGEO, 2015) and Galetzka et al (Science, 2015).*

**Keywords:** Earthquake dynamics, Gorkha earthquake, elastic and anelastic deformation, postseismic deformation

## Zooming into the earthquake zone: An analogue model for seismotectonic plate interfaces.

Michael Rudolf<sup>1</sup>, Matthias Rosenau<sup>1</sup>, Zahra Amirzada<sup>2</sup>, Onno Oncken<sup>1</sup>

<sup>1</sup>) Helmholtz Centre Potsdam, German Research Centre for Geosciences (GFZ), Telegraphenberg, D-14473 Potsdam, Germany

<sup>2</sup>) Universiteit Utrecht, Netherlands

Corresponding author: michael.rudolf@gfz-potsdam.de

S4- Seismic cycle & Earthquake dynamics (Oral)

### Introduction:

The majority of earthquake activity is focused along complex fault networks that operate on a lithospheric scale. During an earthquake the frictional behavior of the slipping fault segment changes and weakens the frictional contact between the plates. These changes in frictional properties of faults can be characterized by rate-and-state friction theory originally introduced by Dieterich (1979) and Ruina (1983). Rate-and-state theory allows the assignment of different frictional conditions like stable, unstable, and transitional to individual fault segments. The interplay of fault conditions (loading rate, pressure), geometry and slip behavior, including fault creep, makes it difficult to model such a process especially over multiple time and length scales. Here we present an experimental approach to understand seismotectonics including an analogue model combined with numerical modelling

### Setup:

In our setup we are using a fault analogue composed of country walls represented by ballistic gelatin (25-30wt%, pig skin) and a fault core or damage zone made of glass beads. Two different geometries are realized using a ring-shear tester and a shear box (Figure 1). The ring-shear tester imposes a simple shear geometry with controlled shear rates ( $10^{-6}$  -  $10^{-3}$  s<sup>-1</sup>) and uniform normal loads (0.5 - 20 kPa). The shear box provides a pure shear vice configuration mimicking a strike-slip fault with a free surface and a vertical pressure gradient as well as a controlled far-field loading. The latter also holds the possibility to include a rheological layering of the model, e.g. using silicone oil (PDMS, G30M) as viscoelastic lower crust. During the experiments the loading forces and surface deformation are monitored using force-transducers and a PIV-camera setup. In the ring-shear tester we monitor the fault surface (fault normal view) while in the shear box the fault trace and adjacent surface of the elastic medium is monitored (map view).

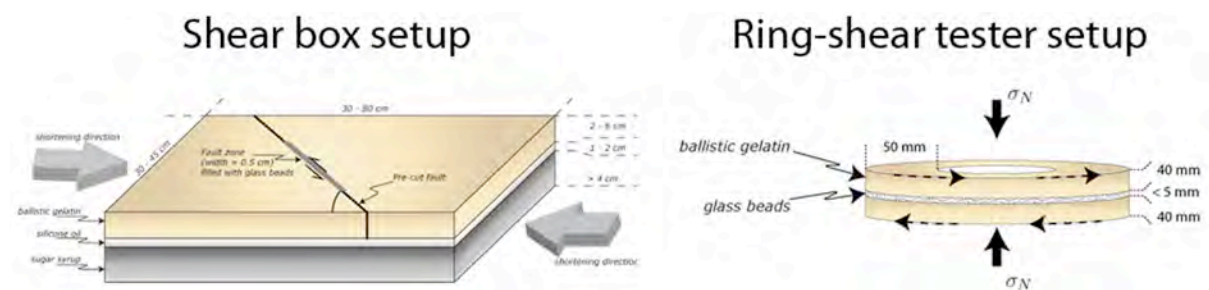


Figure 1: Analogue model setup using glass beads between gelatin as shear zone analogue. The left setup has additional layers of silicone and sugar syrup to model the ductile rheology of lower crust and mantle.

### Preliminary Results:

Both models show periodic slip events occurring alongside with fault creep and “out of sequence” activity akin to foreshocks on the fault. Foreshock activity results in Gutenberg-Richter like statistics ( $b \sim 1$ ) superimposed by a bump reflecting the periodic system-wide events. We observe no aftershocks on the fault but occasionally transient afterslip and creep that changes systematically over the interseismic period. Generally the periodic slip events represent failure of the complete fault area while foreshocks are fractional failures occurring on small patches. We observe both bilateral and unilateral ruptures which occur as slip pulses or cracks. The resulting fault and surface displacement maps show a strong similarity to natural coseismic fault motion obtained by GPS (Figure 2) and are consistent with elastic dislocation model prediction. Furthermore, the recurrence intervals and stress drops can be scaled to the natural prototype. The displacement on the fault zone shows a sequential migration of an individual slip event along the shear zone, starting in regions where the local shear rate is high. Occasionally, a short break in slip propagation can be observed, followed by a complete failure of the whole shear zone.

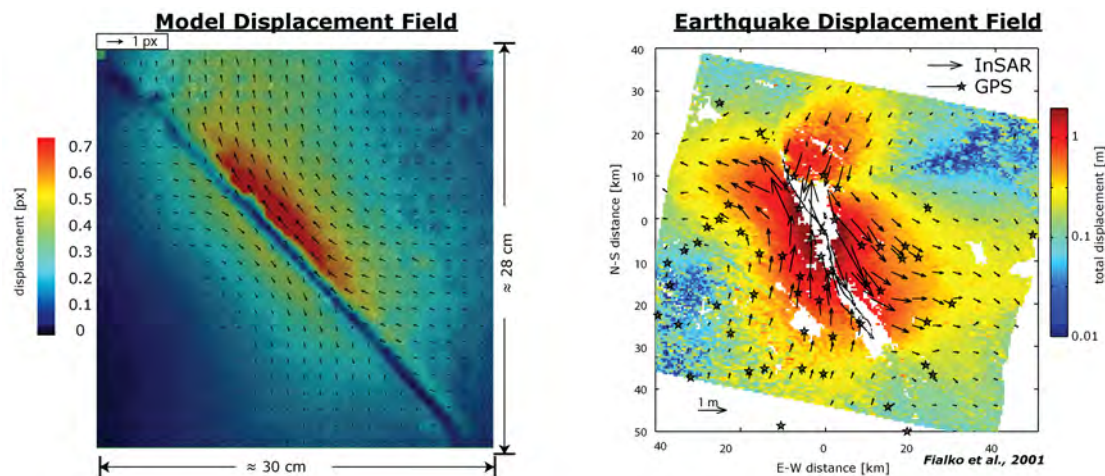


Figure 2: Comparison of a model displacement field (left) resulting from digital image correlation and a natural earthquake displacement field (right). Right image is taken from Fialko et al. (2001).

### Outlook:

The modeling results are combined with numerical rate-and-state models (QDYN, Luo et al. 2011) using physical parameters from the experiment. This enables us to explore a wide range of parameters and to draw connections between the parameters that control the behavior of the earthquake system.

### References:

- Dieterich, J.H., 1979. Modeling of Rock Friction 1. Experimental results and constitutive equations, *Journal of Geophysical Research: Solid Earth*, 84(B5), 2161-2168.
- Fialko, Y., Simons, M., and Agnew, D., 2001. The complete (3-D) surface displacement field in the epicentral area of the 1999 MW7.1 Hector Mine Earthquake, California, from space geodetic observations. *Geophysical Research Letters*, 28(16), 3063-3066.
- Luo, Y., Ampuero, J. P., 2011. Numerical Simulation of Tremor Migration Triggered by Slow Slip and Rapid Tremor Reversals, AGU Fall Meeting 2011, Abstract S33C-02
- Ruina, A., 1983. Slip instability and state variable friction laws. *Journal of Geophysical Research: Solid Earth*, 88(B12), 10359-10370.

**Keywords:** analogue modeling, seismotectonics, rate-and-state friction, fault zones.

## **How subduction velocity and seismogenic zone width tune the seismic behavior of subduction megathrusts: insights from analog and numerical models**

Fabio Corbi<sup>1</sup>, Robert Herrendorfer<sup>2</sup>, Francesca Funicello<sup>3</sup> and Ylona Van Dinther<sup>2</sup>

<sup>1</sup>) University of Montpellier, Géosciences Montpellier Laboratory, Montpellier, France.

<sup>2</sup>) Institute of Geophysics, ETH Zurich, Sonneggstrasse 5, CH-8092, Zurich, Switzerland.

<sup>3</sup>) Roma Tre University, Laboratory of Experimental Tectonics, Dip. Scienze, Rome, Italy.

Corresponding author: [fabio.corbi3@gmail.com](mailto:fabio.corbi3@gmail.com)

S4- Seismic cycle & Earthquake dynamics (Oral)

### **Abstract:**

Seismic characteristics of subduction megathrusts have been related to various geodynamic parameters. However, correlations are generally weak and difficult to interpret due to the short instrumental record and multi-parameter influence. Here we use benchmarked against each other analog- and numerical models to investigate how subduction velocity  $V_s$  and the width of the seismogenic zone  $W$  control seismic rate  $\tau$ , maximum magnitude  $M_{max}$  and moment release rate MRR.

The models create thousands of years long timeseries of stress build up and release via frictional instabilities (i.e., modeled earthquakes). We find that  $W$  is inversely correlated with  $\tau$  and directly correlated with  $M_{max}$  and MRR.  $V_s$  is directly correlated with  $\tau$  and MRR. We also find that  $M_{max}$  is independent from  $V_s$ . By random sampling our time series we suggest that a minimum span of 1 to 5 times the characteristic recurrence time (or even longer timeseries in case of outliers) would be needed to observe at least one event that rupture the 80% of the maximum rupture width.

**Keywords:** Subduction megathrust earthquakes, Subduction velocity, Width of the seismogenic zone.

## Effect of Subduction Zone Parameters on Maximum Magnitude of Earthquakes: Seismic Cycle Modelling

Iskander A. Muldashev<sup>1,2</sup> and Stephan V. Sobolev<sup>1,2</sup>

<sup>1</sup>) GFZ German Research Centre for Geosciences, Potsdam, Germany

<sup>2</sup>) Institute of Earth and Environmental Science, University of Potsdam, Potsdam-Golm, Germany

Corresponding author: [muldashev@gfz-potsdam.de](mailto:muldashev@gfz-potsdam.de)

S4- Seismic cycle & Earthquake dynamics (Oral)

### Introduction:

There are different opinions about the role of subduction zone parameters in producing great earthquakes (Heuret et al., 2011, 2012).

The aim of this study is to estimate maximum magnitudes of earthquakes in subduction zones and their dependence on various subduction zone parameters by using a modeling approach. To do so we model seismic cycles of great megathrust earthquakes in the subduction zone using finite element numerical technique that employs elasto-visco-plastic rheology consistent with laboratory data and is capable to model both geological and seismic-cycle time-scale deformation in lithosphere (Sobolev and Muldashev, 2016).

### Model approach:

First, we make the model setup shown in Fig. 1, by modeling subduction process in the geological time-scale ( $10^7$  years). We use 2D version of thermomechanical finite element numerical code SLIM3D (Popov and Sobolev, 2008) to model subduction during 7-10 Mln years. To do so we employ visco-elasto-plastic rheology with constant low (0.01-0.05) friction coefficient in the uppermost part of the subduction slab, that is consistent with the idea of high pore-fluid pressure in subduction channel. The time step in such model is  $10^4$  years. As a result we get the subduction model with appropriate stress distribution.

Second, we employ classic aging rate-and-state rheology (Dieterich, 1972) in the subduction channel and introduce adaptive time-step procedure with maximum time-step of 5 years. The model generates spontaneous earthquake sequences and adaptive time-step integration procedure varies time step from 40 seconds at instability (earthquake), and gradually increases it to 5 years during postseismic relaxation.

$$\frac{\partial \tau}{\partial \sigma_n} = \mu = \mu^* + a \ln \left( \frac{V}{V^*} \right) + b \ln \left( \frac{\theta V^*}{L} \right),$$
$$\frac{d\theta}{dt} = 1 - \frac{\theta V}{L}.$$

where  $\mu$  and  $\mu^*$  are friction and static friction respectively.  $a$  and  $b$  are parameters for rate and state friction law.  $V$  is velocity of slip on the fault,  $V^*$  is quasi-static (or reference) velocity i.e. the velocity at which  $\mu = \mu^*$ .  $L$  is the critical slip distance and  $\theta$  is the state variable.

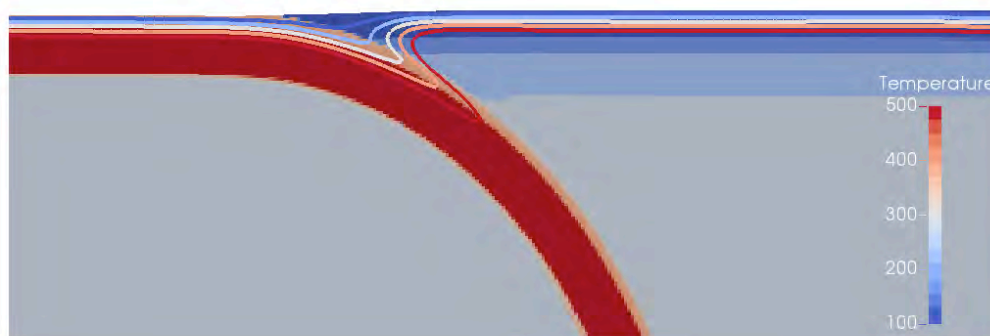


Figure 1: Setup of the 2D model of a subduction zone. Colours represent material phases. Seismogenic zone is limited by width  $W$ . Dipping angle of the seismogenic zone equals  $\theta$ . Wireframe represents temperature distribution in the range from  $100^\circ$  to  $500^\circ$ . Kinematic boundary conditions are prescribed on the bottom of the model.

### Parameter sensitivity:

We calibrate rate and state parameters ( $a$ ,  $b$  and  $L_{cr}$ ) using rupture parameters of Chile 1960 Great Earthquake (Mw 9.3, Moreno et al, 2009), its expected recurrence time of about 400 years (Scholz & Campos, 2012), data on the lithospheric structure (Dzierma, Y. et al, 2012) and thermal field of the region (Currie, 2006) as well as estimation of the friction coefficient in subduction channel from long-term tectonic evolution model.

Using the calibrated parameters we perform a series experiments with different slab geometries, convergence rates etc. The modelling results will be presented and compared with the observations.

### References:

- Heuret A. et al. Physical characteristics of subduction interface type seismogenic zones revisited. *Geochemistry Geophysics Geosystems (G3)* **12**, (2011).
- Heuret A. et al. Relation between subduction megathrust earthquakes, trench sediment thickness and upper plate strain. *Geophys. Res. Lett.* **39**, (2012).
- Popov A. A. & Sobolev S. V., SLIM3D: A tool for three-dimensional thermomechanical modelling of lithospheric deformation with elasto-visco-plastic rheology. *PEPI* **171**, (2008).
- Dieterich, J., Time-dependence of rock friction. *J. Geophys. Res.* **77**, (1972).
- S.V. Sobolev and I.A. Muldashev, Modelling Seismic Cycles of Megathrust Earthquakes Across the Scales, Submitted, (2016).
- Moreno, M. S., Bolte, J., Klotz, J. & Melnick, D. Impact of megathrust geometry on inversion of coseismic slip from geodetic data: Application to the 1960 Chile earthquake. *Geophys. Res. Lett.* **36**, (2009).
- Scholz, C. H., & Campos, J. The seismic coupling of subduction zones revisited. *J. Geophys. Res.* **117**, (2012).
- Dzierma, Y. et al. Seismicity near the slip maximum of the 1960 Mw 9.5 Valdivia earthquake (Chile): Plate interface lock and reactivation of the subducted Valdivia Fracture Zone. *J. Geophys. Res.* **117**, (2012).
- Currie, C. A. & Hyndman, R. D. The thermal structure of subduction zone back arcs. *J. Geophys. Res.* **111**, (2006).

## Unified cycles of Earthquakes with off-fault deformation

James D. P. Moore<sup>1</sup>, Sylvain Barbot<sup>1</sup>, Valère Lambert<sup>1</sup>, Peng Dongju<sup>1</sup>, Tim Stern<sup>2</sup>, and Qiu Qiang<sup>1</sup>.

<sup>1</sup>) Earth Observatory of Singapore (EOS), Nanyang Technological University, 50 Nanyang Avenue, Block N2-01a-15, Singapore 639798.

<sup>2</sup>) Victoria University, Wellington, New Zealand

Corresponding author: earth@jamesdpmoore.com

S4 session: Seismic cycle & Earthquake dynamics (Oral)

Studies of geodetic data across the earthquake cycle indicate a wide range of mechanisms contribute to cycles of stress buildup and relaxation. Both on-fault rate and state friction and off-fault rheologies can contribute to the observed deformation; in particular the postseismic transient phase of the earthquake cycle. One problem with many of these models is that there is a wide range of parameter space to be investigated, with each parameter pair possessing their own tradeoffs. This becomes especially problematic when trying to model both on-fault and off-fault deformation simultaneously. The computational time to simulate these processes simultaneously using finite element and spectral methods can restrict parametric investigations.

We present a novel approach to simulate on-fault and off-fault deformation simultaneously using analytical Green's functions for distributed deformation at depth [Barbot, Moore and Lambert., 2016]. This allows us to jointly explore dynamic frictional properties on the fault, and the plastic properties of the bulk rocks (including grain size and water distribution) in the lower crust with low computational cost. These new displacement and stress Green's functions can be used for both forward and inverse modelling of distributed shear, where the calculated strain-rates can be converted to effective viscosities.

We also present a case study utilising our new Green's functions for distributed deformation and the associated code, Unicycle. Here, we draw insight from the postseismic geodetic observations following the 2015 Mw 7.8 Gorkha earthquake. We forward model afterslip using rate and state friction on the megathrust geometry with the two ramp-décollement system presented by Hubbard et al., (pers. comm., 2015) and viscoelastic relaxation using recent experimentally derived flow laws with transient rheology and the thermal structure from [Cattin et al., 2001]. The calculated strain-rates can be converted to effective viscosities. The postseismic deformation brings new insights into the distribution of brittle and ductile crustal processes beneath Nepal.

Finally, we illustrate a number of other applications for these Green's functions, including inverting for rheological properties in the Sumatran-Andaman arc using geodetic measurements of the postseismic transient following the 2004 Mw 9.1 Sumatra-Andaman earthquake, and inverting for crustal stretching at Taupo, New Zealand, between 2000 and 2012 [Hamling, 2015] using permanent GPS stations.

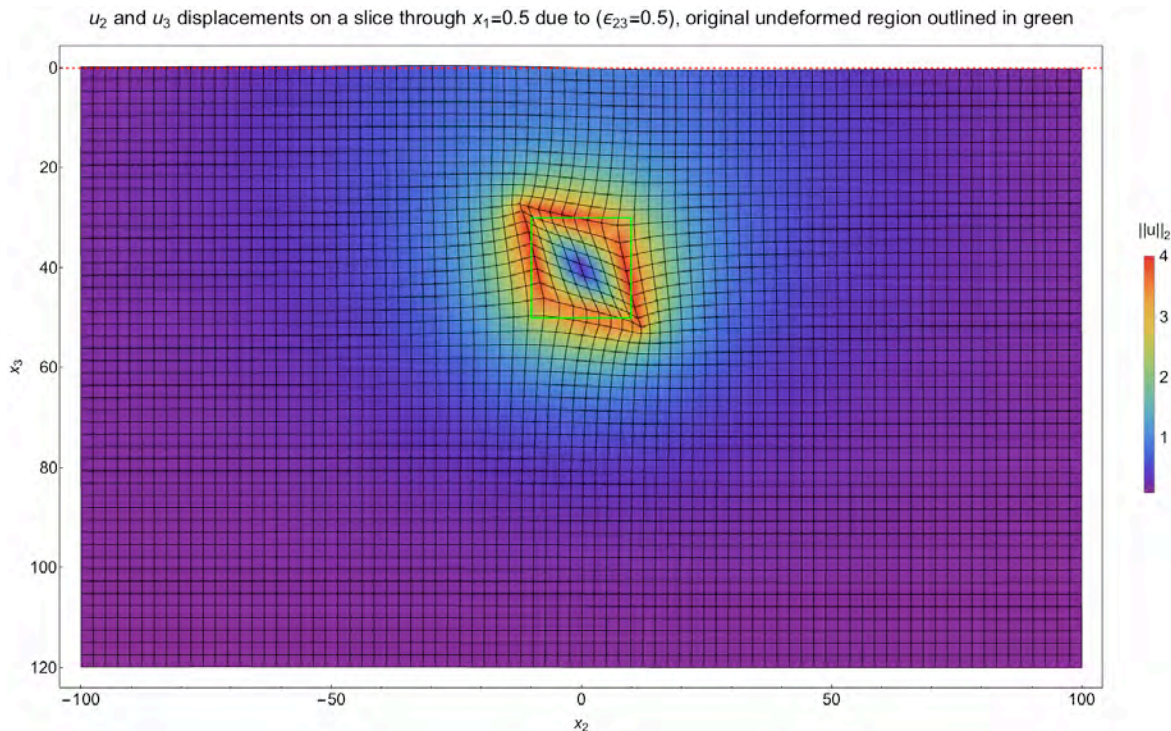


Figure 1: Horizontal ( $u_2$ ) and vertical ( $u_3$ ) displacement due to shear of a buried cube in the  $e_{23}$  direction. Units are self-consistent (m or km etc). Initial surface of  $z=0$  shown with dashed red line, and original undeformed cross section of the cube outlined in green. Original cube dimensions  $20 \times 20 \times 20$  centered at  $(x_1, x_2, x_3) = (0, 0, 40)$ . Analytic expressions evaluated on a grid to show mesh deformation.

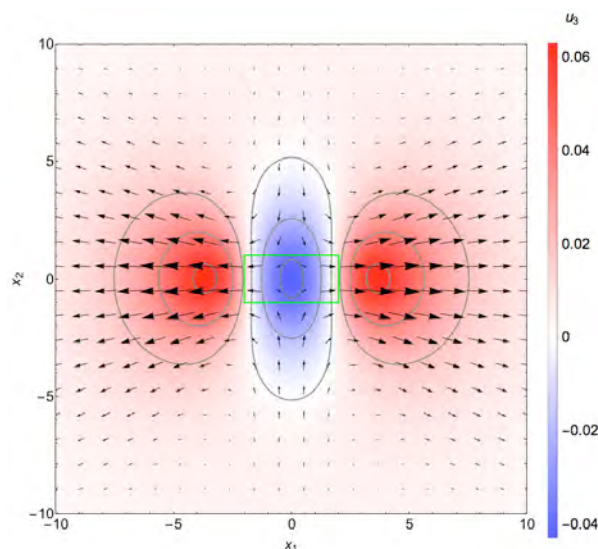


Figure 2: Plan view of surface displacements due to horizontal rifting ( $e_{22}=1$ ) of a cube. Vertical displacements are shaded, whilst horizontal displacements are given by black arrows. Location of buried cube outlined in green. Original cube dimensions  $4 \times 2 \times 2$  centered at  $(x_1, x_2, x_3) = (0, 0, 3)$ . Dimensions are normalised.

## References:

- Barbot S., Moore J. D. P., Lambert V. 2016. Displacements and Stress Associated with Distributed Inelastic Deformation in a Half Space. BSSA, Submitted.
- Cattin R., Martelet G., Henry P., Avouac J. P., Diament M., Shakya T. R. 2001. Gravity anomalies, crustal structure and thermo-mechanical support of the Himalaya of Central Nepal. Geophysical Journal International, Volume 147, Issue 2, 381-392.

Hamling, I. J., Hreinsdottir S., Fournier N. 2015 The ups and downs of the TVZ: Geodetic observations of deformation around the Taupo Volcanic Zone, New Zealand, *Journal of Geophysical Research: Solid Earth*, Volume 120, Issue 6, 4667-4679.

**Keywords:** Earthquake cycle, Green's functions, distributed deformation, rheology.

## Plate convergence rate controls earthquake-size distribution of mountain belts

Luca Dal Zilio<sup>1</sup>, Ylona van Dinther<sup>1</sup>, Taras V. Gerya<sup>1</sup>

<sup>1</sup>) Institute of Geophysics, ETH Zurich, 8092 Zurich, Switzerland

Corresponding author: luca.dalzilio@erdw.ethz.ch

S4 - Seismic cycle & Earthquake dynamics (Oral)

Maximum earthquake magnitude and the rate of seismic activity differ among orogenic mountain belts. This variation is generally attributed to factors such as tectonic structures and stress and strain distribution. However, the processes by which great earthquakes are variably partitioned in space, time, and magnitude, are still strongly debated. Here we show that the seismic behaviour of continent-continent orogenic belts is controlled by the plate convergence rate. We demonstrate this using a tectonically realistic seismo-thermomechanical (STM) modelling approach that considers the long-term deformation, self-consistent collisional orogeny and the short-term seismic cycle.

We developed a two-dimensional, continuum-based STM-model of continental collision, which incorporates a strongly rate-dependent friction formulation and visco-elasto-plastic rheology. The model setup consists of two continental plates separated by an oceanic plate, in which the incipient subduction phase is followed by collisional orogeny.

Results from the post-subduction collisional orogeny show the development of a wide collisional zone (Fig. 1a) dominated by nappe stacking of crustal material in the orogenic wedge and back-thrusting in the retro-wedge. The short-term seismicity pattern (Fig. 1b) shows physically consistent emergence of complex rupture paths. The seismic cycle on seismogenic faults involves long periods of elastic strain and stress accumulation, driven by aseismic ductile deformation at depth, which is ultimately released by sudden fault slip events.

Numerical experiments indicate that the thickness of the brittle layer increases in proportion to the convergence rate, which in turn controls the rupture width, the consequent growth of slip and the maximum earthquake magnitude. Analysing all spontaneous rupture events, we demonstrate that the frequency-size distribution, the corresponding  $b$  value and the maximum earthquake magnitude positively correlate with the plate convergence rate (Fig. 2a). This is a key observational feature of seismicity, which is typically not reproduced in seismic cycle models, and implies a first-order physical control of the convergence rate on the seismicity of mountain belts.

These results quantitatively agree with the observed seismicity patterns within the Alps, Apennines, Zagros and Himalaya (Fig. 2b). In contrast, geometry and tectonic structure of the orogen are observed to play a second-order role. In addition we show that the hypocenter location of earthquakes deepens from the upper to the lower crust as the convergence rate increases. Based on these assessments, we propose that the convergence rate, as well as the temperature and the strain rate (to which the convergence rate is tied), are the parameters most strongly controlling brittle strength and the depth of the seismogenic zones in orogenic mountain belts.

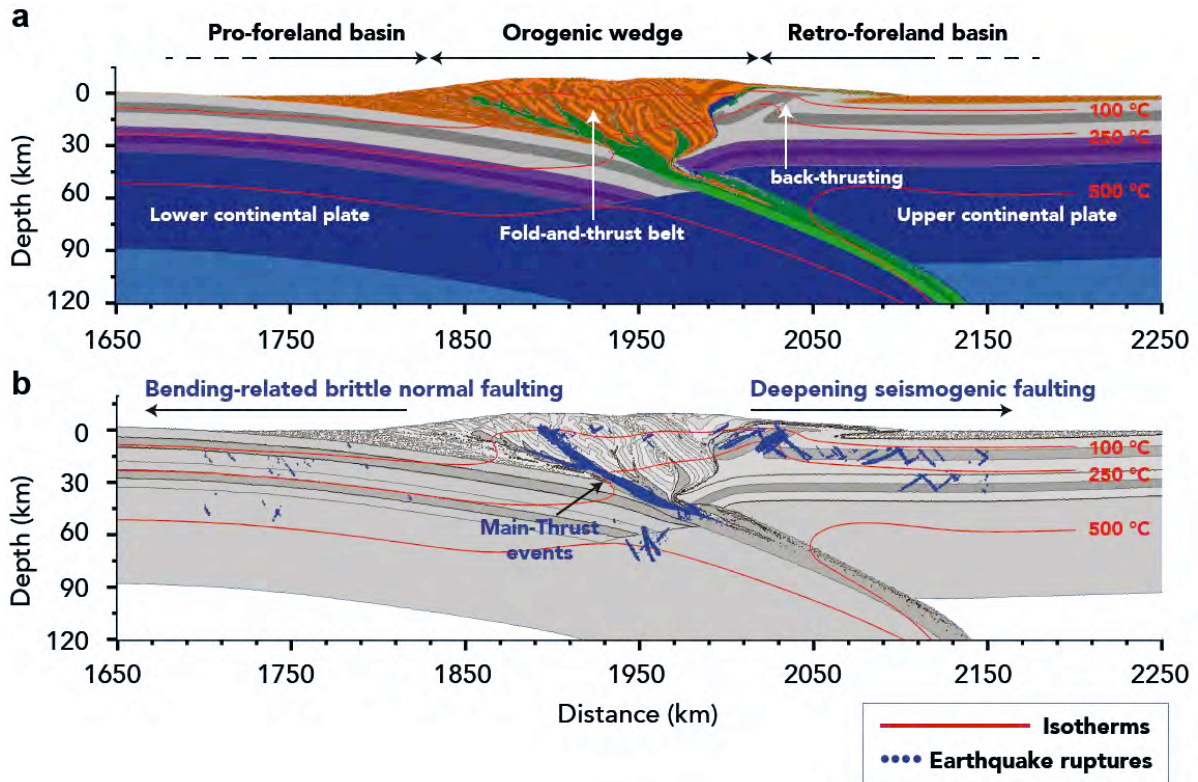


Figure 1. (a) Compositional map showing the characteristics of mountain belt reference model. (b) Short-term spatial evolution of rupture events in the pro-wedge, orogenic wedge and retro-wedge domains.

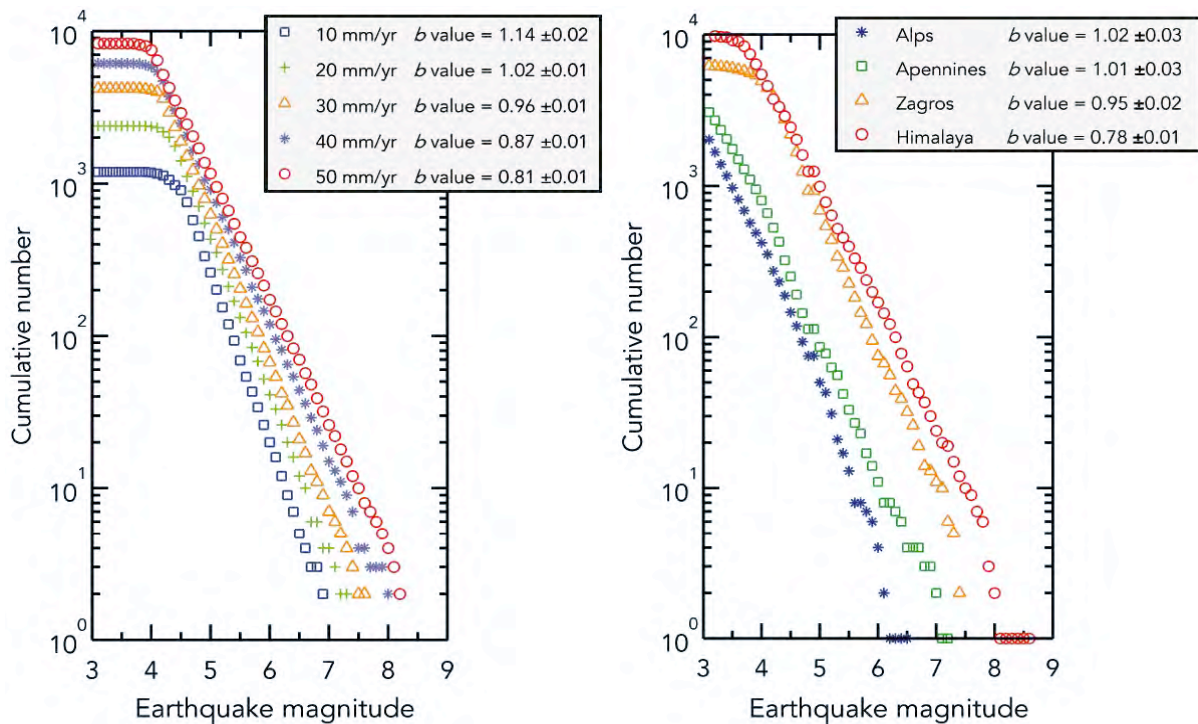


Figure 2. Earthquake-size distribution and  $b$  value estimation of (a) the four major continent-continent orogenic mountain belts and (b) of the two dimensional, quasi static simulations of seismic cycle, assuming plate convergence rates from 10 to 50 mm/yr.

## **Role of coseismic damage and asthenosphere relaxation on the relations between fault length, damaged zone thickness and width of splay fault fans**

Jean Paul Ampuero<sup>1</sup> and Xiaolin Mao<sup>1</sup>

<sup>1</sup>) Seismological Laboratory, California Institute of Technology, Pasadena, California, USA

Corresponding author: ampuero@gps.caltech.edu

S4- Seismic cycle & Earthquake dynamics (Oral)

### **Introduction:**

How earthquakes interact with the evolution of fault zone structure is an open question that motivates emerging efforts to integrate dynamic rupture and long-term crustal deformation modeling. Here, we investigate scaling relations between fault structural properties from the perspective of dynamic and quasi-static mechanical processes involved in fault system evolution. In particular, we develop basic fracture mechanics theory to explain first-order fault zone scaling observations. Faults are surrounded by damaged zones whose properties vary with fault maturity and length. Faults develop an “inner damage zone” in their vicinity (< few 100 m), usually characterized by micro-fracture observations, and an “outer damage zone” at a larger scale comprising macroscopic fault branches forming splay fault fans. For relatively short faults, the thickness of these two damage zones scales with fault length. However, for long faults their empirical scaling is very different: the inner damage zone thickness saturates, whereas the outer damage zone thickness does not (Savage and Brodsky, 2011; Perrin et al., 2016a). Here we present theoretical considerations that help explain this scaling difference and shed light on the mechanisms and time scales governing the evolution of fault structure.

### **Inner damage zone: short-term damage processes lead to thickness saturation:**

Inner damage zones can significantly affect earthquake rupture, enhance near-field ground motions and facilitate fluid transport in the crust. Fault zone trapped waves can generate pulse-like rupture and oscillatory rupture speed, and facilitate supershear ruptures and steady rupture propagation at speeds that are unexpected in homogeneous media (Huang et al., 2011, 2014, 2015; Perrin et al., 2016b). The effects of a fault damage zone crucially depend on its thickness. Field observations of inner damage zone thickness as a function of cumulated slip show linear scaling at small slip but saturation at large slip, with maximum thickness of a few 100 m. Ampuero and Mao (2016) developed fracture mechanics theory, supported by dynamic rupture simulations with off-fault inelastic deformation, that predicts saturation of inner damage zone thickness due to the finite depth of the seismogenic crust (Figure 1, left). In essence, the stress intensity factor at a rupture front, which controls the distance reached by the large off-fault stresses that cause damage, depends on the shortest characteristic length of the rupture, which is limited by the seismogenic depth. The model implies that short-term (co-seismic) processes play a dominant role on the evolution of the inner damage zone. It also provides relations between damage scaling properties and the overall stress at which faults operate.

### **Outer damage zone: long-term viscous relaxation prevents thickness saturation:**

Field observations indicate that outer damage zone width scales with parent fault length, without saturation (Perrin et al., 2016a). Here, we propose a fracture mechanics interpretation of this observation (Figure 1, right). The stress intensity factor at the tips of a fault cutting through the whole depth of an elastic plate (the lithosphere) overlying a linear viscoelastic half-space (the asthenosphere) is time-dependent and shows two regimes. At short times, it depends on seismogenic depth, as expected in an elastic half-space (see above). At times much longer than the viscous relaxation time of

the asthenosphere, it depends on rupture length, as expected for a through-going crack in a thin elastic plate decoupled from the mantle (essentially a 2D plane strain configuration). The growth of splay fault fans is a long-term process, possibly driven by stress concentration near the propagating tip of the main fault governed by the long-term scaling of the stress intensity factor. This view predicts a scaling between outer damage zone width and fault length, consistent with the geological observations.

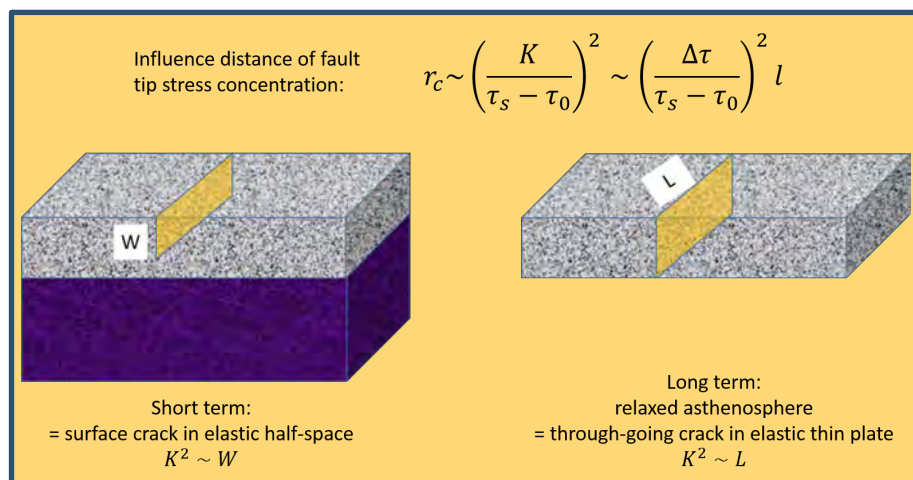


Figure 1: Relation between damage zone thickness ( $r_c$ ) and fault length ( $L$ ) predicted by fracture mechanics. Left: If damage is dominated by short-term processes, Earth behaves as an elastic half-space and  $r_c$  eventually saturates at a value proportional to seismogenic depth ( $W$ ). Right: If damage is controlled by long-term processes, the lithosphere decouples from the asthenosphere and  $r_c$  scales with  $L$  without saturation.

### References:

- Ampuero, J. P., and Mao, X., 2016. Upper limit on damage zone thickness controlled by seismogenic depth, submitted to AGU monograph on "Fault Zone Dynamic Processes: Evolution of Fault Properties During Seismic Rupture".
- Huang, Y., and Ampuero, J. P., 2011. Pulse-like ruptures induced by low-velocity fault zones, *J. Geophys. Res.*, 116, B12307, doi:10.1029/2011JB008684.
- Huang, Y., Ampuero, J. P., and Helmberger, D. V., 2014. Earthquake ruptures modulated by waves in damaged fault zones, *J. Geophys. Res.*, 119 (4), 3133–3154, doi:10.1002/2013JB010724.
- Huang, Y., Ampuero, J. P., and Helmberger, D. V., 2015. The potential for supershear earthquakes in damaged fault zones - Theory and observations, *Earth Planet. Sci. Lett.*, 433, 109–115, doi:10.1016/j.epsl.2015.10.046.
- Perrin, C., Manighetti, I., and Gaudemer, Y., 2016. Off-fault tip splay networks: A genetic and generic property of faults indicative of their long-term propagation, *C. R. Geosci.*, 348, 52–60, doi: 10.1016/j.crte.2015.05.002.
- Perrin, C., Manighetti, I., Ampuero, J. P., Cappa, F. and Gaudemer, Y., 2016. Location of largest earthquake slip and fast rupture controlled by along-strike change in fault structural maturity due to fault growth, *J. Geophys. Res.*, 121 (5), 3666–3685, doi:10.1002/2015JB012671.
- Savage, H. M., and E. E. Brodsky (2011), Collateral damage: Evolution with displacement of fracture distribution and secondary fault strands in fault damage zones, *J. Geophys. Res.*, 116, B03405, doi: 10.1029/2010JB007665.

**Keywords:** Damage zones, splay faults, earthquakes, fracture mechanics.

## Interpreting strike-slip fault interseismic deformation with elasto-plastic models

Olivier Cavalié<sup>1</sup>, Alexandre Chemenda<sup>1</sup>, Mathilde Vergnolle<sup>1</sup>, Stéphane Bouissou<sup>1</sup>, Bertrand Delouis<sup>1</sup>

<sup>1</sup>) University of Nice Sophia Antipolis, Lab. Géoazur, Valbonne, France

Corresponding author: ocavalié@geoazur.unice.fr

S4 – Seismic cycle and Earthquake dynamics (PS7)

### Introduction:

Geological and geophysical observations provide limited information on the 3-D structure, formation and evolution of faults. Faults are characterized by a complex 3-D architecture with different segments and branches that can be reactivated at different periods of the fault evolution. Microseismicity shows that faults are not simple zero-thickness interfaces, but are several dozen kilometer-thick zones where material undergoes damage or irreversible inelastic deformation. On the other hand, interseismic deformations revealed by geodetic measurements (GPS and InSAR) are typically interpreted as elastic and modelled as a dislocation buried at depth and slipping at constant rate below a certain locking depth. The analytical solution for such elastic model shows that, for a strike slip fault, the across-fault displacement profile corresponds to an arctangent function. Almost 200 estimates of locking depth made over more than 100 faults have been done using this model (Wright et al., 2013). Most of them give values between 10-15 km that would correspond to the depth of the crust seismogenic section. Other studies suggest much lower locking depth. Creeping events on the fault (or its part) are then evoked to explain those lower values. In this study, we explore the impact of inelastic deformation during the interseismic phase and notably how it impacts the deformation gradient across a strike-slip fault..

### Modeling results:

The model represents a layer (Fig. 1a) with elasto-plastic properties. The layer is subjected to a gravity force that generates the initial stresses. Along the  $y$ -parallel vertical boundaries, free slip conditions are applied. Along the  $y$ -normal boundaries, kinematic conditions are imposed to simulate an infinite model in the  $y$ -direction. A shear stress,  $\tau_{zy}$  that increases progressively during deformation, is applied to the layer bottom, which is fixed in the  $z$ -direction.

During the initial stages of the model's evolution, its response is purely elastic. At a certain stage, the inelastic deformation starts at the surface in the axial (along  $y$ ) area and rapidly becomes deeper and wider (Fig 1b). At the next stage, a dense set of parallel deformation localization bands (incipient faults) is formed. The whole band set first evolves uniformly, and then one observes a sort of “band selection” process: most of bands die, while others continue evolving. At the last stage of the model deformation one can observe 3 main segments as well as secondary (splay) branches (Fig. 1c). At all deformation stages a wide zone (with width of several layer thicknesses) is involved in inelastic deformation/damage. Fig 2b shows that the arctangent-type shape of the  $u_y$  profile becomes progressively sharper (the displacement gradient becomes larger) with time.

### Comparison with geodetic measurement:

The North and East Anatolian faults (NAF and EAF, respectively) are good examples confirming this shape evolution (Cavalié and Jonsson, 2014). For the NAF, at the location where the last ruptures occurred in 1949 and 1992, the across-fault displacement rate gradient is relatively low and corresponds to a locking depth of 14 km. For the EAF, where the last rupture occurred in the 19th century, this gradient is much higher, with the predicted locking depth of only 3 km (Cavalié and

Jonsson, 2014). For such high displacement rate gradients, that require very small locking depths with a purely elastic model, aseismic slip in the seismogenic zone is postulated. But we show here that a more physically sound solution exists by tacking into account the inelastic deformation in a wide fault zone.

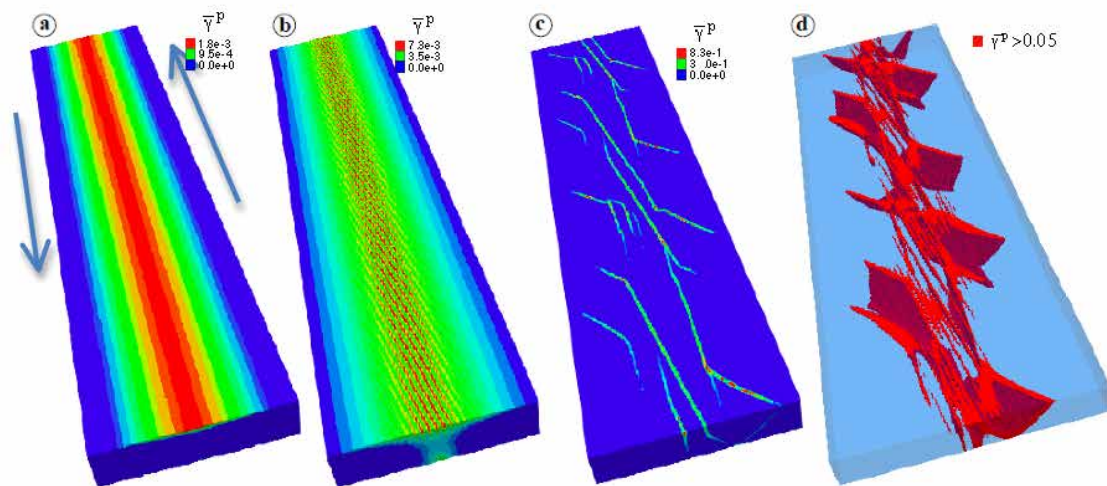


Fig1 : (a to c) Evolution of inelastic deformation and faulting,  $\bar{\gamma}^P$ , and resulting 3-D fault architecture (d, corresponding to the evolutionary stage c).

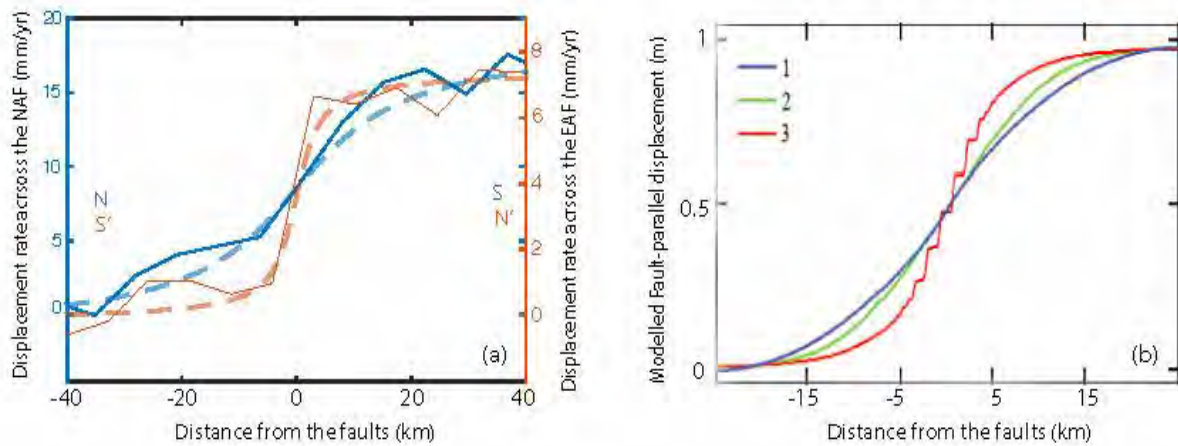


Figure 2: (a) Profiles of displacement rate across the north Anatolian fault (blue lines) and the east Anatolian fault (red lines). Solid lines correspond to the observed (InSAR) displacement rates, dashed lines represent the best-fit elastic model solutions. (b) Along-y-axis profiles of the incremental displacement  $u_y$  at different stages of the model's evolution (see Fig. 1). 1, Purely elastic deformation stage; 2 and 3, successive stages with inelastic deformation.

**References:**

Cavalié O. and Jónsson S., 2014. Block-like plate movements in eastern Anatolia observed by InSAR, *Geophys. Res. Lett.*, 41, 36-31, 2014.

Chemenda, A. et al, 2016. Numerical model of formation of a 3-D strike-slip fault system, *Comptes Rendus Geosciences*, 348, 61-69.

Wright, T., Elliott J., Wang H., Ryder I., 2013. Earthquake cycle deformation and the Moho: Implications for the rheology of continental lithosphere, *Tectonophysics*, 609, 504-523.

**Keywords:** Faulting, Strike-slip, Fault evolution, Finite-difference modeling.

## Control of barrier width on asperities synchronization and genesis of great subduction megathrust earthquakes: insights from 3D analog models

Fabio Corbi<sup>1</sup>, Francesca Funicello<sup>2</sup>, Silvia Brizzi<sup>2</sup>, Elenora Van Rijsingen<sup>1,2</sup>, Serge Lallemand<sup>1</sup>, Stephane Dominguez<sup>1</sup> and Rodolphe Cattin<sup>1</sup>

<sup>1</sup>) University of Montpellier, Géosciences Montpellier Laboratory, Montpellier, France.

<sup>2</sup>) Roma Tre University, Laboratory of Experimental Tectonics, Dip. Scienze, Rome, Italy.

Corresponding author: fabio.corbi3@gmail.com

S4- Seismic cycle & Earthquake dynamics (PS7)

### Abstract:

The world largest earthquakes occur on the subduction megathrust: the interface between the subducting and overriding plates. The mechanical properties of megathrusts vary spatially and temporally for various reasons e.g., presence of geometrical irregularities or stress fluctuations due to past earthquakes. Such variations result in areas prone to hosting large seismic slip aka asperities and areas where the rupture propagation is inhibited aka barriers. According to the “asperity model” [Lay and Kanamori, 1981], the magnitude of an earthquake depends on the possibility for asperities to synchronize and fail simultaneously during the same event. Clear examples of asperities synchronization episodes include the 1960 Chile earthquake (Mw= 9.5) and the 2004 Sumatra–Andaman earthquake (Mw=9.2), where multiple (> 4) high slip patches have been imaged by inversion of geological and geophysical data [Moreno et al., 2009; Subaraya et al., 2006]. The mechanism that promotes asperities synchronization is debated and remains obscure mainly due to the short time interval that is available in the instrumental (both geodetic and seismological) record.

Here we use analog models focusing on the control of barrier width on asperities synchronization. The main advantage of analog models is the possibility to reproduce 10<sup>5</sup> yr long time series of seismicity in a convenient experimental time using a simple but physically self-consistent model. In our models, a gelatin wedge (the analog of the overriding plate) is underthrust by a planar, 10° dipping aluminum slab (the analog of the subducting plate) containing two rectangular patches with velocity weakening friction acting as seismic asperities. The width of the velocity strengthening friction area D between the two asperities (i.e., the analog barrier) is varied systematically in the 2.5-10 cm range. The experiments are monitored from top view and the images processed by means of standard particle image velocimetry PIV. The velocity field is then used to derive the earthquake source parameters.

The models reproduce tens of episodic trenchward slip episodes (the analog earthquakes) alternated by relatively longer and slower periods of landward displacements (analog of interseismic stages). The magnitude of the analog earthquakes is in the Mw6.0 – Mw8.5 range. We observe both ruptures arrested by the barrier and ruptures able to overcome it. The latter represent clear examples of synchronized asperities. The cumulative slip distribution of the synchronized asperities rupture shows two high slip patches separated by a low slip region similarly to the 2010 Maule (Mw=8.8) and the 2005 Nias (Mw=8.6) earthquakes [Konca et al., 2008; Vigny et al., 2011]. We find that the degree of asperity synchronization is a function of D. When D>6.25 cm (which is equivalent to ~40 km in nature) only mono-asperity ruptures with Mw<7.5 are observed. When D≤6.25 cm a fraction of the simulated earthquakes are synchronized asperities failures and Mw>8.0 events are observed.

Future efforts will be devoted to linking the synchronization process to: a) static Coulomb stress changes during the coseismic phase and b) degree of plate locking in the preceding interseismic stage.

Our models may allow a better understanding of the asperities synchronization process, potentially contributing to forecasting the extent of future earthquakes based on geodetically derived pattern of interseismic coupling.

## References:

- Lay, T., and H. Kanamori 1981. An asperity model of large earthquake sequences, *Earthquake Prediction: An International Review* 4.
- Moreno, M. S., J. Bolte, J. Klotz, and D. Melnick, 2009. Impact of megathrust geometry on inversion of coseismic slip from geodetic data: Application to the 1960 Chile earthquake, *Geophys. Res. Lett.*, 36(16), 1–5, doi:10.1029/2009GL039276.
- Subarya, C., M. Chlieh, L. Prawirodirdjo, J.-P. Avouac, Y. Bock, K. Sieh, A. J. Meltzner, D. H. Natawidjaja, and R. McCaffrey, 2006. Plate-boundary deformation associated with the great Sumatra-Andaman earthquake, *Nature*, 440(7080), 46–51, doi:10.1038/nature04522.
- Konca, a O. et al., 2008. Partial rupture of a locked patch of the Sumatra megathrust during the 2007 earthquake sequence, *Nature*, 456(7222), 631–5, doi:10.1038/nature07572.
- Vigny, C., et al. 2011. The 2010 Mw 8.8 Maule megathrust earthquake of Central Chile, monitored by GPS, *Science*, 332(6036), 1417–21, doi:10.1126/science.1204132.

**Keywords:** megathrust earthquakes, asperities synchronization, barrier, slip distribution.

## A new multilayered visco-elasto-plastic experimental model to study strike-slip fault seismic cycle

Y. Caniven<sup>1</sup>, S. Dominguez<sup>1</sup>, R. Soliva<sup>1</sup>, R. Cattin<sup>1</sup>, M. Peyret<sup>1</sup>, C. Romano<sup>1</sup>

<sup>1</sup>Géosciences Montpellier Laboratory, University of Montpellier, Montpellier, France

Corresponding author: [stephane.dominguez@gm.univ-montp2.fr](mailto:stephane.dominguez@gm.univ-montp2.fr)

S4 - Seismic cycle & Earthquake dynamics (PS7)

Nowadays, technological advances in satellite imagery measurements as well as the development of dense geodetic and seismologic networks allow for a detailed analysis of surface deformation associated with active fault seismic cycle. However, the study of earthquake dynamics faces several limiting factors related to the difficulty to access the deep source of earthquake and to integrate the characteristic time scales of deformation processes that extend from seconds to thousands of years. To overcome part of these limitations and better constrain the role and couplings between kinematic and mechanical parameters, we have developed a new experimental setup dedicated to the study of seismic cycle crustal deformation associated to strike-slip faulting.

Our analog model integrates simple but realistic tectonics and kinematics boundary conditions together with a multilayer visco-elasto-plastic rheology simulating the upper and lower crust deformation behavior. The analog model is formed by three superimposed layers of different analog materials whose physical properties were selected to simulate the mechanical behavior of an idealized continental crust (Figure 1). The basal layer is 3 cm thick and is made of a viscoelastic silicone compound (Polydimethyl-siloxane polymer PDMS-SGM 36, Dow Corning Ltd., viscosity about 50 kPa s at room temperature). The silicone layer allows for simulating the viscous deformation and strain-hardening behavior of the lower crust (depth > 10–15 km). The intermediate layer is 4 to 6 cm thick and it is made of a high-resilience Polyurethane foam (Young modulus =  $95 \pm 10$  kPa, Poisson ratio =  $0.06 \pm 0.02$ , shear modulus =  $45 \pm 5$  kPa,  $V_p = 100$  m/s,  $V_s = 68$  m/s). The foam has a high elasticity, which largely dominates its mechanical behavior. Its viscosity is unknown but considered as high enough to be neglected in the process of model scaling. The foam allows for the simulation of the elastic deformation that characterizes the upper crust (depth < 10–15 km) mechanical behavior at the time scale of the seismic cycle. The brittle/ductile transition corresponds to a, 2–3 mm thick, impregnation of the silicone into the base of the polyurethane foam, insuring a strong coupling whose mechanical properties depend also on model velocity boundary conditions (elastic loading rate). The uppermost layer is 0.25 to 0.5 cm thick and is formed by a granular material mixture (silica powder and graphite). It represents the very upper kilometers of the shallow crust where deformation is considered as essentially brittle.

Another originality of our approach is the use of numerical modeling algorithms to investigate the distribution and evolution of strain and stress at the surface and at depth, along the fault plane.

First results, based on more than 50 experiments, show that our model succeed in reproducing the deformation mechanisms and surface kinematics associated to the main phases of the seismic cycle as defined by the elastic rebound theory [Reid, 1910]: - Model interseismic deformation is characterized by either total or partial locking of the fault associated to episodic aseismic creep events. Model surface kinematics can be predicted using the Savage and Burford [1973] analytical formulation which validate the good analogy with nature.

- Coseismic deformation is characterized by almost instantaneous fault slip events that present a broad variability in size and location along the fault. Here also, surface kinematics associated to these microquakes is consistent to those predicted using half-space elastic dislocation numerical modeling. - Finally, the postseismic deformation exhibits after-slip on the fault plane and can be also associated to

viscoelastic relaxation of the simulated lower crust due to the mechanical readjustment at the brittle-ductile transition.

Consequently, we consider that model scaling, despite inevitable dissimilarities, is satisfactory and allow extrapolation of first-order experimental results to nature taking into account intrinsic model limitations. Some scientific results have been already obtained and are in the process of submission.

They concern interesting relations between fault mechanical behavior and the role of some key parameters such as the normal stress, the loading rate, and the frictional heterogeneity along the fault. Future technical developments are on the way, mainly to improve model scaling and to access to coseismic rupture propagation analysis. Moreover, we plan to test specific devices to measure the vertical component of displacement (laser holography), accelerations, and stresses (microsensors) during experiments.

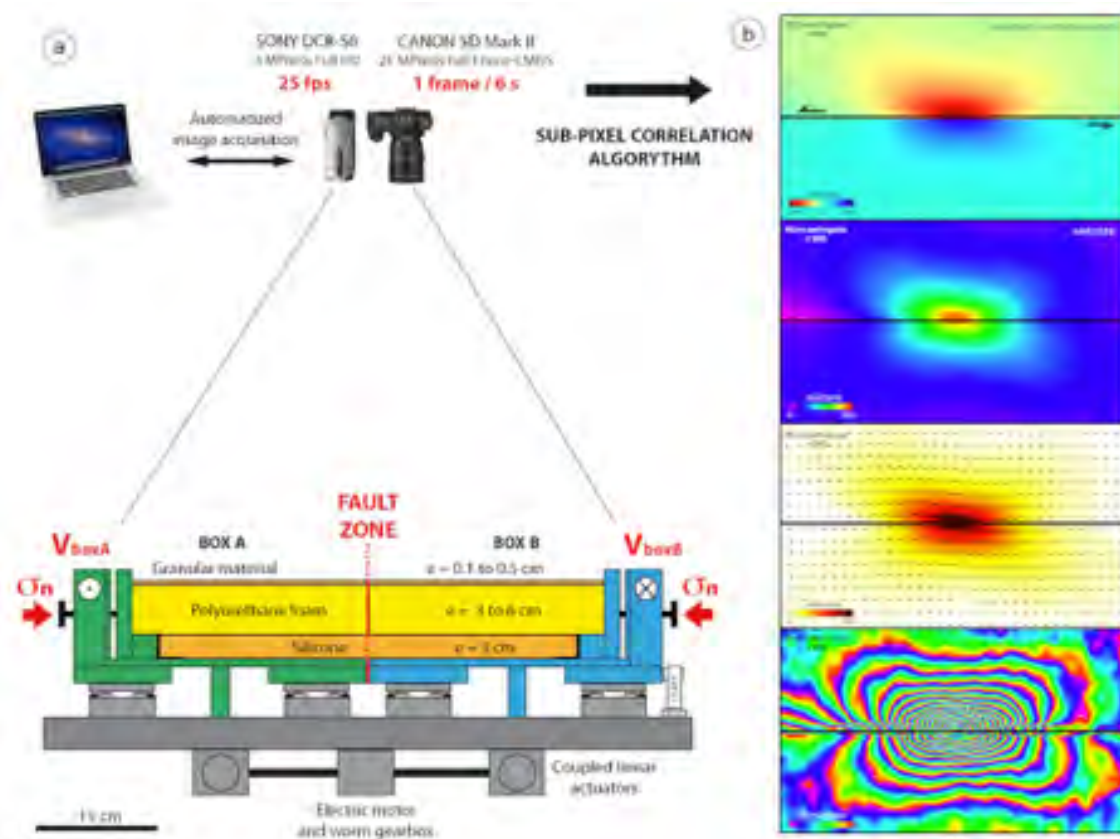


Figure 1: Schematic cross section of the experimental device showing its internal mechanical structure, the geometry of analog material layers and how boundary conditions (initial normal stress and loading rate) are controlled. (b) Model surface horizontal displacements are monitored using subpixel image correlation technique. Numerical modeling tools are used to analyze model deformation at the surface and at depth.

Reid, H. F. (1910), The mechanics of the earthquake, the California Earthquake of April 18, 1906, in Report of the State Earthquake Investigation Commission, vol. 2, 192 pp., Carnegie Institution of Washington, Washington, D. C.

Savage, J. C., and R. O. Burford (1973), Geodetic determination of relative plate motion in central California, *J. Geophys. Res.*, 78(5), 832–845, doi:10.1029/JB078i005p00832.

**Keywords:** Analogue modeling, seismic cycle, earthquake dynamics, strike-slip fault.

## **A visco-elastic model to study experimentally megathrust seismic cycle in subduction tectonic settings.**

S. Dominguez<sup>1</sup>, S. Mazzotti<sup>1</sup>, R. Cattin<sup>1</sup>, M. Peyret<sup>1</sup>, S. Lallemand<sup>1</sup>, J. Malavieille<sup>1</sup>, R. Soliva<sup>1</sup>, C. Romano<sup>1</sup>

<sup>1</sup>Géosciences Montpellier Laboratory, University of Montpellier, Montpellier, France

Corresponding author: [stephane.dominguez@gm.univ-montp2.fr](mailto:stephane.dominguez@gm.univ-montp2.fr)

S4 - Seismic cycle & Earthquake dynamics (PS7)

### **Abstract:**

Subduction megathrust earthquakes, such as the 2004 Sumatra-Andaman or the 2011 Tohoku earthquakes, generate heavy economic and human losses. Their study represents a major societal and scientific challenge. However, several limiting factors, related to the difficulty to analyze deformation undersea, to access deep source of earthquake and to integrate the characteristic time scales of seismic processes, must be overcome first.

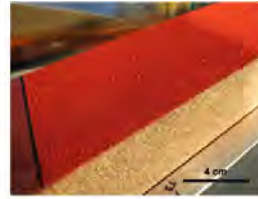
With this aim, we have developed an experimental approach to complement numerical modeling techniques that are classically used to analyze available geological and geophysical observations and measurements of subduction earthquakes. The main goal of this project is to validate a kinematically and mechanically first-order scaled analogue model of a subduction zone capable of reproducing megathrust earthquakes and realistic seismic cycle deformation phases.

Our approach differs from pre-existing experimental devices by several points: we build a large experimental device to avoid boundary effects and study lateral variations; we use a realistic model rheology (multi-layered elasto-visco-plastic), we take into consideration the elastic deformation of the subducting oceanic plate and finally, we model the seismogenic zone by testing different frictional plate interface to modify seismic coupling.

Preliminary results show that our subduction model succeeds in reproducing the deformation phases associated to the seismic cycle (interseismic elastic loading, coseismic rupture and post-seismic relaxation).

By studying model kinematics and mechanical behavior, we expect to improve our understanding of seismic deformation processes and better constrain the role of physical parameters (fault friction, rheology, ...) as well as boundary conditions (loading rate,...) on seismic cycle and megathrust earthquake dynamics.

We expect that results of this project will lead to significant improvement on interpretation of geophysical data, satellite observations and seismological records.

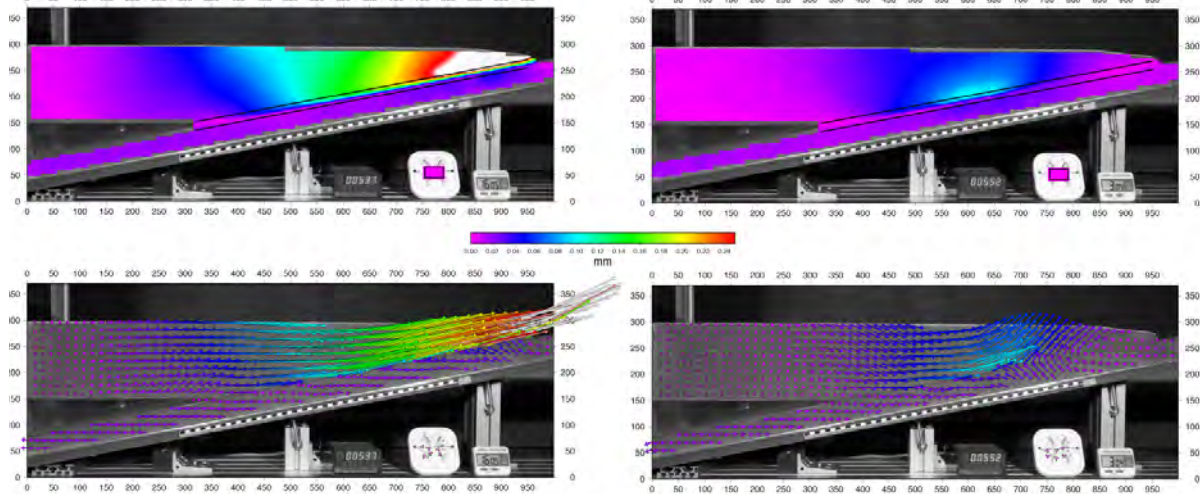


**NATURE**  
 Rigidity Modulus ( $G$ ) = 30 GPa  
 Poisson coefficient ( $\nu$ ) = 0.2  
 Upper Mantle Viscosity =  $10^{18}$  Pa s

**MODEL**  
 Foam rigidity Modulus ( $G$ ) = 90 kPa  
 Poisson coefficient ( $\nu$ ) = 0.05  
 Silicone (SGM36) viscosity = 30-50 kPa s

**FIRST ORDER SCALING**  
 $L^*$  1 cm = 3+/- 1 km  
 $T^*$  1s = 1-5 years  
 $\tau^*$  1s = 5-10 s

EXPERIMENTAL SET-UP and BOUNDARY CONDITIONS : Model kinematics is monitored using sub-pixel spectral correlation of camera images. Friction properties of the seismogenic zone are controlled using foam coating.



SLIP EVENTS VARIABILITY : Frictional properties of the subduction interface (seismogenic zone) allow for the generation of megathrust microquakes rupturing the whole interface but also isolated intermediate microquakes rupturing a limited part of the seismogenic zone. Interface locking, creeping events, as well as slow microquakes are also observed. Note that thanks to the visco-elastic coupling, subsidence is well simulated.

**Keywords:** Analogue modeling, seismic cycle, earthquake dynamics, Subduction megathrust, fault

## Seismic amplification due to topography: preliminary results of a gelatin model

Octavi Gómez-Novell<sup>1</sup> and María Ortuño<sup>1</sup>

<sup>1</sup>) RISKNAT and GEOMODELS group. Universitat de Barcelona. Facultat de Geologia, 08028, Barcelona, Spain.

Corresponding author: maria.ortuno@ub.edu

S4- Seismic cycle & Earthquake dynamics (PS7)

### Introduction:

The topographic effect causes seismic wave amplification on the top of the mountains. This amplification reportedly produces more damage on the infrastructures of these parts of the reliefs and for this reason this effect has been widely studied using mainly numerical and experimental approximations (Massa et al., 2014). However, it has never been studied using analogue modelling. This study aims to start pointing out the main issues and results of carrying out this type of modelling. To do so, two gelatin analogue models have been made in order to achieve a correct scaling of crust's elastic parameters and acoustic waves have been used in order to reproduce seismic P-wave propagation. This has been done considering that the gelatin is efficient to simulate the earth's crust and run laboratory models related to seismicity (e.g.; Kavanagh et al., 2013; Schellart and Strak, 2016). The experiments have been performed in the models allowing the observation of attenuation by geometrical spreading and topographic amplification in most of the acoustic signals. The experimental setup also affects the signals for some configurations producing anomalies in the attenuation and amplification tendencies.

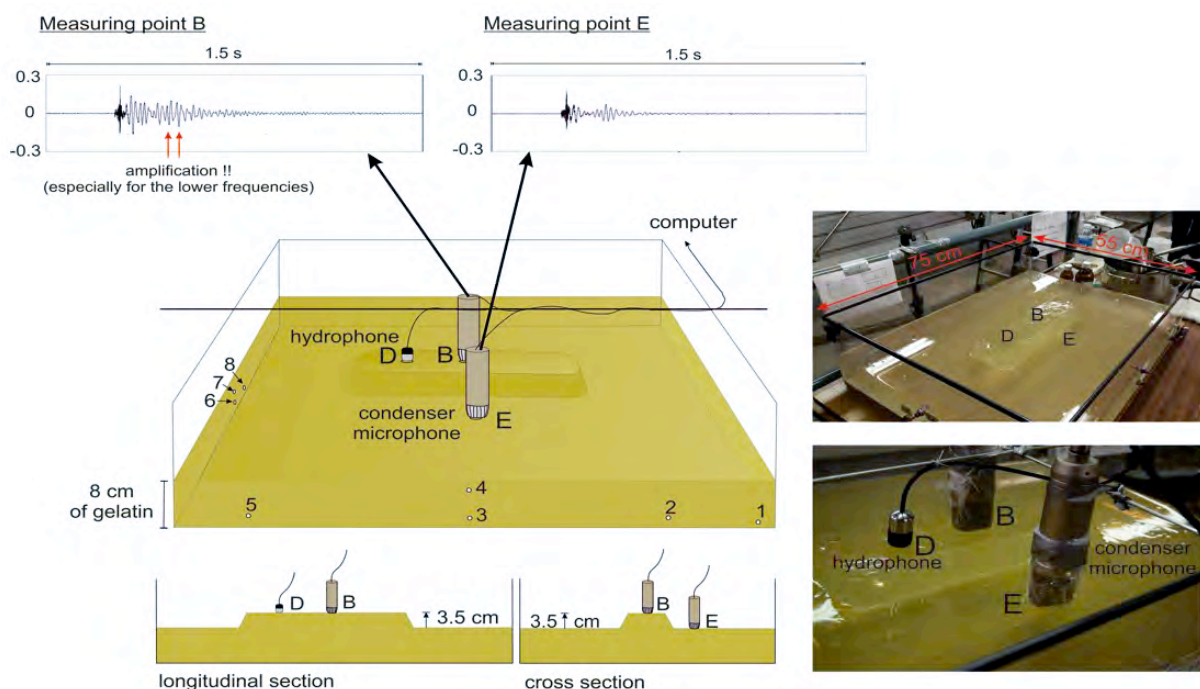


Figure 1. Configuration of one of the models that have been made in order to study the topographic amplification of the acoustic waves. Left: The model scheme includes a 3D view and two cross sections of the model, where the topographic relief and the position of the microphones and the points where the compressed-

*air is injected (1 to 8) are shown. In the upper part, the acoustic records obtained are shown. Topographic amplification can be recognized at the top of the topography, especially for the waves with lower frequency. Right: Detailed photographs of the model are included.*

## **Preliminary results and model limitations:**

Measurements of the acceleration in the model's surface have also been performed, but these don't show any enhanced motions at the top of the relief. The amplification depends on the frequency of the acoustic waves, thus the waves with wavelengths more similar to the mountain's length are the most amplified (12% to 28% of maximum amplification), which is in agreement with most of the studies. Nevertheless, the limitations of this study must be taken into account when it comes to relating the processes in the model with the natural ones. The absence of shear waves in the experimental runs and scaling problems, especially for the acoustic wave frequencies, constitute the main limitations of this study. However, the fact that some processes identified in the model actually occur in the nature, ensure the validity of the method at least from a qualitative perspective. Several improvements must be applied in this method in order to obtain better results and get more useful clues for the natural hazard assessment in the future.

## **References:**

- Gómez-Novell, O. (2016). Analogue modeling of the topographic effect: results and limitations of a pilot study. Unpublished Msc thesis. Universitat de Barcelona, 25 pp.
- Kavanagh, J. L., Menand, T. and Daniels, K. A. (2013). Gelatine as a crustal analogue: Determining elastic properties for modelling magmatic intrusions. *Tectonophysics*, 582, 101–111.
- Massa, M., Barani, S. and Lovati, S. (2014). Overview of topographic effects based on experimental observations: Meaning, causes and possible interpretations. *Geophysical Journal International*, 197 (3), 1537–1550.
- Schellart, W.P. and Strak, V. (2016). A review of analogue modelling of geodynamic processes: Approaches, scaling, materials and quantification, with an application to subduction experiments. *Journal of Geodynamics*, 100, 7-32.

**Keywords:** Gelatin analogue modeling, seismic amplification, topographic effect, acoustic waves.

## **Control of geometrical and mechanical parameters on strike-slip fault segmentation: insights from sandbox experiments.**

Marthe Lefèvre<sup>1</sup>, Pauline Souloumiac<sup>2</sup>, Nadaya Cubas<sup>3</sup> and Yann Klinger<sup>1</sup>

<sup>1</sup>) IPGP - CNRS, Sorbone Paris Cité, Université Paris Diderot, Paris, France

<sup>2</sup>) University of Cergy Pontoise, Lab. Géosciences et Environnement, Cergy-Pontoise, France

<sup>3</sup>) University of Pierre et Marie Curie, IStEP, Paris, France

Corresponding author: mlefevre@ipgp.fr (corresponding author)

S4- Seismic cycle & Earthquake dynamics (PS7)

Co-seismic continental strike-slip ruptures are usually segmented, with segments of varying orientation bounded by fault bends and step overs. The length of segments has been shown to vary from 18km to 25km, independently of the regional tectonic setting (Klinger, 2010). These observations led the author to suggest that the thickness of the seismogenic crust could control this structural scaling. Here, to test this hypothesis, we use analog modeling and seek for the parameters controlling the length of strike-slip fault segments. The formation of strike-slip faults has been thoroughly described by Tchalenko (1970).

We know that theoretically the first structures to appear are en échelon Riedel shears that then rotate, before being abandoned in favor of horizontal shears linking the Riedels that will end up forming the strike-slip fault. These horizontal shears would represent the fault segments described by Klinger (2010). However, no study has been conducted so far to characterize the parameters controlling the distance between Riedel shears or the segment length. We here test and quantify the effect of the sand pack thickness as well as the internal and basal frictions on the length of segments. We then compare our results to natural case to conclude on their potential relationship with the seismogenic thickness.

### **Sandbox apparatus and experimental procedure:**

Sandbox prototype:

The specific sandbox for Riedel experiments is composed of two PVC plates simulating the base of the upper crust. One plate is movable and can be pushed forward to simulate a sinistral strike-slip fault at the base of the model thanks to a lead screw. The other plate is fixed. The dimensions of the box (80x210cm) are large enough to ensure that a significant part of the observations escapes boundary effects. The sand pack is flat and the edges are free. Top view photos are taken every 0.5 mm.

Parametric study description:

We test sand pack varying from 2 to 6 cm thick. To get different internal frictions, the sand is poured in two different mods: (1) sedimented with a sand distributor used to achieve a uniform sand density and a high internal friction (CV32):  $\phi_{int}=43.7^\circ$  and (2) by sprinkling and scraping the sand pack for a lower friction (CV32):  $\phi_{int}=35.6^\circ$ . A third type of sand with a different grain size range (Ga39) is also tested:  $\phi_{int}=33.4^\circ$ . Two different basal frictions were tested:  $\phi_b=13^\circ$  (sand/PVC) and  $\phi_b=18^\circ$  (sand/Alkor foil®). For each experiment, three parameters are measured: the spacing between Riedels (S), the Riedels' length (L) and the angle ( $\phi$ ) formed by the Riedel and the direction of the strike slip fault at the base of the model (Fig. 1). Since experiments need to be repeated several times to obtain satisfactory statistical results and to provide a correlation between parameters, 45 experiments were run for this study.

### **Experimental results:**

On one hand, the thickness of the sand pack has a significant influence on the Riedels spacing. The thicker the sand layer is, the greater the spacing is (and implicitly longer). The thickness and the average spacing between Riedels appear to be linearly correlated (slope  $\sim 1.5$ ) (Fig 1).

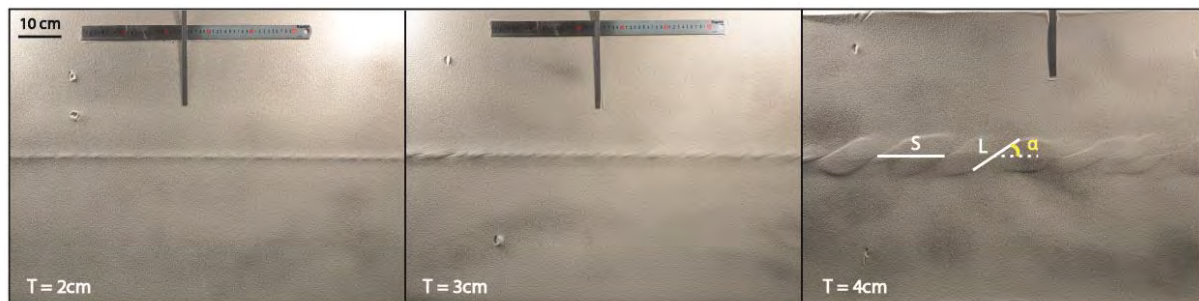


Figure 1: Three top views with various thicknesses ( $T$ ). The sand used is CV32 sedimented ( $\phi_{int} = 43.7^\circ$ ). The measurements are highlighted. The shear amount is the same for the three experiments.

On the other hand, keeping the thickness of sand constant and varying internal friction, the parameters (slope and intercept) of the relation linking length of segment with distance varies, although the relation remains linear. In fact we show that the larger the sand internal friction is, the longer the spacing is (Fig.2); a frictional variation of 0.1 corresponds to a slope variation equal to 0.25. Furthermore, it seems that basal friction has no influence on the Riedels.

Finally, considering a standard internal friction for the upper crust, this study shows that we are able to retrieve the same length-over-thickness ratio as for the natural case.

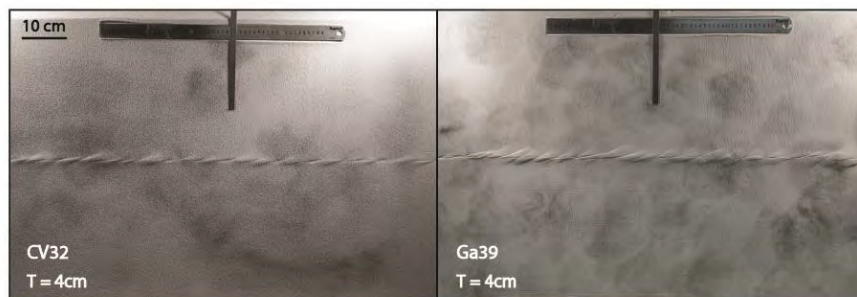


Figure 2: Top views with two different sands ( $T$  constant). Left: sand CV32 poured ( $\phi_{int} = 33.4^\circ$ ), right: sand Ga39 poured ( $\phi_{int} = 35.6^\circ$ ). The shear amount is the same for the two experiments.

## References:

- Klinger Y. 2010. Relation between continental strike-slip earthquake segmentation and thickness of the crust, *J. Geophys. Res.*, 115, B07306, doi:10.1029/2009JB006550.
- Tchalenko 1970. Similarities between shear-zones of different magnitudes. *Geological Society of America Bulletin* 81, Pages 1625–1640.

**Keywords:** Fault segmentation, Riedels, earthquake, sandbox modeling.

## Impact of surface processes on the location of large seismogenic faults in Taiwan

Jacques Malavieille<sup>1-3</sup>, Alfredo Taboada<sup>1-3</sup>, Chya-Yu Lu<sup>2-3</sup>, Marta Limoncelli<sup>4</sup> and Giancarlo Molli<sup>5</sup>

<sup>1</sup>) Univ. Montpellier, UMR 5243, F-34095, Montpellier, France.

<sup>2</sup>) Dept. of Geology, National Taiwan University, Taipei, Taiwan.

<sup>3</sup>) LIA D3E, C.N.R.S.-M.O.S.T. France-Taiwan International Laboratory

<sup>4</sup>) Univ. degli Studi di Milano, Italia.

<sup>5</sup>) Università di Pisa, Dipartimento di Scienze della Terra, Via S.Maria, 53, 56126 Pisa, Italy

Corresponding author: jacques.malavieille@gm.univ-montp2.fr

### S4- Seismic cycle & Earthquake dynamics (PS7)

In Taiwan, due to the high convergence rate (8 ~ 9 cm/yr) between Eurasia and Philippine Sea Plate (PSP), deformation and erosion rates are extreme (horizontal shortening > 2 cm/yr on seismogenic faults with vertical motions up to 3 cm/yr). Catastrophic erosion involving landslides induced by typhoons and earthquakes, have sculpted in a few million years the sharp relief of the island. Looking at the location of big earthquakes ( $M > 7$ ), they occur in the frontal part of the orogen and along the arc-continent plate boundary (yellow stars Fig. 1). If we consider the middle term deformation kinematics, most of the shortening is accounted for by just a few major faults on the western foreland side of the wedge and along its backside hinterland against the Philippine Sea upper-plate (Fig. 2a); about 4 cm/yr are absorbed across the frontal faults, whereas on the backside ~3 cm/yr are absorbed on the onshore Longitudinal Valley faults and ~2 cm/yr offshore within the PSP along the submerged flank of the Coastal Range. On the opposite, little horizontal shortening occurs within the main body of the wedge due to a strong partitioning of deformation. Such a kinematic pattern closely matches the behavior of experimental erosional wedges with décollements (Fig. 2b).

Experiments are analyzed to investigate the effects of erosion on the active bivergent orogenic wedge of Taiwan. The model, has been submitted to erosion under flux steady state conditions, to simulate an erosion pattern close to what is expected in Taiwan for the long term. The presence of a weak layer (made with glass microbeads) that mimic décollement in the entering sequence, favors strain partitioning. Basal accretion of thrust units develops an antiformal nappe stack, whose growth and location is enhanced by erosion. A rapid uplift of underplated material occurs in the rear part of the wedge controlled by backthrusting, whereas frontal accretion characterizes the front of the growing prism. With continued shortening, a zone of fast exhumation develops in the retrowedge, it is controlled by underplating and the major backthrust. The whole material resting above the abandoned décollement is passively uplifted without suffering horizontal shortening.

It suggests that the main mechanisms of growth can be described by frontal accretion in the foreland Foothills and basal accretion of tectonic units at depth under the hinterland. Intra-crustal décollements involving flats and ramps and inherited structures localized within the subducting continental margin of Eurasia favor such a style of deformation partitioning and wedge growth. Basal accretion is at the origin of rapid uplift and exhumation of wedge material accounting for most of the vertical component of deformation. Early décollements are then passively uplifted and folded during continuous underplating processes. Thus, a direct relationship exists between tectonics (shortening inducing the partitioning between horizontal and vertical displacements on faults) and surface processes contributing to huge material transfer. Such a coupling has important consequences (Fig. 2c): - The

main seismogenic faults are located at the boundaries of the wedge both in front (foothills) and along its backpart (in the Longitudinal valley and offshore). - Most of the deformation that is responsible for the rapid uplift of the hinterland is taken into account by aseismic ductile strain at depth. Both, the high heat flow and the low seismicity observed beneath the Central Range, are consistent with this behavior at the scale of the orogen.

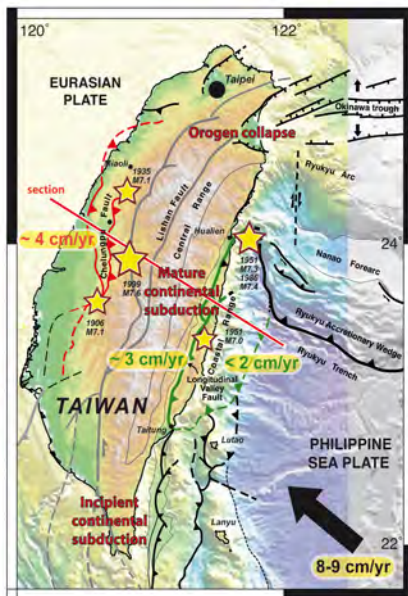


Figure 1 : see explanation in the text

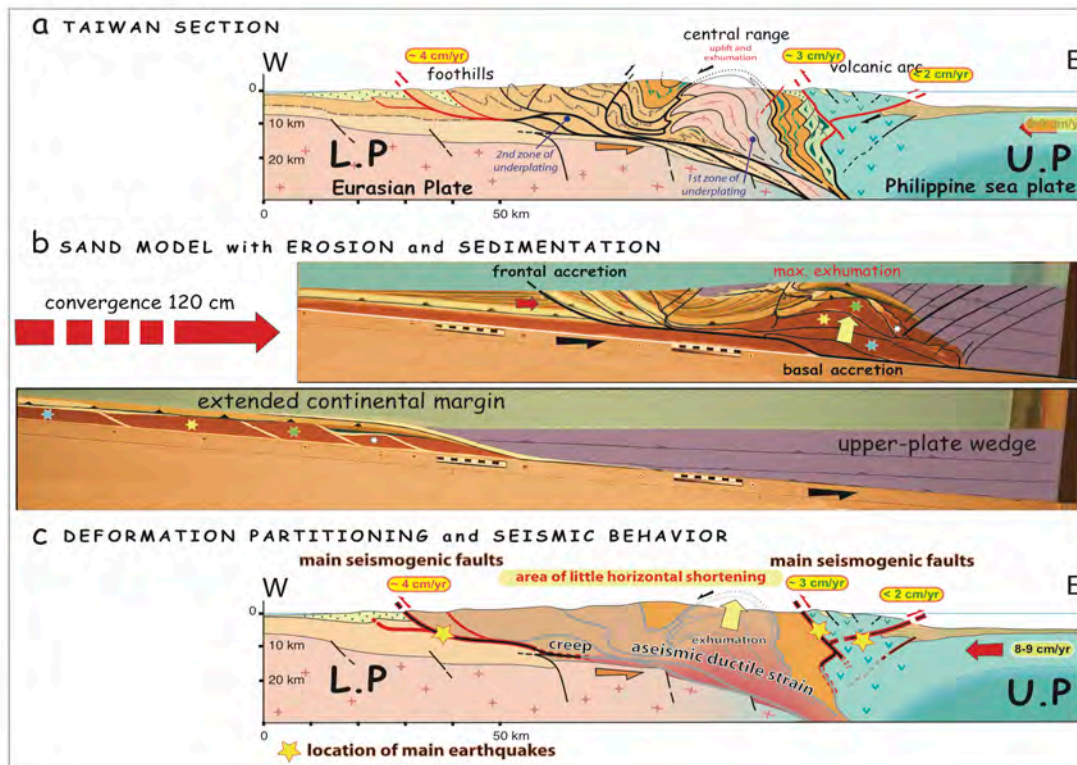


Figure 2: See explanation in the text.

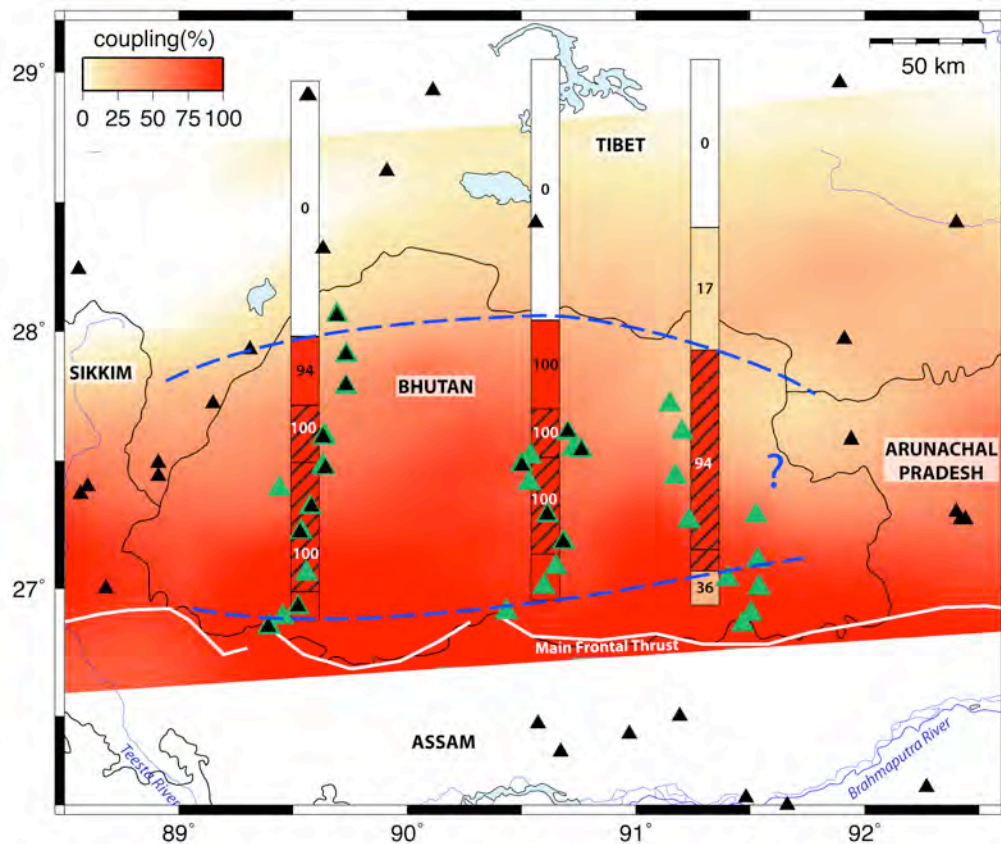
## Evidence of interseismic coupling variations along the Himalayan arc from new GPS data in Bhutan

Anais Marechal, Stephane Mazzotti, Rodolphe Cattin, Gael Cazes, Philippe Vernant, Dowchu Drukpa, Kinzang Thinley, Alizia Tarayoun, Romain Le Roux-Mallouf, Bal Bahadur Thapa, Phuntsho Pelgay, Jampel Gyeltshen, Erik Doerflinger, and Stéphanie Gautier

Corresponding author: anais.marechal@gm.univ-montp2.fr

S4- Seismic cycle & Earthquake dynamics (PS7)

Although the first-order pattern of present-day deformation is well resolved across the Himalayas, irregular data coverage limits detailed analyses of spatial variations of interseismic coupling. We provide the first high-resolution GPS velocity field for the Bhutan Himalaya. Combined with published data, these observations show strong East - West variations in geometry and coupling between central and eastern Bhutan. In contrast with previous suggestions of uniform interseismic coupling along the Himalayan arc, we identify significant lateral variations: In western and central Bhutan, the fully coupled segment is ~ 120 km large with an abrupt downdip transition, whereas in eastern Bhutan the fully coupled segment is only ~ 100 km large and is limited updip and downdip by partially creeping segments. This is the first observation along the Himalayan arc of decoupling on the upper ramp, with important implications for large earthquake surface rupture and seismic hazard.



## Seismic cycle modeling on evolving faults: The question of fault branching

Simon Preuss, Taras Gerya, Ylona van Dinther, Jean Paul Ampuero, Yannick Caniven

ETH Zürich, Switzerland

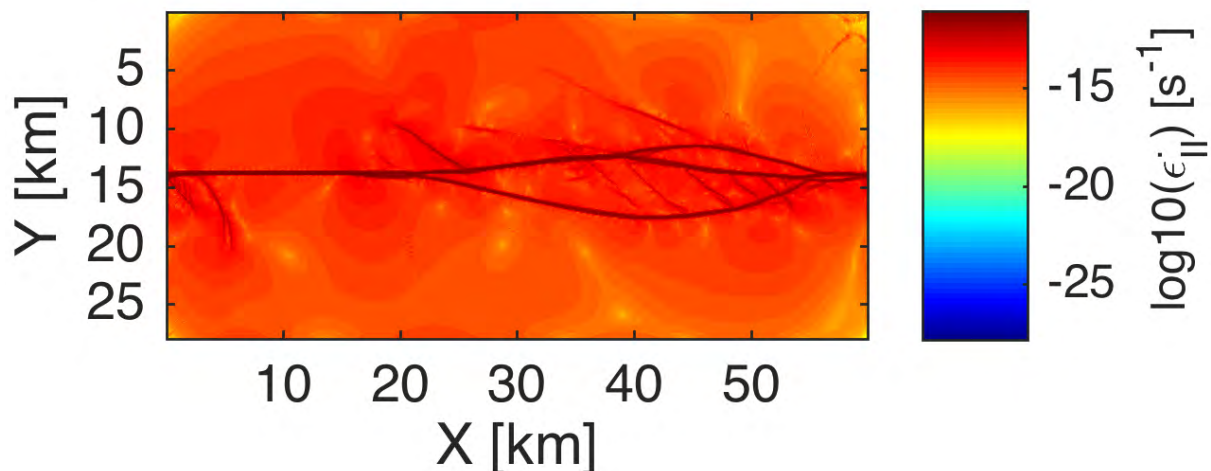
Corresponding author: sipreuss@ethz.ch

S4- Seismic cycle & Earthquake dynamics (PS7)

Even in well documented fault zone regions like California, ~30% of the total displacement occurs off the main fault and large earthquakes have generated on unknown fault branches (e.g. 2010 Baja California earthquake). A severe issue is the determination of their location and estimation of their potential risk as well as proneness to rupture.

To answer such questions we first need a better physical understanding of the long-term evolution of branching fault structures. Our goal is to quantify the parameters influencing branching structure. In our approach we will bridge long-term fault structure evolution and short-term seismicity generation using the tools of Seismo-Thermo-Mechanical (STM) modeling (van Dinther et al., 2013).

To start, we adopt a model with 2D plane view mature strike-slip geometry based on the laboratory model of Caniven et al. (2015) using visco-elasto-plastic material behavior to investigate and compare seismicity patterns and evolution. The numerical simulation results are comparable to the ones of the lab model and reproduce stick-slip behavior, seismic events, nucleation and propagation of ruptures. Next, we implemented strain weakening of cohesion to analyze evolving fault structure in a 2D top view natural scale model. First results of this model show more complex fault pattern giving rise to Riedel shears, R' shears and sub parallel faults isolated by offsets from the main fault. Linkage of en échelon fault segments causes extensional bends and contractional bends.



*Evolving fault in a transform setting (plotted is the second invariant of the strain rate).*

Finally, these results will be compared to a 2D and 3D long-term geodynamic thermo-mechanical model in terms of fault structure on the surface to analyze the role of a visco-plastic structure with depth and short term seismic cycle. Once we have an appropriate setup to study the problem of fault branching, we ultimately plan to explore the role of different friction, material and tectonic parameters on branching structure.

## How does subducting seafloor roughness relate to the seismogenic behaviour of subduction zones?

Elenora van Rijnsingen<sup>1,2</sup>, Serge Lallemand<sup>1</sup>, Michel Peyret<sup>1</sup>, Diane Arcay<sup>1</sup>, Francesca Funicello<sup>2</sup>, Stephane Dominguez<sup>1</sup>, Fabio Corbi<sup>1</sup>

<sup>1</sup> Geosciences Montpellier, CNRS, Montpellier University, France

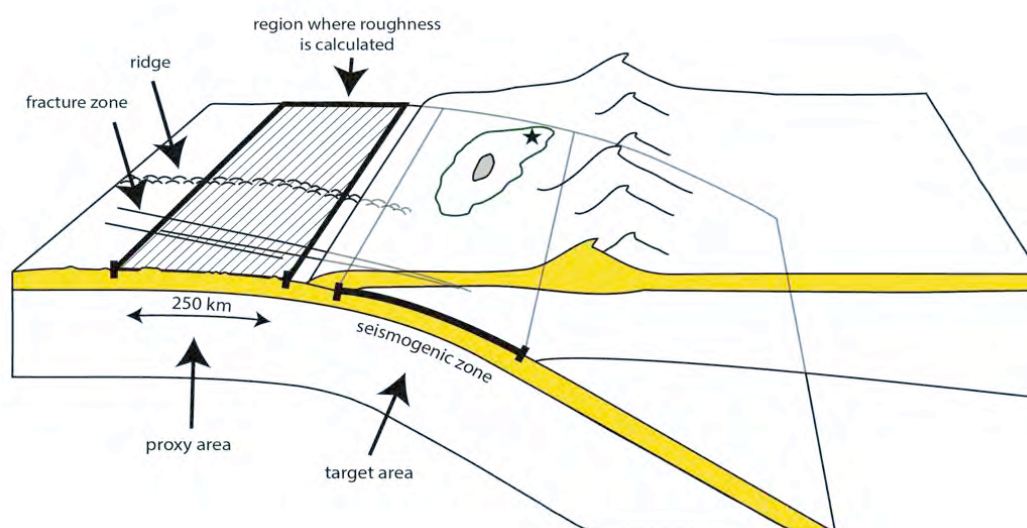
<sup>2</sup> LET – Laboratory of Experimental Tectonics, University Roma Tre, Italy

Corresponding author: [elenora.vanrijsingen@uniroma3.it](mailto:elenora.vanrijsingen@uniroma3.it)

### S4- Seismic cycle & Earthquake dynamics (PS7)

From rupture models obtained from previous (very large) earthquakes, it is known that the coseismic energy release during an earthquake is not distributed homogeneously within the rupture area. It is actually a patchwork of high slip areas (asperities) and areas with low to no slip. This indicates that there is also an inhomogeneity in the strength distribution along the plate interface, a variation of strong areas which tend to generate seismic behaviour (potential asperities) and weak, aseismic areas (Lay et al. 1982; Beck & Ruff 1984). This configuration of weak and strong areas within the subduction interface influences the nucleation point of an earthquake, but more importantly, the propagation. The area of a rupture plays an important role in the determination of an earthquake's moment magnitude (Kanamori, 1983). Hence, if an earthquake has the possibility to propagate over a large distance, it is likely to be a large one.

The alternation of strong and weak regions is influenced by the roughness of the seafloor (e.g. subducting seamounts; Wang & Bilek 2014), but also subducted sediments and fluids in the subduction channel may play an important role. In this study we focus on the role of seafloor roughness on the seismogenic behaviour in subduction zones. On a global scale, we will investigate the relationship between rupture distributions of previous very large earthquakes ( $M_w > 8.0$ ) and the roughness of the seafloor in order to better understand (future) seismogenic behaviour in subduction zones.



*Schematic overview of the approach.*

We developed a technique to characterize the roughness of the seafloor seaward of the trench, which we use as a proxy for the seafloor roughness within the seismogenic zone (e.g. Basset & Watts, 2015). We define the roughness at short (12-20 km) and long (80-100 km) wavelengths, in order to look at different topographic features that may play a role in the seismogenic behaviour of the subduction zone. These roughness values will be compared with earthquake rupture distributions gathered for very large earthquakes which occurred worldwide along the subduction thrust fault. With this approach we aim to come up with a first-order relationship between the seafloor roughness and the seismogenic behaviour of subduction zones.

**References:**

- Basset, D., & Watts, A. (2015). Gravity Anomalies, crustal structure, and seismicity at subduction zones: 1. Seafloor roughness and subducting relief. *Geochemistry Geophysics Geosystems*, 1508–1540. <http://doi.org/10.1002/2014GC005685>.Key
- Beck, S. L., & Ruff, L. J. (1984). The rupture process of the Great 1979 Colombia Earthquake: Evidence for the asperity model. *Journal of Geophysical Research: Solid Earth*, 89(B11), 9281–9291. <http://doi.org/10.1029/JB089iB11p09281>
- Kanamori, H. (1983). Magnitude scale and quantification of earthquakes. *Tectonophysics*, 93(3–4), 185–199. [http://doi.org/10.1016/0040-1951\(83\)90273-1](http://doi.org/10.1016/0040-1951(83)90273-1)
- Lay, T., Kanamori, H., & Ruff, L. (1982). The Asperity Model and the Nature of Large Subduction Zone Earthquakes. *Earthquake Prediction Research*, 1, 3–71.
- Wang, K., & Bilek, S. L. (2014). Invited review paper: Fault creep caused by subduction of rough seafloor relief. *Tectonophysics*, 610, 1–24. <http://doi.org/10.1016/j.tecto.2013.11.024>

## Shocks in a Box 3D: Analogue modelling of along strike seismotectonic segmentation and synchronization of subduction zone forearcs

Matthias Rosenau<sup>1</sup>, Ehsan Kosari<sup>1</sup> and Onno Oncken<sup>1</sup>

<sup>1</sup>) Helmholtz Centre Potsdam, GFZ German Research Centre for Geosciences, Potsdam, Germany

Corresponding author: rosen@gfz-potsdam.de

S4 - Seismic Cycle & Earthquake dynamics (PS7)

### Introduction:

Subduction zones hosts the largest earthquakes on earth with moment magnitudes exceeding 9. Great earthquakes are exclusively generated by interplate slip along the shallow parts (< 50 km depth) of the megathrust which accommodates plate convergence on the long time scale. Following the great Sumatra earthquake in 2004 continuous effort has been spent to develop analog and numerical models of subduction zone seismotectonics. The large range in time scales involved in the process, from earthquake rupture (seconds) to forearc tectonics (Ma), make this process a challenge for modelling.

### Experimental approach:

First analogue models by Rosenau et al. (2009) were quasi-2D and used elastoplastic, granular material to allow for both elastic deformation (seismic cycles) and plastic deformation (tectonics) to occur and to mimic across strike seismotectonic evolution of subduction zone forearcs (“Shocks in a box”). They demonstrated how shortening is localized updip and downdip of the seismogenic zone over several seismic cycles and may lead to the formation of the typical forearc anatomy with forearc basins enclosed between the coastal forearc high and the outer arc high (Figure 1). In a feedback mechanism, strongly segmented forearcs tend to generate more periodic earthquakes than unsegmented forearcs do (Rosenau and Oncken, 2009).

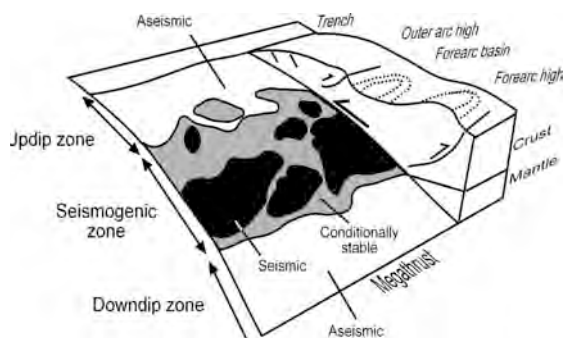


Figure 2: Conceptual view of seismotectonic forearc segmentation.

Here we present first results from a 3D realization of this approach. We use a compressional wedge composed of rice, sugar and rubber pellets on top a rubber belt. Rice has the capability to generate stick-slip events analogue to earthquake instabilities due to its velocity weakening friction. Patches of rice along the base of the wedge represent seismogenic areas (i.e. asperities). Sugar has velocity strengthening friction and is used as basal material to define aseismically creeping areas (i.e. barriers to rupture). Rubber pellets mixed with sugar makes the bulk of the elastoplastic wedge material. We monitor the wedge deformation using Particle Image Velocimetry (Adam et al., 2005) at variable spatial and temporal resolutions to account for the multispectral character of deformation.

## Experimental observations & analysis:

Because of the intrinsically non-plain strain character of elastic deformation even orthogonal convergence leads to along strike segmentation of subduction zone forearcs into topographic highs and lows. Over several seismic cycles shortening localizes along the periphery of the seismogenic patches at depth (Figure 2 a, b). As segmentation evolves earthquakes become more periodic and start to synchronize (Fig. 2c). Based on numerical analysis using elastic dislocation model we found that synchronization is an effect of stress coupling, i.e. coseismic static stress changes leads to clock advance in neighboring segments.

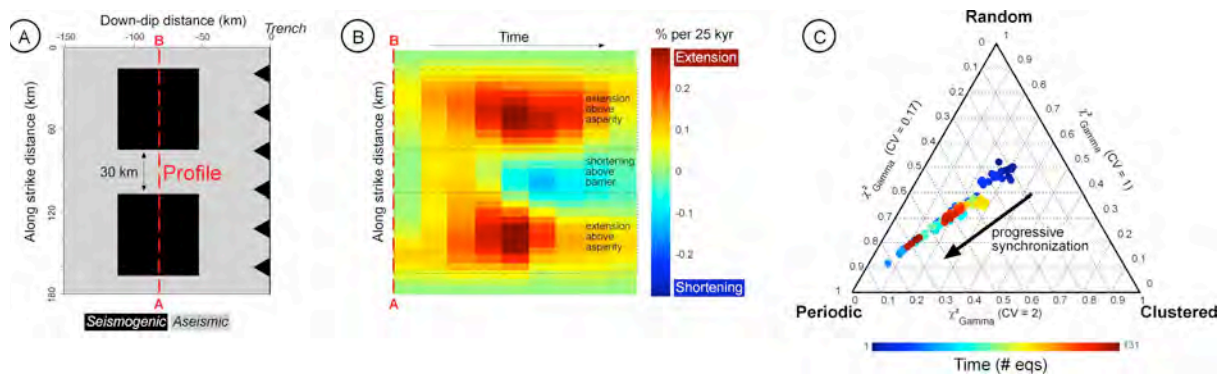


Figure 2: Observations in an analogue model of subduction zone seismotectonics: A) Setup of the model with two seismogenic patches embedded in an aseismically creeping megathrust. B) Spatiotemporal plot of surface deformation. C) Evolution of earthquake sequences towards synchronized characteristic events.

## Outlook:

Based on the current orthogonal convergence models which generate symmetric deformation patterns, we plan to realize 3D seismotectonic models of transpressional wedges to simulate oblique convergence. We hypothesize to see asymmetries in the evolving structural and topographic features.

## References:

- Adam, J., O. Oncken, N. Kukowski, J. Lohrmann, S. Hoth, J. L. Urai, W. van der Zee, J. Schmatz, B. Wieneke, and K. Pfeiffer (2005), Shear localisation and strain distribution during tectonic faulting - New insights from granular-flow experiments and high-resolution optical image correlation techniques, *Journal of Structural Geology*, 27(2), 183-301, doi:10.1016/j.jsg.2004.08.008
- Rosenau, M., J. Lohrmann, and O. Oncken (2009), Shocks in a box: An analogue model of subduction earthquake cycles with application to seismotectonic forearc evolution, *Journal of Geophysical Research-Solid Earth*, 114, 20, B01409, doi: 10.1029/2008jb005665.
- Rosenau, M., and O. Oncken (2009), Fore-arc deformation controls frequency-size distribution of megathrust earthquakes in subduction zones, *Journal of Geophysical Research-Solid Earth*, 114, 12, B10311, doi: 10.1029/2009jb006359.

**Keywords:** Analogue modelling, subduction zone, megathrust earthquakes, seimotectonics, forearc basins, synchronization, characteristic earthquakes, elastoplastic deformation, PIV.

## Rupture envelopes of fault systems

Roger Soliva<sup>1</sup>, Frantz Maerten<sup>2</sup>, Laurent Maerten<sup>2</sup>, Jussi Mattila<sup>3</sup>

<sup>1</sup>Geosciences Montpellier, Université de Montpellier, Campus Triolet, CC060, Place Eugène Bataillon, 34095 Montpellier Cedex 05, France.

<sup>2</sup>Schlumberger, 340 rue Louis Pasteur, 34790 Grabels, France.

<sup>3</sup>Posiva Oy, Olkiluoto, 27160 Eurajoki, Finland

Corresponding author: soliva@gm.univ-montp2.fr

S4 - Rheology, strain localization, folding and faulting (PS7)

### Abstract:

The fact that inherited fault systems show strong variability in their 3D shape provides good reasons to consider the strength of the Earth's brittle crust as variably anisotropic. We quantify this strength anisotropy as a function of fault system complexity. Real fault system geometries are analysed with a numerical 3D boundary-element model based on frictional theory and linear elasticity (Figure 1).

Using variables such as friction, cohesion, stress state and especially its orientation, we define rupture envelopes for fault systems, for which shape is directly related to the fault system complexity and the value of friction coefficient on fault surfaces.

This technique is applied to the realistic geological conditions of the Olkiluoto high-level nuclear waste repository (Finland) and provides new perspective to assess seismic hazard and to study the strength of the brittle crust.

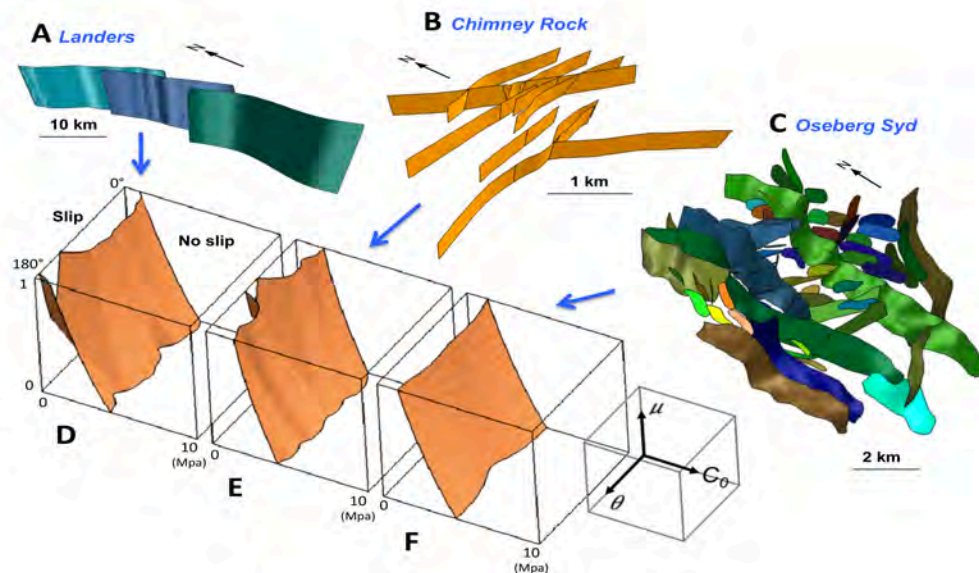


Figure 1: Examples of 3D fault system geometry, from a simple to a very complex case, and related rupture envelopes. A The Landers strike-slip fault segments. B The Chimney rock conjugate strike-slip fault system. C The Oseberg Syd normal fault system. D, E and F are rupture envelopes for each fault system, defining fault system stability for variable uniaxial stress orientation ( $\theta$ ), static friction ( $\mu$ ) and cohesion ( $C_0$ ) on fault surfaces.

**Keywords:** Fault system, strength, rupture envelope, friction, geomechanics.

## Localization of deformation and seismicity in intraplate domains: Reactivation of crustal and lithospheric paleo-structures

Alizia Tarayoun<sup>1</sup>, Stéphane Mazzotti<sup>1</sup>, Frédéric Gueydan<sup>1</sup>

<sup>1</sup>) Université de Montpellier, 34090, France.

Corresponding author: alizia.tarayoun@hotmail.fr

S4- Seismic cycle & Earthquake dynamics (PS7)

The St Lawrence valley, eastern part of Canada has known a succession of two complete Wilson cycles leading to a strong tectonic heritage. We can observe in this area, but also in other intraplate domains, numerous earthquakes. This is not explained by the plate tectonics theory, which proposes rigid plates leading to the concentration of the deformation at plate boundaries. The mechanisms involved in intra-continental deformation are poorly known at present and still discussed. A theory suggests that intraplate deformation is due to the reactivation of crustal and lithospheric paleo-structures. Yet, a question rises. Can structural inheritance explain the deformation observed?

We therefore propose to precisely characterize the variation of strain rates measured by GPS in the St Lawrence valley. This region suffered five earthquakes with a magnitude above 6 between the XVII and XIX centuries.

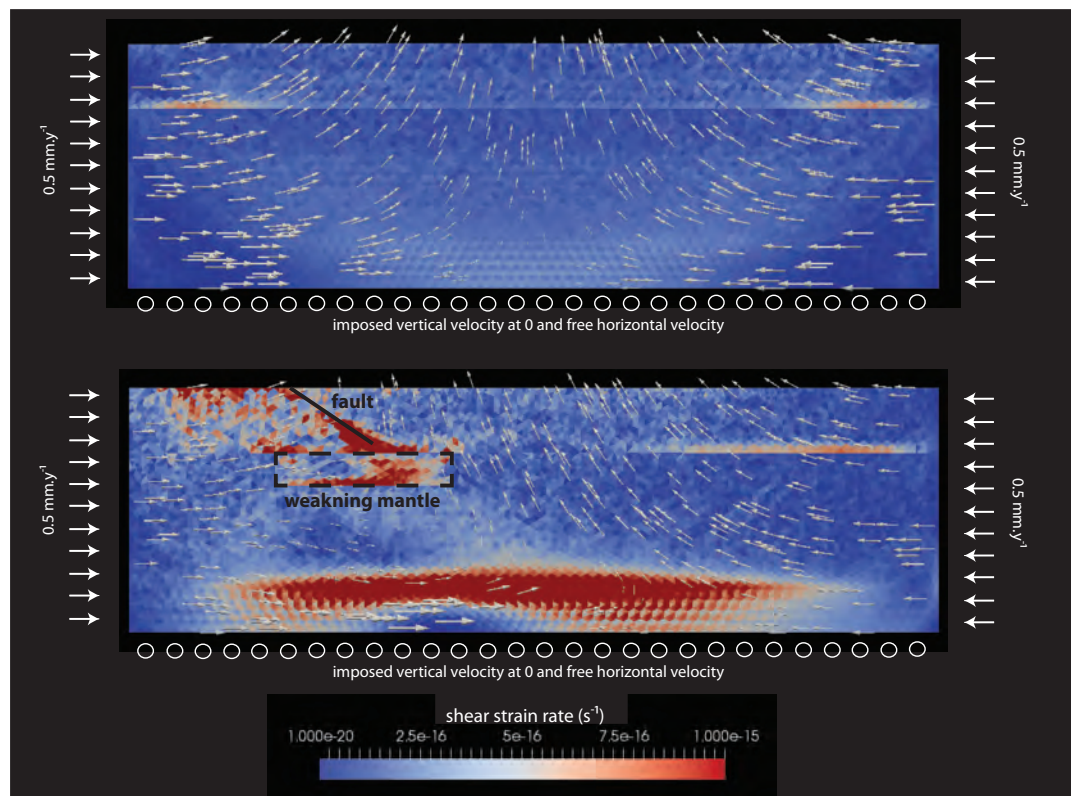


Figure 1: Elasto-visco-plastic models representing a 500 km long and 150 km thick lithosphere including a crust of 40 km thickness. We use rheology of quartz and olivine in the crust and the mantle, respectively. Vectors inside the model show the displacement field. Top: Model without structural inheritance. The surface strain rates are between  $10^{-20}$  and  $2.5 \cdot 10^{-16} \text{ s}^{-1}$ . Bottom: Model with structural inheritance. Weakening localizes the deformation and allows a strain rate of  $10^{-15} \text{ s}^{-1}$  typical of intra-plate domains.

In order to improve our understanding of these earthquakes, we propose to develop a mechanical numerical model representing the lithosphere behaviour in intraplate domains. This model integrates the different forces acting on lithospheric scale, the rheology of the lithosphere as well as tectonic heritage. These models will be validated by newly measured GPS strain rates.

## **S5 – Rheology, strain localization, folding and faulting**

The deformation of the lithosphere beyond elastic limits is strongly nonlinear and involves material damage leading to ductile and/or viscous flow. The damage typically results in strain localization, fracturing, folding, and faulting. These are complex processes that are sensitive to rock-mechanic properties that in turn depend on the rock type, loading conditions, temperature, presence of fluids. Laboratory rock tests, field studies as well as analogue and numerical modeling conducted at different time and length scales help to understand these processes. A topical issue here is the question of strain localization at the origin of faulting.

Another key problem is a definition of constitutive laws from both experimental and theoretical studies considering the scale issues. These laws are implemented into numerical codes and taken into account when scaling analogue models. In this session, we welcome papers on all the aforementioned approaches and particularly those (1) contributing to better understand/describe the rheology of lithosphere and its layers, (2) focusing on the quantification of the mechanical parameters governing strain localization, (3) addressing the scaling problems in both analogue and numerical modeling.

**Conveners** : Frantz Maerten (Schlumberger-MpTC, France) and Marcel Frehner (ETH, Switzerland).

### **Keynote speaker:**

**"Experimental analysis of strain transients in a heterogeneous semi-brittle system: Implications for tectonics"** by Jacqueline Reber (Dept. of Geological and Atmospheric Sciences Iowa State University, USA) - [jreber@iastate.edu](mailto:jreber@iastate.edu)

## **Experimental analysis of strain transients in a heterogeneous semi-brittle system: Implications for tectonics**

Jacqueline E. Reber<sup>1</sup>, Luc L. Lavier<sup>2</sup>

<sup>1</sup>) Iowa State University, Department of Geological and Atmospheric Sciences, Ames, Iowa, USA

<sup>2</sup>) University of Texas at Austin, UTIG, Jackson School of Geoscience, Austin, Texas, USA

Corresponding author: jreber@iastate.edu

S5 – Rheology, strain localization, folding and faulting (Oral)

### **Introduction:**

Tectonic motions leading to destructive earthquakes and enigmatic transient slip events are recorded by seismology, geodesy, and paleo-seismology. The magnitude and periodicity of these events are commonly explained by rate and state friction laws that describe slip over fractured surfaces or fault gouge. Friction laws with the added effects of pore fluid pressure, shear heating, and chemical reactions do not take into account that over a wide range of pressure and temperature conditions rocks often deform following a complex mixed brittle-ductile rheology. Field observations of such semi-brittle rocks at the outcrop scale (mm to m) have shown that depending on composition, temperature, and pressure, the formation of fluid-filled brittle fractures and veins precedes and accompanies the development of localized ductile flow. Furthermore, analytical models and analog-material experiments of mixed brittle-ductile rheology show that the coexistence of brittle and viscous material can control some of the physical characteristics of strain transients and slow slip events, such as those observed at subduction zones.

There are two fundamental reasons why it is extremely important to study semi-brittle materials and their behavior during deformation. (1) Semi-brittle materials combine the deformation time scale associated with fracture and earthquakes and the time scale of viscoelastic deformation associated with a flowing ductile crust. (2) Semi-brittle behavior occurs over a wide range of temperature and pressure conditions for many mineral assemblages and might affect deformation processes from the micro to the lithospheric scale. Therefore a wide range of slip behaviors, with time scales ranging from slightly larger than earthquakes (minutes to hours) to time scales similar or smaller than postseismic relaxation and postglacial rebound, are possible in such a semi-brittle system.

### **Physical experiments:**

Physical experiments are a useful approach to investigate complex rheology as they allow for in situ observation of deformation and do not prescribe a priori rules for frictional or viscous responses. We performed experiments on a simple shear apparatus that allows for monitoring the force and the fracture pattern evolution during deformation. As a semi-brittle rock analog we use a visco-elasto-plastic hydrous gel. The gel shows ‘grain size’ reduction along shear fractures and also allows for the opening of mode I fractures. We can vary the yield stress and the bulk viscosity of the gel, which allows for a systematic parameter space testing. Depending on the yield strength of the gel we can observe strain transients that range from constant creep to stick-slip. Here we present results from experiments where we vary the degree of forced localization. We perform experiments on distributed simple shear and compare them to results from experiments with a prescribed localization. This allows us to determine the impact of the fracture pattern and mode of fractures on the strain transients.

### Connecting the experiments to numerical solutions:

We are comparing the characteristic duration of stick-slip and creep events occurring within the experiments with the numerical solutions of both a rate and state model formulation for a frictional interface and a formulation that takes into account the formation of fluid filled fractures in a semi-brittle media explicitly. Both formulations include the tectonic elastic loading of a fault surface including the effects of the loading history. For rate and state the shear elastic loading is balanced by the rate and state shear stresses that are dependent of both the slip velocity and a state variable. For the semi-brittle media the loading is balanced by the formation of fluid filled fractures that accumulate slip as they form. We compare both approaches with the experiments and attempt to determine the range of temperature and pressure conditions and the range of time scales and slip magnitude that both approaches can potentially simulate.

We show that the nature of localized slip and flow in semi-brittle material depends on the initiation and formation of model I and II fractures and does not involve frictional behavior along the fracture walls, supporting an alternative mechanism for the development of tectonic strain transients.

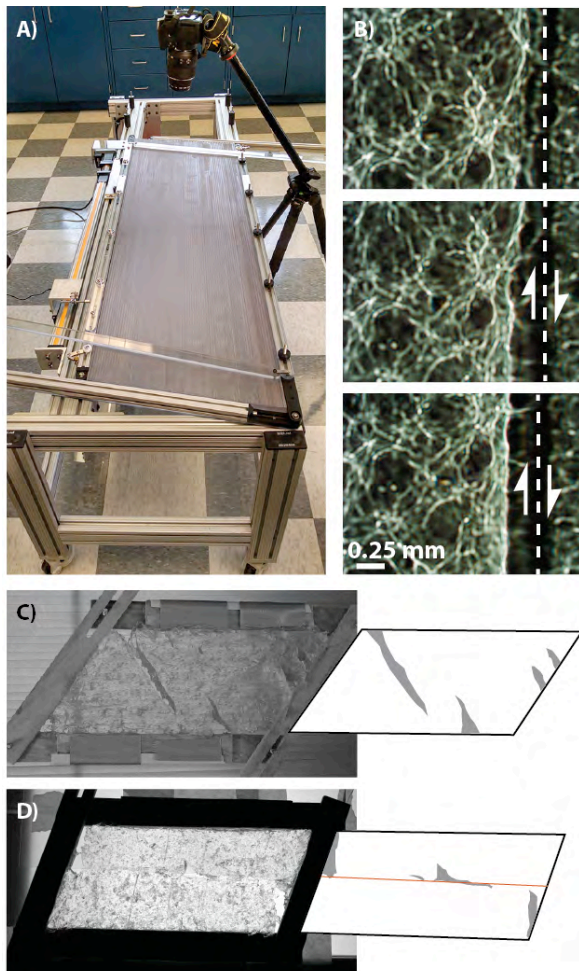


Figure 1: A) The experimental apparatus allows for distributed simple shear as well as localized shear deformation. B) Micro photograph of the experimental rock analog (Carbopol). The dark areas are so called micro-gels that are able to break while the bright areas are behaving in a more viscous manner. With increased deformation a grainsize reduction along the shear plane can be observed. C) Photograph of the experiment with distributed simple shear. Fractures open parallel to  $\sigma_1$ . D) Photograph of experiment where the deformation localization is forced by a velocity jump along the red line. Fractures open as mode I and propagate as mode II in an en echelon array.

**Keywords:** Semi-brittle deformation, Strain transients, Physical simple shear experiments, Analytical fracture slip model.

## Integrating numerical and physical experiments to constrain the evolving work budget of accretionary systems

Jessica McBeck<sup>1</sup>, Michele Cooke<sup>1</sup>, Bertrand Maillot<sup>2</sup>, Pauline Souloumiac<sup>2</sup>

<sup>1</sup>) University of Massachusetts, Amherst, Geosciences Dept., U.S.A.

<sup>2</sup>) University of Cergy Pontoise, Lab. Geosciences et Environnement, Cergy-Pontoise, France

Corresponding author: jmcbeck@geo.umass.edu Rheology,

S5 – Rheology, strain localization, folding and faulting (Oral)

### Introduction:

Tracking the evolution of individual components of the deformational work budget within physical experiments and numerical simulations of accretion can provide insight into how various processes consume or store energy at different stages of deformation. In this contribution, we track the evolution of individual components of the work budget at various stages of accretionary development in numerical simulations of a sandbox accretion experiment. The total work budget of a deforming fault system includes the internal work of deformation,  $W_{int}$ , the work of uplift against gravity,  $W_{grav}$ , the work done against frictional sliding along faults,  $W_{fric}$ , the work required to create new fracture surfaces,  $W_{prop}$ , and the work released as seismic energy,  $W_{seis}$ . The sum of these components is the total external work,  $W_{ext}$ , of the system. *Del Castello & Cooke* [2007] show that accretionary faults can evolve to optimize the total work done in the system, even as individual components of the work budget increase. Between episodes of accretion thrusting,  $W_{grav}$ ,  $W_{int}$  and  $W_{fric}$  monotonically rise, increasing the inefficiency of the system. The development of a new forethrust increases  $W_{int}$ , but decreases  $W_{fric}$  by a greater degree, which then decreases  $W_{ext}$  [*Del Castello & Cooke*, 2007]. The evolution of  $W_{ext}$  throughout deformation provides a framework for predicting the development of new faults within deforming systems [e.g. *Cooke & Madden*, 2014; *Herbert et al.*, 2015].

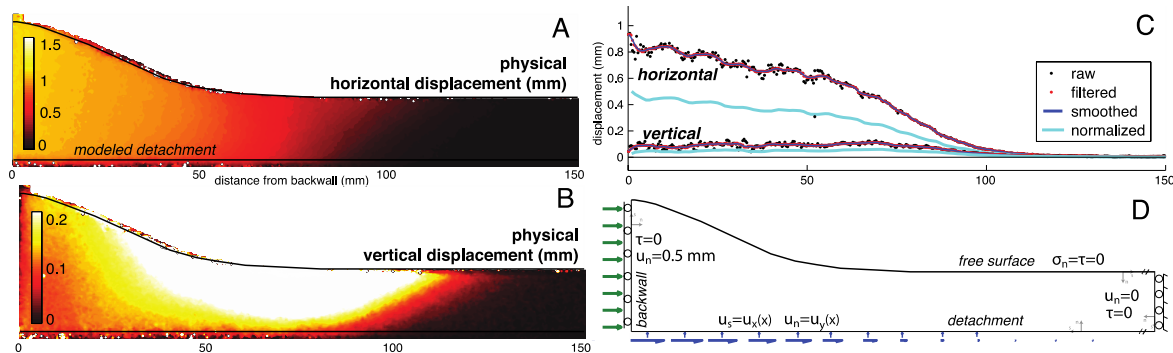


Figure 1: Development of numerical simulation of physical accretion experiment.

### Development of numerical simulations of physical sandbox accretion experiment:

In order to track the evolution of individual work budget components, we simulate stages of fault growth observed in a physical accretion experiment performed at the Université de Cergy-Pontoise tectonic modeling lab. The Fric2D numerical models employed here simulate increments of deformation of the physical sand wedge observed through the glass sidewalls. To simulate this deformation, we calculate the displacement vectors near the physical detachment fault using Particle Image Velocimetry and apply the displacements to the numerical model boundaries (Fig. 1). Laboratory measurements of the analog material determine the model material and fault properties.

We use the topography of the physical wedge at the stages of interest within the experiment as the geometry of the top model boundary. Fric2D solves the quasi-static equations of deformation on each element to determine the displacement and tractions produced by the loading and fracture geometry.

### Evolution of work budget components:

Analysis of the work budget evolution reveals that before any faults develop in the wedge, the system is the least efficient and requires the highest  $W_{ext}$  to accommodate the applied displacements (Fig. 2, system 0). The development of the first backthrust-forethrust pair (system 4) increases the efficiency of the system to a greater extent than either the backthrust (system 1) or forethrust (system 2). Although  $W_{fric}$  and  $W_{grav}$  increase,  $W_{int}$  decreases by a larger magnitude for the model with two thrusts. Consequently, the reduction in off-fault deformation accompanying fault development most significantly controls the efficiency of the system. The wedge requires the least  $W_{ext}$  when it includes the first thrust pair, and the loading conditions simulate the observed basal displacements immediately after the pair develops (system 4). Updating the applied displacements (3 to 4) promotes slip along the new pair and reduces the work done in off-fault deformation, increasing  $W_{fric}$  and decreasing  $W_{int}$ .

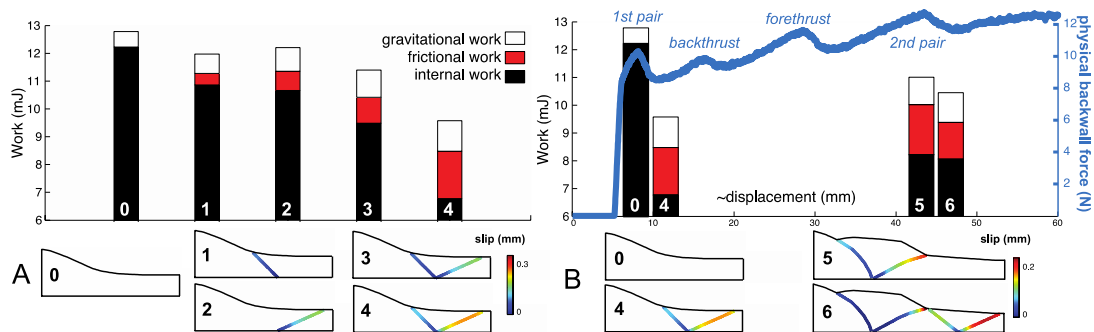


Figure 2: Evolution of work budget components in numerical simulations at 10 mm (A) and 50 mm (B) of shortening, and force measurements in physical experiment (B).

Before the second backthrust-forethrust pair develops (system 5), the  $W_{ext}$  of the modeled system is higher than the model representing the conclusion of the first stage of faulting (system 4). This result is consistent with external force measurements that show increasing force on the moving backwall between episodes of fault growth (Fig. 2B) [e.g., Cubas *et al.*, 2010; Herbert *et al.*, 2015]. Similar to the development of the first backthrust-forethrust pair,  $W_{ext}$  decreases following the development of the second pair (system 6). However, the  $\Delta W_{ext}$  due to the propagation of the second pair is smaller than the first pair because the pre-existing thrust pair continues to slip after the development of the second pair, and consequently, the addition of the new fault pair has less impact on the overall fault network. Consistent with the numerical results, the force curve also shows greater drop associated with the development of the first pair, than the second. Analysis of the evolving work budget provides insight into energy partitioning throughout fracture development, including the energy available to generate frictional melt ( $W_{fric}$ ), the energy required to drive elastic and inelastic processes, such as metamorphic reactions, within the host rock ( $W_{int}$ ), and the energy available for seismic slip ( $W_{seis}$ ).

### References:

- Cooke, M.L., and E. H. Madden, 2014, Is the Earth lazy? A review of work minimization in fault evolution, *JSG*, 66, 334–346. doi:10.1016/j.jsg.2014.05.004.  
Cubas, N., Maillot, B., Barnes, C., 2010, Statistical analysis of an experimental compressional sand wedge. *JSG*, 32, 818–831. doi:10.1016/j.jsg.2010.05.010.

Del Castello, M., and Cooke, M.L., 2007, Underthrusting-accretion cycle: Work budget as revealed by the boundary element method, *JGR*, 113, B12404, 1–14. doi:10.1029/2007JB004997.

Herbert, J.W., M.L. Cooke, P. Souloumiac, E.H. Madden, B.C. Mary and B. Maillot, 2015, The work of fault growth in laboratory sandbox experiments. *EPSL*, 432, 95-102.

**Keywords:** Fault propagation, efficiency, external work, accretionary prism, work budget.

## Initiation and evolution of localized deformation bands in a rock analogue material in triaxial compression tests

Thi Phuong Huyen Tran, Stéphane Bouissou, Alexandre Chemenda and Julien Ambre

University of Nice-Sophia Antipolis, Lab. Geoazur, Valbonne, France

Corresponding: [htran@geoazur.unice.fr](mailto:htran@geoazur.unice.fr)

S5 – Rheology, strain localization, folding and faulting (Oral)

### Introduction:

Rock failure is generally associated with the phenomenon of localization deformation, especially under conditions of low pressure and low temperature. A large amount of experimental tests of rocks performed under axisymmetric compression, covering the whole range of material behavior from brittle to brittle-ductile transition, showed that rock failure starts with the development of shear bands. The number of these strain localization bands increases with the increasing confining pressure. At the onset of brittle-ductile transition, a set of conjugated shear bands is typically formed, and becomes more and more numerous and closely spaced when the shortening of the sample is increased. The angle between shear band and the maximum principal stress direction increases with confining pressure (Bésuelle et al., 2000; Nguyen et al., 2011). However, the evolution of strain localization bands, including the moment and the place of initiation of the first band and then the others, remains poorly known. To predict the onset of the shear localization bands, the bifurcation theory has been developed by Rudnicki and Rice, (1975). The bifurcation analysis certainly provides a useful framework to address the problem of strain localization, but it is not completely clear what are the limits of its application to the behavior of real materials. One of the major criteria of applicability of the theory is a correspondence of the critical hardening modulus predicted theoretically with that measured in the experiments. To make a correct measurement, one has to precisely define the onset of deformation banding and locate it on the stress-strain curve.

In this study, we present new experimental results showing the sequential development of localized deformation bands in a rock analogue material GRAM1. The motivation for this work is to study the mechanisms of the material during deformation by analyzing strain localization initiation and evolution of localized deformation bands from the brittle faulting regime to brittle-ductile transition regime. To do this we performed axisymmetric compression test with a range of confining pressures from 0.1 to 0.3 MPa with the samples made of a low-strength synthetic granular, cohesive, frictional and dilatant rock analogue material GRAM1. The sample can be observed directly through a transparent pressure cell, which allows us to take pictures of the sample during loading and then to apply the Digital Image Correlation (DIC) technic in order to obtain the displacement field and calculate the strains during the sample deformation. We can thus well detect the initiation points and follow the evolution of deformation bands (cf. Figure 1). In each test the deformation bands do not form simultaneously but sequentially and evolve with loading. The inelastic heterogeneous deformation initiated at well positive hardening modulus. In the brittle faulting regime, the first localized deformation band appears around the peak stress with very high velocity of propagation. Shearing corresponds to the drop stress which in turn explains the strain softening of the specimen's response. While in the brittle-ductile transition regime, the first localized deformation bands appears after the peak stress, for negative hardening modulus. During shearing (hardening modulus close to zero), the individual bands exhibit jerky propagation and thickening. The determination of the propagation velocity of major bands shows that the appearance of new strain bands limits the propagation of these major bands. The angle of the deformation bands is measured thanks to the traces on the jacket. The deformation bands pattern on a post-mortem sample corresponds very well with DIC full-field strain results (cf. Figure 2).

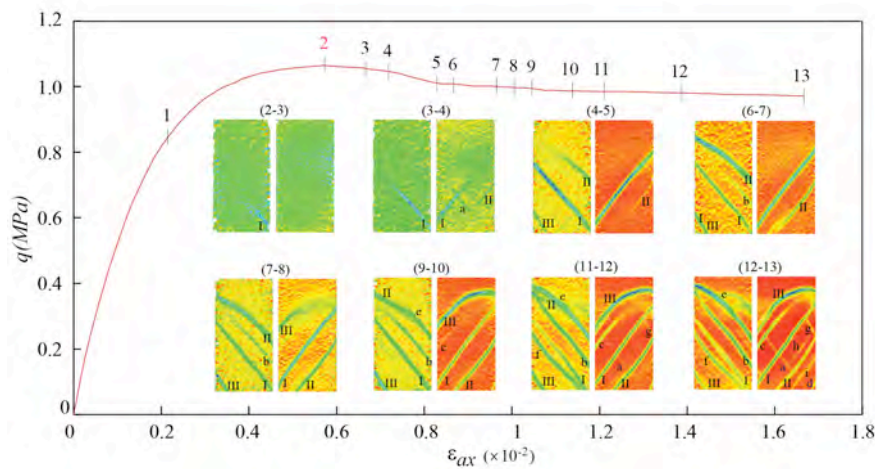


Figure 1: Evolution of localized deformation bands obtained by DIC technic at different increment during the compression test at confining pressure 0.3MPa. Axial deformation maps obtained by two cameras at two opposite sides.

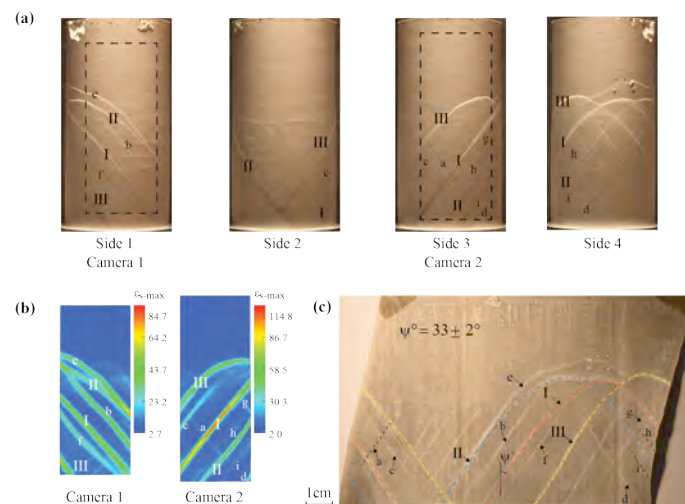


Figure 2: Results from axisymmetric compression test at confining pressure 0.3 MPa. (a) Surfaces of “post-mortem” sample observed from 4 sides, (b) Maximal shear deformation maps obtained by two cameras at two opposite sides, (c) Measurement of the angle of the fracture/deformation band with traces on the jacket.

**References:**

Bésuelle, P., Desrues, J, and Raynaud, S., 2000. Experimental characterisation of the localisation phenomenon inside a Vosges sandstone in a triaxial cell, *International Journal of Rock Mechanics and Mining Sciences*, 37(8): 1223-1237.

Nguyen, S-H, Chemenda, A., Ambre, J., 2011. Influence of the loading conditions on the mechanical response of granular materials as constrained from experimental tests on synthetic rock analogue material, *International Journal of Rock Mechanics and Mining Sciences*, 48(1): 103-115.

Rudnicki, J. W. and Rice, J., 1975. Conditions for the localization of deformation in pressure-sensitive dilatant materials, *Journal of the Mechanics and Physics of Solids*, 23(6): 371-394.

**Keywords:** deformation band, brittle-ductile transition, digital image correlation.

## Quantifying penetrative strain in analogue models of fold-and-thrust belts using anisotropy of magnetic susceptibility (AMS)

Hemin Koyi<sup>1</sup>, Bjarne S.G. Almqvist<sup>1</sup>

<sup>1</sup>Uppsala University, Department of Earth Sciences, Uppsala, Sweden.

Corresponding author: hemin.koyi@geo.uu.se

S5 – Rheology, strain localization, folding and faulting (Oral)

### Introduction:

Three components of deformation (layer-parallel shortening (LPS), folding and thrusting) dominate the evolution of a fold-and-thrust belt. LPS, which is the “invisible” penetrative strain (i.e. layer-parallel compaction; Koyi et al. 2004) is relatively more difficult to quantify compared to the other two components. However, in models, where initial conditions are well known, quantifying LPS is relatively easy (Koyi, 1995, Koyi et al., 2004). Penetrative strain is displayed in the form of for example porosity reduction which, in addition to its significance for understanding tectonic evolution of a fold-and-thrust belt, are of significance for hydrocarbon and groundwater explorations. Anisotropy of magnetic susceptibility (AMS) has been applied to infer penetrative strain in different tectonic environments for more than 50 years, including fold-and-thrust belts (e.g. review by Pares. 2015). However, field AMS measurements may bear some uncertainties related to lack of data on initial stages and the impact of diagenetic and metamorphic alterations. Furthermore, although there exists a clear qualitative correlation between AMS and the strain ellipsoid, there is no consensus in the AMS community for inferring a quantitative correlation between AMS and the strain ellipsoid. In this study, we apply the AMS approach on a series of analogue models shortened from one end in order to quantify penetrative strain at different stages of shortening.

### Experimental setup and AMS measurements:

Experiments consisted of a set of four analogue models that were shortened from one side, from 8 to 33 % (total model length was 60 cm) above a low-friction substrate of fiberglass ( $\mu_b = 0.25$ ). The model material consisted of quartz sand well-mixed with ca 1 volume % of magnetite, both sieved to a grain-size fraction of  $\leq 0.35$  mm. The width and height of the initial models were 37 cm and 2 cm, respectively. Subsequent to shortening the model was carefully wetted, avoiding disturbing the orientation of grains. Plastic cubes (7 cm<sup>3</sup>) were used to sub-sample the model (Fig. 1a). AMS was measured with an MFK1-FA susceptibility bridge, using the semi-automatic spinning method. The measurements yield a symmetric second-rank tensor, from which the magnitude and orientation of principal axes of a susceptibility ellipsoid can be calculated; axes are defined by  $k_1 \geq k_2 \geq k_3$ .

### Results:

During shortening, initially, the sand layers were thickened before they formed a box-fold close to the backstop. Further shortening led to propagation of deformation towards the foreland where new materials were incorporated and new box-folds formed. Models which were shortened up to 33% built a low-tapered wedge (3–4°) reflecting the low basal friction (Fig. 1b).

A primary magnetic fabric is created during preparation of the model. AMS from the undeformed part of the model show a flattening (bedding) fabric with the  $k_3$  axes oriented normal to the horizontal plane and  $k_1$  axes are mainly parallel to side boundaries of the model (Fig. 1a, b). The most compacted part of the model (hinterland), indicate that grains re-orient during deformation and  $k_1$  axes partly rotate perpendicular to the direction of shortening. In addition, the magnetic anisotropy reduces during compaction, indicated by a decrease in values of magnetic foliation and lineation. The undeformed

and compacted parts of the model are separated by a transition zone (Fig. 1c), defined by decreased magnetic anisotropy (Fig. 1d). In shear zones,  $k_1$  axes tend to lie in the thrust plane and parallel to the direction of thrusting, whereas  $k_3$  axes orient perpendicular to this plane.

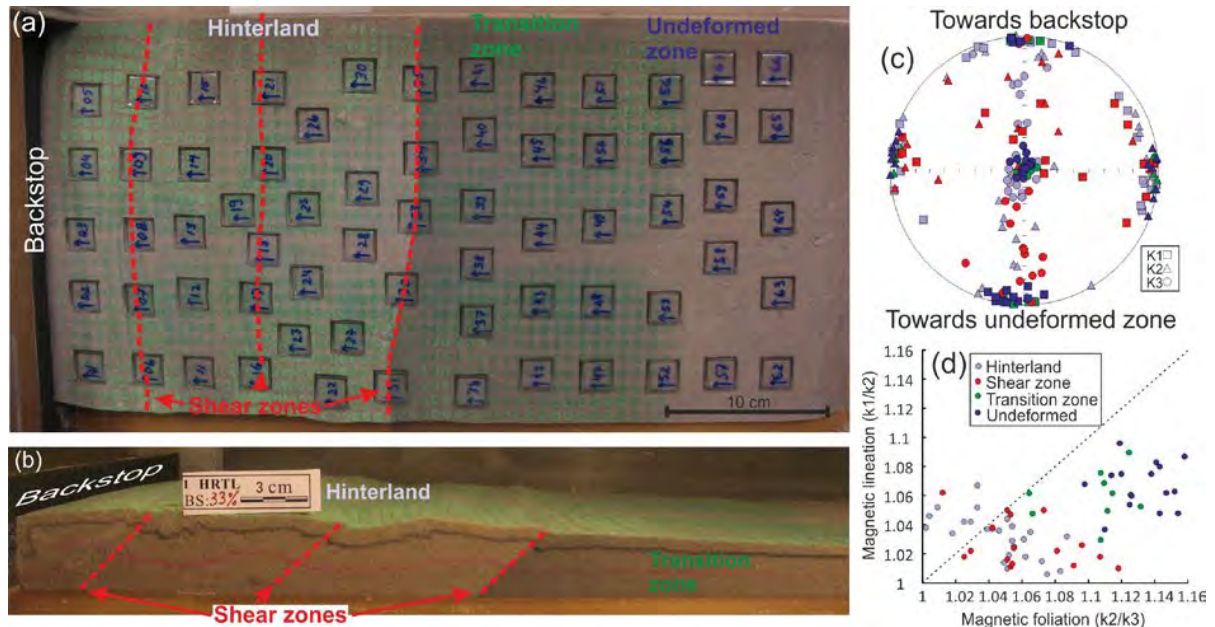


Figure 1: (a) Top view of model 4 at final stage of deformation (33 % shortening) after wetting. The numbered squares are sample locations. A transition zone is marked by shaded area, marking the gradual transition towards the undeformed zone (b) Cross-section of the model. (c) Principal axes of susceptibility ( $k_1 \geq k_2 \geq k_3$ ) shown in a lower hemisphere equal area projection. Colors represent samples from different parts of the model: light blue, hinterland; red, shear zones; green, transition zone; dark blue, undeformed zone. (d) Plot of the magnetic foliation and lineation in different parts of the model.

### Discussion and conclusions:

AMS analysis of samples chosen from different locations of the models (Fig. 1a) depicts both primary and later “tectonic” fabric of the sand layers. Models deformed by different amounts of bulk shortening portray proportional anisotropy reflecting the link between penetrative strain and total shortening. However, the analysis also shows that shortened layers accommodate certain amount of penetrative strain before being folded and thrust. This “initial” tectonic penetrative strain does not show significant change with further bulk shortening of the model as the deformation front propagates towards the foreland where it incorporates and deforms additional materials. Our analysis of systematic modeling indicates the robustness of the AMS approach and the suitability of sand-box models as a testing tool for such applications. It also increases our understanding of how fabric and strain develop in fold-and-thrust belts, where AMS may offer a tool for quantification of penetrative strain.

### References:

- Koyi, H., 1995. Mode of internal deformation in model accretionary wedges. *J. Str. Geol.* 17, 293-300. Koyi et al., 2004. The significance of penetrative strain. *AAPG Mem.* 82, 207-222. Parés, J., 2015. Sixty years of anisotropy of magnetic susceptibility in deformed sedimentary rocks, *Front. Earth Sci.*, 3, doi:10.3389/feart.2015.00004.

**Keywords:** Analogue model, Anisotropy of magnetic susceptibility, penetrative strain.

## On the interference between differently oriented, diachronous thrust fault-related folds: insights from wet clay analog models

Lorenzo Bonini<sup>1</sup>, Gian Andrea Pini<sup>1</sup>, Maurizio Ponton<sup>1</sup>, Anna Del Ben<sup>1</sup>

<sup>1</sup>) University of Trieste, Department of Mathematics and Geosciences

Corresponding author:

S5 – Rheology, strain localization, folding and faulting (Oral)

### Introduction:

Taking into account the effect of pre-existing structures, such as folds or faults, on the subsequent development of new structures is fundamental to reconstruct the tectonic history of an area. The presence of mechanical anisotropies is indeed one of the primary factors that may impact on the evolution of tectonic systems. In many areas worldwide, today contractional structures developed in anisotropic settings where anisotropies consist of inherited structures, such as thrusts and folds. These pre-existing structures may affect the evolution of new structures because: 1) previously formed faults act as a thin, mechanical discontinuities; 2) folds change the shape of the volume involved in the contractional processes and, as a consequence, the distribution of the topographic load. In this study we aim to evaluate the role of a pre-existing thrust fault-related fold on the evolution of a subsequent, non-coaxial contractional structure.

### Experimental procedures and strategy:

To study the role of a pre-existing thrust ramp on the subsequent development of a non-coaxial thrust ramp we perform a series of wet clay analog model. We use an 80x60 cm claybox in which a pre-existing fault is simulated precutting the clay cake before the experiment (Fig. 1). This is made using a recently developed method that is able to introduce thin cuts in the clay pack simulating a fault surface (Cooke et al., 2013; Bonini et al., 2014; Bonini et al., 2015; Bonini et al., 2016). The wet clay is a mixture of kaolin (China Clay) with a water content of 60%. The selected strain rate is 0.005 mm/second. Under these experimental conditions, 1 cm in our models is about 1 km in nature. The clay pack is 5 cm thick and represents 5 km in nature. The experimental apparatus is designed to force the nucleation of the new thrust ramp inserting a velocity discontinuity at the base of the box (Fig. 1).

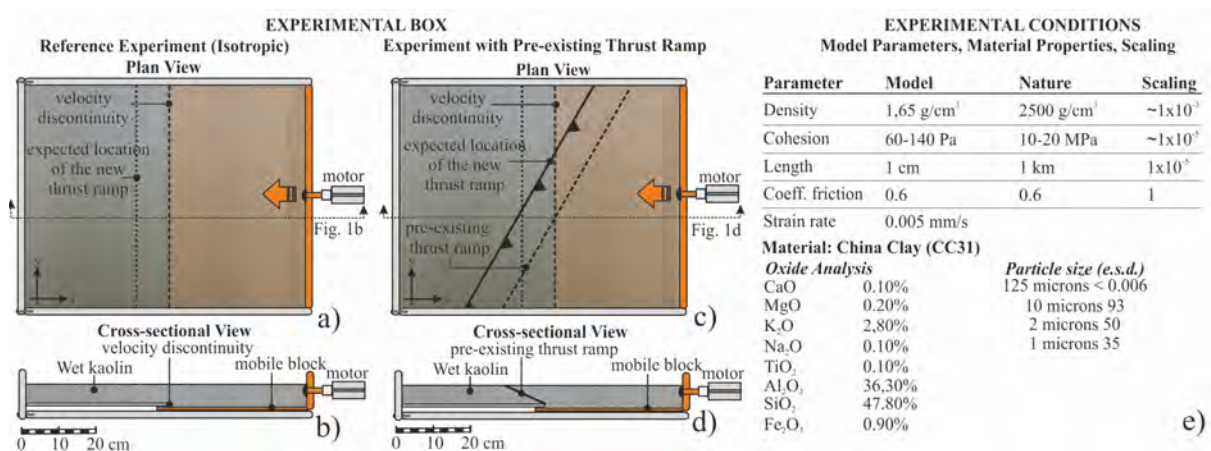


Figure 1. a), b), c), d). Plan view and cross-sectional view of the experimental apparatus. a), and b), represent a different view of the initial setup of the experiment without inserted discontinuities used as reference. c) and d) represent an example of the experiments with an inserted pre-existing thrust ramp. e) Table showing the experimental conditions and material parameters.

We perform five experiments with different initial setups. In the first experiment none pre-existing structure (precut) has been inserted; we use that as a reference for the other experiments with precuts. In the other experiments, the inserted thrust ramps take a different orientation with respect to the strike of velocity discontinuity, namely is differently oriented with respect to the expected new thrust ramp. The precut in these experiments form an angle of 45°, 60°, 75°, 90°, respectively (Fig. 1). All experiments have been performed in the new analogue modeling laboratory hosted at the University of Trieste, and developed in the framework of a collaborative project between the University of Trieste, Department of Mathematics and Geosciences and the Istituto Nazionale di Oceanografia e Geofisica Sperimentale (OGS).

### Experimental results and conclusions:

The experimental results allow to evaluate the role of pre-existing thrust ramp differently oriented with respect to a new thrust ramp. All the results of the experiments with the inserted thrust ramp are different with respect to the isotropic experiment, namely the reference experiment. In the experiments where the strike-angle between the pre-existing fault and the velocity discontinuity is lower (e.g. 30°), most of the shortening is accommodated by the reactivation of the pre-existing fault. Conversely, in the experiments with a relatively high strike-angle the amount of shortening accommodated by folding and fracturing increased. After the experimental phase, we compare these results with a natural case located in South-Eastern Alps where the Alpine thrusts overprint the pre-existing Dinaric thrusts with different orientations. We found a good correlation between experiments and nature.

We believe that using wet clay with the inserted discontinuity simulating a pre-existing fault is an effective method to study and evaluate the role of a pre-existing thrust ramp on the subsequent development of a contractional structure developed under differently oriented stress field. In fact, the use of wet clay allows to analyze the evolution of fold-related faults in a more effective way with respect to other dry granular, analog materials (e.g. quartz sand) because wet clay has a higher cohesion that promote folding and not only faulting.

### References:

- Bonini, L., Di Bucci, D., Toscani, G., Seno, S., Valensise, G., 2014. On the complexity of surface ruptures during normal faulting earthquakes: excerpts from the 6 April 2009 L'Aquila (Central Italy) earthquake (Mw 6.3). *Solid Earth* 5, 389–408. <http://dx.doi.org/10.5194/se-5-389-2014>.
- Bonini, L., Basili, R., Toscani, G., Burrato, P., Seno, S., Valensise, G., 2015. The role of preexisting discontinuities in the development of extensional faults: an analog modeling perspective. *J. Struct. Geol.* 74, 145–158. <http://dx.doi.org/10.1016/j.jsg.2015.03.004>.
- Bonini, L., Basili, R., Toscani, G., Burrato, P., Seno, S., Valensise, G., 2016. The effects of pre-existing discontinuities on the surface expression of normal faults: Insights from wet clay analog modeling. *Tectonophysics*, <http://dx.doi.org/10.1016/j.tecto.2015.12.015>
- Cooke, M.L., Schottenfeld, M.T., Buchanan, S.W., 2013. Evolution of fault efficiency at restraining bends within wet kaolin analog experiments. *J. Struct. Geol.* 51, 180–192.

## The initiation and development of folding and boudinage structures can be treated within a unified energy bifurcation theory for layered ductile materials

Max Peters<sup>1,\*</sup>, Marco Herwegh<sup>2</sup>, Martin K. Paesold<sup>3</sup>, Thomas Poulet<sup>4</sup>, Klaus Regenauer-Lieb<sup>5</sup> and Manolis Veveakis<sup>4,5,\*</sup>

<sup>1</sup>) Karlsruhe Institute of Technology, Institute of Applied Geosciences, Geothermics, Germany

<sup>2</sup>) Institute of Geological Sciences, University of Bern, Switzerland

<sup>3</sup>) Formerly at: School of Mathematics and Statistics, University of Western Australia, Australia

<sup>4</sup>) CSIRO Energy and Resources Group, Australia

<sup>5</sup>) School of Petroleum Engineering, University of New South Wales, Australia

Corresponding author: max.peters@kit.edu

S5 – Rheology, strain localization, folding and faulting (Oral)

### Introducing an alternative theory for folding and boudinage:

In classical mechanics, folding and boudinage are regarded as a geometric problem. This means that an initial infinitesimal small imperfection amplitude grows, which ultimately leads to localization through a process known as wavelength selection. One drawback of this approach using a linearized material response is that folding and boudinage develop for different material parameters or power-law exponents. In the past, this complication has led to a discussion about the applicability of such approaches to localized structures in real rocks (Hobbs et al., 2010 and references therein).

Here, we are concerned with a more generic localization theory, i.e. strain localization out of steady-state conditions inside a homogeneous material at a critical material parameter and deformation rate (e.g. Regenauer-Lieb and Yuen, 2003; Peters et al., 2015). In this framework considering energy flows and microphysical processes, instability arises out of the constitutive description itself for a critical amount of shear heating and layer thickness (Gruntfest, 1963).

### The concept of alternating boundary conditions:

The implementation of the coupled thermo-mechanical 2-D finite element model comprises an elastic and rate-dependent *von Mises* plastic rheology (Peters et al., 2016). The underlying system of equations is solved in a 3-layer pure shear box for constant velocity and isothermal boundary conditions, using the open-source finite element software *REDBACK* (for details refer to Poulet et al., in press). In order to examine the transition from stable to localized creep, we study how material instabilities are related to energy bifurcations, which arise independently of the sign of the stress conditions imposed on the boundaries, whether in compression or extension. The onset of localization is determined by a critical amount of shear heating, termed *Gruntfest* number, when dissipative work by temperature-sensitive creep translated into heat overcomes the diffusive capacity of the layer of a given thickness. Through an additional mathematical bifurcation analysis using constant stress boundary conditions, we test whether both structures develop at a same critical *Gruntfest* number.

### Numerical bifurcation results:

By means of alternating boundary conditions and parameter sensitivity studies, the numerical experiments reveal that folding develops for the same material parameters and power-law exponent as boudinage, by only inverting the sign of displacement. Boudinage and folding instabilities occur when the mechanical work, which is translated into heat, overcomes the diffusive capacity of the layer. Consequently, both instabilities develop for the same critical *Gruntfest* number (Peters et al., 2016). Further, we find that boudinage instability emerges for values of the stress exponent below  $n < 5$  and

especially for a *Newtonian* response ( $n = 1$ ) of the layer. This finding implies that not only can folding and boudinage instabilities be treated as the same energy bifurcation, but also that the energy theory predicts boudinage in cases where classical theories anticipate no growth of the structure.

### Discussion:

The existence of a single critical dissipation number to describe the initiation of folding and boudinage provides a solid basis for explaining complex geological observations. Since the critical material parameters and boundary conditions for both structures to develop are found to coincide, the initiation of localized deformation in mechanically strong layered media within a weaker matrix can be captured by means of a unified theory for localization in ductile materials. For an appropriate set of material properties, local changes of boundary conditions can be considered sufficient to trigger both sets of instabilities close to each other. In this energy framework, neither intrinsic nor extrinsic material weaknesses are required, as the nucleation process of strain localization arises out of homogeneous conditions.

This finding allows us to approach localization problems as coupled rheological bifurcations and to describe folding and boudinage structures as the same energy attractor of ductile deformation. In future, our study will allow geologists to extract critical material parameters and deformation conditions of rate- and temperature-sensitive creep directly from field observations.

### References:

- Gruntfest, I.J., 1963. Thermal feedback in liquid flow; plane shear at constant stress. *Transactions of the Society of Rheology* 7. doi:10.1122/1.548954.
- Hobbs, B.E., Regenauer-Lieb, K., Ord, A., 2010. Folding with thermal mechanical feedback: another reply. *Journal of Structural Geology* 32. doi:10.1016/j.jsg.2009.10.005.
- Peters, M., Herwegh, M., Paesold, M.K., Poulet, T., Regenauer-Lieb, K., Veveakis, M., 2016. Boudinage and folding as an energy instability in ductile deformation. *Journal of Geophysical Research Solid Earth*, 121, doi:10.1002/2016JB012801.
- Peters, M., Veveakis, M., Poulet, T., Karrech, A., Herwegh, M., Regenauer-Lieb, K., 2015. Boudinage as a material instability of elasto-visco-plastic rocks. *Journal of Structural Geology* 78. doi.org/10.1016/j.jsg.2015.06.005.
- Poulet, T., Paesold, M.K., Veveakis, M., in press. Multi-physics modelling for fault mechanics using REDBACK: a parallel open-source simulator for tightly coupled problems. *Rock Mechanics and Rock Engineering*. doi:10.1007/s00603-016-0927-y [http://github.com/pou036/redback.git].
- Regenauer-Lieb, K., Yuen, D.A., 2003. Modeling shear zones in geological and planetary sciences: solid- and fluid thermal-mechanical approaches. *Earth-Science Reviews* 63. doi:10.1016/S0012-8252(03)00038-2.

**Keywords:** Boudinage and folding theory, Thermo-mechanical feedbacks, Layered materials, Shear heating, Numerical methods.

## **Porous rock deformation: from localized brittle behavior to compaction bands formation – insights from laboratory experiments and numerical modeling**

Antoine B. Jacquey<sup>1,2</sup>, Mauro Cacace<sup>1</sup>, Guido Blöcher<sup>1</sup>, Harald Milsch<sup>1</sup>, Fiorenza Deon<sup>3</sup> and Magdalena Scheck-Wenderoth<sup>1,2</sup>

<sup>1</sup>) GFZ – German Research Centre for Geosciences, Potsdam, Germany

<sup>2</sup>) RWTH Aachen University, Aachen, Germany

<sup>3</sup>) Delft University of Technology, Delft, Netherlands

Corresponding author: antoine.jacquey@gfz-potsdam.de

S5 – Rheology, strain localization, folding and faulting (Oral)

Hydraulic stimulation of geothermal wells is often used to increase heat extraction from deep geothermal reservoirs. Initiation and propagation of fractures due to pore pressure build-up increase the effective permeability of the porous medium. Understanding the processes controlling the initiation of fractures, the evolution of their geometries and the hydro-mechanical impact on transport properties of the porous medium is therefore of great interest for geothermal energy production. In this study, we will present an approach starting from laboratory results of tri-axial experiments on sandstones, micro-structure analysis and numerical modeling aiming to better understand and identify the processes controlling micro-cracking and strain localization.

### **Laboratory experiments:**

Three tri-axial experiments under drained conditions were conducted on cylindrical samples of the Bentheimer sandstone under different confinements. The first experiment under low confinement led to a clear shear failure. The second one with high confinement showed more homogeneous deformation with initiation of shear-induced compaction bands. The last one with an intermediate confinement showed a transitional regime between the two firsts. Continuous porosity measurements were conducted during these experiments. It can be observed from these experiments that the deformation behavior ranging from homogeneous compaction to localized features is depending on the confining pressure. To better identify the physical processes controlling the different deformation behaviors, several micro-structure analyses were conducted including Scanning Electron Microscope (SEM) (see Figure 1) and three-dimensional CT scanning. These analyses showed evidences of micro-cracking and presence of a damage zone around the localized features. Some evidences of pore collapse were also identified.

### **Modeling strategy:**

A unifying model for deformation of porous rocks dealing with the physical processes mentioned above will be presented. By mean of a damage variable and an appropriate plasticity model, modeling of the hardening and softening of the elastic stiffness of the porous rock as representation of micro-cracking can be achieved. Localization of deformation is considered by introducing viscous deformation with damage and stress-dependent viscosity. Hydro-mechanical coupling is also considered by introducing appropriate porosity and permeability dependencies.

This model has been implemented in an in-house simulator GOLEM, which is based on the **Multiphysics Object-Oriented Simulation Environment (MOOSE)**. Calibration strategy for such model will be presented by mean of the experimental results previously conducted.

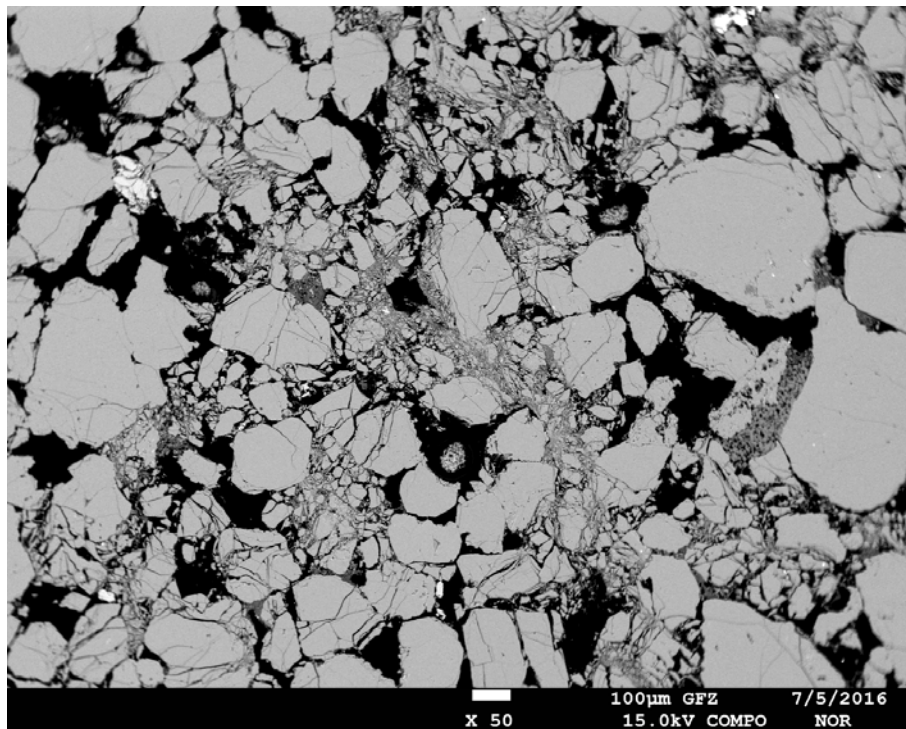


*Figure 1: SEM picture of the Bentheimer sandstone sample after the tri-axial experiment with 70 MPa of confining pressure. Micro-cracking of the grains as well as damage zones are observed.*

**Keywords:** Localized deformation, Damage plasticity model, Hydro-Mechanical coupling, MOOSE.

## Description of new dry granular materials of variable cohesion and friction coefficient: implications for laboratory modelling of the brittle crust

M.M. Abdelmalak<sup>1</sup>, C. Bulois<sup>2</sup>, R. Mourgues<sup>3</sup>, O. Galland<sup>4</sup>, J.-B. Legland<sup>3</sup>, C. Gruber<sup>3</sup>

<sup>1</sup>) CEED, Department of Geosciences, University of Oslo, Oslo, Norway

<sup>2</sup>) Ecole Normale Supérieure de Paris, Paris, France

<sup>3</sup>) L.P.G., UMR-CNRS 6112 - Université du Maine, Le Mans, France

<sup>4</sup>) Physics of Geological Processes, Department of Geosciences, University of Oslo, Oslo, Norway

Corresponding author: m.m.abdelmalak@geo.uio.no

S5 - Rheology, strain localization, folding and faulting (PS7)

Cohesion and friction coefficient are fundamental parameters for scaling brittle deformation in laboratory models of geological processes. However, they are commonly not experimental variable, whereas (1) rocks range from cohesion-less to strongly cohesive and from low friction to high friction and (2) strata exhibit substantial cohesion and friction contrasts. This *brittle paradox* implies that the effects of brittle properties on processes involving brittle deformation cannot be tested in laboratory models. Solving this paradox requires the use of granular materials of tunable and controllable brittle properties.

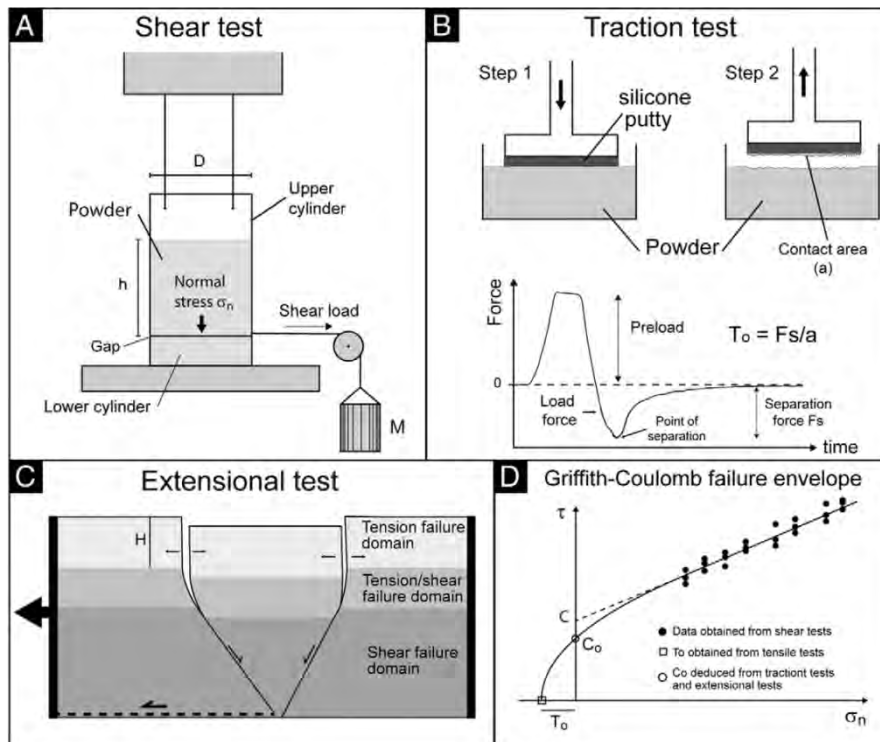


Figure 1: Schematic drawings of the measurements setups used in this study (Abdelmalak et al., 2016). A. Hubbert-type shear box for shear test measurements. B. Traction tests. C. Extensional test setup. D. Schematic graph of the composite Griffith-Coulomb failure envelope displaying characteristic measurements from shear tests (black dots), traction tests (open square) and combined traction/extensional tests (open circle).

In this contribution, we describe dry mixtures of fine-grained cohesive, high friction silica powder (SP) and low-cohesion, low friction glass microspheres (GM) that fulfill this requirement (Abdelmalak et al., 2016). We systematically estimated the cohesions and friction coefficients of mixtures of variable proportions using two independent methods (Figure 1): (1) a classic Hubbert-type shear box to determine the extrapolated cohesion ( $C$ ) and friction coefficient ( $\mu$ ), and (2) direct measurements of the tensile strength ( $T_0$ ) and the height ( $H$ ) of open fractures to calculate the true cohesion ( $C_0$ ). The combination of these methods enabled us to constrain both the linear part of the Mohr-Coulomb failure envelope and the curved Griffith failure envelope, allowing us to calculate the true cohesion ( $C_0$ ) of the materials (Figure 1D).

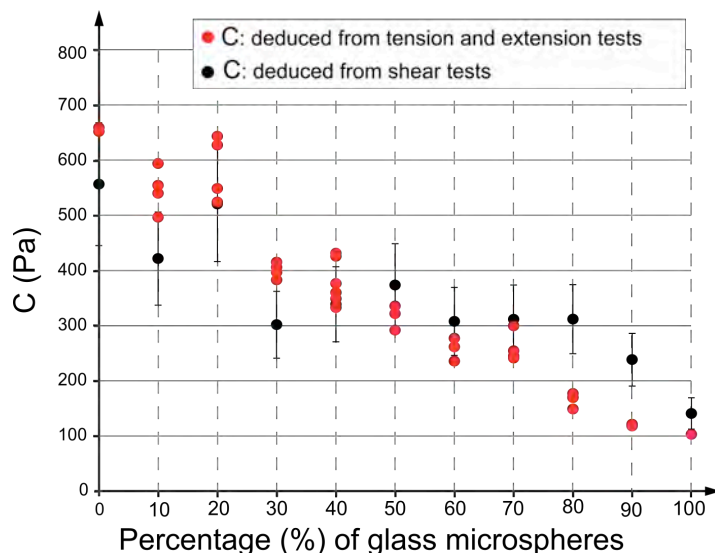


Figure 2: Comparison of extrapolated cohesion ( $C$ ) deduced from shear tests (black dots) and from tensile/extensional tests (red dots) (Abdelmalak et al., 2016).

The measured values of cohesion increase from 100 Pa for pure GM to 600 Pa for pure SP, with a sub-linear trend of the cohesion with the mixture GM content (Figure 2). The two independent cohesion measurement methods, from shear tests and tension/extensional tests, yield very similar results of extrapolated cohesion ( $C$ ) and show that both are robust and can be used independently. The measured values of friction coefficients increase from 0.5 for pure GM to 1.05 for pure SP. The use of these granular material mixtures now allows to test (1) the effects of cohesion and friction coefficient in homogeneous laboratory models and (2) to test the effect of brittle layering on brittle deformation, as demonstrated by preliminary experiments. Therefore, the brittle properties become, at last, experimental variables.

## References:

Abdelmalak, M.M., Bulois, C., Mourgues, R., Galland, O., Legland, J.B., Gruber, C., 2016. Description of new dry granular materials of variable cohesion and friction coefficient: Implications for laboratory modeling of the brittle crust. *Tectonophysics*.

**Keywords:** Laboratory models, brittle properties, cohesion, friction coefficient, tensile strength, dry Coulomb granular materials, layered models.

## Subduction initiation at fracture zone : conditions and various modes

Sarah Abecassis<sup>1</sup>, Diane Arcay<sup>1</sup> and Serge Lallemand<sup>1</sup>

<sup>1</sup>) Géosciences Montpellier, University of Montpellier, CNRS, Antilles University, France

Corresponding author: abecassis@gm.univ-montp2.fr

S5 - Rheology, strain localization, folding and faulting (PS7)

### Introduction:

We aim at understanding the processes leading to incipient subduction at an oceanic fracture zone (FZ), including the specific situation of a transform fault (TF). In nature, we observe 3 subduction initiation modes at a FZ or a TF as shown by the following examples: old oceanic lithosphere has been inferred to subduct in the Izu-Bonin-Mariana case (Stern et al., 2012 ; Lallemand, 2016); young oceanic lithosphere appears to start to subduct south of New Zealand (“Hjort” and “Puysegur”, Meckel, 2005); subduction initiated but rapidly aborted along the Gagua ridge, east of Taiwan (Deschamps et al., 1998).

### Model set-up:

To better assess the conditions controlling the process of subduction initiation, we perform experiments using a 2D numerical thermo-mechanical code (Christensen, 1992) at the scale of upper mantle. A non-Newtonian rheology and a brittle behavior are both modelled. Using active markers advection, two lithologies are tracked within the simulation box: an horizontal crust layer is imposed at the box surface and overlies the underneath lithospheric and asthenospheric mantle. The crust is significantly weaker than the mantle both in the brittle and ductile realms. At the center of the model surface, a vertical weakness zone (WZ) is imposed to mimick the FZ contact between the two oceanic plates of different ages. The simulated WZ has the same physical properties as the oceanic crust. We apply a constant and identical convergence velocity on both oceanic plates far away from the WZ.

We explore two different sets of parameters. The first one determines the oceanic plates set-up (plate age offset, younger lithosphere age, convergence rate). The second parameters set describes the FZ characteristics (width and depth, thermal state). The explored FZ geometry is based on an extended study of natural TF characteristics. In nature, the thermal structure in the vicinity of the TF/FZ results from competing effects (enlargement by thermal conduction vs shortening by strike-slip kinematics and local gravitational instability) that cannot be completely modelled in 2D. We thus impose by hand the width of the thermal transition (TT) between the 2 oceanic plates and vary it to test its influence.

### Results:

We obtain 3 modes of convergence: (1) old oceanic lithosphere subduction, (2) young oceanic lithosphere subduction, and (3) short-lived or no subduction. Successful subduction occurs following a phase of progressive strain localization at the WZ, that generally starts as soon as simulation begins. Subduction fails when deformation do not localize near the WZ but rather in the vicinity of the applied kinematic boundaries. The modelled subduction initiation onsets ( $t_i$ ) range from 0.52 to 10 Myr, corresponding to convergence lengths varying from 21 to 100 km, for a total convergence rate of 1 to 3 cm/yr.

The main studied parameter influences are as follows : If convergence velocity is high or not applied, subduction does not occur. Strong offset of oceanic plate age seems to impede subduction initiation, at least for shallow to moderately deep WZ. However, for strong age contrasts, increasing the TT width

promotes subduction initiation. When the WZ bottom is deepened, the subduction mode changes from old lithosphere subduction to young lithosphere subduction (fig.1). As the temperature at the WZ bottom increases consequently to the WZ deepening, a threshold in WZ temperature, ranging from 712 to 791°C, may control the subduction polarity. The subduction polarity may be explained by the evolution of mechanical parameters such as stress and strain.

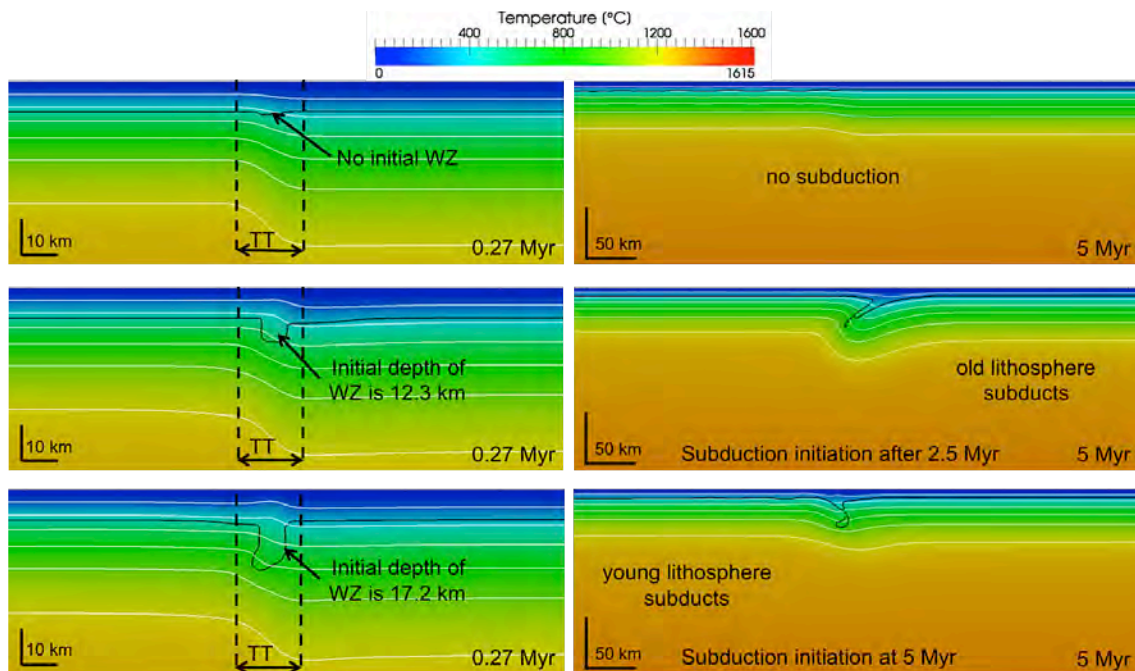


Figure 1: Three numerical simulations with the same initial conditions (total convergence velocity = 1 cm/yr, thermal transition (TT) width = 10 km, oceanic lithosphere of 5 Myr (left plate) versus 10 Myr (right plate)), except for the depth of the weakness zone (WZ) at simulation start (displayed at 0.27 Myr after convergence initiation on the left panels). The right panels exhibit the convergence state after 5 Myr. Temperature field is shown. White solid lines : isotherms each 200°C. Black solid line is the crust-mantle limit.

## References:

- Christensen (1992) An eulerian technique for thermomechanical modelling of lithospheric extension. *J. Geophys. Res.*, V.97,10 February 1992, n°B2, doi:10.1029/91JB02642
- Deschamps et al. (1998) A detailed study of the Gagua Ridge : A fracture zone uplifted during a plate reorganisation in the Mid-Eocene. *Marine Geophys. Res.* V.20, October 1998, p.403-423, doi: 10.1023/A:1004650323183
- Lallemand (2016) Philippine sea plate inception, evolution and consumption with special emphasis on the early stage of Izu-Bonin-Mariana subduction. *Prog. Earth Planet Sci.*, 3:15, 12 May 2016, doi: 10.1186/s40645-016-0085-6
- Meckel et al. (2005) Influence of cumulative convergence on lithospheric thrust fault development and topography along the Australian-Pacific plate boundary south of New Zealand, *Geochem. Geophys. Geosyst.*, 6, Q09010, doi:10.1029/2005GC000914.
- Stern et al. (2012) To understand subduction initiation, study forearc crust : to understand forearc crust, study ophiolites. *Lithosphere* V.4, 16 May 2012, p.469-483, doi:10.1130/L183.1

**Keywords:** Subduction initiation, fracture zone, rheology, diffuse deformation, deformation localisation, numerical modelling.

## **Sandbox and ERT studies on normal faults - An example of laboratory geomodelling**

Halil Bölük, M. Erkan Karaman and Azimuddin Mirza

Akdeniz University, Department of Geological Engineering, Antalya, Turkey

Corresponding author: halilboluk@akdeniz.edu.tr

S5- Rheology, strain localization, folding and faulting (PS7)

### **Introduction :**

Sandbox experiments are the most useful and practical methods for modelling the faults in laboratory. It can be seen and modelled the deformation when a force applied to material. The sandbox mechanism is designed glass-walled to see and digitize all deformation.

In this study, all deformation on material was recorded and digitized to create a model with not only seen changes but also a special electrical resistivity tomography (ERT) device. So it will be possible to compare with ERT from an active fault in real. Furthermore, results of this study was compared with reverse faults data gathered by authors on previous studies.

### **Material and Methods:**

Sandbox mechanism is so simple, old and known device to modelling faults on laboratory (Coelho et. al. 2008, Nishiyama et.al. 2014) Describing the deformation on crust can be easy by simple experiments with it. In this work, a specially designed device was used to create ERT profiles. This device is computer controlled and has a power of 144 watts (72 Volt – DC and 2 Ampere). Wenner – Alpha array was chosen to gather resistivity data. Res2D software was used to interpret gathered data.

In sandbox, different grain size material (fine to medium) was used to simulate the crust. This material was colored with toner to enhance the visibility and was consolidated with plaster to trace its behavior.

### **Results:**

The experiments were performed in three steps. Firstly, undeformed material was digitized and an ERT profile was created (Figure 1-a and 1-b). Then, in second step, deformation was occurred (vertical deformation was 0.5 cm, figure 1-c and 1-d) when the forces applied. Digitizing and ERT process were made on this half-deformed material. Finally, when vertical deformation reached 1cm and fault could be seen clearly (Figure 1-e and 1-f) and all the measurement process repeated again.

Created ERT profiles are compared with digitized graphs and previous ERT profiles. Resultly;

- Laboratory scale ERT studies are so helpful to understand the behavior of crust.
- Prediction of break up time of a normal fault is possible with 4d resistivity (ERT profile in second step).
- Normal and reverse faults are shows similar pattern on ERT profiles just before breaking-up

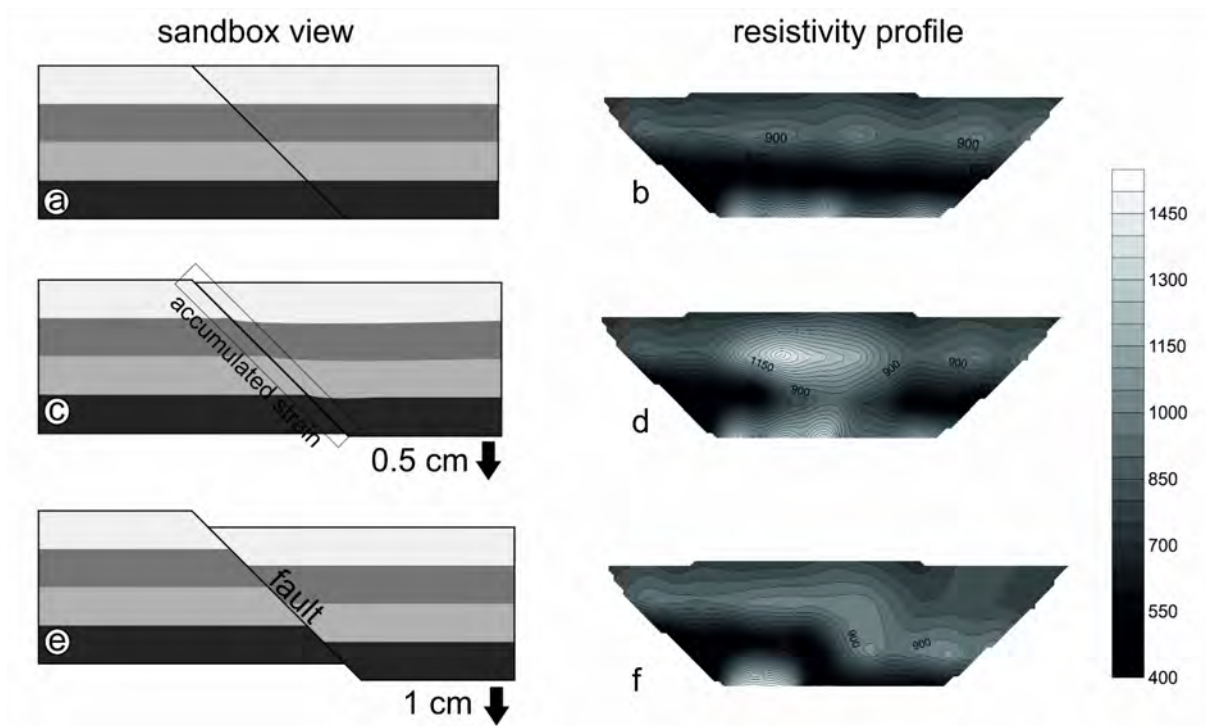


Figure 1: Steps of sandbox experiments and ERT process.

#### References:

- Coelho, S. and Passchier, C., "Mohr-cyclides, a 3D representation of geological tensors: The examples of stress and flow," *J. Struct. Geol.*, vol. 30, no. 5, pp. 580–601, May 2008.
- Nishiyama, S., Ohnishi, Y., Ito, H., and Yano, T., "Mechanical and hydraulic behavior of a rock fracture under shear deformation," *Earth, Planets Sp.*, vol. 66, no. 1, p. 108, Sep. 2014.

**Keywords:** Sandbox, electric resistivity, normal fault.

## Fold axis rotation during transpressional folding: Insights from numerical modeling and application to the Zagros Simply Folded Belt

Marcel Frehner<sup>1</sup>

<sup>1</sup>) Geological Institute, ETH Zurich, Switzerland

Corresponding author: marcel.frehner@erdw.ethz.ch

S5 - Rheology, strain localization, folding and faulting (PS7)

### Introduction:

Transpression is a combination of strike-slip deformation and shortening orthogonal to the deformation zone. Transpressional structures generally form in response to obliquely convergent plate motions. Whereas transpression in the upper crust is dominantly accommodated by faulting, viscous parts of the lithosphere accommodate transpression dominantly by folding. In some cases, transpressional strain is geographically partitioned (Tikoff and Teyssier, 1994) between a strike-slip domain lacking major shortening structures and a neighboring pure-shear domain (e.g., fold-and-thrust belt) lacking major strike-slip structures.

Transpressional folding is inherently 3D; hence the growth and rotation of folds during transpression as a function of the convergence angle is investigated using 3D numerical finite-element models (Figure 1; Frehner, in press). The studied model setup comprises upright single-layer buckle folds in Newtonian materials, which grow from an initial point-like perturbation due to a combination of in-plane shortening and shearing (i.e., transpression).

### Results:

The numerical study suggests that fold axes are always parallel to the major horizontal principal strain axis ( $\lambda_{\max}$ ), and that sequential folds appearing later form parallel to already existing folds and rotate with the major horizontal principal strain axis with increasing strain. This suggests that fold axes are not passive material lines and that fold hinge migration occurs during transpression.

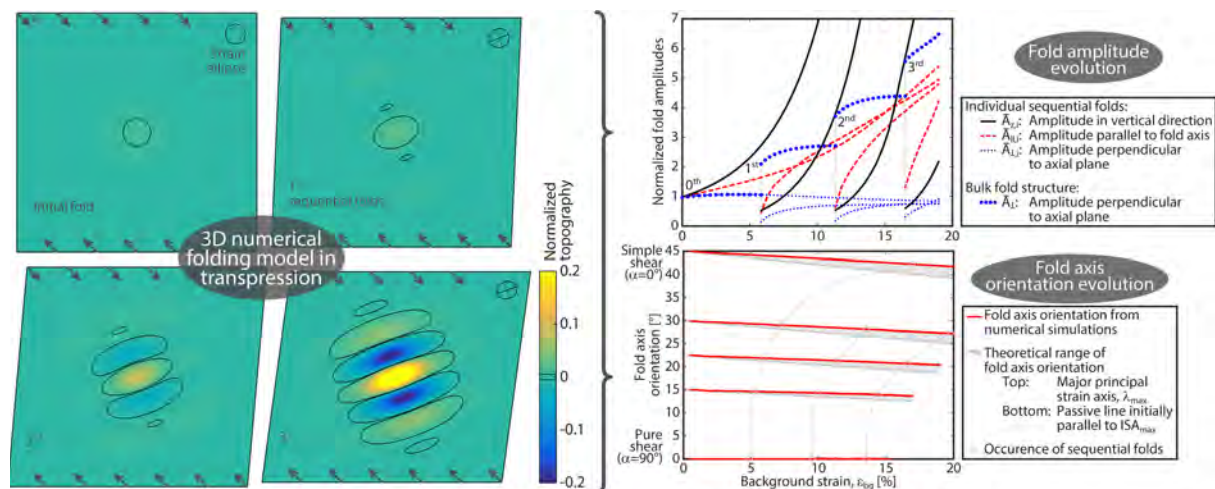


Figure 1: Graphical abstract of main results. Left: Top view snapshots of example simulation with a convergence angle,  $\alpha=45^\circ$ . With increasing background strain, the fold structure grows in all three dimensions. Top right: From the numerical simulation the fold amplitude evolution is calculated in three directions: vertical (fold

growth), parallel to the fold axis (fold elongation) and perpendicular to the axial plane (sequential fold growth). Bottom right: Fold axis orientation in map view with increasing background strain for different convergence angles ( $\alpha=0^\circ-90^\circ$ ). For all cases, the fold axis is always parallel to the major principal strain axis,  $\lambda_{max}$ ; hence it is not a passive marker line.

Because the fold axis is always parallel to  $\lambda_{max}$ , there is an analytical triangular relationship between the convergence angle, the amount of strain, and the fold axis orientation. If two of these values are known, the third can be determined. Importantly, this relationship is independent of the viscosities and viscosity ratios involved in the folded layers.

**Application to the Zagros Simply Folded Belt:**

For the Zagros Simply Folded Belt (ZSFB) in NE Iraq, the far-field convergence angle (from GPS; Vernant and Chéry, 2006) is  $\alpha=35^\circ$ . Strain is partitioned between the ZSFB and the bounding fault system. However, the degree of partitioning is disputed, ranging from full partitioning ( $\alpha=90^\circ$  in the ZSFB; Talebian and Jackson, 2004) to intermediate partitioning ( $\alpha=60^\circ$  in the ZSFB; Vernant and Chéry, 2006). Zero strain partitioning ( $\alpha=35^\circ$  in the ZSFB) is unrealistic because some strike-slip movement along the MZT-MRF-system is clearly documented (Talebian and Jackson, 2002).

The above mentioned triangular relationship is applied to the Zagros fold-and-thrust-belt to estimate the degree of strain partitioning between the ZSFB and the bordering strike-slip fault-system (Figure 2). Despite some data scatter, the orientation of the majority of fold axes indicates a convergence angle within the ZSFB of  $\alpha=60^\circ-90^\circ$ , confirming the proposed range. However, the data covers this entire range; hence it is not clear which end-member model is more appropriate.

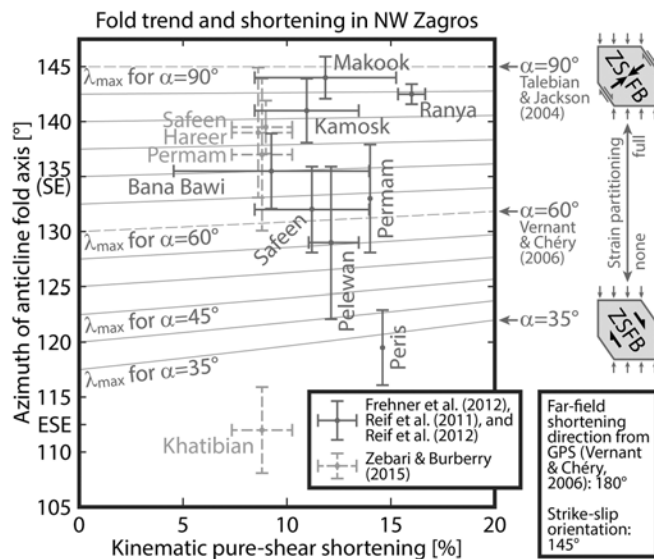


Figure 2: Fold axis orientations plotted versus kinematic strain estimates of anticlines in the ZSFB (NE Iraq). In the background, the theoretical fold axis orientation,  $\lambda_{max}$ , is plotted for different convergence angles. End-member convergence angles are sketched on the right based on the far-field shortening direction and strike-slip fault orientation; they are  $90^\circ$  (pure shear) for full strain partitioning and  $35^\circ$  for zero strain partitioning.

**References:**

Frehner M.: 3D fold growth in transpression. Tectonophysics, doi:10.1016/j.tecto.2016.01.002.  
 Talebian M. and Jackson J., 2004: A reappraisal of earthquake focal mechanisms and active shortening in the Zagros mountains of Iran. Geophysical Journal International 156, 506–526.  
 Tikoff B. and Teyssier C., 1994: Strain modeling of displacement-field partitioning in transpressional orogens. Journal of Structural Geology 16, 1575–1588.

Vernant P. and Chéry J., 2006: Mechanical modelling of oblique convergence in the Zagros, Iran.  
Geophysical Journal International 165, 991–1002.

**Keywords:** Buckle folds, Transpression, Fold growth, Hinge migration, Fold rotation, Zagros fold-and-thrust-belt.

## Structural inheritance during multilayer buckle folding: How pre-existing asymmetries result in parasitic folds with wrong vergence

Marcel Frehner<sup>1</sup> and Timothy Schmid<sup>1</sup>

<sup>1</sup>) Geological Institute, ETH Zurich, Switzerland

Corresponding author: marcel.frehner@erdw.ethz.ch

S5 - Rheology, strain localization, folding and faulting (PS7)

### Introduction:

Parasitic folds are typical structures in geological multilayer folds; they are characterized by a small wavelength and are situated within folds with larger wavelength (Ramberg, 1963; Frehner and Schmalholz, 2006). Parasitic folds exhibit a characteristic asymmetry (or vergence; i.e. S-, Z-, or M-folds) reflecting their structural relationship to the larger-scale fold.

Here we (Frehner and Schmid, 2016) investigate if and how a pre-existing asymmetry (e.g., from sedimentary structures or folds from a previous tectonic event) can be inherited during buckle folding to form alleged parasitic folds with wrong vergence. We conduct 2D finite-element simulations of Newtonian multilayer folding. The applied model setup comprises a thin layer containing the pre-existing asymmetry sandwiched between two thicker layers, all embedded in a lower-viscosity matrix and subjected to layer-parallel shortening. During ongoing layer-parallel shortening and buckling, we track the asymmetry's amplitude with respect to the larger-scale fold median line.

### Results:

Typical results demonstrate that during the early folding stages the geometrical asymmetry both grows in amplitude and intensifies its asymmetry (increasing skew angle) (Figure 1). However, at later folding stages, when the larger-scale fold also macroscopically amplifies, the asymmetry de-amplifies and reduces its skew angle again.

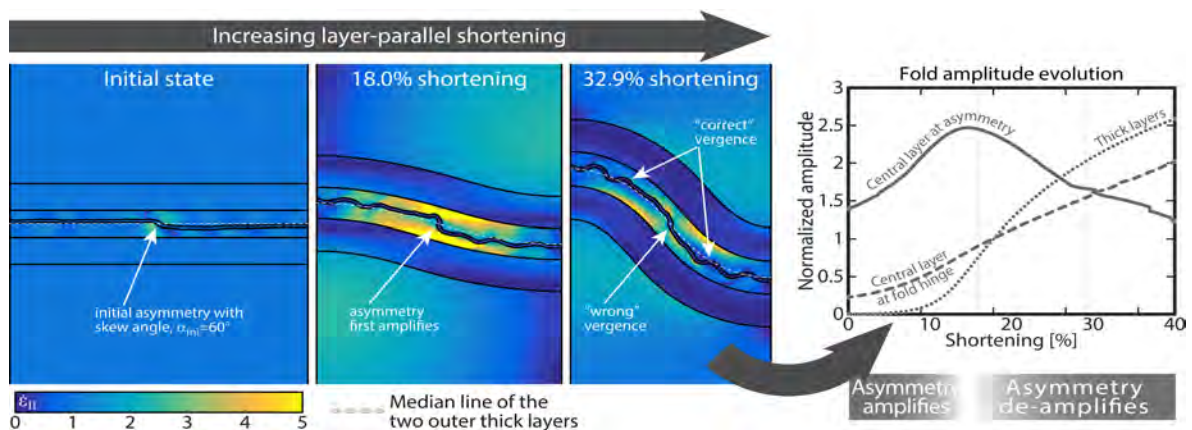


Figure 1: Graphical abstract of the main results. Left: Simulation snapshots visualizing the evolution of the multilayer system containing an initial geometrical asymmetry of the central thin layer. Colors: second invariant of the strain rate tensor,  $\epsilon_{II}$ . Dashed white line: larger-scale median line. The initial asymmetry survives the early stages of buckle folding, which results in an alleged parasitic fold with wrong vergence, alongside true parasitic folds with correct vergence. Right: From the numerical simulation, different (normalized) fold amplitude evolutions can be calculated. Shown are the amplitude of the larger-scale fold (thick layers; dotted line), as well as the amplitude of the central thin layer at the larger-scale fold hinge (dashed line) and at the larger-scale fold limb (i.e., amplitude of the initial asymmetry; solid line).

We systematically vary the intensity of the initial geometrical asymmetry (open to tight; Figure 2A) and its position on the larger-scale fold (from fold hinge to fold limb; Figure 2B). We investigate how the efficiency of de-amplification is controlled by the interplay between larger-scale and smaller-scale fold amplification.

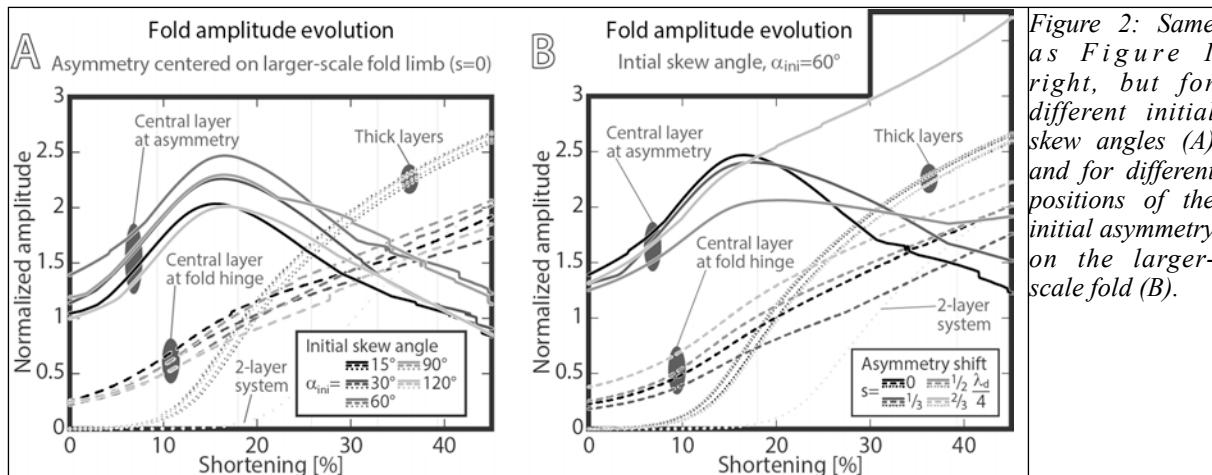


Figure 2: Same as Figure 1 right, but for different initial skew angles (A) and for different positions of the initial asymmetry on the larger-scale fold (B).

### Discussion & Conclusions:

When the two outer thick layers buckle and amplify to finite amplitudes, two processes work against the asymmetry: (i) layer-perpendicular flattening (i.e., pure shear between the two thick layers) and (ii) the rotational component of flexural flow folding (i.e., simple shear between the two thick layers). Both processes promote de-amplification and unfolding of the pre-existing asymmetry.

We conclude that pre-existing folds that are open, exhibit low amplitude, and/or are situated on the limb of the larger-scale fold are prone to de-amplification and may disappear during buckling of the multilayer system. Large-amplitude and/or tight to isoclinal folds and/or folds situated close to the hinge of the larger-scale fold may be inherited and develop into alleged parasitic folds with wrong vergence resembling type 3 fold interference patterns.

### References:

- Frehner M. and Schmalholz S.M., 2006: Numerical simulations of parasitic folding in multilayers. *Journal of Structural Geology* 28, 1647–1657.
- Frehner M. and Schmid T., 2016: Parasitic folds with wrong vergence: How pre-existing geometrical asymmetries can be inherited during multilayer buckle folding. *Journal of Structural Geology* 87, 19–29.
- Ramberg H., 1963: Evolution of drag folds. *Geological Magazine* 100, 97–110.

**Keywords:** Parasitic folds, Buckle folds, Fold vergence, Asymmetric folds, Structural inheritance, Finite-element method.

## Topography controlled sill intrusions: Modeling magma propagation in the crust

Ayleen Gaete<sup>1</sup>, Mehdi Nikkhoo<sup>1</sup> and Thomas R. Walter<sup>1</sup>

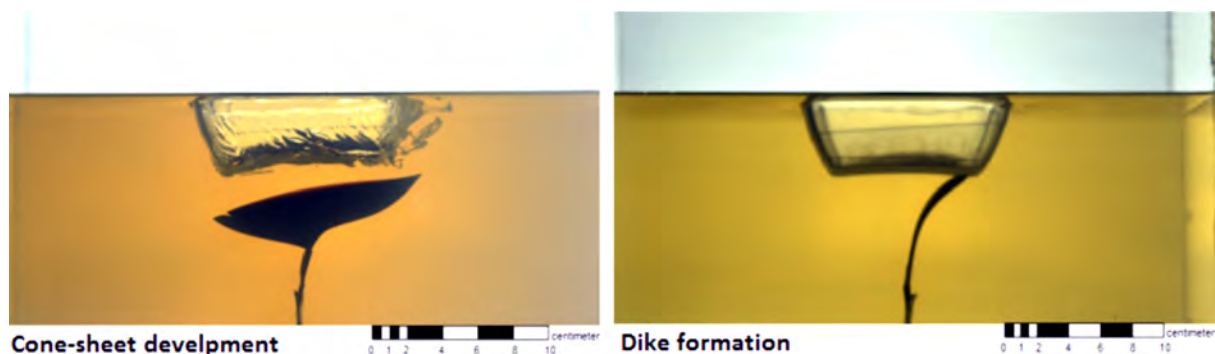
<sup>1</sup>Physics of Earthquakes and Volcanoes, GFZ German Research Centre for Geosciences, Telegrafenberg, 14473 Potsdam, Germany.

Corresponding author: [agaete@gfz-potsdam.de](mailto:agaete@gfz-potsdam.de)

S5 - Rheology, strain localization, folding and faulting (PS7)

### Abstract:

Plumbing system in volcanoes and the process relative to continental crust building are a consequence of the magma transport and storage through the crust, where the common mechanisms observed are laminar intrusions, such as dikes and sills. The emplacement and propagation of these intrusions are thought to be influenced by topographic load that can control the magma transport and dike arrest as well as the development of reservoirs.



Here we analyze possible sheet intrusion mechanisms associated to unloading topography. We are performing hydrofracture experiments in gelatin, an elastic medium allowing to represent the properties of the crust. Fracturing is realized by injection of dyed water, creating hydrofractures that propagate and arrest, change their shape and geometry in dependence of the surrounding stress field.

Experiments reveal the influence of unloading stress on the injection paths. Varying the geometrical and dynamic parameters governing the system we found that dikes form when the fracture toughness associated to gelatin concentration is significant compared to the gravitational stress controlled by the unloading topography. Dikes bend and develop into saucer shaped geometries when the gravitational stress governs over fracture toughness.

**Keywords:** Analog modeling, gelatin, stress field, sheet intrusion, saucer shaped sill, dike.

## Initiating subduction at (weak) fracture zones : a numerical approach

Yann Heurtebize<sup>1</sup>, Fanny Garel<sup>1</sup>, Rhodri Davies<sup>2</sup>, Sarah Abécassis<sup>1</sup>, Diane Arcay<sup>1</sup>, Serge Lallemand<sup>1</sup>

<sup>1</sup>) Géosciences Montpellier, University of Montpellier, Montpellier, France

<sup>2</sup>) Research School of Earth Sciences, Australian National University, Canberra, ACT, Australia

Corresponding author: [garel@gm.univ-montp2.fr](mailto:garel@gm.univ-montp2.fr) (corresponding author)

S5 - Rheology, strain localization, folding and faulting (PS7)

Subduction zones link surface plate motions to deep mantle convection, but the detail of how subduction (rarely?) initiates remains elusive. Several geodynamic contexts have been proposed for subduction initiation, for example : oceanic fracture zones (Hall et al., 2003, Leng and Gurnis, 2011), passive margins (Regenauer-Lieb et al., 2001 ; Nikolaeva et al., 2010), vertical or horizontal asthenospheric flow (Burov and Cloetingh, 2001 ; Lu et al., 2015). Studies have highlighted the crucial role of strain localization for plate weakening, for example through shear heating (Thielmann and Kaus, 2012) or water-induced lubrication (Regenauer-Lieb et al., 2001).

Using the finite-element thermo-mechanical code Fluidity, we investigate here the process of subduction initiation at a weak fracture zone, putting into contact two plates of different ages, with the thermal and rheological discontinuity reinforced by a shallow weak zone. We evidence two possible scenarios for subduction initiation.

Scenario 1 exhibits an asthenosphere upwelling between the two lithospheric plates, leading to a pseudo-back-arc spreading (similar to results of Leng and Gurnis, 2011). Scenario 2 results from strain-localization at the interface between the two lithospheric plates (similar to results of Doin and Henry, 2001; Thielmann and Kaus, 2012 – see also the poster by Abécassis et al. in this session). We find that parameterization of weak zone properties, of plate ages, and of plate and asthenosphere rheology controls the occurrence and the dynamic scenario of subduction initiation.

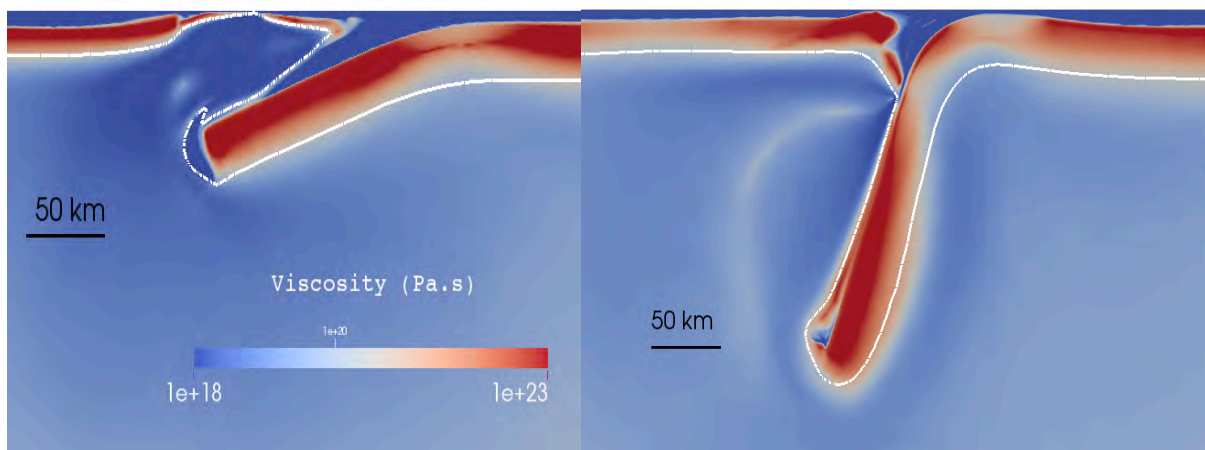


Figure 1: Scenarios 1 (left) and 2 (right) for subduction initiation. The background color is a logarithmic scale for viscosity, and the white line represents the 1300 K isotherm contour.

**References:**

- Burov, E., Cloetingh, S., 2010, Plume-like upper mantle instabilities drive subduction initiation, *Geophysical Research Letters*, 37, L03309, <http://dx.doi.org/doi:10.1029/2009GL041535>
- Doin, M.-P., Henry, P., 2001, Subduction initiation and continental crust recycling: the roles of rheology and eclogitization, *Tectonophysics*, 342, 163-191, [http://dx.doi.org/doi:10.1016/S0040-1951\(01\)00161-5](http://dx.doi.org/doi:10.1016/S0040-1951(01)00161-5)
- Hall, C. E., Gurnis, M., Sdrolias, M., Lavier, L. L., Müller, R. D., 2003, Catastrophic initiation of subduction following force convergence across fracture zones, *Earth and Planetary Science Letters*, 212, 15-30, [http://dx.doi.org/doi:10.1016/S0012-821X\(03\)00242-5](http://dx.doi.org/doi:10.1016/S0012-821X(03)00242-5)
- Leng, W., Gurnis, M., 2011, Dynamics of subduction initiation with different evolutionary pathways, *Geochemistry, Geophysics, Geosystems*, Q12018, <http://dx.doi.org/doi:10.1029/2011GC003877>
- Lu, G., Kaus, B. J. P., Zhao, L., Zheng, T., 2015, Self-consistent subduction initiation induced by mantle flow, *Terra Nova*, 27, 130–138, <http://dx.doi.org/doi:2010.1111/ter.12140>
- Nikolaeva, K., Gerya, T. V., Marques, F. O., 2010, Subduction initiation at passive margins: Numerical modeling, *Journal of Geophysical Research*, 115, B03406, <http://dx.doi.org/10.1029/2009JB006549>
- Regenauer-Lieb, K., Yuen, D. A., Branlund, J., 2001, The Initiation of Subduction: Criticality by Addition of Water?, *Science*, 294, 578, <http://dx.doi.org/10.1126/science.1063891>
- Thielmann, M., and Kaus, B. J. P., 2012, Shear heating induced lithospheric-scale localization: Does it result in subduction?, *Earth and Planetary Science Letters*, 359-360, 1-13, <http://dx.doi.org/10.1016/j.epsl.2012.10.002>

**Keywords:** Subduction, subduction initiation, plate and asthenosphere rheology, strain localisation, numerical modelling.

## Stress distribution around complex salt structures: A new approach using fast 3D boundary element method

Laurent Maerten<sup>1</sup> and Frantz Maerten<sup>1</sup>

<sup>1</sup>) Schlumberger, Montpellier, France laurent.maerten@slb.com Session S5, Rheology, strain localization, folding and faulting

Corresponding author: FMaerten@slb.com

S5 - Rheology, strain localization, folding and faulting (PS7)

### Abstract:

During the last decade geologists and engineers have used the Finite Element Method (FEM) with elasto-plastic or visco-plastic behavior to simulate salt in order to gain a better understanding of the *in-situ* stress distribution. However, building such FEM models can become time consuming and challenging, especially when complex geometry is involved, and modeling elaborated non-linear salt behavior can take hours to days to process.

We have developed a different approach using a fast 3D Boundary Element Method (BEM) (Maerten et al., 2014). Instead of using non-linear mechanical behavior of salt, we use the assumption that salt can be viewed as a pressurized cavity for which unknown parameters such as far field stress and salt pressure gradient are inverted using available data such as observed natural fracture (*e.g.*, joints, faults...) or recorded stress data (*e.g.*, breakout, LOT, micro-seismicity...) associated to past or actual deformation around salt.

To verify this approach, BEM results have been validated against known 3D analytical solution for pressurized spherical cavity (Neuber, 1946) and compared to published (Figure 1), more complex, 3D FEM salt models (Luo et al., 2012; Sanz and Dasari, 2010). The efficiency of this new approach, in terms of model construction and mechanical simulation, is demonstrated through a natural example of faults associated to salt diapirs in the Gulf of Mexico (Figure 2).

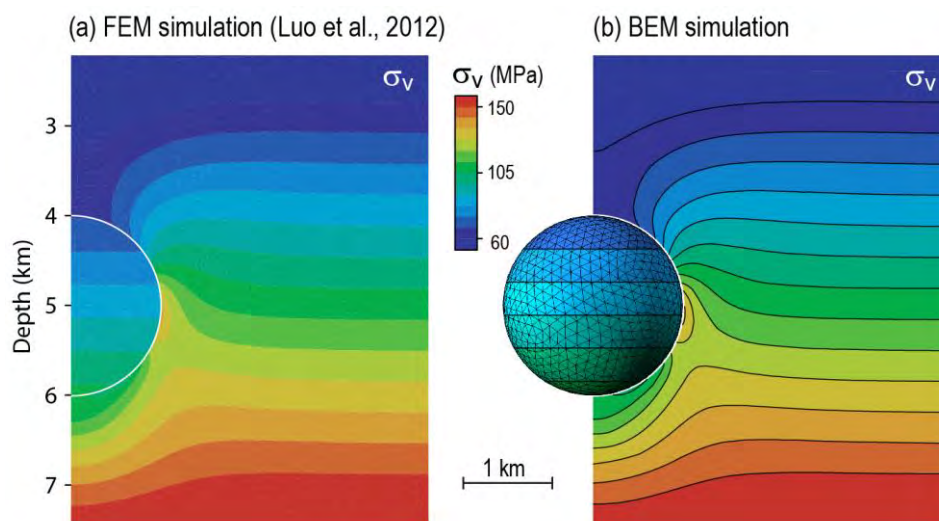


Figure 1: Comparison between iBem3D solution (right) and FEM solution from Luo et al., 2012 (left).

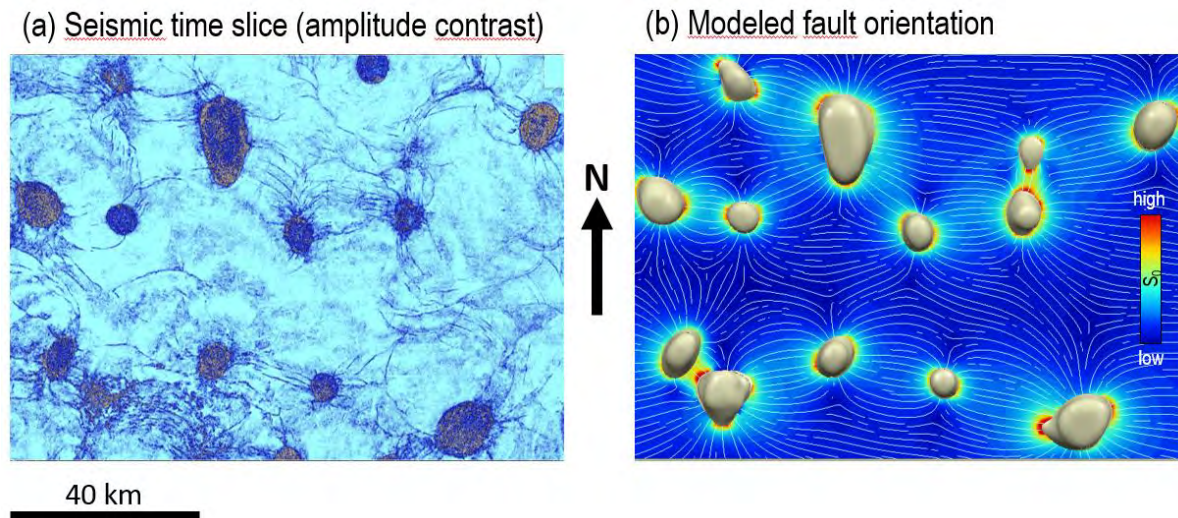


Figure 2: Comparison between (a) the seismic data (time slice at  $z=5\text{km}$ ) and (b) the geomechanical simulation results for the Gulf of Mexico. Maximum Coulomb shear stress ( $S_o$ ) is plotted on the map on the right as well as the orientation of the model shear planes.

#### References:

- Luo, G., Nikolinakou, M.A., Flemings, P.B., and Hudcok, M.R., 2012. Geomechanical modeling of stresses adjacent to salt bodies: Part 1-Uncoupled models, AAPG bulletin, 96(1), 43-64.
- Maerten, F., Maerten, L., Pollard, D.D., 2014. iBem3D, a three-dimensional iterative boundary element method using angular dislocations for modeling geologic structures, Computers and Geosciences, 72, 1-17.
- Neuber, H., 1946. Theory of Notch Stresses, Edwards eds, Ann Arbor, Michigan, p. 181.
- Sanz, P.F. and Dasari, G.R., 2010. Controls on in situ stresses around salt bodies, ARMA, 10-169, 1-12.

**Keywords:** Salt diapirs, boundary element method, stress, elasticity, faults.

## **Estimating the rheological properties of the oceanic asthenosphere using geodetic data**

Sagar Masuti<sup>1</sup>, Sylvain Barbot<sup>1</sup>, Shun-Ichiro Karato<sup>2</sup>, Nachiket Kapre<sup>3</sup>, Lujia Feng<sup>1</sup>, Paramesh Banerjee<sup>1</sup>

<sup>1</sup>Earth Observatory of Singapore, Nanyang Technological University, Singapore, <sup>2</sup>Yale University, Department of Geology and Geophysics, New Haven, CT, USA, <sup>3</sup>School of Computer engineering, Nanyang Technological University, Singapore.

Corresponding author: SAGARSHR001@e.ntu.edu.sg

S5 - Rheology, strain localization, folding and faulting (PS7)

Olivine is the most abundant and weakest mineral in Earth's asthenosphere. The stress-strain rate relation for olivine is believed to govern the rheology of the asthenosphere. The rheological parameters of olivine have been studied extensively in laboratories under hydrous and anhydrous conditions for both diffusion and dislocation creep regimes. Here, we provide an estimate of some of the rheological parameters of olivine in the dislocation creep regime using postseismic geodetic observations following the 2012 Mw 8.6 Wharton Basin earthquake in the Indian Ocean.

The event involved ruptures on complex conjugate faults with coseismic slip reaching 60 km depth, indicating a thick, dry lithosphere in the Wharton Basin. We build a three-dimensional model of postseismic deformation with afterslip in the brittle upper mantle and viscous flow in the asthenosphere.

We use laboratory estimates as the prior information and a nonlinear Burgers model to explore the rheological parameters of olivine such as water content, activation volume, activation energy, and temperature. We find that a minimum water content of  $1600 \text{ H}/10^6 \text{ Si}$  at mantle temperature of 1400 °C, indicating the stratification of water content (dry lithosphere over wet asthenosphere). In addition, a higher activation volume is needed to explain the observations, implying a thin high viscous layer in the Wharton Basin.

## The initiation and development of folding and boudinage structures can be treated within a unified energy bifurcation theory for layered ductile materials

Max Peters<sup>1,\*</sup>, Marco Herwegh<sup>2</sup>, Martin K. Paesold<sup>3</sup>, Thomas Poulet<sup>4</sup>, Klaus Regenauer-Lieb<sup>5</sup> and Manolis Veveakis<sup>4,5,\*</sup>

<sup>1</sup>) Karlsruhe Institute of Technology, Institute of Applied Geosciences, Geothermics, Germany

<sup>2</sup>) Institute of Geological Sciences, University of Bern, Switzerland

<sup>3</sup>) Formerly at: School of Mathematics and Statistics, University of Western Australia, Australia

<sup>4</sup>) CSIRO Energy and Resources Group, Australia

<sup>5</sup>) School of Petroleum Engineering, University of New South Wales, Australia

Corresponding author: max.peters@kit.edu

S5 - Rheology, strain localization, folding and faulting (PS7)

### Introducing an alternative theory for folding and boudinage:

In classical mechanics, folding and boudinage are regarded as a geometric problem. This means that an initial infinitesimal small imperfection amplitude grows, which ultimately leads to localization through a process known as wavelength selection. One drawback of this approach using a linearized material response is that folding and boudinage develop for different material parameters or power-law exponents. In the past, this complication has led to a discussion about the applicability of such approaches to localized structures in real rocks (Hobbs et al., 2010 and references therein).

Here, we are concerned with a more generic localization theory, i.e. strain localization out of steady-state conditions inside a homogeneous material at a critical material parameter and deformation rate (e.g. Regenauer-Lieb and Yuen, 2003; Peters et al., 2015). In this framework considering energy flows and microphysical processes, instability arises out of the constitutive description itself for a critical amount of shear heating and layer thickness (Gruntfest, 1963).

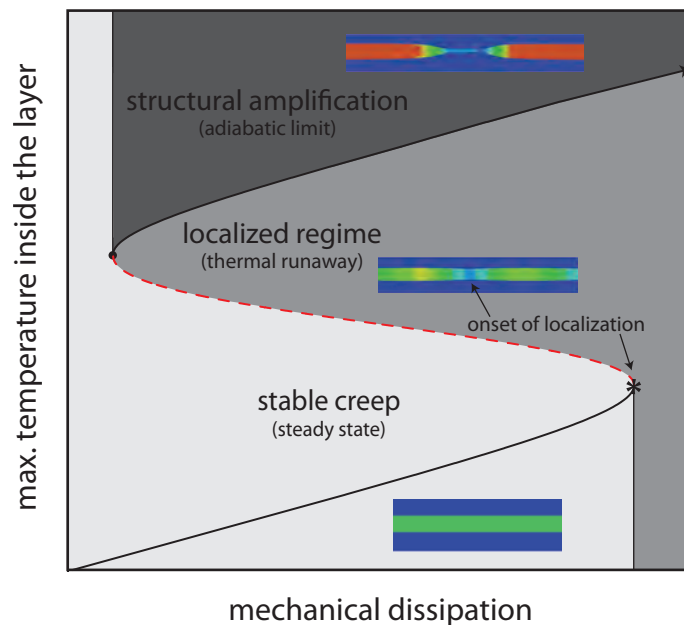
### The concept of alternating boundary conditions:

The implementation of the coupled thermo-mechanical 2-D finite element model comprises an elastic and rate-dependent *von Mises* plastic rheology (Peters et al., 2016). The underlying system of equations is solved in a 3-layer pure shear box for constant velocity and isothermal boundary conditions, using the open-source finite element software *REDBACK* (for details refer to Poulet et al., in press). In order to examine the transition from stable to localized creep, we study how material instabilities are related to energy bifurcations, which arise independently of the sign of the stress conditions imposed on the boundaries, whether in compression or extension. The onset of localization is determined by a critical amount of shear heating, termed *Gruntfest* number, when dissipative work by temperature-sensitive creep translated into heat overcomes the diffusive capacity of the layer of a given thickness. Through an additional mathematical bifurcation analysis using constant stress boundary conditions, we test whether both structures develop at a same critical *Gruntfest* number.

### Numerical bifurcation results:

By means of alternating boundary conditions and parameter sensitivity studies, the numerical experiments reveal that folding develops for the same material parameters and power-law exponent as boudinage, by only inverting the sign of displacement. Boudinage and folding instabilities occur when

the mechanical work, which is translated into heat, overcomes the diffusive capacity of the layer. Consequently, both instabilities develop for the same critical *Gruntfest* number (Peters et al., 2016). Further, we find that boudinage instability emerges for values of the stress exponent below  $n < 5$  and especially for a *Newtonian* response ( $n = 1$ ) of the layer. This finding implies that not only can folding and boudinage instabilities be treated as the same energy bifurcation, but also that the energy theory predicts boudinage in cases where classical theories anticipate no growth of the structure.



### Discussion:

The existence of a single critical dissipation number to describe the initiation of folding and boudinage provides a solid basis for explaining complex geological observations. Since the critical material parameters and boundary conditions for both structures to develop are found to coincide, the initiation of localized deformation in mechanically strong layered media within a weaker matrix can be captured by means of a unified theory for localization in ductile materials. For an appropriate set of material properties, local changes of boundary conditions can be considered sufficient to trigger both sets of instabilities close to each other. In this energy framework, neither intrinsic nor extrinsic material weaknesses are required, as the nucleation process of strain localization arises out of homogeneous conditions.

This finding allows us to approach localization problems as coupled rheological bifurcations and to describe folding and boudinage structures as the same energy attractor of ductile deformation. In future, our study will allow geologists to extract critical material parameters and deformation conditions of rate- and temperature-sensitive creep directly from field observations.

### References:

- Gruntfest, I.J., 1963. Thermal feedback in liquid flow; plane shear at constant stress. *Transactions of the Society of Rheology* 7. doi:10.1122/1.548954.
- Hobbs, B.E., Regenauer-Lieb, K., Ord, A., 2010. Folding with thermal mechanical feedback: another reply. *Journal of Structural Geology* 32. doi:10.1016/j.jsg.2009.10.005.
- Peters, M., Herwegh, M., Paesold, M.K., Poulet, T., Regenauer-Lieb, K., Veveakis, M., 2016. Boudinage and folding as an energy instability in ductile deformation. *Journal of Geophysical Research Solid Earth*, 121, doi:10.1002/2016JB012801.

- Peters, M., Veveakis, M., Poulet, T., Karrech, A., Herwegh, M., Regenauer-Lieb, K., 2015. Boudinage as a material instability of elasto-visco-plastic rocks. *Journal of Structural Geology* 78. doi.org/10.1016/j.jsg.2015.06.005.
- Poulet, T., Paesold, M.K., Veveakis, M., in press. Multi-physics modelling for fault mechanics using REDBACK: a parallel open-source simulator for tightly coupled problems. *Rock Mechanics and Rock Engineering*. doi:10.1007/s00603-016-0927-y [<http://github.com/pou036/redback.git>].
- Regenauer-Lieb, K., Yuen, D.A., 2003. Modeling shear zones in geological and planetary sciences: solid- and fluid thermal-mechanical approaches. *Earth-Science Reviews* 63. doi:10.1016/S0012-8252(03)00038-2.

**Keywords:** Boudinage and folding theory, Thermo-mechanical feedbacks, Layered materials, Shear heating, Numerical methods.

## Development of slip partitioning within wet kaolin and dry sand oblique-convergence experiments

Kevin Toeneboehn<sup>1</sup>, Michele Cooke<sup>1</sup>, Karen Leever<sup>2</sup>

<sup>1</sup>) University of Massachusetts, Amherst, Geosciences Dept., U.S.A.

<sup>2</sup>) Helmholtz Centre Potsdam GFZ, Potsdam, Germany

Corresponding author: cooke@geo.umass.edu

S5 - Rheology, strain localization, folding and faulting (PS7)

### Introduction:

Slip partitioned systems, or fault systems that accommodate oblique convergence with different slip rake on two or more faults, are well documented (e.g. *Haq & Davis, 1997; Leever et al., 2011*). Slip partitioning can occur at multiple scales within the crust and ranges from local convergence within restraining bends (e.g., the Transverse Ranges of the southern San Andreas Fault) to thousands of kilometers across along subduction zones such as the Great Sumatra Fault or median tectonic line of Japan (e.g., *Bowman et al., 2003; Jones & Wesnousky, 1992; Fitch, 1972*). Carefully scaled physical experiments using crustal analog materials inform our understanding of fault evolution because we can control the loading and directly observe the ensuing deformation.

Previous experiments in dry sand show that convergence angle and fault strength control the initiation and maintenance of slip partitioning (McClay & Bonora, 2001; Leever et al., 2011; Haq & Davis, 2010). Leever et al. (2011) demonstrate using a conveyor style convergence device that slip partitioning in dry sand develops in three stages: early strain accumulation, oblique-slip faulting, and finally partitioning along strike-slip and oblique-slip faults. Haq & Davis, 2010 also use dry sand and show slip partitioning above a strike-slip dislocation with convergence angles as high as 60° from margin parallel. These experiments superpose regional contraction and localized strike-slip and do not capture the oblique dislocation of a subduction zone. We simulate oblique convergence using blocks with 30° dipping contacts under the clay or sand (Figure 1) where the overlying crust is obliquely thrust over the subducting slab.

### Experiment Set-Up:

Although dry sand has many benefits as an analog for modeling crustal processes (e.g. strain-rate independence, strength scaling, ease of use) its lack of cohesion favors the growth of new faults over fault reactivation. In contrast to dry sand, the non-zero cohesion of wet kaolin produces long-lived fault structures that easily reactivate. Under similar loading, experiments in wet kaolin produce fewer faults than dry sand and exhibit greater degree of fault reactivation (*Cooke et al., 2013*). These properties of wet kaolin are particularly important for modeling the evolution of fault systems as the abandonment and reactivation of individual fault segments approximates the evolution of faults in the crust.

Scaled experiments using both dry sand and wet kaolin with identical boundary conditions provide insights on the role of material properties in slip partitioning. We test convergence angles ranging from 5° to 45° and document the slip partitioning using high-resolution images. Digital image correlation from the images, combined with stereovision techniques, provides the incremental horizontal displacement and uplift fields. These state of the art methods provide complete slip vectors for the faults, constrain fault dip and provide strain fields surrounding the faults. Additionally, in both experiments we implement force gauges to record fault normal stress changes associated with the onset of faulting.

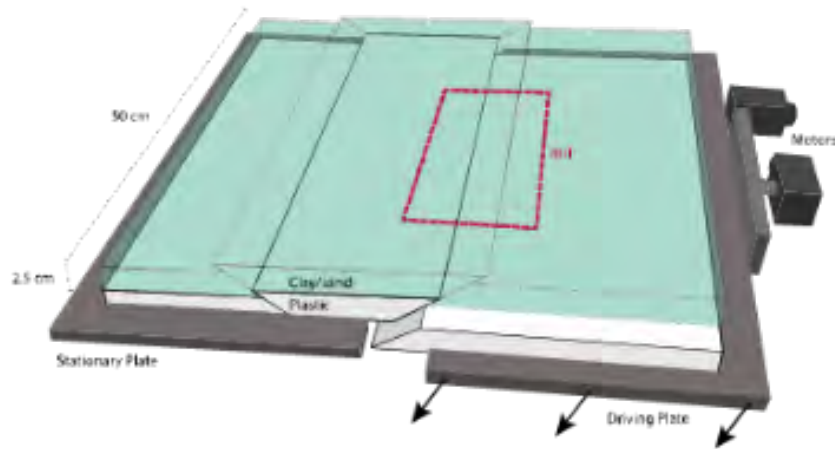


Figure 1: Schematic of experiment has three plastic blocks with abutting  $30^\circ$  contacts and 2.5 cm of overlying wet kaolin clay or dry sand. The blocks are positioned on two plates: one fixed and the other moved by two orthogonal stepper motors. Two cameras mounted above the model capture high-resolution images of the region of interest (ROI) shown in the red-dashed box.

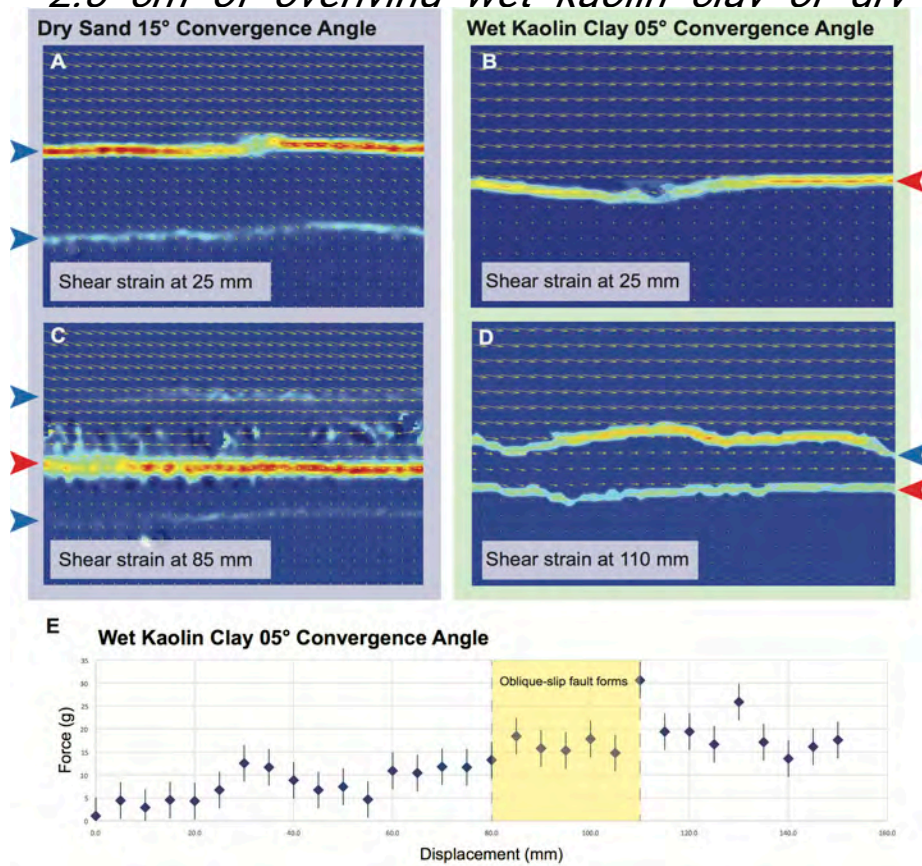


Figure 2: (A-D) Incremental shear strain for experiments in dry sand and wet kaolin clay. Note early slip partitioning (85 mm) in the sand experiments along active oblique-slip fore and back-thrusts (blue arrows) and late-stage through-going strike-slip fault (red arrow). Slip partitioning develops later in the  $05^\circ$  clay experiment (110 mm) with an oblique-slip fore-thrust (blue) and strike-slip fault (red arrow). E) Force data from a  $05^\circ$

*convergence angle experiment in wet kaolin reveals an increase in force immediately preceding the formation of the fore-thrust.*

**Results:**

The evolution of faulting differs between the experiments with dry sand and wet kaolin. Early within the dry sand experiment, an oblique-slip forethrust-backthrust pair forms at approximately 25 mm of total plate displacement followed by the addition of a late stage through-going strike-slip fault at around 85 mm plate displacement (Fig. 2A,C). These results are consistent with oblique convergence dry sand experiments that use a conveyor device (Leever et al., 2011). In contrast, wet kaolin under shallow convergence angles first produces a strike-slip fault at around 25 mm of plate displacement (Fig. 2B). As convergence accumulates in the kaolin, a new forethrust forms dipping toward the underlying discontinuity. No backthrust forms in the wet kaolin. The delay of strike-slip development in the dry sand may owe to diffusion of the mode III stresses around the basal dislocation so that the first faults form in response to the compression (thrust pair) rather than shear.

The lack of cohesion in dry sand allows this material to develop three active slip-partitioned faults while the wet kaolin experiment has only two active faults with commensurate lesser total active fault surface area. The greater cohesion of the kaolin tempers its ability to produce multiple active faults. Within the kaolin, the forethrust only grows after significant accumulation of compression, as revealed by the force measurements (Fig. 2E). Once the strike-slip fault and forethrust develop, the wet kaolin system can sustain slip partitioning without the development of additional faults. Thus, the cohesion of the clay, which may be similar to crustal rock strength, may facilitate the maintenance of slip partitioned fault systems.

**References:**

- Cooke, Michele L., Mariel T. Schottenfeld and Steven W. Buchanan, 2013. Evolution of Fault Efficiency at Restraining Bends within Wet Kaolin, *Journal of Structural Geology*.
- Leever, K. A., Gabrielsen, R. H., Sokoutis, D. and Willingshofer E., 2011. The effect of convergence angle on the kinematic evolution of strain partitioning in transpressional brittle wedges: Insight from analog modeling and high-resolution digital image analysis. *Tectonics*, 30, 1–25.
- Haq, S. S., & Davis, D. M., 2010. Mechanics of fore-arc slivers: Insights from simple analog models. *Tectonics*, 29(5).

**Keywords:** Transpression, slip partitioning, fault evolution, convergence angle, PIV, stereo vision, clay, sand.

## **S6- Dynamics of sedimentary Basins, Fluids & Georeservoirs**

Surface sedimentary rocks are the locus of many human underground activities. Industrial issues concern the exploration, extraction, and storage of hydrocarbons, heat, nuclear waste, or CO<sub>2</sub>, while societal issues point to the evaluation of the environmental risk (pollution, seismicity, soil stability). The sedimentary records also give first order informations about plate tectonics, relief dynamics and paleoenvironment evolution. In all cases, modeling techniques are challenged to improve their efficiency and/or precision in order to simulate more completely the various data (surface, wells, seismics).

Numerical modeling techniques face the challenges of integrating pore pressure, fluid flow, temperature and chemical reactions in highly strained media with large displacement jumps (faults), in particular in 3D. Complementary physical modeling techniques are now developing towards more quantitative protocols and measurements, and better controlled rheologies.

This session welcomes contributions involving numerical or physical basin modeling to study basin formation and deformation (including fold-and-thrust belts and accretionary prisms), the structural and thermal evolution of georeservoirs, or the fluid production and migration, from both fundamental and industrial perspectives.

**Conveners:** Jean-Claude Ringenbach (Total, France) and Giacomo Corti (NRC, Roma, Italy).

### **Keynote speaker:**

**"On the use (and potential abuse) of models in Earth Science with application to inferring sedimentary basin dynamics"** by Guy Simpson (University of Geneva, Switzerland) - [Guy.Simpson@unige.ch](mailto:Guy.Simpson@unige.ch)

## **On the use (and potential abuse) of models in Earth Science with application to inferring Sedimentary Basin Dynamics**

Guy Simpson

Department of Earth Science, University of Geneva

Corresponding autor: [Guy.simpson@unige.ch](mailto:Guy.simpson@unige.ch)

S6- Dynamics of sedimentary Basins, Fluids & Georeservoirs (Keynote)

Because geological processes act on time and length scales that make direct observations difficult, *models* are commonly used to explain geological observations or to infer long-term behaviour that is otherwise virtually impossible to study. These models can take many different forms: for example, they may be mathematical and solved analytically or numerically or they may be analogue models investigated in a laboratory. In any case, a model represents an abstraction of a far more complex real system and an important question is whether a model reveals anything useful about the system it is intended to represent. To answer this question, a number of issues much be addressed.

First, which observations is a model aiming to explain? This step can be critical, since some observations may be ‘favoured’ in comparison to others, which might then influence the choice of model. Second, a model must be formulated and studied (solved). In the case of a numerical model, this step involves firstly deciding on the governing equation(s) (which may be no easy task) and then obtaining an accurate solution to the equation(s) (which is an entirely separate issue that can also be extremely challenging). Finally, one must decide how the model results can be applied to the real system being modelled. Clearly, a model could potentially produce beautiful and very interesting results but that these results may have little relevance to the real system being modelled. Although most of these issues will be familiar to the scientists who actually construct the models, they may be less obvious to scientists specialising in other tools but who are interesting in applying model results.

In this presentation I will illustrate some of these issues using two different problems that are relevant to understanding the dynamics of sedimentary basins. The first problem concerns the modelling of foreland sedimentary basin profiles along the margins of collisional mountain belts while the second problem deals with the modelling of how sediment flux signals linked to climate variability are transmitted downstream and eventually recorded in sedimentary basins. As we will see, it is possible to arrive at quite different, though apparently reasonable conclusions, depending on which model is chosen and how the data being modelled in the first place is interpreted. These examples demonstrate that considerable caution should be exercised when using results of models to make inferences about natural systems.

## Numerical simulation of multiphase flows in porous media

Andrey Afanasyev, Oleg Melnik

Institute of Mechanics, Moscow State University, Moscow, Russia

Corresponding author: melnik@imec.msu.ru

S6- Dynamics of sedimentary Basins, Fluids & Georeservoirs (Oral)

### Introduction:

We present results of numerical simulations conducted by the MUFITS (Multiphase Filtration Transport Simulator, Afanasyev, 2013.) software developed in the Institute of Mechanics, Moscow State University. MUFITS is a noncommercial reservoir simulator for analysis of non-isothermal multiphase multicomponent flows in porous media. The simulator is designed for parallel compositional simulations using both laptops and supercomputers. MUFITS can accommodate geologic, petrophysical and thermophysical data of the real-world complexity.

MUFITS has several EOS modules for prediction PVT properties of reservoir fluids:

**BINMIXT** module for modelling non-isothermal three-phase flows of binary mixtures. The properties are specified by the thermodynamic potential of the mixture, which is calculated before hydrodynamic simulations. The potential is used in conditional extremum problem, which corresponds to the entropy maximum condition in thermodynamic equilibrium. By using this formulation, MUFITS can determine single-, two-, and three-phase equilibriums of the mixture under sub- and supercritical conditions. The primary variables are the pressure, the mixture total enthalpy and the composition. The system singularities in the vicinity of critical thermodynamic conditions are eliminated if these variables are used. Therefore, the simulator can avoid dramatic timestep cuts for hydrodynamic simulations under near-critical conditions.

**BLACKOIL** module for modelling petroleum reservoirs using extended Black-oil approach. The module is capable of single-phase, two-phase and three-phase flows of water, oil and hydrocarbon gas. The gas condensate option is available. This module can be used for analysis of various aspects of oil production.

**GASSTORE** module for modelling underground CO<sub>2</sub> storage, hydrocarbon gas storage and some geothermal scenarios. The module covers three-component three-phase flows of water, salt and gas components. The permeability reduction due to salt precipitation can be simulated.

**T2EOS1** module for modelling non-isothermal single-component flows of water and steam under subcritical thermodynamic conditions. Phase transitions between water and steam are taken into account. This module can be used in hydrothermal applications.

MUFITS can accommodate complex geological setting of the reservoir like heterogeneity, folds or faults. The simulator can load the corner-point grids commonly used in the reservoir simulation industry. The simulator can also automatically create cartesian or radial. The local grid refinement, faults and aquifer options are available among others.

The simulations can be performed in parallel using supercomputers. From the very outset of MUFITS development, the simulator was designed for parallel simulation using MPI interface. This ensured a very good scaling of the computational problems. The estimates show that up to 32 processes there is a linear acceleration of the simulations for a problem comprising several hundred thousand cells.

MUFITS takes a free formatted input data file, which contains the simulation schedule description. The description is formulated using keywords syntax. Both the numeric model parameters and the computation options can be specified in the input data file. The properties in the form of functions are specified by tables.

### Applications:

We discuss several applications of MUFITS for CO<sub>2</sub> sequestration problems (Afanasyev, 2013), dynamics of a hydrothermal system (Afanasyev et al., 2015), interaction of a kimberlitic pipe with alternation of olivine to serpentinite (Afanasyev et al., 2014), volcano syn-eruptive degassing (Melnik et al., 2016) and preliminary results of MUFITS application to porphyry copper deposit formation.

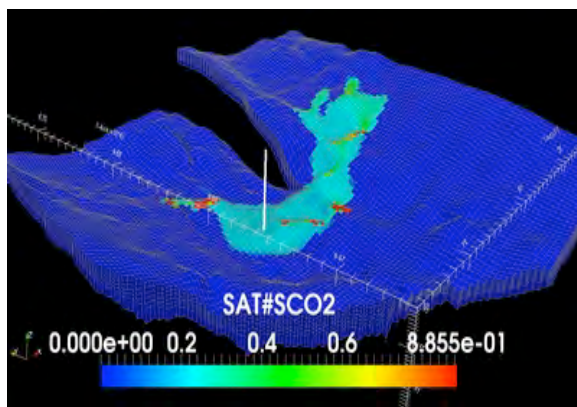


Figure 1: Simulation of CO<sub>2</sub> injection in the Johansen formation using a real-scale geological model of the formation. The model comprises 11 layers of grid blocks. There are 5 vertical faults in the model. We simulate two scenarios of CO<sub>2</sub> injection in this formation for two different locations of the injection well in the region of depression. The duration of the injection period is 100 years while the post-injection period, considered in here, is 2500 years. The injection results in two-phase buoyancy-driven flows of the formation water and supercritical CO<sub>2</sub>. The CO<sub>2</sub> plume spreading along the caprock is strongly affected by the complicated geological settings.

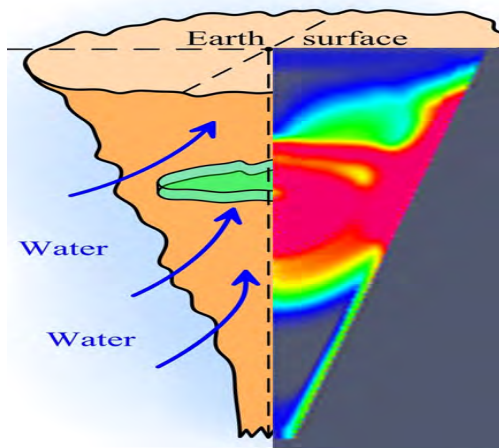


Figure 2: Kimberlite volcanism involves the emplacement of olivine-rich volcanoclastic deposits into volcanic vents or pipes. Kimberlite deposits are typically pervasively serpentinised as a result of the reaction of olivine and water within a temperature range of 130–400 °C or less. We present a model for the influx of ground water into hot kimberlite deposits coupled with progressive cooling and serpentinisation. Large-pressure gradients cause influx and heating of water within the pipe with horizontal convergent flow in the host rock and along pipe margins, and upward flow within the pipe centre. Complete serpentinisation is predicted for wide ranges of permeability of the host rocks and kimberlite deposits. For typical pipe dimensions, cooling times are centuries to a few millennia. Excess volume of serpentine results in filling of pore spaces, eventually inhibiting fluid flow.

### References:

- Afanasyev, A.A., 2013. Application of the Reservoir Simulator MUFITS for 3D Modelling of CO<sub>2</sub> Storage in Geological Formations, Energy Procedia. 40, P.365-374. DOI: 10.1016/j.egypro.2013.08.042.
- Afanasyev A., Costa A., Chiodini G., 2015. Investigation of hydrothermal activity at Campi Flegrei caldera using 3D numerical simulations: extension to high temperature processes. J. Volcanology Geothermal Res. 299: 68-77. DOI: 10.1016/j.jvolgeores.2015.04.004.

Afanasyev, A., Melnik, O., Poritt, L., Schumacher, J., Sparks, R.S.J. 2014. Hydrothermal alteration of kimberlite by convective flows of external water. *Contributions to Mineralogy and Petrology*. 168:1038. DOI: 10.1007/s00410-014-1038-y.

Melnik, O., Afanasyev, A., Zarin G., 2016 .Magma degassing during eruption through water-saturated porous rocks. *Doklady Physics* 61(5):235-238 DOI: 10.1134/S1028335816050074

**Keywords:** reservoir simulation, non-isothermal porous flows, hydrothermal systems, CO<sub>2</sub> sequestration.

## Testing numerical codes for the simulation of 3D thermal convection in faulted geothermal systems

Fabien Magri<sup>1,2</sup>, Mauro Cacace<sup>3</sup>, Olaf Kolditz<sup>1</sup>, Wenqing Wang<sup>1</sup> and Norihiro Watanabe<sup>1</sup>

<sup>1</sup>) Helmholtz Centre for Environmental Research (UFZ), Department of Environmental Informatics (ENVINF) Permoserstraße 15, D04318 Leipzig, Germany;

<sup>2</sup>) Freie Universität Berlin, Hydrogeology, Malteserstr 74-100, 12249 Berlin, Germany

<sup>3</sup>) GFZ – German Research Centre for Geosciences, Telegrafenberg 14473 Postdam, Germany

Corresponding author: fabien.magri@ufz.de

S6- Dynamics of sedimentary Basins, Fluids & Georeservoirs (Oral)

### Summary:

Onset of thermal convection of a single-phase fluid in a vertical fault enclosed in impermeable rocks was considered in a full 3D approximation by Wang et al. (1987). A fundamental result of those investigations was to demonstrate how highly permeable faults allow for onset of free thermal convection even under a normal geothermal gradient. In contrast to simple homogenous 1D and 2D systems, no appropriate analytical solutions exist to test against numerical models of more complex 3D systems that account for variable fluid density and viscosity as well as permeability heterogeneity (e.g. presence of faults). Owing to the importance of thermal convection for the transport of energy and minerals, the development of a benchmark test for density/viscosity driven flow is crucial to ensure that the applied numerical models accurately simulate the physical processes at hands.

The presented study proposes a 3D test case for the simulation of thermal convection in a faulted system that accounts for temperature dependent fluid density and viscosity. The linear stability analysis recently developed by Malkovsky and Magri (2016) is used to estimate the critical Rayleigh number above which thermal convection is triggered.

The numerical simulations are carried out using the finite element technique. OpenGeoSys (Kolditz et al., 2012) and Moose (Gaston et al., 2009) results are compared to those obtained using the commercial software FEFLOW (Diersch, 2014) to test the ability of widely applied codes in matching both the critical Rayleigh number and the dynamical features of convective processes (e.g., Fig. 1). The methodology and Rayleigh expressions given in this study can be applied to any numerical model that deals with 3D geothermal processes in faulted basins.

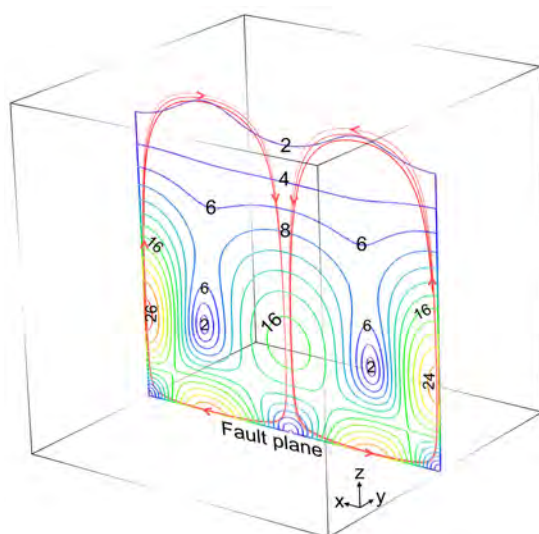


Figure 1: Darcy velocity field displaying thermal convection within a fault plane (modified after Malkovsky and Magri, 2016) The scale of the Darcy velocity is  $1e-9$  m/s and the contour interval is 2.

**References:**

- Kolditz, O., Bauer, S., Bilke, L., Böttcher, N., Delfs, J. O., Fischer, T., U. J. Görke, T. Kalbacher, G. Kosakowski, McDermott, C. I., Park, C. H., Radu, F., Rink, K., Shao, H., Shao, H.B., Sun, F., Sun, Y., Sun, A., Singh, K., Taron, J., Walther, M., Wang, W., Watanabe, N., Wu, Y., Xie, M., Xu, W., Zehner, B., 2012. OpenGeoSys: an open-source initiative for numerical simulation of thermo-hydro-mechanical/chemical (THM/C) processes in porous media. *Environmental Earth Sciences*, 67(2), 589-599.
- Diersch, H. J, 2014. FEFLOW Finite Element Modeling of Flow, Mass and Heat Transport in Porous and Fractured Media, Springer-Verlag Berlin Heidelberg, ISBN 978-3-642-38738-8.
- Gaston D., Newman C., Hansen G., Lebrun-Grandie D, 2009. MOOSE: A parallel solution framework for coupled systems of nonlinear equations. *Nucl. Engrg. Design*, 239, 1,768-1778
- Malkovsky, V. I., Magri, F., 2016. Thermal convection of temperature-dependent viscous fluids within three-dimensional faulted geothermal systems: estimation from linear and numerical analyses, *Water Resour. Res.*, 52, 2855–2867, doi:10.1002/2015WR018001.
- Wang, M., Kassoy, D. R., and Weidman, P. D., 1987. Onset of convection in a vertical slab of saturated porous media between two impermeable conducting blocks, *International Journal of Heat and Mass Transfer*, 30(7), 1331-1341, doi:10.1016/0017-9310(87)90165-7.

**Keywords:** Thermal convection, benchmark, numerical model, fault, geothermal energy.

## **Influence of basement topography on compressive deformation**

Typhaine Caër<sup>1</sup>, Pauline Souloumiac<sup>1</sup>, Pascale Leturmy<sup>1</sup> and Bertrand Maillot<sup>1</sup>

<sup>1</sup>) University of Cergy Pontoise, Lab. Geosciences et Environnement, Cergy-Pontoise, France

Corresponding author: typhaine.caer@u-cergy.fr

S6 Dynamics of sedimentary Basins, Fluids & Georeservoirs (Oral)

### **Introduction:**

It is classically admitted that faults propagate from the depth toward the surface whatever the scale of observation. In an orogen for example, the deformation propagates using shallower and shallower décollements. However fold-and-thrust belts can develop in area prefractured by extensive tectonics. In such cases, the fold-and-thrust belt has formed along a non-planar décollement level disrupted by downward and upward steps. We study the behavior of the compressive deformation that encountered a downward step in the décollement due to basement relief. Does this step systematically generate an abandonment of décollement level? Is it possible to propagate the deformation on the deepened part of the décollement?

### **Method:**

#### *Numerical modeling*

The numerical analysis was carried out with the software OptumG2 using the kinematic approach of the Limit Analysis theory. We realize a parametric study of a prototype composed by a sedimentary bulk in which a décollement level,  $d$ , is disrupted and deepened by a normal fault, that separates this décollement in two parts,  $d_{upper}$  and  $d_{lower}$ .

#### *Sandbox modeling*

The same prototype is reproduced in sandbox in order to validate numerical results by some experiments. The box used is 40 cm length and 28 cm width. The material of the bulk has been modeled by the CV32 sand and the décollement level by Alkor foil®. The base of the model is composed of a paperboard step. The topography is composed of a prism close to the pushing wall and a plateau.

### **Results:**

#### *Numerical results*

Using the limit analysis theory, we demonstrate that for a given set of physical parameters,  $d_{lower}$ , can be reactivated depending on the height of the offset and on the topography above it (Fig. 1). We show that if the topography above the step is completely flat, even a very small step will stop the propagation of the deformation. A low friction on the décollement favors the activation of  $d_{lower}$  while a high friction refrains it. A pre-existing ramp at the upper corner of the step refrains the activation of  $d_{lower}$ , especially if it has a low friction.

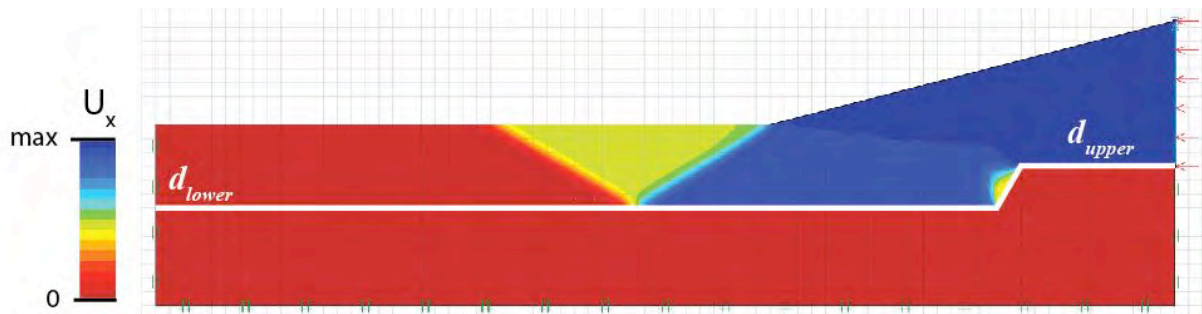


Figure 1: Mechanical result with OptumG2. The deformation propagates beyond the step on  $d_{lower}$ .

### Sandbox results

By sandbox experiments, we validate the results of some precise cases of the numerical parametric study and we illustrate the general behavior in evolution of a deformation that encounter a disruption in the décollement. We show that a step represents a slowdown in the propagation of the deformation front. It acts as a catching point that localizes a ramp until the created topography is sufficient to block the ongoing deformation on this ramp allowing its propagation farther along the lowered portion of the décollement level (Fig. 2). The resulting tectonic style is composed of a stack of faults separated from the following structures by a plateau.

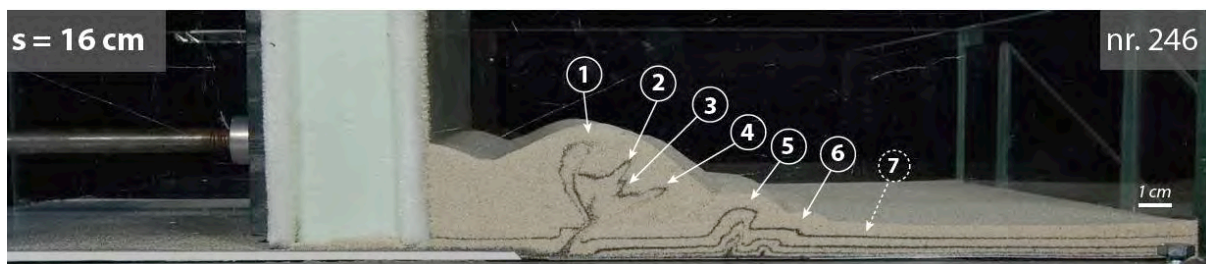


Figure 2: Sandbox result of the evolution of a thrust sequence that encounters a décollement step.

**Keywords:** Limit analysis, sandbox, basement topography, fold-and-thrust belts.

## How syntectonic erosion and sedimentation control the kinematic evolution of a multidecollement fold and thrust zone: Analogue modeling of folding in the southern subandean of Bolivia.

Romain DARNAULT<sup>(1)</sup>, Jean-Paul CALLOT<sup>(2)</sup>, Jean-François BALLARD<sup>(3)</sup>, Jean-Marie MENGUS<sup>(1)</sup>, Jean-Claude Ringenbach<sup>(3)</sup>

(1) IFP Energies nouvelles – 1-4 avenue de Bois Préau, 92852 Rueil-Malmaison, France.

(2) UPPA, I.P.R.A. Avenue de l'Université BP 1155, 64013 Pau Cedex, France.

(3) TOTAL – Exploration Technologies, Avenue Larribau, 64018 Pau Cedex, France.

Corresponding author: romain.darnault@ifpen.fr

S6 Dynamics of sedimentary Basins, Fluids & Georeservoirs (Oral)

Several analogue modeling studies have been conducted during the past fifteen years to discuss the effects of sedimentation and erosion on Foreland Fold and Thrust Belts (FFTB), of which a few have focused on the kilometric scale (Malavieille et al., 1993; Nalpas et al., 1999; Barrier et al., 2002; Pichot and Nalpas, 2009). The influence of syn-deformation sedimentation and erosion on the structural evolution of FFTB has been clearly shown. Here, we propose to go further in this approach by studying a more complex system with a double decollement level. The natural study case is the Bolivian sub-Andean thrust and fold belt, which presents all the required criteria, such as the double decollement level. A set of analogue models performed under a CT-scan have been performed to test the influence of several parameters on a fold and thrust belt system, of which: (i) the spatial variations in the sediment input, (ii) the spatial variations in the erosion rate, (iii) the relative distribution of sedimentation between foreland and hinterland. These experiments led to the following observations:

1. The upper decollement level acts as a decoupling level in case of increased sedimentation rate: it results in the verticalization of the shallower part (above the upper decollement level) while the deeper parts are not impacted.
2. Similarly, the increase in the erosion rate involves the uplift of the deeper part (below the upper decollement level) whereas the shallower parts are not impacted.
3. A high sedimentation rate in the foreland involves a fault and fold vergence reversal, followed by a back-thrusting of the shallower part.
4. A high sedimentation rate in the hinterland favors thrust development toward the foreland in the shallower parts.

### References:

- Barrier, L., Nalpas, T., Gapais, D., Proust, J.-N., Casas, A., Bourquin, S., 2002. Influence of syntectonic sedimentation on thrusts geometry. Field examples from the Iberian Chain (Spain) and analogue modeling. *Sedimentary Geology* 146, 91–104.
- Malavieille, J., Larroque, C., Calassou, S., 1993. Experimental modelling of tectonic/sedimentation relationships between forearc basin and accretionary wedge. *C. R. Acad. Sci. Paris* 316, 1131e1137.
- Pichot T., Nalpas T., 2009. Influence of synkinematic sedimentation in a thrust system with two decollement levels; analogue modelling. *Tectonophysics* 473, 466-475.

## **High-resolution numerical modelling to resolve fluid pathways generation in porous rocks**

Ludovic Räss<sup>1</sup>, Thibault Duretz<sup>1</sup> and Yuri Podladchikov<sup>1</sup>

<sup>1</sup>) University of Lausanne, Institute of Earth Sciences, Lausanne, Switzerland  
ludovic.raess@unil.ch

Corresponding author: ludovic.raess@unil.ch

S6- Dynamics of sedimentary Basins, Fluids & Georeservoirs (Oral)

### **Introduction:**

Vertical pipe structures are widely observed in many subsurface reservoirs on Earth. Because of their economical interest, an important number of geophysical surveys are performed in these regions. The acquired seismic cross-sections provide reliable data about the shape and the main characteristics of those vertical pipes; their elevated permeability makes them preferential pathways for fast vertical fluid flow. Besides the qualitative understanding of those features, there is a need to quantitatively understand the viable physical mechanisms leading to the formation of these high permeability pipes.

### **Method:**

In that context, we propose a physical model that predicts the formation and the evolution of high permeability pipes in porous media. We designed a finite difference model that strongly couples a Stokes solver to a nonlinear Darcy flow, in two and three dimensions (2D and 3D). We also take into account in our models porosity-dependant permeability and rheologies that are representative of common reservoir rock types. The 2D model is implemented using a Newton based solver in Matlab. The 3D model uses an iterative matrix free scheme that runs in parallel on multiple graphical processing units (GPUs) using C-Cuda and MPI.

### **Results:**

We conduct numerical simulations and show the formation and propagation of high permeability and high porosity pipes as a natural outcome of the coupling of the solid matrix deformation to fluid flow (Figure 1). We discuss the treatment of multi-physics coupling and the importance of accurately resolving the nonlinearities. We finally show that the Newton based and the matrix free approaches converge to identical results. Both approaches capture the generation and evolution of fluid pathways. In that context, matrix free algorithms are attractive because they are performing very well on HPC implementations in 3D and are very comprehensible.

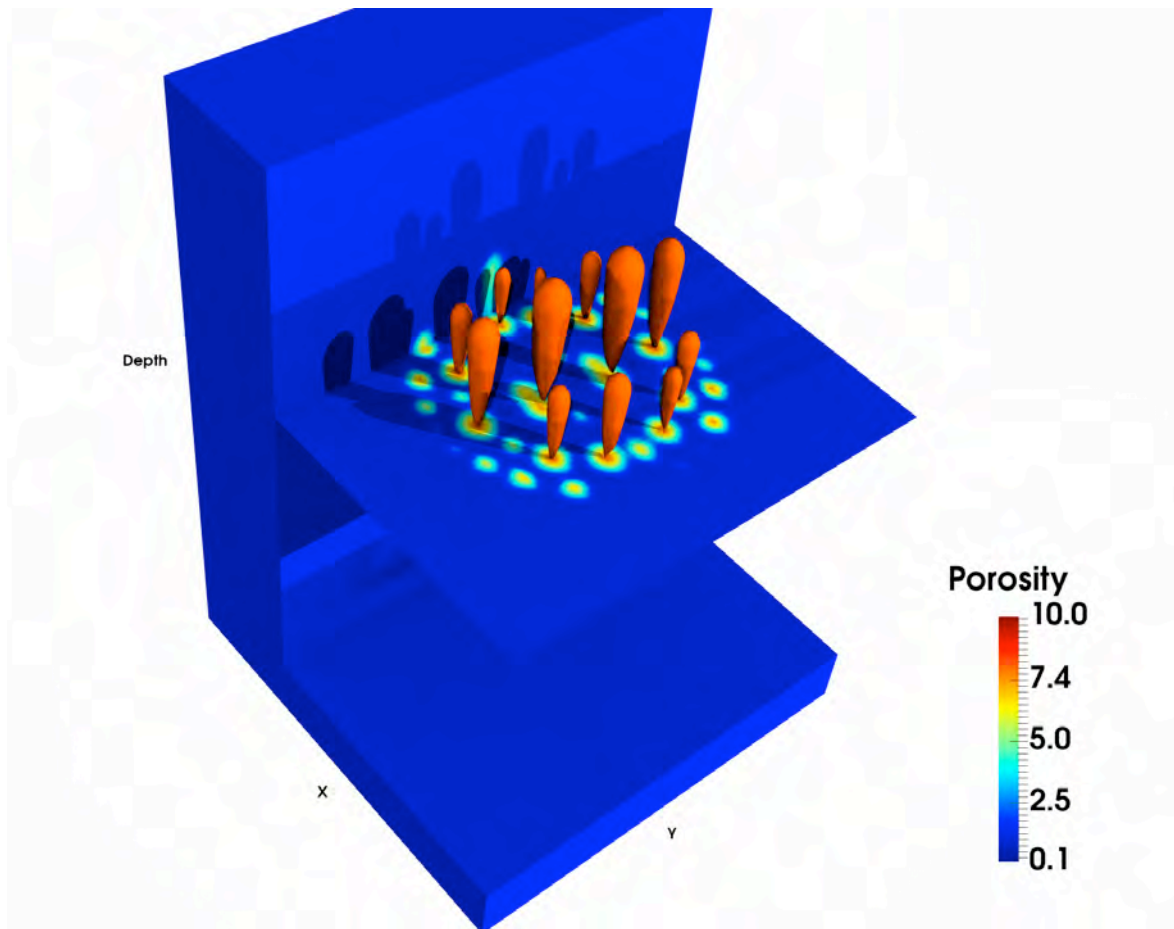


*Figure 1: 3D normalized porosity distribution of a fluid filled visco-elasto-plastic deforming porous media sample compacting under gravity. The initial porosity distribution, a 3D ellipsoid, evolves into distinct pipe structures of elevated porosity and permeability. Fluid flow within these pipes increases more than two orders of magnitude compared to background values.*

**Keywords:** Fluid pathways, pipe structures, two-phase solver, finite-differences, high-resolution, GPU.

## Impact of an interbedded viscous *décollement* on the along-strike segmentation of fold-and-thrust belts: insights from analogue modeling.

Sandra Borderie<sup>1</sup>, Fabien Graveleau<sup>1</sup>, César Witt<sup>1</sup> and Bruno C. Vendeville<sup>1</sup>

<sup>1</sup>) Univ. Lille, CNRS, Univ. Littoral Côte d'Opale, UMR 8187, LOG, Laboratoire d'Océanologie et de Géosciences, F 59000 Lille, France

Corresponding author: sandra.borderie@gmail.com

S6 - Dynamics of sedimentary Basins, Fluids & Georeservoirs (Oral)

Fold-and-thrust belts can be segmented both across and along strike because of diverse factors, including tectonic and stratigraphic inheritance. Along-strike stratigraphic changes in the foreland are classically observed and very often cause a curvature of the deformation front. Although the parameters controlling this curvature are well documented, the structural interactions and mutual influences between adjacent provinces displaying contrasting rheologies are much less analyzed. To investigate this issue, we performed a set of analogue experiments in a compressional box. Models were shortened above a basal frictional detachment (glass microbeads) and segmentation was tested by having a region in which a viscous level (silicone polymer) was interbedded within the sedimentary cover (dry sand). Two models made with and without the interbedded viscous levels provided end-member tests. By changing the relative width of the frictional (F) and viscous (V) provinces, we characterized geometrically and kinematically the dynamic interactions between both provinces.

Our results indicate that there are reciprocal influences between V and F provinces. First, the deformation kinematics in the V province is impacted by the presence of the adjacent F province. This influence depends on the width of the V province. Indeed, narrow V provinces display in sequence propagation of shallow thrusts, whereas wide V provinces display an out-of-sequence mode of deformation propagation. This results in the deformation front to reach lately the external *décollement* pinchout in the former case, but to reach it much more rapidly in the latter. In the latter case (wide V province), once deformation has reached the external *décollement* pinchout, the trend of younger thrusts in the V province near the lateral limit between the adjacent provinces are oblique with respect to the direction of shortening.

In addition, the structural style in the V provinces is significantly impacted by the adjacent F province. It notably triggers the distinction between three distinct structural styles along strike. Indeed, far from the F province, structures are primarily of salt-massif type. They do not seem to be influenced by the F province because they correspond to the structural style observed in the end-member V model. Towards the F province, deformation changes gradually to a zone of purely forethrusts (foreland verging thrusts), and finally to a highly faulted zone with both fore- and backthrusts.

Second, along-strike segmentation in the foreland stratigraphy affects the deformation kinematics of thrusts rooting at depth in the basal frictional *décollement*. In one-province end-member models, the deep deformation front is located very much backward in the V model, but is located extremely forward in the F model. In the two-province models (adjacent F and V provinces), the position of the deformation front at depth in the F province is much more backward than in the end-member model. Similarly, the position of the deep deformation front in the V province is much more forward than in the end-member model. Therefore, two adjacent F and V provinces influence mutually the dynamics of propagation of the deep deformation front by restraining it backward in the F province and pushing it forward in the V province.

Finally, we compare our experimental results with natural examples in the Kuqa basin (Southern Tian Shan, China), or the Franklin Mountains (NW Canada), which allow a better understanding of the dynamics of salt-bearing fold-and-thrust belts.

**Keywords:** Analogue modeling, fold-and-thrust belt, along-strike segmentation, viscous décollement.

## **Burial history characterization of Ordovician reservoir (Bir Ben Tartar Formation) in South Remada region (South east of Tunisia)**

Imen Arfaoui<sup>1</sup>, Anis Belhaj Mohamed<sup>2</sup>, Najet Slim-Shimi<sup>3</sup>, Moncef Saidi<sup>4</sup> and Mabrouk Montacer<sup>4</sup>

<sup>1</sup>) University of Gabes, Research Unit of Géosystèmes, Géoressources, Géoenvironnements, Tunisia

<sup>2</sup>) Tunisian petroleum company, Lab. of Organic geochemistry, Tunis, Tunisia

<sup>3</sup>) University of Tunis, Head of geology department, Tunis, Tunisia

<sup>4</sup>) Tunisian petroleum company, Head of Lab. of Organic geochemistry, Tunis, Tunisia

<sup>5</sup>) University of Gabes, Head of Research Unit of Géosystèmes, Géoressources, Géoenvironnements, Tunisia

Corresponding author: imenarfaoui1@outlook.fr

S6- Dynamics of sedimentary Basins, Fluids & Georeservoirs (PS7)

### **Introduction:**

The Northern side of Ghadames basin is known as the most important petroleum province. Geochemical data, in South Remada region, indicates that the hot shale layer of the Tannezuft Formation is the main source rock which has been charged the Ordovician reservoir. According to Ghnima (1993), this formation represents the origin of 80-90% Paleozoic sourced hydrocarbons on the entire Saharan Platform.

The reconstruction of the burial history and thermal history of this layer was established by coupling two different disciplines:

The 1D geochemical modeling of the well localized in Bir Ben Tartar Region, and the microthermometry by measuring the homogenization temperature of the fluid inclusions trapped into the quartz grains of the Ordovician reservoir. The found results provide important clues to remodel the diagenetic events observed over time.

### **Geochemical modeling:**

According to the model made by the BasinMod-1D software, we deduce that the heat flow varies between 60 °C and 80 °C (Fig.1), related to a thickness of 84m in Silurian series in Bir Tartar region.

During the Ordovician in the same region, the widespread extension and crustal thinning are expected to cause an increase in heat flow, which is estimated on average 100 ° C.

This variation of the heat flow over time can be explained by the presence of major structural events that have affected the study area. Indeed the Hercynian compression leads to a significant crustal thickening inducing rapid reduction of heat flow (Makhous, 2001).

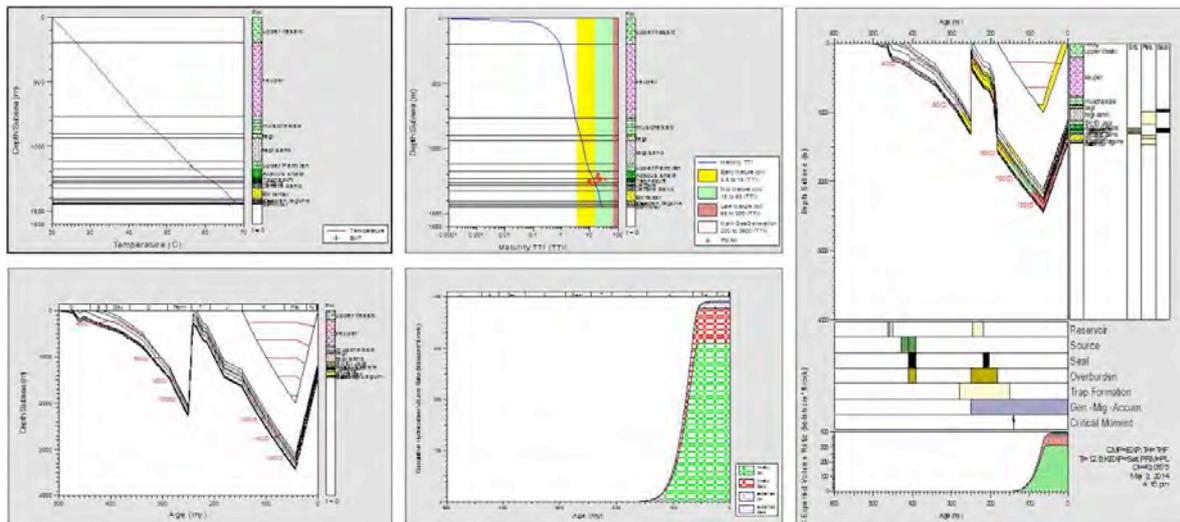


Figure 1: Basin modeling and Petroleum Event Chart of Bir Ben Tartar well

**Fluid Inclusions assessment:**

Fluid inclusions analyzed by microthermometry are also known as indicative of trapping conditions and petroleum fluid flow. The high density and low pressure describe the trapping physical characteristics of mineral Banking (Fluid inclusions are trapped in detrital quartz grain, well-rounded morphology). The measured salinity is high, on average  $\approx 25\%$  weight eq. NaCl (Fig.2). This external fluid is acid circulating in the Ordovician reservoir may come from the Silurian source rock which has expelled fluids rich in organic acids during the landfill (Tournier, 2010). These burial temperatures are consistent with the homogenization temperatures measured in aqueous two-phase fluid inclusions (surrounding of  $102^\circ\text{C}$ ).

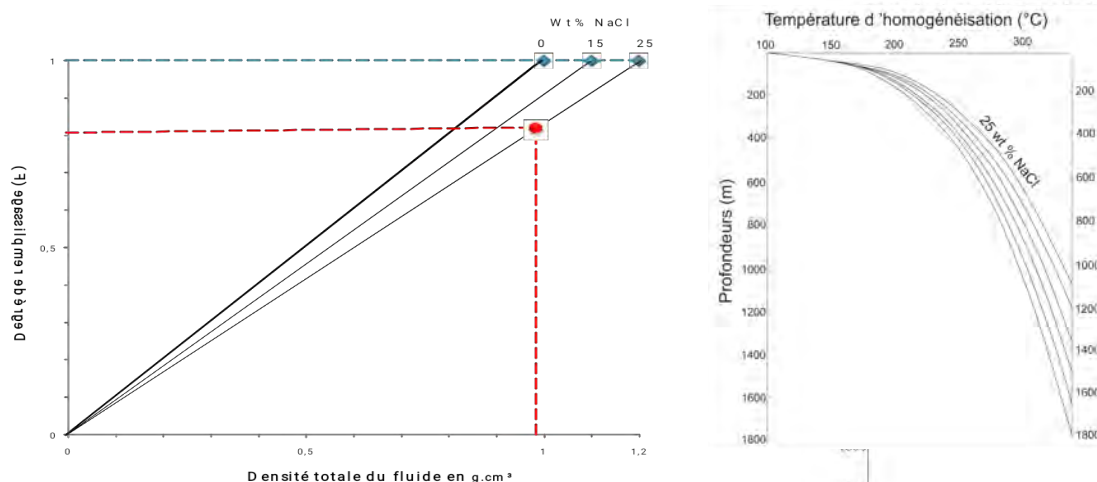


Figure 2: Relationship between the degree of charging ( $F$ ) at  $25^\circ\text{C}$  and the total density of the inclusions for different solutions of NaCl (Clifton H. et al., 1985).

**References:**

Clifton H., Shepherd T.J., Rankin A.H. & Alderton D.H.M. (1985): A practical guide to fluid inclusion studies, 222p.

- Ghénima R. (1993): Etude des roches mères paléozoïques du bassin de Ghadamès. Modélisation de la migration des hydrocarbures et application à l'étude du gisement d'El Borma. Thèse de l'Université d'Orléans, 276p.
- Makhous M., (2001): the formation of hydrocarbon deposits in the North African Basins. Geological and Geochemical Conditions, Springer, 329p.
- Tournier F. (2010): Mécanismes et contrôles des phénomènes diagénétiques en milieu acide dans les grès de l'Ordovicien glaciaire du bassin de Sbaa, Algérie. Thèse de doctora de l'université de Paris Sud, 403p.

**Keywords:** Modeling, Geochemistry, reservoir, Petroleum, Fluid Inclusion.

## Mechanical restoration of gravity-driven deformations using Limit Analysis Theory: the Baram delta in NW Borneo.

Josselin Berthelon<sup>1</sup>, Xiaoping Yuan<sup>2</sup>, Antoine Bouziat<sup>3</sup>, Pauline Souloumiac<sup>1</sup>, Bertrand Maillot<sup>1</sup> and Tristan Cornu<sup>4</sup>

<sup>1</sup>) University of Cergy Pontoise, Lab. Geosciences et Environnement, Cergy-Pontoise, France

<sup>2</sup>) Laboratoire de Géologie, UMR 8538, CNRS, École Normale Supérieure, Paris, France

<sup>3</sup>) IFP Energies nouvelles, 1 & 4 Avenue de Bois Préau, Rueil-Malmaison, France

<sup>4</sup>) TOTAL, CSTJF, Avenue Larribau, Pau, France

Corresponding author: josselin.berthelon@live.fr

### S6- Dynamics of sedimentary Basins, Fluids & Georeservoirs (PS7)

The Baram Delta System, Brunei, NW Borneo, is a tertiary delta system nested in the crustal-scale Borneo collapse system (Sapin et al, 2010) (Figure 1a). The margin failure is accommodated by proximal extension and distal shortening corresponding to gravity spreading above a miocene shale décollement (Figure 1b). In the offshore Baram delta, seismic resolution and well-correlations are lacking to thoroughly describe the calendar of the late pliocene-pleistocene gravity-driven deformations, in order to reduce structural uncertainties of the kinematic scenarios of basin deformation.

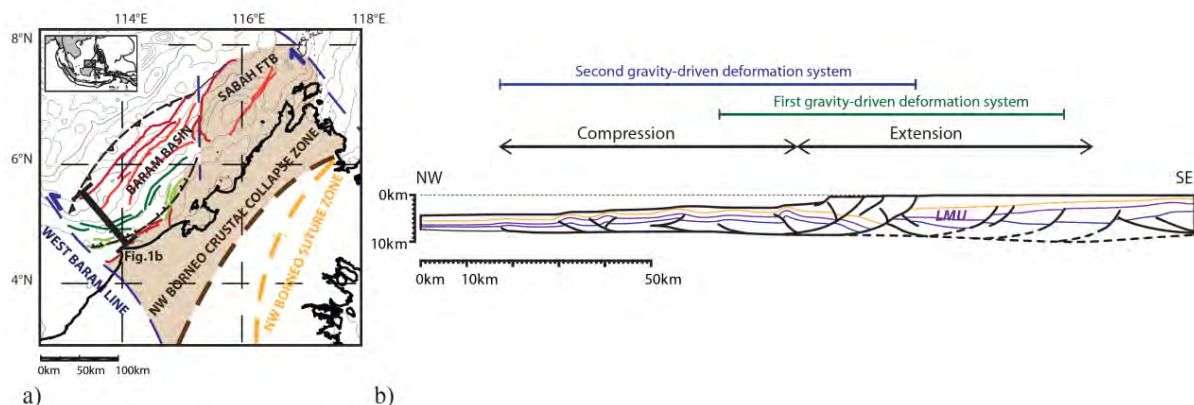


Figure 1: a) Tectonic map of N.W. Borneo and b) interpreted depth-converted seismic section of the Baram Delta (modified from Sapin, 2010).

In this work, we aim to restore the geological evolution of the Plio-Pleistocene Baram Delta, respecting mechanical equilibrium, volume conservation and the maximum rock strength. These gravity-driven deformations are constrained using the kinematic approach of limit analysis, considering geological materials as overpressured Coulomb frictional materials. SLAMTec (Sequential Limit Analysis Method for Tectonic) is a forward method that detects at each increment of sedimentation a possible gravitational collapse, with an optimum normal fault and thrust-fold emplacement, and updates the basin geometry using a set of geometrical rules (Mary et al, 2013; Yuan, in prep.).

1782 simulations are run to explore the influence of the sedimentation processes, fluid overpressure and sediments internal friction angle on the Plio-Pleistocene gravity-driven deformations. Boundary conditions consist of two fixed walls, a décollement angle ( $\beta$ ) of  $1.8^\circ$  and a topographic slope ( $\alpha$ ) divided in three segments of  $0^\circ$ ,  $2^\circ$  and  $-0.8^\circ$ . The sedimentation model is defined by three parameters:

proximal aggradation, distal aggradation and shelf progradation, tested respectively from 2.5 to 3.5km, 1 to 2km and 25km to 35km. The explored bulk and décollement effective friction angles ( $\phi'b$ ;  $\phi'd$ ) are comprised between  $9^\circ$  to  $14^\circ$  and 0.05° to 0.7°. Assuming dry internal friction angles of  $20^\circ$  and  $10^\circ$  for the bulk and décollement, it corresponds to a fluid overpressure gradient ( $\Delta\lambda$ ) ranging respectively from 0.42 to 0.31 and 0.577 to 0.54. Model results show that a high fluid overpressure is necessary to create the conditions for gravitational collapse, while the margin stability is critically linked to the rates of shelf aggradation and progradation. Eight quantitative criteria are defined to grade the 1782 models compared to the available data. As in the inversion theory approach, these are used to point the models that match the best the interpreted seismic section (Figure 1b). One of these models is displayed in Figure 2.

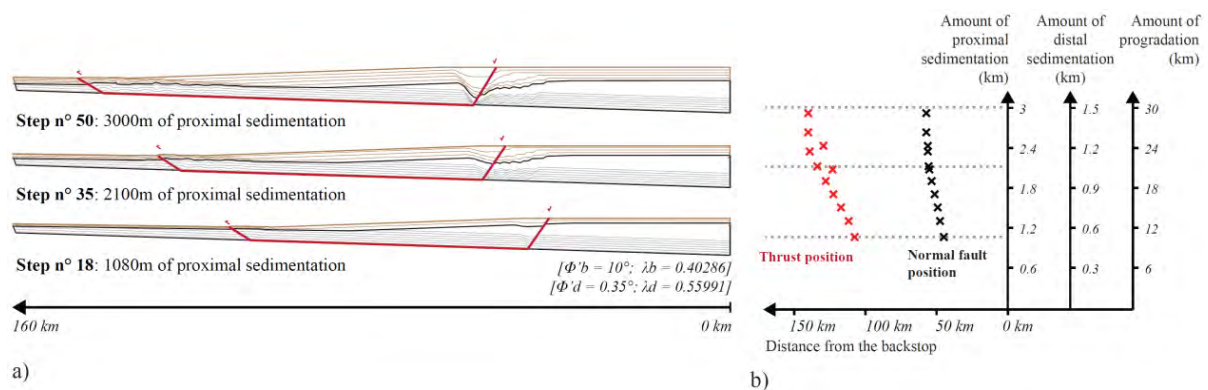


Figure 2: a) Modeled evolution of the Brunei collapsed system for  $[\phi'd=0.35^\circ; \phi'b=10^\circ]$  and b) Position of the normal fault/thrust fault couples during the sedimentation.

In this example, the major structural features of the Brunei margin have been successfully modeled. However, the two successive gravity-driven systems observed in Figure 1b cannot be explained with constant parameters. We suggest that evolutionary sedimentation and mechanical parameters are necessary to model this structural feature. As such, this study highlights the existence of distinct deformation sequences during the Plio-Pleistocene in the Baram delta, each characterized by different sedimentation models and/or pore pressure values. The lessons learned from this work are used to conceive a “mechanically balanced” structural restoration, including information on the fluids overpressure, sedimentation model and mechanical parameters that controlled its evolution.

## References:

- Mary, B., Maillot, B., Leroy, Y., 2013. Deterministic chaos in frictional wedges revealed by convergence analysis, *Int. J. Numer. Anal. Method Geomech.*, 37(17),
- Sapin, F., 2010. Impact du couple érosion/sédimentation sur la structuration d'un prisme d'accrétion : L'exemple du prisme NO Borneo Approche géologique, sismique et thermique (PhD thesis). UPMC, Paris
- Yuan, XP, Leroy YM, Maillot B. Reappraisal of gravity instability conditions for offshore wedges: consequences for overpressures in the Niger Delta, in preparation.

**Keywords:** Brunei, gravity-driven deformations, mechanical restoration, numerical modeling.

## Late extension in compressional wedges above an interbedded weak, viscous *décollement*: results from analogue modeling

Sandra Borderie<sup>1</sup>, Bruno C. Vendeville<sup>1</sup>, Fabien Graveleau<sup>1</sup> and César Witt<sup>1</sup>

<sup>1</sup> Univ. Lille, CNRS, Univ. Littoral Cote d'Opale, UMR 8187, LOG, Laboratoire d'Océanologie et de Géosciences, F 59000, France

Corresponding author: sandra.borderie@gmail.com

S6- Dynamics of sedimentary Basins, Fluids & Georeservoirs (PS7)

Extension during convergence is a structural process commonly encountered in different geodynamic settings, such as accretionary wedges subjected to tectonic erosion, or mountain belts undergoing post-orogenic collapse. This has been investigated with experimental models at the scale of doubly-vergent wedges (Bonini et al., 2000; Buck and Sokoutis, 1994; Haq and Davis, 2008); but not thoroughly at the scale of fold-and-thrust belts. During an experimental investigation carried out on the behavior of segmented fold-and-thrust belts induced by stratigraphic inheritance in the foreland series, unexpected shallow normal faulting occurred during the latest stages. The models comprised one basal frictional *décollement* (glass microbeads) and one upper viscous *décollement* embedded in the cover (silicone polymer) (Fig. 1).

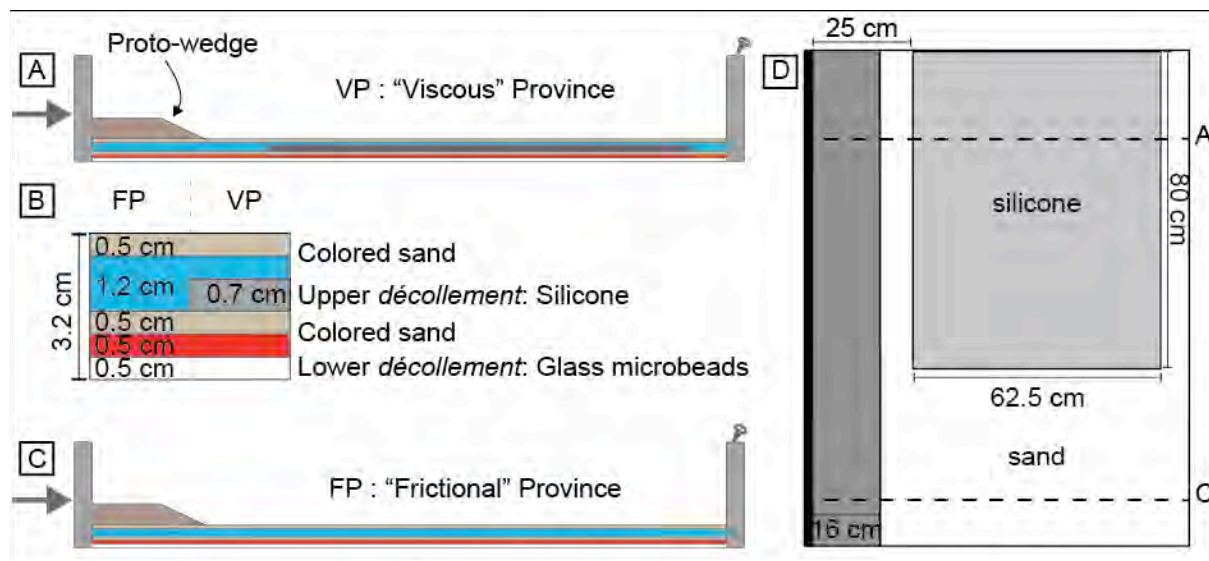


Figure 1: Boundary conditions of a two-province model. A to C: With and without an interbedded silicone *décollement* in the foreland. D: Map-view of the silicone location in one of the models.

Extension took place during the late stages of the experiments (about after 20 cm of shortening) and it was localized at the transition zone between the rear domain of the wedge and the frontal fold-and-thrust belt that detached on the upper viscous *décollement* (Fig. 2-A). Normal faults strike parallel to the compressional structures and mainly dip toward the foreland. They root in the viscous *décollement* and are locally contemporary to diapiric piercement, leading to the formation of silicone tongue (Fig. 2-B). Through a series of parametrized experiments dedicated to constrain the timing of formation of these extensional structures, we could evidence that these normal faults appear once the bulk shortening in the rear domain has created enough uplift of the internal zone by antiformal

stacking and enough forelandward tilting of the upper viscous *décollement*. These two latter mechanisms are direct consequences of the whole wedge dynamics that links the thrust fault dynamics in the upper shallow sedimentary sequence and the thrust dynamics of the deep layers. The occurrence of this extension depends on the initial position of the upper viscous *décollement* and notably the position of the internal pinchout with respect to the position of the backstop. Additional tests have also demonstrated that this extension is prevented by sedimentation. We compare our experimental findings with natural examples of accretionary systems across the world (e.g. the Mediterranean ridge).

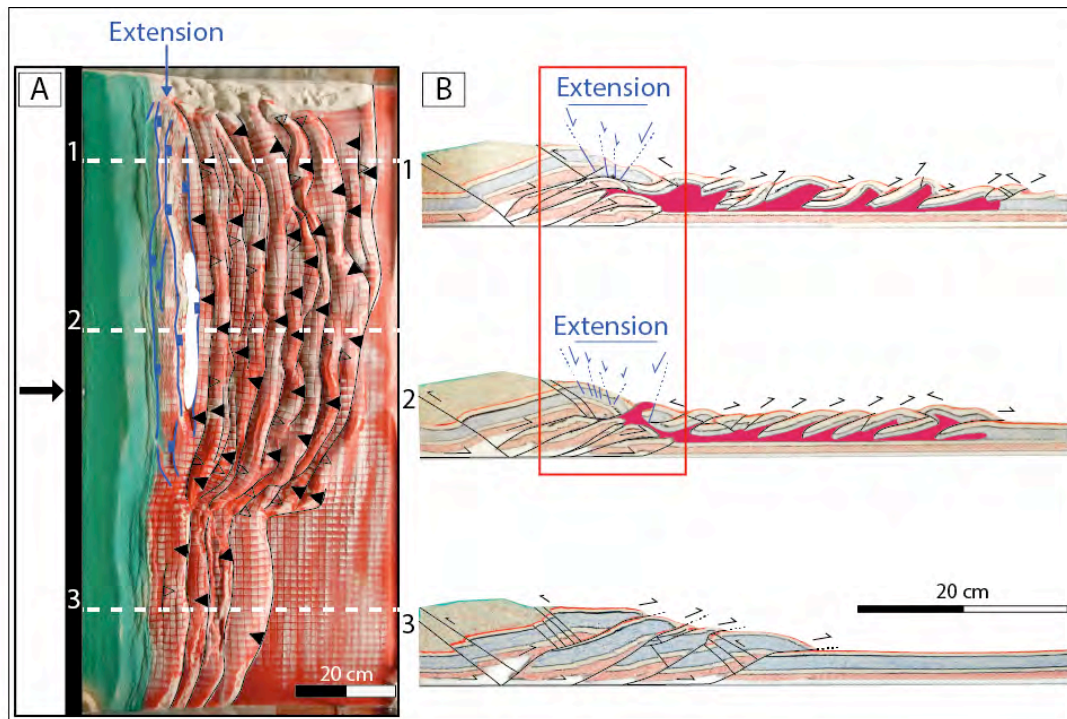


Figure 2: A: Final stage in map-view of a two-province model (see boundary conditions Fig. 1-D). Empty triangles are for backthrusts, full triangles are for forethrusts. Normal faults are in blue. B: Serial cross sections of the model (see location in A). Normal faults are located at the transition between the inner and the outer part of the wedge. They root in the silicone upper *décollement*.

### References:

- Bonini, M., Sokoutis, D., Mulugeta, G., Kattrivanos, E., 2000. Modelling hanging wall accommodation above rigid thrust ramps. *J. Struct. Geol.* 22, 1165–1179.
- Buck, W.R., Sokoutis, D., 1994. Analogue model of gravitational collapse and surface extension during continental convergence. *Nature* 369, 737–740. doi:10.1038/369737a0
- Haq, S.S., Davis, D.M., 2008. Extension during active collision in thin-skinned wedges: Insights from laboratory experiments. *Geology* 36, 475–478.

**Keywords:** Analogue modeling, fold-and-thrust belts, syncontractional extension, salt *décollement*.

## Along-strike structural coupling in fold-and-thrust belts controlled by lateral changes in basal *décollement* strength: results from analogue modeling

Sandra Borderie<sup>1</sup>, Fabien Graveleau<sup>1</sup>, Bruno C. Vendeville<sup>1</sup>, César Witt<sup>1</sup> and Alexandra Skrubelj<sup>1</sup>

<sup>1</sup> Univ. Lille, CNRS, Univ. Littoral Cote d'Opale, UMR 8187, LOG, Laboratoire d'Océanologie et de Géosciences, F 59000, France

Corresponding author: sandra.borderie@gmail.com

S6- Dynamics of sedimentary Basins, Fluids & Georeservoirs (PS7)

Fold-and-thrust belts can be segmented along-strike because of changes in the lithology of the basal *décollement* in the foreland. This change can be generated by sedimentary variations along the strike in the initial filling, for instance when a viscous evaporite level evolves laterally toward a frictional detrital layer. Such variations in basal *décollement* strength classically lead to a curvature of the deformation front (Cotton and Koyi, 2000) and to the development of a complex transfer zone between adjacent foreland domains (Calassou et al., 1993). Although several parameters controlling this curvature have been well documented (Marshak, 2004), the structural and kinematics interactions between adjacent provinces having contrasting rheologies have been investigated much less.

In order to answer to this question, we carried out a set of analogue models in a 60 cm wide and 90 cm long experimental box (Fig. 1). We used medium quartz sand and a silicone polymer to model frictional and viscous natural rheologies, respectively. Boundary conditions were designed to test how fold-and-thrust belt dynamics change as a function of the relative width of the adjacent viscous and purely frictional provinces. We built a total of four models: 1) two end-member models with either a purely frictional or a viscous *décollement* across the entire model's width (Fig. 1 D-E); and 2) two intermediate models comprising 1/3 and 2/3 of either a viscous or purely frictional *décollement* (Fig 1 F-G). Models were all laterally lubricated using a silicone coating along the glass sidewall in order to reduce lateral edge effects.

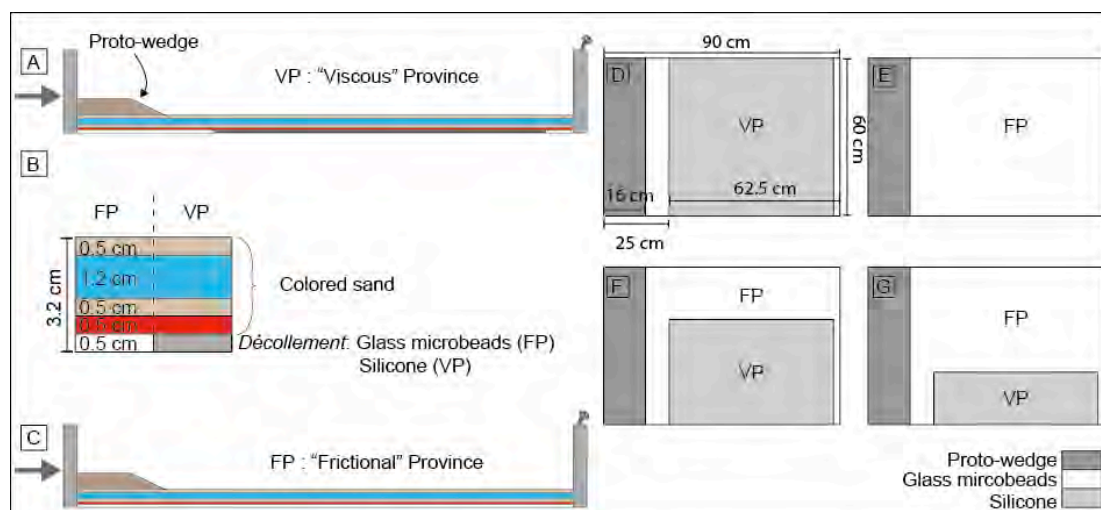


Figure 1: Boundary conditions of the set of models. A to C: Side views of the box filling with or without a viscous *décollement* in the foreland. D to G: Map views of the location of the rheological provinces (frictional and viscous provinces). D: 100% frictional, E: 100% viscous, F: 66% frictional / 33% viscous and G: 66% frictional / 33% viscous

Deformed models indicate that regardless of the relative width of the purely frictional vs viscous province, the deformation style and kinematic of the frictional province is not impacted significantly by the adjacent viscous province. By contrast, the deformation kinematics in the viscous provinces is significantly influenced by the presence or absence of an adjacent frictional province. Indeed, deformation kinematics in the viscous province is typically “out of sequence” in the one-province end-member model having a viscous *décollement* all across its width (Fig. 2.A). It becomes “in sequence” in both two-province models (Fig. 2.B-C). Therefore, this suggests that a purely frictional province prevents the deformation in the adjacent viscous province from propagating rapidly outward (and thus “out-of-sequence”) because of the lateral friction that opposes the advance of the deformation front. Interestingly, no significant change in the structural style was observed in the viscous provinces despite the change in deformation propagation sequence.

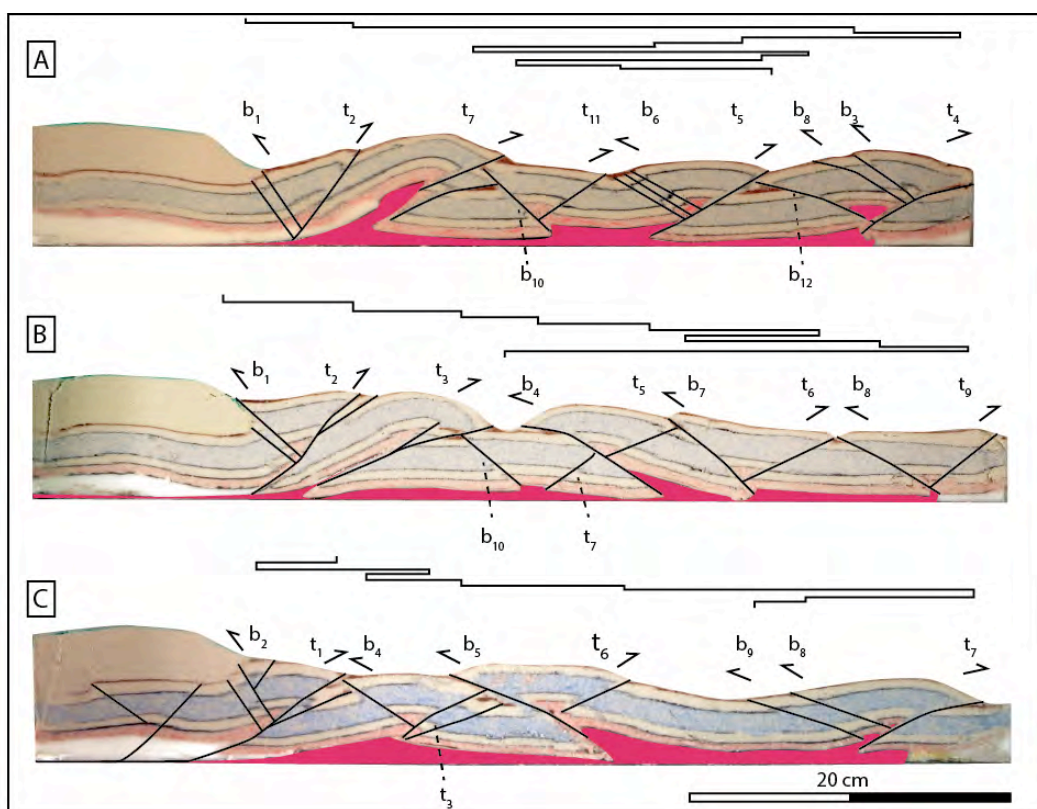


Figure 2: Final cross-sections of three viscous provinces. The viscous *décollement* is in pink, the thrusts are in black. The deformation sequence is given by numbered forethrusts (*t*), backthrusts (*b*), and by the lines above the cross-sections. A: Cross-section in the 100% viscous model. Deformation propagates rapidly to the silicone pinchout and is out of sequence. B and C: Cross-sections in the 66% and 33% viscous model, respectively. Deformation propagates lately to the silicone pinchout and is in sequence.

### References:

- Calassou, S., Larroque, C., Malavieille, J., 1993. Transfer zones of deformation in thrust wedges: an experimental study. *Tectonophysics* 221, 325–344.
- Cotton, J.T., Koyi, H.A., 2000. Modeling of thrust fronts above ductile and frictional detachments: application to structures in the Salt Range and Potwar Plateau, Pakistan. *Geol. Soc. Am. Bull.* 112, 351–363.

Marshak, S., 2004. Salients, Recesses, Arcs, Oroclines, and Syntaxes - A Review of Ideas Concerning the Formation of Map-view Curves in Fold-thrust Belts. *Thrust Tecton. Hydrocarb. Syst. AAPG AAPG Mem.* 82, 131–156.

**Keywords:** Analogue modeling, Fold-and-thrust belt, along-strike segmentation, viscous décollement

## **Coupled Thermo-Hydraulic (TH) modelling of geothermal systems – a review from the geothermal facility at Groß Schönebeck, North Germany**

Mauro Cacace<sup>1</sup>, Guido Blöcher<sup>1</sup>, Norihiro Watanabe<sup>3</sup>, Antoine Jacquy<sup>1</sup>, Florian Wellmann<sup>2</sup>, Ernst Huenges<sup>1</sup>, Magdalena Scheck-Wenderoth<sup>1,2</sup>

<sup>1</sup>) GFZ – German Research Centre for Geosciences, Potsdam Germany

<sup>2</sup>) RWTH Aachen University, Aachen Germany

<sup>3</sup>) Helmholtz Centre for Environmental Research UFZ Leipzig, Germany

Corresponding author: mauro.cacace@gfz-potsdam.de

S6- Dynamics of sedimentary Basins, Fluids & Georeservoirs (PS7)

Determining transport processes in natural faulted and fractured geological systems has been receiving increasing attention for different applications in geosciences. Examples comprise oil and gas and geothermal recovery and CO<sub>2</sub> capture and sequestration. In this study, we present the results from recent efforts in modelling coupled thermal and hydraulic processes occurring in complex natural settings comprising a heterogeneous sedimentary matrix structure, discrete geological discontinuities, i.e. faults and fractures, and geothermal wells. We use novel modelling concepts to integrate into forward dynamic models details of 3D geological architecture of faulted/fractured geological systems at different scales (from regional to the reservoir scale). As such, these models enable to fully account for the coupling between non-linear physical hydro-thermal processes given their proper temporal and spatial scales and to specifically investigate and quantify interactions between discrete flow paths through and across faults and fractures and within the porous rock matrix.

### **Regional scale models:**

We carried out numerical coupled hydraulic and thermal simulations focusing on the region of Brandenburg, Northeast German Basin. The goal of this study is to investigate the impact of major fault zones on the groundwater circulation system and on the thermal field for the area of Brandenburg in northeast Germany. For this purpose, two regional fault zones – the Gardelegen and Lausitz Escarpments – have been integrated into an existing 3D structural of the study area. The study has indicated specific yet unclear interactions between major fault zones and neighboring sediments. The hydrodynamic and thermal influence of faults is structurally linked to their internal permeability architecture and the nature of hydrogeological connectivity with hosting heterogeneous sediments. Highly permeable fault zones focusing and channeling fluid flow has a strong impact on both the thermal and pressure field in the surrounding sedimentary domains. In contrast, low permeable fault zones impact only on the pressure evolution of the nearby sediments. Depending on the fault permeability structure, their geometry, fault zones may dynamically interact with the regional groundwater circulation in quite distinct ways giving rise to the formation of domains of abnormal pressures and thermal anomalies, which may extend further in the surrounding porous host matrix.

### **Reservoir scale models:**

The results from regional studies have shed new information on the large-scale hydrodynamics of sedimentary basins characterized by major fault zones in their interior. In addition to the regional picture, existing fault zones and fractured domains modify the overall reservoir permeability structure and therefore change the flow dynamics of the reservoir. Apart for an accurate description of the parameter space, to correctly simulate operating scenarios under different working conditions requires a detailed representation of the geometry of the target formations comprising local inhomogeneity characterizing the natural system.

Recent numerical modelling studies focused on improving our understanding of the geothermal reservoir dynamics at the Groß Schönebeck geothermal reservoir. In these studies, TH numerical forward simulations of the reservoir behavior during geothermal fluid injection and production have been carried out. These have been combined with an integrative study aiming at identifying uncertainties in the geological data in order to evaluate their influence on the outcome of the process simulation. The results have demonstrated that existing fault zones and induced fractures modify the overall reservoir permeability structure and therefore change the flow dynamics of the reservoir, see Fig. 1. This has a great impact on the productivity of the same reservoir, which can be enhanced or reduced depending on the fracture network architecture and their location with respect to the producing well.

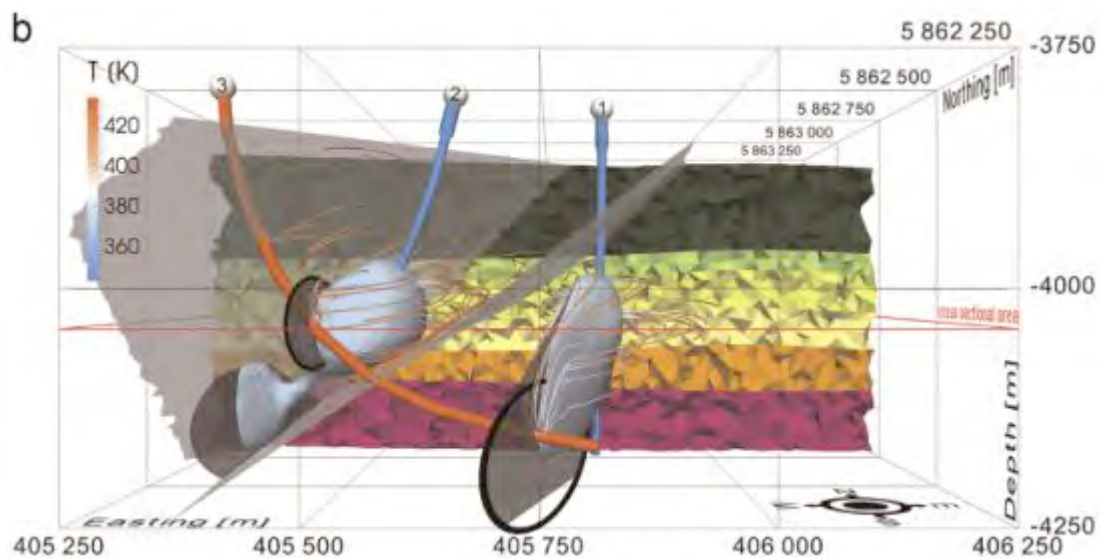


Figure 1: Example of a simulation results after 30 years for the Groß Schönebeck geothermal reservoir.

The results, as constrained against available data, demonstrate the relevance of the approach to improve current predictive capabilities of reservoir models with a combined consideration of their uncertainties in rock properties and structural features.

Based on the results obtained for the current situation of the reservoir, additional simulations have been carried out with the aim to find optimal well designs to improve both its performance and long-term sustainability. This latter study shows that a hybrid concept combining both matrix and fracture-dominated flow paths between the production and the injection wells could significantly increase the reservoir productivity and prolongs the time before the onset of thermal breakthrough.

Ongoing work focuses on integrating additional processes that have yet to be fully quantified. These include mechanical-chemical processes related to the presence of free gas and two-phase flow in the reservoir (e.g. nearby the well screen), chemical precipitates in the wellbore, chemical alteration of the porous matrix, and mechanical sustainability of hydraulically induced fractures and barrier effects of internal fault zones which could harm the sustainability of the overall system under production.

**Keywords:** Geothermal Reservoir Analysis, Coupled Thermal and Hydraulic Processes, Numerical Modelling, Groß Schönebeck.

## Physicochemical characterization of Miocene sands of Bou Chebka (Kasserine: South West of Tunisia) and industrial valorization assessment

I. Maâlla<sup>1</sup>, A. Sebei<sup>1</sup>, S. Boussen<sup>1,2</sup>, F. Chaabani<sup>1</sup>, M. E. Gaied<sup>1,3</sup>

<sup>1</sup>) Mineral Resources and Environment Laboratory, University of Tunis El Manar Faculty of Sciences of Tunis, Department of Geology, University Campus, 2092 Tunis, Tunisia.

<sup>2</sup>) National Office of Mines, Energy Street No. 24 Z.I. Charguia I, Tunis, Tunisia.

<sup>3</sup>) Higher Institute of Fine Arts in Sousse.

Corresponding author: imenmaala@gmail.com

S6- Dynamics of sedimentary Basins, Fluids & Georeservoirs (PS7)

### Abstract:

The study area is located in the Kasserine region to end of western-central part of Tunisia, named “Bou Chebka” region. It’s characterized by the largest sands deposits extra-siliceous in Tunisia: sands and sandstones of Beglia formation, extending into the region of Jebel Chaambi- Jebel Semmama-Bou Chebka. They are considered in quantity and quality as the best silica sand deposit. It is typified by its high silica content, to very low levels of impurities and by their remarkable granularity.

The research was interested to a multidisciplinary study to investigate the potential of extra siliceous, Serravallian – Tortonian, sands of Bou Chebka region, and estimate its use in industrial field, mainly in glassware. The morphoscopic analysis of detrital series shows that the useful fraction (100 - 630 microns) consists essentially transparent quartz grains, translucent to opaque. The densimetric separation identified very small quantities of some heavy minerals: tourmaline, staurolite and Zircon.

The mineralogical study of the total rock, by X-ray diffraction, shows that the sands are rich in quartz with low levels of feldspars. Chemical analysis of sand shows very high levels of SiO<sub>2</sub> corresponding to an extra siliceous sand (SiO<sub>2</sub> ≈ 98 %). Other major elements show low levels. However, contents of iron (Fe<sub>2</sub>O<sub>3</sub>), and coloring elements (TiO<sub>2</sub>) are slightly higher. By setting attrition sand processing parameters, the results demonstrated a decrease of Fe<sub>2</sub>O<sub>3</sub> (0, 04 %) and an increase in the SiO<sub>2</sub> content of about 99, 5 %. Geological sands reserves identified in Bou Chebka field are very important. It can be used in the manufacture of certain types of semi-white glass, colored glassware and glass wool.

The sustainability of the operation can be provided by the reservations contained in the immediate and natural extensions of these industrial sands. This site contains an ideal sands deposit, which is amenable to exploitation by quarry to produce multiple industrial use, in particular the manufacture of glass.

**Keywords:** The sands, Mineralogy, Chemistry, Attrition, Glassware.

## **Formation of ophiolite-bearing tectono-sedimentary mélanges in accretionary wedges by gravity driven submarine erosion: Insights from analogue models and case studies**

Malavieille Jacques<sup>1,2</sup>, Molli Giancarlo<sup>3</sup>, Genti Manon<sup>1</sup>, Dominguez Stephane<sup>1,2</sup>, Taboada Alfredo<sup>1,2</sup>, Beysac Olivier<sup>4</sup>, Vitale-Brovarone Alberto<sup>4</sup>, Lu Chia-Yu<sup>5,2</sup>, Chen Chih-Tung<sup>5</sup>

<sup>1</sup>) Université de Montpellier, Géosciences Montpellier, 34095 Montpellier cedex 5, France

<sup>2</sup>) LIA D3E, C.N.R.S.-M.O.S.T. France-Taiwan International Laboratory

<sup>3</sup>) Università di Pisa, Dipartimento di Scienze della Terra, Via S.Maria, 53, 56126 Pisa, Italy

<sup>4</sup>) Sorbonne Universités - UPMC Univ Paris 06, Institut de Minéralogie, de Physique des Matériaux, et de Cosmochimie (IMPMC), UMR CNRS 7590, 4 Place Jussieu, F-75005 Paris, France

<sup>5</sup>) National Taiwan University, Department of Geosciences, Taipei, Taiwan.

Corresponding author: malavie@gm.univ-montp2.fr

S6- Dynamics of sedimentary Basins, Fluids & Georeservoirs (PS7)

### **Introduction:**

Orogenic wedges locally present chaotic tectonostratigraphic units that contain exotic blocks of various size, origin, age and lithology, embedded in a sedimentary matrix. The occurrence of ophiolitic blocks, sometimes huge, in such “mélanges” raises questions on i) the mechanisms responsible for the incorporation of oceanic basement rocks into an accretionary wedge and ii) the mechanisms allowing exhumation and redeposition of these exotic elements in “mélanges” during wedge growth.

### **Analogue modelling:**

To address these questions, we present the results of a series of analog experiments performed to characterize the processes and parameters responsible for accretion, exhumation and tectonosedimentary reworking of oceanic basement lithospheric fragments in an accretionary wedge. The experimental setup is designed to simulate the interaction between tectonics, erosion and sedimentation. Different configurations are applied to study the impact of various parameters, such as irregular oceanic floor due to structural inheritance, or the presence of layers with contrasted rheology that can affect deformation partitioning in the wedge (frontal accretion vs basal accretion) influencing its growth (Fig. 1). Image correlation technique allows extracting instantaneous velocity field, and tracking of passive particles. Using the particle paths determined on models the pressure-temperature path of mélange units or elementary blocks can be discussed.

### **Case studies and tectonic model:**

The experimental results are then compared with observations from ophiolite-bearing mélanges in Taiwan (Lichi and Kenting mélanges) and Raman spectroscopy of carbonaceous material (RSCM) Thermometry data on rocks from the northern Apennines (Casanova mélange). A geological scenario is proposed following basic observations (Fig. 2). The tectonic evolution of the retroside of doubly vergent accretionary wedges is mainly controlled by backthrusting and backfolding. The retro wedge is characterized by steep slopes that are prone to gravitational instabilities. It triggers submarine landslides inducing huge mass transfers. This erosion combined with backthrusting could favour exhumation of the ophiolitic fragments formerly accreted at the base of the wedge along the rough

seafloor-sediments interface. Such an exhumed material can be reworked and deposited as debris-flows in proximal basins located at the foot of the retowedge slope forming a tectono-sedimentary mélangé. These syntectonic basins are continuously deformed and involved in prograding backthrusting-induced deformation.

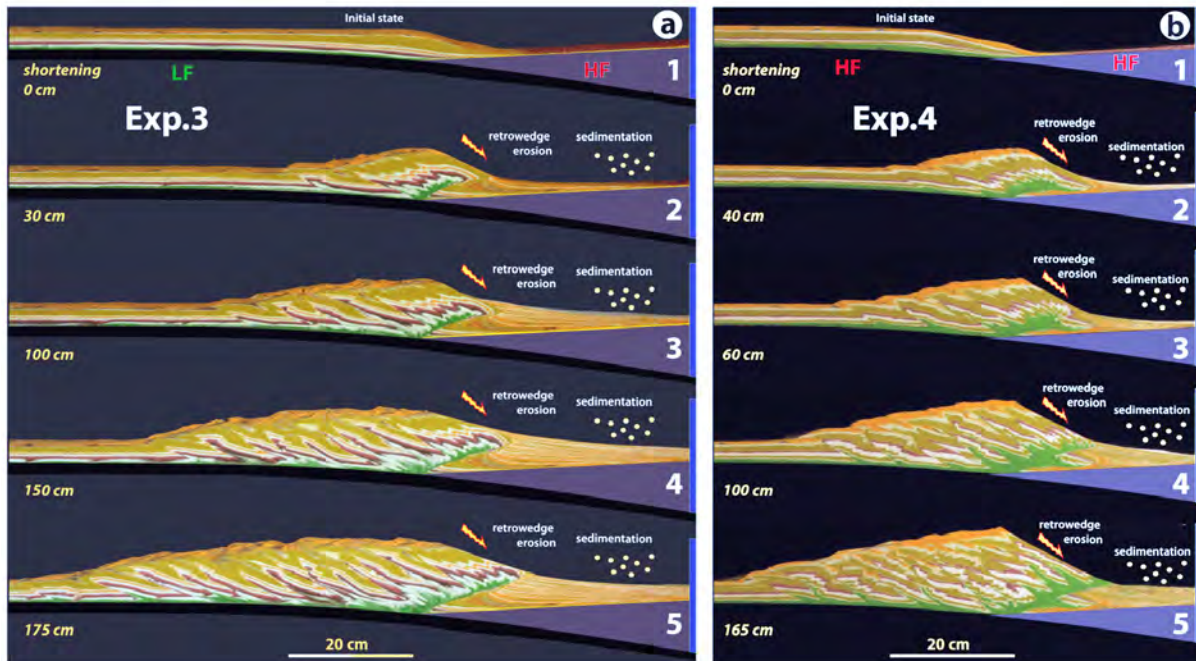


Figure 1: Evolutionary stages of experiments 3 and 4 outlining the impact of basal friction on wedge dynamics and exhumation.

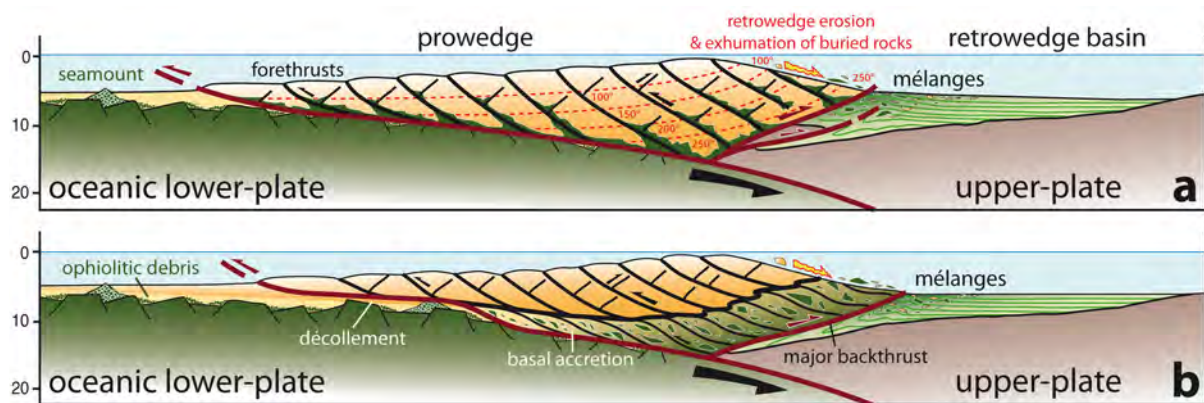


Figure 2: Cartoon illustrating the proposed model for exhumation and redeposition of ophiolitic debris and wedge rocks as tectono-sedimentary mélanges in the retowedge setting. Major backthrusting and gravity driven submarine erosion allows exhumation and deposition of exotic blocks in the syn-tectonic retowedge basin. a) First setting, the wedge grows by frontal accretion of imbricated thrust units. The red dotted lines suggest the shape of isotherms registered by peak temperature thermometry. b) Second setting, deformation partitioning occurs, the wedge grows by frontal accretion and basal accretion at depth.

**Keywords:** Tectono-sedimentary mélanges, ophiolites, analog modeling, Raman spectrometry, submarine erosion, Casanova mélangé, Apennines, Kenting & Lichi mélanges, Taiwan.

## Plate flexure and the development of depositional cycles in sedimentary basins: The Steer rears its head.

Moore, J. D. P.<sup>1,2</sup>, Watts, A. B.<sup>2</sup>

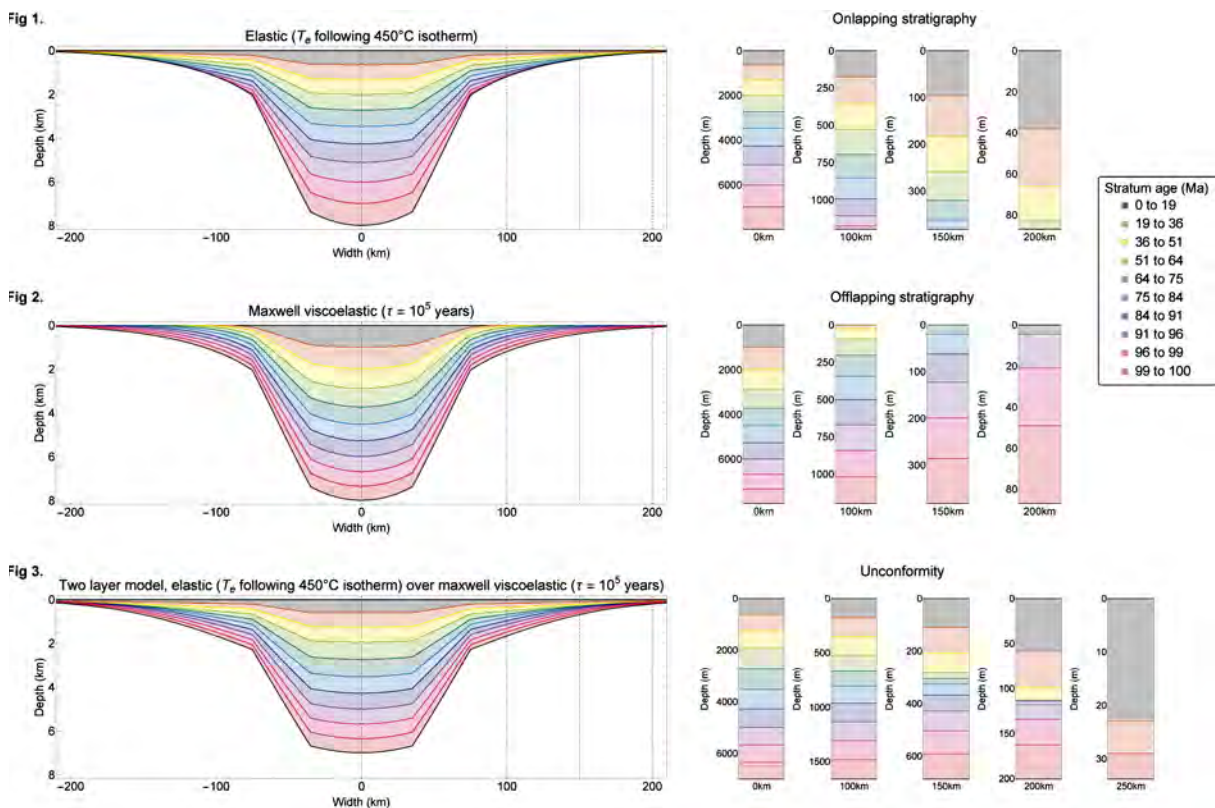
<sup>1</sup>Earth Observatory of Singapore, Nanyang Technological University, Singapore 639798.

<sup>2</sup>Department of Earth Sciences, University of Oxford

Corresponding author: earth@jamesdpmoore.com

S6- Dynamics of sedimentary Basins, Fluids & Georeservoirs (PS7)

Backstripping studies of biostratigraphic data from deep wells show that sediment loading is one of the main factors controlling the subsidence and uplift history of sedimentary basins. Previous studies based on single layer models of elastic and viscoelastic plates overlying an inviscid fluid have shown that sediment loading, together with a tectonic subsidence that decreases exponentially with time, can explain the large-scale ‘architecture’ of rift-type basins and, in some cases, details of their internal stratigraphy such as onlap and offlap. One problem with these so-called ‘steer’s head’ models is that they were based on a simple rheological model in which the long-term strength of the lithosphere increased with thermal age. Recent oceanic flexure studies, however, reveal that the long-term strength of the lithosphere depends not only on thermal age, but also load age.



We have used the thermal structure based on plate cooling models, together with recent experimentally-derived flow laws, to compute the viscosity structure of the lithosphere and a new

analytical model to compute the flexure of a multilayer viscoelastic plate by a trapezoid-shaped sediment load at different times since basin initiation. The combination of basin subsidence and viscoelastic flexural response results in the fluctuation of the depositional surface with time. In our new analytical model, we can replicate a range of stratigraphic patterns from onlap to offlap with a continuum of transitional behaviour.

This transition regime can produce a basin in which onlap dominates its early evolution while offlap dominates its later evolution with an unconformity separating the two different stratal patterns. The model also elucidates the behaviour of the depositional surface which can shallow, deepen, or cycle between the two. Cycles of sedimentation occur throughout the geological column, although they are arguably best developed in the Carboniferous cyclothem of Europe and North America.

Therefore, when consideration is given to the fact that the long-term strength of the lithosphere depends on *both* thermal and load age we are able to produce stratal geometries that not only closely resemble stratigraphic observations, but do not require either long-term sea-level or sediment flux changes in order to explain them.

## The impact of the Messinian Salinity Crisis on Petroleum Systems – A Modelling Perspective

Martin Neumaier<sup>1</sup>, Abdulaziz Al-Balushi<sup>2</sup>, Alastair J. Fraser<sup>2</sup> and Christopher A.-L. Jackson<sup>2</sup>

<sup>1</sup>) Schlumberger, Montpellier, France

<sup>2</sup>) Imperial College, London, United Kingdom

Corresponding author: mneumaier@slb.com

S6- Dynamics of sedimentary Basins, Fluids & Georeservoirs (PS7)

### Modelling the Messinian Salinity Crisis:

The offshore Levant Basin demonstrates one of the most phenomenal natural examples of a working petroleum system associated with a relatively rapid unloading and loading cycle caused by the Messinian Salinity Crisis (MSC). In this study (Al-Balushi et al. 2016, in press), 2D basin modelling suggests that the geologically instantaneous water unloading of c. 2070 m and subsequent rapid salt deposition and refill impact the subsurface pore pressure, temperature and other petrophysical parameters in the underlying sediments (Figure 1). The pressure drop is modelled to be instantaneous, whereas the impact on temperature is more of a transient response.

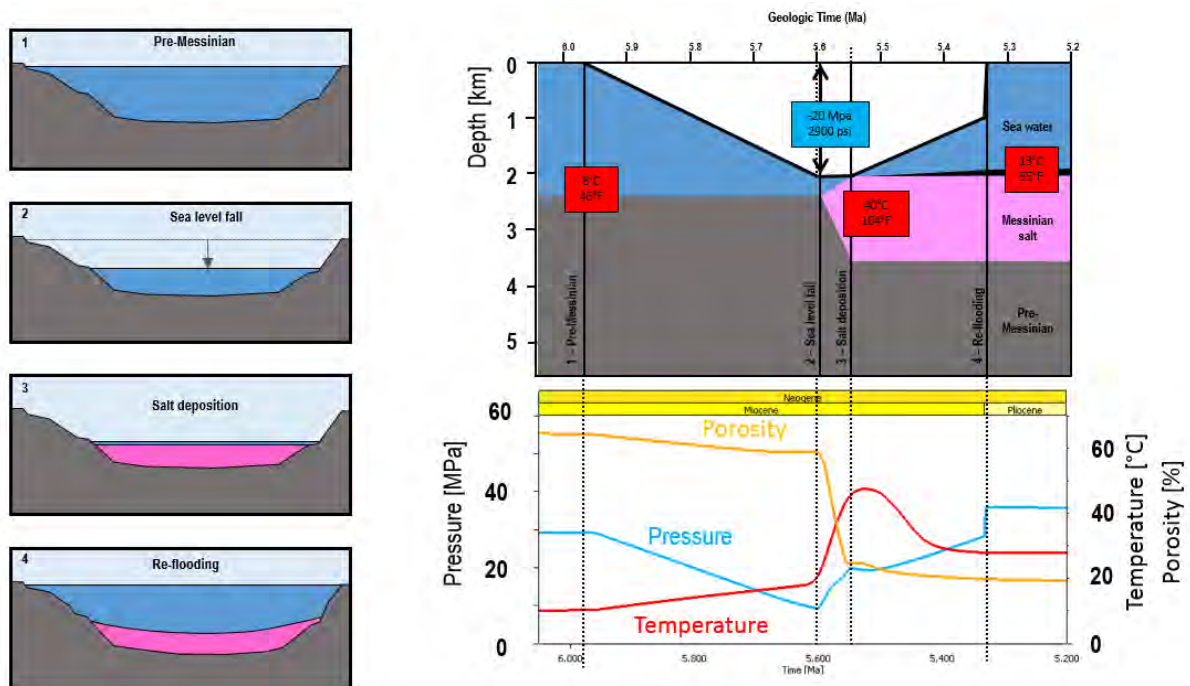


Figure 1: Conceptual model of the Messinian sea level drop and salt precipitation with results of pressure, temperature and compaction modelling.

### Impact on Petroleum Systems:

This has important consequences for the shallow sub-Messinian biogenic petroleum system, which is assumed to have experienced fluid brecciation associated with massive fluid escape events. Deeper Oligo-Miocene sediments are far less affected, thus indicating a "preservation window" for biogenic gas accumulations, which hosts the recent discoveries (Tamar, Leviathan, Aphrodite; Figure 2). Hydrocarbon accumulations of a "bubblepoint oil" composition are modelled to have experienced a phase change followed by gas cap expansion during the drawdown, with the pressure drop being the primary control. This study suggests that seal-limited traps are expected to have undergone a catastrophic seal failure, resulting in a series of pockmarks in the vicinity of the Messinian salt.

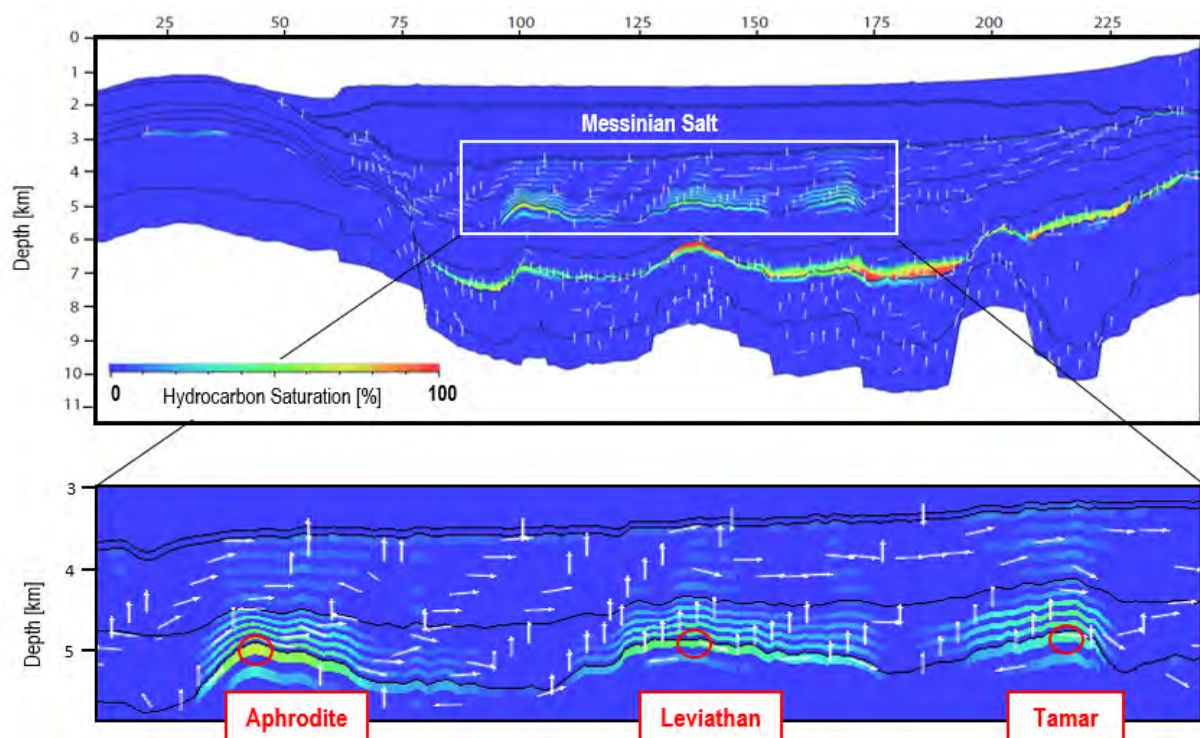


Figure 2: Cross section with hydrocarbon saturations resulting from petroleum systems modeling.

### References:

Al-Balushi, A., Neumaier, M., Fraser, A. J., Jackson, C. A. L., 2016. The impact of the Messinian Salinity Crisis on the petroleum system of the Eastern Mediterranean: a critical assessment using 2D-petroleum system modelling. *Petroleum Geoscience* (in press)

**Keywords:** Mediterranean Sea, Messinian Salt, Levant Basin, Pockmarks, Fluids, Biogenic Gas, Petroleum Systems, Tamar.

## **Salt tectonics in thick-skinned extensional and strike-slip settings: recognising strike-slip reactivation of the extensional basins in the Southern North Sea**

Jeroen Smit<sup>1</sup>, Renaud Bouroullec<sup>2</sup>, Stefan Peeters<sup>1,2</sup>, Dagmar Smit<sup>1</sup>, Bram Scheffers<sup>1</sup> en Dimitrios Sokoutis<sup>1</sup>

<sup>1</sup>) Earth Science Department, Utrecht University, PO Box 80.021, 3508 TA Utrecht, the Netherlands

<sup>2</sup>) TNO Energy, P.O. Box 80015, NL-3508 TA Utrecht, The Netherlands

Corresponding author: [j.h.w.smit@uu.nl](mailto:j.h.w.smit@uu.nl)

S6- Dynamics of sedimentary Basins, Fluids & Georeservoirs (PS7)

### **Introduction:**

The Southern North Sea is dissected by a series of Permian-Triassic and Jurassic extensional basins that are strongly influenced by salt tectonics, related to a thick layer of Late Permian Zechstein evaporites that decouples the Mesozoic basin-fill from the Paleozoic basement. Although the current tectonic setting and crustal structure of the Southern North Sea results from repeated tectonic activity over the past 400 My, most of the fault network was already established before the late Carboniferous Variscan orogeny. The southern North Sea's segmentation in several basins, platforms and highs was completed after the Permian-Triassic and Late Jurassic rifting phases (e.g. Ziegler et al., 1990). The Permian-Triassic and Late Jurassic extensional basins were partly inverted during Late Cretaceous and Paleogene convergence. The current basin fill reflects only part of the tectonic history due to salt tectonics and several erosion phases.

Logically, a network of parallel extensional basins of the same age is interlinked by strike-slip faults and strike-slip motion should therefore be a general feature. However, like in most cases, the recognition of strike-slip displacement in the North Sea is not obvious and further complicated by fault reactivation and salt tectonics. Moreover, the evaporites cause a strong decrease in seismic resolution, limiting the seismic resolution below the Zechstein.

### **Modelling of strike-slip reactivation:**

To better understand the localisation and mechanics of strike slip reactivation in extensional salt-tectonic basins, a series of tectonic laboratory experiments was performed. We however started our experimental study with experiments on post-rift salt tectonics in light of the many salt walls and diapirs in the Southern North Sea and their possible role in accommodating strike-slip deformation. The early stages of salt tectonics in thick-skinned extension has been studied rather well (e.g., Nalpas and Brun, 1993), less is known about the further development of ductile structures after the seize of regional extension.

Because we are unaware of experimental studies that focussed on salt tectonics in strike-slip settings, besides the application to pull-apart basins (e.g. Smit et al., 2008), we investigated the evolution and the internal and external structure of salt tectonics in pure strike slip systems in the second series.

A final series focussed on reactivation in strike slip of extensional basins. The models demonstrate that the presence of a weak layer in a pre-formed basin has a profound effect on the deformation pattern when the preformed basin is subjected to strike-slip deformation. Results are applied to the North Sea Central Graben.

## References:

- Nalpas, T., Brun, J.P., 1993. Salt flow and diapirism related to extension at crustal scale. New insights into salt tectonics. *Tectonophysics* 228, 349-362.
- Smit, J., Brun, J.P., Fort, X., Cloetingh, S., Ben-Avraham, Z., 2008. Salt tectonics in pull-apart basins with application to the Dead Sea Basin. *Tectonophysics* 449, 1-16.
- Ziegler, P.A., 1990. *Geological Atlas of Western and Central Europe*, 2nd. Ed. . Shell Int. Pet. Mij., distributed by Geol. Soc. Publ. House, Bath.

**Keywords:** North Sea, thick-skinned, thin-skinned, reactivation, strike-slip, extension, brittle-ductile coupling, tectonic laboratory experiments.

## Interrelation between surface and basement heat flow in sedimentary basins

Alban Souche<sup>1,2</sup>, Daniel W. Schmid<sup>1,2</sup>, Lars Rüpke<sup>3</sup>

<sup>1</sup>) GeoModelling Solutions, Hardturmstrasse 120, 8005 Zürich, Switzerland

<sup>2</sup>) Physics of Geological Processes, University of Oslo, Norway 3) GEOMAR, Helmholtz Center for Ocean Research Kiel.

Corresponding author: Germany [alban.souche@geo.uio.no](mailto:alban.souche@geo.uio.no)

S6 – Dynamics of sedimentary Basins, Fluids & Georeservoirs (PS7)

### Introduction:

A number of key processes in sedimentary basins are temperature-controlled. Examples include source rock maturation, quartz cementation, and smectite to illite transformation. These processes are particularly relevant for petroleum system analysis as they affect the generation of hydrocarbons, fluid pressure development, and reservoir quality.

Modeling the thermal evolution of a sedimentary basin involves solving the transient heat equation, which requires the specification of initial and boundary conditions. Within the crust, and more generally within the entire lithosphere, a relatively constant boundary condition through geological time scale is the ~1300 °C isotherm defining the Lithosphere-Asthenosphere-Boundary (LAB). Petroleum System Models (PSM) are, however, designed to resolve sedimentation processes within a specific region of interest where the heat equation is solved at basin-scale and far away from the LAB.

Therefore, PSM rely on the assumption of a basement heat flow boundary condition. There are several drawbacks in using such boundary condition: 1) the basement heat flow is usually unknown and may evolve during the basin formation, and 2) the basement heat flow can be influenced by thermal feedbacks from sedimentary processes (Rüpke et al., 2013). Regarding these limitations, several geodynamic models can be used to approximate a value of the basement heat flow, ranging from the classic McKenzie model (McKenzie, 1978, Jarvis and McKenzie, 1980) to fully dynamic margin models (e.g., Huismans and Beaumont, 2011). However, these lithospheric-scale geodynamic models often neglect the basin-scale sedimentation processes.

In this study, we calculate the basement and surface heat flow in a sedimentary basin by taking into account both basin-scale and lithospheric-scale thermal processes using a tailored 1D finite element model. Our model domain extended through the entire lithosphere, where the thermal boundaries are relatively well constrained, and is greatly refined toward the surface to accurately account for the formation of the basin and solve for the basin-scale thermal processes. We will illustrate the importance of taking into account the thermal processes operating on both scales simultaneously with the “classical” example of a rift basin formation. We will also assess the relevance of using surface heat flow measurements for the calibration of the basement heat flow into PSM and show that a simple relationship between surface and basement heat flow only exists in thermal steady state.

### Results – thermal structure of a rift basin:

Here we model the thermal structure of a rift basin created by isostatic compensation after uniform stretching of the lithosphere. We systematically quantify the effect of the transient thermal processes inherent to basin formation, such as sedimentation and compaction driven fluid flow, on the evolution of the basement and surface heat flow.

Figure 1a shows the temperature evolution of the 10 first km of the model where the black line represents the depth of the forming basin. The corresponding evolution of the basement and surface heat flow are plotted Figure 1b. To illustrate the importance of the sedimentary processes in the thermal evolution of the system, we compare our results with the heat flow prediction from McKenzie model, which neglects the presence of sediments in the basin.

Two important observations can be made; 1) sedimentation processes may lead to a reduction of the surface and basement heat flow at the initial stage of rifting, and 2) a decoupling between surface and basement heat flow may be expected during syn-rift and shortly after post-rift.

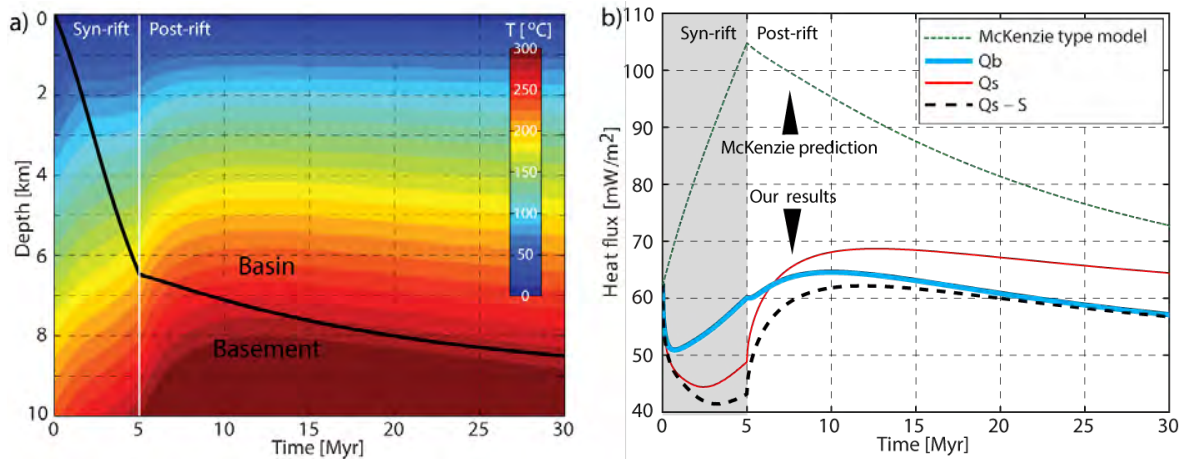


Figure 1: a) Temperature evolution during syn-rift (5 Ma, stretching factor 2) and post-rift in the upper 10 km of the model. b) Corresponding evolution of the basement heat flow ( $Q_b$ ), surface heat flow ( $Q_s$ ), and corrected surface heat flow ( $Q_s - S$ ) calculated in our model compared to the surface/basement heat flow predicted by McKenzie model where thermal disequilibrium and sedimentation processes are neglected.

Our results show that resolving sedimentation processes in basin modeling is crucial, with the thermal impact of sediment deposition being at least as important as rifting induced basement heat flow variations.

### References:

- Huismans, R., and Beaumont, C., 2011. Depth-dependent extension, two-stage breakup and cratonic underplating at rifted margins, *Nature*, 473, 74-78.
- Jarvis, G. T., and McKenzie, D., 1980. Sedimentary basin formation with finite extension rates, *Earth and Planetary Science Letters*, 48, 439-459.
- McKenzie, D., 1978. Some remarks on the development of sedimentary basins, *Earth and Planetary Science Letters*, 40, 25-32.
- Rüpke, L. H., Schmid D. W., Perez-Gussinye, M., and Hartz E., 2013. Interrelation between rifting, faulting, sedimentation, and mantle serpentinization during continental margin formation - including examples from the Norwegian Sea. *Geochemistry Geophysics Geosystems*, 14, 4351-4369.

**Keywords:** Basin modeling, surface/basement heat flow evolution, sedimentation processes, rifting.

## **Sandbox modelling of foredeep deformation and application to the Southern Alps Northern Apennines system**

Claudio Turrini<sup>1</sup> and Giovanni Toscani<sup>2</sup>

<sup>1</sup>) CT GeolConsulting, St. Germain-en-Laye, 78100, France

<sup>2</sup>) University of Pavia, Dipartimento di Scienze della Terra e dell' Ambiente, Italy

Corresponding author: [clturri@wanadoo.fr](mailto:clturri@wanadoo.fr)

S6 - Dynamics of sedimentary Basins, Fluids & Georeservoirs (PS7)

The Po Valley (northern Italy) is a rather peculiar foreland-foredeep tectonic system. Indeed, from Oligocene to present the region was the contemporaneous foredeep to the Southern Alps and the Northern Apennines belts which intermittently advanced towards the south and the north respectively, while deforming across a common foreland.

During the related geodynamic events, the northernmost sector of the Adria microplate (present-day Po Valley) was (i) colliding against the Eurasian plate, (ii) counterclock-rotating around a pivot-zone likely placed in the western zone of the Adria indenter and (iii) giving rise to the Southern Alps and the Northern Apennines tectonic arcs, now buried by Plio-Pleistocene sediments.

In the attempt to simulate the Cenozoic fold-and-thrust tectonics across the basin, we carried out a set of sand-box models where a curved shape backstop was used to reproduce the Alpine-age rotational geodynamics that happened in the region. Intermediate deformation steps were surveyed through model surface scan, while internal sections have been carried out at the end of the simulation process. Results from the experiments suggested the possible evolution of the Po Valley structural arcs and they allowed the associated deformation geometries and mechanisms to be reconstructed in the 3D space.

Once the role of the Mesozoic, inherited pre-compressional structures distribution is accepted as a key factor for the initiation and development of the Po Valley buried arc, our sandbox models suggest that arc-shaped thrust fronts can be produced simply as a function of

1. the centripetal belt rotation around the pivot-zone and towards a common foreland-foredeep region,
2. the displacement gradient, decreasing towards the pivot, that is acquired by the different tectonic arcs as shortening increases during the deformation progression.

The experiments throw some new insights about deformation partitioning inside such a three-dimensional complex tectonic setting that can eventually be used as analogs to other similar settings, worldwide.

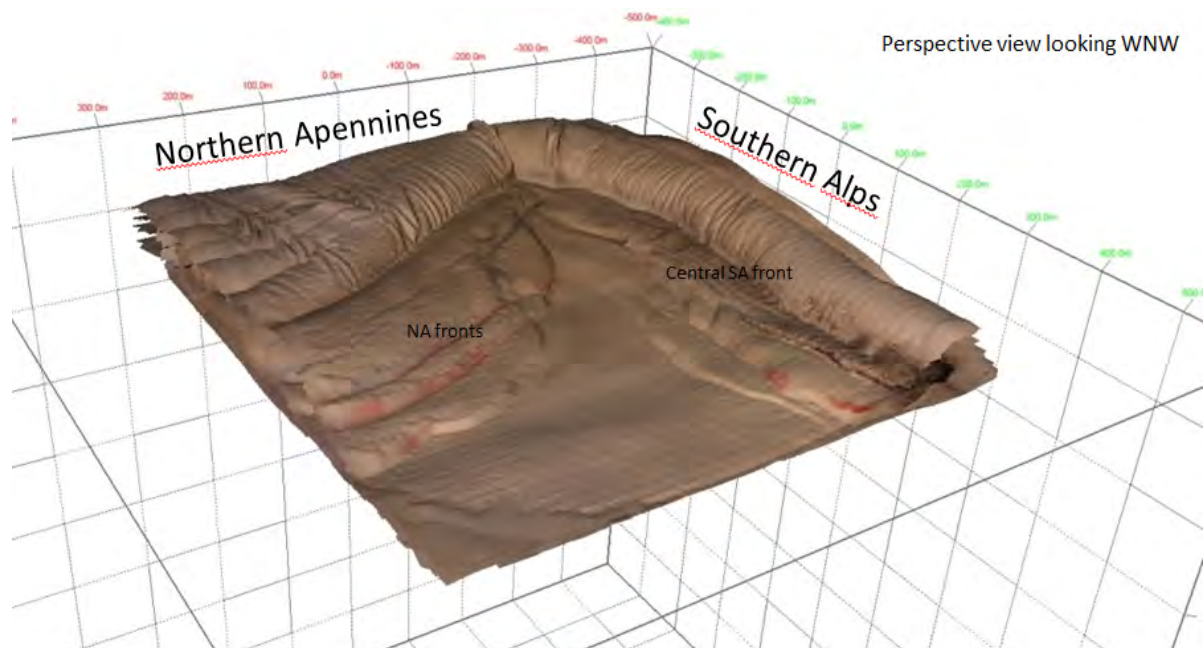


Figure 1: Map pictures of different steps of the model have been overlapped on corresponding digital surface scan.

**Keywords:** Po Plain, Analogue Models, Foredeep Deformations, Structural arcs.

## **Contribution of the spatial distribution and geostatistics in the study of waters geochemistry of wadi meliane, in the capital of Tunisia**

Asma Yahyaoui<sup>1,2</sup>, Rim Ben Amor<sup>1</sup>, Myriam Abidi<sup>1</sup>, Moncef Gueddari<sup>1</sup>, Lassaad Chouba<sup>2</sup>

<sup>1</sup>) Geochemistry and Environmental Geology Laboratory, Geology Department, Faculty of Sciences of Tunis, University campus, 2092 Tunis, Tunisia.

<sup>2</sup>) Laboratory of Marine Affairs, INSTM, Fishing Port of Goulette, 2060, Tunis, Tunisia.

Corresponding author: asma.yahyaoui@gmail.com

S6 - Dynamics of sedimentary Basins, Fluids & Georeservoirs (PS7)

### **Abstract:**

Wadi Meliane is the second major rivers of Tunisia, it opens in the sea at the coast of the Rades. It is particularly affected by the problem of the growing population and the continuous development of industry and agriculture. Wadi Meliane is subject to important risks of pollution in both urban and industrial discharges and, threatening the quality of its waters.

The objective of this study is to contribute the spatial distribution and geostatistics in the study of geochemistry wadi Meliane and identifying natural and anthropogenic factors that control its evolution, and to estimate the degree of pollution of waterways.

To achieve our goals, a sampling campaign was conducted and water samples were collected. These samples were subject to analysis of physico-chemical parameters, nutrients, evaluation parameters of the organic chemical pollution and major elements.

The use of ArcGIS allowed to mount space distribution of different elements and demonstrate the concentrations of elements according to the rate of pollution.

The principal component analysis allowed to highlight the correlation between the different parameters and differentiate areas of the water quality in the study area, showing that the degree of concentration varies from one site to another according varies with the distance away from the source of pollution.

**Keywords:** Geochemistry, Wadi Meliane, ArcGIS, Spatial distribution, Principal component analysis.

## **Modelling of shales and maturation of organic matter by the using of the mechanism of phase transition in physical models.**

Alain Zanella<sup>1</sup>, Salomé Larmier<sup>2</sup> and Régis Mourgues<sup>1</sup>

<sup>1</sup>) Laboratoire de Planétologie et Géodynamique, LPG – UMR CNRS 6112 - Université du Maine, Le Mans, France

<sup>2</sup>) Master 1, Géosciences Montpellier – UMR 5243 - Université de Montpellier 2, France

Corresponding author: alain.zanella@univ-lemans.fr

S6 - Dynamics of sedimentary Basins, Fluids & Georeservoirs (PS7)

### **Abstract:**

The maturation of organic matter within shales is a complex phenomenon, which can be described as a simple mechanism of phase transition (from solid to fluid). During this geological process, hydrocarbons that are fluids (as oil and/or gas) are generated from the solid particles of the immature organic matter. This phenomenon leads to a fluid overpressure within the pore space of the source rock as well as a hydraulic fracturing when the fluid pressure exceeds the lithostatic pressure. The geometry of the fracture network essentially consists of multiple bedding-parallel fractures filled by fibrous calcite (often called beef veins).

Nowadays, physical models, able to generate a fluid from solid particles, are mainly the best approach to study these mechanisms. Thus in such models, a mechanism of phase transition is used to generate a liquid by an increasing of the temperature and therefore no injector system is required to add a fluid in these models. To simulate a source rock, a mixture of silica powder and beeswax microspheres is used. This granular and isotropic material is porous but impermeable. With this experimental approach, the study of mechanisms of fluid overpressures and hydraulic fracturing became more adapted but the scaling of the physical models are still not clearly done and all of intrinsic source rocks parameters, as the anisotropy, are not taking in account. However, the anisotropy of shales seems to be a key parameter in the shape of the hydraulic fracturing network.

In such a context, we decided to perform (1) series of shear tests on the previous analogue materials, and (2) to develop news materials that will better take in account the rheology of a source rock. The shear tests have been performed on several mixtures composed by different proportions of silica powder and beeswax microspheres (respectively 30%, 40% and 50% by volume of beeswax), as well as different temperatures (from 20°C to the melting point of wax ~62°C). The proportions of beeswax are in volume and allow us to simulate different concentration of organic matter in a source rock. The different temperatures simulate the different maturity degrees of the source rock.

In addition of the previous materials, we developed new granular materials constituted with a mixture of silica powder, wax flakes and micas. The flakes of wax and the micas allow us to create an anisotropic material, which is still impermeable with interstitial silica particles. With the using of these materials in different proportions, we are able to control the organic content, the anisotropic degree and the permeability of our analogue source rock. Thus, sources rocks are better considered in experimental models.

**Keywords:** Source rocks, hydraulic fracturing, phase transitions, organic matter.